WILEY-VCH

Edited by
Teresa M.V.D. Pinho e Melo and Marta Pineiro

Heterocycles

Synthesis, Catalysis, Sustainability, and Characterization

Heterocycles

Heterocycles

Synthesis, Catalysis, Sustainability, and Characterization

Edited by Teresa M.V.D. Pinho e Melo and Marta Pineiro

WILEY-VCH

Editors

Prof. Teresa M.V.D. Pinho e Melo
University of Coimbra
Coimbra Chemistry Centre (CQC)
Department of Chemistry
Rua Larga
3004-535 Coimbra
Portugal

Prof. Marta Pineiro
University of Coimbra
Coimbra Chemistry Centre (CQC)
Department of Chemistry
Rua Larga
3004-535 Coimbra
Portugal

Cover Image: Courtesy of Teresa M.V.D. Pinho e Melo and Marta Pineiro

Library of Congress Card No.: applied for

British Library Cataloguing-in-Publication Data
A catalogue record for this book is available from the British Library.

Bibliographic information published by the Deutsche Nationalbibliothek
The Deutsche Nationalbibliothek lists this publication in the Deutsche Nationalbibliografie; detailed bibliographic data are available on the Internet at <http://dnb.d-nb.de>.

Print ISBN: 978-3-527-34886-2
ePDF ISBN: 978-3-527-83199-9
ePub ISBN: 978-3-527-83201-9
oBook ISBN: 978-3-527-83200-2

Typesetting Straive, Chennai, India
Printing and Binding

Printed on acid-free paper

Contents

Preface

Heterocyclic chemistry plays a central role in organic chemistry, being the field with the greatest impact in terms of applications. Heterocycles are widely present in many naturally occurring compounds and are particularly relevant in the pharmaceutical and agrochemical industries besides being important materials in other industrial applications. Therefore, it does not come as a surprise that an impressive number of contributions on heterocyclic chemistry appear each year aiming at the development of novel and more sustainable synthetic methodologies and to achieve higher structural diversity to meet the demands of the various heterocycles' applications.

The planning of the book had *Synthesis, Catalysis, Sustainability and Characterization* as the main guidelines. The ***Synthetic Methods*** include chapters on selected "hot topics" covering the state-of-the-art on synthetic approaches to heterocycles. The choice of themes was based on the relevance of the transformations with regard to the high potential already demonstrated and prospects for new developments. They comprise the following topics: chiral heterocycles via enantioselective photochemical reactions, heterocycles via dearomatization reactions, and an overview of synthetic strategies toward heterocyclic macrocycles and medium-sized rings. Special focus was also given to ***Catalytic Methods*** with chapters on organocatalysis, transition-metal catalysis, and biocatalysis.

At present, the relevance of green chemistry is justified by the inclusion of selected topics on ***Sustainability*** in the context of the synthesis of heterocyclic compounds. Multicomponent synthesis, synthesis from renewable resources, synthesis in nonconventional reaction media, mechanochemistry, and flow chemistry are covered.

The book includes a chapter on the use of matrix isolation spectroscopy as a tool for structural ***Characterization*** and for unprecedented mechanistic insights on reactions involving heterocyclic compounds. The final chapter is a comprehensive overview on oxygen heterocycles *Characterization* by NMR spectroscopy, with great practical utility for those working with these scaffolds.

The book is aimed at advanced-level readers and specialists in the area of heterocyclic chemistry. This includes researchers from academia and students of advanced courses on Organic Chemistry, Medicinal Chemistry, and Green Chemistry, as well as researchers in the field of Fine Chemical Industry.

This feature of having topics covering cutting-edge research on heterocyclic chemistry was only possible due to contributions from an outstanding international team of 30 authors, which are gratefully acknowledged, making *Heterocycles – Synthesis, Catalysis, Sustainability, and Characterization* a unique book that we hope will become a reference in the area of Heterocyclic Chemistry.

University of Coimbra, Coimbra
22 March 2022

Teresa M.V.D. Pinho e Melo
Marta Pineiro

1

Heterocyclic Compounds in Enantioselective Photochemical Reactions

Norbert Hoffmann

Université de Reims Champagne-Ardenne, CNRS, ICMR, Equipe de Photochimie, UFR Sciences, B.P. 1039, Reims 51687, France

1.1 Introduction

The present chapter deals with different key topics. Heterocyclic compounds play a central role in many domains of chemistry such as the search of new biologically active compounds in pharmaceutical and agricultural chemistry [1]. Also, many new materials such as semiconducting compounds contain heterocyclic moieties [2]. In these domains, a large structural diversity and molecular complexity is highly needed. Here, traditional methods of organic synthesis find their limits. Photochemical reactions extend such limits. As electronic excitation completely changes the chemical reactivity of compounds or whole family of compounds [3], products, which cannot be synthesized by more conventional methods become accessible and are of high interest for application in the field of bioactive compounds [4, 5]. Furthermore, the outcome of known reactions, especially catalytic reactions, can be improved when they are carried out under photochemical conditions. Based on the enormous quantity of recent and past results in the field of photochemical reactions, it makes sense to subdivide chemical reactions into two classes: reactions that occur in the electronic ground state and reactions in which electronic excitation is involved. From the economic and ecological point of view, photochemical reactions are particularly interesting, since many of them can be carried out without an additional chemical reagent. The photon is considered as a traceless reagent [6, 7]. For these reasons, these reactions are now highly appreciated in chemical and pharmaceutical industry [8–10].

Stereoselectivity also plays a central role in organic synthesis. Biological activity and material properties strongly depend on the stereochemistry of chemical compounds. Sooner or later, almost all synthesis methods will face this problem. In the past, photochemical reactions have been considered as being inherently stereo-unselective. It was thought that the high energy uptake by light absorption induces uncontrolled relaxation processes that lead to unselective reactions with large amounts of degradation either of the substrates or the photoproducts [11].

Heterocycles: Synthesis, Catalysis, Sustainability, and Characterization, First Edition.
Edited by Teresa M.V.D. Pinho e Melo and Marta Pineiro.

In this regard, it must however be pointed out that stereoselective and stereospecific photochemical reactions have been known from the very beginning of this research area [12, 13]. The controlled dissipation of the high electronic excitation energy in photochemical reactions is the reason for the high stereoselectivity in such reactions [11]. In particular, photochemical reactions can be conducted enantioselectively in chiral supramolecular structures [14, 15]. Enantiopure compounds are obtained in different ways: they can be prepared directly from other chiral precursors such as natural products ("chiral pool") or by optical resolution using different types of chromatography or crystallization techniques. Asymmetric syntheses using chiral auxiliaries, which are removed after the stereoselective reaction, also provide enantiopure compounds. Asymmetric catalysis and enzymatic catalysis directly yield enantioenriched compounds. A chiral enantiopure environment in a supramolecular structure or in a crystal may be the inductor of chirality in asymmetric reactions. In the present chapter, methods will be discussed leading directly to enantiopure heterocyclic compounds via photochemical reactions.

1.2 Asymmetric Catalysis with Chiral Templates

Photochemical substrates may be complexed with chiral structures that induce chirality [16]. A typical example is described in Scheme 1.1 [17]. The quinolone derivative **1** carrying a pyrrolidine moiety undergoes an intramolecular cyclization leading to the spirocyclic indolizidine compound **6**. The substrate is complexed with the enantiopure Kemp acid derivative (**2**) via hydrogen bonds between two lactam

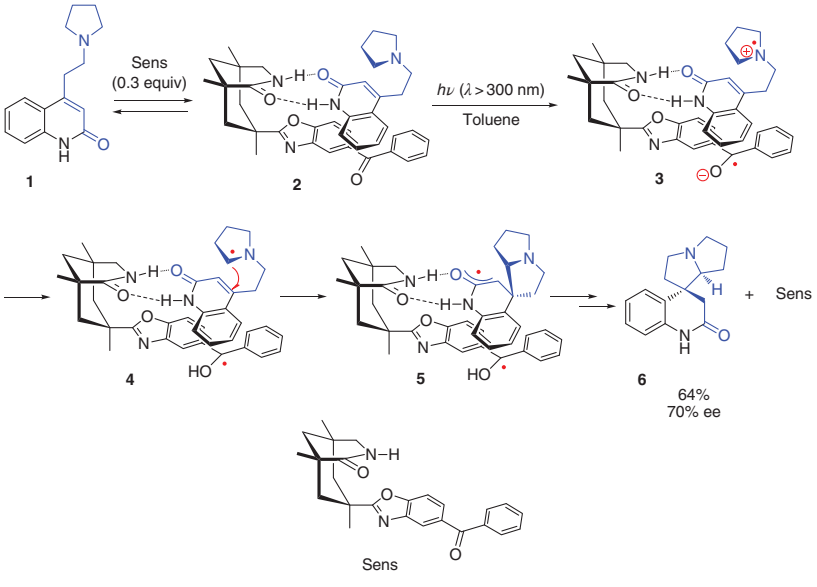

Scheme 1.1 Enantioselective synthesis of a spirocyclic indolizidine compound induced by a photochemical electron transfer.

moieties. In this arrangement, the pyrrolidine approaches the reaction center mainly by one diastereotopic half-space. In this complex, the shielding group acts also as an aromatic ketone sensitizer (sens). After photochemical excitation of the latter, electron transfer from the tertiary amine moiety to the ketone leads first to a radical ion pair **3** and after proton transfer to intermediate **4** [18]. The nucleophilic α-aminoalkyl radical attacks with 70% of stereoselectivity the electrophilic double bond of the quinolone moiety. Thus, an electrophilic oxoallyl radical is generated affording the diradical intermediate **5**. The final product **6** results from a hydrogen transfer from the ketyl radical to the oxoallyl radical. It must be pointed out that in the present case this step is favored because it is an intramolecular process. In these radical steps, polar effects play an important role [19–21]. In the corresponding intermolecular stereoselective reactions, these effects contribute essentially to the efficiency of these processes [18]. The intermolecular addition of tertiary amines to indolone derivatives with an exocyclic electron-deficient olefinic double bond has been carried out with similar Kemp acid derivatives [22]. In this case, however, ruthenium or iridium complexes have been used as external photoredox catalysts that were excited by visible light absorption.

Using a similar chiral sensitizer, an intramolecular [2+2] photocycloaddition has been carried out with high enantioselectivity (Scheme 1.2) [23]. The quinolone derivative **7** is transformed, under visible light irradiation, into a complex polycyclic compound **8** containing a pyrrolidine moiety. It must be pointed out that the same [2+2] photocycloaddition is also induced by UV irradiation via direct light absorption but no chiral induction takes place. It is therefore necessary to choose a sensitizer that absorbs in the visible domain of the light spectrum to ensure enantioselectivity. The thioxanthone derivative **9** absorbs in the visible light region and transfer its triplet energy to the complexed substrate (**10**). Again, this complexation occurs via hydrogen bonds between the two lactams of the substrate and the Kemp acid moiety of the sensitizer. In this structure the olefinic double bond in the side chain approaches the reactive center of the quinolone almost only by one

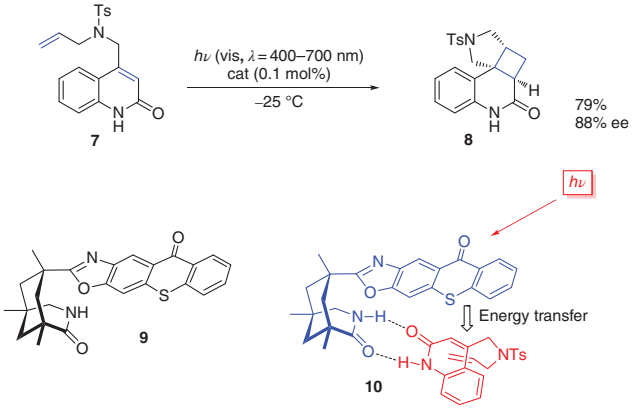

Scheme 1.2 Construction of a pyrrolidine moiety using an enantioselective [2+2] photocycloaddition. Source: Alonso and Bach [23] / John Wiley & Sons.

diastereotopic half-space. Similar asymmetric reactions have been performed with 3-alkylquinolones carrying a 4-*O* alkene side chain. In this case, tetrahydrofuran moieties are formed [24].

The substrate can also be complexed to a metal or a strong coordinating atom. In such a case, chirality is induced by a chiral ligand sphere [25]. In this context, chiral Lewis acid **11** was used to catalyze the asymmetric intramolecular [2+2] photocycloaddition of the dihydropyridinone derivative **12** (Scheme 1.3) [26]. In this reaction, a δ-valerolactam moiety (**13**) is formed. By complexation with a Lewis acid, the absorption maximum of compound **12** is shifted from 290 to 350 nm. Using fluorescent lamps with an emission λ_{max} = 366 nm, complex **14** was excited almost exclusively since the noncomplexed substrate **12** does not absorb light in this spectral range. Thus, the formation of racemic product as background reaction is suppressed. In the complex **14**, the approach of the olefin to the reaction center again occurs by one diastereotopic half-space.

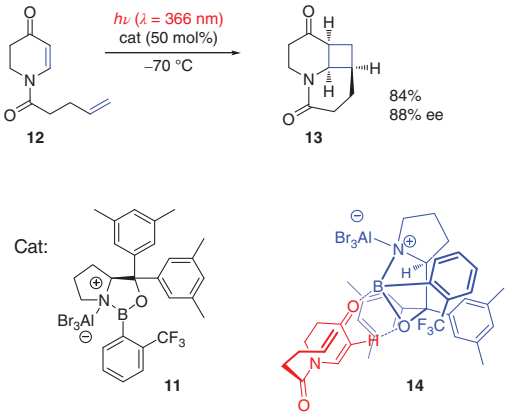

Scheme 1.3 Enantioselective Lewis acid catalysis of an intramolecular [2+2] photocycloaddition reaction. Source: Brimioulle and Bach [26] / American Association for the Advancement of Science.

α,α,α′,α′-Tetraaryl-2,2-disubstituted 1,3-dioxolane-4,5-dimethanols (TADDOLs, e.g. **23**) are capable of complexing numerous substrates via hydrogen bonds [27]. When a photochemical substrate is complexed with such compounds, chirality can be induced. Under these conditions, when the flavone derivative **15** was irradiated with the diphenyl butadiene **16**, a [2+3] cycloaddition took place, leading to compounds **17** and **18** (Scheme 1.4) [28]. After reduction with $NaBH_4$, compounds **19** and **20** were isolated in good yields. Furthermore, the major diastereoisomer **19** was obtained in high enantioselectivity, and recrystallization led to almost enantiopure samples. The high enantioselectivity of the photochemical reaction was explained by the structure of complex **21**, which strongly favors the attack of the olefin by only one diastereotopic half-space. Interestingly, when the sterically much less encumbered chiral alcohol **22** was added instead of the TADDOL compound

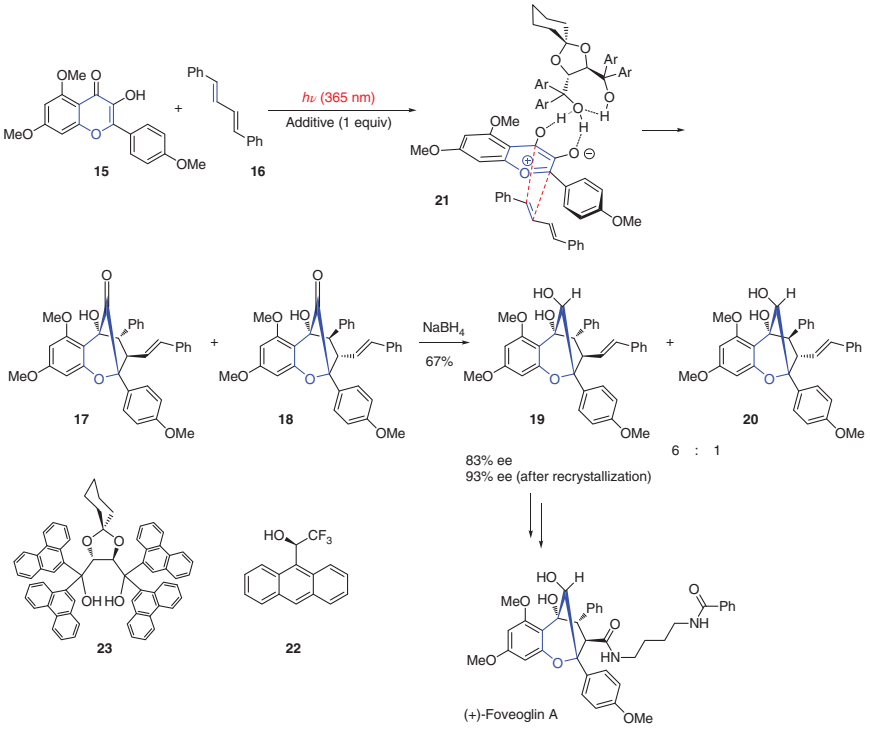

Scheme 1.4 Asymmetric synthesis of (–)-foveoglin A using ESIPT-promoted [2+3] cycloaddition with a flavone derivative. Source: Wang et al. [28] / John Wiley & Sons.

23, an efficient chiral induction was still observed. The high enantioselectivity observed with hydrogen bond complexes can also be explained by the fact that excited state intramolecular proton transfer (ESIPT) plays a key role in the reaction mechanism [29]. In fact, it was shown that the cycloaddition occurred at the triplet state of **15** and that most probably single electron transfer is involved. Compound **19** was transformed into (+)-foveoglin A, which is the enantiomer of a natural product. This compound family plays an important role in medicinal chemistry as they possess anticancer and antiviral activities.

The cyclization reaction of two alkynes and one nitrile function is a convenient method for the preparation of pyridine compounds [30]. It can be carried out under particular mild conditions when simple and inexpensive cobalt catalysts such as **24** are used (Scheme 1.5) [31]. Under irradiation with visible light, the formation of the cobaltacyclopentadiene intermediate **25** is accelerated, and the addition of the nitrile leading to the intermediate **26** or **27** becomes the rate-determining step. The consumption of the nitrile substrate becomes the first-order reaction step. Under these particularly mild conditions, a variety of pyridine derivatives have been synthesized possessing fragile substituents (Figure 1.1) [32]. Asymmetric catalysis was also successfully performed. The cyclopentadienyl ligand in the

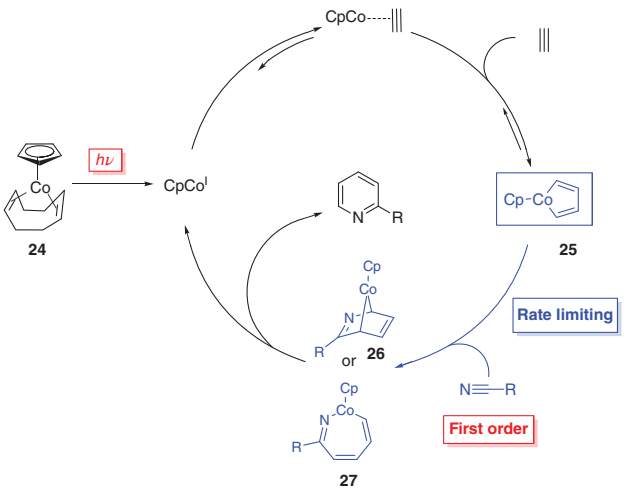

Scheme 1.5 Visible light-supported cobalt-catalyzed [2+2+2] cycloaddition applied to the synthesis of pyridines.

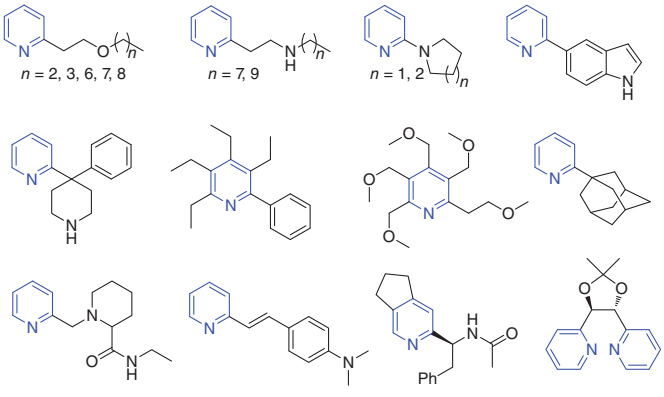

Figure 1.1 Pyridines that have been synthesized under mild conditions using photochemically promoted cobalt-catalyzed [2+2+2] cycloaddition.

cobalt catalyst was replaced by chiral analogs, best results being obtained with catalyst **28** (Scheme 1.6) [33]. With this reaction axial chirality can be efficiently induced as shown by the transformation of compound **29** into naphthyl pyridine **30**. Similar reactions have been carried out starting from 2-alkoxy-1-naphthonitriles **31** using different chiral cobalt complexes as catalysts. Either diines were used, leading to tetracyclic compounds **32**, or 2 equiv of a monoalkyne were employed, yielding the corresponding tricyclic products **33**. In this part of the study, the chiral catalysts **ent-28**, **34**, **35**, **36**, and **37** have also been tested. The study of this type of chirality, atropisomerism, has recently gained particular attention in photochemistry [34].

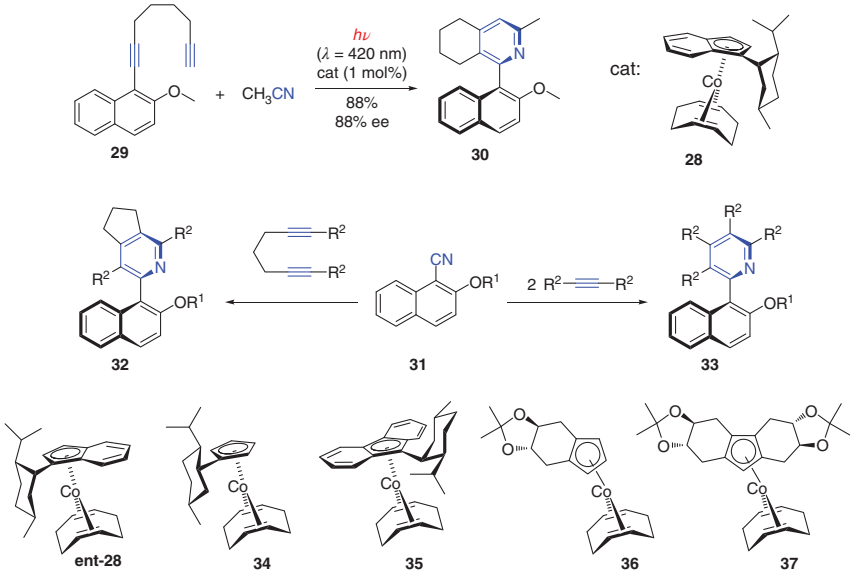

Scheme 1.6 Visible light-supported asymmetric [2+2+2] cycloaddition using chiral cobalt catalysts.

1.3 Asymmetric Photo-Enzyme Catalysis

Enzyme catalysis is a general method to produce enantiomerically enriched or pure compounds. Many such transformations need multi-enzyme systems that complicate the application to organic synthesis. In some cases, however, the replacement of one or more enzyme activities by a chemical transformation facilitates the transformations. As they tolerate a large variety of reaction conditions, photochemical reactions were efficiently applied in this context [35].

The Baeyer–Villiger monooxygenase (BVMO) asymmetrically catalyzes the transformation of ketones into esters or lactones in the case of cyclic ketones (Scheme 1.7) [36]. This enzyme contains a flavin adenine dinucleotide (E-FAD_{red}) unit, which reduces molecular oxygen into hydrogen peroxide capable of oxidizing the ketone substrate. The oxidized flavin species (E-FAD_{ox}) is reduced by nicotinamide adenine dinucleotide phosphate(H) (NADPH). The resulting nicotinamide adenine dinucleotide phosphate ($NADP^+$) is reduced via a glucose dehydrogenase-catalyzed reaction. This second enzyme activity can be replaced by adding flavin (FAD) to the reaction mixture. The reduced form of the nonbound FAD_{red} is capable of reducing the enzyme-bound E-FAD_{ox}. At the excited state, FAD_{ox} (generated by irradiation with visible light) is easily reduced via electron transfer from a sacrificial electron donor such as ethylenediaminetetraacetic acid (EDTA).

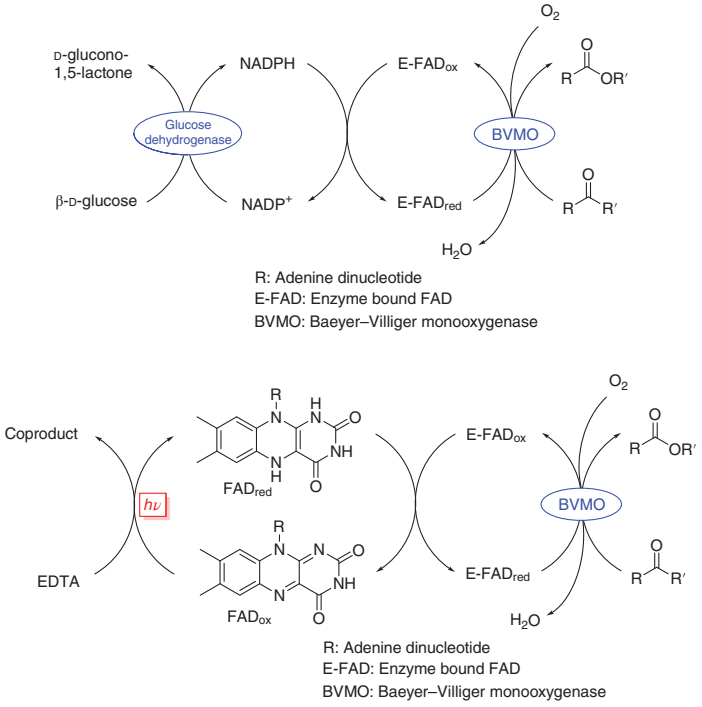

Scheme 1.7 Replacement of the glucose dehydrogenase by a simple photoredox catalytic system based on nonbound FAD.

Under these conditions the asymmetric Baeyer–Villiger reaction was carried out with the racemic 2-phenylcyclohexanone **38** (Scheme 1.8) [37]. Only the *R*-enantiomer was oxidized, and the phenylcaprolactone **39** was obtained in high enantioselectivity. The racemic cyclobutanone derivative **40** has been transformed under the same conditions. Interestingly both enantiomers were oxidized but different outcomes were observed. The α-*S*-enantiomer yields the bicyclic butyrolactone **41**, whereas the α-*R*-enantiomer is transformed into regioisomer **42**. Both compounds are formed in high enantioselectivity. Compound **41** is the expected regioisomer of a Baeyer–Villiger reaction. Depending on the stereochemistry of the starting ketone, the enzyme activity is therefore capable of directing the regioselectivity of the reaction [38]. It should be pointed out that under such reaction conditions, hydrogen peroxide is generated in low stationary concentration that reduces the enzyme degradation [39].

Combined photo- and enzyme catalysis was also carried out with alcohol dehydrogenases (ADH) [40]. These enzymes use NAD(P)H/NAD(P)$^+$ as cofactor [41]. In order to optimize the enzyme activity, this cofactor system must be regenerated [42]. One of the hydroxyl functionalities of the achiral diol **43** is dehydrogenated to an aldehyde by horse liver alcohol dehydrogenase (HLADH) with molecular oxygen (Scheme 1.9) [43]. Cyclization leads to the lactol **44**, a reversible step. In a second dehydrogenation also catalyzed by HLADH, the lactol is oxidized

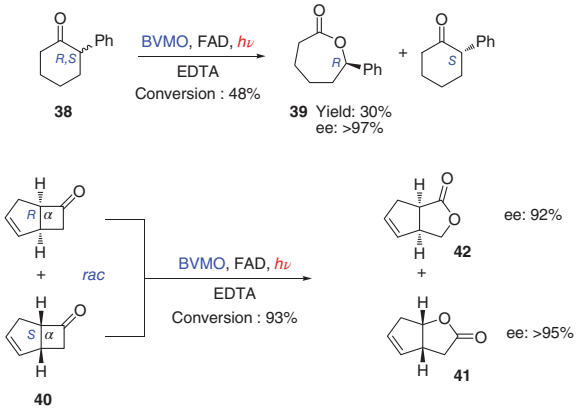

Scheme 1.8 Enzyme-catalyzed enantioselective Baeyer–Villiger reaction applied to the synthesis of lactones. Source: Hollmann et al. [37] / John Wiley & Sons.

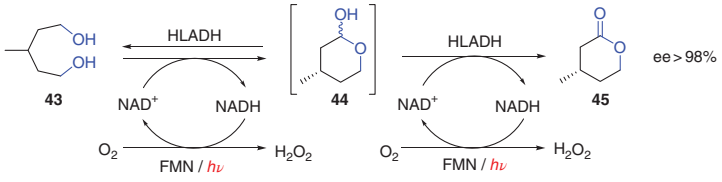

Scheme 1.9 Enantiospecific oxidation of the achiral diol **43** to 4-methyl-δ-valerolactone **45** using a photobiocatalytic process. Source: Rauch et al. [43] / Royal Society of Chemistry.

to the 4-methyl-δ-valerolactone **45**, obtained with complete enantioselectivity. In these steps, hydrogen is transferred to NAD^+ and NADH is formed. NAD^+ is regenerated by hydrogen transfer to oxygen leading to hydrogen peroxide. This step is photocatalyzed by flavin mononucleotide (FMN). The irradiation was carried out with blue LED ($\lambda_{max} = 465$ nm). Under similar reaction conditions and using a flavin-dependent "ene"-reductase, a variety of lactams have been obtained in high enantioselectivity [44].

The combination of enzymatic reactions with photochemical, in particular photoredox processes, offers numerous perspectives for organic synthesis [45]. This combination is a particularly efficient approach in connection with sustainable or green chemistry. As these processes are the basis of photosynthesis in green plants, they have been suggested of potential relevance for a sustainable chemical industry by G. Ciamician more than 100 years ago [46]. It was the beginning of green chemistry [47] although it has been almost forgotten over the decades.

1.4 Asymmetric Photochemical Reactions in Crystals

Asymmetric synthesis is often based on selection of conformations. An efficient method to do this is to carry out reactions at the crystalline state. Molecular

symmetry and crystallography are strongly linked [48]. Particularly impressive photochemical reactions have been reported with achiral substrates that crystallize in Sohncke space groups [49, 50]. When achiral compounds crystallize in these space groups, most frequently, one enantiopure conformer is present in such homochiral crystals [51, 52].

When α-ketoamides **46** are irradicated at the solid state, the hydroxy-β-lactams **47** are obtained in high enantioselectivity (Scheme 1.10) [53]. After light absorption, a hydrogen atom is transferred from an isopropyl group to the α-keto function leading to the diradical **48**. Radical cyclization yields the final product **47**. All these reaction steps occur under conformational control exerted by the crystal environment. In most cases, enantiomeric excesses (ee) were higher than 90%. In the case of Ar = Ph, the substrate crystallized in the chiral space group $P2_12_12_1$ [54]. Irradiation of the homochiral crystals yields product **47** (Ar = Ph) in 93% ee, which crystallized in the same space group $P2_12_12_1$. Both enantiomers have been selectively prepared choosing the corresponding homochiral crystals of the substrate. Under similar conditions the achiral α,β-unsaturated thioamide **49** was transformed into the thio-β-lactam **50** [55]. After photochemical excitation, a hydrogen was transferred from one of the benzyl positions into the β-position of the cyclohexene moiety (**51**). Radical combination yields the final product **50**. The starting product crystallized in the $P2_1$ space group, and when homochiral crystals were irradiated, one enantiomer of **50** was obtained in high enantiomeric excess. It is noteworthy that, when compound **49** was irradiated in solution, the same product **50** was isolated but as a racemic mixture along with side products [56]. Various other examples of this approach to chiral compounds have been reported [57].

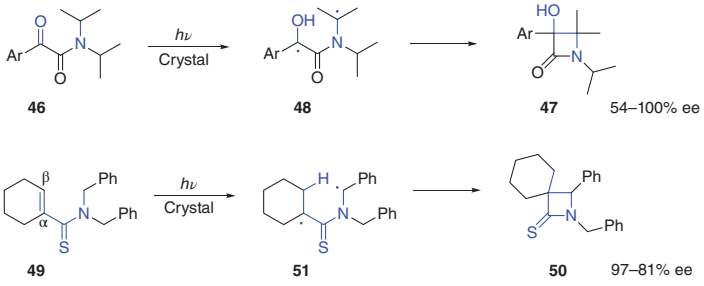

46 48 47 49 51 50

Scheme 1.10 Synthesis of β-lactams using absolute asymmetric synthesis with homochiral crystals of the achiral substrates. Each enantiomer has been selectively produced from the corresponding homochiral crystal of the substrate.

This method for the production of only one enantiomer without external chiral induction is part of absolute asymmetric synthesis. Using particular crystallization methods, e.g. seeding crystallization with the desired homochiral crystal, the achiral starting compound can be selectively transformed into only one of the homochiral crystals [58]. It should further be pointed out that such solid-state photochemical reactions can also be carried out on larger scale when suspensions are irradiated [59].

A certain control of the crystal symmetry can be obtained by attaching a homochiral element to the substrate. In this case, the number of possible space groups is reduced to 65 (Sohncke groups). A defined chiral environment is thus created around the photochemical substrate [48–51]. In order to obtain enantiomerically pure or enriched photochemical products, the chiral element should not be covalently bonded to the photochemical substrate [60]. In this context, ammonium salts of chiral amines and α-ketoamide **52** carrying a carboxylate function have been prepared, and the crystalline phase was irradiated (Scheme 1.11) [61]. In most cases, the resulting hydroxyl β-lactams **53** have been obtained in high yield and enantioselectivity. The oxooxazolidine derivatives **54** were formed in minor amounts. Both enantiomers of carboxylates **53** or **54** have been obtained as major stereoisomers depending on the configuration of the chiral ammonium cation. The absolute configuration of the carboxylates has not been determined in this study.

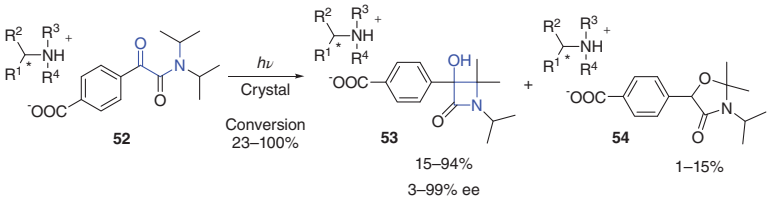

Scheme 1.11 Synthesis of β-lactams by irradiation of crystalline chiral ammonium salts. Source: Natarajan et al. [61] / American Chemical Society.

A similar norbornene **55** derivative has been transformed under the same conditions (Scheme 1.12) [62]. Upon irradiation, the carbonyl is added to the alkene function leading to the triplet 1,4-diradical intermediate **56**, which is a typical intermediate of the Paternò–Büchi reaction [63]. Such intermediates may undergo C—C bond formation leading to oxetanes. Bond cleavage of the newly formed C—O bond (b) can also take place regenerating the starting compound. This reaction step plays a key role in the stereoselective Paternò–Büchi reaction in solution [11, 64]. However, in the present case, a C—C bond (a) of the norbornene moiety is cleaved, yielding the final product **57**, a bicyclic dihydrofuran derivative. In most cases, high stereoselectivity was observed. The reaction is a photo-Claisen rearrangement [65] with intersystem crossing taking place.

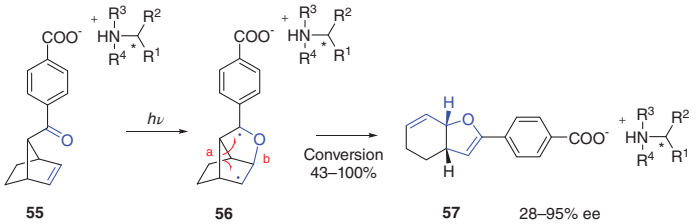

Scheme 1.12 Asymmetric photo-Claisen rearrangement by irradiation of crystalline chiral ammonium salts. Source: Xia et al. [62] / American Chemical Society.

1.5 Crystalline Inclusion Complexes

As pointed out earlier, TADDOLs are auxiliaries that efficiently induce chirality without being covalently bonded to the reacting molecule [27]. Using co-crystallization of these compounds with substrates of photochemical reactions is an interesting strategy for asymmetric synthesis [66, 67]. Crystals of TADDOLs are host structures with cavities that can be filled by guest molecules. When co-crystallized with a TADDOL derivative in a 1 : 1 ratio, the furoic acid amide **58** undergoes enantioselectively photocycloaddition yielding the quinolinone compound **59** (Scheme 1.13) [68]. Due to its polar mesomeric structure **60**, the amide constitutes a 6π system with benzene and furan moieties. Therefore, it undergoes conrotatory photocyclization leading to **61**. The final product **59** is formed via a tautomerization step. The same reaction was carried out with the acrylanilide derivative **62** (Scheme 1.13). Co-crystals of a 1 : 1 ratio with the same TADDOL have been irradiated. Again, the quinolinone compound (**63**) was obtained in high enantiomeric excess. Guest molecules can interact principally in two different ways with the TADDOL host matrix. They can approach the host molecules with their polar face, which may lead to the formation of hydrogen bonds. This was observed for the furoic acid amide **58** (Figure 1.2a). Guest molecules may also interact with the aryl substituents of the TADDOLs. In such cases, van der Waals, π–π-stacking, or

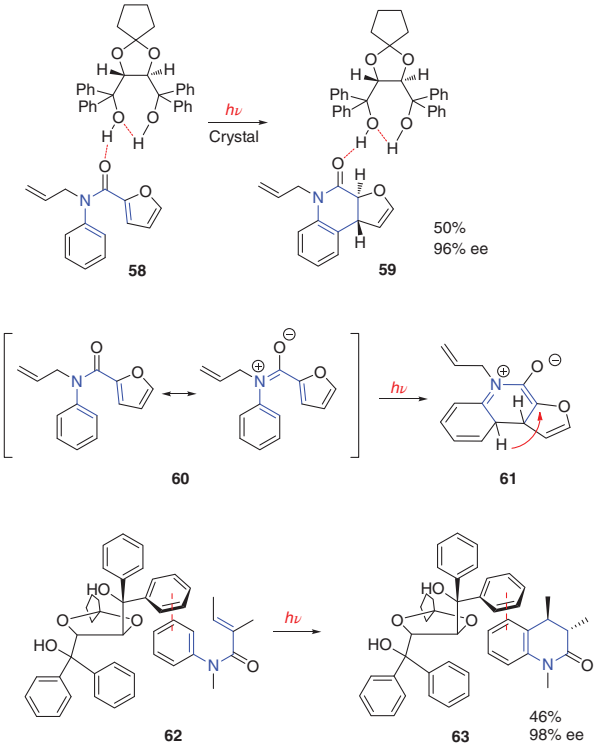

Scheme 1.13 Photocyclization in TADDOL co-crystals yielding quinolones in high enantioselectivity. Source: Toda et al. [68] / American Chemical Society.

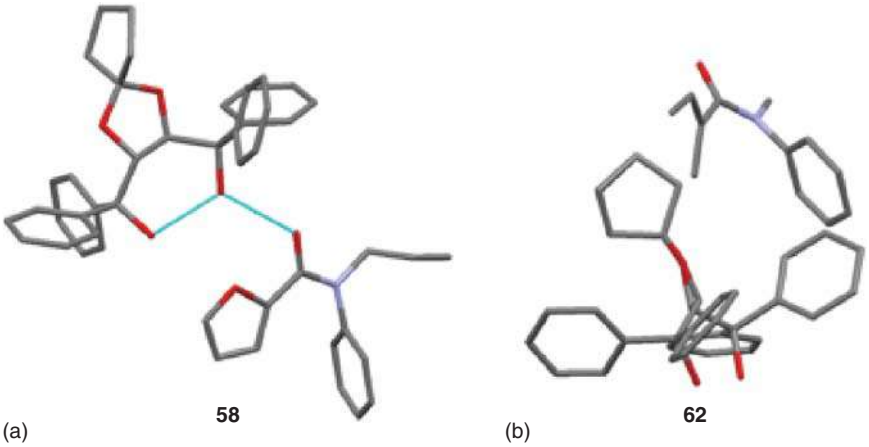

Figure 1.2 X-ray structures of compound **58** (a) and **62** (b) in 1 : 1 co-crystals with a TADDOL (compare Scheme 1.13).

edge-to-face interactions [69] can be observed. This may be the case in the reaction of compound **62** (Figure 1.2b).

Numerous photochemical reactions have been performed using cyclodextrins inclusion complexes [15, 70]. In water solution, cyclodextrins form such complexes with a variety of organic molecules. However, in many cases when β-cyclodextrin is used, the inclusion complexes are less soluble, and the corresponding suspensions, powders, or films are irradiated. In this context, a suspension of the 1 : 1 complex of β-cyclodextrin and the azepinone **64** has been irradiated with UV light (Scheme 1.14) [71]. The photochemical product **65** was hydrogenated, and the corresponding bicyclic γ-butyrolactam **66** was isolated in good yields and moderate enantioselectivity. Similar results have been obtained when films of the inclusion complex were irradiated. When the photochemical reaction of **64** in the presence of β-cyclodextrin was carried out in solution, followed by hydrogenation, **66** was isolated as a racemic mixture. Obviously, under these conditions, no inclusion of **66** takes place.

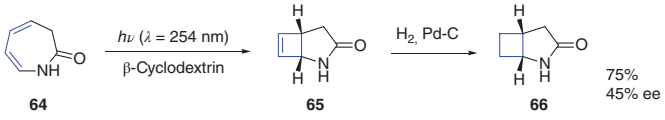

Scheme 1.14 Photocyclization of the dihydroazepinone **64** as part of an inclusion complex with β-cyclodextrin. Source: Mansour et al. [71] / American Chemical Society.

1.6 Inclusion in Zeolites

Zeolites are inorganic crystalline porous materials that absorb small- or medium-sized molecules depending on the cavity size [72]. They are frequently used as catalysts. Concerning photochemical reactions, they have been used as a

host structure for organic molecules [73, 74]. The photocyclization of pyridones **67** to the bicyclic β-lactams **68** has been performed in super cages of MY zeolites, where M are different alkali metal ions (Scheme 1.15) [75]. In order to create a chiral environment, inclusion into the super cages of MY zeolite of (−)-norephedrine or (−)-ephedrine together with the substrate **67** was carried out. In order to assure maximum interaction with the chiral inductor, the aminoalcohols were used in a 10-fold excess. In cases of larger substituents R, the bicyclic β-lactams **68** have been obtained with enantiomeric excesses up to 53%. The confinement of the non-covalently bonded chiral inductor with the pyridone substrates reduces the number of conformers. The proximity of the chiral inductor directs this selection in an enantioselective way. It must be pointed out that when the same reactions were carried out in solution, almost no chiral induction was observed. The reaction was also performed with pyridone substrates in which chiral amine derivatives were covalently bonded. In such cases, significant diastereoselectivity was observed when compounds were absorbed by Y zeolites.

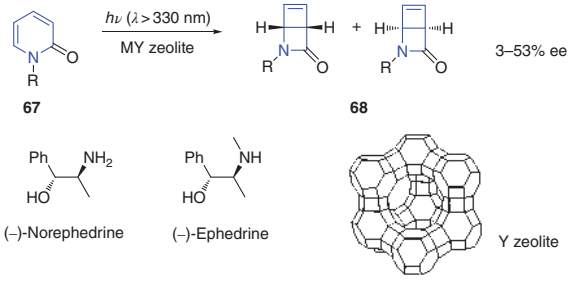

Scheme 1.15 Photochemical transformation of pyridones **67** to bicyclic β-lactams **68** co-absorbed with chiral aminoalcohols in Y zeolites. Source: Sivasubramanian et al. [75] / Royal Society of Chemistry.

1.7 Memory of Chirality

In many stereoselective reactions, the chiral information is transferred from a chiral center, for example, a chiral carbon atom, to the reaction center [76]. The resulting products are formed with diastereoselectivity. In some cases, however, such a chiral center is destroyed, and the chiral information is conserved (memory of chirality) in more or less stable conformers or other non-covalent interactions. In this way, such reactions become stereo- or enantioselective. Such phenomena are part of chiral memory effects [77, 78]. In this context, the proline derivative **69** has been irradiated in an acetone/water mixture (Scheme 1.16) [79]. Under these conditions, sensitization occurs via triplet energy transfer from photochemical excited acetone to **69**. Intramolecular electron transfer occurs from the carboxylate functionality to the phthalimide moiety (**70**). Immediate decarboxylation takes place and an α-aminoalkyl radical (**71**) is generated. In this reaction step, the chiral information at the former proline moiety is lost. Radical cyclization leads to the final product

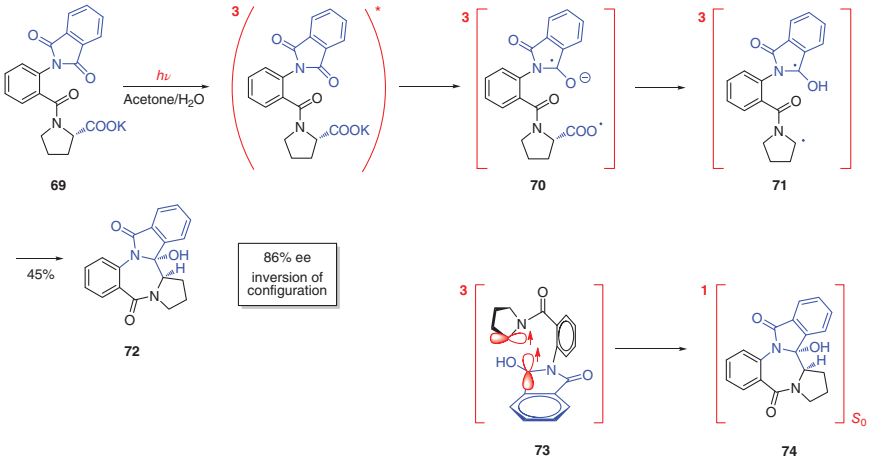

Scheme 1.16 Observation of a memory of chirality effect in a decarboxylative photocyclization. Source: Griesbeck et al. [79] / John Wiley & Sons.

72 with high enantioselectivity. It must be pointed out that the chiral information was conserved in relatively rigid conformations and transferred with inversion of configuration. This effect is explained by the fact that the spin multiplicity changes in this step. The triplet diradical **73** is transformed into the final product in its singlet state **74**. Radical combination and intersystem crossing concomitantly occur when the radical carrying p orbitals in the diradical are orthogonally oriented as depicted in structure **73** [80]. Such an arrangement increases spin–orbit coupling. As shown for the present and other examples, such an interaction has a significant impact on the stereoselectivity of these reactions [81]. In a similar electrochemical reaction, which takes place at the singlet ground state, almost the same enantioselectivity was observed but with retention of configuration at the pyrrolidine moiety [78, 82]. Memory of chirality effects have been observed in a variety of photochemical reactions involving radical intermediates [83].

1.8 Conclusion and Perspectives

Enantioselective synthesis of heterocyclic compounds plays an important role in many domains such as the search of new biologically active compounds for use in medicine or agriculture or for the preparation of new materials. Photochemical reactions significantly contribute to this research field. Currently, template-supported or organometallic catalysis is intensively investigated with considerable impact in photoredox catalysis and photosensitization [84, 85]. Enzyme catalysis represent an efficient method for the preparation of enantiopure compounds, among them many heterocyclic compounds. Photochemical reactions can simplify the catalytic systems. In many cases, the use of coenzymes has been replaced by simple photochemical processes. Solid-state photochemistry is an efficient method to control the equilibrium of conformers in an enantioselective way. Consequently, many of such

reactions are carried out with high or complete enantioselectivity. This research domain provides interesting perspectives for material science. Photochemistry of heterocyclic compounds also contributes to basic understanding of chemical reactivity. Memory of chirality is observed in some of these reactions. For example, the influence of spin–orbit coupling, the conformational rigidity on enantioselectivity, has been discussed in this context. It should also be pointed out that supramolecular structures [14] or supramolecular catalysis [86] play a key role in most of these reactions. Among the reaction discussed in this chapter, asymmetric photoredox catalytic reactions and photochemically modified enzymatic reactions are certainly the most attractive methods for application in organic synthesis. In the context of sustainable chemistry, photochemical reaction with crystalline substrate is particularly interesting since no solvent is needed [66, 87].

References

1 (a) Dinges, J. and Lamberth, C. (ed.) (2012). *Bioactive Heterocyclic Compound Classes – Pharmaceuticals*. Weinheim: Wiley-VCH. (b) Lamberth, C. and Dinges, J. (ed.) (2012). *Bioactive Heterocyclic Compound Classes – Agrochemicals*. Weinheim: Wiley-VCH. (c) Krämer, W., Schirmer, U., Jeschke, P., and Witschel, M. (ed.) (2012). *Modern Crop Protection Compounds*, 2e, vol. 1–3. Weinheim: Wiley-VCH.

2 Ostroverkhova, O. (ed.) (2019). *Handbook of Organic Materials for Electronic and Photonic Devices*, 2e. Duxford: Elsevier.

3 (a) Klán, P. and Wirz, J. (2009). *Photochemistry of Organic Compounds*. Chichester: Wiley. (b) Buzzetti, L., Crisenza, G.E.M., and Melchiorre, P. (2019). Mechanistic studies in photocatalysis. *Angew. Chem. Int. Ed.* 58: 3730–3747. https://doi.org/10.1002/anie.201809984.

4 Lefebvre, C., Fortier, L., and Hoffmann, N. (2020). Photochemical rearrangements in heterocyclic chemistry. *Eur. J. Org. Chem.* 2020: 1393–1404. https://doi.org/10.1002/ejoc.201901190.

5 (a) Hoffmann, N. (2008). Photochemical reactions as key steps in organic synthesis. *Chem. Rev.* 108: 1052–1103. https://doi.org/10.1021/cr0680336. (b) Bach, T. and Hehn, J.P. (2011). Photochemical reactions as key steps in natural product synthesis. *Angew. Chem. Int. Ed.* 50: 1000–1052. https://doi.org/10.1002/anie.201002845. (c) Kärkäs, M.D., Porco, J.A., and Stephenson, C.R.J. (2016). Photochemical approaches to complex chemotypes: application in natural product synthesis. *Chem. Rev.* 116: 9683–9747. https://doi.org/10.1021/acs.chemrev.5b00760.

6 Turro, N.J. and Schuster, G. (1975). Photochemical reactions as a tool in organic synthesis. *Science* 187: 303–312. https://doi.org/10.1126/science.187.4174.303.

7 (a) Hoffmann, N. (2012). Photochemical reactions of aromatic compounds and the concept of the photon as a traceless reagent. *Photochem. Photobiol. Sci.* 11: 1613–1641. https://doi.org/10.1039/C2PP25074H. (b) Oelgemöller, M.,

Jung, C., and Mattay, J. (2007). Green photochemistry: production of fine chemicals with sunlight. *Pure Appl. Chem.* 79: 1939–1947. https://doi.org/10.1351/pac200779111939.

8 Li, P., Terrett, J.A., and Zbieg, J.R. (2020). Visible-light photocatalysis as an enabling technology for drug discovery: a paradigm shift for chemical reactivity. *ACS Med. Chem. Lett.* 11: 2120–2130. https://doi.org/10.1021/acsmedchemlett.0c00436.

9 Bonfield, H.E., Knauber, T., Lévesque, F. et al. (2020). Photons as a 21st century reagent. *Nat. Commun.* 11: 804. https://doi.org/10.1038/s41467-019-13988-4.

10 Michelin, C., Lefebvre, C., and Hoffmann, N. (2019). Les réactions photochimiques à l'échelle industrielle. *Actual. Chim.* 436: 19–27.

11 Oelgemöller, M. and Hoffmann, N. (2016). Studies in organic and physical photochemistry – an interdisciplinary approach. *Org. Biomol. Chem.* 14: 7392–7442. https://doi.org/10.1039/C6OB00842A.

12 Roth, H.D. (1989). The beginnings of organic photochemistry. *Angew. Chem. Int. Ed.* 28: 1193–1207. https://doi.org/10.1002/anie.198911931.

13 (a) Rau, H. (1983). Asymmetric photochemistry in solution. *Chem. Rev.* 83: 535–547. https://doi.org/10.1021/cr00057a003. (b) Inoue, Y. (1992). Asymmetric photochemical reactions in solution. *Chem. Rev.* 92: 741–770. https://doi.org/10.1021/cr00013a001. Chiral Photochemistry. (c) Inoue, Y. and Ramamurthy, V. (ed.) (2004). *Chiral Photochemistry*. New York: Marcel Dekker. (d) Griesbeck, A.G. and Meierhenrich, U. (2002). Asymmetric photochemistry and photochirogenesis. *Angew. Chem. Int. Ed.* 41: 3147–3154. https://doi.org/10.1002/1521-3773(20020902)41:17<3147::AID-ANIE3147>3.0.CO;2-V. (e) Meggers, E. (2015). Asymmetric catalysis activated by visible light. *Chem. Commun.* 51: 3290–3301. https://doi.org/10.1039/C4CC09268F.

14 (a) Ramamurthy, V. and Sivaguru, J. (2016). Supramolecular photochemistry as a potential synthetic tool: photocycloaddition. *Chem. Rev.* 116: 9914–9993. https://doi.org/10.1021/acs.chemrev.6b00040. (b) Ramamurthy, V. and Mondal, B. (2015). Supramolecular photochemistry concepts highlighted with select examples. *J. Photochem. Photobiol. C* 23: 68–102. https://doi.org/10.1016/j.jphotochemrev.2015.04.002. (c) Vallavoju, N. and Sivaguru, S. (2014). Supramolecular photocatalysis: combining confinement and non-covalent interactions to control light initiated reactions. *Chem. Soc. Rev.* 43: 4084–4101. https://doi.org/10.1039/C3CS60471C.

15 Yang, C. and Inoue, Y. (2014). Supramolecular photochirogenesis. *Chem. Soc. Rev.* 43: 4123–4123. https://doi.org/10.1039/C3CS60339C.

16 Brimioulle, R., Lenhart, D., Maturi, M.M., and Bach, T. (2015). Enantioselective catalysis of photochemical reactions. *Angew. Chem. Int. Ed.* 54: 3872–3890. https://doi.org/10.1002/anie.201411409.

17 Bauer, A., Westkämper, F., Grimme, S., and Bach, T. (2005). Catalytic enantioselective reactions driven by photoinduced electron transfer. *Nature* 436: 1139–1140. https://doi.org/10.1038/nature03955.

18 (a) For detailed discussion of the mechanism see:Bertrand, S., Hoffmann, N., Humbel, S., and Pete, J.P. (2000). Diastereoselective tandem addition-cyclization

reactions of unsaturated tertiary amines initiated by photochemical electron transfer (PET). *J. Org. Chem.* 65: 8690–8703. https://doi.org/10.1021/jo001166l. (b) Hoffmann, N. and Görner, H. (2004). Photoinduced electron transfer from *N*-methylpyrrolidine to ketones and radical addition to an electron-deficient alkene. *Chem. Phys. Lett.* 383: 451–455. https://doi.org/10.1016/j.cplett.2003.11.045. (c) Hoffmann, N., Bertrand, S., Marinković, S., and Pesch, J. (2006). Efficient radical addition of tertiary amines to alkenes using photochemical electron transfer. *Pure Appl. Chem.* 78: 2227–2246. https://doi.org/10.1351/pac200678122227. (d) Griesbeck, A.G., Hoffmann, N., and Warzecha, K.D. (2007). Photoinduced-electron-transfer chemistry: from studies on PET processes to applications in natural product synthesis. *Acc. Chem. Res.* 40: 128–140. https://doi.org/10.1021/ar068148w.

19 Fischer, H. and Radom, L. (2001). Factors controlling the addition of carbon-centered radicals to alkenes – an experimental and theoretical perspective. *Angew. Chem. Int. Ed.* 40: 1340–1371. https://doi.org/10.1002/1521-3773(20010417)40:8<1340::AID-ANIE1340>3.0.CO;2-%23.

20 (a) Roberts, B.P. (1999). Polarity-reversal catalysis of hydrogen-atom abstraction reactions: concepts and applications in organic chemistry. *Chem. Soc. Rev.* 28: 25–35. https://doi.org/10.1039/A804291H. (b) Ravelli, D., Fagnoni, M., Fukuyama, T. et al. (2018). Site-selective C–H funtionalization by decatungstate anion photocatalysis: syntergistic control by polar and steric effects. *ACS Catal.* 8: 701–713. https://doi.org/10.1021/acscatal.7b03354.

21 (a) Hoffmann, N. (2015). Electron and hydrogen transfer in organic photochemical reactions. *J. Phys. Org. Chem.* 28: 121–136. https://doi.org/10.1002/poc.3370. (b) Hoffmann, N. (2016). Photochemical electron and hydrogen transfer in organic synthesis: the control of selectivity. *Synthesis* 48: 1782–1802. https://doi.org/10.1055/s-0035-1561425.

22 Lenhart, D., Bauer, A., Pöthig, A., and Bach, T. (2016). Enantioselective visible-light-induced radical-addition reactions to 3-alkylidene indolin-2-ones. *Chem. Eur. J.* 22: 6519–6523. https://doi.org/10.1002/chem.201600600.

23 Alonso, R. and Bach, T. (2014). A chiral thioxanthone as an organocatalyst for enantioselective [2+2] photocycloaddition reactions induced by visible light. *Angew. Chem. Int. Ed.* 53: 4368–4371. https://doi.org/10.1002/anie.201310997.

24 (a) Li, X., Jandl, C., and Bach, T. (2020). Visible-light-mediated enantioselective photoreactions of 3-alkylquinolones with 4-*O*-tethered alkenes and allenes. *Org. Lett.* 22: 3618–3622. https://doi.org/10.1021/acs.orglett.0c01065. (b) Cauble, D.F., Lynch, V., and Krische, M.J. (2003). Studies on the enantioselective catalysis of photochemically promoted transformations: "Sensitizing Receptors" as chiral catalysts. *J. Org. Chem.* 68: 15–21. https://doi.org/10.1021/jo020630e.

25 Zhang, L. and Meggers, E. (2017). Steering asymmetric Lewis acid catalysis exclusively with octahedral metal-centered chirality. *Acc. Chem. Res.* 50: 320–330. https://doi.org/10.1021/acs.accounts.6b00586.

26 Brimioulle, R. and Bach, T. (2013). Enantioselective Lewis acid catalysis of intramolecular enone [2+2] photocycloaddition reactions. *Science* 342: 840–843. https://doi.org/10.1126/science.1244809.

27 Seebachn, D., Beck, A.K., and Heckel, A. (2001). TADDOLs, their derivatives, and TADDOL analogues: versatile chiral auxiliaries. *Angew. Chem. Int. Ed.* 40: 92–138. https://doi.org/10.1002/1521-3773(20010105)40:1<92::AID-ANIE92>3.0.CO;2-K.

28 Wang, W., Clay, A., Krishnan, R. et al. (2017). Total syntheses of isomeric aglain natural products foveoglin A and perviridine B: excited-state intramolecular proton-transfer photocycloaddition. *Angew. Chem. Int. Ed.* 56: 14479–14482. https://doi.org/10.1002/anie.201707539.

29 Roche, S.P., Cencic, R., Pelletier, J., and Porco, J.A. Jr. (2010). Biomimetic photocycloaddition of 3-hydroxyflavones: synthesis and evaluation of rocaglate derivatives as inhibitors of eukaryotic translation. *Angew. Chem. Int. Ed.* 49: 6533–6538. https://doi.org/10.1002/anie.201003212.

30 (a) Heller, B. and Hapke, M. (2007). The fascinating construction of pyridine ring systems by transition metal-catalysed [2+2+2] cycloaddition reactions. *Chem. Soc. Rev.* 36: 1085–1094. https://doi.org/10.1039/B607877J. (b) Gläsel, T. and Hapke, M. (2020). Cobalt-catalysed [2+2+2] cycloadditions. In: *Cobalt Catalysis in Organic Synthesis* (ed. T. Gläsel and M. Hapke), 287–335. Weinheim: Wiley-VCH https://doi.org/10.1002/9783527814855.ch9.

31 (a) Schulz, W., Pracejus, H., and Oehme, G. (1989). Photoassisted cocyclization of acetylene and nitriles catalyzed by cobalt complexes at ambient temperature and normal pressure. *Tetrahedron Lett.* 30: 1229–1232. https://doi.org/10.1016/S0040-4039(00)72722-5. (b) Heller, B., Heller, D., and Oehme, G. (1996). Systematic investigation of the photocatalytic alkyne-nitrile heterotrimerisation to pyridine. *J. Mol. Catal. A* 110: 211–219. https://doi.org/10.1016/1381-1169(96)00158-6.

32 (a) Heller, B., Sudermann, B., Fischer, C. et al. (2003). Facile and racemization-free conversion of chiral nitriles into pyridine derivatives. *J. Org. Chem.* 68: 9221–9225. https://doi.org/10.1021/jo030206t. (b) Heller, B., Sudermann, B., Buschmann, H. et al. (2002). Photocatalyzed [2+2+2]-cycloaddition of nitriles with acetylene: an effective method for the synthesis of 2-pyridines under mild conditions. *J. Org. Chem.* 67: 4414–4422. https://doi.org/10.1021/jo011032n.

33 (a) Gutnov, A., Heller, B., Fischer, C. et al. (2004). Cobalt(I)-catalysed [2+2+2] cycloaddition of alkynes and nitriles: synthesis of enantiomerically enriched atropoisomers of 2-arylpyridines. *Angew. Chem. Int. Ed.* 43: 3795–3797. https://doi.org/10.1002/anie.200454164. (b) Hapke, M., Kral, K., Fischer, C. et al. (2010). Asymmetric synthesis of axially chiral 1-aryl-5,6,7,8-tetrahydroquinolines by cobalt-catalysed [2+2+2] cycloaddition reaction of 1-aryl-1,7-octadiynes and nitriles. *J. Org. Chem.* 75: 3993–4003. https://doi.org/10.1021/jo100122d.

34 Kumarasamy, E., Ayitou, A.J.L., Vallavoju, N. et al. (2016). Tale of twisted molecules. atropselective photoreactions: taming light induced asymmetric transformations through non-biaryl atropisomers. *Acc. Chem. Res.* 49: 2713–2724. https://doi.org/10.1021/acs.accounts.6b00357.

35 (a) Ni, Y. and Hollmann, F. (2016). Artificial photosynthesis: hybrid systems. *Adv. Biochem. Eng. Biotechnol.* 159: 137–158. https://doi.org/10.1007/10_2015_5010. (b) Maciá-Agulló, J.A., Corma, A., and Garcia, J. (2015). Photocatalysis: the power of combining photocatalysis and enzymes. *Chem. Eur. J.*

21: 10940–10959. https://doi.org/10.1002/chem.201406437. (c) Burek, B.O., Bormann, S., Hollmann, F. et al. (2019). Hydrogen peroxide driven biocatalysis. *Green Chem.* 21: 3232–3249. https://doi.org/10.1039/C9GC00633H.

36 (a) Hollmann, F., Kara, S., Opperman, D.J., and Wang, Y. (2018). Biocatalytic synthesis of lactones and lactams. *Chem. Asian J.* 13: 3601–3610. https://doi.org/10.1002/asia.201801180. (b) Alphand, V. and Wohlgemuth, R. (2010). Application of Baeyer–Villiger monooxygenase in organic synthesis. *Curr. Org. Chem.* 14: 1928–1965. https://doi.org/10.2174/138527210792927519. (c) Mihovilovic, M.D. (2006). Enzyme mediated Baeyer–Villiger oxidations. *Curr. Org. Chem.* 10: 1265–1287. https://doi.org/10.2174/138527206777698002. (d) Mihovilovic, M.D., Müller, B., and Stanetty, P. (2002). Monooxygenase-mediated Baeyer–Villiger oxidations. *Eur. J. Org. Chem.* 2002: 3711–3730. https://doi.org/10.1002/1099-0690(200211)2002:22<3711::AID-EJOC3711>3.0.CO;2-5.

37 Hollmann, F., Taglieber, A., Schulz, F., and Reez, M.T. (2007). A light-driven stereoselective biocatalytic oxidation. *Angew. Chem. Int. Ed.* 46: 2903–2906. https://doi.org/10.1002/anie.200605169.

38 (a) Krow, G.R. (1993). The Baeyer–Villiger oxidation of ketones and aldehydes. *Org. React.* 43: 251–798. https://doi.org/10.1002/0471264180.or043.03. (b) Renz, M. and Meunier, B. (1999). 100 Years of Baeyer–Villiger oxidations. *Eur. J. Org. Chem.* 1999: 737–750. https://doi.org/10.1002/(SICI)1099-0690(199904)1999:4<737::AID-EJOC737>3.0.CO;2-B.

39 Perez, D., Grau, M.M., Arends, I.W.C.E., and Hollmann, F. (2009). Visible light-driven and chloroperoxidase-catalyzed oxygenation reactions. *Chem. Commun.* 6848–6850. https://doi.org/10.1039/B915078A.

40 Gargiulo, S., Arends, I.W.C.E., and Hollmann, F. (2011). A photoenzymatic system, for alcohol oxidation. *ChemCatChem* 3: 338–342. https://doi.org/10.1002/cctc.201000317.

41 Kroutil, W., Mang, H., Edegger, K., and Faber, K. (2004). Biocatalytic oxidation of primary and secondary alcohols. *Adv. Synth. Catal.* 346: 125–142. https://doi.org/10.1002/adsc.200303177.

42 (a) Chenault, H.K. and Whitesides, G.M. (1987). Regeneration of nicotinamide cofactors for use in organic synthesis. *Appl. Biochem. Biotechnol.* 1: 147–197. https://doi.org/10.1007/BF02798431. (b) Hollmann, F., Arends, I.W.C.E., and Buehler, K. (2010). Biocatalytic reactions for organic synthesis: nonconventional regeneration methods. *ChemCatChem* 2: 762–782. https://doi.org/10.1002/cctc.201000069.

43 Rauch, M., Schmidt, S., Arends, I.W.C.E. et al. (2017). Photobiocatalytic alcohol oxidation using LED light sources. *Green Chem.* 19: 376–379. https://doi.org/10.1039/C6GC02008A.

44 Biegasiewicz, K.F., Cooper, S.J., Gao, X. et al. (2019). Photoexcitation of flavoenzymes enables a stereoselective radical cyclization. *Science* 364: 1166–1169. https://doi.org/10.1126/science.aaw1143.

45 (a) Some recent examples: Zhang, W., Fernandez Fueyo, E., Hollmann, F. et al. (2019). Combining photo-organo redox- and enzyme catalysis facilitates asymmetric C—H bond functionalization. *Eur. J. Org. Chem.* 2019: 80–84. https://

doi.org/10.1002/ejoc.201801692. (b) Page, C.G., Cooper, S.J., DeHovitz, J.S. et al. (2021). Quaternary charge-transfer complex enables photoenzymatic intermolecular hydroalkylation of olefins. *J. Am. Chem. Soc.* 143: 97–102. https://doi.org/10.1021/jacs.0c11462. (c) Sandoval, B.A., Clayman, P.D., Oblinsky, D.G. et al. Photoenzymatic reductions enabled by direct excitation of flavin-dependent "Ene"-reductases. *J. Am. Chem. Soc.* https://doi.org/10.1021/jacs.0c11494. (d) Chen, J., Guan, Z., and He, Y.H. (2019). Photoenzymatic approaches in organic synthesis. *Asian J. Org. Chem.* 8: 1775–1790. https://doi.org/10.1002/ajoc.201900427.

46 (a) Ciamician, G. (1908). Sur les actions de la lumière. *Bull. Soc. Chim. Fr.* 3: i–xxvii. (b) Ciamician, G. (1912). The photochemistry of the future. *Science* 36: 385–394. https://doi.org/10.1126/science.36.926.385.

47 (a) Albini, A. and Fagnoni, M. (2008). 1908 Giacomo Ciamician and the concept of green chemistry. *ChemSusChem* 1: 63–66. https://doi.org/10.1002/cssc.200700015. (b) Albini, A. and Fagnoni, M. (2004). Green chemistry and photochemistry were born at the same time. *Green Chem.* 6: 1–6. https://doi.org/10.1039/B309592D.

48 Jacques, J., Collet, A., and Wilen, S.H. (1994). *Enantiomers, Racemates, and Resolutions*. Malabar: Krieger Publishing Company. (Copyright 1981, John Wiley and Sons, Inc.).

49 Nespolo, M., Aroyo, M.I., and Souvignier, B. (2018). Crystallographic shelves: space-group hierarchy explained. *J. Appl. Cryst.* 51: 1481–1491. https://doi.org/10.1107/S1600576718012724.

50 Levkin, P.A., Torbeev, V.Y., Lenev, D.A., and Kostyanovsky, R.G. (2006). Homo- and heterochirality in crystals. *Top. Stereochem.* 25: 81–134. https://doi.org/10.1002/0471785156.ch4.

51 Sakamoto, M. (2006). Spontaneous chiral crystallization of achiral materials and absolute asymmetric photochemical transformation using the chiral crystalline environment. *J. Photochem. Photobiol. C* 7: 183–196. https://doi.org/10.1016/j.jphotochemrev.2006.11.002.

52 Kuroda, R. (2004). Circular dichroim in the solid state. In: *Chiral Photochemistry* (ed. Y. Inoue and V. Ramamurthy), 385–413. New York: Marcel Dekker.

53 (a) Toda, F., Yagi, M., and Soda, S.I. (1987). Formation of a chiral β-lactam by photocyclisation of an achiral oxo amide in its chiral crystalline state. *J. Chem. Soc., Chem. Commun.* 1413–1414. https://doi.org/10.1039/C39870001413. (b) Toda, F. and Miyamoto, H. (1993). Formation of chiral β-lactams by photocyclisation of achiral *N*,*N*-diisopropylarylglyoxylamides in their chiral crystalline form. *J. Chem. Soc., Perkin Trans.* I: 1129–1132. https://doi.org/10.1039/P19930001129.

54 Sekine, A., Hori, K., Ohashi, Y. et al. (1989). X-ray structural studies of chiral β-lactam formation from an achiral oxo amide using the chiral-crystal environment. *J. Am. Chem. Soc.* 111: 697–699. https://doi.org/10.1021/ja00184a045.

55 Sakamoto, M., Takahashi, M., Kamiya, K. et al. (1996). Crystal-to-crystal solid-state photochemistry: absolute asymmetric β-thiolactam synthesis from an

achiral α,β-unsaturated thioamide. *J. Am. Chem. Soc.* 118: 10664–10665. https://doi.org/10.1021/ja961878m.

56 Sakamoto, M., Kimura, M., Shimoto, T. et al. (1990). Photochemical reaction of *N*,*N*-dialkyl-α,β-unsaturated thioamides. *J. Chem. Soc., Chem. Commun.* 1214–1215. https://doi.org/10.1039/C39900001214.

57 Sakamoto, M., Takahashi, M., Arai, W. et al. (2000). Solid-state photochemistry: absolute asymmetric β-thiolactam synthesis from achiral *N*,*N*-dibenzyl-α,β-unsaturated thioamides. *Tetrahedron* 56: 6795–6804. https://doi.org/10.1016/S0040-4020(00)00501-9.

58 Kellogg, R.M. (2017). Practical stereochemistry. *Acc. Chem. Res.* 50: 905–914. https://doi.org/10.1021/acs.accounts.6b00630.

59 Veeman, M., Resendiz, M.J.E., and Garcia-Garibay, M.A. (2006). Large-scale photochemical reactions of nanocrystalline suspensions: a promising green chemistry method. *Org. Lett.* 8: 2615–2617. https://doi.org/10.1021/ol060978m.

60 Scheffer, J.R. and Xia, W. (2005). Asymmetric induction in organic photochemistry via the solid-state ionic chiral auxiliary approach. *Top. Curr. Chem.* 254: 233–262. https://doi.org/10.1007/b101000.

61 Natarajan, A., Wang, K., Ramamurthy, V. et al. (2002). Control of enantioselectivity in the photochemical conversion of α-oxoamides into β-lactam derivatives. *Org. Lett.* 4: 1443–1446. https://doi.org/10.1021/ol025700i.

62 Xia, W., Yang, C., Patrick, B.O. et al. (2005). Asymmetric synthesis of dihydrofurans via a formal retro-Claisen photorearrangement. *J. Am. Chem. Soc.* 127: 2725–2730. https://doi.org/10.1021/ja043254j.

63 (a) Frénau M, Hoffmann N. The Paternò–Büchi reaction—mechanisms and application to organic synthesis. *J. Photochem. Photobiol. C* 2017; 33: 83–108. https://doi.org/10.1016/j.jphotochemrev.2017.10.002. (b) D'Auria M. The Paternò–Büchi reaction – a comprehensive review. *Photochem. Photobiol. Sci.* 2019; 18: 2297–2362. https://doi.org/10.1039/C9PP00148D. (c) Abe M. Formation of a four-membered ring: oxetanes. In: Albini A, Fagnoni M, editors. *Handbook of Synthetic Photochemistry*: Weinheim: Wiley-VCH; 2010. p 217–239. https://doi.org/10.1002/9783527628193.ch7.

64 Buschmann, H., Scharf, H.D., Hoffmann, N. et al. (1989). Chiral induction in photochemical reactions. 10. The principle of isoinversion: a model of stereoselection developed from the diastereoselectivity of the Paternò–Büchi reaction. *J. Am. Chem. Soc.* 111: 5367–5373. https://doi.org/10.1021/ja00196a048.

65 Galindo, F. (2005). The photochemical rearrangement of aromatic ethers a review of the photo-Claisen reaction. *J. Photochem. Photobiol. C* 6: 123–138. https://doi.org/10.1016/j.jphotochemrev.2005.08.001.

66 (a) Toda, F. (1988). Reaction control of guest compounds in host–guest inclusion complexes. *Top. Curr. Chem.* 149: 211–238. https://doi.org/10.1007/3-540-19338-3_5. (b) Tanaka, K. and Toda, F. (2000). Solvent-free organic synthesis. *Chem. Rev.* 100: 1025–1074. https://doi.org/10.1021/cr940089p.

67 Koshima, H. (2004). Chiral solid-state photochemistry including supramolecular approaches. In: *Chiral Photochemistry* (ed. Y. Inoue and V. Ramamurthy), 485–531. New York: Marcel Dekker.

68 Toda, F., Miyamoto, H., Kanemoto, K. et al. (1999). Enantioselective photocyclization of *N*-alkylfuran-2-carboxanilides to *trans*-dihydrofuran derivatives in inclusion crystals with optically active host compounds derived from tartaric acid. *J. Org. Chem.* 64: 2096–2102. https://doi.org/10.1021/jo982099m.

69 Jennings, W.B., Farrell, B.M., and Malone, J.F. (2001). Attractive intramolecular edge-to-face interactions in flexible organic molecules. *Acc. Chem. Res.* 34: 885–894. https://doi.org/10.1021/ar0100475.

70 Rekharsky, M.V. and Inoue, Y. (1998). Complexation thermodynamics of cyclodextrins. *Chem. Rev.* 98: 1875–1918. https://doi.org/10.1021/cr970015o.

71 Mansour, A.T., Buendia, J., Xie, J. et al. (2017). β-Cyclodextrin-mediated enantioselective photochemical electrocyclization of 1,3-dihydro-2*H*-azepin-2-one. *J. Org. Chem.* 82: 9832–9836. https://doi.org/10.1021/acs.joc.7b01300.

72 (a) Weitkamp, J. and Puppe, L. (ed.) (1999). *Catalysis and Zeolites*. Berlin/Heidelberg: Springer-Verlag. (b) Chester, A.W. and Derouane, E.G. (ed.) (2009). *Zeolite Characterization and Catalysis*. Dordrecht: Springer. (c) Pariente, J.P. and Sánchez-Sánchez, M. (ed.) (2018). *Structure and Reactivity of Metals in Zeolite Materials*. Cham: Springer Nature https://doi.org/10.1007/978-3-319-98905-1.

73 (a) Ramamurthy, V. (2019). Achiral zeolites as reaction media for chiral photochemistry. *Molecules* 24: 3570. https://doi.org/10.3390/molecules24193570. (b) Sivaguru, S., Nathrajan, A., Kaanumalle, L.S. et al. (2003). Asymmetric photoreactions within zeolites: role of confinement and alkali metal ions. *Acc. Chem. Res.* 36: 509–521. https://doi.org/10.1021/ar020269i.

74 Scaiano, S.C. and García, M. (1999). Intrazeolite photochemistry: toward supramolecular control of molecular photochemistry. *Acc. Chem. Res.* 32: 783–793. https://doi.org/10.1021/ar9702536.

75 Sivasubrmanian, K., Kaanumalle, L.S., Uppili, S., and Ramamurthy, V. (2007). Value of zeolites in asymmetric induction during photocyclization of pyridines, cyclohexadiones and naphthalenones. *Org. Biomol. Chem.* 5: 1569–1576. https://doi.org/10.1039/B702572F.

76 For such cases models have been developed to quantify chiral induction: Ruch, E. and Ugi, I. (1969). The stereochemical analogy model – a mathematical theory of dynamic stereochemistry. *Top. Stereochem.* 4: 99–125. https://doi.org/10.1002/9780470147139.ch3.

77 (a) Alezra, V. and Kawabata, T. (2016). Recent progress in memory of chirality (MOC): an advanced chiral pool. *Synthesis* 48: 2997–3016. https://doi.org/10.1055/s-0035-1562441. (b) Zhao, H., Hsu, D.C., and Carlier, P.R. (2005). Memory of chirality: an emerging strategy for asymmetric synthesis. *Synthesis* 1–16. https://doi.org/10.1055/s-2004-834931. (c) Gloor, C.S., Dénès, F., and Renaud, P. (2016). Memory in reactions involving monoradicals. *Free Radical Res.* 50: S102–S1114. https://doi.org/10.1080/10715762.2016.1232485.

78 Kramer, W.H. and Griesbeck, A.G. (2008). The same and not the same: chirality, topicity, and memory of chirality. *J. Chem. Educ.* 85: 701–709. https://doi.org/10.1021/ed085p701.

79 Griesbeck, A.G., Kramer, W., and Lex, J. (2001). Diastereo- and enantioselective synthesis of pyrrolo[1,4]benzodiazepines through decarboxylative

photocyclization. *Angew. Chem. Int. Ed.* 40: 577–579. https://doi.org/10.1002/1521-3773(20010202)40:3<577::AID-ANIE577>3.0.CO;2-L.

80 (a) Salem, L. and Rowland, C. (1972). The electronic properties of diradicals. *Angew. Chem. Int. Ed.* 11: 92–111. https://doi.org/10.1002/anie.197200921. (b) Carlacci, L., Doubleday, D. Jr., Furlani, T.R. et al. (1987). Spin-orbit coupling in biradicals. Ab initio MCSCF calculations on trimethylene and the methyl–methyl radical pair. *J. Am. Chem. Soc.* 109: 5323–5329. https://doi.org/10.1021/ja00252a004. (c) Michl, J. (1996). Spin-orbit coupling of biradicals. 1. The 2-electron-in-2-orbitals model revisited. *J. Am. Chem. Soc.* 118: 3568–3579. https://doi.org/10.1021/ja9538391.

81 (a) Griesbeck, A.G., Abe, M., and Bondock, S. (2004). Selectivity control in electron spin inversion processes: regio- and stereochemistry of Paternò–Büchi photocycloadditions as a powerful tool for mapping intersystem crossing processes. *Acc. Chem. Res.* 37: 919–928. https://doi.org/10.1021/ar040081u. (b) Griesbeck, A.G., Mauder, H., and Stadtmüller, S. (1994). Intersystem crossing in triplet 1,4-biradicals: conformational memory effects on the stereoselectivity of photocycloaddition reactions. *Acc. Chem. Res.* 27: 70–75. https://doi.org/10.1021/ar00039a002.

82 (a) Wanyoike, G.N., Onomura, O., Maki, T., and Matsumura, Y. (2002). Highly enhanced enantioselectivity in the memory of chirality via acyliminium ions. *Org. Lett.* 4: 1875–1877. https://doi.org/10.1021/ol025865r. (b) Onomura, O. (2016). Aliphatic nitrogen-containing compounds, amines, amino alcohols, and amino acids. In: *Organic Electrochemistry*, 5e (ed. O. Hammerich and B. Speiser), 1103–1119. Boca Raton: CRC Press.

83 (a) For selected examples see: Šumanovac Ramljak, T., Sohora, M., Antol, I. et al. (2014). Memory of chirality in the phthalimide photocyclization. *Tetrahedron Lett.* 55: 4078–4081. https://doi.org/10.1016/j.tetlet.2014.05.118. (b) Sinicropi, A., Barbosa, F., Basosi, R. et al. (2005). Mechanism of the Norrish–Yang photocyclization reaction of an alanine derivative in the singlet state: origin of the chiral-memory effect. *Angew. Chem. Int. Ed.* 44: 2390–2393. https://doi.org/10.1002/anie.200461898. (c) Sakamoto, M., Kawanishi, H., Mino, T. et al. (2006). Photochemcial asymmetric synthesis of phenyl-bearing quaternary chiral carbons using chiral-memory effect on β-hydrogen abstraction by thiocarbonyl group. *Chem. Commun.* 4608–4610. https://doi.org/10.1039/B608513J. (d) Bonache MA, López P, Martín-Martínez M, García-López MT, Cativiela C, González-Muñiz R. Stereoselective synthesis of amino acid-derived β-lactams. Experimental evidence for TDDOL as a memory of chirality enhancer. *Tetrahedron* 2006; 62: 130–138. https://doi.org/10.1021/ja0378299. (e) Mori, T., Saito, H., and Inoue, Y. (2003). Complete memory of chirality upon photodecarboxylation of mesityl alkanoate to mesitylalkane: theoretical and experimental evidence for cheletropic decarboxylation via a spiro-lactonic transition state. *Chem. Commun.* 2302–2303. https://doi.org/10.1039/B305267B.

84 Michelin, C. and Hoffmann, N. (2018). Photosensitization and photocatalysis – perspectives in organic synthesis. *ACS Catal.* 8: 12046–12055. https://doi.org/10.1021/acscatal.8b03050.

85 (a) Stephenson, C.R.J., Yoon, T.P., and MacMillan, D.W.C. (ed.) (2018). *Visible Light Photocatalysis in Organic Chemistry*. Weinheim: Wiley-VCH. (b) König, B. (ed.) (2020). *Chemical Photocatalysis*, 2e. Berlin: De Gruyter.

86 (a) Bhattacharyya, A., De Sarkar, S., and Das, A. (2021). Supramolecular engineering and self-assembly strategies in photoredox catalysis. *ACS Catal.* 11: 710–733. https://doi.org/10.1021/acscatal.0c04952. (b) Baruah, J.B. (2019). *Principles and Advances in Supramolecular Catalysis*. Boca Raton: CRC Press.

87 (a) Mishra, M.K., Ramamurty, U., and Desiraju, G.R. (2016). Mechanical property of molecular solids. *Curr. Opin. Solid State Mater. Sci.* 20: 361–370. (b) Toda F, editor. Organic solid state reactions. *Top. Curr. Chem.* Vol.254; 2005, https://doi.org/10.1007/b98357. (c) Kaupp, G. (2003). Solid-state molecular synthesis: complete reactions without auxiliaries based on the new solid-state mechanism. *CrystEngComm* 5: 117–133. https://doi.org/10.1039/B303432A.

2

Heterocycles via Dearomatization Reactions

Alexey M. Starosotnikov and Maxim A. Bastrakov

N.D. Zelinsky Institute of Organic Chemistry RAS, Leninsky prosp. 47, Moscow, 119991, Russia

2.1 Introduction

Dearomatization is an organic reaction implying addition to arenes or hetarenes accompanied by permanent loss of their aromaticity. It has become a challenging research topic in modern synthetic organic chemistry and one of the most powerful methods for conversion of simple aromatic substrates into diverse structurally complex systems. Attractiveness and elegancy of the dearomative approach comes from the well-known inert nature of (het)arenes in addition reactions. This feature provides motivation for the search and development of new methods to overcome the resonance stabilization energy and to disrupt the aromaticity. In many syntheses dearomatization of readily available aromatic starting compounds is preferable in comparison with construction from aliphatic or alicyclic precursors since it may significantly shorten the synthetic routes.

The most widely recognized examples of dearomatization are Birch reduction [1], ozonolysis of arenes [2, 3], and hydrogenation. Significant interest to dearomatizing methodology rose in 2000s and has been increasing during the last decade. According to the Web of Science citation database (www.webofknowledge.com), the annual number of publications related to "dearomatization" has grown from about 30 in 2008 to more than 330 in 2020.

Dearomatization is widely used for construction of fused heterocyclic systems. It has been frequently applied to the total synthesis of natural compounds, such as strychnine [4], griseofulvin [5], (–)-communesin F [6], cortistatin [7], platensimycin [8], vinigrol [9], and many others.

It is difficult to overestimate the importance of heterocyclic compounds. Regardless of natural or synthetic origin, they have gained wide appreciation as pharmaceuticals and dyes. The great potential of dearomatization reactions provides an easy access to various condensed heterocyclic skeletons directly from simple and readily available (hetero)aromatics. In most cases quaternary carbon centers are formed; therefore, catalytic asymmetric dearomatizations allow construction of enantio- and/or diastereoenriched annulated, spiro-, or bridged heterocyclic compounds, including numerous privileged scaffolds for medicinal chemistry.

Heterocycles: Synthesis, Catalysis, Sustainability, and Characterization, First Edition.
Edited by Teresa M.V.D. Pinho e Melo and Marta Pineiro.

A number of reviews and monographs should be mentioned dedicated to some special related topics such as dearomatization via transition metal complexes [10, 11], asymmetric dearomatization reactions [12], dearomatization in the synthesis of complex natural products [13], nucleophilic dearomatizing reactions [14], and synthesis of spiro compounds via radical dearomatization [15].

This chapter encompasses *dearomatization* methods elaborated mainly within the last decade and promoted by addition (or cycloaddition) to aromatic hydrocarbons and heterocycles *with formation of a new heterocyclic ring*. There are two main dearomatizing approaches leading to formation of a heterocycle: annulation (Scheme 2.1a) and spirocyclization (Scheme 2.1b). In turn, annulation can be achieved by means of either cycloaddition (generally [3+2] and [4+2]) or intramolecular nucleophilic or radical addition to aromatic double bonds. Due to numerous literary sources existing on this topic, the scope of the current chapter is limited by the typical processes yielding isolable dearomatized products, while those cases where they are formed as intermediates further transformations are not considered.

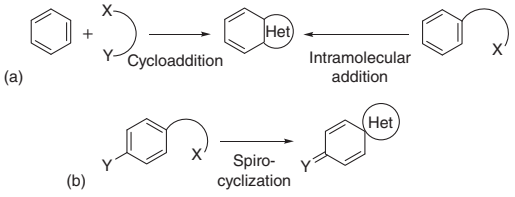

Scheme 2.1 General strategies for the synthesis of heterocycles via dearomatization reactions.

2.2 Annulation of Heterocycles via Dearomative Cycloaddition to Arenes and Hetarenes

2.2.1 [3+2] Cycloaddition

1,3-Dipolar cycloaddition is a basic method for construction of a wide range of five-membered heterocycles by the reactions of various dipoles with multiple C—C or C—heteroatom bonds as dipolarophiles. In some circumstances aromatic "double" bonds of arenes or hetarenes may act as 2π-components in cycloadditions. In these cases annulation of another heterocycle is possible along with dearomatization of an existing aromatic moiety. For this reason the lower the aromaticity of (het)arene is, the more readily cycloaddition reactions proceed. Indoles and other five-membered benzoheterocycles bearing electron-withdrawing groups are the most studied in [3+2] annulations. Indeed, carbon–carbon double bonds of these heterocycles activated by electron-withdrawing groups are rather reactive and prone to add dipoles and other electron-rich species under mild conditions. However, reactions of benzenoid aromatics with 1,3-dipoles were also reported. In this subsection various [3+2] annulations will be

considered, including true pericyclic and formal [3+2] cycloadditions and related reactions.

A stereoselective annulation of the tetrahydrofuran ring through palladium-catalyzed asymmetric dearomative formal [3+2] cycloaddition of epoxybutenes to nitrobenzoheterocycles was developed by You and coworkers [16, 17] (Scheme 2.2). The authors have synthesized wide range of new polycyclic derivatives with easily transformable functional groups and thus made this methodology potentially useful for organic synthesis and medicinal chemistry. Both 2- and 3-nitro heterocycles gave cycloadducts in high yields. The authors were able to tune the diastereoselectivity by changing the polarity of the solvent: in toluene the reactions gave predominantly *cis*-adducts, whereas in the more polar MeCN, the stereoselectivity was inversed to give *trans*-diastereomers. The observed stereocontrol was explained by different rate-limiting steps for reactions in two different solvents. The ligand screening was performed, and phosphinooxazoline (PHOX) ligands with fine-tuned electronic and steric characteristics were found to provide the best enantioselectivity in up to 95% ee.

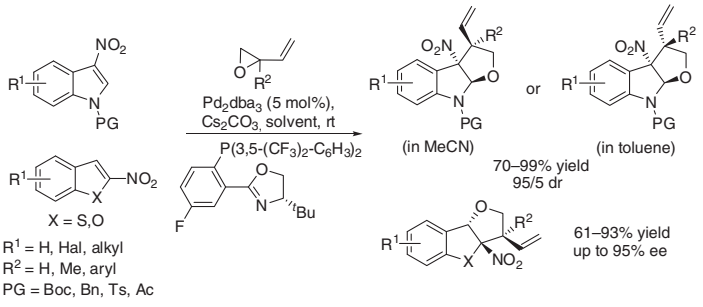

Scheme 2.2 You's Pd-catalyzed stereoselective annulation of the tetrahydrofuran ring.

An approach to densely functionalized tetrahydropyrrolo[2,3-*b*]indolines based on dearomative Pd-catalyzed [3+2] cycloaddition to N-protected 3-nitroindoles was reported by Rivinoja et al. [18] and Suo et al. [19] (Scheme 2.3). *N*-Tosyl-2-vinylaziridine acted as the 1,3-zwitterionic dipole precursor. These two-step formal cycloadditions proceed smoothly on a gram scale with excellent diastereoselectivity. Configuration of the tertiary carbon stereocenter bearing a vinyl group

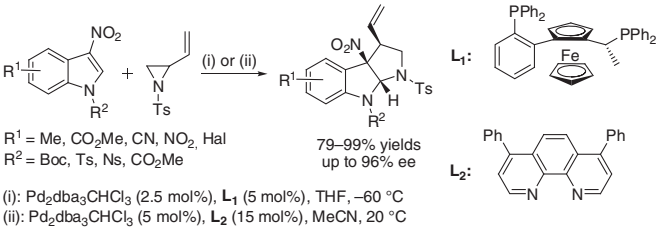

Scheme 2.3 Diastereo- and enantioselective cycloaddition of 2-vinylaziridine to 3-niroindoles.

depends on the ligand and especially on the substituent at position 4 of indole core. It was noticed [18] that in the case of phenanthroline BPhen ligand, four-unsubstituted indoles gave *trans*-products, while 4-*R*-3-nitroindoles provided *cis*-cycloadducts depicted in Scheme 2.3. On the other hand, the enantioselective version of these transformations performed by Suo et al. [19] using a phosphine Walphos-type ligand at −60 °C allowed the synthesis of *cis*-adducts in high yields, dr and ee.

Isomeric tetrahydropyrrolo[3,4-*b*]indolines with two adjacent quaternary carbon stereocenters were synthesized by You and coworkers [20] via $Fe(OTf)_3$-catalyzed reaction between *N*-tosylaziridines and 2,3-dialkylindoles (Scheme 2.4). Mechanistically, the reaction includes coordination of $Fe(OTf)_3$ with both alkoxycarbonyl groups of the aziridine followed by ring opening with formation of a stabilized azomethine ylide and its subsequent stepwise [3+2] annulation. The process features cheap catalyst, mild conditions, and operational simplicity providing complex heterocyclic scaffolds in one step in acceptable yields.

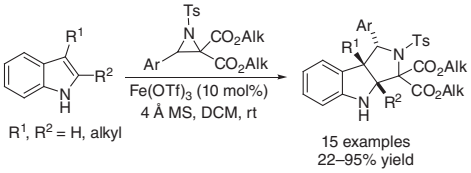

Scheme 2.4 You's synthesis of tetrahydropyrrolo[3,4-*b*]indolines.

2-Nitrobenzofurans [21] and 3-nitro-*N*-tosylindoles [22] react with stabilized azomethine ylides resulting in dearomative formal [3+2] cycloaddition with formation of a pyrrolidine ring (Scheme 2.5). The dipoles were generated from glycine-derived imino esters and Cs_2CO_3 as base. High stereoselectivity was achieved using a chiral Cu(I)/(S,S_p)-*i*Pr-Phosferrox catalyst for benzofurans and PyBidine/$Cu(OTf)_2$ catalyst in the case of 3-nitroindoles. These reactions provided an efficient method for construction of diverse and complex chiral-fused pyrrolidine compounds. The products were obtained in high yields, diastereo- and enantioselectivities, with broad scope for both substrates and dipoles. The *exo*′-selectivity of the formal cycloaddition was explained by a stepwise Michael/Mannich reaction and supported by experimental results [22].

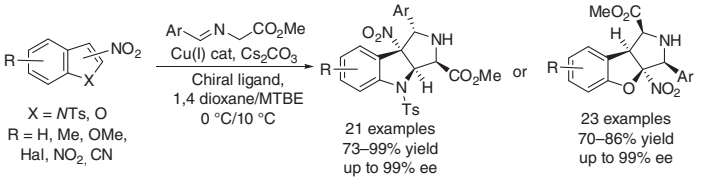

Scheme 2.5 Reactions of 2-nitrobenzofurans and 3-nitroindoles with amino ester-derived imines.

Reactions between 2- or 3-nitroindoles and unstabilized *N*-alkyl azomethine ylides generated *in situ* from *N*-alkyl glycine and paraformaldehyde in refluxing

toluene afforded hexahydropyrrolo[3,4-*b*]indoles in good to excellent yields [23] (Scheme 2.6). Presence of two strong electron-withdrawing groups (in particular, nitro group) in the pyrrole ring is essential since no reaction was observed in the case of *N*-benzyl-3-nitro-, *N*-phenylsulfonyl-, and 3-cyano- *N*-(phenylsulfonyl)indoles. Regardless of relatively drastic conditions and excess of dipole precursor, the elimination of nitrous acid was not observed.

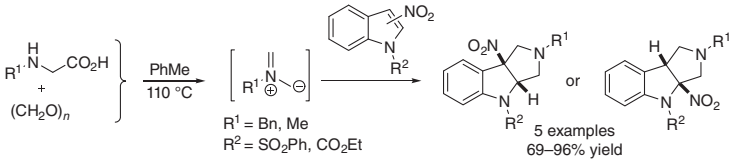

Scheme 2.6 Reactions of 2- and 3-nitroindoles with *N*-alkyl azomethine ylides.

Asymmetric dearomative [3+2] cyclization of indoles with 1,4-benzoquinone under chiral phosphoric acid catalysis gave enentioenriched benzofuroindolines with high regioselectivity [24]. Availability of the starting materials, mild reaction conditions, and broad scope of compounds obtained make this protocol efficient and useful for asymmetric construction of pharmaceutically oriented benzofuro[2,3-*b*]indoline derivatives (Scheme 2.7a). Another example of dearomative annulation of a heterocycle to indole core was reported by Lu and coworkers [25]. 3-Alkyl- and 2,3-dialkylindoles undergo metal-free formal [3+2] cycloaddition with azoalkenes, leading to chiral pyrroloindoline derivatives (Scheme 2.7b). Application of the previously mentioned chiral phosphoric acid catalysis led to the formation of multifunctional pyrroloindolines under mild conditions in high yields and with excellent enantioselectivities.

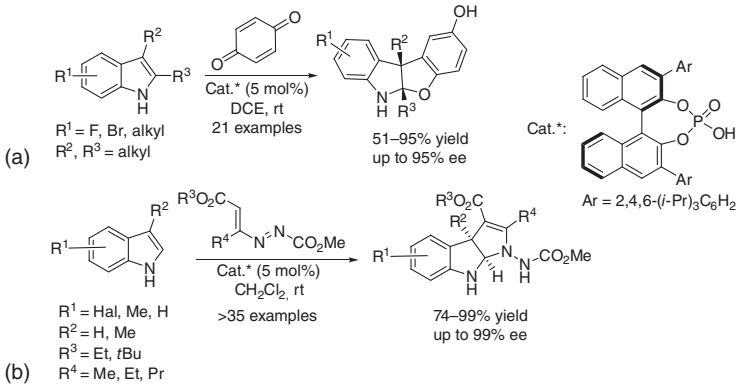

Scheme 2.7 Synthesis of benzofuroindolines (a) and pyrroloindolines (b) via [3+2] cyclizations.

2-Aminocyclopropane-1,1-dicarboxylates represent an interesting example of C_3-components for [3+2] cycloaddition to C=N double bonds of hetarenes.

The enantioselective dearomative [3+2] cycloaddition to benzazoles has been developed recently by Zhang et al. [26] (Scheme 2.8). In the presence of a copper complex derived from $Cu(OTf)_2$ and a chiral bisoxazoline ligand, a series of hydropyrrolo-benzazole derivatives containing quaternary stereogenic centers was obtained in high yields and enantioselectivity. The products proved to be useful precursors of important heterocyclic skeletons, such as 1,5-benzothiazepine and pyrrolo-benzothiazine.

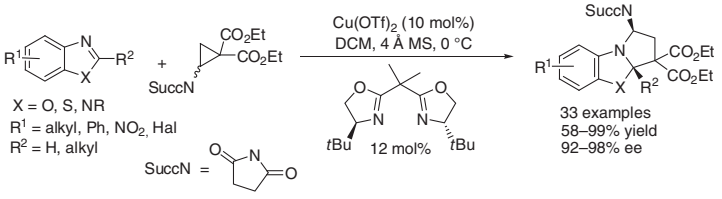

Scheme 2.8 Asymmetric [3+2] cycloaddition of benzoazoles with aminocyclopropanes.

In 2017, Waser's group reported on a simple method for the preparation of benzo-fused tetrahydroindolizine derivatives by dearomative ytterbium(III)-catalyzed [3+2] cycloaddition of pyridines, isoquinolines, or quinolines with donor–acceptor aminocyclopropanes [27]. High yields and diastereomer ratios > 20 : 1 along with broad substrate scope were achieved (Scheme 2.9). The reaction was found to be scalable, and further functionalizations of the obtained products were performed, thus opening an access to more complex biologically prospective molecules.

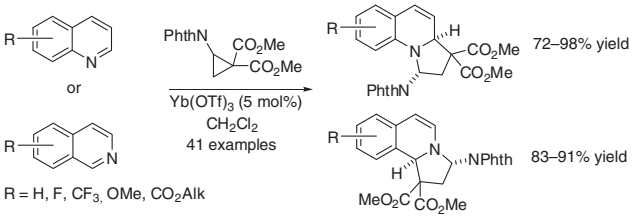

Scheme 2.9 Waser's diastereoselective synthesis of tetrahydroindolizines.

Jiang and coworkers developed a new strategy for the dearomatization of isoquinolines [28] (Scheme 2.10). They implemented formal [3+2] cycloaddition of *N*-aryl α-amino acids with isoquinoline *N*-oxides via visible light-driven reactions using bis(5-methoxythienyl)dicyanopyrazine as the photoredox catalyst. As a result a series of diazabicyclo[3.2.1]octane-based N-heterocyclic compounds were obtained in high yields. The proposed reaction mechanism included generation of an α-aminoalkyl radical from the α-amino acid and its addition to isoquinoline-*N*-oxide followed by reduction to give intermediate **I**. After protonation with 1,1,3,3-tetramethyl guanidine as a proton shuttle, cation **II** undergoes intramolecular Mannich reaction. This approach represents the first example of *N*-aryl α-amino acids used as 1,2-synthons in organic chemistry.

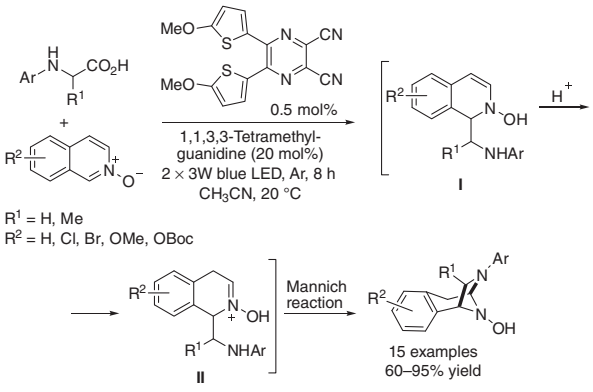

Scheme 2.10 Photoredox-catalyzed reactions of isoquinoline-*N*-oxides with *N*-aryl α-amino acids.

Asymmetric [3+2] cycloaddition of 2-nitrobenzofurans with cyclic azomethine ylides, catalyzed by a copper complex derived from $Cu(OAc)_2$ and a chiral diphosphine ligand, was proposed by Wang et al. [29]. Dearomatization of a furan ring with formation of a bridged pyrrolidine ring provided a series of fused polycyclic 8-azabicyclo[3.2.1]octane derivatives in high yields (75–91%) with enantioselectivities up to 98% (Scheme 2.11). The developed method is a direct synthetic approach to fused polycyclic tropane scaffolds. The ease of product transformations and scalability of the reactions were demonstrated.

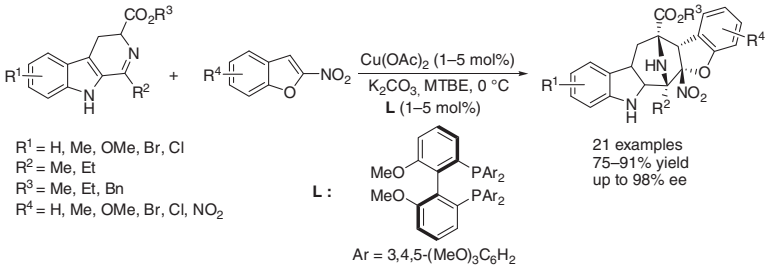

Scheme 2.11 Dearomative [3+2] cycloaddition reactions of 2-nitrobenzofurans.

In situ generated *N*-benzyl azomethine ylide readily reacts with benzofurans, benzothiophenes, and indoles bearing electron-withdrawing substituents (Scheme 2.12). These dearomative [3+2] cycloadditions were found to be diastereoselective giving rise to a series of functionalized fused tricyclic pyrrolidine derivatives in good yields under mild reaction conditions [30–32].

Highly electrophilic 3,5-dinitropyridines [33] and nitroazolopyridines [34] undergo double cycloaddition with nonstabilized *N*-alkyl azomethine ylides (Scheme 2.13). It was found that aromatic C—C as well as C=N bonds of pyridine rings bearing nitro groups in imidazo- and triazolopyridine derivatives may act as dipolarophiles toward nucleophilic 1,3-dipoles so that addition of 2 equiv of

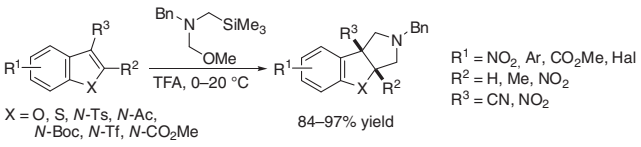

Scheme 2.12 Dearomative annulations of pyrrolidine ring to five-membered benzo-fused heterocycles.

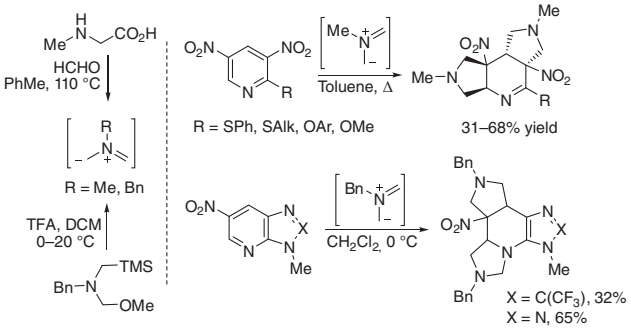

Scheme 2.13 Double [3+2] cycloaddition of *N*-alkyl azomethine ylides to nitropyridines.

azomethine ylide becomes possible. As a result, a number of polycyclic pyrrolidine derivatives were synthesized in moderate yields. Complete diastereoselectivity of the process was observed in both cases: *cis*-addition of two dipoles occurred from the opposite sides of the pyridine plane.

The previously mentioned examples of [3+2] annulation include reactions of 1,3-dipoles or related intermediates to heterocycles, which obviously exhibit less aromatic character than benzene derivatives. However, similar processes for benzenoid aromatics are also known. For instance, 1,3-dipolar cycloadditions of azomethine ylides to aromatic dipolarophiles were reviewed recently by Ryan [35].

Shevelev and coworkers found the first example of 1,3-dipolar cycloaddition of unstabilized azomethine ylides to C=C(NO_2) bonds of nitroarenes [36, 37]. It was shown that 4,6-dinitrobenzoazoles as well as 6,8-dinitroquinoline react with *N*-methyl azomethine ylide to give products of double [3+2] cycloaddition – decahydropyrrolo[3,4-*e*]isoindoles in moderate to good yields (Scheme 2.14a). Later [38], similar reactivity of *N*-benzyl azomethine ylide toward 7-substituted-4-nitrobenzofuroxans was observed (Scheme 2.14b). As expected, in both cases the bis-adducts were formed diastereoselectively through *trans*-annulation of two pyrrolidine rings but as racemic mixtures. The dipoles were generated as it is shown in Scheme 2.13.

In continuation of this research, reactions of *N*-alkyl azomethine ylides with various functionalized nitrobenzoazoles and dinitroquinolines (Scheme 2.15) were studied [39–41]. 4-Nitro- and 5-nitrobenzofurazans, thiadiazoles, and selenadiazoles readily undergo dearomative [3+2] annulation of a pyrrolidine ring to the C=C(NO_2) fragment (Scheme 2.15a). On the other hand, 5,7-dinitroquinolines with arylamino group at position 8 (Scheme 2.15b) also gave monoadducts

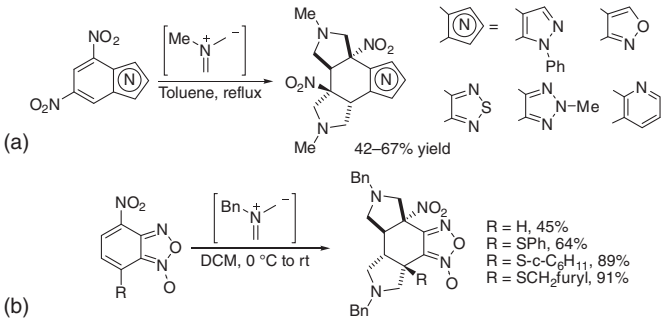

Scheme 2.14 Double [3+2] cycloaddition of *N*-alkyl azomethine ylides to nitroarenes.

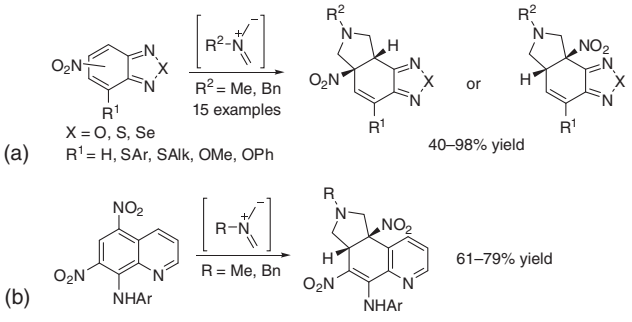

Scheme 2.15 [3+2] Cycloaddition of *N*-alkyl azomethine ylides to nitroarenes.

despite the presence of two nitro groups (compare with Scheme 2.14a). Thus, a method for the synthesis of condensed tetrahydroisoindole derivatives has been developed.

S.R. Piettre et al. showed that non-stabilized *N*-benzyl azomethine ylide reacts smoothly at room temperature with a variety of uncomplexed aromatic carbocycles and heterocycles [32, 42]. Formation of the adduct was observed for those aromatic compounds containing at least two electron-withdrawing substituents (an example is shown on Scheme 2.16). This method affords highly functionalized polycyclic structures in moderate to good yields. In most cases, the second cycloaddition step occurs on the opposite face to that occupied by the first newly formed pyrrolidine ring. DFT calculations indicate that a concerted mechanism features a low activation barrier compared with an alternative cycloaddition process involving a nitrobenzene radical anion and an azomethine ylide radical cation.

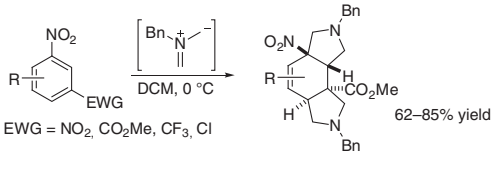

Scheme 2.16 Reactions of *N*-benzyl azomethine ylide with nitrobenzene derivatives.

Intramolecular dearomative [3+2] cycloaddition to nitroaromatics was reported by Wales et al. (Scheme 2.17) [43]. Reactions of 3,5-dinitrobenzyloxy- and 3,5-dinitrobenzyl aminobenzaldehydes with N-substituted α-amino acids resulted in the formation of unprecedented benzoazepine-fused isoindolines. The fragment C=C(NO_2) acted as dipolarophile interacting with the tethered azomethine ylide, formed from an amino acid and an aldehyde, to give a pyrrolidine moiety. Subsequent aromatization gave the final products in moderate to high yields. This method is scalable and gives products with a nitro group ready for further transformations; some of those were performed, such as reduction, N-deprotection, and others.

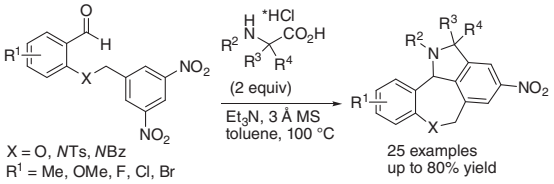

Scheme 2.17 Intramolecular [3+2] cycloadditions of azomethine ylides with dinitroarenes. Source: Wales et al. [43]/American Chemical Society.

Finally, a promising synthetic approach to benzopyrano-fused natural products such as flavonoids was proposed by Takata and coworkers [44] (Scheme 2.18). Chlorination of 2-phenoxybenzaldehyde oximes with NCS in the presence of Et_3N resulted in formation of the corresponding nitrile *N*-oxides, which underwent intramolecular 1,3-dipolar cycloaddition to the neighboring benzene ring under refluxing $CHCl_3$. The dearomatization led to *peri*-annulated isoxazolines in moderate to high yields.

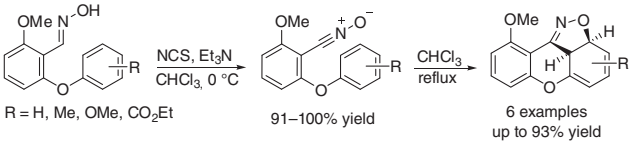

Scheme 2.18 Intramolecular dearomative [3+2] cycloaddition of nitrile *N*-oxides.

2.2.2 [4+2] Cycloaddition

[4+2] and [3+2] cycloadditions are isoelectronic [$_\pi4_s+_\pi2_s$] processes; therefore, it is not surprising that potential 2π-substrates for both transformations generally belong to the same classes. Formation of new heterocycles via Diels–Alder reactions of (het)arenes is possible by interaction of either azadienes with the C=C double bond of (het)arenes or all-carbon electron-rich dienophiles with the heterodiene fragment of (het)arenes. Thus, selected highly electrophilic nitroarenes and five-membered benzo-fused heterocycles are able to undergo [4+2] cycloaddition as dienophiles (normal electron demand, NED) as well as heterodienes (inverse

electron demand, IED) acting as conjugated nitroalkenes [45]. The publications of Terrier and coworkers [46, 47] appear to be the first major contribution to understanding such transformations. It was found that reactions of highly electrophilic 4,6-dinitrobenzofuroxan with equimolar amount of indene or ethyl vinyl ether proceeded smoothly at ambient temperature, giving oxazine-*N*-oxides fused to the benzofuroxan system (Scheme 2.19). Formally, the C=C—NO_2 fragment of the aromatic system acts as heterodiene; however, the suggested mechanism is either a two-step (through σ-complex) or a concerted reaction through a cyclic transition state, i.e. IED [4+2] cycloaddition.

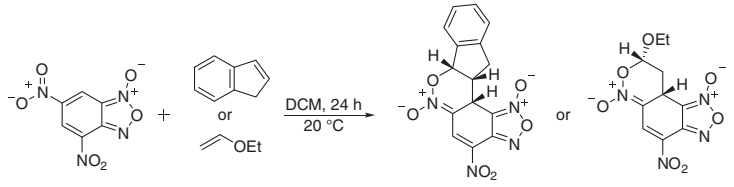

Scheme 2.19 4,6-Dinitrobenzofuroxan as heterodiene in IED Diels–Alder reactions.

More recently Shevelev and coworkers reported on a number of structurally similar "superelectrophilic" nitrobenzofuroxans annulated with azole or azine rings, which were found to undergo Diels–Alder reactions with ethyl vinyl ether [41, 48–52]. Reactions represent diastereoselective dearomative annulations of an oxazine-*N*-oxide moiety (Scheme 2.20a). In addition, the same authors found that 4,6-dinitrobenzo[*c*]isoxazole readily underwent double IED [4+2] cycloaddition with ethyl vinyl ether (Scheme 2.20b) [53]. In this case, two oxazine fragments were annulated to the benzene ring giving rise to the corresponding bis-cycloadduct with dr 90 : 10.

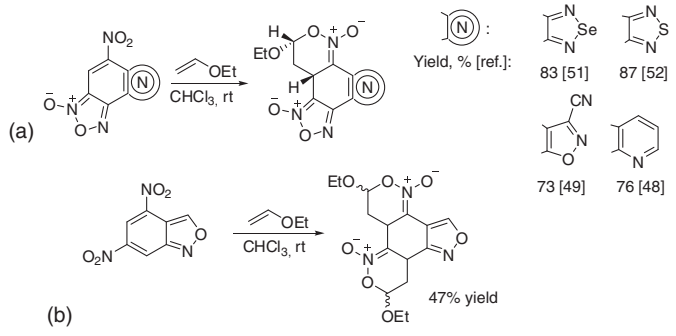

Scheme 2.20 Reactions of highly electrophilic nitroaromatics with ethyl vinyl ether.

An interesting example of dearomatizing [4+2] cycloaddition of indoles was reported by Chataigner and coworkers [54]. It was shown that 3-nitroindole can be involved in thiourea-catalyzed cascade [4+2]/[3+2] cycloadditions under high pressure. The intermediate [4+2] adduct represents a cyclic nitronate, i.e. a

1,3-dipole, which further reacts with acrylate to give a polycyclic indoline derivative in 90% yield with dr 63 : 37 with predominance of the *cis*-isomer (Scheme 2.21). A number of chiral thiourea catalysts were used to evaluate the stereochemistry of the cycloaddition process. It turned out that chiral catalysts have only little influence on the diastereomeric ratios of the second cycloaddition, and the enantiomeric excess of 28% or less could be reached.

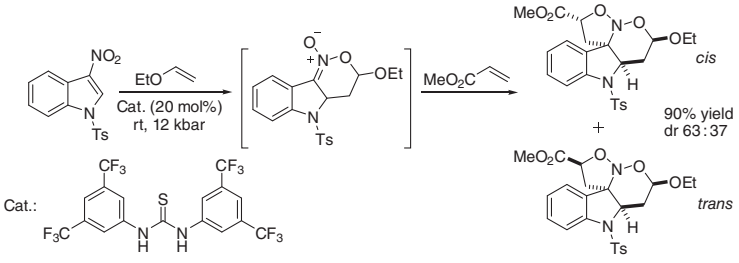

Scheme 2.21 Thiourea-catalyzed dearomatizing [4+2] cycloaddition of 3-nitroindole.

Formal [4+2] cycloaddition of 3-nitroindoles with ethynyl benzoxazinanones was developed by You in two versions: Cu(I) catalyzed [55] and metal free (Scheme 2.22) [56]. Propargylic dearomatization of indole via a copper–allenylidene intermediate followed by *cis*-annulation of the six-membered ring gave 5*H*-indolo[2,3-*b*]quinolines in high yields and diastereoselectivity under mild conditions [55]. The metal-free formal [4+2] cycloaddition was postulated to proceed via aza-*ortho*-quinone methides generated *in situ* from ethynyl benzoxazinanones in the presence of a base [56]. Due to stabilizing secondary orbital interactions, an *endo*-selective cyclization is favored resulting in the formation of *trans*-adducts. The authors proposed this aza-Diels–Alder reaction to proceed as a stepwise process.

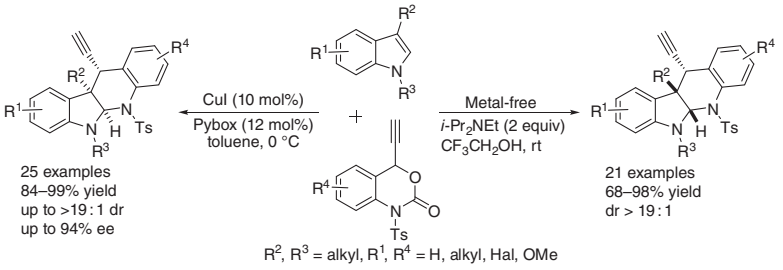

Scheme 2.22 Formal [4+2] cycloaddition of 3-nitroindoles with ethynyl benzoxazinanones. Source: Shao et al. [56]/John Wiley & Sons.

Similar heterocyclic systems were synthesized in 2020 by Hyland and coworkers [57]. They demonstrated that diastereoselective Pd-catalyzed formal [4+2] cycloaddition between 3-nitroindoles and N-unprotected vinyl benzoxazinones resulted in the formation of densely functionalized tetrahydro-5*H*-indolo[2,3-*b*]

quinolines (Scheme 2.23). *Trans*-annulated products were isolated in high yields and dr > 98 : 2.

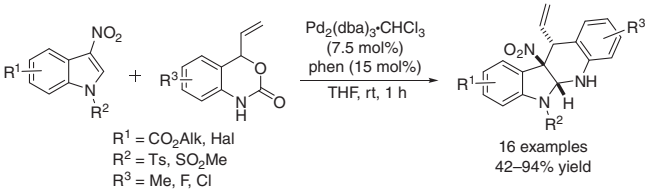

Scheme 2.23 Pd-catalyzed formal [4+2] cycloaddition of 3-nitroindoles with vinyl benzoxazinones.

Dearomative annulation of partially hydrogenated pyridazine ring to functionalized indoles was reported by Xu [58]. The authors developed an efficient metal-free method for the synthesis of tetrahydro-1*H*-pyridazino[3,4-*b*]indoles by the reaction between indoles and α-bromohydrazones (Scheme 2.24). Systematic study revealed the great influence of electronic and steric effects of the substrate and reagents on the reaction. A plausible reaction mechanism includes conversion of bromohydrazone to 1,2-diaza-1,3-diene under the action of a base and further IED aza-Diels–Alder reaction.

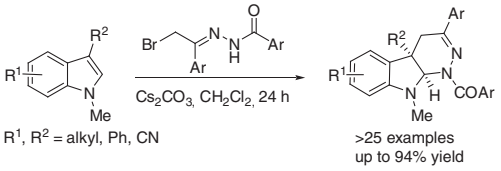

Scheme 2.24 Xu's dearomative annulation of pyridazine ring to indoles.

Reactions of indoles with 1,2-diaza-1,3-dienes under Zn(II) catalysis proceed as formal dearomative [4+2] or [3+2] cycloaddition depending on the nature of substituents (Scheme 2.25) [59]. 2,3-Unsubstituted indoles with cyclic diazadienes gave pyridazine annulations in [4+2] fashion, while 2,3-dialkylindoles with linear azoalkenes provided [3+2] adducts – tetrahydropyrrolo[2,3-*b*]indoles. Interestingly, the DFT study revealed that [4+2] cycloadditions are concerted asynchronous, whereas [3+2] reactions proceed through a stepwise mechanism. Among the main

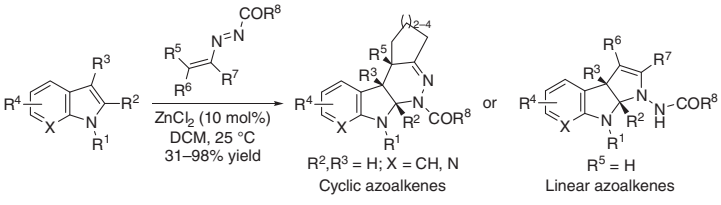

Scheme 2.25 Formal dearomative cycloadditions of 1,2-diaza-1,3-dienes to indoles. Source: Ciccolini et al. [59]/American Chemical Society.

features of these interactions are high chemo- and diastereoselectivities, which allowed preparing a broad product scope in moderate to good yields.

In 2016, You described an example of intramolecular Pd-catalyzed dearomatization of substituted indoles [60]. The reaction of indoles with allyl carbonate containing an alcohol side chain proceeds in a cascade fashion with formation of tetrahydropyran ring providing polycyclic bridged indoline derivatives (Scheme 2.26). Application of chiral phosphoramidite ligands allowed implementing enantioselective reactions in up to 95% ee.

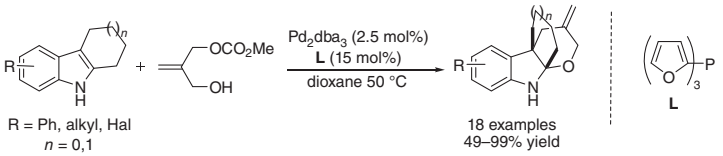

Scheme 2.26 Intramolecular Pd-catalyzed dearomatization of substituted indoles.

A metal-free dearomatization of substituted furans was developed by Mo and coworkers [61]. [4+2] Cycloaddition of aza-*o*-quinone methides (generated *in situ* from *o*-(tosylamino)chloromethylbenzenes) to furan ring led to densely functionalized furo[3,2-*b*]quinolines (Scheme 2.27). The use of 2 equiv of azadiene provided double cycloaddition to both furan double bonds to give furo[2,3-*b* : 4,5-*b*′]diquinolines. High regio- and diastereoselectivities of the process were demonstrated.

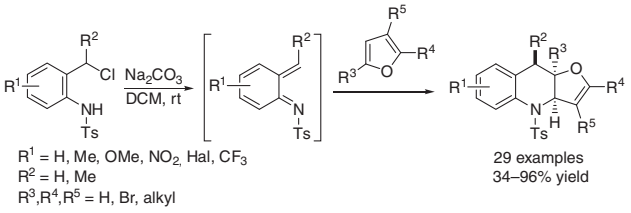

Scheme 2.27 [4+2] Cycloaddition of aza-*o*-quinone methides to furans.

Photoinduced dearomatization of arenes accomplished through an intramolecular cycloaddition with aza-*o*-xylylenes was contributed by Kutateladze and coworkers [62] (Scheme 2.28). This unprecedented method for photo-dearomatization of a tethered benzene ring playing a role of dienophile provided rapid access to novel *peri*-annulated heterocycles via simultaneous formation of five- and six-membered heterocyclic rings.

Visible light-activated dearomatization of pyridines was described by Glorius and coworkers [63]. They studied dearomative energy transfer-catalyzed [4+2] cycloaddition of pyridine-containing cinnamoyl amides using polymer-immobilized Ir-based photocatalyst (Scheme 2.29). The mechanism supported by both kinetic studies and DFT calculations includes promotion of the ground-state alkene moiety to the triplet excited state followed by direct cycloaddition to a pyridine

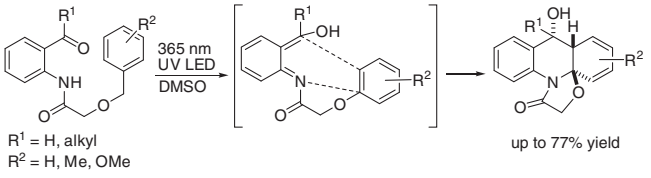

Scheme 2.28 Photoinduced intramolecular cycloaddition of aza-*o*-xylylenes.

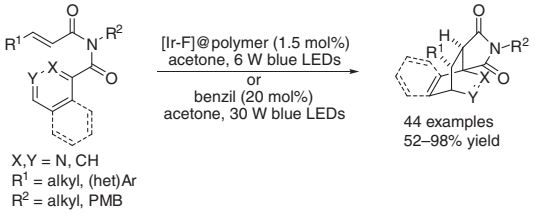

Scheme 2.29 Direct dearomative [4+2] cycloaddition of pyridines.

ring. This method provided functionalized isoquinuclidine derivatives in high yields. The broad substrate scope along with facile scalability and functional group tolerance makes this approach efficient and useful.

2.2.3 Other Cycloadditions

N-Iminoquinolinium ylides undergo Pd-catalyzed dearomative [4+3] cycloaddition with 2-(hydroxymethyl)allyl *tert*-butylcarbonates to give novel seven-membered saturated heterocycles with three heteroatoms and exocyclic C=C double bond [64] (Scheme 2.30). Similar cyclizations were also performed using substituted isoquinolinium ylides as starting compounds.

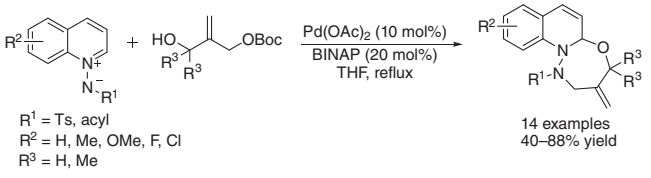

Scheme 2.30 Pd-catalyzed dearomative [4+3] cycloaddition of *N*-iminoquinolinium ylides.

Recently Zhai's group developed a method for the synthesis of pyridothiazepines via 1,5-dipolar cycloaddition reaction between pyridinium 1,4-zwitterionic thiolates and terminal activated allenes conducted under thermal conditions [65] (Scheme 2.31). The same authors reported on a synthesis of pyridothiazines using pyridinium 1,4-zwitterionic thiolates and α-functionalized bromoalkanes via formal [5+1] cycloaddition [66]. Thiazine derivatives were found to be quite unstable and underwent oxidation and ring-contraction/desulfuration when in air (Scheme 2.31).

In 2019, recent developments on the [5+2] cycloadditions and their application in the synthesis of natural products containing seven-membered heterocycles

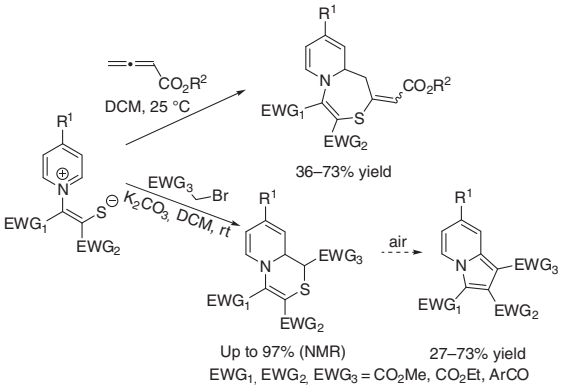

Scheme 2.31 Cycloaddition reactions of pyridinium 1,4-zwitterionic thiolates.

were reviewed by Ding and coworkers [67]. In particular, this review summarized advances in dearomative [5+2] cycloadditions of indoles, pyrylium salts, pyridinium, and quinolinium ylides. It also contains other examples of formation of new heterocycles via dearomatization reactions.

2.3 Intramolecular Addition to Aromatic Double Bonds Leading to Heterocycles

An original dearomative approach to pyrrolo[3,4-*b*]indoles was proposed by Gribble and coworkers [68]. Treatment of 2-bromoindole-3-carboxamide derivative with tri-*n*-butyltin hydride and AIBN gave 3,4-dihydropyrrolo[3,4-*b*]indole-1(2*H*)-one via annulation of the pyrrolidine ring (Scheme 2.32). The reaction is supposed to proceed through homolytic debromination followed by formation of *N*-methylene radical, which undergoes 5-endo-*trig*-cyclization to give tricyclic product in 51% yield.

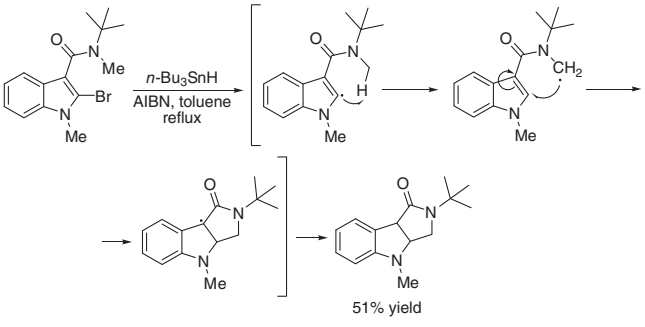

Scheme 2.32 Intramolecular radical cyclization of indole-3-carboxamide.

Another example of intramolecular dearomative cyclization of indoles leading to fused eight-membered aza-heterocycles was reported recently by Yuan et al. [69].

The process deals with intramolecular ZnI_2-catalyzed alkylation of indoles at C-2 with annulations of the tetrahydroquinoline core and subsequent ring expansion on reacting with acylacetylenes in the presence of a base (Scheme 2.33). This approach was applied recently to the synthesis of related series of indoline-fused eight-membered azaheterocycles containing chromene moiety [70].

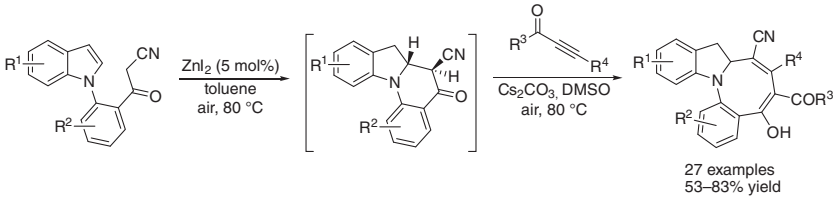

Scheme 2.33 Intramolecular dearomative cyclization of indoles and subsequent ring expansion.

Pd-catalyzed 2,3-difunctionaliztion of indoles and benzofurans with simple boronic acids and TEMPO as an oxidant leads to *syn*-annulation of five- to seven-membered rings with simultaneous dearomatization of the initial pyrrole or furan cycles (Scheme 2.34) [71]. For the series of derivatives bearing carboxylic acid-substituted side chains, high diastereoselectivity was observed, which depends on the specific substituent. The proposed mechanism includes formation of aryl–Pd complex and electrophilic palladation of a heterocycle at C3 position and 1,2-migration of ArPd followed by intramolecular trapping of the corresponding cation by the acid. Subsequent reductive elimination gives β-aryl lactones generally in moderate yields.

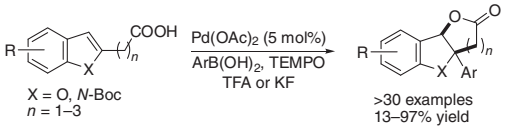

Scheme 2.34 Dearomative annulation of lactones to indoles and benzofurans. Source: Ramella et al. [71]/John Wiley & Sons.

Liu et al. reported on an electrochemical method for regioselective dearomative annulations of N-protected indole and benzofuran derivatives [72]. Reactions with α,ω-diols and dithiols as well as mixed *O*-,*S*-bis-nucleophiles afforded indolines or 2,3-dihydrobenzofurans condensed with various saturated heterocycles (Scheme 2.35). The significant tolerance of functional groups in the heteroarene fragment to the reaction conditions is mentioned, even in the case of iodide, hydroxyl, azide, amide, cyano, or carbonyl. On the basis of experimental results, a plausible mechanism was proposed, suggesting that the reactions proceed through the anodic oxidation of indole with formation of a radical cation, which then reacts with bis-nucleophile depending on the nature of a particular reactant. In the case of *S*-nucleophiles, anodic oxidation of thiol to *S*-radical occurs followed

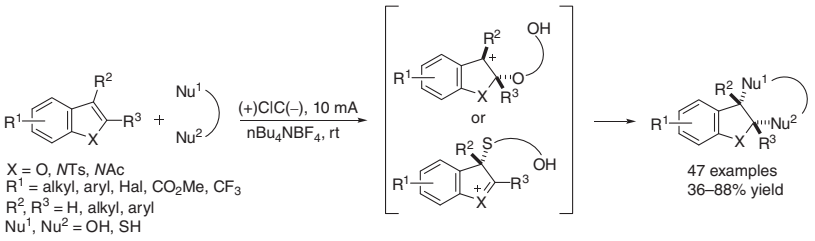

Scheme 2.35 Electrochemical annulation of saturated O- and S-heterocycles.

by radical cross-coupling and intramolecular nucleophilic addition. Otherwise, the indole radical cation reacts with the *O*-nucleophile to give a C3-centered radical, which is then oxidized to carbocation and attacked with hydroxyl to form C—O bond.

A catalytic protocol for the construction of 1,4-cyclohexadiene-fused sultams has been reported very recently [73]. Starting from quite simple sulfonyl enamides, a carboamination/radical dearomatization cascade allowed to assemble complex polycyclic structures (Scheme 2.36). Closure of two heterocyclic rings (pyrrolidinone and sultam) was achieved with high diastereoselectivity and moderate to good yields. As a result, a photoredox-mediated strategy was developed as an atom- and step-economy synthesis of complex molecular frameworks.

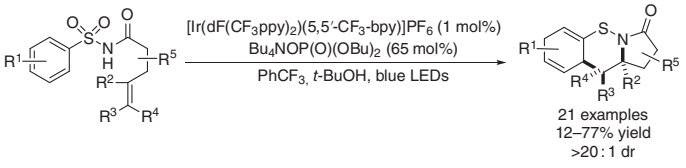

Scheme 2.36 Photoredox-catalyzed cyclization of *N*-arylsulfonyl amides.

Reactions of 4-(aminoethyl)-1-naphthol with aryl bromides under Pd/Q-Phos-catalysis produced structurally diverse benzomesembrine derivatives by means of dearomative pyrrolidine ring closure [74]. This intermolecular arylative dearomatization followed by intramolecular aza-Michael addition provides tricyclic structures with two adjacent stereocenters (Scheme 2.37).

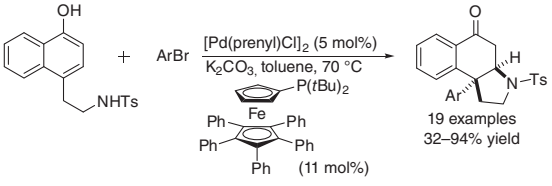

Scheme 2.37 Dearomative arylation/annulation of pyrrolidine ring to four-substituted 1-naphthol.

2.4 Dearomative Spirocyclizations

This subsection is devoted to the synthesis of spiroheterocycles by means of dearomatization of arenes or hetarenes. Spiro-containing compounds are of considerable importance, owing to their potential application in medicinal chemistry. They have been isolated from plants, marine sponges, and other biological sources. Natural products containing spirocarbocycles [75] and spirooxindoles [76, 77] have been reviewed. Oxidative dearomatizing spirocyclization of substituted phenols is one of the most straightforward and popular approaches to spiroheterocycles (see Scheme 2.1b). It can be nicely illustrated by the synthesis of spirooxazolines from various simple 4-hydroxybenzylamides (Scheme 2.38) [78]. Employing aryl iodide as the precatalyst and MCPBA as oxidant in hexafluoro-2-propanol at room temperature furnished *in situ* generated iodine(III) species, which on coordination with phenol oxygen atom initiated spirocyclization. 1-Substituted 2-naphthol derivatives behave similarly giving target spirooxazolines in moderate yield.

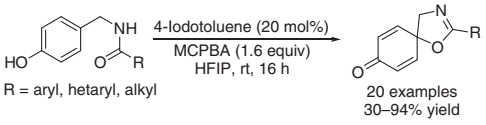

Scheme 2.38 Synthesis of spirooxazolines via oxidative dearomatization of phenols. Source: Umair Tariq and Moran [78]/John Wiley & Sons.

Another relevant example comprising iodine-mediated spirocyclization in the *ortho*-position of naphthols and phenols deals with formation of spirolactone under ammonium hypoiodite/oxone catalysis [79] (Scheme 2.39a). Reactions proceed under mild conditions in the presence of chiral quaternary ammonium iodides to afford the corresponding spirolactones in high yield and enantioselectivity. Spirocyclization with formation of a tetrahydrofuran ring under the action of $PhI(OAc)_2$ was also reported for substituted phenol [80] (Scheme 2.39b).

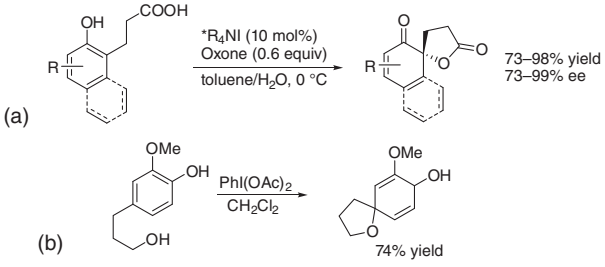

Scheme 2.39 Spirocyclizations with formation of tetrahydrofuran ring.

A series of 4-spiro-β-lactam-3-carbonitriles was synthesized by Abdellaoui and Xu from *N*-benzyl-*N*-(4-hydroxyphenyl)cyanoacetamides via intramolecular oxidative

dearomative cyclization using $PhI(OAc)_2$ as an oxidant and KOH as a base [81] (Scheme 2.40). The authors proposed the cyclization mechanism as a sequence of nucleophilic *ipso*-addition and oxidative dearomatization.

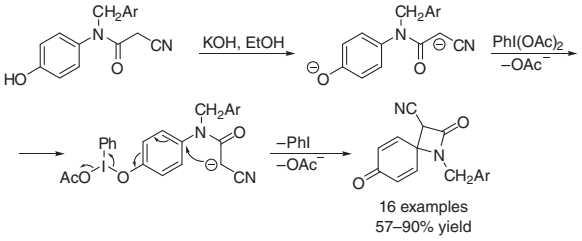

Scheme 2.40 Oxidative dearomatization as an approach to 4-spiro-β-lactams.

In addition to hypervalent iodine oxidative spiro-heterocyclizations, another efficient methodology for dearomatization of phenols was developed [82]. It deals with nucleophilic attack of amines, azides, and hydroperoxides onto *para*-position of phenols or position 1 of 2-naphthols in the presence of phenyl trimethyl ammonium tribromide (PTAB). In particular, reactions of 2-(4-hydroxyphenyl)propionates with benzylamine in the presence of PTAB provided *N*-benzyl spirolactams in good yields (Scheme 2.41).

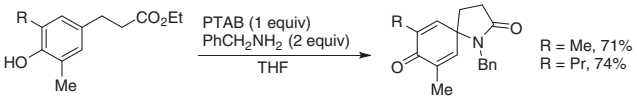

Scheme 2.41 Synthesis of spirolactams by means of dearomative spirocyclization.

Similar spirolactams were obtained in moderate to good yields using visible light-induced dearomative amidation of phenol derivatives [83]. Substituted 3-(4-methoxyphenyl)-*N*-arylpropanamides in the presence of Ru-catalyst and acetoxybenzoiodoxole (BI-OAc) irradiated with 5 W blue LED underwent intramolecular cyclization to yield corresponding spirolactams (Scheme 2.42a). Moreover, the elaborated conditions were employed for the synthesis of indole-containing spirocycles

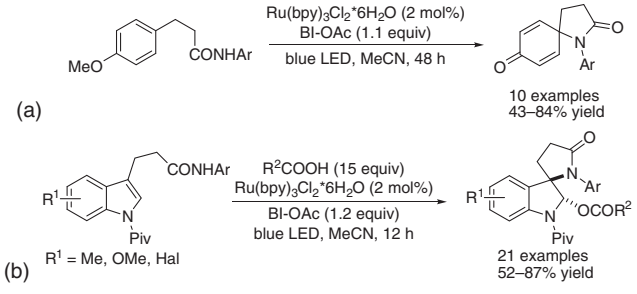

Scheme 2.42 Ru-catalyzed synthesis of *N*-aryl spirolactams.

via dearomative oxamidation (Scheme 2.42b). This efficient protocol exhibited exclusive diastereoselectivity due to steric reasons along with broad substrate scope.

Dearomatization approach to access 3-acyl/alkylspiro[4.5]trienones was proposed by Reddy and coworkers [84] (Scheme 2.43). A sequence of silver-catalyzed decarboxylative acylation (alkylation)/spirocyclization of *N*-arylpropiolamides resulted in the formation of functionalized 3-acyl(alkyl)spiro[4.5]trienones in good to excellent yields. Potassium peroxodisulfate was found to be the best oxidant for the process. A plausible reaction mechanism includes conversion of α-keto acids into acyl radicals, which triggers the dearomatization step with formation of a cyclohexadienone radical. The latter is oxidized to oxonium cation with $S_2O_8^{2-}$ followed by attack by a nucleophile (H_2O) and elimination of MeOH. This approach was successfully extended to the synthesis of 6,7-dihydro-3*H*-pyrrolo[2,1-*j*]quinoline-3,9-diones (Scheme 2.43).

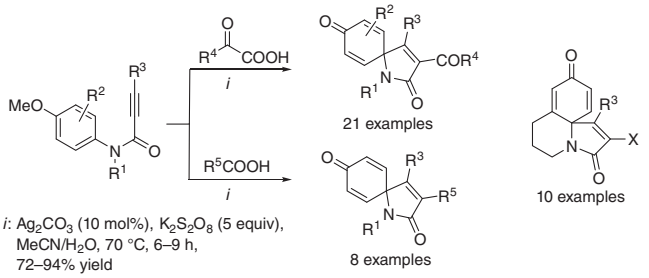

Scheme 2.43 Dearomatization approach to 3-acyl/alkylspiro[4.5]trienones.

Transition metal-free synthesis of spiroisoxazolines from aryl (thio)ethers and (thio)phenols was accomplished in one-step manner including oximation/oxidative dearomatization cascade [85]. In this case air was used as an oxidant, and the process features mild conditions, high yields, and cheap reagents. The proposed reaction sequence initiated with formation of the oxime derivatives, which underwent dearomative spirocyclization catalyzed by nitrosonium ion, using air as the terminal oxidant (Scheme 2.44).

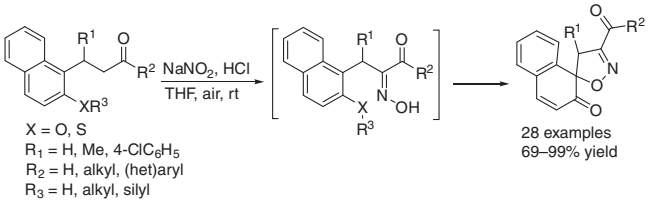

Scheme 2.44 Transition metal-free synthesis of spiroisoxazolines.

Similar approach has been applied to *p*-substituted (thio)ethers and phenols. An aerobic oxidative dearomatization of the corresponding oximes catalyzed by TEMPO and $NaNO_2$ afforded spiro-cyclohexadienone isoxazoline derivatives in

high yields [86] (Scheme 2.45). Ambient oxygen utilized as green oxidant as well as broad substrate scope and mild reaction conditions make the elaborated protocol attractive for synthetic purposes.

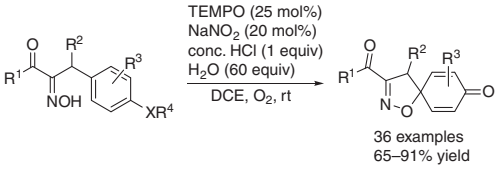

Scheme 2.45 Dearomative approach to spiro-cyclohexadienone isoxazoline derivatives.

Intramolecular phenol dearomatization was utilized in the synthesis of nitrogen-fused polycyclic compounds [87]. Substituted tyramine derivatives were subjected to acid-promoted spirocyclization via *ipso*-Friedel–Crafts allenylation followed by treatment with TBAF, which afforded both indole and cyclopropane moieties in one step (Scheme 2.46). The developed step-economy approach provided an access to structurally uncommon systems potentially interesting as scaffolds for drug discovery.

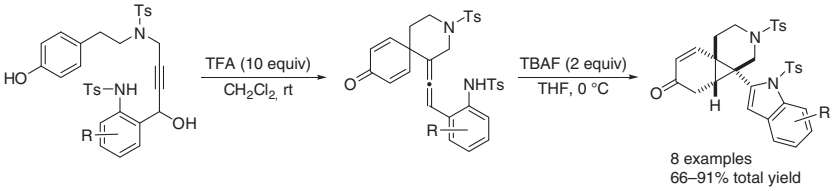

Scheme 2.46 Spirocyclization of tyramine derivatives.

Tandem dearomatization of a furan ring followed by acetalization represents an easy access to 1,6-dioxaspiro[4.4]non-3-enes [88]. Thus, addition of a catalytic amount of TsOH to the corresponding furylpropionic aldehydes caused formation of a carbocation, which was then trapped by a formyl group followed by acetal formation (Scheme 2.47). This novel protocol for the synthesis of acetal-spiroacetal-enol ethers expands the range of synthetic applications of furan derivatives as building blocks.

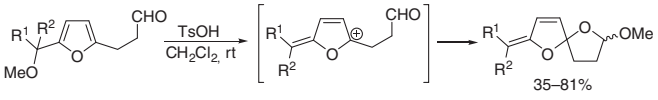

Scheme 2.47 Synthesis of 1,6-dioxaspiro[4.4]non-3-enes.

Intramolecular spirocyclization of 4-aminoethylpyridines afforded 3,9-diazaspiro[5.5]undecanes in moderate yields [89]. This pathway includes electrophilic activation of a pyridine ring with ethyl chloroformate and its further

dearomatization by nucleophilic addition in the presence of $Ti(O^iPr)_4$ (Scheme 2.48). As a result of the process, a piperidine ring is formed, while the initial pyridine cycle is converted into 1,4-dihydropyridine.

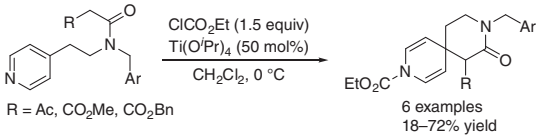

Scheme 2.48 Electrophilic activation and dearomatization of pyridines.

Dearomative radical spirocyclization of *N*-benzyl trichloroacetamides using copper(I) chloride as a mediator under microwave irradiation gave rise to 2-azaspiro[4.5]decanes as 3 : 2 mixture of diastereomers by means of β-lactam ring closure [90]. Allylic chlorine atom of the intermediate in aqueous medium is readily replaced by hydroxyl function (Scheme 2.49). It was demonstrated that the presence of a bulky substituent on the nitrogen favors the cyclization process.

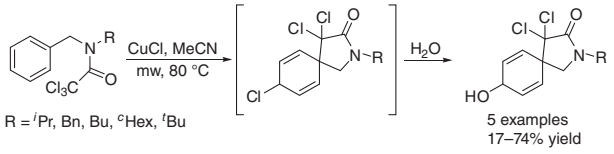

Scheme 2.49 CuCl-mediated spirocyclization of *N*-benzyl trichloroacetamides.

Another example of dearomatization leading to the formation of spiroheterocycle was reported by Feng and coworkers [91]. Fused spiroindolines with three stereocenters were synthesized by the reaction of 3-(2-isocyanoethyl)indoles with alkylidene malonates catalyzed by chiral *N*,*N*′-dioxide/Mg(II) complex. The process includes Michael/Friedel–Crafts cascade, which afforded a variety of polycyclic spiroindolines in excellent yields and stereoselectivity (Scheme 2.50). It was found that addition of $NaBAr^F_4$ resulted in improvement of enantioselectivity (ee 81–96%).

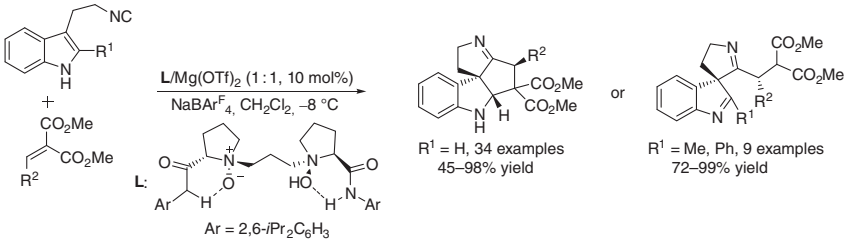

Scheme 2.50 Synthesis of polycyclic spiroindolines via dearomatization.

Sequential catalytic asymmetric dearomatization/reduction reactions were successfully exploited for highly efficient synthesis of spiroindolines with three contiguous stereogenic centers [92]. Vicinal tertiary and quaternary carbon stereocenters are

formed during iridium-catalyzed allylic dearomatization, while reduction of the relatively unstable intermediate spiroindolenine provided another stereocenter at C-2 of the indole core (Scheme 2.51).

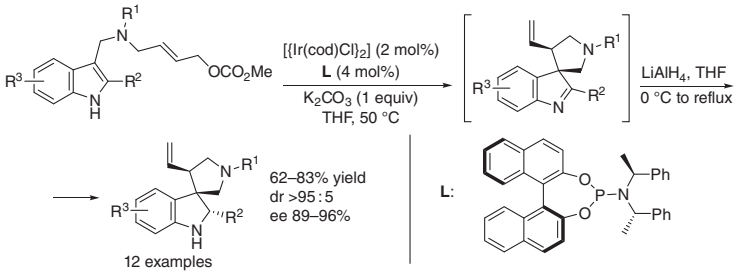

Scheme 2.51 Synthesis of spiroindolines via asymmetric dearomatization/reduction sequence.

Synthesis of polycyclic spiroindolines by dearomatizing annulations of *N*-sulfonyltriazoles reported by Bora et al. [93] includes Rh(II)-catalyzed triazole ring opening and subsequent dearomatization of a pyrrole ring with formation of spiropiperidine and annulated pyrroline rings in one synthetic step (Scheme 2.52). Protective group at the indole nitrogen atom was found to play a crucial role in the process: electron-donating groups favor the reaction, while electron-withdrawing groups failed to give the desired product. Carrying out the reaction in enantioselective manner (in the presence of 3 mol% Rh_2(S-BNP)$_4$) provided promising enantiomeric ratio of 73.3 : 26.7.

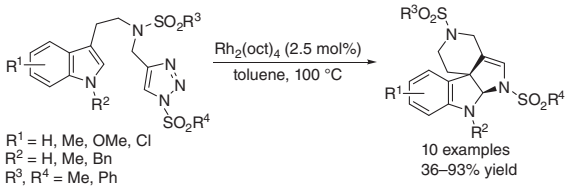

Scheme 2.52 Synthesis of spiroindolines by dearomatizing annulations of *N*-sulfonyltriazoles.

Yokoe et al. developed an efficient approach to dispirocyclic systems by means of dearomative domino double spirocyclization of 1,4-disubstituted benzenes [94]. It was found that (4-aminopropyl)phenyl amides of propiolic acid react with NIS in the presence of silver trifluoroacetate, giving rise to diastereoenriched tricyclic products (Scheme 2.53). It seems reasonable that the process is triggered by electrophilic iodination of the terminal alkyne, formation of 3,4-pyrroline-2-one moiety, followed by a second spirocyclization with pyrrolidine ring formation. HFIP was proved to be the most suitable solvent to achieve diastereoselective formation of the products. This unprecedented construction of two spirocyclic centers in one step enables diazadispiro[4.2.48.25]tetradecatriene system to be accessible in a simple fashion.

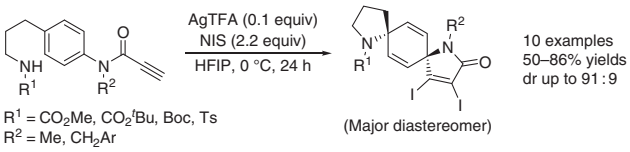

Scheme 2.53 Dearomative domino double spirocyclization of 1,4-disubstituted benzenes.

2.5 Conclusion and Perspectives

The dearomatization strategy probably represents the most convenient and efficient pathway to the wide variety of spiro- and fused heterocyclic ring systems. This approach delivers more concise synthetic routes to target molecules due to considerable increase of complexity at the dearomatization step. It seems very useful, in particular, for the total synthesis of natural products as well as pharmaceutically oriented compounds. One of the significant advantages of dearomatizing approach is the possibility of construction of several quaternary carbon stereocenters using chiral organocatalysts. Many examples considered in this chapter feature functional group tolerance and high yields along with excellent stereoselectivities. However, there are methods using strong oxidants, which impose certain restrictions on the substitution patterns of the final products. In addition, the majority of dearomative spirocyclizations are still limited to racemic reactions. Therefore, further development of dearomatization methodology toward heterocycles, especially spirocyclizations, is highly desirable.

Rapid increase in number of publications observed over the past 10 years indicates an unambiguous interest to the mentioned processes, which in turn will certainly stimulate the future development in the area. Implementation of modern practical methods, such as visible light-induced and microwave-assisted synthesis, would promote dearomatization to become a general pathway to numerous highly important classes of heterocyclic systems.

Acknowledgments

This work was supported by the Russian Science Foundation (Grant 19-73-20259).

References

1 Birch, A.J. (1944). Reduction with dissolving metals. Part I. *J. Chem. Soc.* 430–436. https://doi.org/10.1039/JR9440000430.

2 Bailey, P.S., Bath, S.S., Dobinson, F. et al. (1964). Ozonolysis of naphthalenes. The aromatic products. *J. Org. Chem.* 29: 697–702. https://doi.org/10.1021/jo01026a042.

3 Mandeville, W.H. and Whitesides, G.M. (1986). Synthesis of a water-soluble derivative of cyclohexatriacontan-1,2,13,14,25,26-hexone. *J.Org. Chem.* 51: 3257–3261. https://doi.org/10.1021/jo00367a002.

4 Woodward, R.B., Cava, M.P., Ollis, W.D. et al. (1954). The total synthesis of strychnine. *J. Am. Chem. Soc.* 78: 4749–4751. https://doi.org/10.1021/ja01647a088.

5 Day, A.C., Nabney, J., and Scott, A.I. (1960). The total synthesis of griseofulvin. *Proc. Chem. Soc.* 284–285. https://doi.org/10.1039/PS9600000261.

6 Zuo, Z., Xie, W., and Ma, D. (2010). Total synthesis and absolute stereochemical assignment of (–)-communesin F. *J. Am. Chem. Soc.* 132: 13226–13228. https://doi.org/10.1021/ja106739g.

7 Frie, J.L., Jeffrey, C.S., and Sorensen, E.J. (2009). A hypervalent iodine-induced double annulations enables a concise synthesis of the pentacyclic core structure of the cortistatins. *Org. Lett.* 11: 5394–5397. https://doi.org/10.1021/ol902168g.

8 McGrath, N.A., Bartlett, E.S., Sittihan, S., and Njardarson, J.T. (2009). A concise ring-expansion route to the compact core of platensimycin. *Angew. Chem. Int. Ed.* 48: 8543–8546. https://doi.org/10.1002/anie.200903347.

9 Yang, Q., Draghici, C., Njardarson, J.T. et al. (2014). Evolution of an oxidative dearomatization enabled total synthesis of vinigrol. *Org. Biomol. Chem.* 12: 330–344. https://doi.org/10.1039/C3OB42191K.

10 Harman, W.D. (1997). The activation of aromatic molecules with pentaammineosmium(II). *Chem. Rev.* 97: 1953–1978. https://doi.org/10.1021/cr940316n.

11 Pape, A.R., Kaliappan, K.P., and Kuendig, E.P. (2000). Transition-metal-mediated dearomatization reactions. *Chem. Rev.* 100: 2917–2940. https://doi.org/10.1021/cr9902852.

12 You, S.-L. (ed.) (2016). *Asymmetric Dearomatization Reactions*. Weinheim, Germany: Wiley-VCH.

13 Roche, S.P. and Porco, J.A. Jr., (2011). Dearomatization strategies in the synthesis of complex natural products. *Angew. Chem. Int. Ed.* 50: 4068–4093. https://doi.org/10.1002/anie.201006017.

14 Lopez Ortiz, F., Iglesias, M.J., Fernandez, I. et al. (2007). Nucleophilic dearomatizing (D_NAr) reactions of aromatic C,H-systems. A mature paradigm in organic synthesis. *Chem. Rev.* 107: 1580–1691. https://doi.org/10.1021/cr030207l.

15 Yang, W.-C., Zhang, M.-M., and Feng, J.-G. (2020). Recent advances in the construction of spiro compounds via radical dearomatization. *Adv. Synth. Catal.* 362: 4446–4461. https://doi.org/10.1002/adsc.202000636.

16 Cheng, Q., Zhang, F., Cai, Y. et al. (2018). Stereodivergent synthesis of tetrahydrofuroindoles through Pd-catalyzed asymmetric dearomative formal [3+2] cycloaddition. *Angew. Chem. Int. Ed.* 57: 2134–2138. https://doi.org/10.1002/anie.201711873.

17 Cheng, Q., Zhang, H.-J., Yue, W.-J., and You, S.-L. (2017). Palladium-catalyzed highly stereoselective dearomative [3+2] cycloaddition of nitrobenzofurans. *Chem* 3: 428–436. https://doi.org/10.1016/j.chempr.2017.06.015.

18 Rivinoja, D.J., Gee, Y.S., Gardiner, M.G. et al. (2017). The diastereoselective synthesis of pyrroloindolines by Pd-catalyzed dearomative cycloaddition of

vinylaziridine to 3-nitroindoles. *ACS Catal.* 7: 1053–1056. https://doi.org/10.1021/acscatal.6b03248.

19 Suo, J.-J., Liu, W., Du, J. et al. (2018). Diastereo- and enantioselective palladium-catalyzed dearomative [3+2] cycloaddition of 3-nitroindoles. *Chem. Asian J.* 13: 959–963. https://doi.org/10.1002/asia.201800133.

20 Liu, H., Zheng, C., and You, S.-L. (2014). $Fe(OTf)_3$ catalyzed annulation of 2,3-disubstituted indoles with aziridines. *Chin. J. Chem.* 32: 709–714. https://doi.org/10.1002/cjoc.201400178.

21 Liang, L., Niu, H.-Y., Wang, D.-Ch. et al. (2019). Facile synthesis of chiral [2,3]-fused hydrobenzofuran via asymmetric Cu(I)-catalyzed dearomative 1,3-dipolar cycloaddition. *Chem. Commun.* 55: 553–556. https://doi.org/10.1039/c8cc09226e.

22 Awata, A. and Arai, T. (2014). PyBidine/copper catalyst: asymmetric exo'-selective [3+2] cycloaddition using imino ester and electrophilic indole. *Angew. Chem. Int. Ed.* 53: 10462–10465. https://doi.org/10.1002/anie.201405223.

23 Roy, S., Kishbaugh, T.L.S., Jasinski, J.P., and Gribble, G.W. (2007). 1,3-Dipolar cycloaddition of 2- and 3-nitroindoles with azomethine ylides. A new approach to pyrrolo[3,4-*b*]indoles. *Tetrahedron Lett.* 48: 1313–1316. https://doi.org/10.1016/j.tetlet.2006.12.125.

24 Zhang, L., Hu, J., Xu, R. et al. (2019). Catalytic asymmetric dearomative [3+2] cyclization of 1,4-quinone with 2,3-disubstituted indoles. *Adv. Synth. Catal.* 361: 5449–5457. https://doi.org/10.1002/adsc.201901035.

25 Mei, G.-J., Tang, X., Tasdan, Y., and Lu, Y. (2020). Enantioselective dearomatization of indoles by an azoalkene-enabled (3+2) reaction: access to pyrroloindolines. *Angew. Chem. Int. Ed.* 59: 648–652. https://doi.org/10.1002/anie.201911686.

26 Zhang, M.-C., Wang, D.-C., Xie, M.-S. et al. (2019). Cu-catalyzed asymmetric dearomative [3+2] cycloaddition reaction of benzazoles with aminocyclopropanes. *Chem* 5: 156–167. https://doi.org/10.1016/j.chempr.2018.10.003.

27 Preindl, J., Chakrabarty, S., and Waser, J. (2017). Dearomatization of electron poor six-membered N-heterocycles through [3+2] annulation with aminocyclopropanes. *Chem. Sci.* 8: 7112–7118. https://doi.org/10.1039/c7sc03197a.

28 Liu, X., Yin, Y., and Jiang, Z. (2019). Photoredox-catalyzed formal [3+2] cycloaddition of *N*-aryl α-amino acids with isoquinoline *N*-oxides. *Chem. Commun.* 55: 11527–11530. https://doi.org/10.1039/c9cc06249a.

29 Wang, Z., Wang, D.-C., Xie, M.-S. et al. (2020). Enantioselective synthesis of fused polycyclic tropanes via dearomative [3+2] cycloaddition reactions of 2-nitrobenzofurans. *Org. Lett.* 22: 164–167. https://doi.org/10.1021/acs.orglett.9b04108.

30 Wang, K.-K., Xie, Y.-X., Li, Y.-L. et al. (2020). Dearomative [3+2] cycloaddition reaction of nitrobenzothiophenes with nonstabilized azomethine ylides. *RSC Adv.* 10: 28720–28724. https://doi.org/10.1039/d0ra05687a.

31 Manneveau, M., Tanii, S., Gens, F. et al. (2020). Dearomatization of 3-cyanoindoles by (3+2) cycloaddition: from batch to flow chemistry. *Org. Biomol. Chem.* 18: 3481–3486. https://doi.org/10.1039/D0OB00582G.

32 Lee, S., Diab, S., Queval, P. et al. (2013). Aromatic C=C bonds as dipolarophiles: facile reactions of uncomplexed electron-deficient benzene derivatives and other aromatic rings with a non-stabilized azomethine ylide. *Chem. Eur. J.* 19: 7181–7192. https://doi.org/10.1002/chem.201201238.

33 Bastrakov, M.A., Kucherova, A.Y., Fedorenko, A.K. et al. (2017). Dearomatization of 3,5-dinitropyridines – an atom-efficient approach to fused 3-nitropyrrolidines. *Arkivoc* (part 3): 181–190. https://doi.org/10.3998/ark.5550190.p010.185.

34 Starosotnikov, A.M., Ilkov, K.V., Bastrakov, M.A. et al. (2020). Mild and efficient addition of carbon nucleophiles to condensed pyridines: influence of structure and limits of applicability. *Chem. Heterocycl. Compd.* 56: 92–100. https://doi.org/10.1007/s10593-020-02628-1.

35 Ryan, J.H. (2015). 1,3-Dipolar cycloaddition reactions of azomethine ylide with aromatic dipolarophiles. *Arkivoc* 160–183. https://doi.org/10.3998/ark.5550190.p008.928.

36 Bastrakov, M.A., Starosotnikov, A.M., Pechenkin, S.Y. et al. (2010). Double 1,3-dipolar cycloaddition of *N*-methyl azomethine ylide to meta-dinitrobenzene annelated with nitrogen aromatic heterocycles. *J. Heterocyclic Chem.* 47: 893–896. https://doi.org/10.1002/jhet.423.

37 Konstantinova, L.S., Bastrakov, M.A., Starosotnikov, A.M. et al. (2010). 4,6-Dinitrobenzo[*c*]isothiazole: synthesis and 1,3-dipolar cycloaddition to azomethine ylide. *Mendeleev Commun.* 20: 353–354. https://doi.org/10.1016/j.mencom.2010.11.018.

38 Starosotnikov, A.M., Bastrakov, M.A., Kachala, V.V. et al. (2018). Unusual pericyclic reactivity of 4-nitrobenzofuroxans in 1,3-dipolar cycloaddition with *N*-benzyl azomethine ylide – a new example of multiple C—C-bond forming transformations. *ChemistrySelect* 3: 9773–9777. https://doi.org/10.1002/slct.201802117.

39 Starosotnikov, A.M., Bastrakov, M.A., Pechenkin, S.Y. et al. (2011). 1,3-Dipolar cycloaddition of unstabilized *N*-methyl azomethine ylide to nitrobenzene annelated with azoles. *J. Heterocyclic Chem.* 48: 824–828. https://doi.org/10.1002/jhet.599.

40 Pechenkin, S.Y., Starosotnikov, A.M., Bastrakov, M.A. et al. (2012). 4-R-7-nitrobenzofurazans in [3+2] cycloaddition reactions with *N*-methyl azomethine ylide. *Russ. Chem. Bull.* 61: 74–77. https://doi.org/10.1007/s11172-012-0011-z.

41 Bastrakov, M.A., Starosotnikov, A.M., Kachala, V.V. et al. (2015). Facile dearomatization of nitroquinolines through [3+2] and [4+2] cycloaddition reactions. *Asian J. Org. Chem.* 4: 146–153. https://doi.org/10.1002/ajoc.201402207.

42 Lee, S., Chataigner, I., and Piettre, S.R. (2011). Facile dearomatization of nitrobenzene derivatives and other nitroarenes with *N*-benzyl azomethine ylide. *Angew. Chem. Int. Ed.* 50: 472–476. https://doi.org/10.1002/anie.201005779.

43 Wales, S.M., Rivinoja, D.J., Gardiner, M.G. et al. (2019). Benzoazepine-fused isoindolines via intramolecular (3+2)-cycloadditions of azomethine ylides with dinitroarenes. *Org. Lett.* 21: 4703–4708. https://doi.org/10.1021/acs.orglett.9b01580.

44 Yonekawa, M., Koyama, Y., Kuwata, S., and Takata, T. (2012). Intramolecular 1,3-dipolar cycloaddition of nitrile *N*-oxides accompanied by dearomatization. *Org. Lett.* 14: 1164–1167. https://doi.org/10.1021/ol300125s.

45 Shevelev, S.A. and Starosotnikov, A.M. (2013). Pericyclic [4+2] and [3+2] cycloaddition reactions of nitroarenes in heterocyclic synthesis. *Chem. Heterocycl. Compd.* 49: 92–115. https://doi.org/10.1007/s10593-013-1233-1.

46 MacCormack, P., Halle, J.-C., Pouet, M.-J., and Terrier, F. (1988). Unusual structure in Meisenheimer complex formation from the highly electrophilic 4,6-dinitrobenzofuroxan. *J. Org. Chem.* 53: 4407–4409. https://doi.org/10.1021/jo00253a044.

47 Halle, J.-C., Vichard, D., Pouet, M.-J., and Terrier, F. (1997). A new cycloaddition process involving nitro group participation in polynitroaromatic chemistry. *J. Org. Chem.* 62: 7178–7182. https://doi.org/10.1021/jo9704570.

48 Bastrakov, M.A., Starosotnikov, A.M., Kachala, V.V. et al. (2014). 5-Nitro-7,8-furoxanoquinoline: a new type of fused nitroarenes possessing Diels–Alder reactivity. *Mendeleev Commun.* 24: 203–205. https://doi.org/10.1016/j.mencom.2014.06.004.

49 Bastrakov, M.A., Starosotnikov, A.M., Kachala, V.V. et al. (2015). 3-*R*-4-Nitro-6,7-furoxanobenzo[*d*]isoxazoles – a new type of condensed nitroarenes capable of Diels–Alder reaction. *Chem. Heterocycl. Compd.* 51: 496–499. https://doi.org/10.1007/s10593-015-1726-1.

50 Steglenko, D.V., Shevelev, S.A., Kletskii, M.E. et al. (2015). Quantum-chemical and NMR study of nitrofuroxanoquinoline cycloaddition. *Chem. Heterocycl. Compd.* 51: 838–844. https://doi.org/10.1007/s10593-015-1785-3.

51 Bastrakov, M.A., Starosotnikov, A.M., Pavlov, A.A. et al. (2016). Synthesis of novel polycyclic heterosystems from 5-nitro[1,2,5]selenadiazolo[3,4-*e*]benzofuroxans. *Chem. Heterocycl. Compd.* 52: 690–693. https://doi.org/10.1007/s10593-016-1950-3.

52 Bastrakov, M.A., Starosotnikov, A.M., Pavlov, A.A. et al. (2016). Synthesis of novel polycyclic heterosystems based on 5-nitro[1,2,5]thiadiazolo[3,4-*e*]benzofuroxan. *Mendeleev Commun.* 26: 217–219. https://doi.org/10.1016/j.mencom.2016.04.013.

53 Starosotnikov, A.M., Leontieva, M.A., Bastrakov, M.A. et al. (2010). Super-electrophilic nature of 4,6-dinitrobenzo[*c*]isoxazole (4,6-dinitroanthranil) in [4+2]-cycloaddition reactions and σ^H-complex formation. *Mendeleev Commun.* 20: 165–166. https://doi.org/10.1016/j.mencom.2010.05.014.

54 Andreini, M., De Paolis, M., and Chataigner, I. (2015). Thiourea-catalyzed dearomatizing [4+2] cycloadditions of 3-nitroindole. *Catal. Commun.* 63: 15–20. https://doi.org/10.1016/j.catcom.2014.07.042.

55 Shao, W. and You, S.-L. (2017). Highly diastereo- and enantioselective synthesis of tetrahydro-5*H*-indolo[2,3-*b*]quinolines through copper-catalyzed propargylic dearomatization of indoles. *Chem. Eur. J.* 23: 12489–12493. https://doi.org/10.1002/chem.201703443.

56 Shao, W., Xu-Xu, Q.-F., and You, S.-L. (2020). Highly diastereoselective synthesis of polycyclic indolines through formal [4+2] propargylic cycloaddition of indoles

with ethynyl benzoxazinanones. *Chem. Asian J.* 15: 2462–2466. https://doi.org/10.1002/asia.202000640.

57 Bird, M.J., Wales, S.M., Richardson, C., and Hyland, C.J.T. (2020). Palladium-catalyzed decarboxylative formal (4+2) cycloaddition of vinyl benzoxazinanones with 3-nitroindoles. *Synlett* 31: 916–924. https://doi.org/10.1055/s-0040-1707995.

58 Cao, W.-B., Xu, X.-P., and Ji, S.-J. (2017). Synthesis of fused indoline heterocycles via dearomatization of indoles with α-bromohydrazones: a systematic study on the substrates. *Org. Biomol. Chem.* 15: 1651–1654. https://doi.org/10.1039/c6ob02362b.

59 Ciccolini, C., Mari, G., Gatti, F.G. et al. (2020). Synthesis of polycyclic fused indoline scaffolds through a substrate-guided reactivity switch. *J. Org. Chem.* 85: 11409–11425. https://doi.org/10.1021/acs.joc.0c01489.

60 Gao, R.-D., Xu, Q.-L., Zhang, B. et al. (2016). Palladium(0)-catalyzed intermolecular allylic dearomatization of indoles by a formal [4+2] cycloaddition reaction. *Chem. Eur. J.* 22: 11601–11604. https://doi.org/10.1002/chem.201602691.

61 Lei, L., Yao, Y.-Y., Jiang, L.-J. et al. (2020). Synthesis of furo[3,2-*b*]quinolines and furo[2,3-*b*:4,5-*b*′]diquinolines through [4+2] cycloaddition of aza-*o*-quinone methides and furans. *J. Org. Chem.* 85: 3059–3070. https://doi.org/10.1021/acs.joc.9b02953.

62 Kuznetzov, D.M., Mukhina, O.A., and Kutateladze, A.G. (2016). Photoassisted synthesis of complex molecular architectures: dearomatization of benzenoid arenes with aza-*o*-xylylenes via an unprecedented [2+4] reaction topology. *Angew. Chem. Int. Ed.* 55: 6988–6991. https://doi.org/10.1002/anie.201602288.

63 Ma, J., Strieth-Kalthoff, F., Dalton, T. et al. (2019). Direct dearomatization of pyridines via an energy-transfer-catalyzed intramolecular [4+2] cycloaddition. *Chem* 5: 2854–2864. https://doi.org/10.1016/j.chempr.2019.10.016.

64 Dai, W., Li, C., Liu, Y. et al. (2020). Palladium-catalyzed [4+3] dearomatizing cycloaddition reaction of *N*-iminoquinolinium ylides. *Org. Chem. Front.* 7: 2612–2617. https://doi.org/10.1039/d0qo00320d.

65 Cheng, B., Zhang, X., Li, H. et al. (2020). Synthesis of pyridothiazepines via a 1,5-dipolar cycloaddition reaction between pyridinium 1,4-zwitterionic thiolates and activated allenes. *Adv. Synth. Catal.* 362: 4668–4672. https://doi.org/10.1002/adsc.202.

66 Cheng, B., Zhang, X., Li, Y. et al. (2020). Synthesis of indolizines from pyridinium 1,4-zwitterionic thiolates and α-functionalized bromoalkanes *via* a stepwise [(5+1)-1] pathway. *Chem. Commun.* 56: 8396–8399. https://doi.org/10.1039/d0cc03446k.

67 Gao, K., Zhang, Y.-G., Wang, Z., and Ding, H. (2019). Recent developments on the [5+2] cycloadditions and their application in natural product synthesis. *Chem. Commun.* 55: 1859–1878. https://doi.org/10.1039/c8cc09077g.

68 Badenock, J.C., Fraiser, H.L., and Gribble, G.W. (2018). A new approach to pyrrolo[3,4-*b*]indole ring system. *Arkivoc* (part v): 140–149. https://doi.org/10.24820/ark.5550190.p010.584.

69 Yuan, Y., Wang, Y., Mu, Y. et al. (2020). Synthesis of aza-eight-membered ring-fused indulines initiated by Zn-catalyzed C2 alkylation of indoles and

subsequent base-promoted ring expansion. *Org. Lett.* 22: 6532–6536. https://doi.org/10.1021/acs.orglett.0c02307.

70 Mu, Y., Yuan, Y., Wang, Y. et al. (2020). Synthesis of indoline-fused eight-membered azaheterocycles through Zn-catalyzed dearomatization of indoles and subsequent base-promoted C–C activation. *Org. Biomol. Chem.* 18: 6916–6926. https://doi.org/10.1039/d0ob01626h.

71 Ramella, V., He, Z., Daniliuc, C.G., and Studer, A. (2016). Palladium-catalyzed dearomatizing difunctionalization of indoles and benzofurans. *Eur. J. Org. Chem.* 2268–2273. https://doi.org/10.1002/ejoc.201600194.

72 Liu, K., Song, W., Deng, Y. et al. (2020). Electrooxidation enables highly regioselective dearomative annulations of indole and benzofuran derivatives. *Nat. Commun.* 11: 3. https://doi.org/10.1038/s41467-019-13829-4.

73 McAtee, R.C., Noten, E.A., and Stephenson, C.R.J. (2020). Arene dearomatization through a catalytic N-centered radical cascade reaction. *Nat. Commun.* 11: 2528. https://doi.org/10.1038/s41467-020-16369-4.

74 Xu, R.-Q., Gu, Q., and You, S.-L. (2017). Construction of the benzomesembrine skeleton: palladium(0)-catalyzed intermolecular arylative dearomatization of α-naphthols and subsequent aza-Michael reaction. *Angew. Chem. Int. Ed.* 56: 7252–7256. https://doi.org/10.1002/anie.201703674.

75 Smith, L.K. and Baxendale, I.R. (2015). Total synthesis of natural products containing spirocarbocycles. *Org. Biomol. Chem.* 13: 9907–9933. https://doi.org/10.1039/C5OB01524C.

76 Hong, L. and Wang, R. (2013). Recent advances in asymmetric organocatalytic construction of 3,3′-spirocyclic oxindoles. *Adv. Synth. Catal.* 355: 1023–1052. https://doi.org/10.1002/adsc.201200808.

77 Singh, G.S. and Desta, Z.Y. (2012). Isatins as privileged molecules in design and synthesis of spiro-fused cyclic frameworks. *Chem. Rev.* 112: 6104–6155. https://doi.org/10.1021/cr300135y.

78 Umair Tariq, M. and Moran, W.J. (2020). Spirooxazoline synthesis by an oxidative dearomatizing cyclization. *Eur. J. Org. Chem.* 5153–5160. https://doi.org/10.1002/ejoc.202000840.

79 Uyanik, M., Kato, T., Sahara, N. et al. (2019). High-performance ammonium hypoiodite/oxone catalysis for enantioselective oxidative dearomatization of arenols. *ACS Catal.* 9: 11619–11626. https://doi.org/10.1021/acscatal.9b04322.

80 Quideau, S., Pouysegu, L., Oxoby, M., and Looney, M.A. (2001). 2-Alkoxyarenol-derived orthoquinols in carbon-oxygen, carbon–nitrogen and carbon–carbon bond-forming reactions. *Tetrahedron* 57: 319–329. https://doi.org/10.1016/S0040-4020(00)00939-X.

81 Abdellaoui, H. and Xu, J. (2014). Versatile synthesis of 4-spiro-*b*-lactam-3-carbonitriles via the intramolecular nucleophilic cyclization of *N*-(*p*-hydroxyphenyl) cyanoacetamides. *Tetrahedron* 70: 4323–4330. https://doi.org/10.1016/j.tet.2014.05.008.

82 Sarkar, D., Kumar Ghosh, M., Rout, N., and Kuila, P. (2017). "A Jack of Trio"-robust one-pot metal free oxidative amination, azidation and peroxidation of phenols. *New J. Chem.* 41: 3715–3718. https://doi.org/10.1039/c7nj00169j.

83 Wu, L., Hao, Y., Liu, Y. et al. (2020). Visible-light-induced dearomative oximination of indole derivatives and dearomative amidation of phenol derivatives. *Chem. Commun.* 56: 8436–8439. https://doi.org/10.1039/d0cc03506h.

84 Raji Reddy, C., Kolgave, D.H., Subbarao, M. et al. (2020). Ag-catalyzed oxidative *ipso*-cyclization via decarboxylative acylation/alkylation: access to 3-acyl|alkyl-spiro[4.5]trienones. *Org. Lett.* 22: 5342–5346. https://doi.org/10.1021/acs.orglett.0c01588.

85 Chen, D., He, T., Huang, Y. et al. (2020). Synthesis of spiroisoxazolines via an oximation/dearomatization cascade under air. *Org. Lett.* 22: 4429–4434. https://doi.org/10.1021/acs.orglett.0c01429.

86 Chen, D., Wang, Y., Cai, X.-M. et al. (2020). Synthesis of spiroisoxazolines via TEMPO/$NaNO_2$-catalyzed aerobic oxidative dearomatization. *Org. Lett.* 22: 6847–6851. https://doi.org/10.1021/acs.orglett.0c02372.

87 Yokosaka, T., Nemoto, T., Nakayama, H. et al. (2014). Synthesis of nitrogen-containing fused-polycyclic compounds from tyramine derivatives using phenol dearomatization and cascade cyclization. *Chem. Commun.* 50: 12775–12778. https://doi.org/10.1039/c4cc04809a.

88 Yin, B.-L., Lai, J.-Q., Huang, L. et al. (2012). Easy access to acetal-spiroacetal-enol ethers by tandem dearomatization of a furan ring and acetalization. *Synthesis* 44: 2567–2574. https://doi.org/10.1055/s-0032-1316548.

89 Parameswarappa, S.G. and Pigge, F.C. (2011). Synthesis of substituted 3,9-diazaspiro[5.5]undecanes via spirocyclization of pyridine substrates. *Tetrahedron Lett.* 52: 4357–4359. https://doi.org/10.1016/j.tetlet.2011.06.055.

90 Diaba, F., Montiel, J.A., Martinez-Laporta, A., and Bonjoch, J. (2013). Dearomative radical spirocyclization from *N*-benzyltrichloroacetamides revisited using a copper(I)-mediated atom transfer reaction leading to 2-azaspiro[4.5]decanes. *Tetrahedron Lett.* 54: 2619–2622. https://doi.org/10.1016/j.tetlet.2013.03.019.

91 Zhao, X., Liu, X., Mei, H. et al. (2015). Asymmetric dearomatization of indoles through a Michael/Friedel-Crafts-type cascade to construct polycyclic spiroindolines. *Angew. Chem. Int. Ed.* 54: 4032–4035. https://doi.org/10.1002/anie.201410814.

92 Zhuo, C.-X., Zhou, Y., Cheng, Q. et al. (2015). Enantioselective construction of spiroindolines with three contiguous stereogenic centers and chiral tryptamine derivatives via reactive spiroindolenine intermediates. *Angew. Chem. Int. Ed.* 54: 14146–14149. https://doi.org/10.1002/anie.201507193.

93 Bora, P.P., Lu, Z.-L., Chen, L., and Kang, Q. (2016). Rh(II)-catalyzed intramolecular dearomatizing annulations of *N*-sulfonyl-1,2,3-triazoles: synthesis of polycyclic spiroindolines. *Tetrahedron* 72: 1467–1471. https://doi.org/10.1016/j.tet.2016.01.049.

94 Yokoe, H., Mizumura, Y., Sugiyama, K. et al. (2020). Rapid access to dispirocyclic scaffolds enabled by diastereoselective intramolecular double functionalization of benzene rings. *Chem. Asian J.* 15: 4271–4274. https://doi.org/10.1002/asia.202001179.

3

Strategies for the Synthesis of Heterocyclic Macrocycles and Medium-Sized Rings

William P. Unsworth and Thomas C. Stephens

University of York, Department of Chemistry, York YO10 5DD, UK

3.1 Introduction

Functionalized macrocycles (12+ membered rings) and medium-sized rings (8–11-membered rings) have important applications in a wide array of scientific fields and technologies. In the vast majority of cases, these large-ring molecules are also heterocyclic, with the heteroatoms often playing a key role in their function, whether that be as drugs, agrochemicals, ligands, sensors, or part of molecular machines (Figure 3.1) [1, 2]. Naturally, this has propagated the development of several methods for the synthesis of large-ring heterocyclic systems, with key concepts and selected highlights summarized in this chapter.

Ring size, and its effect on the efficiency of cyclization reactions, is central to any discussion about the synthesis of macrocycles and medium-sized rings. Cyclization reactions based on an intramolecular bond-forming step are among the most efficient reactions in synthetic chemistry; performing a reaction in an intramolecular sense can result in significant kinetic and thermodynamic benefits compared with the analogous intermolecular processes. Thus, cyclization reactions are often easier and more efficient than the equivalent intermolecular reactions, especially for the formation of 5- and 6-membered ring systems (e.g. **1** → **2**, Scheme 3.1a). However, cyclization to form larger rings is typically far less straightforward [1f]. In macrocyclization reactions, greater loss of entropy (e.g. compared with the equivalent 6-membered ring cyclization) and/or unfavorable conformational effects can provide a major barrier to cyclization (**3** → **4**, Scheme 3.1b), and if the rate of cyclization is sufficiently slow, the equivalent intermolecular coupling (**3** → **5**), or other side reactions can out-compete the desired transformation [3]. Medium-sized ring cyclization reactions are also susceptible to the same problems, and indeed in many cases, medium-sized rings are more difficult to prepare than macrocycles, in view of the additional challenge associated with their typically high levels of transannular strain [4].

Countering unwanted intermolecular reactions and other unwanted side processes is the key challenge to overcome when developing new methods for the

Heterocycles: Synthesis, Catalysis, Sustainability, and Characterization, First Edition.
Edited by Teresa M.V.D. Pinho e Melo and Marta Pineiro.

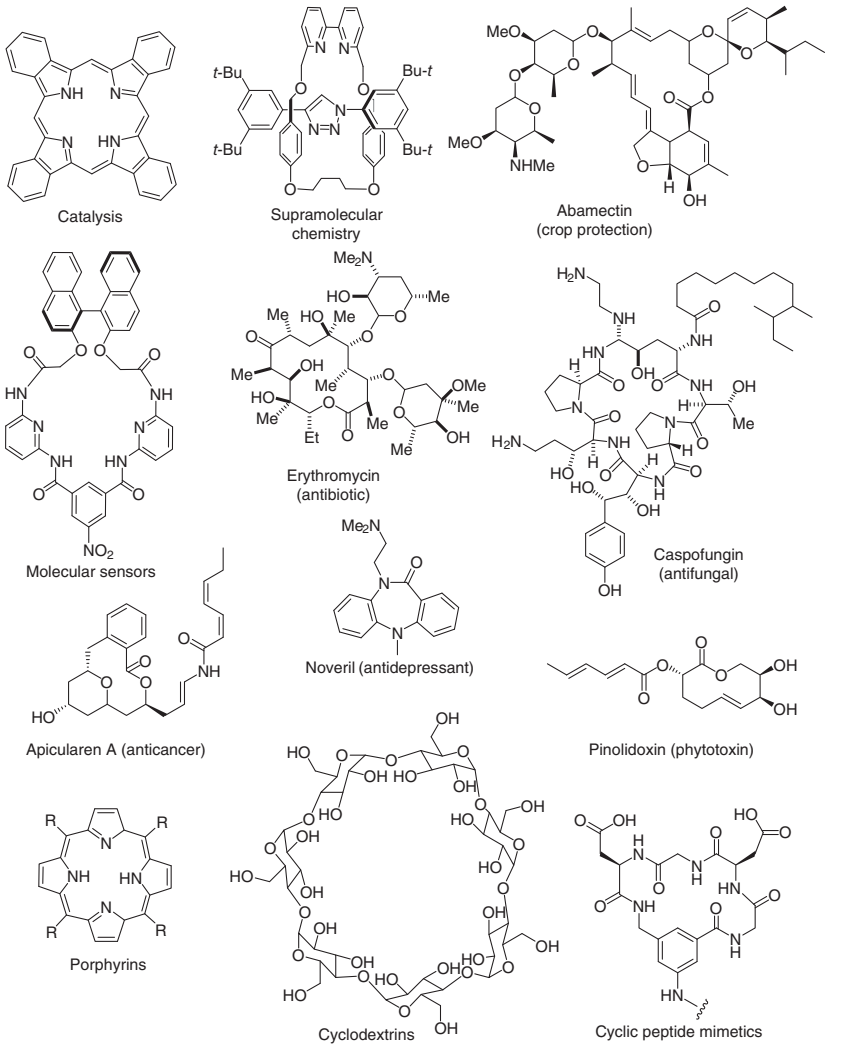

Figure 3.1 Important heterocyclic macrocycles and medium-sized rings. Source: Refs. [1, 2].

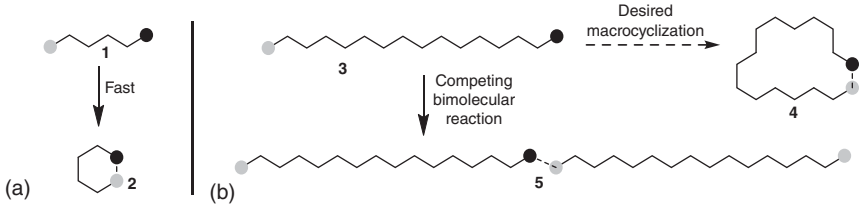

Scheme 3.1 Normal-sized ring cyclization (a) vs. macrocyclization (b).

synthesis of heterocyclic macrocycles and medium-sized rings. This chapter is devoted to summarizing some of the best strategies to achieve this. The simplest (and most commonly used) method to counter this problem is to perform macrocyclization reactions at high dilution. High dilution conditions can limit the negative impact of intermolecular coupling by reducing the frequency of intermolecular collisions while (generally) having a much smaller effect on the desired intramolecular reaction. However, while this approach has been successful in many cases [5], including in systems featured in this chapter, such processes have poor green/economic credentials and are generally impractical on large scale, even after taking measures to avoid side reactions. They can also be low yielding and are highly substrate dependent, so alternative methods that avoid dilution are desirable.

We start this chapter by summarizing the current state of the art in high dilution and pseudo-high dilution methods for heterocyclic macrocycle synthesis. We then go on to detail methods for which high dilution is not required, by taking advantage of conformational and/or template effects. Ring-expansion methods are next covered, and we end by considering medium-sized rings separately as special cases.

3.2 High Dilution and Pseudo-High Dilution Methods

3.2.1 Traditional High Dilution/Slow Addition Methods

In theory, virtually any bond-forming chemical process can be modified to make heterocyclic macrocycles and medium-sized rings, for example, by running the reaction at increased dilution and/or via slow addition of the starting materials [5]. However, some methodologies are turned to more frequently than others when making large rings, and Yamaguchi macrolactonization (and related methods) falls into this category [6]. These reactions operate via initial activation of the carboxylic acid of a seco acid starting material **7**, through formation of a mixed anhydride species (e.g. **8**), followed by lactonization via the tethered alcohol to form the lactone product **9**. DMAP is often included as a nucleophilic catalyst in such processes (step not shown), and the reactions are done at high dilution, usually involving slow, dropwise addition of the seco acid into a solution of the reagent **6** and base/DMAP, sometimes over of a period of several hours (Scheme 3.2). Several variations of classical Yamaguchi methods are known, with Steglich and Mukaiyama–Corey–Nicolaou esterifications among the most prominent [6b].

Macrolactonization reactions have been used extensively in multiple total syntheses due to their broad applicability, functional group tolerance, and compatibility with high dilution conditions, and hence the lactone C—O bond is often chosen as the key ring-closing disconnection when planning syntheses of complex macrolactones [6b]. An impressive example can be found in the total synthesis of (−)-amphidinolide E (**19**), reported by Costa, Vilarrasa, and coworkers [7], where a Kita–Trost macrolactonization is utilized (Scheme 3.3). In this study, sulfone **10** was reacted with aldehyde **11** in a Julia–Kocienski olefination, to afford the

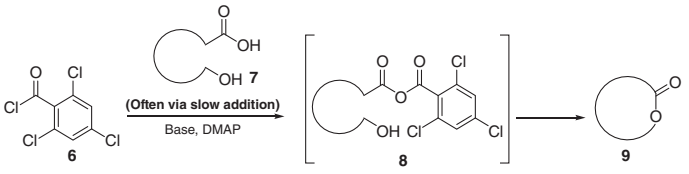

Scheme 3.2 Yamaguchi macrolactonization.

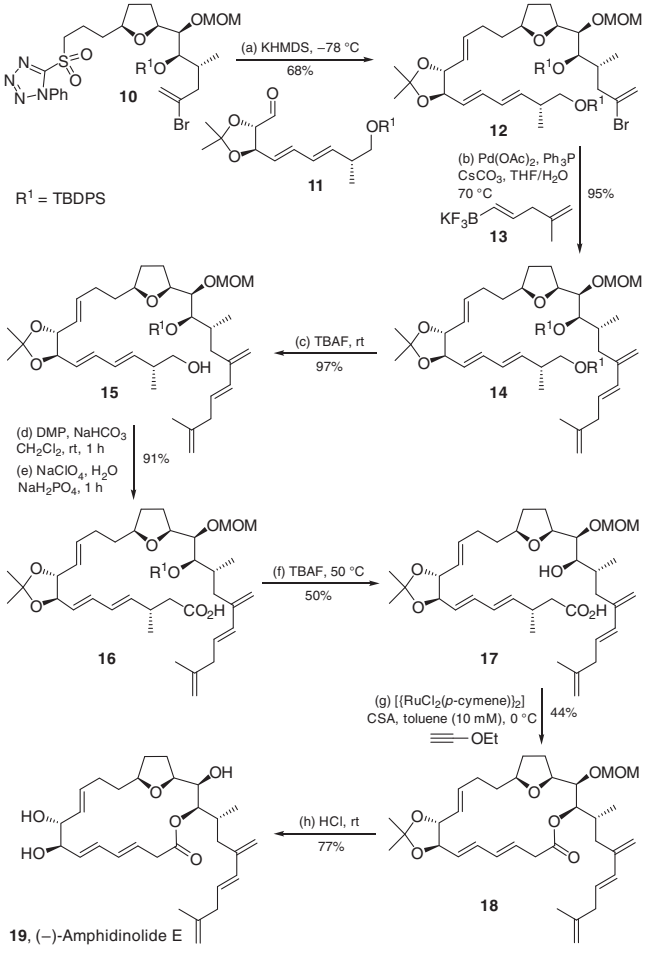

Scheme 3.3 The total synthesis of (–)-amphidinolide E (**19**).

E-alkene **12**, with this step followed by palladium-catalyzed Suzuki–Molander coupling with trifluoroborate fragment **13**. Cleavage of the TBDPS protecting group using TBAF afforded alcohol **15**, and oxidation of the alcohol to the corresponding carboxylic acid was done via a two-stage Dess–Martin oxidation (to generate the aldehyde) followed by a Pinnick oxidation to form carboxylic acid **16** in 91% overall yield. Removal of the TBDPS at the hindered C-17 position required treatment

with TBAF at elevated temperatures to form the key seco acid precursor **17**. The macrocyclization step was initially tried using a Yamaguchi lactonization but was unsuccessful. As a result, various alternative lactonization methods were tested, with the Kita–Trost reaction delivering lactone **18** in the highest yield (44%). Finally, global deprotection was performed using HCl, affording (−)-amphidinolide E (**19**) in 77% yield. There are many options available for the synthetic chemist to choose from when undertaking a macrolactonization reaction, and this is arguably both a strength and a weakness of the approach; as seen in this total synthesis, it is reassuring to know that alternatives are available if the original conditions fail, but predicting which conditions will work best in any given case is challenging.

Mitsunobu reactions rival Yamaguchi-type approaches for broad utility in macrolactonization [8]. Of the many examples that could have been chosen to illustrate this point, its use by De Brabander and coworkers in the total synthesis of peloruside A (**24**) is instructive (Scheme 3.4) [9]. Thus, aldehyde **20** was reacted with the boron enolate of ketone **21**, in a highly stereoselective aldol addition. Meerwein's salt was then used to methylate this newly formed secondary alcohol in excellent yield and chemoselectivity. Enone **22** was reduced using a Corey–Bakshi–Shibata (CBS) reduction, and subsequent ester hydrolysis yielded carboxylic acid **23**. Then, slow addition of **23** (as a dilute 30 mM solution in THF) to a dilute solution (50 mM) of PPh_3 and DIAD enabled the desired Mitsunobu cyclization to proceed in 47% yield step (e) only. Global deprotection under acidic conditions completed the synthesis of peloruside A (**24**).

High dilution ring-closing metathesis (RCM) is also widely used in the synthesis of heterocyclic macrocycles and medium-sized rings [10]. First described by Villemin et al. [10a], but developed and popularized as a synthetic tool for large ring synthesis most notably by Grubbs and Schrock, RCM is a powerful method when making larger rings [10b]. It is based on the coupling of simple

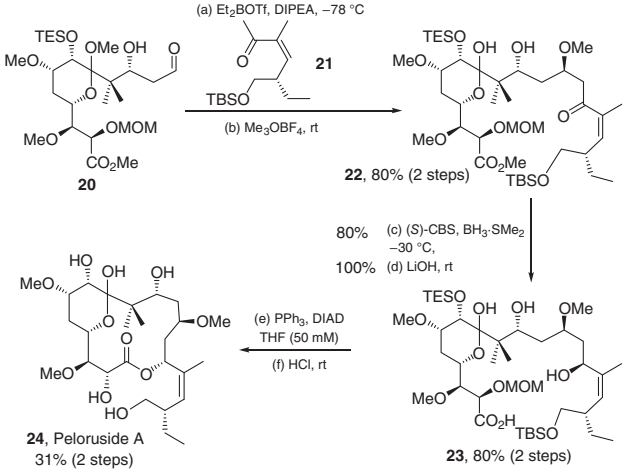

Scheme 3.4 Total synthesis of peloruside A (**24**) using a high dilution Mitsunobu macrolactonization. Source: Liao et al. [9]/Wiley.

tethered alkenes and has been used in many total syntheses of medium-sized rings and macrocycles (e.g. floresolide [10c], (−)-balanol A [10d], (+)-migrastatin [10e], and others [10f]), with its good functional group tolerance, compatibility with high dilution conditions, and the wide range of available catalysts, all being important contributors to its popularity. The geometry of the alkene product has been historically problematic, with mixtures of both *Z*- and *E*-alkenes often being produced in large ring sizes. However, more recently, remarkably selective catalysts able to impart excellent *E*- and *Z*-selective RCM have been developed, meaning that most selectivity problems can be solved via prudent choice of catalyst and reaction conditions [11]. A powerful example of a *Z*-selective RCM can be seen in Yu, Wang, and coworkers' total synthesis of (−)-nakadomarin A (**34**) (Scheme 3.5) [11b]. As part of this route, 1,3-dicarbonyl **25** was treated with cinchona alkaloid **26** to induce highly stereoselective Michael addition with furan **27**, to form **28** as a single diastereomer. A Mannich-type reaction of **28** with formaldehyde and amine **29** was used to form spirocyclic lactam **30**, which required a further six steps to produce tetracyclic diene **31**, ready for the RCM step. This was done using tungsten alkylidene catalyst **32**, and high dilution (1 mM) and under vacuum to remove volatile olefin by-products, enabling macrocycle **33** to be formed in excellent yield with high (97 : 3) *Z*-/*E*-selectivity. A further six steps completed the synthesis of (−)-nakadomarin A (**34**).

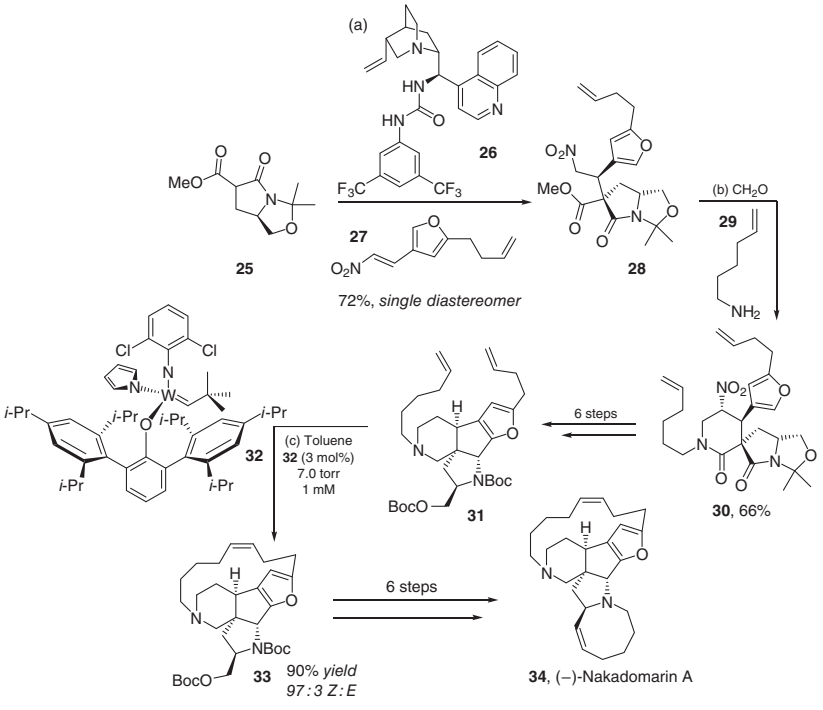

Scheme 3.5 Synthesis of (−)-nakadomarin A using Z-selective RCM catalyst. Source: Yu et al. [11b]/Springer Nature.

Many other transformations have also been put to regular use in macrocyclization reactions to form heterocycles. Huisgen-type 1,3-dipolar cycloaddition reactions between an azide and alkyne to generate 1,2,3-triazoles are popular [12], especially in biological applications (for an example, see Section 3.2.2 of this chapter). Other commonly used reaction classes include peptide bond formation [1], alkyne metathesis [13], Diels–Alder reactions [14], Horner–Wadsworth–Emmons-type reactions [15], and various palladium-catalyzed cross-coupling processes [16]. In simple terms, reactions that are considered to be good and reliable in synthetic chemistry in general tend also to be those that are used most widely in high-dilution macrocyclization reactions. This makes sense – macrocycle and medium-sized ring synthesis is hard – for the reasons outlined earlier in this chapter, so it stands to reason that synthetic chemists tend to choose comparatively straightforward bond-forming methods in order to reduce the overall challenge of the already difficult transformation. Nonetheless, synthetic strategies that enable larger rings to be made that avoid high dilution have the potential to both improve the practicality of the synthesis and enable more challenging transformations to be performed. Therefore, the remainder of this chapter will focus on recent progress on the development of such methods, starting with so-called "pseudo-dilution" methods, before going on to describe methods in which dilution is not required at all.

3.2.2 Solid-Supported Methods

Performing macrocyclization on a solid support can create "pseudo-dilution" conditions in which solvent volumes can be reduced compared with the analogous solution phase reactions. This is most often performed by localizing the linear cyclization precursors on a resin [17]. Problems associated with unwanted intermolecular reactions are not entirely avoided using this method (e.g. cross-linking of solid-supported coupling partners can still occur if the resin is overloaded), but it can still have significant practical advantages, especially in the peptide field, where solid phase peptide synthesis (SPPS) techniques are used routinely. An instructive example of this approach can be seen in the work of Lokey and coworkers, who utilized a copper-catalyzed cycloaddition, as part of a solid-supported synthesis of macrocyclic peptide mimetics (Scheme 3.6) [18]. For example, using standard SPPS, a 2-chlorotrityl chloride resin-supported alkyne amino acid derivative **35** was coupled with leucine fragment **36**, and this was repeated twice to generate tetramer **38**. Azido-leucine **39** was then coupled using HOAT and DCC to afford azido alkyne **40**. Copper-catalyzed 1,3-dipolar cycloaddition was then performed, while the peptide was still attached to the resin to form macrocycle **41**. Subsequent removal from the resin was done using 1% TFA, affording the cyclic peptide mimetic, **42**, in 25% overall yield. This reliable on-resin cyclization method has been used to make many other cyclic peptide mimetics, including for library synthesis, in which bioassay was possible directly from the crude products.

3.2.3 Phase Separation

Another pseudo-dilution strategy for macrocycle synthesis was reported in 2011 by Collins and Bédard. This method enables a Glaser–Hay coupling macrocyclization to

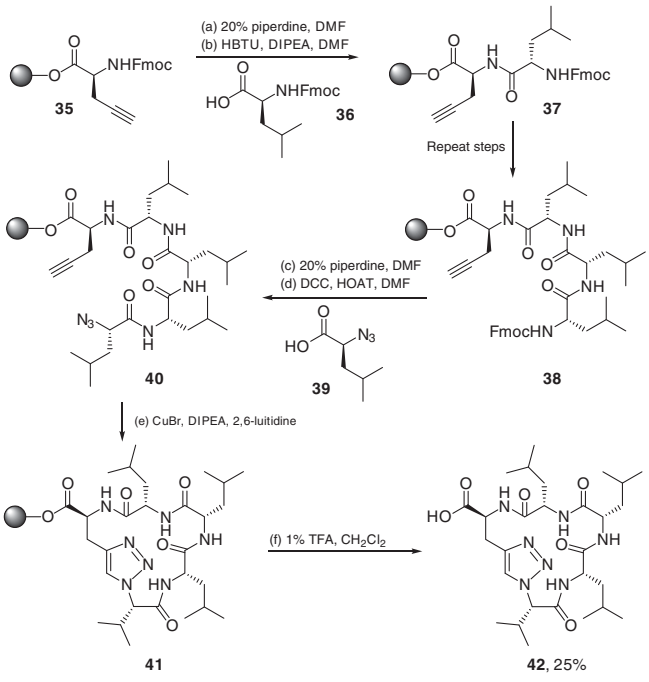

Scheme 3.6 Cycloaddition in the solid-phase synthesis of small cyclic peptide mimetics. Source: Turner et al. [18]/American Chemical Society.

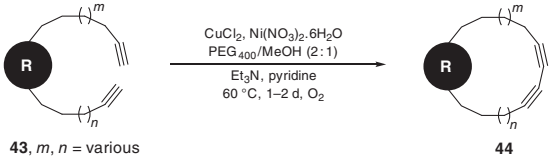

Scheme 3.7 Phase separation in macrocyclic Glaser–Hay coupling. Source: Bédard and Collins [19]/American Chemical Society.

be performed at increased concentrations (0.03 M) by exploiting phase separation of the reaction catalyst and substrate as an alternative to dilution (Scheme 3.7) [19]. A mixed copper/nickel-based cocatalyst system is used in a biphasic solvent mixture of methanol and PEG_{400}. This was shown to solubilize the copper–pyridine complexes integral to the cross-coupling reaction and proved to be a successful method to generate effective low concentrations of reactive linear intermediates, therefore promoting macrocyclization rather than intermolecular coupling. This alternative method of controlling dilution effects enabled the synthesis of various diyne-macrocycles of the form **44** from linear starting materials **43** with no apparent conformational preferences to undergo cyclization, at concentrations that result in polymerization when conducted in a single homogeneous phase.

3.3 Methods Designed to Impart More Favorable Cyclization Conformations

3.3.1 The Importance of Conformation on Macrocyclization

Conformation plays a pivotal role on the efficiency of macrocyclization reactions but predicting the conformation of long linear molecules is challenging. The unpredictable nature of macrocyclization reactions can be a major source of frustration for researchers working on macrocycle synthesis, with strategies that appear equally viable on paper often leading to very different synthetic outcomes – in simple terms, sometimes you may get lucky, but other times not! For example, as part of a build/couple/pair diversity-oriented synthesis study, Marcaurelle and coworkers reported that 12-membered lactone **47** was formed in a relatively modest 33% yield when cyclized using an S_NAr reaction (from **45**), but when the same lactone was formed using a macrolactamization procedure (from **46**), the yield was greatly improved to 83% (Scheme 3.8) [20]. Both synthetic procedures would be expected to perform reliably when considering the bond-forming steps in isolation, hence the large difference in yield is likely to be a consequence of the differing conformations of the linear starting materials. This highlights the difficulty of predicting macrocyclization efficiency, even when using high dilution conditions.

Recognizing that a substrate class has a natural predisposition to undergo macrocyclization (and making use of this feature when it does) is important in macrocycle synthesis. The syntheses of some heterocyclic macrocycles are trivial and have been known and studied for decades; for example, classical methods for the synthesis of porphyrins such as TPP **51** are easily performed on large scale via multicomponent reactions. Although relatively dilute conditions are usually required to minimize polypyrrole formation, the reactions are still considerably more straightforward than typically macrocyclization processes (Scheme 3.9a) [21]. In the case of porphyrins, it is easy to rationalize that with their rigid structure and high number of sp^2 hybridized centers, macrocyclization becomes more favorable

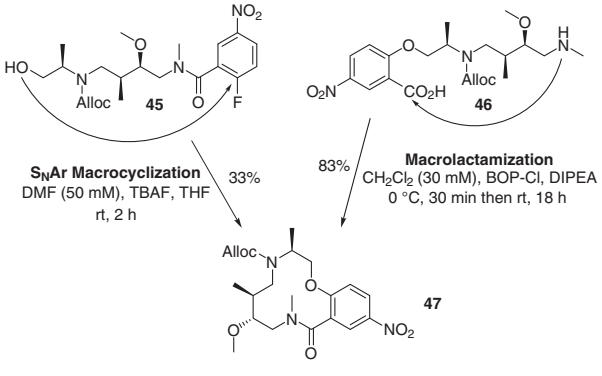

Scheme 3.8 The contrasting success of different cyclization strategies to make macrocycle **47**. Source: Fitzgerald et al. [20]/American Chemical Society.

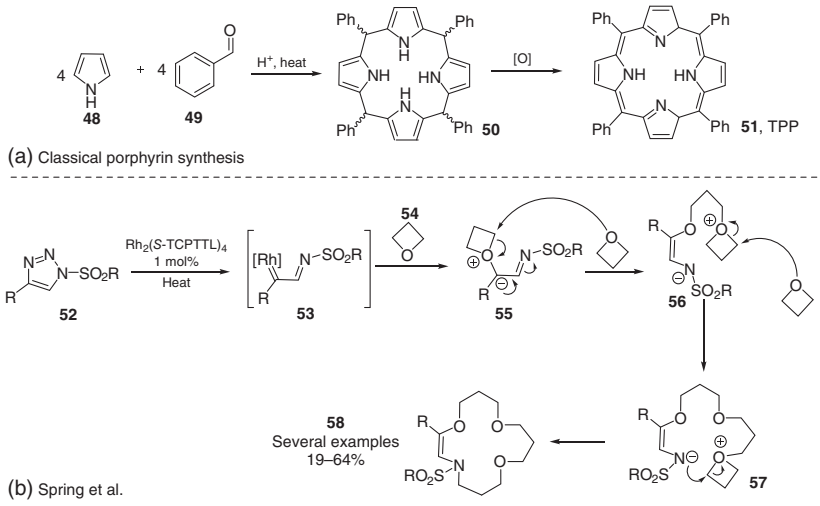

Scheme 3.9 (a) Classical porphyrin synthesis; (b) controlled cascade reaction of oxetanes with α-iminocarbenes to form macrocycles **58**. Source: Guarnieri-Ibáñez et al. [22]/Royal Society of Chemistry.

once a certain ring size (i.e. pyrrole **48** and aldehyde units) is reached and hence a suitable geometry/conformation can be attained. However, porphyrins are not unique in this regard, and similar traits can also be found in more surprising systems. For example, Spring and coworkers reported a remarkable overall [3+4+4+4] polycondensation reaction for the synthesis of 15-membered macrocyclic polyethers of the type **58** (Scheme 3.9b) [22]. The proposed mechanism is based on sequential oxetane nucleophilic attack and ring opening, initiated by formation of a Rh(II) carbenoid. The fact that the reaction typically operates via the incorporation of exactly three oxetane units, clearly demonstrates that the cyclization of this scaffold (i.e. **57** → **58**) is more kinetically favorable than larger/smaller alternatives. Control studies suggest that the metal does not influence the outcome of the selectivity of the reaction, seemingly ruling out chelation control (see Section 3.3.3); thus in this system it appears that the preference for the 15-membered ring product is substrate controlled.

Electrostatic interactions can also help favor the macrocyclization of some substrate classes; for example, in linear peptides, attractive ion pair interactions between the oppositely charged N- and C-termini mean that stable conformations amenable to cyclization can usually be adopted relatively easily [23]. However, these components cannot react on their own, and because peptide coupling reagents result in the loss of the zwitterionic character of the peptide, the ion pair interaction is lost, which tends to disfavor macrocyclization (**59** → **60**, Scheme 3.10a). An ingenious way to circumvent this problem was introduced by Yudin and coworkers in 2010 [24]. This process starts with the condensation of the linear peptide with aldehyde **61** to form an iminium intermediate **62**. Like the precursor peptide, this intermediate is zwitterionic, and this property facilitates macrocyclization via reaction with *tert*-butyl isocyanide in an Ugi-like process to form **63**, which itself quickly rearranges to form the

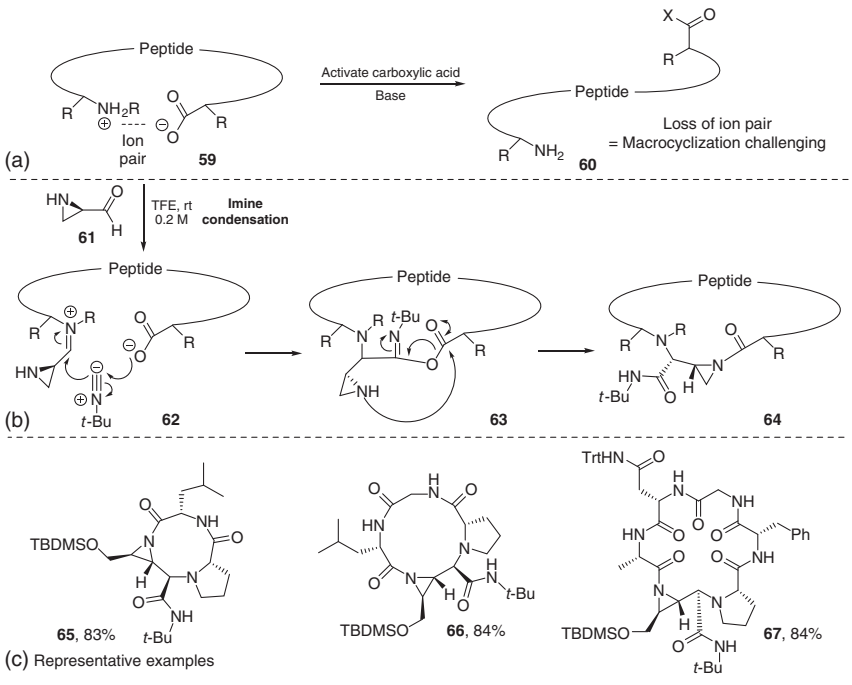

Scheme 3.10 Macrocyclization of linear peptides enabled by zwitterionic molecules.

desired product **64** (Scheme 3.10b). High yields of both medium-sized and macrocyclic peptides (e.g. **65–67**, Scheme 3.10c) can be obtained using this method, under mild conditions and without having to resort to high dilution (the reaction is performed at RT and 0.2 M concentration).

An alternative approach in which macrocyclization is also promoted by non-covalent interactions was described recently by Leboeuf and Force, but in this study via formally neutral species (Scheme 3.11) [25]. The overall method is related to the Yamaguchi macrolactonization in that it also involves formation of a mixed anhydride intermediate **70** (cf. **8** in Scheme 3.2). Using Leboeuf's method, cheap and readily available pentafluorobenzoyl chloride **69** is used to activate the seco acid linear starting material **68**. Its cyclization to form lactone **71** is then proposed to be facilitated by a π-lone pair interaction (**70**) or a π–π interaction (not shown), which helps to bring the reactive sites into closer proximity. Many successful examples were reported, in which the new method and reagent **69** consistently outperform more traditional Yamaguchi macrolactonization reagents and conditions.

3.3.2 Structural Features to Bias Cyclization Conformation

Structural features able to bias the conformation of linear starting materials toward cyclization are an advantage in any macrocyclization process, but they are especially important in the synthesis of cyclic peptides or cyclic peptide mimetics. One of the reasons why macrocyclization of linear peptides is often so challenging is

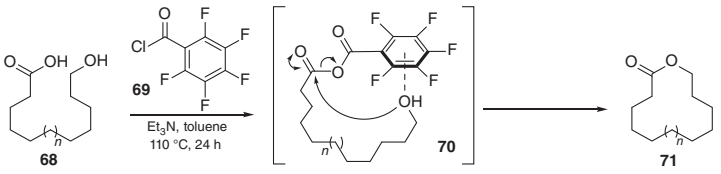

Scheme 3.11 Macrolactonization driven by supramolecular interactions. Source: Force et al. [25]/Wiley.

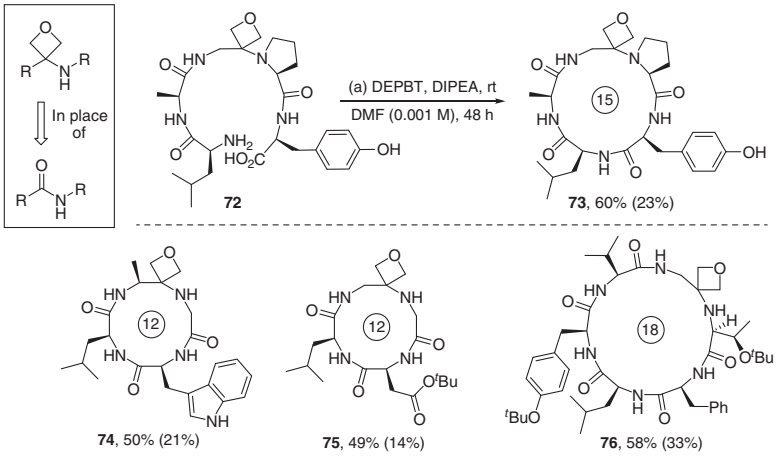

Scheme 3.12 Macrocyclization of small peptides enabled by oxetane incorporation (yields in parentheses are for the cyclization of the parent peptides).

the conformational rigidity of their amide bonds. Linear amides typically adopt a *Z*-geometry, which usually does not lead to a conformation conducive to cyclization. However, certain amino acid sequences are known that typically favor the adoption of linear conformations more amenable to macrocyclization, by helping to bring the two ends of the molecule closer together, for example, by incorporating "turns" into the linear peptide using features such as pseudoproline, N-alkylated, and/or D-amino acids [26].

Knowledge and application of turn-inducing elements is certainly important in peptide science, but the requirement to have a particular sequence of amino acids is a limitation in scenarios where these groups are not required in the products. An interesting alternative approach was developed by Shipman and coworkers, who demonstrated that an oxetane unit can be used in place of an amide as a turn inducing moiety (Scheme 3.12, box) [27]. The amino oxetane fragment mimics an amino acid and can be introduced using two separate strategies with orthogonal deprotection conditions. Generally, high dilution conditions were still needed to obtain good yields of macrocycle, but significant yield improvements were observed when using the oxetane-containing peptides (for a comparison, yields for formation of the analogous parent peptides are included in parentheses). Multiple oxetane-containing macrocycles in challenging ring sizes can be made: tetra-, penta-, and hexapeptides,

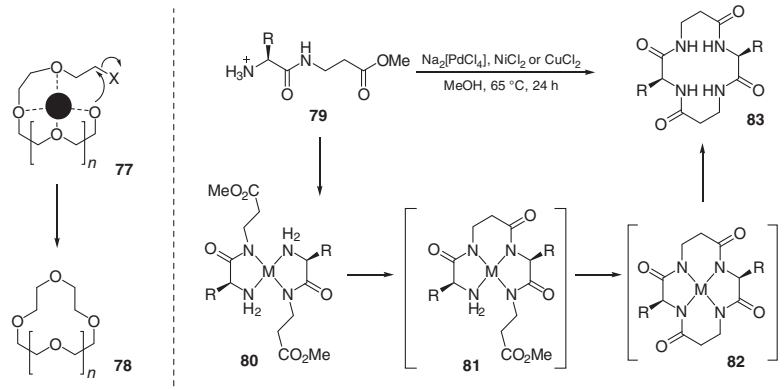

Scheme 3.13 (a) Classical crown ether synthesis; (b) templated synthesis of cyclic tetrapeptides **83** from nonactivated peptide esters on metal centers, where M denotes the metal.

e.g. **73–76** have been prepared using this method, intriguingly with similar IC_{50} values to those of the parent cyclic peptides.

3.3.3 Templated Macrocyclization

Metals can be used to chelate and pre-organize a linear substrate into a reactive conformation, facilitating cyclization to form macrocyclic heterocycles [28]. Templated synthesis benefits from both kinetic and thermodynamic effects that can favor cyclization over dimerization [29]. Perhaps the most well-known example of templated synthesis is for the synthesis of macrocyclic polyethers, better known as crown ethers – indeed, these are arguably the most famous class of heterocyclic macrocycles of all. Originally reported by Pedersen while working at DuPont [30], countless examples of the synthesis of polycyclic ethers via reactions of the type **77** → **78** have been disclosed, usually based on chelation of a group I metal cation (typically where $M^+ = Li^+$, Na^+, or K^+, Scheme 3.13a) [28]. Conceptually related strategies can also be used to form more functionalized heterocyclic macrocycles, for example, as demonstrated in a study by Beck and coworkers, in which cyclic tetrapeptides can be prepared via the initial coordination of dipeptide derivatives **79**, to a Ni(II), Pd(II), or Cu(II) templates [31]. The resulting metal complex **80** goes on to participate in templated cyclization (**80** → **81** → **82**) from nonactivated esters. Upon acidic workup, the metal can be removed alongside the desired macrocyclic tetrapeptide **83** (Scheme 3.13b).

3.4 Ring-Expansion Methods

For the reasons set out earlier (see Scheme 3.1), end-to-end cyclization reactions to make heterocyclic macrocycles and medium-sized rings are often complicated

by competing intermolecular side reactions. Many of the methods described throughout this chapter up to this point are based on strategies designed to improve end-to-end macrocyclization, either by making cyclization more favorable (e.g. using templates) or by making bimolecular reactions less favorable (e.g. using dilution/pseudo-dilution methods). Ring-expansion approaches are different, as rather than trying to improve the difficult end-to-end macrocyclization step, they allow it to be completely avoided.

Many such approaches have been used successfully for the synthesis of heterocyclic macrocycles and medium-sized rings, with heteroatoms often playing a key role in the rearrangement. Several review articles have been published on ring-expansion methods in general and should be consulted for more detail [32], with selected highlights included in the following text. Pericyclic reactions are often used to drive the key ring-expansion/rearrangement process, for example, via electrocyclic ring opening, as illustrated in a clever 2-carbon ring expansion reported by Li, Sun, and coworkers (Scheme 3.14a) [33]. Thus, upon treatment with a suitable Lewis acid, both cyclic acetals and cyclic aminals (**84**, where X = O or NTs) can be converted in 2-carbon homologated products **90**, via formation of a reactive oxonium species (**86**, X = O) followed by a formal [2+2] cycloaddition and subsequent electrocyclic ring-opening sequence. A similarly impressive 3-carbon ring-expansion method, reported by Schmid and Schmid [34], enables S-heterocycles to be prepared via an elegant alkylation/2,3-sigmatropic rearrangement approach (**92** → **93** → **94**, Scheme 3.14b). An interesting feature of this method is that further iterations of the same process can be performed on the product, thus enabling further ring expansion to be performed relatively easily (**94** → **97** → **98**). Four-carbon ring expansion can also be achieved using 3,3-sigmatropic rearrangement chemistry. This was exemplified by another iterative approach, which was reported by Back and coworkers [35] (Scheme 3.14c). The key step in this approach involved the reaction of 2-vinylpyrrolidine **99** with an acetylenic sulfone to form a zwitterion **100**, which undergoes 3,3-aza-cope rearrangement *in situ* to produce 4-carbon homologated enamine product **101**. Following additional steps (**101** → **105**), a second ring expansion was performed in the same way, to 13-membered aza-cycle **107**, which was subsequently converted into the natural product motuporamine A **108**.

Ring-expansion processes based on side chain insertion are another major class used for the synthesis of heterocyclic macrocycles and medium-sized rings [32]. Side chain insertion reactions typically involve the attachment of a linear side chain to a cyclic system containing a nucleophilic motif (usually a heteroatom such as O, N) to promote ring expansion via a rearrangement reaction. Reactions of this type tend to be reversible and hence under thermodynamic control. This means that ring size can have a major bearing on the outcomes of the reactions, as is illustrated in a seminal study by Corey and coworkers (Scheme 3.15a) [36]. Thus, while the reaction of nine-membered ring lactone **109a** with 1 mol% of *para*-toluenesulfonic acid results in facile ring expansion to form 12-membered ring **110a**, the expansion of the shorter eight-membered homolog **109b** was significantly slower and lower yielding. The seven-membered ring lactone **110c** failed to undergo ring expansion

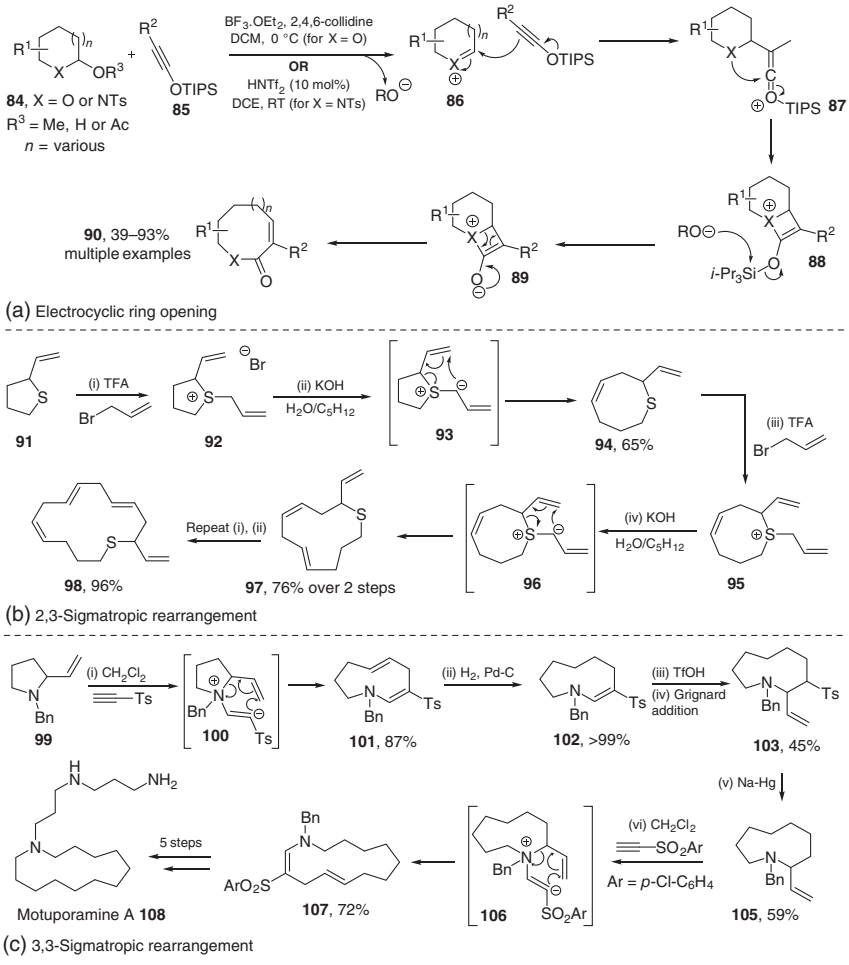

Scheme 3.14 Pericyclic ring-expansion reactions. Source: Zhao et al. [33].

at all. The successful expansion of **109a** into **110a** is presumably being driven by the relative instability of the nine-membered ring (i.e. reactions involving the conversion of medium-sized rings → macrocycle are generally thermodynamically favorable), whereas the shorter homologs are associated with ring size changes that are less favorable. This illustrates a common feature of side chain insertion ring-expansion reactions – that they tend to be more favorable when applied to larger ring systems. Hesse and coworkers produced a series of important works based on large ring expansions of this type [32a], for example, the sequence shown in Scheme 3.15b, which features examples of the two main types of transamidation ring expansion developed by this group (**112** → **113** and **115** → **116**) [37].

The work of Hesse (and others) helped to inspire research in our own group on the Successive Ring Expansion (SuRE) of cyclic β-ketoesters and lactams (Scheme 3.16) [38]. These methods enable iterative ring expansion to be achieved via a sequence

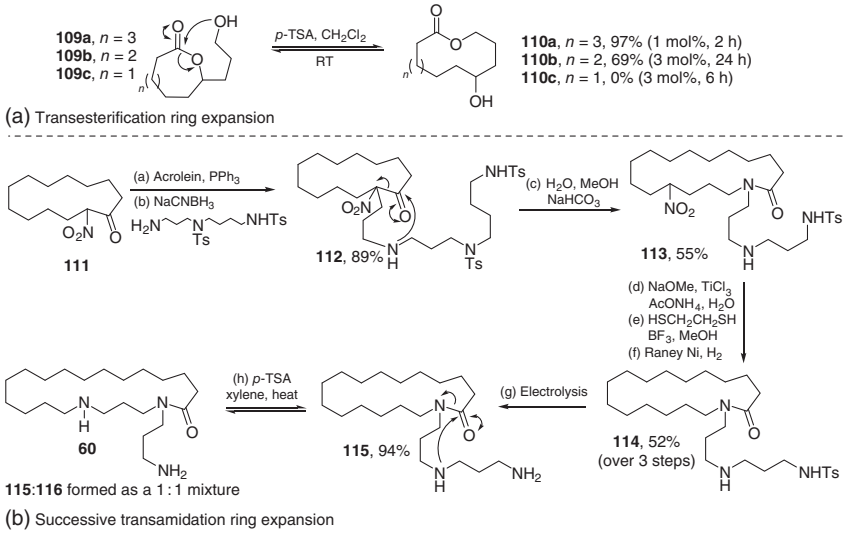

Scheme 3.15 Side chain insertion ring-expansion reactions. Source: Corey et al. [36]/American Chemical Society.

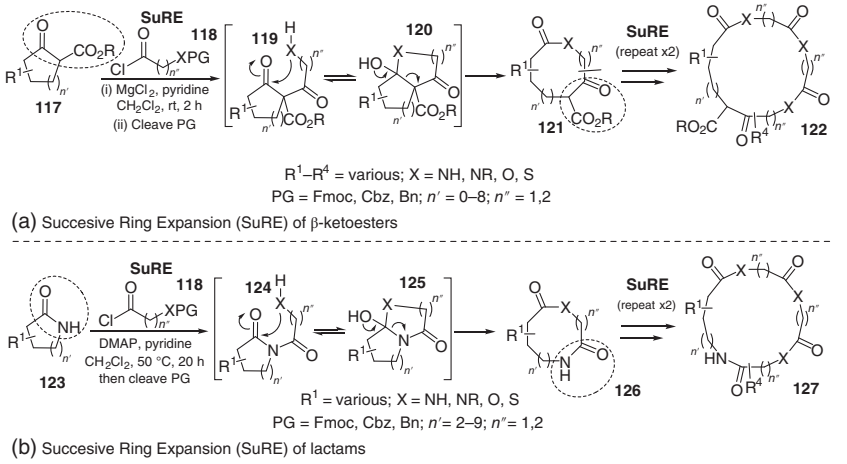

Scheme 3.16 Successive Ring Expansion (SuRE). Source: Refs. [38].

of acylation, protecting group cleavage and spontaneous ring expansion via the rearrangement reactions shown (**119** → **120** → **121** and **124** → **125** → **126**), using both β-ketoesters and lactams as starting materials. High yielding 3- and 4-atom ring expansion can be achieved on a wide range of starting ring sizes, using protected amino acid, hydroxy acid, and thiol acid-derived acid chlorides as acylating agents. These ring expansions were designed so that they can be performed iteratively, expanding by 3 or 4 atoms each time (**121** → **122** and **126** → **127**); regeneration of the initial reactive moiety (i.e. the circled β-ketoester and lactam motifs) upon rearrangement is a key design feature, thus allowing subsequent iterations to be

performed without additional synthetic effort. Large macrocyclic heterocycles can therefore be prepared containing specific amino/hydroxy/thiol acid sequences using the SuRE approach.

3.5 Medium-Sized Rings: Special Cases

Medium-sized ring heterocycles are commonly found in bioactive natural products and medicinally important molecules [4, 39]. In contrast to normal-sized rings (5–7-membered) and macrocycles (12+-membered rings), the relative rigidity and 3D spatial properties of medium-sized (8–11-membered) rings often imparts them with attractive properties in medicinal chemistry, such as improved binding, oral bioavailability, and cell permeability [40]. These attractive features have helped boost interest in the synthesis and applications of medium-sized rings and macrocycles for medicinal purposes. However, medium-sized rings are often especially challenging to synthesize compared with analogous larger or smaller ring systems, with the kinetic and thermodynamic barriers associated with their synthesis typically being higher than for other rings sizes [41]. Medium-sized rings are generally sufficiently large that synthesis via cyclization of a linear precursor is often associated with significant loss of entropy, but they are small enough to experience destabilizing transannular interactions and strain [3a].

Despite the synthetic challenges, many innovative methods directed toward the synthesis of medium-sized ring heterocycles have nonetheless been developed. A more detailed account on these methods can be found in various review articles [4, 39, 42], with selected recent developments described in this section. The use of "SnAP" (Sn amino protocol) reagents **129**, as developed and introduced by Bode and coworkers, is a prominent example (Scheme 3.17a) [43]. Thus, it was shown that SnAP reagents of the form **129** can react with aldehydes **128** to form eight- and nine-membered ring heterocycles **131**. The overall yields in some cases are lower than those obtained when preparing analogous normal-sized rings (as would be expected), but nonetheless, the direct synthesis of various products **131** in a single operation is still impressive. There are also some parallels to be seen in the application of silyl-Prins reactions to make eight-membered ring cyclic ethers **135**, as reported by Barbero and coworkers (Scheme 3.17b) [44]. In both studies, the efficiency of the key bond-forming steps in the cyclization are able to overcome the additional thermodynamic challenges associated with making medium-sized ring products.

Palladium-catalyzed annulation reactions have also been shown to be powerful methods to construct medium-sized rings, as is illustrated in an intriguing 2020 report by Peng, Han, and coworkers on the regiodivergent synthesis of seven- and nine-membered ring cyclic ethers and amines from allylidenemalononitriles **136** and vinylethylene carbonates **137** (Scheme 3.18) [45]. Thus, upon reaction with a Pd(0) catalyst, the two reaction components couple to form a key intermediate **138**, which then proceeds to cyclize, either via a formal [5+4] annulation to form nine-membered ring products **139** or a formal [5+2] annulation to form

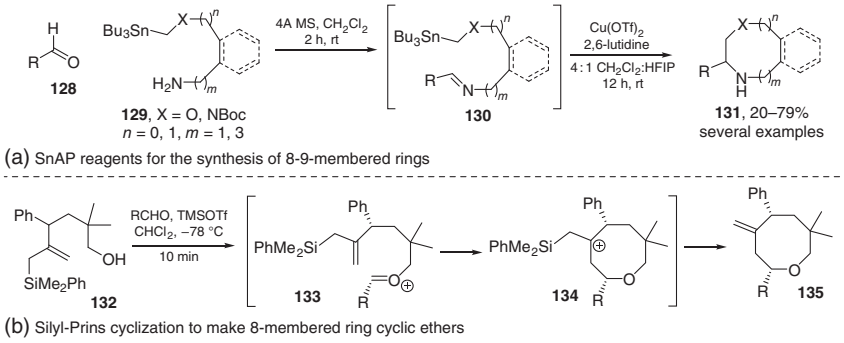

Scheme 3.17 Direct syntheses of eight- and nine-membered heterocycles from aldehydes and annulation reagents. Source: Vo et al. [43]/Springer Nature; Poza-Diez and Barbero [44]/Wiley.

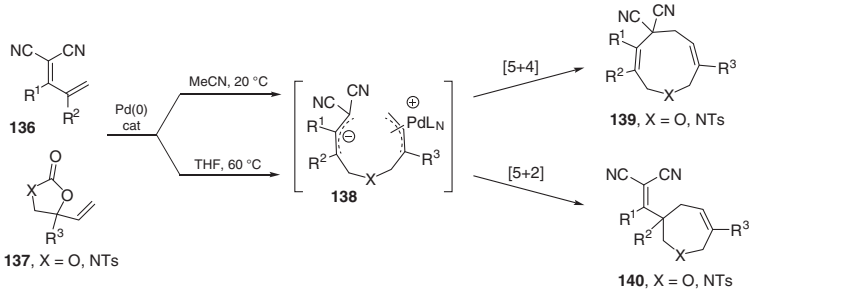

Scheme 3.18 Regiodivergent construction of medium-sized heterocycles from vinylethylene carbonates and allylidenemalononitriles. Source: Zhang et al. [45]/Royal Society of Chemistry.

seven-membered ring products **140**, depending on the reaction conditions used. Several high yielding examples of both divergent pathways were reported.

As with macrocycles, ring-expansion methods also have utility for the synthesis of medium-sized ring heterocycles. For such approaches to be successful, it is important that there is a clear thermodynamic imperative for rearrangement to occur. This is because based on ring size alone, the conversion of normal- into medium-sized rings is usually "uphill" thermodynamically, and for ring-expansion reactions to be exergonic overall, this thermodynamic cost must be "repaid" in some other way. This idea is demonstrated in work by Clayden and coworkers, who have shown that Smiles-type rearrangements of reactive lithiated species of the form **142** can be used as an effective way to make medium-sized azacycles **144** (Scheme 3.19a) [46]. Stabilization of the negative charge upon rearrangement (**142** → **143**) provides the driving force for ring expansion in this case. Neutralization of positive charge can also help to promote ring expansion, as shown in a study from our own group on cyclization/ring-expansion cascade reactions to make medium-sized lactams and lactones **147** (Scheme 3.19b) [47]. Ring expansion can also be driven by the formation of stable aromatic products, as demonstrated by Tan

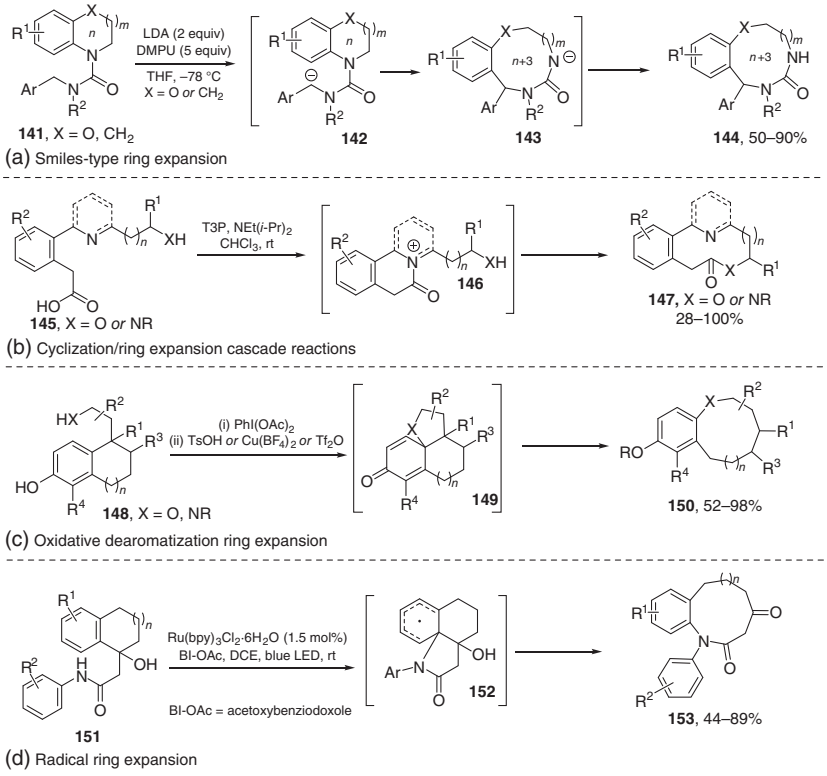

Scheme 3.19 Ring-expansion methods to prepare medium-sized ring heterocycles. Source: Ref. [46] and Lawyer et al. [47]/Wiley.

and coworkers, who used an innovative oxidative dearomatization ring-expansion (ODRE) strategy to make a diverse array of medium-sized scaffolds for bioassay [40a]. Reactive radical intermediates can also promote powerful ring-expansion reactions, exemplified by a series of studies by Liu and coworkers [48], typified by their efficient photocatalytic $n+3$ ring-expansion strategy to form medium-sized lactams **153**, via the generation of nitrogen centered radicals using visible-light photoredox catalysis (Scheme 3.19d) [48d].

3.6 Conclusions and Perspectives

Macrocyclic and medium-sized rings with appropriately located heteroatoms have a long history in applied areas of science, spanning medicinal chemistry, supramolecular chemistry, catalysis, and many more [1, 2]. Interest in these applied areas continues to grow, and therefore establishing an efficient toolbox of reactions to prepare diversely functionalized heterocyclic macrocycles and medium-sized rings is a very important endeavor. In this chapter, a small selection of methods are summarized, ranging from high dilution and templating strategies to the use of solid supports

and ring-expansion reactions. With an appreciation of all these contrasting methods, synthetic chemists are well placed to devise effective syntheses of a broad array of useful large ring heterocycles.

Dedication

Dedicated to the memory of Prof Éric Marsault – a giant in the field of heterocyclic macrocycles and their application in medicinal chemistry.

References

1 For application in medicinal chemistry, see: (a) Driggers EM, Hale SP, Lee J, Terrett NK. The exploration of macrocycles for drug discovery – an underexploited structural class. *Nat. Rev. Drug Discovery* 2008;7: 608–624. doi:https://doi.org/10.1038/nrd2590; (b) Marsault E, Peterson ML. Macrocycles are great cycles: applications, opportunities, and challenges of synthetic macrocycles in drug discovery. *J. Med. Chem.* 2011;54: 1961–2004. doi:https://doi.org/10.1021/jm1012374; (c) Ghadiri MR, Granja JR. Ion channel models based on self-assembling cyclic peptide nanotubes. *Acc. Chem. Res.* 2013;46: 2955–2965. doi:https://doi.org/10.1021/ar400061d; (d) Giordanetto F, Kihlberg J. Macrocyclic drugs and clinical candidates: what can medicinal chemists learn from their properties? *J. Med. Chem.* 2014;57: 278–295. doi:https://doi.org/10.1021/jm400887j; (e) Yudin AK. Macrocycles: lessons from the distant past, recent developments, and future directions. *Chem. Sci.* 2015;6: 30–49. doi:https://doi.org/10.1039/C4SC03089C; (f) Marsault, E. and Peterson, M.L. (2017). *Practical Medicinal Chemistry with Macrocycles*. Wiley-VHC.

2 For other applications, see: (a) Ema T, Tanida D, Sakai T. Versatile and practical macrocyclic reagent with multiple hydrogen-bonding sites for chiral discrimination in NMR. *J. Am. Chem. Soc.* 2007;129: 10591–10596. doi:https://doi.org/10.1021/ja073476s; (b) Griffiths KE, Stoddart JF. Template-directed synthesis of donor/acceptor [2]catenanes and [2]rotaxanes. *Pure Appl. Chem.* 2008;80: 485–506. doi:https://doi.org/10.1351/pac200880030485; (c) Evans NH, Beer PD. Progress in the synthesis and exploitation of catenanes since the Millennium. *Chem. Soc. Rev.* 2014;43: 4658–4683. doi:https://doi.org/10.1039/C4CS00029C; (d) Xue M, Yang Y, Chi X, Yan X, Huang F. Development of pseudorotaxanes and rotaxanes: from synthesis to stimuli-responsive motions to applications. *Chem. Rev.* 2015;115: 7398–7501. doi: https://doi.org/10.1021/cr5005869; (e) Byrne JP, Blasco S, Aletti AB, Hessman G, Gunnlaugsson T. Formation of self-templated 2,6-bis(1,2,3-triazol-4-yl)pyridine [2]catenanes by triazolyl hydrogen bonding: selective anion hosts for phosphate. *Angew. Chem. Int. Ed.* 2016;55: 8938–8943. doi:https://doi.org/10.1002/anie.201603213; (f) Sato K, Itoh Y, Aida T. Columnarly assembled liquid-crystalline peptidic macrocycles unidirectionally orientable over a large area by an electric field. *J. Am. Chem. Soc.* 2011;133: 13767–13796. doi:https://doi.org/10.1021/ja203894r; (g) Neal EA, Goldup SM.

Chemical consequences of mechanical bonding in catenanes and rotaxanes: isomerism, modification, catalysis and molecular machines for synthesis, *Chem. Commun.* 2014;50: 5128–5142. doi:https://doi.org/10.1039/C3CC47842D.

3 (a) Illuminati G, Mandolini L. Ring closure reactions of bifunctional chain molecules. *Acc. Chem. Res.* 1981;14: 95–102. doi:https://doi.org/10.1021/ar00064a001; (b) Fastrez J. Macrocyclization versus polymerization in polycondensation reactions under high-dilution conditions: a theoretical study. *J. Phys. Chem.* 1989;93: 2635–2642. doi:https://doi.org/10.1021/j100343a077; (c) White CJ, Yudin, AK. Contemporary strategies for peptide macrocyclization. *Nat. Chem.* 2011;3: 509–524. doi:https://doi.org/10.1038/nchem.1062; (d) Collins JC, James K. Emac – a comparative index for the assessment of macrocyclization efficiency. *Med. Chem. Commun.* 2012;3: 1489–1495. doi:https://doi.org/10.1039/C2MD20176C.

4 Clarke AK, Unsworth WP. A happy medium: the synthesis of medicinally important medium-sized rings via ring expansion. *Chem. Sci.*, 2020;11: 2876–2881. doi:https://doi.org/10.1039/d0sc00568a.

5 For examples in synthesis, see references 1a–f, and: (a) Unsworth WP, Gallagher KA, Jean M, Schmidt JP, Diorazio LJ, Taylor RJK. Direct imine acylation: synthesis of the proposed structures of 'Upenamide. *Org. Lett.* 2013;15: 262–265. doi:https://doi.org/10.1021/ol3030764; (b) Shen X, Nguyen TT, Koh MJ, Xu D, Speed AWH, Schrock RR, Hoveyda AH. Kinetically E-selective macrocyclic ring-closing metathesis. *Nature* 2017;541: 380–385. doi:https://doi.org/10.1038/nature20800.

6 (a) Inanaga J, Hirata K, Saeki H, Katsuki T, Yamaguchi M. A rapid esterification by means of mixed anhydride and its application to large-ring lactonisation. *Bull. Chem. Soc. Jpn.* 1979;52: 1989–1993. doi:https://doi.org/10.1246/bcsj.52.1989; (b) Parenty A, Moreau X, Campagne J-M. Macrolactonisations in the total synthesis of natural products. *Chem. Rev.* 2006;106: 911–939. doi:https://doi.org/10.1021/cr0301402.

7 Bosch L, Mola L, Petit E, Saladrigas M, Esteban J, Costa AM, Vilarrasa J. Formal total synthesis of amphidinolide E. *J. Organomet. Chem.* 2017;82: 11021–11034. doi:https://doi.org/10.1021/acs.joc.7b01973.

8 (a) Mitsunobu O, Yamada M. Preparation of esters of carboxylic and phosphoric acid via quaternary phosphonium salts. *Bull. Chem. Soc. Jpn.* 1967;40: 2380–2382. doi:https://doi.org/10.1246/bcsj.40.2380; (b) But TYS, Toy PH. The Mitsunobu reaction: origin, mechanism, improvements, and applications. *Chem. Asian J.*, 2007;2: 1340–1355. doi:https://doi.org/10.1002/asia.200700182.

9 Liao X, Wu Y, De Brabander JK. Total synthesis and absolute configuration of the novel microtubule-stabilizing agent peloruside A. *Angew. Chem. Int. Ed.* 2003;42: 1648–1652. doi:https://doi.org/10.1002/anie.200351145.

10 (a) Villemin D. Synthese de macrolides par methathese. *Tetrahedron Lett.*, 1980;21: 1715–1718. doi:https://doi.org/10.1016/S0040-4039(00)77818-X; (b) Hassan MA. Recent applications of ring-closing metathesis in the synthesis of lactams and macrolactams. *Chem. Commun.*, 2010;46: 9100–9106. doi:https://doi.org/10.1039/C0CC03122D; (c) Nicolaou KC, Xu H. Total synthesis

of floresolide B and Δ6,7-Z-floresolide B. *Chem. Commun.*, 2006: 600–602. doi:https://doi.org/10.1039/B517385J; (d) Fürstner A, Thiel OR. Formal Total synthesis of (−)-balanol: concise approach to the hexahydroazepine segment based on RCM. *J. Org. Chem.*, 2000;65: 1738–1742. doi:https://doi.org/10.1021/jo991611g; (e) Gaul C, Njardarson JT, Danishefsky SJ. The total synthesis of (+)-migrastatin. *J. Am. Chem. Soc.* 2003;125: 6042–6043. doi:https://doi.org/10.1021/ja0349103; (f) Lecourt C, Dhambri S, Allievi L, Sanogo Y, Zeghbib N, Ben Othman R, Lannou M-I, Sorin G, Ardisson J. Natural products and ring-closing metathesis: synthesis of sterically congested olefins. *J. Nat. Prod. Rep.*, 2018;35: 105–124. doi:https://doi.org/10.1039/C7NP00048K.

11 (a) Marx VM, Herbert MB, Keitz BK, Grubbs RH. Stereoselective access to Z and E macrocycles by ruthenium-catalyzed Z-selective ring-closing metathesis and ethenolysis. *J. Am. Chem. Soc.*, 2013;135: 94–97. doi:https://doi.org/10.1021/ja311241q; (b) Yu M, Wang C, Kyle AF, Jakubec P, Dixon DJ, Schrock RR, Hoveyda AH. Synthesis of macrocyclic natural products by catalyst-controlled stereoselective ring-closing metathesis. *Nature*, 2011;479: 88–93. doi:https://doi.org/10.1038/nature10563.

12 Pehere, A.D. and Abell, A.D. (2017). The synthesis of peptide-based macrocycles by Huisgen cycloaddition. In: *Practical Medicinal Chemistry with Macrocycles* (ed. E. Marsault and M.L. Peterson). Wiley.

13 Neuhaus CM, Liniger M, Stieger M, Altmann K-H. Total synthesis of the tubulin inhibitor WF-1360F based on macrocycle formation through ring-closing alkyne metathesis. *Angew. Chem. Int. Ed.*, 2013;52: 5866–5870. doi:https://doi.org/10.1002/anie.201300576.

14 Zapf CW, Harrison BA, Drahl C, Sorensen EJ. A Diels–Alder macrocyclization enables an efficient asymmetric synthesis of the antibacterial natural product abyssomicin C. *Angew. Chem. Int. Ed.*, 2005;44: 6533–6537. doi:https://doi.org/10.1002/anie.200502119.

15 Kodama M, Shiobara Y, Sumitomo H, Matsumura K, Tsukamoto M, Harada C. Total syntheses of marchantin A and riccardin B, cytotoxic bis(bibenzyls) from liverworts. *J. Org. Chem.*, 1988;53: 72–77. doi:https://doi.org/10.1021/jo00236a015.

16 Ronson, T.O., Unsworth, W.P., and Fairlamb, I.J.S. (2017). Palladium-catalyzed synthesis of macrocycles. In: *Practical Medicinal Chemistry with Macrocycles* (ed. E. Marsault and M.L. Peterson). Wiley.

17 (a) Franzyk H, Christensen MK, Jørgensen RM, Meldal M, Cordes H, Mouritsen S, Bock K. Constrained glycopeptide ligands for MPRs. Limitations of unprotected phosphorylated building blocks. *Bioorg. Med. Chem.* 1997;5: 21–40. doi:https://doi.org/10.1016/S0968-0896(96)00194-0; (b) Andersen MO, Shelat AA, Guy RK. A solid-phase approach to the phallotoxins: total synthesis of [Ala^7]-phalloidin. *J. Org. Chem.* 2005;70: 4578–4584. doi:https://doi.org/10.1021/jo0503153; (c) Xu W-L, Cui AL, Hu X-X, You X-F, Li Z-R, Zheng J-S A new strategy for total solid-phase synthesis of polymyxins. *Tetrahedron Lett.* 2015;56: 4796–4799. doi:https://doi.org/10.1016/j.tetlet.2015.06.056; (d) Kim SJ, McAlpine SR. Solid phase versus solution phase synthesis of heterocyclic macrocycles. *Molecules*, 2013;18: 1111–1121. doi:https://doi.org/10.3390/molecules18011111.

18 Turner RA, Oliver AG, Lokey RS. Click chemistry as a macrocyclization tool in the solid-phase synthesis of small cyclic peptides. *Org. Lett.*, 2007;9: 5011–5014. doi:https://doi.org/10.1021/ol702228u.

19 Bédard AC, Collins SK. Phase separation as a strategy toward controlling dilution effects in macrocyclic Glaser–Hay couplings. *J. Am. Chem. Soc.* 2011;133: 19976–19981. doi:https://doi.org/10.1021/ja208902t.

20 Fitzgerald ME, Mulrooney CA, Duvall JR, Wei J, Suh BC, Akella LB, Vrcic A, Marcaurelle LA. Build/couple/pair strategy for the synthesis of stereochemically diverse macrolactams via head-to-tail cyclization. *ACS Comb. Sci.* 2012;14: 89–96. doi:https://doi.org/10.1021/co200161z.

21 Hiroto S, Miyake Y, Shinokubo H. Synthesis and functionalization of porphyrins through organometallic methodologies. *Chem. Rev.* 2017;117: 2910–3043. doi:https://doi.org/10.1021/acs.chemrev.6b00427.

22 Guarnieri-Ibáñez A, Medina F, Besnard C, Kidd SL, Spring DR, Lacour J. Diversity-oriented synthesis of heterocycles and macrocycles by controlled reactions of oxetanes with α-iminocarbenes. *Chem. Sci.* 2017;8: 5713–5720. doi:https://doi.org/10.1039/C7SC00964J.

23 Schmuck C, Wienand W. Highly stable self-assembly in water: ion pair driven dimerisation of a guanidiniocarbonyl pyrrole carboxylate zwitterion. *J. Am. Chem. Soc.* 2003;125: 452–459. doi:https://doi.org/10.1021/ja028485+.

24 Hili R, Rai V, Yudin AK. Macrocyclization of linear peptides enabled by amphoteric molecules. *J. Am. Chem. Soc.* 2010;132: 2889–2891. doi:https://doi.org/10.1021/ja910544p.

25 Force G, Perfetto A, Mayer, RJ, Ciofini I, Leboeuf D. Macrolactonisation driven by a pentafluorobenzoyl group. *Angew. Chem. Int. Ed.*, 2021;60: 19843–18851. doi: https://doi.org/10.1002/anie.202105882

26 Martí-Centelles, V, Pandey MD, Burguete MI, Luis SV. Macrocyclization reactions: the importance of conformational, configurational, and template-induced preorganisation. *Chem. Rev.*, 2015;115: 8736–8834. doi:https://doi.org/10.1021/acs.chemrev.5b00056.

27 Roesner S, Saunders GJ, Wilkening I, Jayawant E, Geden JV, Kerby P, Dixon AM, Notman R, Shipman M. Macrocyclisation of small peptides enabled by oxetane incorporation. *Chem. Sci.*, 2019;10: 2465–2472. doi:https://doi.org/10.1039/C8SC05474F.

28 Gerbeleu, N.V., Arion, V.B., and Burgess, J. (1999). *Template Synthesis of Macrocyclic Compounds*. Weinheim: Wiley-VCH Verlag GmbH.

29 Chambron JC, Dietrich-Buchecker CO, Hemmert C, Khemiss A-K, Mitchell D, Sauvage J-P, Weiss J. Interlacing molecular threads on transition metals. *Pure Appl. Chem.*, 1990;62: 1027–1034. doi:https://doi.org/10.1351/pac199062061027.

30 Pedersen C J. Cyclic polyethers and their complexes with metal salts. *J. Am. Chem. Soc.* 1967;89: 7017. doi:https://doi.org/10.1021/ja01002a035.

31 Haas K, Ponikwar W, Nöth H, Beck W. Facile synthesis of cyclic tetrapeptides from nonactivated peptide esters on metal centers. *Angew. Chem. Int. Ed.*, 1998;37: 1086–1089. doi: https://doi.org/10.1002/(SICI)1521-3773(19980504)37:8<1086::AID-ANIE1086>3.0.CO;2-V.

32 For general reviews of ring expansion reactions, see reference 4 and: (a) Hesse, M. (1991). *Ring Enlargement in Organic Chemistry*. Weinheim: Wiley-VCH; (b) Donald JR, Unsworth WP. Ring-expansion reactions in the synthesis of macrocycles and medium-sized rings. *Chem. Eur. J.* 2017;23: 8780–8799. doi:https://doi.org/10.1002/chem.201700467; (c) Prantz K, Mulzer J. Synthetic applications of the carbonyl generating Grob fragmentation. *Chem. Rev.* 2010;110: 3741–3766. doi:https://doi.org/10.1021/cr900386h; (d) Stephens TC, Unsworth WP. Consecutive ring-expansion reactions for the iterative assembly of medium-sized rings and macrocycles. *Synlett* 2020;31: 133–146. doi:https://doi.org/10.1055/s-0037-1611500.

33 (a) Zhao W, Li Z, Sun J. A new strategy for efficient synthesis of medium and large ring lactones without high dilution or slow addition. *J. Am. Chem. Soc.* 2013;135: 4680–4683. doi: https://doi.org/10.1021/ja400883q; (b) Zhao W, Qian H, Li Z, Sun J. Catalytic ring expansion of cyclic hemiaminals for the synthesis of medium-ring lactams. *Angew. Chem. Int. Ed.* 2015;54: 10005–10008. doi:https://doi.org/10.1002/anie.201504926.

34 Schmid R, Schmid H. Repetierbare Ringerweiterungen durch [2,3]-sigmatropische Umlagerungen in cyclischen Allylsulfonium-allyliden; Synthese von mittleren und grossen Thiacyclen. Vorläufige Mitteilung. *Helv. Chim. Acta* 1977;60, 1361–1366. doi:https://doi.org/10.1002/hlca.19770600424.

35 Weston MH, Nakajima K, Back TG. Tandem conjugate additions and 3-aza-cope rearrangements of tertiary allyl amines and cyclic α-vinylamines with acetylenic sulfones. Applications to simple and iterative ring expansions leading to medium and large-ring nitrogen heterocycles. *J. Org. Chem.* 2008;73: 4630–4637. doi:https://doi.org/10.1021/jo800600a.

36 Corey EJ, Brunelle DJ, Nicolaou KC. A translactonisation route to macrocyclic lactones. *J. Am. Chem. Soc.* 1977;99: 7359–7360. doi:https://doi.org/10.1021/ja00464a047.

37 Wälchli R, Guggisberg A, Hesse M. Ring expansion reactions in the formation of macrocyclic lactams. A synthesis of desoxo-inandenine. *Tetrahedron Lett.* 1984;25: 2205–2208. doi:https://doi.org/10.1016/S0040-4039(01)80211-2.

38 (a) Kitsiou C, Hindes JJ, I'Anson P, Jackson P, Wilson TC, Daly EK, Felstead HR, Hearnshaw P, Unsworth WP. The synthesis of structurally diverse macrocycles by successive ring-expansion. *Angew. Chem. Int. Ed.* 2015;54: 15794–15798. doi:https://doi.org/10.1002/anie.201509153; (b) Baud LG, Manning, MA, Arkless HL, Stephens TC, Unsworth WP. Ring expansion approach to medium-sized lactams and analysis of their medicinal lead-like properties. *Chem. Eur. J.* 2017;23: 2225–2230. doi:https://doi.org/10.1002/chem.201605615; (c) Stephens TC, Lodi M, Steer A, Lin Y, Gill M, Unsworth, WP. Synthesis of cyclic peptide mimetics by the successive ring expansion of lactams. *Chem. Eur. J.* 2017;23: 13314–13318. doi:https://doi.org/10.1002/chem.201703316; (d) Stephens TC, Lawer A, French T, Unsworth WP. Iterative assembly of macrocyclic lactones using successive ring expansion reactions. *Chem. Eur. J.* 2018;24: 13947–13953. doi:https://doi.org/10.1002/chem.201803064; (e) Lawer A, Epton RG, Stephens TC, Palate KY, Lodi M, Marotte E, Lamb KJ, Sangha JK, Lynam JM, Unsworth WP. Evaluating the

viability of successive ring-expansion reactions based on amino acid and hydroxyacid side-chain insertion. *Chem. Eur. J.* 2020;26: 12674–12683. doi:https://doi.org/10.1002/chem.202002164; (f) Palate KY, Epton RG, Whitwood AC, Lynam JM, Unsworth WP. Synthesis of macrocyclic and medium-sized ring thiolactones via the ring expansion of lactams. *Org. Biomol. Chem.* 2021;19: 1404–1411. doi:https://doi.org/10.1039/D0OB02502J.

39 Majumdar KC. Regioselective formation of medium-ring heterocycles of biological relevance by intramolecular cyclization. *RSC Adv.* 2011;1: 1152–1170. doi:https://doi.org/10.1039/C1RA00494H.

40 (a) Bauer RA; Wenderski TA, Tan DS. Biomimetic diversity-oriented synthesis of benzannulated medium rings via ring expansion. *Nat. Chem. Biol.* 2013;9: 21–29. doi:https://doi.org/10.1038/nchembio.1130; (b) Zhao C, Ye Z, Ma Z-X, Wildman SA, Blaszczyk SA, Hu L, Guizei IA, Tang W. A general strategy for diversifying complex natural products to polycyclic scaffolds with medium-sized rings. *Nat. Commun.* 2019;10: 4015. doi:https://doi.org/10.1038/s41467-019-11976-2;

41 Casadei MA, Galli C, Mandolini L. Ring-closure reactions. 22. Kinetics of cyclization of diethyl (.omega.-bromoalkyl)malonates in the range of 4- to 21-membered rings. Role of ring strain. *J. Am. Chem. Soc.* 1984;106: 1051–1056. doi:https://doi.org/10.1021/ja00316a039.

42 Maier ME. Synthesis of medium-sized rings by the ring-closing metathesis reaction. *Angew. Chem. Int. Ed.* 2000;39: 2073–2077. doi:https://doi.org/10.1002/1521-3773(20000616)39:12<2073::AID-ANIE2073>3.0.CO;2-0.

43 Vo, C-VT, Luescher MU, Bode JW. SnAP reagents for the one-step synthesis of medium-ring saturated N-heterocycles from aldehydes. *Nat. Chem.* 2014;6: 310–314. doi:https://doi.org/10.1038/nchem.1878.

44 Poza-Díez, C; Barbero A. Synthesis of O- and N-heterocycles by silyl-Prins cyclization of allylsilanes. *Eur. J. Org. Chem.* 2017: 4651–4665. doi:https://doi.org/10.1002/ejoc.201700644.

45 Zhang X, Li X, Li J-L, Wang Q-W, Zou W-L, Liu Y-Q, Jia Z-Q, Peng F, Han B. Regiodivergent construction of medium-sized heterocycles from vinylethylene carbonates and allylidenemalononitriles. *Chem. Sci.* 2020;11: 2888–2894. doi:https://doi.org/10.1039/C9SC06377C.

46 (a) Hall JE, Matlock JV, Ward JW, Gray KV, Clayden J. Medium-ring nitrogen heterocycles through migratory ring expansion of metalated ureas. *Angew. Chem. Int. Ed.* 2016;55: 11153–11157. doi:https://doi.org/10.1002/anie.201605714; (b) Costil R, Lefebvre Q, Clayden J. Medium-sized-ring analogues of dibenzodiazepines by a conformationally induced smiles ring expansion. *Angew. Chem. Int. Ed.* 2017;56: 14602–14606. doi:https://doi.org/10.1002/anie.201708991.

47 Lawer A, Rossi-Ashton JA, Stephens TC, Challis BJ, Epton RG, Lynam JM, Unsworth WP internal nucleophilic catalyst mediated cyclisation/ring expansion cascades for the synthesis of medium-sized lactones and lactams. *Angew. Chem. Int. Ed.* 2019;58: 13942–13947. doi:https://doi.org/10.1002/anie.201907206.

48 (a) Li Z-L, Li X-H, Wang N, Yang N-Y, Liu X-Y. Radical-mediated 1,2-formyl/carbonyl functionalization of alkenes and application to the construction of medium-sized rings. *Angew. Chem. Int. Ed.* 2016;55: 15100–15104.

doi:https://doi.org/10.1002/anie.201608198; (b) Li L, Li Z-L, Wang F-L, Guo Z, Cheng Y-F, Wang N; Dong X-W, Fang C, Liu J, Hou C, Tan B, Liu X-Y Radical aryl migration enables diversity-oriented synthesis of structurally diverse medium/macro- or bridged-rings. *Nat. Commun.* 2016;7: 13852. doi:https://doi.org/10.1038/ncomms13852; (c) Li L, Li Z-L, Gu Q-S, Wang N, Liu X-Y. A remote C–C bond cleavage–enabled skeletal reorganization: access to medium-/large-sized cyclic alkenes. *Sci. Adv.* 2017;3: e1701487. doi:https://doi.org/10.1126/sciadv.1701487; (d) Wang N, Gu Q-S, Li Z-L, Li Z, Guo Y-L, Guo Z, Liu X-Y. Direct photocatalytic synthesis of medium-sized lactams by C−C bond cleavage. *Angew. Chem. Int. Ed.* 2018;57: 14225–14229. doi:https://doi.org/10.1002/anie.201808890; (e) Wang N, Wang J, Guo Y-L, Li L, Sun Y, Li Z, Zhang H-X, Guo Z, Li Z-L, Liu X-Y. Oximinotrifluoromethylation of unactivated alkenes under ambient conditions. *Chem. Commun.* 2018;54: 8885–8888. doi:https://doi.org/10.1039/C8CC05186K.

4

Organocatalysis in Synthetic Heterocyclic Chemistry

Ángel Cores, Mercedes Villacampa, and J. Carlos Menéndez

Universidad Complutense, Unidad de Química Orgánica y Farmacéutica, Departamento de Química en Ciencias Farmacéuticas, Facultad de Farmacia, Plaza de Ramón y Cajal, s.n., 28040 Madrid, Spain

4.1 Introduction

Heterocycles are the most important single class of compounds in the pharmaceutical and agrochemical industries, comprising more than 60% of products in the market or the pipeline. Due to regulatory reasons associated to their impact on human health, the demand for final product purity in these areas is very high, and, therefore, the development of industrial processes in these areas is highly challenging. In the academic field, as well as with an important industrial projection, the preparation of chiral heterocyclic systems in enantiopure form is one of the main goals in organic synthesis.

Organocatalysis can be defined as the acceleration of chemical reactions by substoichiometric amounts of organic molecules. Although many cases of catalysis with organic molecules were scattered in the literature, the idea of organocatalysis as a unifying concept did not arise until the end of the twentieth century, and the term itself was first proposed by MacMillan in 2000 [1]. Some advantages of organocatalysis over alternative catalytic methods include the low toxicity inherent to the methodology due to the absence of transition metals and the robustness usually displayed by the procedures. Although not exclusively, modern organocatalysis is generally focused on the development of enantioselective reactions.

Although detailed mechanisms will be discussed when the reactions are presented in this chapter, we will give herein a general overview of the main mechanistic aspects of organocatalysts. Many of them are secondary amines such as proline and some of its derivatives, in particular prolinol silyl ethers and imidazolidinones (Scheme 4.1a).

Secondary amines normally act by covalent mechanisms, with the modalities of enamine and iminium catalysis. The mechanism of the reaction of an aldehyde and an electrophile in the presence of proline is shown in Scheme 4.1b as an example of enamine catalysis. In Scheme 4.1c the proline-catalyzed Michael reaction of acrolein with a nucleophile is presented as a representative example of iminium

Heterocycles: Synthesis, Catalysis, Sustainability, and Characterization, First Edition.
Edited by Teresa M.V.D. Pinho e Melo and Marta Pineiro.

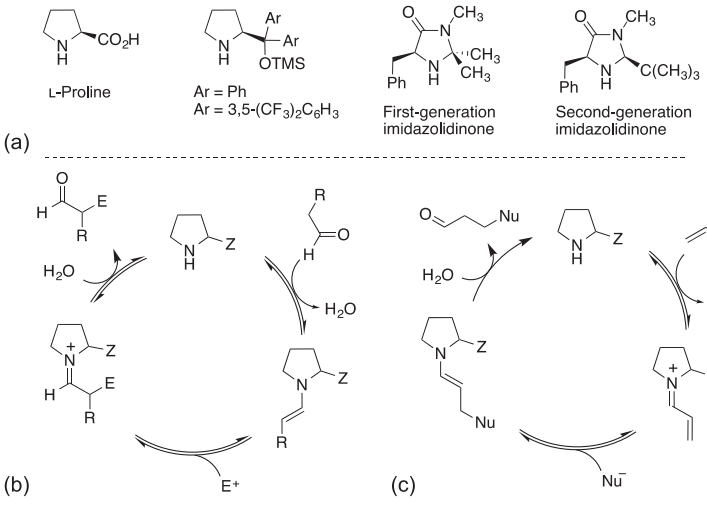

Scheme 4.1 (a) Representative secondary amine covalent organocatalysts. (b) Enamine organocatalysis. (c) Iminium organocatalysis.

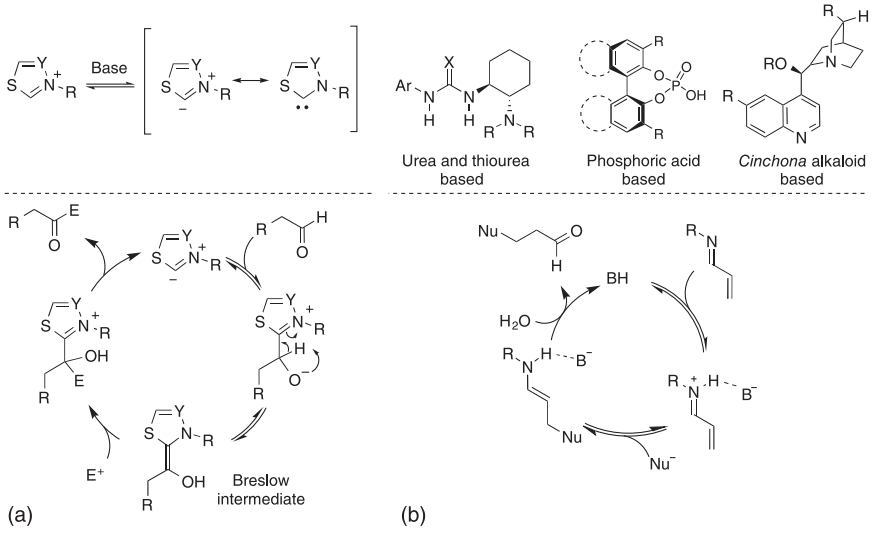

Scheme 4.2 (a) N-Heterocyclic carbene catalysis. (b) Non-covalent organocatalysis.

catalysis. These covalent mechanisms normally require high catalyst loadings, typically 20–30 mol% for proline-derived catalysis.

The usual method for activating carbonyl groups involves the attachment of an electrophilic catalyst, but a reverse strategy (*umpolung*) is also possible. N-heterocyclic carbene (NHC) catalysts, inspired in the natural thiazolium derivative thiamine (vitamin B_1), exhibit such an inverted reactivity and allow the carbonyl carbon to act as a nucleophile. A typical NHC catalytic cycle is shown in Scheme 4.2a.

Other important types of organocatalysts, acting by non-covalent mechanisms, include Brønsted acids, such as chiral binaphthyl-derived phosphoric acids; Brønsted bases, such as *Cinchona* alkaloids and their derivatives; and hydrogen-bonding donors, such as chiral urea and thiourea derivatives (Scheme 4.2b). These non-covalent interactions facilitate low catalyst loadings (down to 0.001 mol%).

4.2 Organocatalytic Synthesis of Five-Membered Heterocycles

4.2.1 Pyrroles and Pyrrolidines

Pyrrole derivatives are common in nature and are very important in materials science and medicinal chemistry. The construction of pyrroles by organocatalytic methods has been recently reviewed [2], and we will give herein a representative example based on the combination of the sila-Stetter and Paal–Knorr reactions in the presence of the thiazolium catalyst **3**. Thus, the sequential three-component reaction between chalcones **1**, acylsilanes **2**, and primary amines in the presence of the thiazolium derivative **3** afforded the polysubstituted pyrroles **4** in a one-pot procedure (Scheme 4.3) [3].

The mechanism proposed for this complex transformation is shown in Scheme 4.4. The sila-Stetter reaction involves the generation of carbene **5** by DBU deprotonation of the thiazolium catalyst **3**. Its addition to the starting acylsilane **2** furnishes intermediate **6**, which undergoes a Brook rearrangement, i.e. a 1,2-silyl group C–O shift, yielding **7**, which is desilylated by the isopropyl alcohol additive to give **8**. The reaction then follows the usual Stetter mechanism by a conjugate addition of **8** to chalcone **1**, leading to intermediate **9**, which is fragmented to yield the regenerated carbene **5** and 1,4-diketone **10**, the starting point for the final Paal–Knorr reaction that furnishes the pyrrole products **4**.

The synthesis of axially chiral pyrroles has been the subject of much recent interest. As an example, an atroposelective synthesis of 1,5-diarylpyrroles **12** developed by Tan and coworkers using chiral phosphoric acid catalyst **11** is shown in Scheme 4.5 [4].

Pyrrolidines and their fused derivatives are also very important structural motifs in natural products and drug candidates [5]. For instance, the pyrrolo[2,3-*b*]indoline framework is present in a large number of bioactive alkaloids and has been the

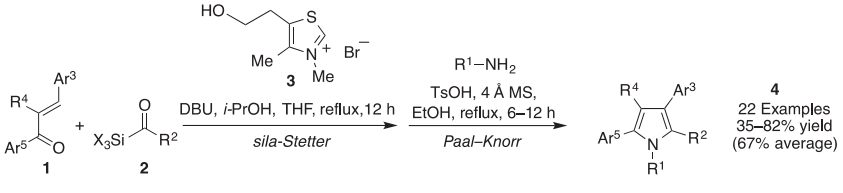

Scheme 4.3 Synthesis of pyrroles from chalcones, acylsilanes, and primary amines.

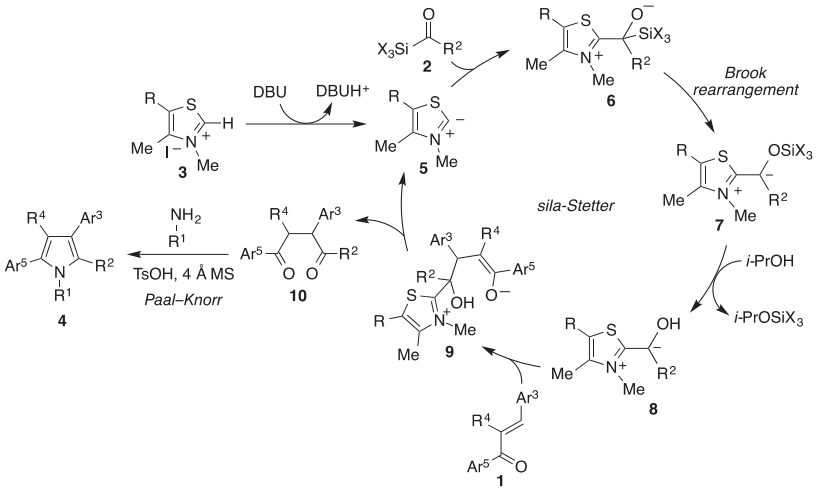

Scheme 4.4 Proposed mechanism for the sila-Stetter/Paal–Knorr sequence leading to pyrroles **4**.

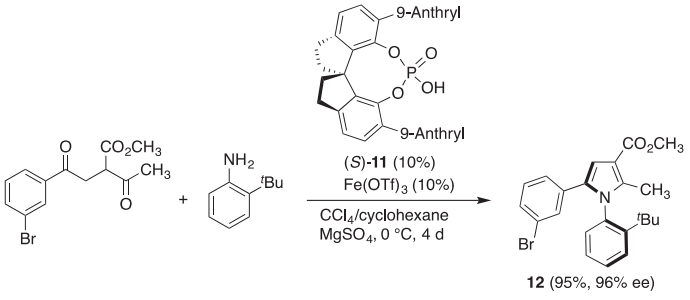

Scheme 4.5 An organocatalytic atroposelective synthesis of 1,5-diarylpyrroles.

subject of much synthetic work. MacMillan reported a brief enantioselective synthesis of the chiral pyrrolo[2,3-*b*]indoline **15** based on the generation of a pyrrolidine ring via an addition–cyclization process of the *N*-prenyltryptamine derivative **13** with acrolein in the presence of the chiral imidazolidinone organocatalyst **14**. Compound **15** was then transformed in three steps into alkaloid (−)-flustramine B (Scheme 4.6) [6].

The mechanism of the key step that generates both stereocenters of the natural product involves iminium catalysis and starts with the reaction of the MacMillan catalyst **14** with acrolein to give intermediate **16**. This electrophile reacts with tryptamine **13** at the C-3 position of the indole ring to furnish **17**, which is cyclized in 5-*exo*-dig fashion to yield the pyrrolo[2,3-*b*]indoline framework. A final hydrolytic step releases aldehyde **18**, a straightforward precursor to **15**, and regenerates the catalyst, thus closing the catalytic cycle (Scheme 4.7).

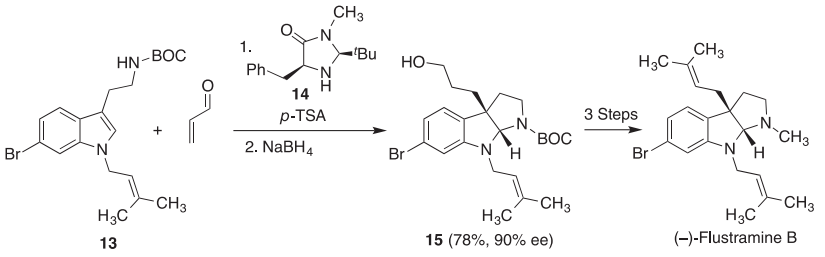

Scheme 4.6 Enantioselective organocatalytic synthesis of (–)-flustramine B.

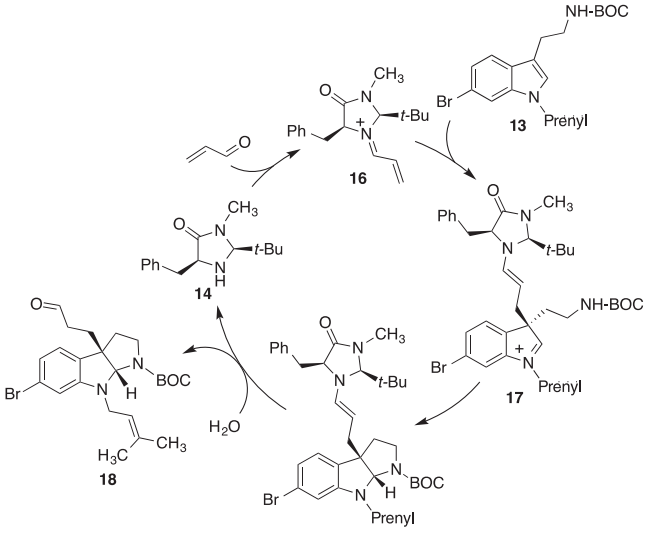

Scheme 4.7 Organocatalytic cycle explaining the formation of the flustramine precursor **18**.

4.2.2 Furan and Benzofuran Derivatives

The tetrahydrofuran and dihydrobenzofuran scaffolds are present in a large variety of natural products including macrolide antibiotics, polyether ionophores, and plant lignans. Many efforts have been done toward their enantioselective synthesis by organocatalytic methods, and we will summarize some representative examples in the following text [7].

Enders and coworkers reported a three-step synthesis of doubly functionalized 2,3,4-trisubstituted tetrahydrofurans, using organocatalysis to promote the key initial step. As shown in Scheme 4.8, treatment of aldehydes **19** and the conjugated nitro olefin **20** in the presence of the Hayashi catalyst **21** afforded the chiral nitroaldehyde **22** through a *si–si* attack of an intermediate enamine onto the nitro olefin. A subsequent carbonyl reduction followed by an intramolecular oxa-Michael reaction afforded the target tetrahydrofuran derivatives **23** [8].

Jørgensen and coworkers have described a one-pot approach to the synthesis of derivatives of the cyclopenta[*b*]benzofuran scaffold (compounds **27**), which

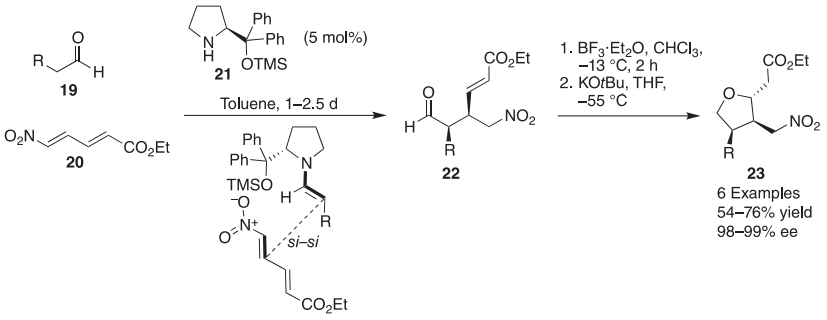

Scheme 4.8 Organocatalytic synthesis of functionalized tetrahydrofurans.

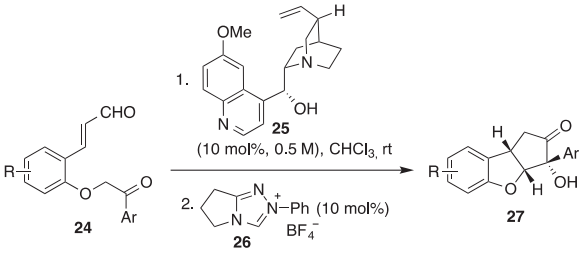

Scheme 4.9 Synthesis of cyclopenta[*b*]benzofurans via an organocatalytic double cyclization approach.

is present in several bioactive natural products such as the flavaglines. These compounds are reached via an intramolecular double cyclization process starting from compounds **24** and require the participation of two catalysts, namely, quinine (**25**) and compound **26**, the precursor of an NHC (Scheme 4.9) [9].

The mechanism proposed involves two orchestrated catalytic cycles, which are shown in Scheme 4.10. Quinine **25**, acting as a base, deprotonates the α-position to the ketone in substrate **24** and the resulting chiral ammonium ion and enolate interact by hydrogen bonding interactions to generate intermediate **28**. The bulk created by the catalyst directs the stereochemistry of the first cyclization, which takes place by way of an intramolecular Michael addition and affords the benzofuran derivative **29**. For the second catalytic cycle, quinine deprotonates **26** to generate carbene **30**, which promotes an intramolecular benzoin condensation that furnishes the final product **27**.

4.3 Organocatalytic Synthesis of Six-Membered Heterocycles

4.3.1 Pyridines, Dihydropyridines, and Piperidines

Pyridines and their reduced and fused derivatives are a large family of heterocyclic structures belonging to the "privileged scaffold" category in drug discovery [10].

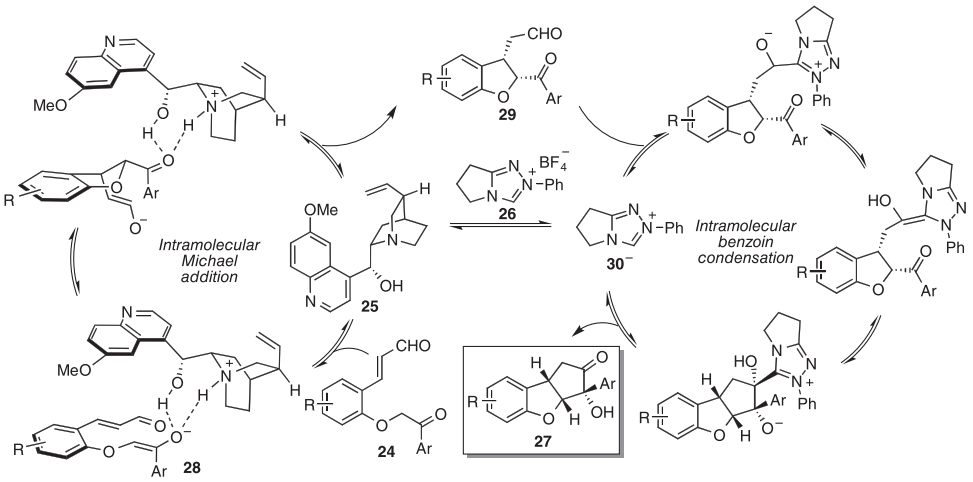

Scheme 4.10 Two catalytic cycles involved in the double cyclization leading to cyclopenta[*b*]benzofurans **27**.

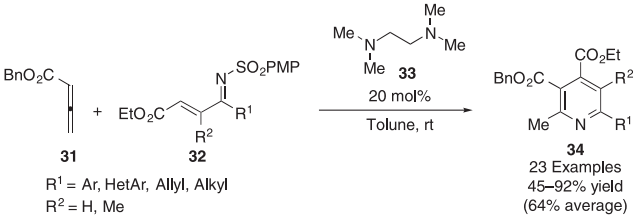

Scheme 4.11 Pyridine synthesis based on an organocatalytic aza-Rauhut–Currier reaction.

These structures may be found in a huge number of compounds and natural products with broad spectra of relevant bioactivities. Usually, pyridines are obtained under thermal conditions or under metal catalysis, but organocatalysis represents a safer alternative to metal-catalyzed reactions, reducing the time and temperature of these reactions, usually allowing to start from less expensive reagents and catalysts and reducing the toxicity associated to some metals [11].

Highly functionalized pyridines **34** with diverse substitution patterns were obtained in good yields by an aza-Rauhut–Currier reaction/cyclization/desulfonation cascade process from allenoates **31** and 1-aza-1,3-dienes **32** in the presence of *N*,*N*,*N*′,*N*′-tetramethylethane-1,2-diamine (TMEDA, **33**) with considerable advantages in terms of catalyst stability and ease of handling over the more usual phosphine catalysts (Scheme 4.11) [12].

The mechanism proposed for this transformation starts with the addition of the catalyst **33** to the starting allenoate **31** to yield the 1,3-dipolar intermediate **35**, which undergoes a Michael addition to the azadiene **32** to furnish **36**, which isomerizes to **37** and undergoes cyclization to **38** and a final aromatization to **34** with concomitant loss of a molecule of sulfonic acid (Scheme 4.12).

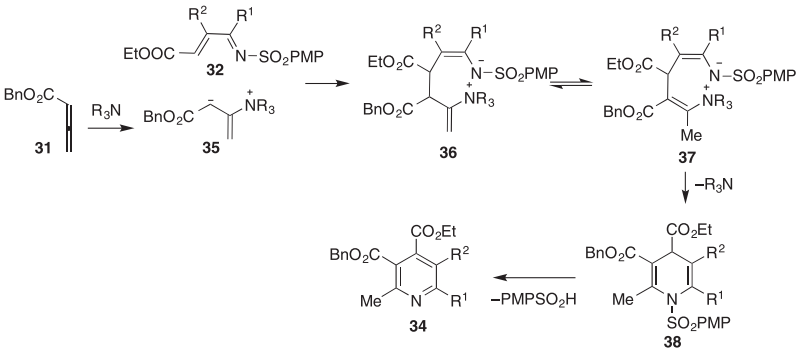

Scheme 4.12 Mechanism of the organocatalytic aza-Rauhut–Currier reaction and subsequent steps.

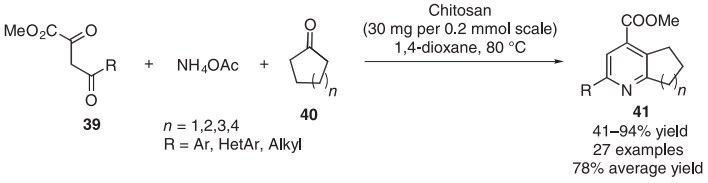

Scheme 4.13 Chitosan-catalyzed Guareschi–Thorpe pyridine synthesis.

Polysaccharides have also been described as promising organocatalysts in pyridine synthesis. An example of this strategy is the preparation of fused pyridines **41** by a chitosan-organocatalyzed heterogeneous Guareschi–Thorpe reaction from β-ketoesters **39**, ammonium acetate, and cyclic ketones **40** (Scheme 4.13). Chitosan is a carbohydrate-based polymer with amino groups exposed in its surface, which gave better results than other amine-based organocatalysts and showed a robust functional group tolerance [13]. The heterogeneous nature of this catalyst enabled its reutilization up to four times without a significant drop in yield.

1,4-Dihydropyridines (DHPs) are pharmacologically very relevant and very important targets for organocatalytic enantioselective synthesis [10, 14]. The Hantzsch reaction, which was first reported in 1881 [15], is still considered as the best method to access symmetrically substituted 1,4-DHPs. In a representative organocatalytic Hantzsch reaction, Kumar and Maurya demonstrated the synthesis of hexahydroquinolines **45** through a four-component reaction between aryl aldehydes **42**, acyclic β-dicarbonyl compounds **43**, dimedone **44**, and ammonium acetate at room temperature under solvent-free conditions (Scheme 4.14) [16]. After a careful optimization, L-proline proved be the best catalyst, leading to products **45** in excellent yields. A related transformation starting from ethyl acetoacetate, 1,3-indanedione, and ammonium acetate was also reported for the synthesis of unsymmetrical fused 1,4-DHPs in the presence of L-proline in water under reflux conditions [17].

The authors proposed two different pathways to explain the isolation of compounds **45**: (i) Proline, via iminium catalysis, promotes the condensation between

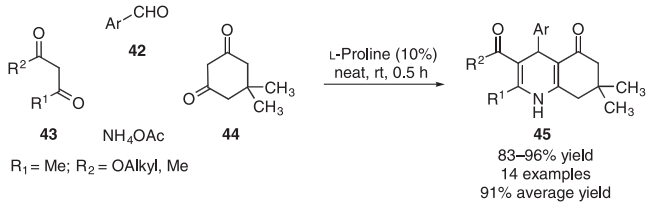

Scheme 4.14 Proline-catalyzed Hantzsch synthesis of unsymmetrical fused dihydropyridines.

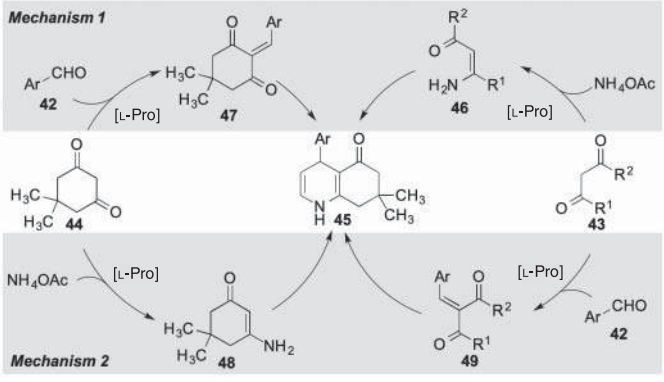

Scheme 4.15 Two mechanistic proposals for the proline-catalyzed Hantzsch synthesis of unsymmetrical fused dihydropyridines.

β-dicarbonyl compound **43** and ammonium acetate. The resulting enaminone **46** reacts with the Knoevenagel product **47**, previously formed by proline-promoted condensation of aldehyde **42** and dimedone **44** (top half of Scheme 4.15); (ii) Dimedone can also react with ammonium acetate, leading to the corresponding enaminone **48**, which then reacts with the Knoevenagel adduct **49**, arising from the condensation of the aldehyde and β-dicarbonyl components (bottom half of Scheme 4.15).

The chirality of DHPs is crucial for their bioactivity profile [18]. Both enantiomers often show different biological activities, and they can even have opposite effects. This was well described for DHP calcium channel blockers and exemplified by (−)-*S*-amlodipine [19], (+)-*S*-manidipine [20], and (−)-*S*-nitrendipine [21], which were more active compared with their respective enantiomers. Thus, the asymmetric synthesis of 1,4-DHPs has become a highly sought goal in medicinal chemistry, and organocatalysis appears as the most promising strategy to achieve it [14].

The first asymmetric organocatalytic Hantzsch DHP synthesis dates back to 2007 and was developed by Renaud and coworkers (Scheme 4.16) [22]. They first established the ability of racemic biphenol-based phosphoric acids (**50a,b**) to catalyze the reaction and **50b** was chosen as a model catalyst to obtain 13 compounds in modest to good yields (32–89%). Then, this study was expanded to three different chiral BINOL-derived phosphoric acid catalysts, observing in one case a selective

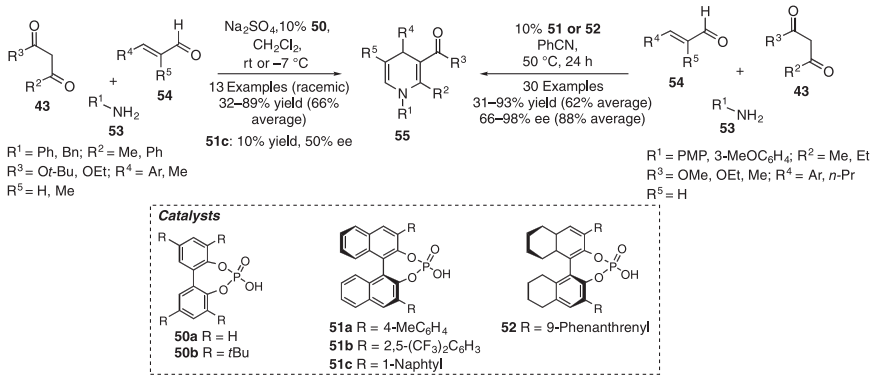

Scheme 4.16 Enantioselective Hantzsch dihydropyridine synthesis catalyzed by chiral phosphoric acids.

Michael addition of the β-enaminoester to the unsaturated aldehyde in a modest 50% ee for the case of catalyst **51c**. After this result, other BINOL-based phosphoric acids (**52**) were successfully studied as catalysts of the multicomponent reaction between 1,3-dicarbonyl compounds **43**, primary amines **53**, and α,β-unsaturated aldehydes **54** to furnish DHPs **55**. The mechanism proposed by the authors starts with the condensation of aldehyde **54** and amine **53** to afford the corresponding α,β-unsaturated imine. This intermediate is activated in iminium form by the chiral phosphoric acid. Then, the 1,3-dicarbonyl compound reacts with the iminium β-position in a enantioselective fashion and after cyclization and subsequent dehydration furnishes the 1,4-DHP **55** in good yields (31–93%) and good to excellent enantioselectivities (66–98%) [23]. Similarly, the use of a chiral BINOL-phosphoric acid catalyst was reported to allow the enantioselective synthesis of hexahydroquinolines [24], but unfortunately these results have not proved reproducible [25].

Jørgensen and coworkers [26] and Kanger and coworkers [27] described asymmetric protocols for the synthesis of 1,4-DHPs (compounds **56**) through amine catalysis, in the presence of the diarylprolinol-TMS ether derivatives **57a**,**b**, either from isolated β-enamines **46** and α,β-unsaturated aldehydes **54** or via a three-component fashion (Scheme 4.17). While both methods enabled the preparation of 1,4-DHPs substituted at the positions 1, 3, and 4, the three-component Jørgensen approach gave poor enantioselectivities in the case of aromatic aldehydes (38–64% ee) compared with the Kanger method (71–96% ee), which also afforded better yields. The three-component transformation is an enantioselective version of a Ce(IV)-catalyzed sequential three-component synthesis of DHPs reported by our group [28].

The three-component protocol were proposed to start with the formation of an iminium cation from the α,β-unsaturated aldehyde. Then, the 1,3-dicarbonyl compound or the corresponding β-enaminone (paths A and B, respectively) reacts selectively with the iminium species from a single face of the molecule. The resulting intermediate then undergoes a cyclization step to afford the 1,4-DHP (Scheme 4.18).

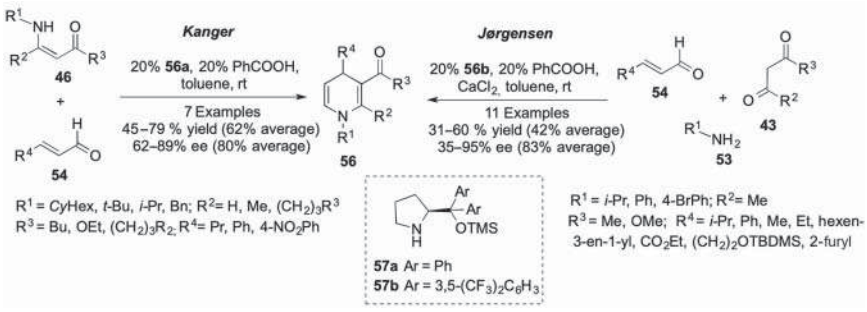

Scheme 4.17 Enantioselective dihydropyridine synthesis catalyzed by diarylprolinol TMS ethers.

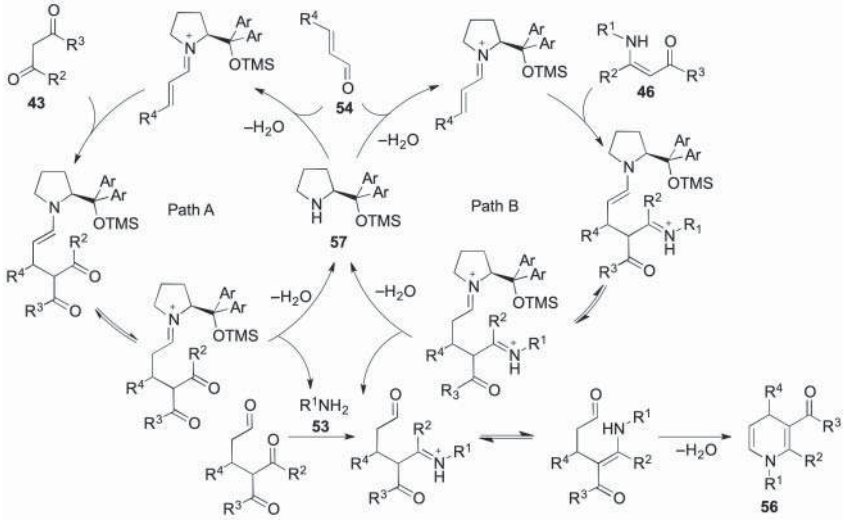

Scheme 4.18 Two catalytic cycles that explain the diarylprolinol TMS ether-catalyzed enantioselective dihydropyridine synthesis.

The Kanger approach followed pathway B, since it started from an isolated enaminone, and a mass spectral study allowed to verify the presence of the proposed intermediates in the reaction mixture.

Takemoto and coworkers introduced a combination of a chiral thiourea and a Brønsted acid to catalyze the same reaction [29]. The best results corresponded to the use of a 1 : 1 mixture of difluoroacetic acid (DFA) and the thiourea **58c** and afforded the 5,6-unsubstituted 1,4-DHPs **56** in good yields (55–96%) and modest to good enantioselectivities (38–80% ee). This reaction was rationalized on the basis of catalyst association by a network of hydrogen bonds between the thiourea moiety and the difluoroacetate anion. The ammonium proton activates the α,β-unsaturated aldehyde and the conjugate base the β-enaminone, promoting the Michael addition in an enantioselective fashion (Scheme 4.19).

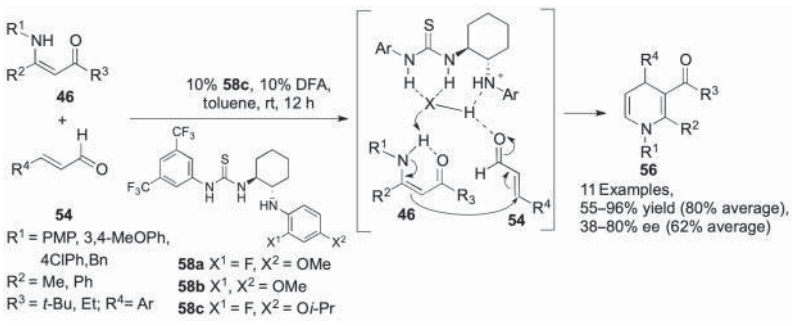

Scheme 4.19 Bicatalytic enantioselective synthesis of 1,4-DHPs in the presence of a chiral thiourea and its proposed mechanism.

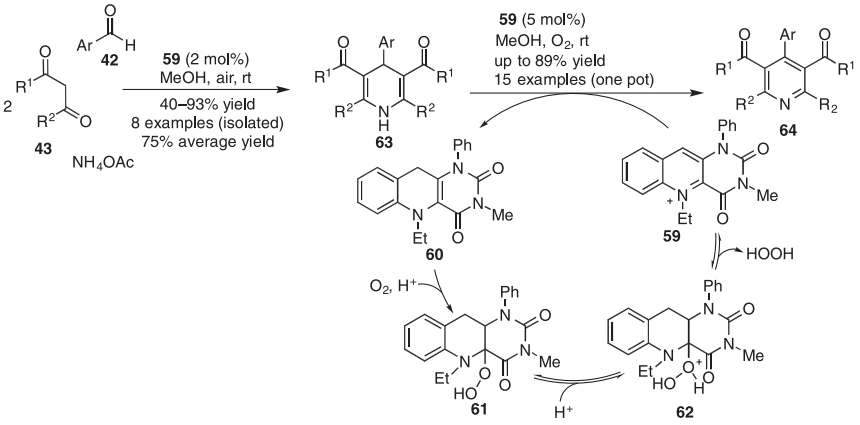

Scheme 4.20 One-pot Hantzsch reaction–dehydrogenation sequence promoted by a synthetic flavin.

We will finally discuss some examples of one-pot procedures comprising a Hantzsch synthesis of dihydropyridines and their oxidation to pyridine. The nature-inspired synthetic flavin **59** is able to catalyze the Hantzsch reaction and also to promote two-electron oxidation processes outside of any enzyme active site [30]. The flavin precatalyst **60** is oxidized by oxygen in an aerobic system leading to **61**, which is transformed into **59** with loss of hydrogen peroxide. Then, **59** oxidizes the Hantzsch DHP **63** to pyridine **64** after acidic activation and regenerates the reduced species **60**, able to start again this redox cycle (Scheme 4.20). This organocatalytic oxidation can be used to achieve direct access to pyridines from acyclic precursors (aldehydes **19**, β-dicarbonyls **43**, and ammonium acetate) or the oxidative process can start from DHP derivatives **63** obtained by other methods.

Bressy, Bugaut, and Rodriguez [31] have taken advantage of the chiral thiourea-catalyzed Hantzsch reaction to develop an atroposelective synthesis of fused pyridine derivatives **66** via an innovative central-to-axial conversion of chirality process [32] starting from the chiral Hantzsch DHPs **65** (Scheme 4.21).

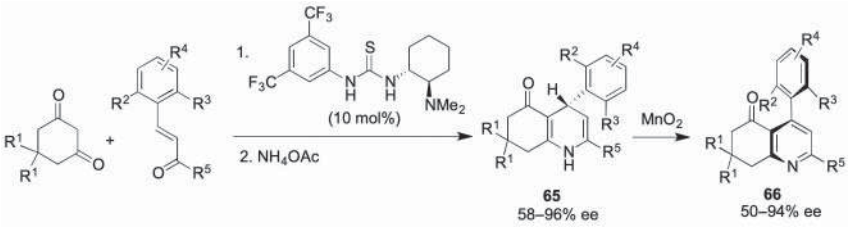

Scheme 4.21 Atroposelective synthesis of pyridines based on an enantioselective Hantzsch dihydropyridine synthesis.

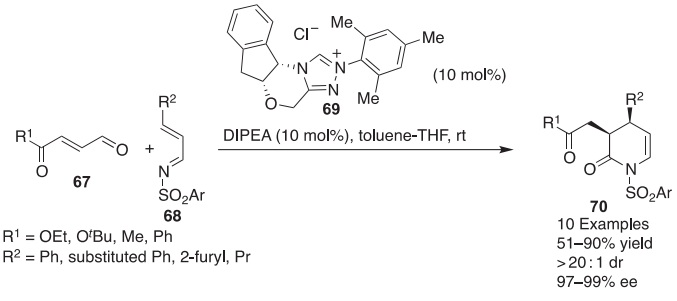

Scheme 4.22 Enantioselective synthesis of 2-pyridones catalyzed by a chiral N-heterocyclic carbene.

Bode reported the first enantioselective aza-Diels–Alder reaction catalyzed by a chiral NHC, which was generated from the *cis*-1,2-aminoindanol-based triazolium salt **69**. The chiral 2-pyridone derivatives **70** were obtained from dicarbonyl compounds **67** and the 1-azadienes **68** in excellent diastereo- and enantioselectivities (Scheme 4.22) [33].

These results were explained by the mechanism summarized in Scheme 4.23. The starting enal **67** reacts with the nucleophilic carbene catalyst **71**, forming the Breslow intermediate **72,** which can also be written as its homoenolate resonance structure. An intramolecular proton transfer then affords **73**, a very electron-rich dienophile that undergoes a Diels–Alder reaction with azadiene **68**, affording the dihydropyridinone derivatives **70** with regeneration of the catalyst. The high diastereoselectivity was rationalized by the preference for an *endo* transition state and the observed high enantioselectivity by the presence of the bulky 1,2-aminoindanol moiety.

Fustero described the synthesis of piperidine derivatives via highly enantioselective intramolecular aza-Michael reactions promoted by the Jørgensen catalyst. This process, which presumably proceeds via the iminium intermediate **74** (Scheme 4.24), was used as the basis for the total synthesis of the piperidine alkaloids (+)-sedamine, (+)-allosedamine, and (+)-coniine [34].

In another organocatalytic route to enantiopure piperidines, Vesely, Moyano, and Ríos reported an efficient and highly enantioselective reaction of α,β-unsaturated aldehydes and a malonamic ester derivative in the presence of the Hayashi catalyst

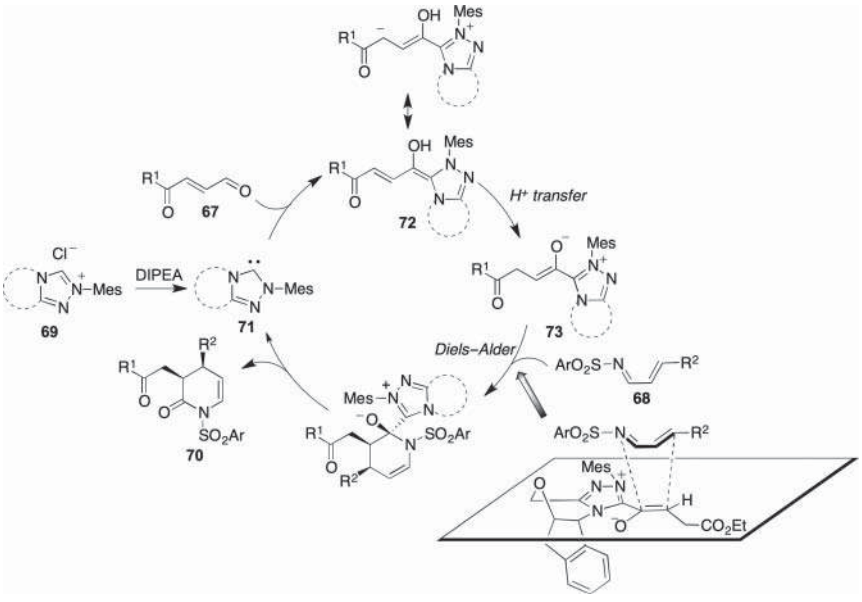

Scheme 4.23 Mechanistic explanation of the enantioselective aza-Diels–Alder reaction leading to chiral 2-pyridones **70**.

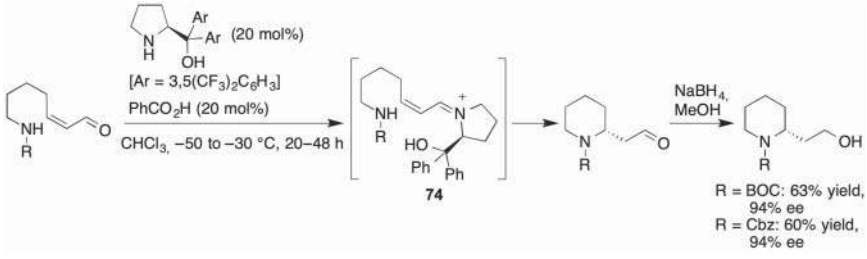

Scheme 4.24 Synthesis of piperidines by an organocatalytic enantioselective intramolecular aza-Michael reaction.

(Scheme 4.25). This methodology allowed a concise formal synthesis of the antidepressant drug paroxetine [35].

4.3.2 Fused Pyridine Derivatives

The 1,2,3,4-tetrahydroquinoline ring system is widespread in nature and is present in a large number of bioactive compounds. One of the main methods for its preparation is the Povarov reaction, i.e. the inverse electron demand formal [4+2] cycloaddition between aromatic imines and electron-rich olefins. Several organocatalytic versions of this reaction have been reported, starting from the enantioselective synthesis of tetrahydroquinolines in the presence of chiral phosphoric acids. One example is the reaction reported by Gong and coworkers, who described a three-component Povarov reaction from anilines, aldehydes, and 2-hydroxystyrene **75**, acting as the

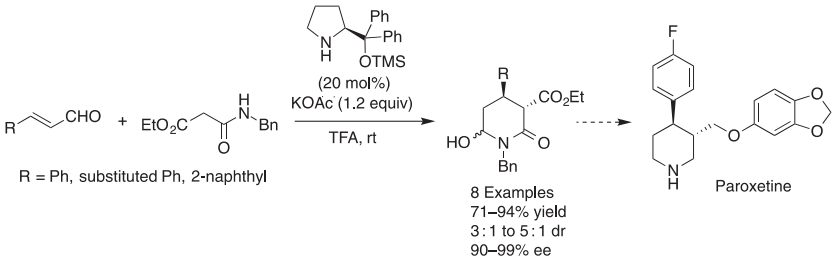

Scheme 4.25 Enantioselective synthesis of piperidines from α,β-unsaturated aldehydes and malonamic esters.

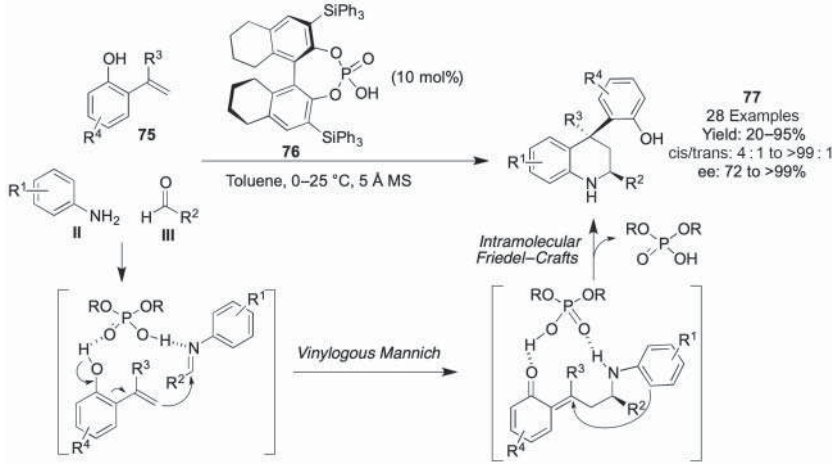

Scheme 4.26 An example of a Povarov reaction catalyzed by a chiral phosphoric acid.

dienophile, in the presence of the chiral phosphoric acid **76**. This reaction furnished *cis* tetrahydroquinolines **77** in 99 : 1 dr and 97% ee [36]. A computational study suggested that this reaction proceeds stepwise and comprises a vinylogous Mannich reaction and an intramolecular Friedel–Crafts cyclization, in which the catalyst activates both the diene and the dienophile (Scheme 4.26).

Jacobsen examined in 2010 a new method to induce enantioselectivity in the Povarov reaction by cooperative Brønsted acid and H-bond donor catalysis [37, 38]. After extensive optimization work, the chiral sulfinamidourea **79** and the strong Brønsted acid *o*-nitrobenzenesulfonic acid **80** were selected as cocatalysts. This catalytic system promoted the Povarov reaction of a broad range of imines **78** and a number of dienophiles, including *N*-vinylpyrrolidones **81**, *N*-benzyloxycarbonyl-2,3-dihydropyrroles **82**, and 2,3-dihydrofuran **83**, and yielded tetrahydroquinolines **84**–**86**, respectively, in good yields and enantioselectivities (Scheme 4.27). A detailed computational mechanistic study led to the proposal of a concerted, nonsynchronous mechanism via the transition state shown in Scheme 4.28, where the sulfinamidourea and triflate groups act as H-bond acceptors and the iminium species as a H-bond donor. The enantioselectivity of

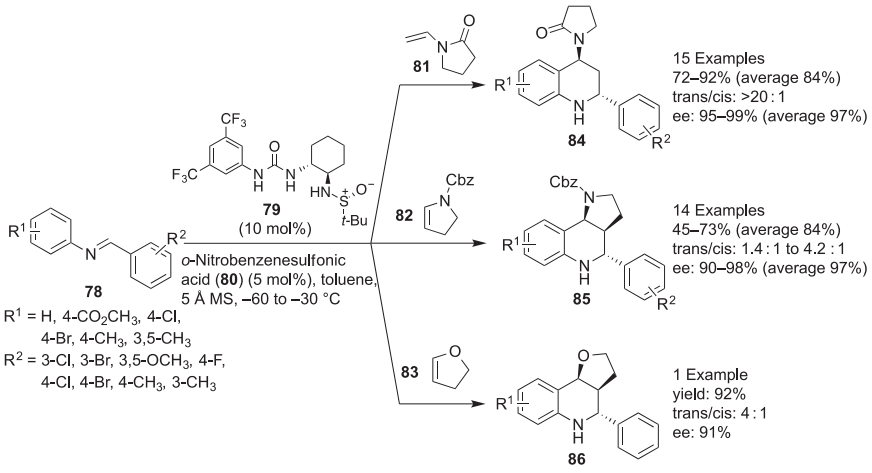

Scheme 4.27 Povarov reactions catalyzed by a chiral thiourea-Brønsted acid combination.

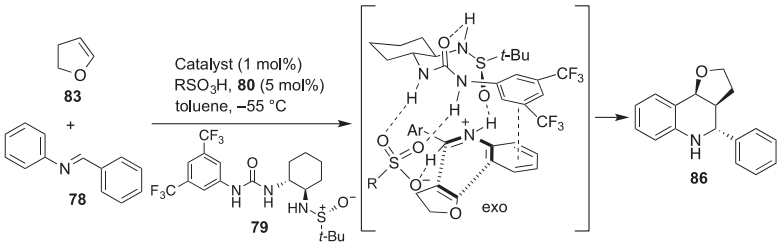

Scheme 4.28 Explanation of the enantioselectivity of the chiral thiourea-promoted Povarov reaction.

the reaction was attributed to stabilizing π–π interactions between the aromatic component of the catalyst and the aryl moiety of the imine coming from the aniline (Scheme 4.28).

As another example of the generation of a tetrahydroquinoline ring system, we will discuss the synthesis of dibenzo[*af*]quinolizine derivatives in racemic form through an amine-catalyzed dehydrogenative domino process starting from *N*-aryltetrahydroisoquinolines **87** and crotonaldehyde **88** in good yields and diastereoselectivities (Scheme 4.29). After optimization, the authors chose the MacMillan imidazolidinone catalyst **89**, together with benzoic acid and DDQ, and the aldehyde function was reduced with sodium borohydride in an additional step to afford the stable compounds **90** [39].

The mechanism proposed for this transformation is summarized in Scheme 4.30 and involves the initial reaction of crotonaldehyde **88** with the secondary amine **89** to yield dienamine **91**. On the other hand, the iminium derivative **92** is formed from oxidation of the starting material **87** by DDQ. This intermediate is trapped by **91** and furnishes the unsaturated iminium ion **93**, which provides **94** by an intramolecular vinylogous Mannich reaction. Finally, the hydrolysis of the enamine would yield the aldehyde **95** while closing the catalytic cycle by regenerating the catalyst **89**.

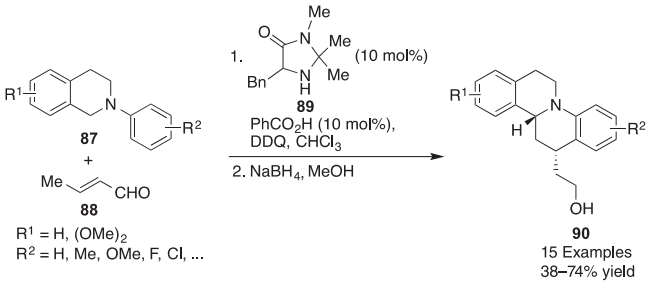

Scheme 4.29 Organocatalytic enantioselective synthesis of dibenzo[*af*]quinolizines.

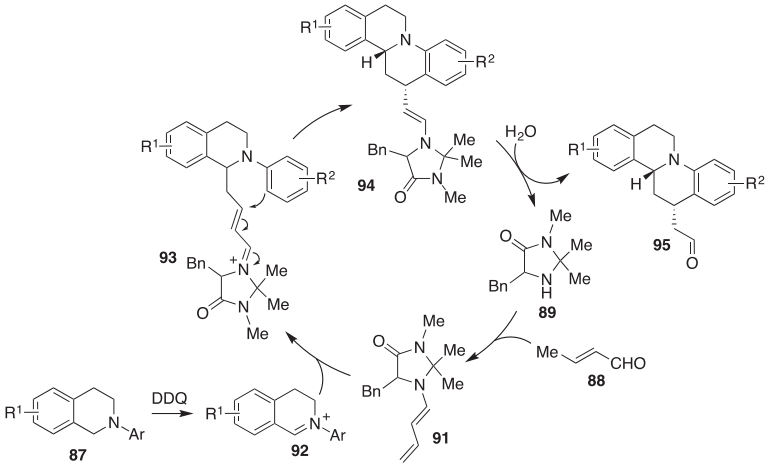

Scheme 4.30 Mechanistic proposal to explain the formation of dibenzo[*af*]quinolizines.

4.3.3 Pyrimidines

The Biginelli reaction is a three-component process starting from aldehydes, β-ketoesters, and urea to yield dihydropyrimidones, which are very interesting compounds from the pharmaceutical point of view. There has been much recent interest in organocatalyzed Biginelli reactions, which have been performed with a large number of catalysts [40]. As an example, the first enantioselective Biginelli reaction, developed by Gong using the chiral phosphoric acid **96** as catalyst, is shown in Scheme 4.31.

4.3.4 Pyran and Fused Pyrans

Pyrans and their polysubstituted and fused systems such as benzopyran, chroman, xanthane, and coumarin, among others, are widespread in natural and unnatural bioactive compounds. Organocatalysis, sometimes combined with the use of multicomponent procedures, offers an attractive approach to synthetize diversely substituted pyran derivatives. An example is the L-proline-catalyzed reaction

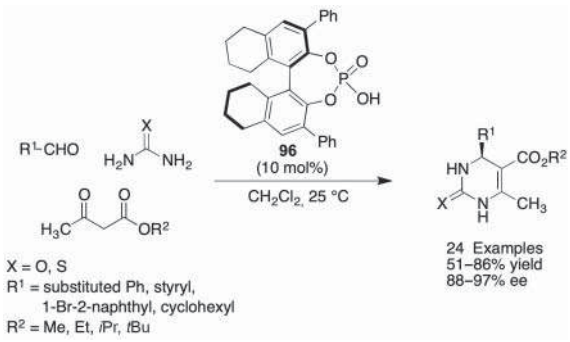

Scheme 4.31 Organocatalytic, enantioselective Biginelli reaction.

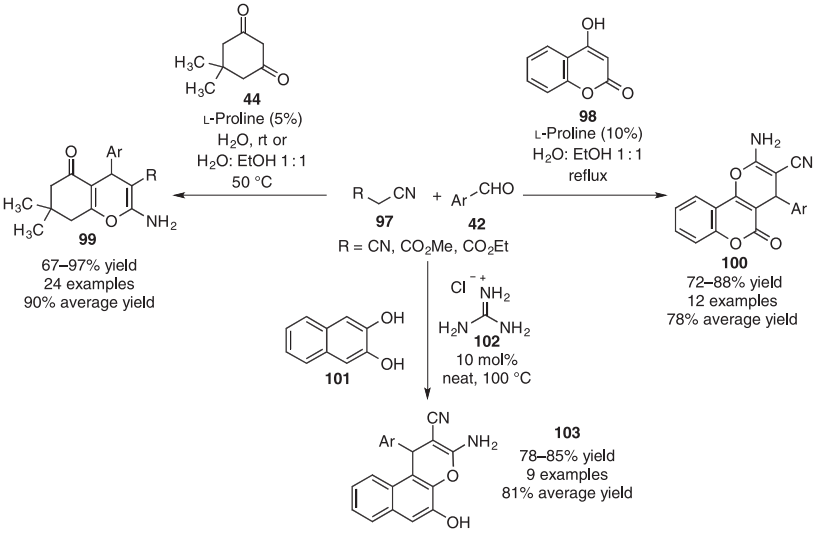

Scheme 4.32 Some organocatalytic syntheses of fused pyran derivatives.

between aromatic aldehydes **42**, active methylene nitriles **97**, and dimedone **44** or 4-hydroxycoumarin **98**, which allow the synthesis of fully and diversely substituted pyran rings by the formation of two bonds in a single operation. The approach described by Movassagh and coworkers [41] explores a wide range of aryl aldehydes and nitriles, leading to fused pyrans **99** in excellent yields. A similar procedure described by Abdolmohammadi and coworkers starts from aromatic aldehydes **42**, 4-hydroxycoumarin **98**, and malononitrile, affording 3,4-dihydropyrano[*c*]chromene derivatives **100** in good yields but in a limited scope compared with the previously described approach [42]. Recently [43], Olyaei et al. describe a similar methodology leading to a new class of benzo[*f*]chromene derivatives **103** starting from 2,3-dihydroxynaphthalene **101**, malononitrile, and aldehydes **42**, using guanidinium chloride (102) as organocatalyst under solvent-free reaction conditions (Scheme 4.32).

A related process catalyzed by proline triflate afforded diversely substituted benzoxanthenes **106** and **107** in good to excellent yields from aldehydes **104**, cyclic 1,3-diketones **105**, and α- or β-naphtol, respectively. The regioisomer formed depends on the naphthol isomer employed in the reaction, with α-naphtol furnishing the benzo[*c*]xanthenes **106** and β-naphtol their benzo[*a*]xanthene regioisomers **107** (Scheme 4.33). Aldehydes with electron-withdrawing or electron-donating substituents were well tolerated, but the use of aliphatic aldehydes, with the exception of 3-butenal, led to failure of the reaction [44].

Organocatalytic cycloaddition reactions have been extensively investigated as one of the most powerful tools for the quick construction of molecules via multiple C—C bond formations in a single step. In particular, the pyran ring can be obtained by a DABCO-catalyzed regioselective [4+2] cycloaddition described by Shi and coworkers (Scheme 4.34) [45]. This procedure was based in the reaction between β,γ-unsaturated α-ketophosphonates and β,γ-unsaturated α-ketoesters **108** with

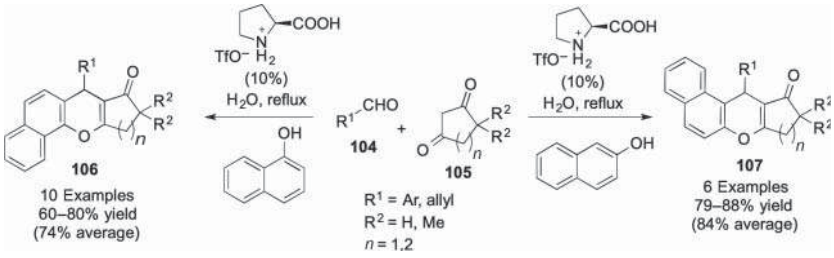

Scheme 4.33 Organocatalytic synthesis of benzoxanthenes.

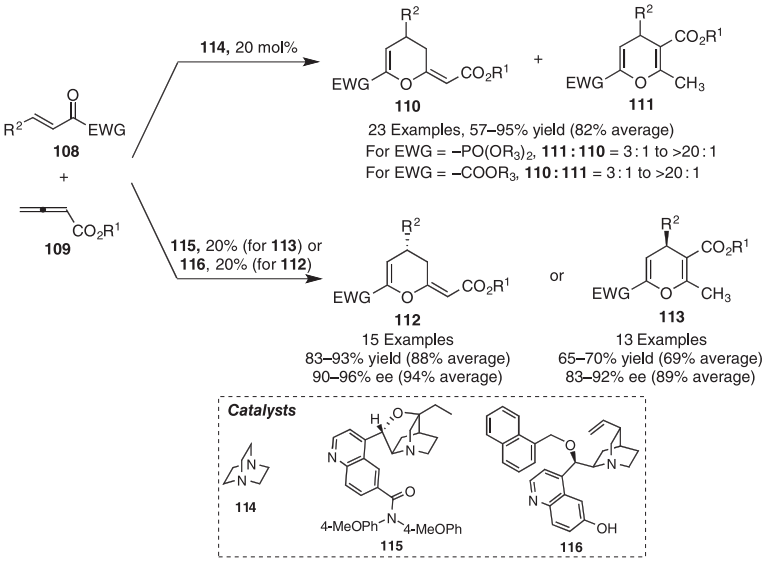

Scheme 4.34 Organocatalytic synthesis of pyran derivatives.

allenic esters **109**, affording the dihydropyran (**110**) and pyran (**111**) derivatives in good yields. The nature of the electron-withdrawing group was critical for the regioselectivity in this reaction. When EWG was a phosphonate, the dihydropyran **111** was favored compared with pyran **110**. However, a switch of EWG to an ester group led to a complete inversion of selectivity. This procedure was adapted to obtain enantioenriched pyran derivatives using different organocatalysts derived from *Cinchona* alkaloids [46]. Compounds **112** and **113** derivatives were obtained in good yields (65–93%) and enantioselectivities (83–96%). Besides their role in the induction of enantioselectivity, these chiral organocatalysts also have a large influence in regioselectivity. Thus, catalyst **115** promotes the formation of pyrans **113**, while dihidropyrans **112** were obtained as single regioisomer in the presence of **114**. The authors explain this full regioselectivity by a steric clash between naphthyl group from the catalyst and phosphonate group of the β,γ-unsaturated system.

4.4 Organocatalytic Synthesis of Seven-Membered Heterocycles

Seven-membered rings are often found in compounds with interesting biological activities, mainly as fused benzo derivatives.

4.4.1 Diazepines and Fused Diazepines

Glorius and coworkers [47] have described the reaction of α,β-unsaturated aldehydes **54** and *N*-Boc hydrazones **117** to afford 1,2-diazepines **118** or pyrazoles **119** just by switching the NHC precatalyst from **69** to **120** (Scheme 4.35). The proposed catalytic cycle is summarized in Scheme 4.36. The extended Breslow intermediates **121** and **122**, formed in the reaction of carbene **120** with aldehyde **54**, can follow two different pathways depending on the precatalyst used. When NHC precursor **69** is employed, intermediate **121** reacts with the *in situ* formed azoalkene **123** to give the acyl azolium **124**, which suffers an intramolecular acylation affording 1,2-diazepines

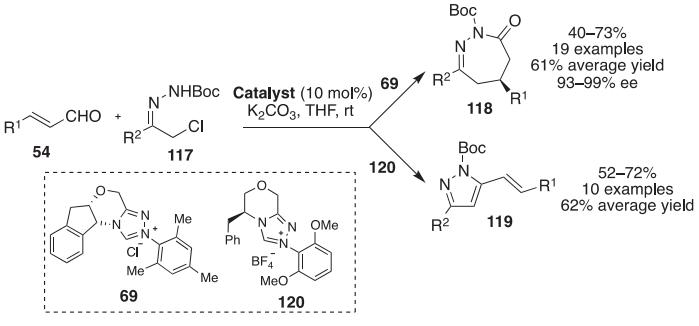

Scheme 4.35 Divergent synthesis of diazapines or pyrazoles under N-heterocyclic carbene catalysis.

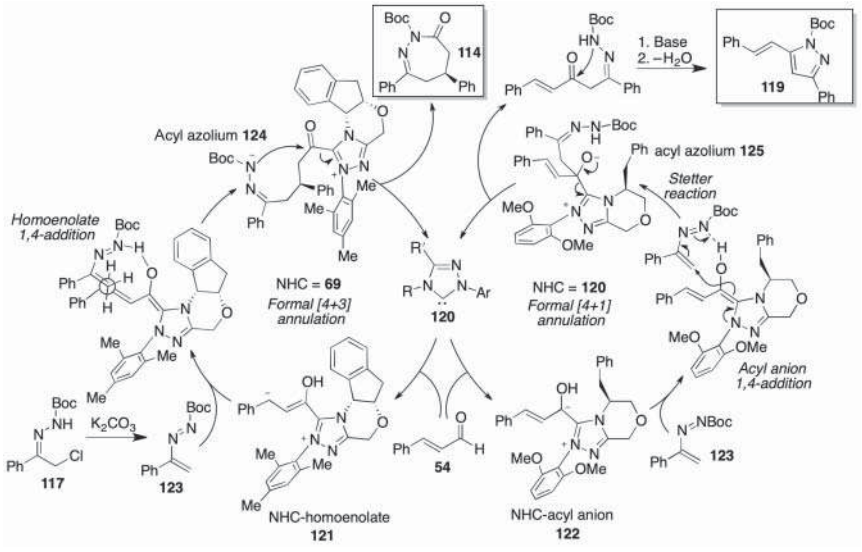

Scheme 4.36 Proposed mechanism for the divergent synthesis of 1,2-diazepines or pyrazoles under NHC catalysis.

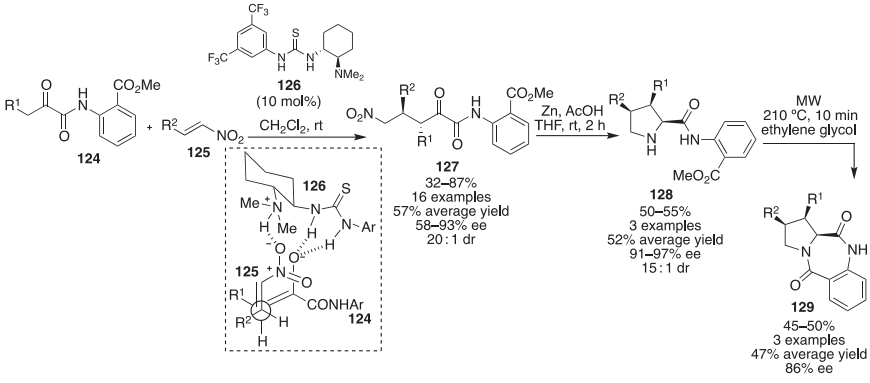

Scheme 4.37 Enantioselective synthesis of pyrrolidines and pyrrolo-1,4-benzodiazepine-2,5-diones based on a chiral thiourea-catalyzed Michael addition.

114. In the presence of NHC precatalyst **120**, intermediate **122** and azoalkene **123** give, through a Stetter reaction, acyl azolium **125**. Regeneration of NHC **120**, followed by an intramolecular cyclization and subsequent dehydration, furnishes pyrazoles **119**.

Rodríguez and coworkers [48] described a three-step enantioselective synthesis of the pyrrolo-1,4-benzodiazepine-2,5-dione framework, which is found in some bioactive natural products, such as asterelenin, aszonalenin, and oxotomamycin. As shown in Scheme 4.37, the reaction of 1,2-ketoamides **124** and nitro olefins **125**, catalyzed by the Takemoto thiourea catalyst **126**, gave the chiral Michael adducts **127** through a *si–re* attack of the (*Z*)-enolate onto the olefin. Treatment of **127** with

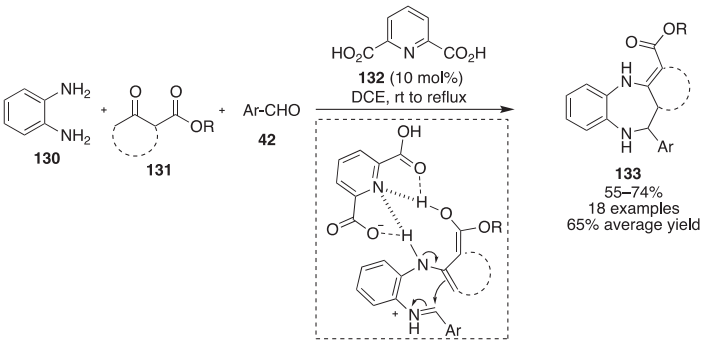

Scheme 4.38 2,6-PDCA-catalyzed multicomponent reaction for the synthesis of 1,5-benzodizepines.

activated Zn in acetic acid afforded pyrrolidines **128** in moderate yields but excellent diastereoselectivity, and these intermediates were finally converted into compounds **129** by heating under microwave irradiation.

Khan and coworkers [49] reported a multicomponent reaction for the preparation of 1,5-benzodizepines **133**, from *o*-phenylenediamine **130**, β-ketoesters **131**, and aromatic aldehydes **42** catalyzed by 2,6-pyridine dicarboxylic acid (2,6-PDCA) **132** (Scheme 4.38). The scope of the reaction admits a wide variety of aromatic aldehydes substituted with electron-withdrawing or electron-donating groups, heterocyclic aldehydes, and acyclic and cyclic β-ketoesters. The proposed mechanism relies on the acidity of **132** and its ability to establish intramolecular hydrogen bonds with the reaction intermediate.

4.4.2 Thiazepines and Fused Thiazepines

The enantioselective preparation of benzothiazepine derivatives has attracted much attention due to their pharmacological relevance, especially in the treatment of cardiovascular diseases. For instance, Asano and Matsubara have described [50] a regio- and enantioselective one-step synthesis of 2-substituted 1,5-benzothiazepines through an asymmetric formal [4+3] cycloaddition. Thus, the reaction of α,β-unsaturated carbonic anhydrides **134** and N-protected aminothiophenols **135** catalyzed by chiral cyclic isothiourea **136** afforded benzothiazepines **137** in good yields and high enantioselectivities. The reaction was assumed to proceed through an acyl ammonium intermediate **138**, generated by the reaction of **134** and the catalyst **136**, which undergoes a sulfa-Michael addition followed by cyclization. Mechanistic studies have suggested that the high regio- and enantioselectivity of this transformation can be attributed to the reversibility of the sulfur-Michael addition (Scheme 4.39). This methodology has also been applied to the enantioselective synthesis of 3-substituted and 3,5-disubstituted 1,5-benzothiazepines using related chiral thioureas as catalysts [51].

Fochi and Bernardi [52] reported an organocatalytic two-step procedure for the preparation of 2,3,4,5-tetrahydro-1,5-benzothiazepines (Scheme 4.40). First,

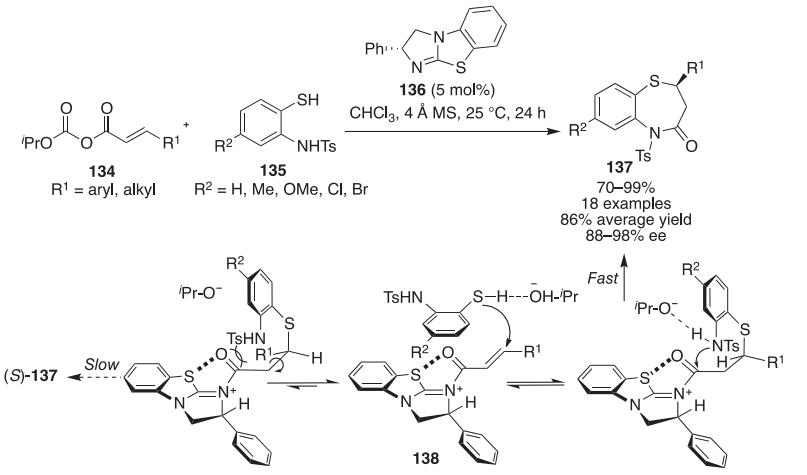

Scheme 4.39 Enantioselective synthesis of 2-substituted 1,5-benzothiazepines catalyzed by a chiral cyclic isothiourea.

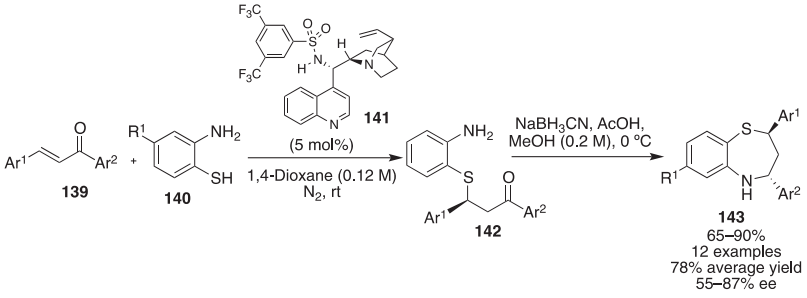

Scheme 4.40 Enantioselective synthesis of 2,3,4,5-tetrahydro-1,5-benzothiazepines.

chalcones **139** undergo a sulfa-Michael addition of 2-aminothioles **140** in the presence of the *Cinchona* organocatalyst **141** to give intermediate **142** with good enantioselectivity. Then, the cyclization step was carried out by a classic reductive amination, which proceeded without racemization.

4.5 Organocatalytic Synthesis of Polyheterocyclic, Bridged, and Spiro Compounds

In this final section we will first discuss some reactions that generate more than one heterocycle in a single operation, leading to polyheterocyclic frameworks. For instance, Perumal [53] has reported the preparation of structurally complex heterocyclic *ortho*-quinones **147** via a L-proline-catalyzed sequential four-component process starting from 2-hydroxynaphthalene-1,4-dione **144**, 3-aminocrotononitrile **145**, phenylhydrazine **146**, and aromatic aldehydes **42** (Scheme 4.41). Among the many solvents tested, water was found to be optimal in terms of yield and reaction

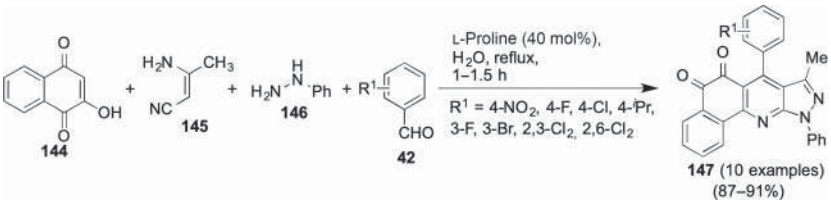

Scheme 4.41 L-Proline-catalyzed four-component synthesis of benzo[*h*]pyrazolo[3,4-*b*]quinoline-5,6(10*H*)-diones.

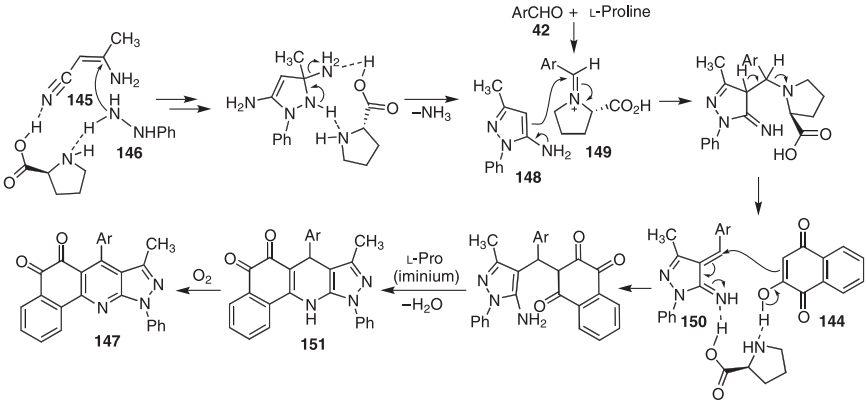

Scheme 4.42 Mechanism proposed to explain the formation of tetracyclic quinones **147**.

time, which was explained by the interaction of free OH groups of water with the organic reactants at the oil–water interface (*on-water* mechanism).

The mechanism proposed to explain the formation of compounds **147** is shown in Scheme 4.42. After an initial proline-facilitated Michael addition of phenylhydrazine **146** to 3-aminocrotononitrile **145**, an 5-*exo*-dig annulation is followed by the elimination of a molecule of ammonia to give 3-methyl-1-phenyl-1*H*-pyrazol-5-amine **148**. In parallel, aldehydes **42** are activated by reaction with L-proline via transformation into the iminium compounds **149**. Both fragments would then be joined by addition–elimination of **148** onto **149**, followed by loss of proline, yielding the pyrazole-derived 1-azadiene **150**. A Michael addition of hydroxynaphthoquinone **144** onto **150** followed by cyclization provides intermediate **151**, whose DHP ring is aromatized via air oxidation to furnish the final *o*-quinone products **147**.

As an example of the enantioselective generation of heterocyclic bridged compounds, Tang and coworkers [54] have developed an enantioselective synthesis of compounds **152**, with the controlled generation of four stereogenic centers via a Michael–aldol domino sequence catalyzed by the proline-related organocatalyst **151** (Scheme 4.43). The reaction was proposed to follow the usual catalytic cycle for enamine organocatalysis, as shown in Scheme 4.44.

Zhao and coworkers have reported the synthesis of the chiral spiro pyrazolone-tetrahydroquinolines **156**, which are of interest because they bear three contiguous

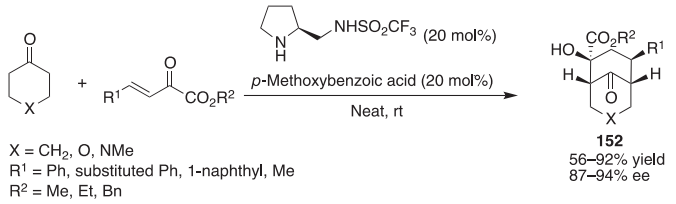

Scheme 4.43 Organocatalytic, enantioselective synthesis of bridged heterocyclic compounds.

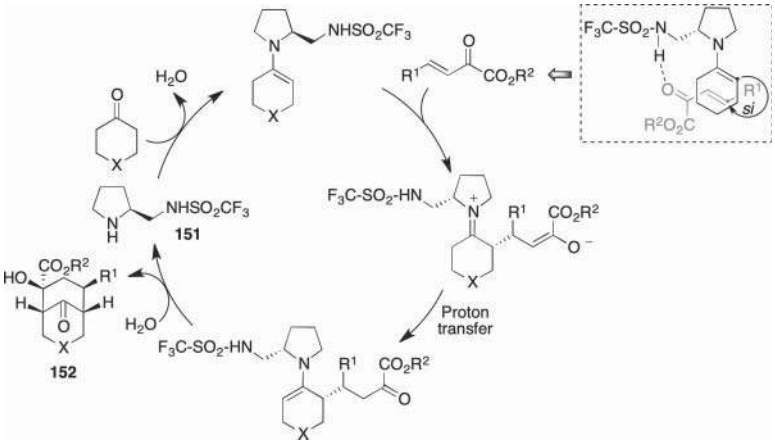

Scheme 4.44 Catalytic cycle proposed to explain the formation of compounds **152**.

stereogenic centers, starting from enones **153** and unsaturated pyrazolones **154** (Scheme 4.45). This transformation, which took place in excellent yields and generally good diastereo- and enantioselectivities, involved an aza-Michael/Michael reaction sequence. The catalyst employed was the chiral bifunctional organocatalyst **155**, which contains both a *Cinchona* alkaloid framework and a squaramide fragment, and was proposed to take place via a hydrogen bonding-stabilized transition state [55].

A stereoselective Michael addition of lactols **158** to electron-deficient 2-methyleneoxindole derivatives **157** promoted by the Hayashi catalyst was combined with a triethylamine-catalyzed Michael/Henry sequential process involving nitrostyrenes **159** to finally afford highly complex spirocyclic oxindole derivatives **160** [56]. These compounds contain six continuous stereogenic centers but their preparation nevertheless proceeded with full diastereoselectivity and excellent enantioselectivity (Scheme 4.46).

The mechanism proposed for this transformation is summarized in Scheme 4.47 and involves an initial Michael addition of enamine **161**, generated from the starting lactol **158** and the catalyst, to oxindole **157** to give intermediate **162**, which is hydrolyzed to **163**. This intermediate then reacts with the third component **159** via a Michael–intramolecular Henry sequence that furnishes the final product **160**.

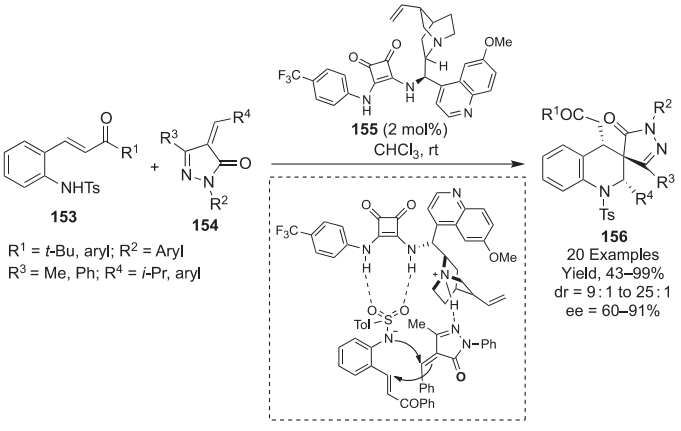

Scheme 4.45 Enantioselective synthesis of spiro pyrazolone-tetrahydroquinolines based on an enantioselective aza-Michael/Michael domino reaction.

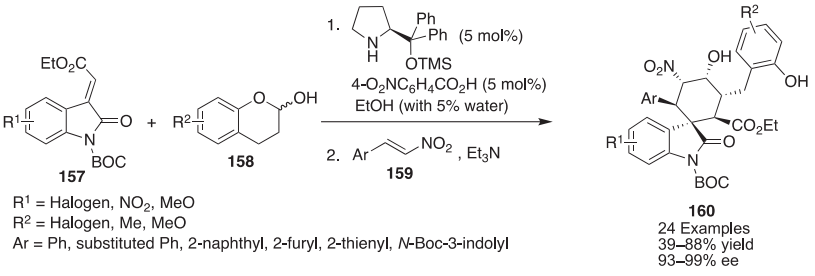

Scheme 4.46 Organocatalytic synthesis of spirocyclic oxindole derivatives **160**.

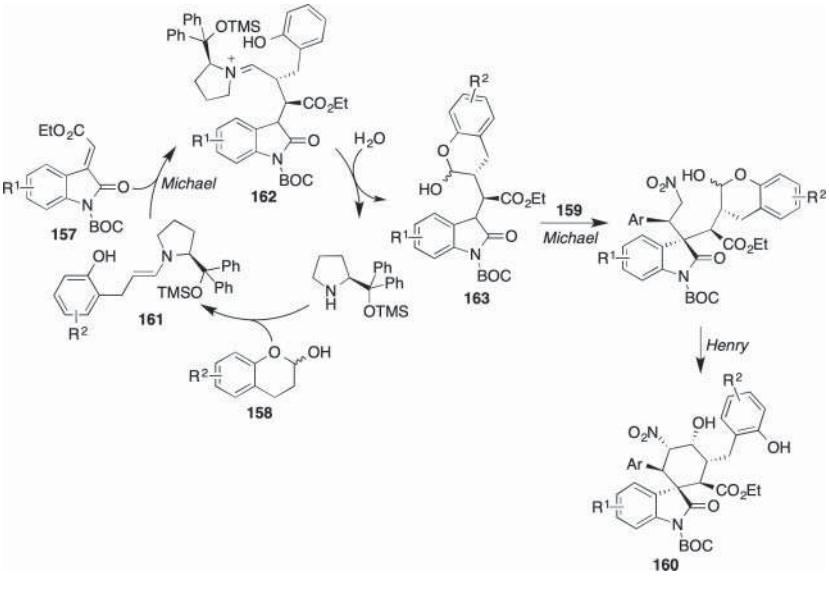

Scheme 4.47 Mechanistic explanation of the formation of compounds **160**.

4.6 Conclusion and Perspectives

Although organocatalysis is a relatively new concept, organocatalytic methods are steadily gaining importance in organic synthesis and in particular in the preparation of heterocycles, allowing the efficient assembly of many biologically relevant frameworks. Enantioselective organocatalysis is particularly promising for the construction of libraries formed by structurally diverse and complex chiral heterocyclic systems. Regarding future prospects, the synergic combination of organocatalysis with emerging technologies such as electrochemistry, photochemistry, and mechanochemistry can be safely envisioned as frontier topics in the next decade. The application of artificial intelligence to the design of catalysts will presumably also be an area of future growth [57].

Acknowledgments

We gratefully acknowledge financial support from MINECO (grant RTI2018-097662-B-I00).

References

1 Ahrendt, K.A., Borths, C.J., and MacMillan, D.W.C. (2000). New strategies for organic catalysis: the first highly enantioselective organocatalytic Diels–Alder reaction. *J. Am. Chem. Soc.* 122: 4243–4244. https://doi.org/10.1021/ja000092s.

2 Borah, B., Dwivedi, K.D., and Chowhan, L.R. (2021). Recent approaches in the organocatalytic synthesis of pyrroles. *RSC Adv.* 11: 13585–13601. https://doi.org/10.1039/D1RA01690C.

3 Mattson, A.E., Bharadwaj, A.R., Zuhl, A.M., and Scheidt, K.A. (2006). Thiazolium-catalyzed additions of acylsilanes: a general strategy for acyl anion addition reactions. *J. Org. Chem.* 71: 5715–5724. https://doi.org/10.1021/jo060699c.

4 Zhang, L., Zhang, J., Ma, J. et al. (2017). Highly atroposelective synthesis of arylpyrroles by catalytic asymmetric Paal–Knorr reaction. *J. Am. Chem. Soc.* 139: 1714–1717. https://doi.org/10.1021/jacs.6b09634.

5 Han, M.Y., Jia, J.Y., and Wang, W. (2014). Recent advances in organocatalytic asymmetric synthesis of polysubstituted pyrrolidines. *Tetrahedron Lett.* 55: 784–794. https://doi.org/10.1016/j.tetlet.2013.11.048.

6 Austin, J.F., Kim, S.G., Sinz, C.J. et al. (2004). Enantioselective organocatalytic construction of pyrroloindolines by a cascade addition-cyclization strategy: synthesis of (−)-flustramine B. *Proc. Natl. Acad. Sci. U.S.A.* 101: 5482–5487. https://doi.org/10.1073/pnas.0308177101.

7 Chavan, L.N., Mainkar, P.S., and Chandrasekhar, S. (2019). Organocatalytic asymmetric synthesis of tetrahydrofuran and 1,2-dihydrobenzofuran scaffolds. *Eur. J. Org. Chem.* 6890–6910. https://doi.org/10.1002/ejoc.201901067.

8 Enders, D., Wang, C.A., and Greb, A. (2010). Asymmetric synthesis of 2,3,4-trisubstituted functionalised tetrahydrofurans via an organocatalytic Michael addition as key step. *Adv. Synth. Catal.* 352: 987–992. https://doi.org/10.1002/adsc.200900879.

9 Paz, B.M., Li, Y., Thøgersen, M.K., and Jørgensen, K.A. (2017). Enantioselective synthesis of cyclopenta[*b*]benzofurans via an organocatalytic intramolecular double cyclization. *Chem. Sci.* 8: 8086–8093. https://doi.org/10.1039/C7SC03006A.

10 Vachan, B.S., Karuppasamy, M., Vinoth, P. et al. (2020). Proline and its derivatives as organocatalysts for multi-component reactions in aqueous media: synergic pathways to the green synthesis of heterocycles. *Adv. Synth. Catal.* 362: 87–110. https://doi.org/10.1002/adsc.201900558.

11 Egorova, K.S. and Ananikov, V.P. (2017). Toxicity of metal compounds: knowledge and myths. *Organometallics* 36: 4071–4090. https://doi.org/10.1021/acs.organomet.7b00605.

12 Shi, Z. and Loh, T.P. (2013). Organocatalytic synthesis of highly functionalized pyridines at room temperature. *Angew. Chem. Int. Ed.* 52: 8584–8587. https://doi.org/10.1002/anie.201301519.

13 Jaiswal, P.K., Sharma, V., Mathur, M., and Chaudhary, S. (2018). Organocatalytic modified Guareschi–Thorpe type regioselective synthesis: a unified direct access to 5,6,7,8-tetrahydroquinolines and other alicyclic [*b*]-fused pyridines. *Org. Lett.* 20: 6059–6063. https://doi.org/10.1021/acs.orglett.8b02132.

14 Auria-Luna, F., Marqués-López, E., and Herrera, R.P. (2017). Organocatalytic enantioselective synthesis of 1,4-dihydropyridines. *Adv. Synth. Catal.* 359: 2161–2175. https://doi.org/10.1002/adsc.201700300.

15 Hantzsch, A. (1881). Condensationsprodukte aus Aldehydammoniak und Ketonartigen Verbindungen. *Ber. Dtsch. Chem. Ges.* 14: 1637–1638. https://doi.org/10.1002/cber.18810140214.

16 Kumar, A. and Maurya, R.A. (2007). Synthesis of polyhydroquinoline derivatives through unsymmetric Hantzsch reaction using organocatalysts. *Tetrahedron* 63: 1946–1952. https://doi.org/10.1016/j.tet.2006.12.074.

17 Behbahani, F.K. and Alaei, H.S. (2013). L-Proline-catalysed synthesis of functionalized unsymmetrical dihydro-1*H*-indeno[1,2-*b*]pyridines. *J. Chem. Sci.* 125: 623–626. https://doi.org/10.1007/s12039-013-0419-5.

18 Goldmann, S. and Stoltefuss, J. (1991). Effects of chirality and conformation on the calcium antagonist and calcium agonist activities. *Angew. Chem. Int. Ed.* 30: 1559–1578. https://doi.org/10.1002/anie.199115591.

19 Goldmann, S., Stoltefuss, J., and Born, L. (1992). Determination of the absolute configuration of the active amlodipine enantiomer as (−)-*S*: a correction. *J. Med. Chem.* 35: 3341–3344. https://doi.org/10.1021/jm00096a005.

20 Cataldi, M., Taglialatela, M., Palagiano, F. et al. (1999). Effects of manidipine and nitrendipine enantiomers on the plateau phase of K^+-induced intracellular Ca^{2+} increase in GH_3 cells. *Eur. J. Pharmacol.* 376: 169–178. https://doi.org/10.1016/s0014-2999(99)00149-1.

21 Mikus, G., Mast, V., Ratge, D. et al. (1995). Stereoselectivity in cardiovascular and biochemical action of calcium antagonists: studies with the enantiomers of the

dihydropyridine nitrendipine. *Clin. Pharmacol. Ther.* 57: 52–61. https://doi.org/10.1016/0009-9236(95)90265-1.

22 Moreau, J., Duboc, A., Hubert, C. et al. (2007). Metal-free Brønsted acids catalyzed synthesis of functional 1,4-dihydropyridines. *Tetrahedron Lett.* 48: 8647–8650. https://doi.org/10.1016/j.tetlet.2007.10.040.

23 Jiang, J., Yu, J., Sun, X.X. et al. (2008). Organocatalytic asymmetric three-component cyclization of cinnamaldehydes and primary amines with 1,3-dicarbonyl compounds: straightforward access to enantiomerically enriched dihydropyridines. *Angew. Chem.* 120: 2492–2496. https://doi.org/10.1002/anie.200705300.

24 Evans, C.G. and Gestwicki, J.E. (2009). Enantioselective organocatalytic Hantzsch synthesis of polyhydroquinolines. *Org. Lett.* 11: 2957–2959. (retracted).

25 Quinonero, O., Lemaitre, C., Jean, M. et al. (2021). On the enantioselective phosphoric-acid-catalyzed Hantzsch synthesis of polyhydroquinolines. *Org. Lett.* 23: 3394–3398. https://doi.org/10.1021/acs.orglett.1c00866.

26 Franke, P.T., Johansen, R.L., Bertelsen, S., and Jørgensen, K.A. (2008). Organocatalytic enantioselective one-pot synthesis and application of substituted 1,4-dihydropyridines-Hantzsch ester analogues. *Chem. Asian J.* 3: 216–224. https://doi.org/10.1002/asia.200700360.

27 Noole, A., Borissova, M., Lopp, M., and Kanger, T. (2011). Enantioselective organocatalytic aza-ene-type domino reaction leading to 1,4-dihydropyridines. *J. Org. Chem.* 76: 1538–1545. https://doi.org/10.1021/jo200095e.

28 Sridharan, V., Perumal, P.T., Avendaño, C., and Menéndez, J.C. (2007). A new three-component domino synthesis of 1,4-dihydropyridines. *Tetrahedron* 63: 4407–4413. https://doi.org/10.1016/j.tet.2007.03.092.

29 Yoshida, K., Inokuma, T., Takasu, K., and Takemoto, Y. (2010). Catalytic asymmetric synthesis of both enantiomers of 4-substituted 1,4-dihydropyridines with the use of bifunctional thiourea-ammonium salts bearing different counterions. *Molecules* 15: 8305–8326. https://doi.org/10.3390/molecules15118305.

30 Chen, S., Hossain, M.S., and Foss, F.W. Jr. (2013). Bioinspired oxidative aromatizations: one-pot syntheses of 2-substituted benzothiazoles and pyridines by aerobic organocatalysis. *ACS Sustainable Chem. Eng.* 1: 1045–1051. https://doi.org/10.1021/sc4001109.

31 Quinonero, O., Jean, M., Vanthuyne, N. et al. (2016). Combining organocatalysis with central-to-axial chirality conversion: atroposelective Hantzsch-type synthesis of 4-arylpyridines. *Angew. Chem. Int. Ed.* 55: 1401–1405. https://doi.org/10.1002/anie.201509967.

32 For a review of this concept, see:Yang, H. and Chen, J. (2020). Construction of axially chiral compounds via central-to-axial chirality conversion. *Chem. Asian J.* 19: 2939–2951. https://doi.org/10.1002/asia.202000681.

33 He, M., Struble, J.R., and Bode, J.W. (2006). Highly enantioselective azadiene Diels–Alder reactions catalyzed by chiral N-heterocyclic carbenes. *J. Am. Chem. Soc.* 128: 8418–8420. https://doi.org/10.1021/ja062707c.

34 Fustero, S., Jiménez, D., Moscardo, J. et al. (2007). Enantioselective organocatalytic intramolecular aza-Michael reaction: a concise synthesis of (+)-Sedamine,

(+)-allosedamine, and (+)-coniine. *Org. Lett.* 9: 5283–5286. https://doi.org/10.1021/ol702447y.

35 Valero, G., Schimer, J., Cisarova, I. et al. (2009). Highly enantioselective organocatalytic synthesis of piperidines. Formal synthesis of (−)-paroxetine. *Tetrahedron Lett.* 50: 1943–1946. https://doi.org/10.1016/j.tetlet.2009.02.049.

36 Shi, F., Xing, G.J., Tao, Z.L. et al. (2012). An asymmetric organocatalytic Povarov reaction with 2-hydroxystyrenes. *J. Org. Chem.* 77: 6970–6979. https://doi.org/10.1021/jo301174g.

37 Xu, H., Zuend, S.J., Woll, M.G., and Jacobsen, E.N. (2010). Asymmetric cooperative catalysis of strong Brønsted acid-promoted reactions using chiral ureas. *Science* 327: 986–990. https://doi.org/10.1126/science.1182826.

38 Xu, H., Zhang, H., and Jacobsen, E.N. (2014). Chiral sulfinamidourea and strong Brønsted acid–cocatalyzed enantioselective Povarov reaction to access tetrahydroquinolines. *Nat. Protoc.* 9: 1860–1866. https://doi.org/10.1038/nprot.2014.125.

39 Wu, X., Chen, D.F., Chen, S.S., and Zhu, Y.F. (2015). Synthesis of polycyclic amines through mild metal-free tandem cross-dehydrogenative coupling/intramolecular hydroarylation of *N*-aryltetrahydroisoquinolines and crotonaldehyde. *Eur. J. Org. Chem.* 468–473. https://doi.org/10.1002/ejoc.201403375.

40 De Fátima, A., Terra, B.S., da Silva, L. et al. (2015). Organocatalyzed Biginelli reactions: a greener chemical approach for the synthesis of biologically active 3,4-dihydropyrimidin-2(1*H*)-ones/-thiones. In: *Green Synthetic Approaches for Biologically Relevant Heterocycles* (ed. G. Brahmachari), 317–337. Elsevier.

41 Balalaie, S., Bararjanian, M., Amani, A.M., and Movassagh, B. (2006). (*S*)-Proline as a neutral and efficient catalyst for the one-pot synthesis of tetrahydrobenzo[*b*]pyran derivatives in aqueous media. *Synlett* 263–266. https://doi.org/10.1055/s-2006-926227.

42 Abdolmohammadi, S. and Balalaie, S. (2007). Novel and efficient catalysts for the one-pot synthesis of 3,4-dihydropyrano[*c*]chromene derivatives in aqueous media. *Tetrahedron Lett.* 48: 3299–3303. https://doi.org/10.1016/j.tetlet.2007.02.135.

43 Olyaei, A., Shahsavari, M.S., and Sadeghpour, M. (2018). Organocatalytic approach toward the green one-pot synthesis of novel benzo[*f*]chromenes and 12-*H*-benzo[5,6]chromeno[2,3-*b*]pyridines. *Res. Chem. Intermed.* 44: 943–956. https://doi.org/10.1007/s11164-017-3145-7.

44 Li, J., Lu, L., and Su, W. (2010). A new strategy for the synthesis of benzoxanthenes catalyzed by proline triflate in water. *Tetrahedron Lett.* 51: 2434–2437. https://doi.org/10.1016/j.tetlet.2010.02.149.

45 Pei, C.K., Wu, L., Lian, Z., and Shi, M. (2012). DABCO-catalyzed regioselective cyclization reactions of β,γ-unsaturated α-ketophosphonates or β,γ-unsaturated α-ketoesters with allenic esters. *Org. Biomol. Chem.* 10: 171–180. https://doi.org/10.1039/C1OB06507F.

46 Pei, C.K., Jiang, Y., Wei, Y., and Shi, M. (2012). Enantioselective synthesis of highly functionalized phosphonate-substituted pyrans or dihydropyrans through asymmetric [4+2] cycloaddition of β,γ-unsaturated α-ketophosphonates with allenic esters. *Angew. Chem. Int. Ed.* 51: 11490–11494. https://doi.org/10.1002/anie.201206958.

47 Guo, C., Sahoo, B., Daniliuc, C.G., and Glorius, F. (2014). N-Heterocyclic carbene catalyzed switchable reactions of enals with azoalkenes: formal [4+3] and [4+1] annulations for the synthesis of 1,2-diazepines and pyrazoles. *J. Am. Chem. Soc.* 136: 17402–17405. https://doi.org/10.1021/ja510737n.

48 Acosta, P., Becerra, D., Goudedranche, S. et al. (2015). Exploiting the reactivity of 1,2-ketoamides: enantioselective synthesis of functionalized pyrrolidines and pyrrolo-1,4-benzodiazepine-2,5-diones. *Synlett* 1591–1595. https://doi.org/10.1055/s-0034-1378711.

49 Lal, M.R., Basha, S., Sarkar, S., and Khan, A.T. (2013). 2,6-Pyridinedicarboxylic acid as organocatalyst for the synthesis of 1,5-benzodiazepines through one-pot reaction. *Tetrahedron Lett.* 54: 4264–4272. https://doi.org/10.1016/j.tetlet.2013.05.148.

50 Fukata, Y., Asano, K., and Matsubara, S. (2015). Facile net cycloaddition approach to optically active 1,5-benzothiazepines. *J. Am. Chem. Soc.* 137: 5320–5323. https://doi.org/10.1021/jacs.5b02537.

51 Fukata, Y., Yao, K., Miyaji, R. et al. (2017). Asymmetric net cycloaddition for access to diverse substituted 1,5-benzothiazepines. *J. Org. Chem.* 82: 12655–12668. https://doi.org/10.1021/acs.joc.7b02451.

52 Corti, V., Camarero González, P., Febvay, J. et al. (2017). Organocatalytic asymmetric sulfa-Michael addition of 2-aminothiophenols to chalcones: first enantioselective access to 2,3,4,5-tetrahydro-1,5-benzothiazepines. *Eur. J. Org. Chem.* 49–52. https://doi.org/10.1002/ejoc.201601364.

53 Rajesh, S.M., Bala, B.D., Perumal, S., and Menéndez, J.C. (2011). L-Proline-catalysed sequential four-component "on-water" protocol for the synthesis of structurally complex heterocyclic *ortho*-quinones. *Green Chem.* 13: 3248–3254. https://doi.org/10.1039/C1GC15794A.

54 Cao, C.L., Sun, X.L., Kang, Y.B., and Tang, Y. (2007). Enantioselective formal [3+3] annulation for the direct construction of bicyclic skeletons with four stereogenic centers. *Org. Lett.* 9: 4151–4154. https://doi.org/10.1021/ol701669b.

55 Li, J.H. and Du, D.M. (2014). Organocatalyzed cascade aza-Michael/Michael addition for the asymmetric construction of highly functionalized spiropyrazolone tetrahydroquinolines. *Chem. Asian J.* 9: 3278–3286.

56 Li, Z.L., Liu, C., Tan, R. et al. (2016). Organocatalytic, asymmetric [2+2+2] annulation to construct six-membered spirocyclic oxindoles with six continuous stereogenic centers. *Catalysts* 6: 65. https://doi.org/10.3390/catal6050065.

57 Lasaleta, J.M. (2020). Spotting trends in organocatalysis for the next decade. *Nat. Commun.* 11: 3787. https://doi.org/10.1038/s41467-020-17600-y.

5

Transition Metal Catalysis in Synthetic Heterocyclic Chemistry

Dina Murtinho and M. Elisa da Silva Serra

University of Coimbra, Coimbra Chemistry Centre (CQC) and Department of Chemistry, Rua Larga, 3004-535 Coimbra, Portugal

5.1 Introduction

Heterocyclic scaffolds are profusely present in many naturally occurring compounds, biologically active compounds, pharmaceuticals, and other industrially pertinent compounds [1, 2]. Due to their widespread importance and use, the development of efficient reliable synthetic methodologies for the synthesis of the various types of heterocycles is essential. One of the approaches, which is most used for the construction of heterocycles, is metal-catalyzed reactions.

Many reviews have been published on the use of metal catalysts in the synthesis of heterocycles in the recent past, the most abundant involving gold [3–11], rhodium [12–15], silver [16–20], palladium [21–31], and copper [1, 24, 32–47]. The use of copper- and palladium-catalyzed reactions for the specific synthesis of heterocycles has been especially striking, as indicated by over 27 000 hits in the Scopus database when "copper-catalyzed heterocycle synthesis" was used and over 29 000 hits when "palladium-catalyzed heterocycle synthesis," respectively, were used (2015 to the present).

Considering the vast amount of literature on the subject, as well as the diversity of metals and methods, the following discussion will focus on synthetic processes involving palladium- and copper-catalyzed synthesis of heterocyclic compounds, from 2018 to the present.

Among the enormous variety of heterocyclic compounds, greater accent has been placed on the synthetic processes and reactivity of nitrogen heterocycles, including the possibility of their use as intermediates in the synthesis of other compounds due to their widespread use in the most diverse areas. Consequently, this chapter will emphasize synthetic processes used for this type of heterocyclic compounds.

Heterocycles: Synthesis, Catalysis, Sustainability, and Characterization, First Edition.
Edited by Teresa M.V.D. Pinho e Melo and Marta Pineiro.

5.2 Copper-Catalyzed Synthesis of Heterocycles

Copper is one of the most frequently used metals in organic synthesis and catalysis. Due to its abundance, it is an inexpensive metal, and it also has low toxicity. Therefore, its use is more profitable and sustainable compared with many precious metals used in catalytic processes. The chemistry involving copper is extremely varied, depending on the metal's oxidation state. Reactions in which it participates may involve a one-electron mechanism (radical process), a two-electron mechanism (polar process), or even both. Additionally, copper coordinates easily to π-bonds and to heteroatoms, which also motivates its use. As a result, copper catalysts are very efficient in promoting a myriad of reactions, namely, C—C and C—heteroatom bond formation, C—H bond functionalization, metalations, cycloadditions, and click reactions, among others [48].

5.2.1 Fused Heterocycles

Fused heterocyclic compounds are structures of great importance, thus the continued interest in the development of novel efficient synthetic methodologies for obtaining this type of compounds [1, 33, 42, 46, 49, 50]. Fused heterocycles have found application in many areas, namely, in the field of medicinal chemistry, being present in therapeutic agents, as well as in other biologically active natural products. Many of these structures have an aromatic ring fused to heterocycles with one or two nitrogen atoms, such as pyridine, pyrrole, imidazole, and indazole. Several synthetic methodologies have been used to prepare this type of compounds, namely, intermolecular and intramolecular cyclizations, N—N and C—N bond-forming reactions, and cycloadditions, among others.

Indazoles, N-heterocycles with pyrazole and benzene fused rings, are bioisosteres of their indole analogs, with a wide range of biological and pharmaceutical applications [51]. Also an active research field is the use of some of these compounds for bioimaging, photoswitches, and photoacids, among others [52–54]. These compounds have been amply reviewed in the last three years [33, 36, 42, 50].

Indoles, indolines, and oxindoles are structurally similar fused heterocycles composed of a benzene fused to a five-membered nitrogen heterocycle. These structural motifs, especially the chiral versions, may be found in many pharmaceuticals and natural products with biological activity and also have ample application as chiral ligands, auxiliaries, and organocatalysts [42, 55–59]. Consequently, the development of efficient methods for synthesizing these building blocks has been receiving significant attention in industry and academy.

Several examples of the synthesis of these scaffolds through copper-catalyzed borylation have been developed. Li and coworkers have described one of these processes for the synthesis of *cis*-disubstituted chiral indolines, involving the copper-catalyzed intramolecular borylative cyclization of vinyl arenes with *ortho*-imine substituents (Scheme 5.1) [57]. This is referred as the first reported example for asymmetric borylative intramolecular cyclization. In this reaction, the complex promotes the intramolecular cyclization of styrenes having an *ortho*-tethered imine group.

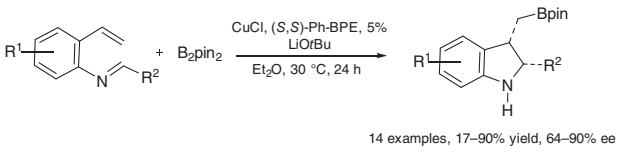

Scheme 5.1 Indolines through intramolecular borylative cyclization of vinyl arenes with *ortho*-imine substituents. Source: Li et al. [58]/John Wiley & Sons.

The reaction of *N*-benzylidene-2-vinylaniline with bis(pinacolato)diboron was studied with various chiral diphosphine ligands and CuCl, using different solvents and reaction temperatures. Optimized reaction conditions were found to be 5 mol% Cu-(*S,S*)-Ph-BPE, LiO^{t}Bu, in diethyl ether at 30 °C for 24 hours. Using these conditions, the substrate scope was studied by varying the substituent on phenyl ring of vinyl arene as well as on the imine moiety. Electron-donating groups on the imine moiety resulted in products with higher ee, while electron-withdrawing groups gave indolines with lower ee. The substituents on the vinyl arene moiety also affected the product ee, albeit in a more variable fashion. The reaction is applicable to various vinyl arenes with an imine moiety at the *ortho*-position, including heterocycles.

The proposed catalytic cycle (Scheme 5.2) involves the initial addition of the copper–Bpin complex (generated from CuCl, LiO^{t}Bu, Bpin) to the alkene giving a benzyl copper species. This, in turn, adds to styrene C=C bond, which then suffers intramolecular addition to the imine giving the product indoline.

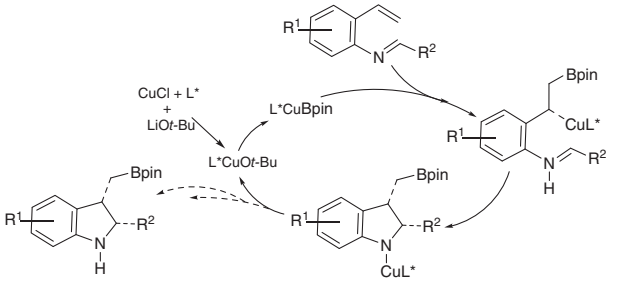

Scheme 5.2 Proposed catalytic cycle for Li's chiral intramolecular borylative cyclization.

The introduction of fluorine atoms in these compounds modifies characteristics such as solubility, metabolic stability, bioavailability, among others, which may lead to greater biological activity. Thus, an efficient procedure for the synthesis of 3-fluoroalkyl indolines has been developed through a copper-catalyzed fluoroalkylation/cyclization of *N*-allyl anilines with fluoroalkyl iodides. The authors synthesized 29 examples in 25–86% yields [60].

A similar procedure for the synthesis of chiral oxindoles through intramolecular borylation is reported by Whyte and collaborators (Scheme 5.3) [59]. 3,3-Disubstituted oxindoles can be synthesized by copper-catalyzed intramolecular borylacylation of vinyl arenes with an *ortho*-tethered carbamoyl substituent. For these substrates, the chiral Cu–SEGPHOS complex was found to be the most efficient catalyst, in the presence of B_2pin_2 and sodium *tert*-butoxide, carrying out the reaction at room temperature for 24 hours in diethyl ether as solvent.

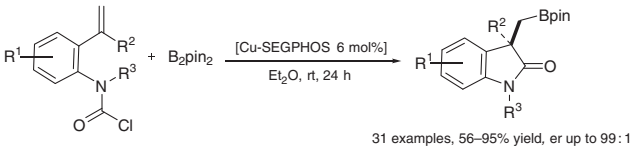

Scheme 5.3 Synthesis of chiral oxindoles through intramolecular borylation. Source: Whyte et al. [60]/John Wiley & Sons.

The scope of the reaction was explored by varying the substituent on phenyl ring of vinyl arene as well as the N-substituent of the carbamoyl moiety, a large variety of substituents being tolerated on both groups. The catalytic cycle is identical to the one described for the intramolecular borylation of the chiral oxindolines. Various alternative strategies for the synthesis of indoles have also been presented by Marchese et al. involving a diverse and broad array of fundamental reactivity as unique advantages. The processes involve the use of Mizoroki–Heck-inspired domino cyclizations, 1,2-addition–cyclization domino sequences, and a multicomponent multicatalyst reaction ((MC)2R) strategy involving C–H functionalization [58].

Table 5.1 presents a summary of additional synthetic methodologies used in the synthesis of fused heterocycles from 2018 to the present.

5.2.2 Five- and Six-Membered N- and N,N-Heterocycles

Five- and six-membered nitrogen heterocycles such as pyrroles, pyrrolidines, imidazoles, oxazoles, pyrazoles, pyridines, piperidines, pyrimidines, and pyrazines are important scaffolds due to their biological activity and synthetic utility. Substituted pyridines, for example, present a wide range of pharmacological activity and additionally are frequently used as organic bases and organocatalysts in synthetic procedures. Pyridine derivatives have also found applications in materials science as organic light-emitting diodes and fluorescent sensors [91, 92]. Table 5.2 summarizes some examples of recent methodologies for the synthesis of these types of structures.

An interesting process for obtaining pyridines, as well as other heterocyclic molecules, involves the use of multicomponent reactions (MCRs), transformations involving at least three easily available components and occurring in a one-pot process. These reactions form a single product, mainly incorporating the atoms of the reagents. MCRs catalyzed by transition metals, namely, copper and palladium, are becoming of growing importance in the design and synthesis of heterocycles [46].

Vodnala and collaborators [91] made use of a simple MCR for the synthesis of 1,6-difunctionalized pyridines through the reaction of simple aliphatic amines, acetophenones, and DMSO, via [2+2+1+1] annulation catalyzed by $Cu(OAc)_2 \cdot H_2O$ (Scheme 5.4).

The optimized reaction conditions were found to be 10 mol% catalyst and 120 °C for 20 hours. DMSO acted as solvent as well as a C1 synthon, while the amine was the nitrogen source. The reaction was found to be very versatile, allowing the use of acetophenones with both electron-withdrawing and electron-donating substituents. Both symmetrical and unsymmetrical 2,6-diarylpyridines could be

Table 5.1 Summary of copper-catalyzed synthetic procedures for nitrogen-based fused heterocycles.

General structure	Reaction type	References
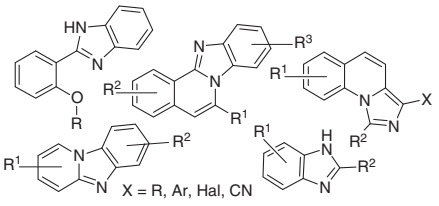	• Microwave-assisted domino reactions • Tandem: annulation/oxidative C–H amination/halogenation, intermolecular Chan–Lam N-arylation/intramolecular arene C–H amination • Diamine–aldehyde coupling • Aerobic three-component cyclizations	[61–66]
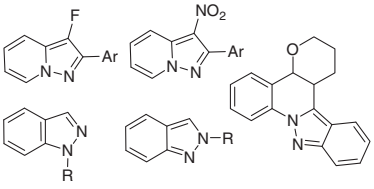	• Oxidative [3+2]-annulation of α-fluoronitroalkenes • Davis–Beirut reaction • Visible light photoredox N—N bond-forming reactions	[67–69]
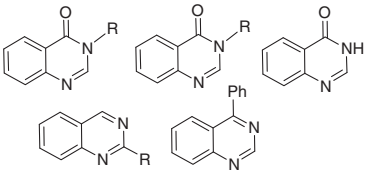	• Oxidative decarboxylative amination • Reaction of 2-aminobenzamides and methanol, O_2 atmosphere • Diamine–aldehyde coupling	[66, 70]
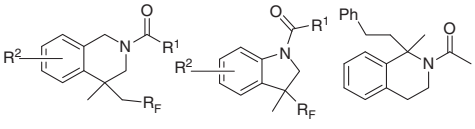	• Fluroalkylation/cyclization • Radical 1,2-benzylarylation	[60, 71]
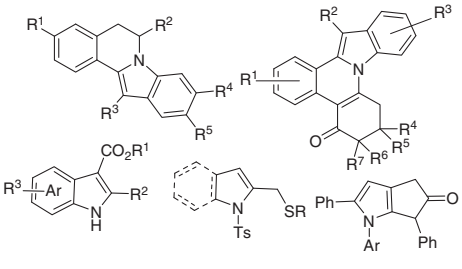	• Cross-dehydrogenative coupling • C–C coupling and cyclization • One-pot tandem Ullmann-type C—N bond formation/intramolecular cross-dehydrogenative coupling • Single-pot aza-Piancatelli/ hydroamination • Intramolecular sulfenoamination of alkenes	[57, 72–75]
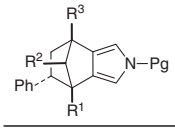	• Enantioselective tandem cyclization–formal [3+2] cycloaddition	[76]

(*continued*)

Table 5.1 (Continued)

General structure	Reaction type	References
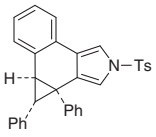	• Enantioselective tandem intramolecular cyclization-initiated cyclopropanation/C–H insertion	[77]
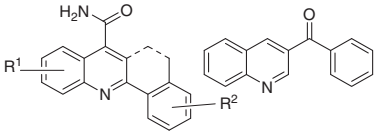	• Domino rearrangement: coupling of isatin ring expansion through cleavage of two C—N bonds • One-pot domino reactions	[78, 79]
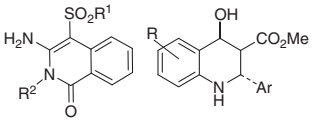	• One-pot Ullmann-type coupling • Stereoselective conjugate borylation/Mannich cyclization	[80, 81]
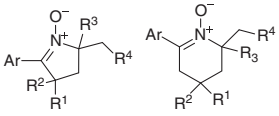	• Cope-type hydroamination	[82]
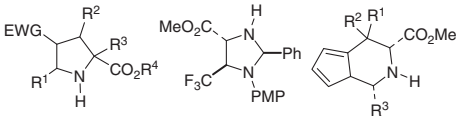	• Asymmetric transformations of N-metalated azomethine ylides as 1,3-dipoles	[83, 84]
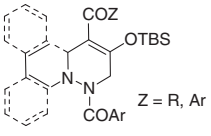	• Chiral [3+3]-cycloaddition	[85]
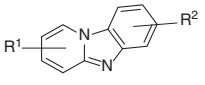	• Tandem radical cyclizations: C—H/C—C bond cleavage and C—C/C—N bond formation	[86]
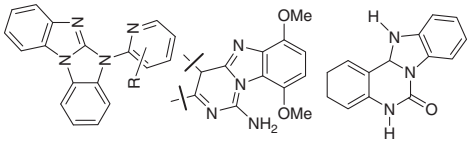	• Intramolecular C–N coupling/intermolecular coupling/cascade sp^2 C–H amination • C(sp^2)–N coupling, cyclization, and oxidation • C—C bond cleavage/double cyclization	[87–90]
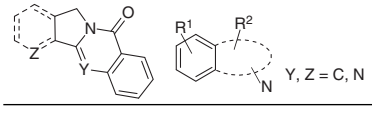	• Photoinduced radical domino cyclization	[49, 50]

Table 5.2 Summary of copper-catalyzed synthetic procedures simple five- and six-membered N- and N,N-heterocycles.

General structure	Reaction type	References
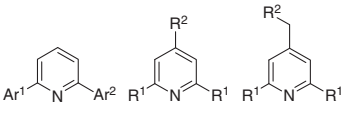	• Regioselective [2+2+1+1] annulation • Oxidative decarboxylative amination	[70, 91]
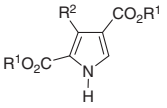	• [3+1+1] Cycloaddition	[93]
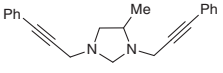	• Annulation/A3-coupling/A3-coupling	[94]
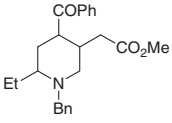	• Cyclizations in the formation of six-membered N-heterocycles	[34]
	• Regio- and enantioselective radical-mediated C–H cyanation	[95]
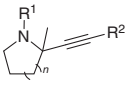	• Cascade intramolecular hydroamination/cyclization	[96]
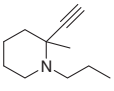	• Condensation/intramolecular cyclization/alkynylation: eco-friendly three-component coupling	[97]
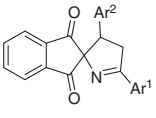	• N—O bond cleavage	[98]
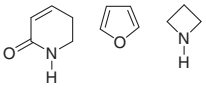	• Tandem cross-coupling/cyclization	[99]
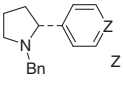	• Suzuki–Miyaura cross-coupling/enantioselective intramolecular hydroamination	[100]
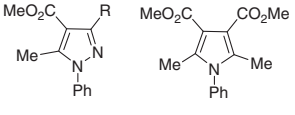	• Oxidant-dependent oxidative radical annulation by sequential C—C and N—N (C—N) bond-forming reactions	[101]
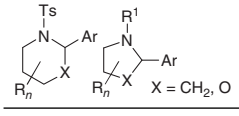	• N–F and C–H activation	[102]

(*continued*)

Table 5.2 (Continued)

General structure	Reaction type	References
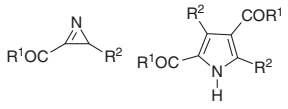	• *In situ* photochemical valence isomerization • Dimerization of acylazirines	[103]
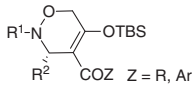	• Chiral [3+3]-cycloaddition	[85]
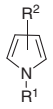	• Reductive N—O bond cleavage/oxidative cyclization	[104]

Scheme 5.4 1,6-Difunctionalized pyridines through MCR.

obtained, depending on if only one or two different acetophenone molecules were used.

Based on mechanistic studies, including GC/MS and deuterium labeling, a reaction mechanism was proposed for the [2+2+1+1] annulation (Scheme 5.5).

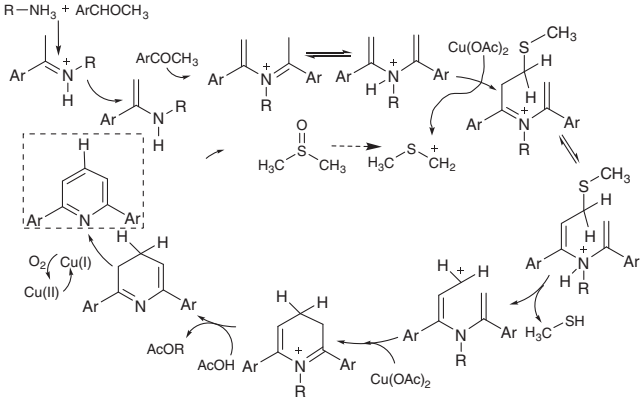

Scheme 5.5 Proposed mechanism for Vodnala's synthesis of 1,6-difunctionalized pyridines.

Initial condensation of acetophenone and propylamine originates an imine intermediate, which tautomerizes to the corresponding enamine. This, in turn, condenses with a second molecule of the ketone and the resulting structure tautomerizes to a new enamine intermediate. Subsequently, it captures the

Pummerer-like intermediate ($MeSCH_2^+$, generated *in situ* from DMSO) followed by a new tautomerization and elimination of methanethiol to give a cationic species, which undergoes copper-catalyzed cyclization to a dihydropyridinium intermediate. Finally, elimination of *n*-propyl acetate and oxidation by Cu(II)/O_2 delivers the final 2,6-diarylpyridine.

Sujatha and coworkers established the first example of an intermolecular ring expansion cascade of azirines with alkynes (Scheme 5.6), originating highly substituted pyridines [92]. The reaction is catalyzed by CuI in the presence of triethylamine, at room temperature for 30 minutes. Concerning the scope of the reaction, it allowed the use of azirines with both electron-withdrawing and electron-donating substituents, while a wide variety of alkynes was also allowed.

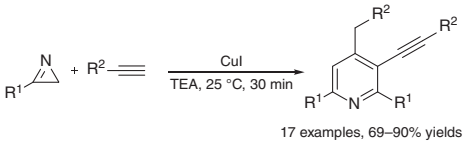

Scheme 5.6 Synthesis of tetrasubstituted pyridines through the intermolecular ring expansion cascade of azirines with alkynes.

The proposed mechanism (Scheme 5.7) for this transformation involves the initial formation of a copper acetylide that undergoes ring-opening with the azirine originating two intermediates, a skipped-yne-imine, and an yne-enamine. The two intermediates react through a copper-assisted hydroalkylation, giving a new intermediate, which subsequently suffers cyclization, elimination of ammonia, and tautomerization, to give the pyridine product. Some of these substituted pyridines have been tested and found to have potent anticancer activity against oral cancer cells.

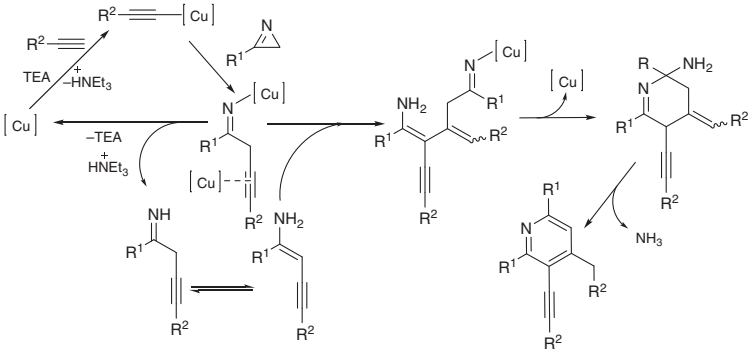

Scheme 5.7 Proposed mechanism for the synthesis of tetrasubstituted pyridines from azirines.

Five- and six-membered N-heterocycles have been synthesized, involving N-metalated azomethine ylides as 1,3-dipoles, to give optically active pyrrolidines and imidazolidines [83, 84]. These reactions involve [3+2], [3+6], and

[3+3] 1,3-dipolar cycloadditions catalyzed by chiral copper catalysts. Illustrative examples of this very versatile synthetic process are the reactions of azomethine ylides with dimethyl maleate in dichloromethane with NEt_3 at 0 °C, catalyzed by Cu-TFBiphamPhos. The initial formation of a copper-*N*-azomethine ylide is followed by its 1,3-dipolar cycloaddition with dimethyl maleate to give pyrrolidines with 4 chiral centers in 41–98% yields and 97–99% ee. When fluorinated imines are used instead of dimethyl maleate, in toluene at −20 °C, with Cu(S,R_P)-PPFOMe, fluorinated imidazolidines result in 50–95% yields and 83–98% ee.

5.2.3 Five- and Six-Membered N,O-Heterocycles

Heterocycles with more than one heteroatom are plentiful in nature. As many other heterocycles, they are present in many natural products, and many have biological activity, thus the importance of novel synthetic procedures for the synthesis of this type of compounds. Table 5.3 presents some recent synthetic procedures for simple, abundant, five- and six-membered N,O-heterocycles.

Oxazoles, isoxazoles, oxazolines, isoxazolines, and oxazolidines are five-membered heterocycles containing one nitrogen and one oxygen atom. All of these structures incorporate compounds that exhibit various types of biological activity. A cascade approach was achieved to obtain oxazoles, namely, thiosubstituted benzoxazoles, by Kotovshchikov et al. The procedure involves the annulation-triggered electrocyclic opening of a 1,2,3-triazole ring generating *in situ* a diazo compound,

Table 5.3 Summary of synthetic procedures simple five- and six-membered N,O-heterocycles.

General structure	Reaction type	References
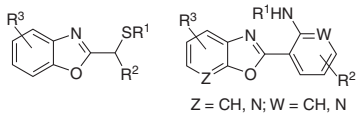 Z = CH, N; W = CH, N	• Cascade coupling domino reactions	[105, 106]
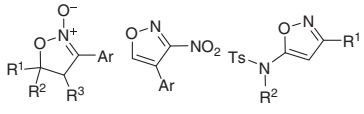	• [3+2] Annulation • Reactions of benzaldehydes with nitromethane • Cyclization	[107–109]
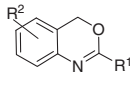	• Coupling	[66]
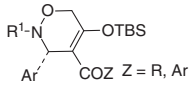 Z = R, Ar	• [3+3] Cycloadditions	[43, 85]
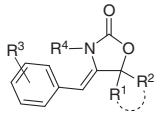	• One-pot multicomponent catalytic addition, hydroamination, and cyclization with consecutive C—C, C—O, and C—N bond formations	[110]

which is subsequently trapped by thiol scaffolds originating products in good yields of up to 91% [105].

A $Cu(OAc)_2$-catalyzed reaction of benzaldehydes with nitromethane yielded 3-nitroisoxazoles through a one-pot cyclization. In this reaction the C–O–N fragment in the isoxazole results from the rearrangement of C–N–O unit nitromethane, the first known example of this type of rearrangement [108].

2-Isoxazoline-*N*-oxides are important synthetic precursors for complex molecules, and their derivatives are found in biologically active agents. The copper-mediated [3+2] radical annulation of alkenes with α-nitrobenzyl bromides has been presented as a synthetic method of forming 2-isoxazoline-*N*-oxides under mild conditions and short reaction times. The usefulness of this synthetic procedure was demonstrated by easy transformation of this type of heterocycle into other N,O-containing heterocyclic compounds [107].

A domino approach has also been used for the synthesis of spirooxazolidinones via a copper-catalyzed catalytic addition, hydroamination, and cyclization sequence involving consecutive C—C, C—O, and C—N bond formations [110].

5.3 Pd-Catalyzed Heterocycle Synthesis

Palladium has been one of the most used metals in organometallic chemistry with wide application in organic synthesis. Numerous C—C and C—N bond-forming reactions, including Sonogashira, Heck, Wacker, and Kumada reactions, among others, can be carried out using palladium as catalyst [111]. It is not surprising, therefore, that it is also widely used in the synthesis of heterocyclic compounds. Palladium metal complexes containing chiral and non-chiral ligands can be applied in a wide range of catalytic heterocycle formation processes, including asymmetric ones. Reactions catalyzed by palladium can usually be carried out under mild conditions and are tolerated by most functional groups (unlike the more conventional methodologies that use high temperatures and are catalyzed by strong acids or bases), which has contributed to the great number of articles that are published annually on palladium-catalyzed synthesis of heterocyclic compounds. Although this metal is not cheap, it is more accessible than platinum or rhodium and is sometimes possible to reuse, which is also a competitive advantage over other transition metals [22, 25, 28].

Palladium can exhibit three oxidation states, Pd(0), Pd(II), and Pd(IV). In general, Pd(0) compounds act as nucleophiles, inserting into chemical bonds in organic compounds (aryls, allylics, vinyl halides, etc.), suffering oxidative addition to Pd(II). Then, in general, a reductive elimination occurs, with formation of a sigma bond and reduction of Pd(II) back to Pd(0). Pd(II) complexes are usually electrophilic and can coordinate with various organic substrates, namely, alkenes, alkynes, and arenes, among others. The complexes formed can be attacked by nucleophiles or activate C—H bonds via palladacycles. Pd-catalyzed activation of C—H bonds is a widely used method for the construction of heterocycles [111, 112].

Heterocycle formation reactions, catalyzed by Pd, have been the subject of numerous review articles in recent years. In the three years covered by this chapter, several reviews have been published on oxygen [21], nitrogen [22, 24–27], or miscellaneous [23, 28–31] heterocycle formation reactions.

Environmental concerns have led to the development of synthetic methodologies with improved atomic efficiency, which allows a greater reduction in production costs and waste. In this context, cascade reactions have been applied to the synthesis of heterocycles, including reactions catalyzed by palladium, which have also been the subject of recent reviews, namely, on the synthesis of indole derivatives [113], 3-methyleneisoindolin-1-ones [114] and in double Heck cyclization reactions for the synthesis of polycyclic compounds [115, 116]. Recently, nanoparticles have also been used as catalysts in organic transformations, namely, in the synthesis of heterocycles. The use of metallic nanoparticles (including palladium) in the synthesis of nitrogen and oxygen heterocycles was the subject of a recent review [117].

5.3.1 Nitrogen Heterocycles

The synthesis of compounds such as indoles, quinolines, carbolines, pyrrolidines, piperidines, phthalazines, pyrazoles, and derivatives of the ones mentioned in the previous paragraphs has been carried out resorting to Pd-catalyzed reactions. Some relevant examples of the construction of five- and six-membered nitrogen containing heterocycles, published between 2018 and 2020, and not discussed in this chapter, are summarized in Tables 5.4 and 5.5. Indole and derivatives are among the most synthesized nitrogen heterocycles; thus, they will be focused on in more detail.

Reductive carbonylation reactions involving *ortho*-substituted nitro arenes and carbon monoxide, catalyzed by transition metals, is a widely used method for the preparation of nitrogen heterocycles, including indoles [23, 143]. The replacement of carbon monoxide by other safer sources, such as formate esters, was studied by Formenti et al. Using 2-nitrocinnamic acid derivatives, phenyl formate, $Pd(CH_3CN)_2Cl_2$ as catalyst, and triethylamine as base, in the presence of 1,10-phenanthroline, it was possible to prepare substituted indoles at 2- and 3-positions, in yields of 45–98% (Scheme 5.8) [145].

The scope of the reaction was extended, namely, to the functionalization of an aromatic C—H bond, formation of a six-membered ring, cyclization of a β-nitrostyrene, and even an intermolecular cyclization reaction.

Kinetic studies have shown that the decarbonylation of the phenyl formate is activated by the base, triethylamine, and not catalyzed by the metal. Thus, a mechanistic proposal was made for this reaction, as described in Scheme 5.9. The first reaction is the decarbonylation of the phenyl formate, followed by a reductive cyclization. After CO formation, the active species of Pd reacts with *o*-nitrostyrene, forming **A**, which undergoes intramolecular cyclization, originating **B**. The latter is converted into species **C**, through hydrogen atom 1.5-shift, which is in equilibrium with *N*-hydroxyindole **D**. The product is generated by a CO deoxygenation, with CO_2 formation and regeneration of the Pd catalyst.

Table 5.4 Construction of five-membered nitrogen heterocycles.

General structure	Reaction type	References
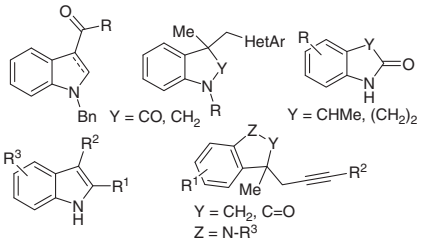	• Tandem reaction • Intramolecular α-arylation • Insertion/cyclization • Reductive cyclization • Domino reaction	[118–122]
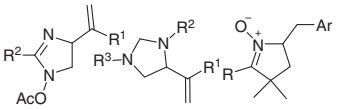	• Cyclization reaction • Cyclization/formal migration [2+3] cycloadditions • Carboannulation	[123–125]
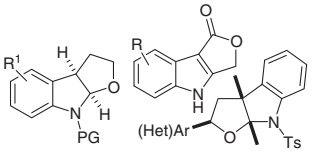	• Dehydrohalogenative cyclization • Enantioselective intermolecular carbohetero functionalization	[126, 127]
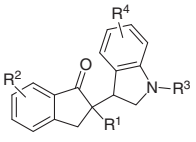	• Tandem reactions	[128]
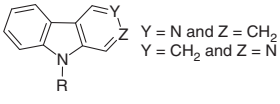	• Domino C–C/C–N coupling/cyclization	[129]
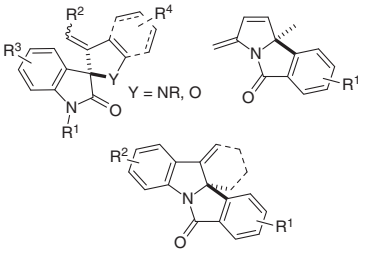	• Enantioselective dearoamative Heck reaction	[130]
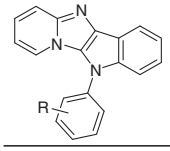	• Domino C–N coupling	[131]

Table 5.5 Construction of six-membered nitrogen heterocycles.

General structure	Reaction type	References
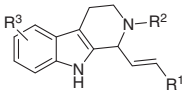	• Alkyne isomerization/C–H activation	[132]
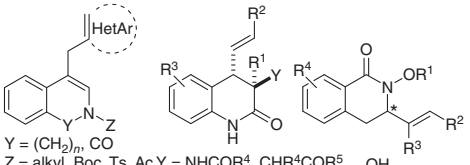	• Intramolecular carbopalladation/C–H allylation • Inverse-electron-demand asymmetric [4+2] cycloadditions • Asymmetric oxidative annulation • Ring-opening/formal 6-*endo*-trig cyclization	[133–136]
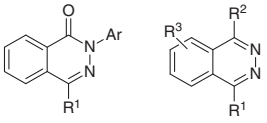	• Intermolecular acylation/nucleophilic condensation	[137]
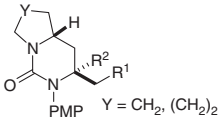	• Alkene carboamination reactions	[138]
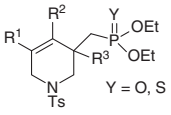	• Cyclizative phosphorylation	[139]
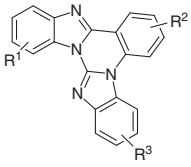	• Cross-dehydrogenative C(sp^2)–H/N–H couplings	[140]
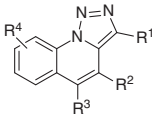	• Intermolecular annulation/arylation cascade	[141]
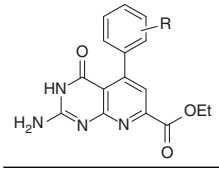	• Cyclization/Pd(II) supported on SBA-15	[142]

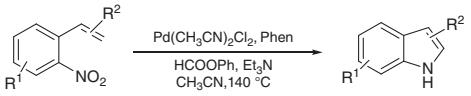

Scheme 5.8 Substituted indoles through reductive carbonylation. Source: Formenti et al. [144]/John Wiley & Sons.

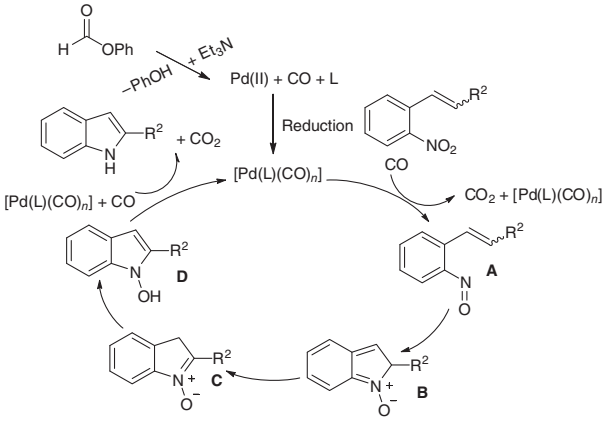

Scheme 5.9 Mechanistic proposal for the reductive carbonylation.

Ramesh et al. refers to the use of a sustainable strategy for the synthesis of indolines, oxindoles, and dihydrobenzofurans, based on a domino reaction, in water, catalyzed by Pd and assisted by microwaves [146]. This strategy involves an intramolecular Heck type reaction, followed by an intermolecular Sonogashira coupling. The reaction conditions were optimized, using 2-iodo-*N*-methyl-*N*-(2-methylallyl)aniline and phenyl acetylene as substrates, 1 mol% of $Pd_2(dba)_3$ as catalyst, 1,8-diazabicyclo[5.4.0]undec-7-ene (DBU) as base, and benzyltriethylammonium chloride (BTEAC) as additive, yielding 98% of the target compound (MW irradiation, 100 °C, 15 minutes, Scheme 5.10).

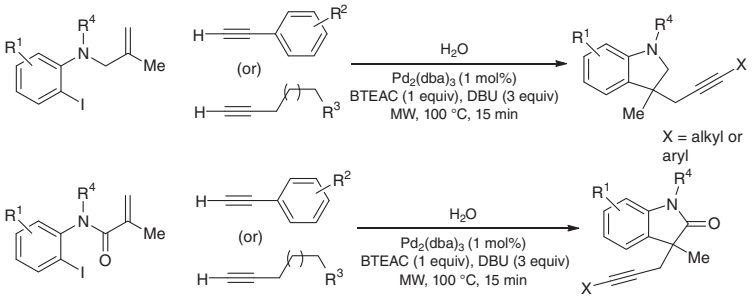

Scheme 5.10 Sustainable Heck–Sonogashira strategy for the synthesis of indolines.

The use of different 2-iodo-*N*-alkyl-*N*-(2-methylallyl)anilines or *N*-(2-iodophenyl)-*N*-alkylmethacrylamide and acetylenes (Scheme 5.10) allowed the synthesis of 21 indolines and 10 3,3-disubstituted oxindoles, in yields of 85–98% and 80–98%, respectively.

The reaction was further extended to the synthesis of dihydrobenzofurans using 1-iodo-2-[(2-methylallyl)oxy]benzene as substrate (20 compounds were prepared, in 80–98% yields). The catalytic cycle of this reaction is described in Scheme 5.11, with Pd(0) insertion occurring in the aromatic C—I bond, forming the aryl-Pd(II) species **A**. Then, an intramolecular Heck reaction takes place, originating **B**. The latter coordinates with acetylene through the π electrons, forming a complex, **C**. Upon elimination of HI, species **D** is formed, followed by reductive elimination via Sonogashira coupling, with product formation and catalyst regeneration.

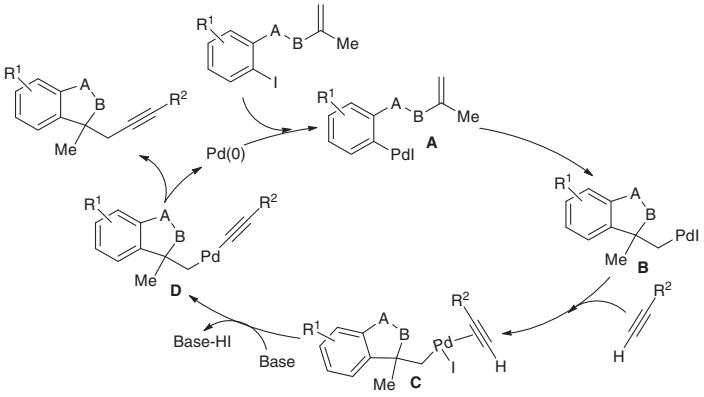

Scheme 5.11 Catalytic cycle for the synthesis of indolines.

Asymmetric reactions are particularly relevant in the field of fine chemistry, especially in medicinal and agrochemical chemistry, which is why the synthesis of chiral heterocyclic compounds has been the subject of numerous publications in recent years, including some indole nitrogen heterocycles. For example, Bai et al. synthesized a series of chiral oxindoles, containing $-CF_3$ substituent groups, through a Heck cyclization/Sonogashira reaction catalyzed by Pd and Cu [144]. Chiral fluorinated compounds are very relevant in medicinal chemistry because they have unique biological properties. In this paper, CF_3-substituted *o*-iodoacrylanilides and terminal alkynes were used as reagents. Several chiral catalysts, generated *in situ* by the reaction of $[(\eta^3\text{-}C_3H_5)PdCl]_2$ with chiral phosphorus ligands, were studied; best results, in terms of enantioselectivity (97% ee; 85% yield), were obtained with ligand **L1**, using *N*-(2-iodophenyl)-*N*-methyl-2-(trifluoromethyl)acrylamide and phenylacetylene as substrates, and the reaction conditions are described in Scheme 5.12. The use of CF_3-substituted *o*-iodoacrylanilides, with different aryl substituents on the nitrogen atom, allowed the formation of a series of products (18) in excellent ee (94–98%) and yields of 40–91%.

The reaction was further extended to the synthesis of non-CF_3-substituted *o*-iodoacrylanilides, 16 compounds having been prepared with ee between 92% and 97% and yields of 80–95%, using the **L2** ligand.

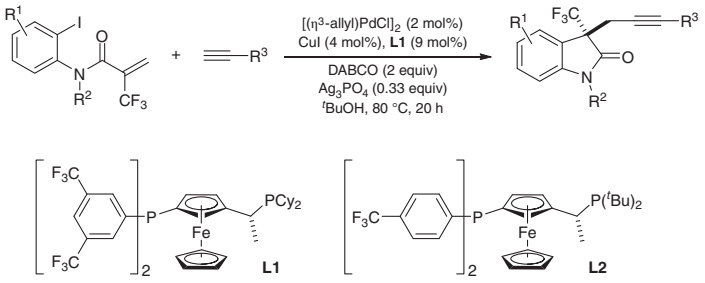

Scheme 5.12 Synthesis of chiral fluorinated oxindoles.

Another strategy for the asymmetric synthesis of indole derivatives, in this case of 3-methyleneindolines (skeleton base of some biologically active and pharmaceutical natural products), has been described by Zhang et al. These authors used an innovative approach for the synthesis of these compounds: the enantioselective intermolecular denitrogenative cyclization reaction of benzotriazoles with allenes and *N*-allenamides [147].

Although denitrogenative cyclization of benzotriazoles with alkynes and alkenes has already been developed by others [148–151], the use of allenes in this reaction, concomitant with the formation of chiral products, had not yet been described. Preliminary studies showed that the best results were obtained using $Pd(dba)_3$, ligand **L3**, and the triflate group as an electron attracting group in benzotriazole.

The reaction with different aryltriazoles and allenes (Scheme 5.13) allowed the preparation of 20 different compounds in high yields and ee (88–97% and 89–98%, respectively). In the case of *N*-allenamides, the best results were obtained with **L4** ligand and using the conditions described in Scheme 5.13. The respective chiral products were obtained in 88–95% yields and 84–95% ee.

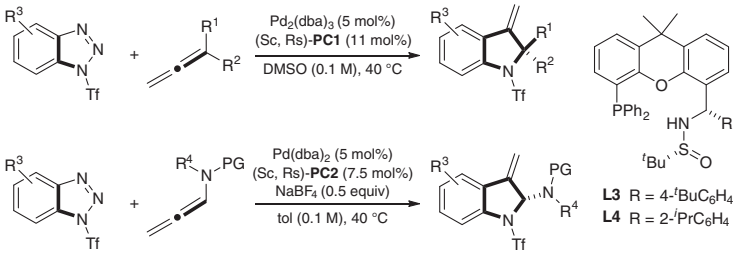

Scheme 5.13 Zhang's synthesis of 3-methyleneindolines.

According to the mechanistic proposal presented by the authors, benzotriazole forms diazonium **A** followed by an oxidative addition to the palladium complex, with elimination of N_2, generating the intermediate **B**. Upon insertion of the allene or allenamide in the carbon–Pd bond, complex **C** is formed, which originates the cyclization products through an allyl substitution, regenerating the catalyst (Scheme 5.14).

In addition to the examples mentioned of Pd-catalyzed indole-based compound synthesis, others have been published in recent years, namely, the

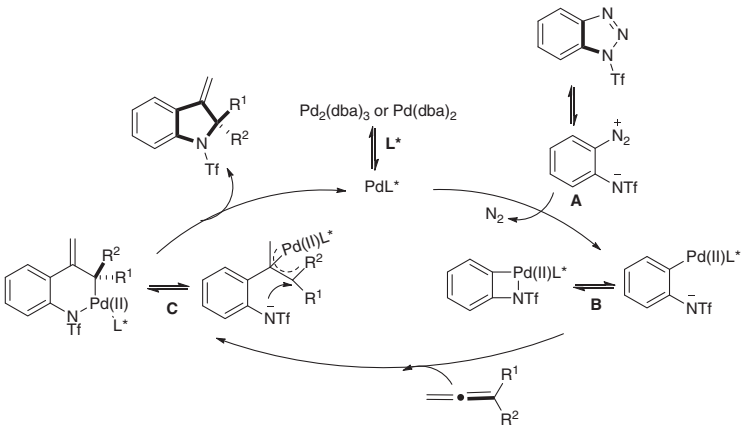

Scheme 5.14 Mechanistic proposal for the synthesis of 3-methyleneindolines.

synthesis of 3-phosphinomethyl 3,3-disubstituted oxindoles through domino Heck/phosphorylation reactions [152, 153], of indoles using Pd/C as a catalyst [154], of 5 and 6-azaindoles [155], and of 3,4-, 3,5- and 3,6-fused indoles [156], among others.

A series of chiral tetrahydroindoles were prepared using $[Pd(\eta^3\text{-}C_3H_5)Cl]_2$/RuPHOX as catalyst and unstable enolizable ketimines and *meso*-diacetatecycloalkenes as substrates, in yields up to 86% and high ee (up to 96%) [157]. In addition to the chiral tetrahydroindoles previously mentioned, the synthesis of N-fused polycyclic indoles, compounds that can exhibit antimalarial, anti-HIV, anticancer, and antibiotic activity, has also been described. Polycyclic indoles were prepared by reacting indolyl-2-carbinols with cyclic β-keto esters, in the presence of Pd/BINOL derivative complexes, originating tetracyclic structures [6−5−5−6] and [6−5−5−5], in yields of 72–99% and 86–99% ee [158].

Saturated nitrogen heterocycles, such as pyrrolidines and piperidines, are present in several pharmaceutical compounds, namely, astemizole, procyclidine, and ramipril. The development of new synthetic methodologies for the preparation of this type of compounds, particularly in the chiral version, remains a challenge. The traditional synthetic methods for these heterocycles usually involve Mitsunobu, Appel, or classic reductive amination reactions. Metal-catalyzed methods, involving hydrogen borrowing or reductive amination, have been used more recently [159]. In the case of Pd, methods involving intramolecular aza-Wacker and aza-Heck reactions have been widely used [160]. Ma et al. through aza-Heck cyclization reactions of alkenyl *N*-(tosyloxy)-carbamates using $Pd_2(dba)_3$ and the ligand **L5** as catalysts, developed a methodology that allows the synthesis of a wide range of pyrrolidines (Scheme 5.15) [162].

The scope of the method allows that substrates with different protecting groups, *N*-Boc or *N*-Cbz, can be used (although the latter leads to slightly lower ee) and alkenes with different degrees of steric hindrance (R^1 can be a methyl group or a more hindered group such as isopropyl). Chiral pyrrolidines were obtained in yields and ee of 54–95% and 88–96%, respectively.

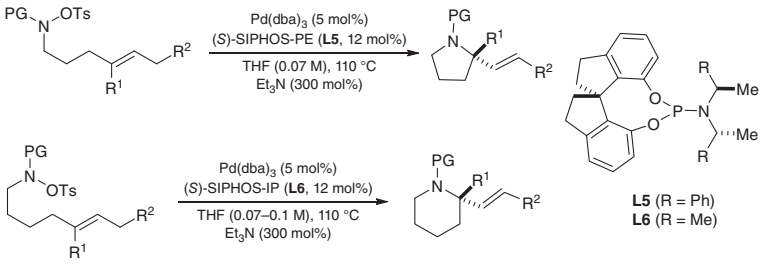

Scheme 5.15 Synthesis of chiral pyrrolidines and piperidines by aza-Heck cyclization. Source: Ma et al. [161]/American Chemical Society.

The synthesis of piperidines using the same methodology proved to be more difficult; however, the replacement of ligand **L5** by less hindered **L6** allowed the synthesis of a set of piperidines with different substituents, with good results (60–84% yield and 82–96% ee), Scheme 5.15.

An additional advantage of this synthetic methodology is that at the end of the synthesis process, the Pd(0) catalyst is released, which allows it to be used in tandem processes. To make this proof of concept, the authors synthesized caulophyllumine B, a natural compound, using a two-step aza-Heck/Heck one-pot tandem process.

Other saturated nitrogen heterocycles were also synthesized using Pd catalysis, namely, 2-pyrrolidinones [163] (by reaction of alkyl isocyanates with 2-acetoxymethyl-3-allyltrimethylsilane through a cycloaddition [3+2] catalyzed by $Pd(dba)_2$/DPEphos), 2-vinylpyrrolidines and 2-vinylpiperidines [161] (by intramolecular amino carbonate cyclization catalyzed by $Pd_2(dba)_3/PPh_3$), and 2,3,6-trisubstituted piperidines [164] (using isoxazolinones as starting reagents and $Pd_2(dba)_3$ as catalyst to obtain 3,4-dihydropyridines, which are reduced to the corresponding piperidines by hydrogenation, using $[Ir(cod)Cl]_2$ as catalyst).

N-Heterocycles containing more than six members and synthesized using Pd catalysts are summarized in Table 5.6.

5.3.2 Oxygen Heterocycles

Like nitrogen heterocycles, oxygen heterocycles are also present in numerous compounds of natural and synthetic origin, namely, in drugs, solvents, and flavors, among others [169, 170]. Oxygen heterocycles with five and six atoms in the ring, including furans and benzofurans, pyranes, chromenes, coumarins, xanthones, dioxanes, and the previously mentioned derivatives, have been widely synthesized using palladium catalysis. Among these various classes of compounds, furan and benzofuran derivatives have been the subject of a greater number of publications in recent years.

Rocaboy et al. synthesized several dihydrobenzofurans by an intramolecular coupling, with the construction of $C(sp^3)$—$C(sp^3)$ bonds from two $C(sp^3)$—H bonds. Starting from *o*-bromophenols and making use of a 1,4-Pd-shift (a strategy initiated by Heck), it was possible to synthesize several dihydrobenzofurans in yields between 41% and 92% (Scheme 5.16) [171]. The reaction is carried out in a sealed

Table 5.6 Construction of *n*-member ($n > 6$) or multiple cycle nitrogen heterocycles.

General structure	Reaction type	References
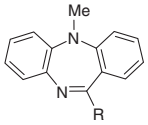	• Insertion/intramolecular C(sp^2)–H activation	[165]
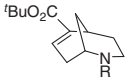	• Tandem diverted Tsuji–Trost process	[166]
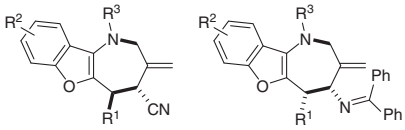	• Asymmetric [4+3] cyclization	[167]
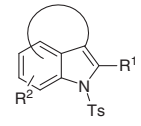 3,4- and 3,5- and 3,6-fused	• Cascade alkyne insertion/C–H activation/amination	[156]
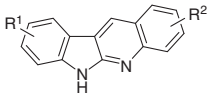	• Dual annulation reaction	[168]

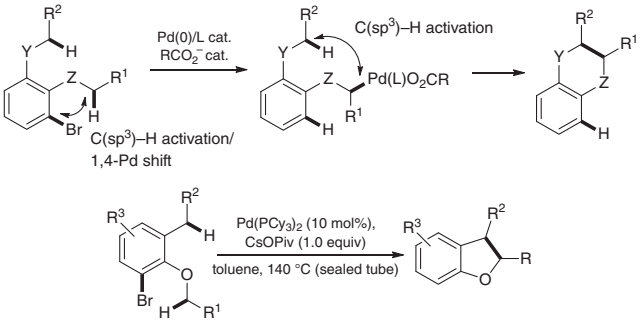

Scheme 5.16 Rocaboy's synthesis of dihydrobenzofurans by intramolecular coupling.

tube, using $Pd(PCy_3)_2$ complex and a stoichiometric amount of cesium pivalate (Scheme 5.16).

The reaction was extended to the use of aryl ketones, allowing the synthesis of the corresponding 2,3-dihydrobenzofuran-3-ols and also the construction of six-membered rings, thus originating several chroman-4-one (using in this case adamantane carboxylic acid as a catalyst, base in stoichiometric amount, 120 °C).

Another interesting example reports the multicomponent synthesis of fully substituted alkylidene-furan-3-(2*H*)-ones using ynones, imines, and aryl iodides [172].

This MCR involves a Mannich reaction, an oxypalladation, and a reductive elimination with the formation of three bonds: one C—O bond and two C—C bonds. The novelty of this synthesis is the use of γ,δ-acetylenic β-ketoesters, presenting both β-keto ester and ynone functions; the former act as nucleophiles in a basic medium, and the latter can be activated by metals and subsequently attacked by nucleophiles.

The reaction was optimized, and it was concluded that the use of $P(OAc)_2$, XantPhos as ligand, in the presence of DIPEA, in acetonitrile at room temperature, allowed the synthesis of alkylidene-furan-3(2*H*)-ones in yields between 43% and 92% (Scheme 5.17).

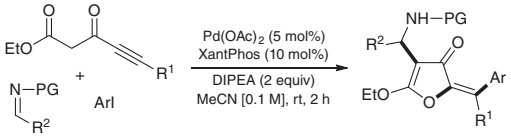

Scheme 5.17 Multicomponent synthesis of alkylidene-furan-3-(2*H*)-ones.

The proposed mechanism for the reaction is described in Scheme 5.18. The first step of the mechanism involves the Mannich reaction between a γ,δ-acetylenic β-ketoester and an imine; in the second step the triple bond of the resulting product coordinates with ArPdI (obtained by the reaction of the Pd(0) species with an aryl iodide), which through a regioselective 5-*exo*-dig oxypalladation gives rise to the vinylpalladium intermediate; in a third stage, this intermediate undergoes a reductive elimination, generating the product and regenerating the Pd(0) species.

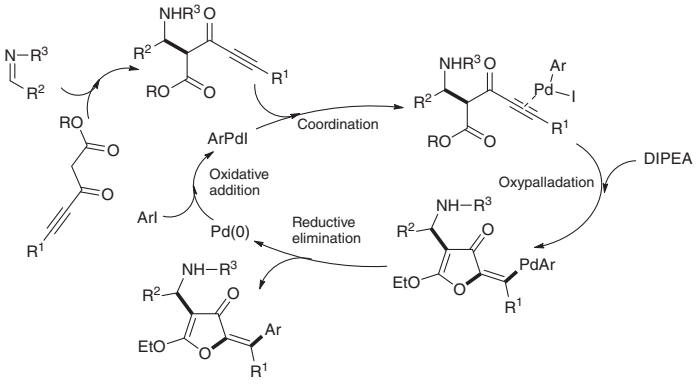

Scheme 5.18 Proposed mechanism for the multicomponent synthesis of alkylidene-furan-3-(2*H*)-ones.

Another example of the construction of five-membered rings, namely, for the synthesis of 3-allylbenzofurans, involving a decarboxylative allylation and a nucleophilic cyclization catalyzed by Pd, has also been reported (Scheme 5.19) [174]. The advantages of this methodology lie in the fact that it is possible to obtain a wide range of products using only $Pd_2(dba)_3$, without the need for any additional

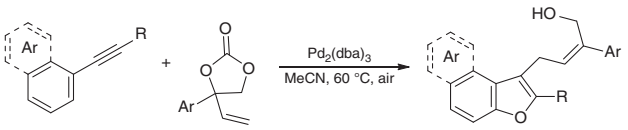

Scheme 5.19 Pd catalyzed synthesis of 3-allylbenzofurans, involving decarboxylative allylation and nucleophilic cyclization. Source: Zhang et al. [173]/American Chemical Society.

ligand or base, and that the reaction takes place under mild conditions, 60 °C, and without inert atmosphere. Using several α-alkynylnaphth-2-ols and vinylethylene carbonates, it was possible to obtain the respective products in yields of 37–82% and stereoselectivities between 2 : 1 and >19 : 1 (*Z*/*E* ratio). The mechanism suggested by the authors involves the decarboxylation of vinylethylene carbonate, forming a Pd-π-allyl intermediate, which then activates the alkyne, followed by a nucleophilic cyclization with proton transfer involving the hydroxyl group of naphthol. The intermediate formed on reductive elimination originates the product and regenerates the catalyst.

Some compounds containing chiral tetrahydrofuran nuclei present biological activity, being present in numerous natural and pharmaceutical products. The synthesis of this type of structures can be carried out using asymmetric catalysis methods, namely, through intermolecular [3+2] cycloadditions of vinyl three-membered heterocycles catalyzed by transition metals (Scheme 5.20). Several dipolarophiles can be used in this reaction, including activated alkenes. Previous work has reported the use of double-activated electron-deficient alkenes or, less commonly, with one activator, containing aryl or alkyl substituents at the β-position. Du et al. reported the use of poorly reactive trisubstituted alkenes with only one activator and containing alkyl or aryl substituents in the α position, as dipolarophiles, for the synthesis of chiral tetrahydrofurans using Pd as catalyst [175].

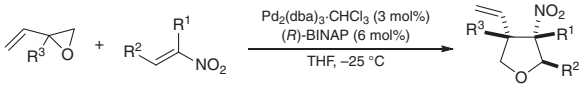

Scheme 5.20 Synthesis of chiral tetrahydrofurans using intermolecular [3+2] cycloadditions.

The asymmetric reaction was carried out using vinyl epoxides and (*E*)-disubstituted nitroalkenes, $Pd_2(dba)_3$, and $CHCl_3$/(*R*)-BINAP as catalyst, in THF at −25 °C. Depending on the type of substituent present on the nitroalkene, products are obtained in diastereoisomeric ratios from 1 : 1 to 20 : 1 and 90–99% ee. Other examples of the synthesis of furan and benzofuran derivatives can be found in Table 5.7.

Chromenes (benzopyranes) and derivatives have a six-membered oxygen heterocycle in their structure and constitute an important class of oxygen heterocycles, which are present in numerous compounds with antitumor, antimicrobial, antituberculosis, and antidiabetic activities, among others [180]. A recent example of

Table 5.7 Construction of five-membered oxygen heterocycles.

General structure	Reaction type	References
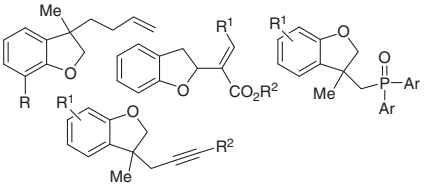	• Arylallylation • Elimination/ intermolecular Heck coupling/ intramolecular allylation cascade reaction • Domino intramolecular Heck cyclization/ intermolecular phosphorylation • Domino reaction	[122, 153, 173, 176]
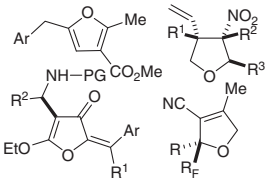	• 5-*exo*-dig cyclization/ coupling/isomerization • Enantioselective [3+2] cycloaddition • [3+2] Cycloaddition • Mannich reaction/ oxypalladation/ reductive elimination	[172, 175, 177, 178]
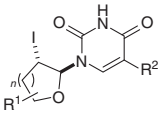	• Enantioselective Wacker-type process	[179]
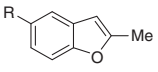	• Cyclization	[154]
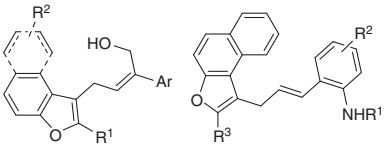	• Decarboxylative allylation/nucleophilic cyclization	[174]
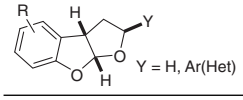	• Enantioselective intermolecular carbo-heterofunctionalization	[127]

the synthesis of this type of compounds has been described by Nikolić et al. [181]. The authors describe the one-pot synthesis of tricyclic compounds containing a CF_3-substituent in the pyrazole (R^2) ring fused with an isochromene. A one-pot two-step procedure was used in which in the first step the pyrazolone is alkylated, and in the second step, the pyran ring is constructed using an intramolecular Pd-catalyzed C–H arylation (Scheme 5.21). Using the one-pot reaction, several 3,5-dihydroisochromene[3,4-*c*]pyrazoles were synthesized in 30–82% yields.

The construction of other *n*-membered ($n > 5$) oxygen heterocycles, using Pd catalysis, is summarized in Table 5.8.

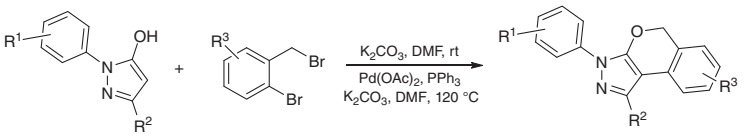

Scheme 5.21 One-pot synthesis of 3,5-dihydroisochromene[3,4-*c*]pyrazoles.

Table 5.8 Construction of *n*-member ($n > 5$) oxygen heterocycles.

General structure	Reaction type	References
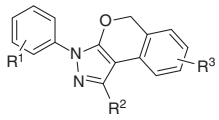	• Direct C–H arylation	[181]
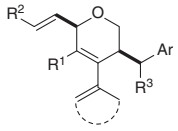	• Stereoselective carbocyclization	[182]
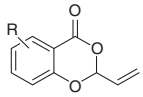	• Intramolecular allylic C–H acetoxylation	[183]
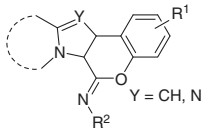	• C(sp^2)–H activation/insertion	[184]
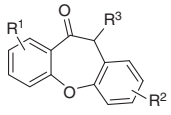	• α-Arylation	[185]

5.3.3 N,O-Heterocycles

Pd-catalyzed alkene carboetherification reactions have been used for the synthesis of oxygen heterocycles, including chiral ones. The use of alkenyl oximes and modified palladium complexes with chiral ligands allows the construction of chiral (N, O) rings, which are present in various bioactive compounds. In this context, Wang et al. [186] and Li et al. [187] recently synthesized several chiral isoxazolines and 1,2-dihydrooxazines using β, γ- and γ, δ-alkenyl oximes, in the presence of Sadphos and SegPhos derived ligands, respectively (Scheme 5.22). 3,5-Disubstituted and 3,5,5-trisubstituted chiral isoxazolines with ee up to 97% and 5,6-dihydro-4*H*-1,2-chiral chiral with ee up to 96% were obtained.

Some other relevant examples of the construction of five- and six-member N,O-heterocycles or of two heterocycles (with N- and O-containing cycles), in the same reaction, and catalyzed by Pd in the 2018–2020 period, are summarized in Table 5.9.

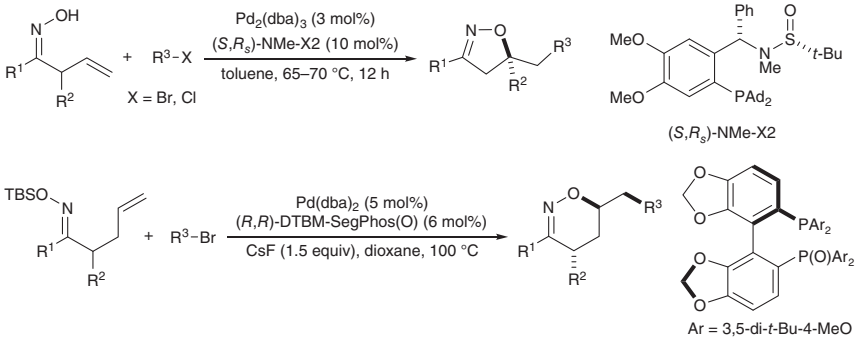

Scheme 5.22 Synthesis of isoxazolines and 1,2-dihydrooxazines by carboetherification of alkenyloximes.

Table 5.9 Construction of one or two N,O-heterocycles.

General structure	Reaction type	References
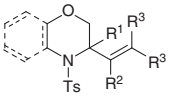	• Enantioselective aza-Wacker-type reaction	[188]
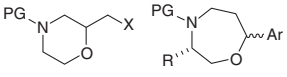 X = Cl, CO_2Me, OCOH, OCOMe	• Oxidative olefin oxyarylation	[189]
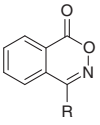	• Intermolecular acylation/ nucleophilic condensation	[137]
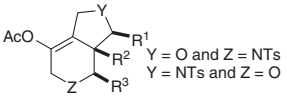 Y = O and Z = NTs Y = NTs and Z = O	• Intramolecular acetoxylative (3+2) annulation	[190]
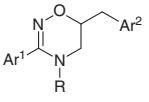	• Carboannulation	[125]
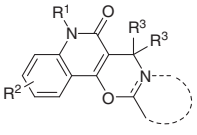	• Carbonylative cascade/CO insertion	[191]
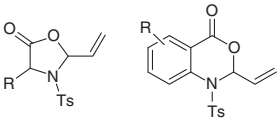	• Intramolecular allylic C–H acetoxylation	[183]
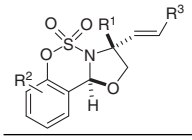	• Asymmetric (3+2) cycloaddition	[192]

5.4 Conclusion and Perspectives

The development of efficient, reliable synthetic methodologies for the synthesis of heterocycles is essential as a consequence of the widespread importance and use of these compounds. Heterocyclic scaffolds are profusely abundant in biologically active compounds, naturally occurring compounds, pharmaceuticals, agrochemicals, and many other industrially relevant compounds. Metal-catalyzed reactions are among the most useful, effective, and advantageous routes to these compounds, a large number of them relying on copper and palladium complexes. This chapter summarizes methods recently referred in the literature for the construction of nitrogen and oxygen heterocycles, mainly of five and six members. Some of the more interesting and different examples are highlighted. The numerous publications on the subject in databases clearly indicate the great interest in metal-catalyzed heterocycle synthesis as well as the continued motivation for exploring new methodologies.

Acknowledgments

Thanks are due to Coimbra Chemistry Centre (CQC), supported by the Portuguese Agency for Scientific Research, "Fundação para a Ciência e a Tecnologia" (FCT) through projects UIDB/00313/2020 and UIDP/00313/2020, and co-funded by COMPETE2020-UE.

References

1 Neto, J.S.S. and Zeni, G. (2020). Ten years of progress in the synthesis of six-membered N-heterocycles from alkynes and nitrogen sources. *Tetrahedron* 76 (4): 130876. https://doi.org/10.1016/j.tet.2019.130876.

2 Pozharskii, A.F., Soldatenkov, A.T., and Katritzky, A.R. (2011). *Heterocycles in Life and Society: An Introduction to Heterocyclic Chemistry, Biochemistry and Applications*. Wiley https://doi.org/10.1002/9781119998372.

3 Zhao, X., Rudolph, M., Asiri, A.M., and Hashmi, A.S.K. (2020). Easy access to pharmaceutically relevant heterocycles by catalytic reactions involving α-imino gold carbene intermediates. *Front. Chem. Sci. Eng.* 14 (3): 317–349. https://doi.org/10.1007/s11705-019-1874-4.

4 Kaur, N., Bhardwaj, P., Devi, M. et al. (2019). Gold-catalyzed C—O bond forming reactions for the synthesis of six-membered O-heterocycles. *SN Appl. Sci.* 1: 903. https://doi.org/10.1007/s42452-019-0920-7.

5 Fürstner, A. (2018). Gold catalysis for heterocyclic chemistry: a representative case study on pyrone natural products. *Angew. Chem. Int. Ed.* 57 (16): 4215–4233. https://doi.org/10.1002/anie.201707260.

6 Kaur, N. (2017). Applications of gold catalysts for the synthesis of five-membered O-heterocycles. *Inorg. Nano-Metal Chem.* 47 (2): 163–187. https://doi.org/10.1080/15533174.2015.1068809.

7 Sugimoto, K. and Matsuya, Y. (2017). Recent applications of gold-catalyzed cascade reactions in total synthesis of natural product. *Tetrahedron Lett.* 58 (47): 4420–4426. https://doi.org/10.1016/j.tetlet.2017.10.029.

8 Huple, D.B., Ghorpade, S., and Liu, R.S. (2016). Recent advances in gold-catalyzed N- and O-functionalizations of alkynes with nitrones, nitroso, nitro and nitroxy species. *Adv. Synth. Catal.* 358 (9): 1348–1367. https://doi.org/10.1002/adsc.201600018.

9 Pan, F., Shu, C., and Ye, L.W. (2016). Recent progress towards gold-catalyzed synthesis of N-containing tricyclic compounds based on ynamides. *Org. Biomol. Chem.* 14 (40): 9456–9465. https://doi.org/10.1039/c6ob01774f.

10 Blanc, A., Bénéteau, V., Weibel, J.M., and Pale, P. (2016). Silver and gold-catalyzed routes to furans and benzofurans. *Org. Biomol. Chem.* 14 (39): 9184–9205. https://doi.org/10.1039/c6ob01468b.

11 Debrouwer, W., Heugebaert, T.S.A., Roman, B.I., and Stevens, C.V. (2015). Homogeneous gold-catalyzed cyclization reactions of alkynes with *N*- and *S*-nucleophiles. *Adv. Synth. Catal.* 357 (14–15): 2975–3006. https://doi.org/10.1002/adsc.201500520.

12 Shilpa, T., Dhanya, R., Saranya, S., and Anilkumar, G. (2020). An overview of rhodium-catalysed multi-component reactions. *ChemistrySelect* 5 (2): 898–915. https://doi.org/10.1002/slct.201904441.

13 Kaur, N., Ahlawat, N., Bhardwaj, P. et al. (2020). Synthesis of five-membered N-heterocycles using Rh based metal catalysts. *Synth. Commun.* 50 (2): 137–160. https://doi.org/10.1080/00397911.2019.1689271.

14 Wang, R., Xie, X., Liu, H., and Zhou, Y. (2019). Rh(III)-catalyzed C—H bond activation for the construction of heterocycles with sp^3-carbon centers. *Catalysts* 9 (10): 823. https://doi.org/10.3390/catal9100823.

15 Chen, W.W. and Xu, M.H. (2017). Recent advances in rhodium-catalyzed asymmetric synthesis of heterocycles. *Org. Biomol. Chem.* 15 (5): 1029–1050. https://doi.org/10.1039/C6OB02021F.

16 Kaur, N., Ahlawat, N., Bhardwaj, P. et al. (2020). Ag-mediated synthesis of six-membered N-heterocycles. *Synth. Commun.* 50 (6): 753–795. https://doi.org/10.1080/00397911.2019.1703196.

17 Kaur, N., Grewal, P., Bhardwaj, P. et al. (2019). Synthesis of five-membered N-heterocycles using silver metal. *Synth. Commun.* 49 (22): 3058–3100. https://doi.org/10.1080/00397911.2019.1655767.

18 Kaur, N. (2019). Gold and silver assisted synthesis of five-membered oxygen and nitrogen containing heterocycles. *Synth. Commun.* 49 (12): 1459–1485. https://doi.org/10.1080/00397911.2019.1575423.

19 Kaur, N. (2019). Application of silver-promoted reactions in the synthesis of five-membered O-heterocycles. *Synth. Commun.* 49 (6): 743–789. https://doi.org/10.1080/00397911.2019.1570525.

20 Kaur, N. (2018). Synthesis of six- and seven-membered and larger heterocylces using Au and Ag catalysts. *Inorg. Nano-Metal Chem.* 48 (11): 541–568. https://doi.org/10.1080/24701556.2019.1567544.

21 Khan, I., Ibrar, A., and Shehzadi, S.A. (2019). Building molecular complexity through transition-metal-catalyzed oxidative annulations/cyclizations: harnessing the utility of phenols, naphthols and 1,3-dicarbonyl compounds. *Coord. Chem. Rev.* 380: 440–470. https://doi.org/10.1016/j.ccr.2018.11.001.

22 Kaur, N. (2019). Applications of palladium dibenzylideneacetone as catalyst in the synthesis of five-membered N-heterocycles. *Synth. Commun.* 49 (10): 1205–1230. https://doi.org/10.1080/00397911.2018.1540048.

23 Choury, M., Lopes, A.B., Blond, G., and Gulea, M. (2020). Synthesis of medium-sized heterocycles by transition-metal-catalyzed intramolecular cyclization. *Molecules* 25 (14): 3147. https://doi.org/10.3390/molecules25143147.

24 Zhang, M., Wang, Q., Peng, Y. et al. (2019). Transition metal-catalyzed sp^3 C–H activation and intramolecular C–N coupling to construct nitrogen heterocyclic scaffolds. *Chem. Commun.* 55 (87): 13048–13065. https://doi.org/10.1039/c9cc06609h.

25 Silva, V.L.M. and Silva, A.M.S. (2019). Palladium-catalysed synthesis and transformation of quinolones. *Molecules* 24 (2): 228. https://doi.org/10.3390/molecules24020228.

26 Kaur, N. (2019). Palladium acetate and phosphine assisted synthesis of five-membered N-heterocycles. *Synth. Commun.* 49 (4): 483–514. https://doi.org/10.1080/00397911.2018.1536213.

27 Kaur, N., Verma, Y., Grewal, P. et al. (2020). Palladium acetate assisted synthesis of five-membered N-polyheterocycles. *Synth. Commun.* 50 (11): 1567–1621. https://doi.org/10.1080/00397911.2020.1723640.

28 Perrone, S., Troisi, L., and Salomone, A. (2019). Heterocycle synthesis through Pd-catalyzed carbonylative coupling. *Eur. J. Org. Chem.* 2019 (29): 4626–4643. https://doi.org/10.1002/ejoc.201900439.

29 Zuo, L., Liu, T., Chang, X., and Guo, W. (2019). An update of transition metal-catalyzed decarboxylative transformations of cyclic carbonates and carbamates. *Molecules* 24 (21): 3930. https://doi.org/10.3390/molecules24213930.

30 Mancuso, R., Della, Ca' N., Veltri, L. et al. (2019). PdI_2-based catalysis for carbonylation reactions: a personal account. *Catalysts* 9: 610. https://doi.org/10.3390/catal9070610.

31 Gabriele B. Synthesis of heterocycles by palladium-catalyzed carbonylative reactions *Advances in Transition-Metal Mediated Heterocyclic Synthesis*, Solé D, Fernández I, editors: Elsevier Inc; 2018. https://doi.org/10.1016/B978-0-12-811651-7.00003-0.

32 Ojha, N.K., Zyryanov, G.V., Majee, A. et al. (2017). Copper nanoparticles as inexpensive and efficient catalyst: a valuable contribution in organic synthesis. *Coord. Chem. Rev.* 353: 1–57. https://doi.org/10.1016/j.ccr.2017.10.004.

33 Romero, A.H. (2019). Fused heteroaromatic rings via metal-mediated/catalyzed intramolecular C–H activation: a comprehensive review. *Top. Curr. Chem.* 377: 21. https://doi.org/10.1007/s41061-019-0246-3.

34 Kaur, N., Verma, Y., Ahlawat, N. et al. (2020). Copper-assisted synthesis of five-membered O-heterocycles. *Inorg. Nano-Metal Chem.* 50 (8): 705–740. https://doi.org/10.1080/24701556.2020.1724144.

35 Kaur, N. (2019). Copper catalyzed synthesis of seven and higher membered heterocycles. *Synth. Commun.* 49 (7): 879–916. https://doi.org/10.1080/00397911.2018.1543780.

36 Janardhanan, J.C., Bhaskaran, R.P., Praveen, V.K. et al. (2020). Transition-metal-catalyzed syntheses of indazoles. *Asian J. Org. Chem.* 9 (10): 1410–1431. https://doi.org/10.1002/ajoc.202000300.

37 Li, W. and Zhang, J. (2020). Synthesis of heterocycles through denitrogenative cyclization of triazoles and benzotriazoles. *Chem. Eur. J.* 26 (52): 11931–11945. https://doi.org/10.1002/chem.202000674.

38 Selvaraj, K., Chauhan, S., Sandeep, K., and Swamy, K.C.K. (2020). Advances in [4+3]-annulation/cycloaddition reactions leading to homo- and heterocycles with seven-membered rings. *Chem. Asian J.* 15 (16): 2380–2402. https://doi.org/10.1002/asia.202000545.

39 Campos, J.F. and Berteina-Raboin, S. (2020). Tandem catalysis: synthesis of nitrogen-containing heterocycles. *Catalysts* 10 (6): 631. https://doi.org/10.3390/catal10060631.

40 Largeron, M. and Nguyen, K.M.H. (2018). Recent advances in the synthesis of benzimidazole derivatives from the oxidative coupling of primary amines. *Synthesis* 50 (2): 241–253. https://doi.org/10.1055/s-0036-1590915.

41 Kazemi, M. and Mohammadi, M. (2020). Magnetically recoverable catalysts: catalysis in synthesis of polyhydroquinolines. *Appl. Organomet. Chem.* 34 (3): 42–48. https://doi.org/10.1002/aoc.5400.

42 Bugaenko, D.I., Karchava, A.V., and Yurovskaya, M.A. (2019). Synthesis of indoles: recent advances. *Russ. Chem. Rev.* 88 (2): 99–159. https://doi.org/10.1070/rcr4844.

43 Marichev, K.O. and Doyle, M.P. (2019). Catalytic asymmetric cycloaddition reactions of enoldiazo compounds. *Org. Biomol. Chem.* 17 (17): 4183–4195. https://doi.org/10.1039/c9ob00478e.

44 Murarka, S. and Antonchick, A.P. (2018). Metal-catalyzed oxidative coupling of ketones and ketone enolates. *Synthesis* 50 (11): 2150–2162. https://doi.org/10.1055/s-0037-1609715.

45 Kerru, N., Gummidi, L., Maddila, S. et al. (2020). A review on recent advances in nitrogen-containing molecules and their biological applications. *Molecules* 25 (8): 1909. https://doi.org/10.3390/molecules25081909.

46 Cherian, R.M., Harry, N.A., Saranya, S. et al. (2019). Copper-catalysed multicomponent syntheses of heterocycles. *Asian J. Org. Chem.* 8 (2): 197–233. https://doi.org/10.1002/ajoc.201800619.

47 Saikia, P. and Gogoi, S. (2018). Isocoumarins: general aspects and recent advances in their synthesis. *Adv. Synth. Catal.* 360 (11): 2063–2075. https://doi.org/10.1002/adsc.201800019.

48 Pal, T., Lahiri, G.K., and Maiti, D. (2020). Copper in efficient synthesis of aromatic heterocycles with single heteroatom. *Eur. J. Org. Chem.* 2020 (44): 6859–6869. https://doi.org/10.1002/ejoc.202000688.

49 Baguia, H., Deldaele, C., Romero, E. et al. (2018). Copper-catalyzed photoinduced radical domino cyclization of ynamides and cyanamides: a unified entry

to rosettacin, luotonin A, and deoxyvasicinone. *Synthesis* 50 (15): 3022–3030. https://doi.org/10.1055/s-0037-1610134.

50 Kaur, N. (2018). Copper catalysts in the synthesis of five-membered N-polyheterocycles. *Curr. Org. Synth.* 15 (7): 940–971. https://doi.org/10.2174/1570179415666180815144442.

51 Dong, J., Zhang, Q., Wang, Z. et al. (2018). Recent advances in the development of indazole-based anticancer agents. *ChemMedChem* 13 (15): 1490–1507. https://doi.org/10.1002/cmdc.201800253.

52 Cheng, Y., Li, G., Liu, Y. et al. (2016). Unparalleled ease of access to a library of biheteroaryl fluorophores via oxidative cross-coupling reactions: discovery of photostable NIR probe for mitochondria. *J. Am. Chem. Soc.* 138 (14): 4730–4738. https://doi.org/10.1021/jacs.5b09241.

53 Janardhanan, J.C., Mishra, R.K., Das, G. et al. (2018). Functionalizable 1*H*-indazoles by palladium catalyzed aza-Nenitzescu reaction: pharmacophores to donor-acceptor type multi-luminescent fluorophores. *Asian J. Org. Chem.* 7 (10): 2094–2104. https://doi.org/10.1002/ajoc.201800413.

54 Travieso-Puente, R., Budzak, S., Chen, J. et al. (2017). Arylazoindazole photoswitches: facile synthesis and functionalization via S_NAr substitution. *J. Am. Chem. Soc.* 139 (9): 3328–3331. https://doi.org/10.1021/jacs.6b12585.

55 Kaur, M., Singh, M., Chadha, N., and Silakari, O. (2016). Oxindole: a chemical prism carrying plethora of therapeutic benefits. *Eur. J. Med. Chem.* 123: 858–894. https://doi.org/10.1016/j.ejmech.2016.08.011.

56 Kirillova, M.S., Miloserdov, F.M., and Echavarren, A.M. (2018). Total syntheses of pyrroloazocine indole alkaloids: challenges and reaction discovery. *Org. Chem. Front.* 5 (2): 273–287. https://doi.org/10.1039/c7qo00786h.

57 Li, D.X., Kim, J., Yang, J.W., and Yun, J. (2018). Copper-catalyzed asymmetric synthesis of borylated cis-disubstituted indolines. *Chem. Asian J.* 13 (17): 2365–2368. https://doi.org/10.1002/asia.201800121.

58 Marchese, A.D., Larin, E.M., Mirabi, B., and Lautens, M. (2020). Metal-catalyzed approaches toward the oxindole core. *Acc. Chem. Res.* 53 (8): 1605–1619. https://doi.org/10.1021/acs.accounts.0c00297.

59 Whyte, A., Burton, K.I., Zhang, J., and Lautens, M. (2018). Enantioselective intramolecular copper-catalyzed borylacylation. *Angew. Chem. Int. Ed.* 57 (42): 13927–13930. https://doi.org/10.1002/anie.201808460.

60 Li, D., Wang, Y., Jia, Z. et al. (2019). Cu-mediated synthesis of indolines and dihydroisoquinolinones through arylperfluoroalkylation of unactivated alkenes. *Eur. J. Org. Chem.* 2019 (30): 4797–4804. https://doi.org/10.1002/ejoc.201900680.

61 Sayyad, N., Cele, Z., Aleti, R.R. et al. (2018). Copper-catalyzed self-condensation of benzamide: domino reactions towards quinazolinones. *Eur. J. Org. Chem.* 2018 (39): 5382–5388. https://doi.org/10.1002/ejoc.201800660.

62 Liu, X., Deng, G., and Liang, Y. (2018). Selective synthesis of benzo[4,5]imidazo[2,1-*a*]isoquinolines via copper-catalyzed tandem annulation of alkynylbenzonitriles with 2-iodoanilines. *Tetrahedron Lett.* 59 (29): 2844–2847. https://doi.org/10.1016/j.tetlet.2018.06.030.

63 Feng, C.T., Wei, H.J., Li, J. et al. (2018). Synthesis of cyanide-functionalized imidazo[1,5-*a*]quinolines via copper-mediated aerobic three-component cyclizations. *Adv. Synth. Catal.* 360 (24): 4726–4730. https://doi.org/10.1002/adsc.201801060.

64 Sandeep, M., Swati Dushyant, P., Sravani, B., and Rajender, R.K. (2018). Direct access to halogenated fused imidazo[1,5-α]*N*-heteroaromatics through copper-promoted double oxidative C–H amination and halogenation. *Eur. J. Org. Chem.* 2018 (23): 3036–3047. https://doi.org/10.1002/ejoc.201800628.

65 Kwak, J.P., Dao, P.D.Q., and Cho, C.S. (2020). Synthesis of 2-aminoquinazoline- and 2-aminopyrimidine-fused hybrid scaffolds by copper-catalyzed C(sp^2)–N coupling and cyclization followed by oxidation. *Eur. J. Org. Chem.* 2020 (23): 3468–3474. https://doi.org/10.1002/ejoc.202000427.

66 Tran, C.B., To, T.A., Vo, Y.H. et al. (2019). A green synthesis of N,N- and N,O-heterocycles using a recyclable catalyst in a bio-based solvent. *ChemistrySelect* 4 (3): 880–883. https://doi.org/10.1002/slct.201804027.

67 Motornov, V.A., Tabolin, A.A., Nelyubina, Y.V. et al. (2020). Copper-mediated oxidative [3+2]-annulation of nitroalkenes and pyridinium imines: efficient synthesis of 3-fluoro- and 3-nitro-pyrazolo[1,5-*a*] pyridines. *Org. Biomol. Chem.* 18 (7): 1436–1448. https://doi.org/10.1039/c9ob02668a.

68 Zhu, J.S., Haddadin, M.J., and Kurth, M.J. (2019). Davis–Beirut reaction: diverse chemistries of highly reactive nitroso intermediates in heterocycle synthesis. *Acc. Chem. Res.* 52 (8): 2256–2265. https://doi.org/10.1021/acs.accounts.9b00220.

69 Hajipour, A.R., Khorsandi, Z., and Bahri, S. (2018). An efficient and inexpensive visible light photoredox copper catalyst for N—N bond-forming reactions: the one-pot synthesis of indazolo[2,3-α]quinolines. *J. Iran. Chem. Soc.* 15 (4): 981–986. https://doi.org/10.1007/s13738-018-1295-1.

70 Niu, B., Li, S., Cui, C. et al. (2019). New strategy for the synthesis of heterocycles via copper-catalyzed oxidative decarboxylative amination of glyoxylic acid. *Eur. J. Org. Chem.* 2019 (48): 7800–7803. https://doi.org/10.1002/ejoc.201901538.

71 Yu, H., Xuan, P., Jiao, M., and Lin, J. (2018). Synthesis of 1,1-disubstituted *N*-acyl tetrahydroisoquinolines from enamides by cascade radical addition and cyclization. *Eur. J. Org. Chem.* 2018 (33): 4565–4570. https://doi.org/10.1002/ejoc.201800748.

72 Martín-García, I. and Alonso, F. (2018). Synthesis of dihydroindoloisoquinolines through copper-catalyzed cross-dehydrogenative coupling of tetrahydroisoquinolines and nitroalkanes. *Chem. Eur. J.* 24 (71): 18857–18862. https://doi.org/10.1002/chem.201805137.

73 Lee, H.K., Dao, P.D.Q., Kim, Y.S., and Cho, C.S. (2018). Synthesis of indolo[2,1-*a*]isoquinolines via copper-catalyzed C–C coupling and cyclization of 2-(2-bromoaryl)-1*H*-indoles with 1,3-diketones. *Synthesis* 50 (16): 3243–3249. https://doi.org/10.1055/s-0036-1591589.

74 Li, Y., Peng, J., Chen, X. et al. (2018). Copper-catalyzed synthesis of multisubstituted indoles through tandem Ullmann-type C–N formation and cross-dehydrogenative coupling reactions. *J. Organomet. Chem.* 83 (9): 5288–5294. https://doi.org/10.1021/acs.joc.8b00353.

75 Ni, Y., Zuo, H., Li, Y. et al. (2018). Copper-catalyzed regioselective intramolecular electrophilic sulfenoamination via Lewis acid activation of disulfides under aerobic conditions. *Org. Lett.* 20 (14): 4350–4353. https://doi.org/10.1021/acs.orglett.8b01803.

76 Hong, F., Chen, Y., Ye, S. et al. (2020). Copper-catalyzed asymmetric reaction of alkenyl diynes with styrenes by formal [3+2] cycloaddition via Cu-containing all-carbon 1,3-dipoles: access to chiral pyrrole-fused bridged [2.2.1] skeletons. *J. Am. Chem. Soc.* 142 (16): 7618–7626. https://doi.org/10.1021/jacs.0c01918.

77 Hong, F.L., Wang, Z.S., Wei, D.D. et al. (2019). Generation of donor/donor copper carbenes through copper-catalyzed diyne cyclization: enantioselective and divergent synthesis of chiral polycyclic pyrroles. *J. Am. Chem. Soc.* 141 (42): 16961–16970. https://doi.org/10.1021/jacs.9b09303.

78 Ramaraju, A., Chouhan, N.K., Ravi, O. et al. (2018). Cu-catalyzed coupling of *o*-acyl oximes with isatins: domino rearrangement strategy for direct access to quinoline-4-carboxamides by C—N bond cleavage. *Eur. J. Org. Chem.* 2018 (23): 2963–2971. https://doi.org/10.1002/ejoc.201800501.

79 Dang, H.V., Le, H.T.B., Tran, L.T.B. et al. (2018). Copper-catalyzed one-pot domino reactions via C—H bond activation: synthesis of 3-aroylquinolines from 2-aminobenzylalcohols and propiophenones under metal-organic framework catalysis. *RSC Adv.* 8 (55): 31455–31464. https://doi.org/10.1039/c8ra05459b.

80 Gong, X., Li, G., Gan, Z. et al. (2019). Sulfonylacetonitriles as building blocks in copper-catalyzed domino reactions: an efficient approach to sulfonated isoquinolin-1(2*H*)-ones. *Asian J. Org. Chem.* 8 (8): 1472–1478. https://doi.org/10.1002/ajoc.201900382.

81 Larin, E.M., Loup, J., Polishchuk, I. et al. (2020). Enantio- and diastereoselective conjugate borylation/Mannich cyclization. *Chem. Sci.* 11 (22): 5716–5723. https://doi.org/10.1039/d0sc02421j.

82 Zhang, M., Liu, S., Li, H. et al. (2019). Copper-catalyzed cope-type hydroamination of nonactivated olefins toward cyclic nitrones: scope, mechanism, and enantioselective process development. *Chem. Eur. J.* 25 (54): 12620–12627. https://doi.org/10.1002/chem.201902683.

83 Wei, L., Chang, X., and Wang, C.J. (2020). Catalytic asymmetric reactions with N-metallated azomethine ylides. *Acc. Chem. Res.* 53 (5): 1084–1100. https://doi.org/10.1021/acs.accounts.0c00113.

84 Adrio, J. and Carretero, J.C. (2019). Stereochemical diversity in pyrrolidine synthesis by catalytic asymmetric 1,3-dipolar cycloaddition of azomethine ylides. *Chem. Commun.* 55 (80): 11979–11991. https://doi.org/10.1039/c9cc05238k.

85 Marichev, K.O., Adly, F.G., Carranco, A.M. et al. (2018). Catalyst choice for highly enantioselective [3+3]-cycloaddition of enoldiazocarbonyl compounds. *ACS Catal.* 8 (11): 10392–10400. https://doi.org/10.1021/acscatal.8b03391.

86 Lv, J., He, Z., Zhang, J. et al. (2018). One-pot synthesis of [1,2,4]triazolo[1,5-*a*]pyridines from azines and benzylidenemalononitriles via copper-catalyzed tandem cyclization. *Tetrahedron* 74 (29): 3996–4004. https://doi.org/10.1016/j.tet.2018.06.002.

87 Subramanian, P. and Kaliappan, K.P. (2020). A one-pot copper-catalyzed 3-fold C—N bond coupling strategy to the synthesis of substituted benzimidazoles. *Eur. J. Org. Chem.* 2020 (44): 6915–6921. https://doi.org/10.1002/ejoc.202000428.

88 Guchhait, S.K. and Saini, M. (2019). Chan-Lam: N-arylation and C–H amination with heteroaromatic ring-NH: an approach to access extended-fused imidazo[1,2-*a*]-pyridines/pyrazines. *New J. Chem.* 44 (2): 308–312. https://doi.org/10.1039/c9nj04966e.

89 Zou, L.H., Yan, C., Shi, K. et al. (2019). Copper-catalyzed C—C bond cleavage/double cyclization of α-ketoamides with *o*-phenylene diamines: synthesis of benzimidazo[1,2-*c*]quinazolin-6-ones. *Eur. J. Org. Chem.* 2019 (47): 7725–7729. https://doi.org/10.1002/ejoc.201901642.

90 Kerdphon, S., Sanghong, P., Chatwichien, J. et al. (2020). Commercial copper-catalyzed aerobic oxidative synthesis of quinazolinones from 2-aminobenzamide and methanol. *Eur. J. Org. Chem.* 2020 (18): 2730–2734. https://doi.org/10.1002/ejoc.202000257.

91 Vodnala, N., Gujjarappa, R., Satheesh, V. et al. (2020). Copper-catalyzed [2+2+1+1] annulation for the regioselective synthesis of 2,6-diarylpyridines via C1-insertion and subsequent cyclization. *ChemistrySelect* 5 (32): 10144–10148. https://doi.org/10.1002/slct.202002968.

92 Sujatha, C., Bhatt, C.S., Ravva, M.K. et al. (2018). Copper-catalyzed ring-expansion cascade of azirines with alkynes: synthesis of multisubstituted pyridines at room temperature. *Org. Lett.* 20 (11): 3241–3244. https://doi.org/10.1021/acs.orglett.8b01090.

93 Tian, Z., Xu, J., Liu, B. et al. (2018). Copper-catalyzed synthesis of polysubstituted pyrroles through [3+1+1] cycloaddition reaction of nitrones and isocyanides. *Org. Lett.* 20 (9): 2603–2606. https://doi.org/10.1021/acs.orglett.8b00798.

94 Zhang, Y., Feng, H., Liu, X., and Huang, L. (2018). A highly chemoselective synthesis of cyclic divalent propargylamines by copper-catalyzed annulation/double A3-couplings. *Eur. J. Org. Chem.* 2018 (17): 2039–2046. https://doi.org/10.1002/ejoc.201800393.

95 Zhang, Z., Zhang, X., and Nagib, D.A. (2019). Chiral piperidines from acyclic amines via enantioselective, radical-mediated δ C–H cyanation. *Chem* 5 (12): 3127–3134. https://doi.org/10.1016/j.chempr.2019.09.010.

96 De Tan, T., Chen, Y.B., Fan, X.Y., and Ye, L.W. (2019). Recent progress in the copper-catalyzed cascade cyclization involving intramolecular hydroamination of terminal alkynes. *Synlett* 30 (18): 2035–2040. https://doi.org/10.1055/s-0037-1611903.

97 Van Beek, W.E., Gadde, K., and Tehrani, K.A. (2018). The use of calcium carbide as acetylene source in a three-component coupling with ω-chlorinated ketones and primary amines. *Chem. Eur. J.* 24 (62): 16645–16651. https://doi.org/10.1002/chem.201803669.

98 Gulati, U., Rajesh, U.C., and Rawat, D.S. (2020). Magnetically recoverable Ni@CuI hybrid nanocatalysts affording spiropyrroline heterocycles from

ketoximes and alkenes. *Asian J. Org. Chem.* 9 (7): 1059–1064. https://doi.org/10.1002/ajoc.202000145.

99 Ji, D., Liu, K., and Sun, J. (2018). Tandem reaction of allenoate formation and cyclization: divergent synthesis of four- to six-membered heterocycles. *Org. Lett.* 20 (23): 7708–7711. https://doi.org/10.1021/acs.orglett.8b03435.

100 Dai, X.J., Engl, O.D., León, T., and Buchwald, S.L. (2019). Catalytic asymmetric synthesis of α-arylpyrrolidines and benzo-fused nitrogen heterocycles. *Angew. Chem. Int. Ed.* 58 (11): 3407–3411. https://doi.org/10.1002/anie.201814331.

101 Jang, S.S., Chang, J.Y., Kang, G.Y., and Youn, S.W. (2019). Oxidant-controlled divergent syntheses of pyrazoles and pyrroles by copper(I)-catalyzed oxidative coupling of β-enamino esters. *Asian J. Org. Chem.* 8 (9): 1668–1673. https://doi.org/10.1002/ajoc.201900351.

102 Bafaluy, D., Muñoz-Molina, J.M., Funes-Ardoiz, I. et al. (2019). Copper-catalyzed N−F bond activation for uniform intramolecular C−H amination yielding pyrrolidines and piperidines. *Angew. Chem. Int. Ed.* 58 (26): 8912–8916. https://doi.org/10.1002/anie.201902716.

103 Paternoga, J. and Opatz, T. (2019). A copper-catalyzed synthesis of pyrroles through photochemically generated acylazirines. *Eur. J. Org. Chem.* 2019 (42): 7067–7078. https://doi.org/10.1002/ejoc.201901176.

104 Yasukawa, N., Kuwata, M., Imai, T. et al. (2018). Copper-catalyzed pyrrole synthesis from 3,6-dihydro-1,2-oxazines. *Green Chem.* 20 (19): 4409–4413. https://doi.org/10.1039/c8gc01373j.

105 Kotovshchikov, Y.N., Latyshev, G.V., Kirillova, E.A. et al. (2020). Assembly of thiosubstituted benzoxazoles via copper-catalyzed coupling of thiols with 5-iodotriazoles serving as diazo surrogates. *J. Organomet. Chem.* 85 (14): 9015–9028. https://doi.org/10.1021/acs.joc.0c00931.

106 Lu, J.Y. (2019). Copper-catalyzed synthesis of 2-aminopyridylbenzoxazoles: via domino reactions of intermolecular N-arylation and intramolecular O-arylation. *RSC Adv.* 9 (24): 13414–13417. https://doi.org/10.1039/c9ra01908a.

107 Iwasaki, M., Ikemoto, Y., and Nishihara, Y. (2020). Synthesis of 2-isoxazoline N-oxides by copper-mediated radical annulation of alkenes with α-nitrobenzyl bromides. *Org. Lett.* 22 (19): 7577–7580. https://doi.org/10.1021/acs.orglett.0c02781.

108 Fu, M., Li, H., Su, M. et al. (2019). Synthesis of 3-nitroisoxazoles via copper acetate-mediated reaction of benzaldehydes with nitromethane. *Adv. Synth. Catal.* 361 (14): 3420–3429. https://doi.org/10.1002/adsc.201900323.

109 Chen, C. and Cui, S. (2019). Iterative assembly of nitrile oxides and ynamides: synthesis of isoxazoles and pyrroles. *J. Organomet. Chem.* 84 (18): 12157–12164. https://doi.org/10.1021/acs.joc.9b01430.

110 Potuganti, G.R., Indukuri, D.R., Nanubolu, J.B., and Alla, M. (2018). Copper-catalyzed domino addition, hydroamination, and cyclization: a multicomponent approach to spiro oxazolidinone derivatives. *J. Organomet. Chem.* 83 (24): 15186–15194. https://doi.org/10.1021/acs.joc.8b02461.

111 Li L, Ji X, Huang H. Pd-catalyzed synthesis of nitrogen-containing heterocycles. In transition metal-catalyzed heterocycle synthesis via C–H activation. Wu X, editor: Wiley-VCH; 2016. 45–64. https://doi.org/10.1002/9783527691920.

112 Wolfe, J.P. and Li, J.J. (2006). An introduction to palladium catalysis. In: *Palladium in Heterocyclic Chemistry, a Guide for the Synthetic Chemist* (ed. J.J. Li and G.W. Gribble), 1–35. Elsevier Science https://doi.org/10.1016/S1460-1567(07)80050-X.

113 Christodoulou, M.S., Beccalli, E.M., Foschi, F., and Giofrè, S. (2020). Pd-catalyzed domino reactions involving alkenes to access substituted indole derivatives. *Synthesis* 52 (19): 2731–2760. https://doi.org/10.1055/s-0040-1707123.

114 Youn, S.W. (2020). Transition-metal-catalyzed annulative coupling cascade for the synthesis of 3-methyleneisoindolin-1-ones. *Synthesis* 52 (6): 807–818. https://doi.org/10.1055/s-0039-1690046.

115 Gabriele, B., Mancuso, R., Veltri, L. et al. (2019). Palladium-catalyzed double cyclization processes leading to polycyclic heterocycles: recent advances. *Eur. J. Org. Chem.* 2019 (31–32): 5073–5092. https://doi.org/10.1002/ejoc.201900481.

116 Ju, B. and Kong, W. (2020). Recent progress in the consecutive double Heck reaction. *Asian J. Org. Chem.* 9 (8): 1154–1161. https://doi.org/10.1002/ajoc.202000230.

117 Dhameliya, T.M., Donga, H.A., Vaghela, P.V. et al. (2020). A decennary update on applications of metal nanoparticles (MNPs) in the synthesis of nitrogen- and oxygen-containing heterocyclic scaffolds. *RSC Adv.* 10 (54): 32740–32820. https://doi.org/10.1039/d0ra02272a.

118 Yue, G., Li, S., Jiang, D. et al. (2020). Syntheses of 3,3-disubstituted dihydrobenzofurans, indolines, indolinones and isochromanes by palladium-catalyzed tandem reaction using $Pd(PPh_3)_2Cl_2$/(±)-BINAP as a catalytic system. *Catalysts* 10: 1084. https://doi.org/10.3390/catal10091084.

119 Kumar, G.S., Singh, D., Kumar, M., and Kapur, M. (2018). Palladium-catalyzed aerobic oxidative coupling of allylic alcohols with anilines in the synthesis of nitrogen heterocycles. *J. Organomet. Chem.* 83 (7): 3941–3951. https://doi.org/10.1021/acs.joc.8b00287.

120 Yang, L., Shi, L., Xing, Q. et al. (2018). Enabling CO insertion into *o*-nitrostyrenes beyond reduction for selective access to indolin-2-one and dihydroquinolin-2-one derivatives. *ACS Catal.* 8 (11): 10340–10348. https://doi.org/10.1021/acscatal.8b02863.

121 Guan, X., Zhu, H., Zhao, Y., and Driver, T.G. (2020). Pd-catalyzed reductive cyclization of nitroarenes with CO_2 as the CO source. *Eur. J. Org. Chem.* 2020 (1): 57–60. https://doi.org/10.1002/ejoc.201901629.

122 Ramesh, K. and Satyanarayana, G. (2020). Propargyl alcohols as alkyne sources: synthesis of heterocyclic compounds under microwave irradiation. *J. Organomet. Chem.* 922: 121350. https://doi.org/10.1016/j.jorganchem.2020.121350.

123 Hu, J., Li, Z., Zhang, X. et al. (2018). Palladium-catalyzed cyclization reaction of oxime acetates and aryl iodides: syntheses of 2-imidazolines. *Org. Lett.* 20 (7): 2116–2119. https://doi.org/10.1021/acs.orglett.8b00696.

124 Yang, Y. and Yang, W. (2018). Divergent synthesis of N-heterocycles by Pd-catalyzed controllable cyclization of vinylethylene carbonates. *Chem. Commun.* 54 (86): 12182–12185. https://doi.org/10.1039/C8CC06945J.

125 Sun, B., Liu, S., Zhang, M. et al. (2019). Pd-catalyzed carboannulation of γ,δ-alkenyl oximes: efficient access to 5-membered cyclic nitrones and dihydroazines. *Org. Chem. Front.* 6 (3): 388–392. https://doi.org/10.1039/c8qo01076e.

126 Jana, S., Bandyopadhyay, M., and Mal, D. (2018). Regioselective synthesis of dihydro-1*H*-furo[*b*]indol-1-ones and their carbanionic reactivity. *Synthesis* 50 (18): 3723–3730. https://doi.org/10.1055/s-0037-1610439.

127 Tao, M., Tu, Y., Liu, Y. et al. (2020). Pd/Xiang-Phos-catalyzed enantioselective intermolecular carboheterofunctionalization under mild conditions. *Chem. Sci.* 11 (24): 6283–6288. https://doi.org/10.1039/d0sc01391a.

128 Yong, W., Li, P., Sheng, R. et al. (2018). Pd-catalyzed one-pot two-step synthesis of 2-(1*H*-indol-3-yl)-2-phenylindolin-3-ones from 2-alkynyl arylazides and indoles. *ChemistrySelect* 3 (41): 11696–11699. https://doi.org/10.1002/slct.201802476.

129 Hung, T.Q., Hieu, D.T., Van Tinh, D. et al. (2019). Efficient access to β- and γ-carbolines from a common starting material by sequential site-selective Pd-catalyzed C–C, C–N coupling reactions. *Tetrahedron* 75 (40): 130569. https://doi.org/10.1016/j.tet.2019.130569.

130 Li, X., Zhou, B., Yang, R.Z. et al. (2018). Palladium-catalyzed enantioselective intramolecular dearomative Heck reaction. *J. Am. Chem. Soc.* 140 (42): 13945–13951. https://doi.org/10.1021/jacs.8b09186.

131 Hung, T.Q., Quan, N.M., Van Dong, H. et al. (2019). Synthesis of 5-aryl-5*H*-pyrido[2′,1′:2,3]imidazo[4,5-*b*]indoles by domino Pd- and Cu-catalyzed C–N coupling reactions. *Synlett* 30 (3): 303–306. https://doi.org/10.1055/s-0037-1611957.

132 Cera, G., Lanzi, M., Balestri, D. et al. (2018). Synthesis of carbolines via palladium/carboxylic acid joint catalysis. *Org. Lett.* 20 (11): 3220–3224. https://doi.org/10.1021/acs.orglett.8b01072.

133 Hédouin, J., Schneider, C., Gillaizeau, I., and Hoarau, C. (2018). Palladium-catalyzed domino allenamide carbopalladation/direct C–H allylation of heteroarenes: synthesis of primprinine and papaverine analogues. *Org. Lett.* 20 (19): 6027–6032. https://doi.org/10.1021/acs.orglett.8b02365.

134 Wang, Y.N., Xiong, Q., Lu, L.Q. et al. (2019). Inverse-electron-demand palladium-catalyzed asymmetric [4+2] cycloadditions enabled by chiral P,S-ligand and hydrogen bonding. *Angew. Chem. Int. Ed.* 58 (32): 11013–11017. https://doi.org/10.1002/anie.201905993.

135 Zhang, T., Shen, H.C., Xu, J.C. et al. (2019). Pd(II)-catalyzed asymmetric oxidative annulation of *N*-alkoxyheteroaryl amides and 1,3-dienes. *Org. Lett.* 21 (7): 2048–2051. https://doi.org/10.1021/acs.orglett.9b00216.

136 Bhattacharya, D., Tomar, R., and Babu, S.A. (2020). Conversion of 2,3-dihydrobenzo[*b*][1,4]dioxine-2-carboxamides to 3-oxoquinolin-2(1*H*)-ones via ring-opening and formal 6-endo-trig cyclization-involved Heck reactions. *Asian J. Org. Chem.* 9 (5): 829–839. https://doi.org/10.1002/ajoc.202000096.

137 Suchand, B. and Satyanarayana, G. (2018). Palladium-catalyzed acylation reactions: a one-pot diversified synthesis of phthalazines, phthalazinones and benzoxazinones. *Eur. J. Org. Chem.* 2018 (19): 2233–2246. https://doi.org/10.1002/ejoc.201800159.

138 Babij, N.R., Boothe, J.R., McKenna, G.M. et al. (2019). Stereocontrolled synthesis of bicyclic ureas and sulfamides via Pd-catalyzed alkene carboamination reactions. *Tetrahedron* 75 (32): 4228–4243. https://doi.org/10.1016/j.tet.2019.04.031.

139 Hong, Y., Liu, W., Dong, M. et al. (2019). Pd(0)-catalyzed cyclizative phosphorylation of (*Z*)-1-iodo-1,6-diene: synthesis of alkylphosphonate and alkylthionophosphonate. *Org. Lett.* 21 (14): 5742–5746. https://doi.org/10.1021/acs.orglett.9b02149.

140 Guo, X., Hu, J., Zhang, M., and Wang, L. (2019). Palladium-catalyzed C(sp^2)–H activation for the formation of C–N bonds: rapid access to benzimidazoquinazolines. *Asian J. Org. Chem.* 8 (3): 417–421. https://doi.org/10.1002/ajoc.201800710.

141 Qiu, H., Zhou, P., Liu, W. et al. (2020). Palladium-catalyzed intermolecular carbopalladation cascade: facile synthesis of [1,2,3]triazolo[1,5-*a*]quinolines from *o*-triazole bromobenzenes and internal alkynes. *ChemistrySelect* 5 (10): 2935–2939. https://doi.org/10.1002/slct.201904238.

142 Ghaedi, A., Bardajee, G.R., Delbari, A.S., and Hekmat, S. (2020). Green and efficient synthesis of new pyrido[2,3-*d*]pyrimidine derivatives using Pd/SBA-15 as a nanocatalyst. *Arkivoc* 2020 (6): 84–93. https://doi.org/10.24820/ARK.5550190.P011.140dummy2.

143 Ferretti, F., Ramadan, D.R., and Ragaini, F. (2019). Transition metal catalyzed reductive cyclization reactions of nitroarenes and nitroalkenes. *ChemCatChem* 11 (18): 4450–4488. https://doi.org/10.1002/cctc.201901065.

144 Bai, X., Wu, C., Ge, S., and Lu, Y. (2020). Pd/Cu-catalyzed enantioselective sequential Heck/Sonogashira coupling: asymmetric synthesis of oxindoles containing trifluoromethylated quaternary stereogenic centers. *Angew. Chem. Int. Ed.* 59 (7): 2764–2768. https://doi.org/10.1002/anie.201913148.

145 Formenti, D., Ferretti, F., and Ragaini, F. (2018). Synthesis of N-heterocycles by reductive cyclization of nitro compounds using formate esters as carbon monoxide surrogates. *ChemCatChem* 10 (1): 148–152. https://doi.org/10.1002/cctc.201701214.

146 Ramesh, K., Basuli, S., and Satyanarayana, G. (2018). Microwave-assisted domino palladium catalysis in water: a diverse synthesis of 3,3′-disubstituted heterocyclic compounds. *Eur. J. Org. Chem.* 2018 (19): 2171–2177. https://doi.org/10.1002/ejoc.201800155.

147 Zhang, P.C., Han, J., and Zhang, J. (2019). Pd/PC-Phos-catalyzed enantioselective intermolecular denitrogenative cyclization of benzotriazoles with allenes

and *N*-allenamides. *Angew. Chem. Int. Ed.* 58 (33): 11444–11448. https://doi.org/10.1002/anie.201904805.

148 Nakamura, L., Nemoto, T., Shiraiwa, N., and Terada, M. (2009). Palladium-catalyzed indolization of *N*-aroylbenzotriazoles with disubstituted alkynes. *Org. Lett.* 11 (5): 1055–1058. https://doi.org/10.1021/ol900113f.

149 Wang, Y., Li, Y., Fan, Y. et al. (2017). Palladium-catalyzed denitrogenative functionalizations of benzotriazoles with alkenes and 1,3-dienes. *Chem. Commun.* 53 (87): 11873–11876. https://doi.org/10.1039/c7cc07543j.

150 Wang, Y., Wang, Z., Chen, X., and Tang, Y. (2018). Palladium-catalyzed denitrogenative cycloadditions and alkenylations of benzotriazoles with alkynes. *Org. Chem. Front.* 5 (19): 2815–2819. https://doi.org/10.1039/c8qo00778k.

151 Teders, M., Pitzer, L., Buss, S., and Glorius, F. (2017). Regioselective synthesis of 2-substituted indoles from benzotriazoles and alkynes by photoinitiated denitrogenation. *ACS Catal.* 7 (6): 4053–4056. https://doi.org/10.1021/acscatal.7b01025.

152 Lu, G., Huangfu, X., Wu, Z. et al. (2019). Palladium-catalyzed domino Heck/phosphorylation towards 3,3-disubstituted phosphinonyloxindoles. *Adv. Synth. Catal.* 361 (21): 4961–4965. https://doi.org/10.1002/adsc.201901100.

153 Ramesh, K. and Satyanarayana, G. (2019). Microwave-assisted domino Heck cyclization and phosphorylation: synthesis of phosphorus containing heterocycles. *Eur. J. Org. Chem.* 2019 (24): 3856–3866. https://doi.org/10.1002/ejoc.201900510.

154 Savvidou, A., IoannisTzaras, D., Koutoulogenis, G.S. et al. (2019). Synthesis of benzofuran and indole derivatives catalyzed by palladium on carbon. *Eur. J. Org. Chem.* 2019 (24): 3890–3897. https://doi.org/10.1002/ejoc.201900577.

155 Son, N.T., Tien, T.A.N., Ponce, M.B. et al. (2020). Synthesis of 5- and 6-azaindoles by sequential site-selective palladium-catalyzed C–C and C–N coupling reactions. *Synlett* 31 (13): 1308–1312. https://doi.org/10.1055/s-0040-1707853.

156 Fan, L., Hao, J., Yu, J. et al. (2020). Hydroxylamines as bifunctional single-nitrogen sources for the rapid assembly of diverse tricyclic indole scaffolds. *J. Am. Chem. Soc.* 142 (14): 6698–6707. https://doi.org/10.1021/jacs.0c00403.

157 Xu, K., Ye, J., Liu, H. et al. (2020). Pd-catalyzed asymmetric allylic substitution annulation using enolizable ketimines as nucleophiles: an alternative approach to chiral tetrahydroindoles. *Adv. Synth. Catal.* 362 (10): 2059–2069. https://doi.org/10.1002/adsc.202000151.

158 Göricke, F. and Schneider, C. (2020). Palladium-catalyzed, enantioselective (3+2)-cycloannulation of β-keto esters with alkylidene 2*H*-indoles toward complex indole-based heterocycles. *Org. Lett.* 22 (15): 6101–6106. https://doi.org/10.1021/acs.orglett.0c02166.

159 Afanasenko, A., Hannah, R., Yan, T. et al. (2019). Ruthenium and iron-catalysed decarboxylative N-alkylation of cyclic α-amino acids with alcohols: sustainable routes to pyrrolidine and piperidine derivatives. *ChemSusChem* 12 (16): 3801–3807. https://doi.org/10.1002/cssc.201901499.

160 Hazelden, I.R., Carmona, R.C., Langer, T. et al. (2018). Pyrrolidines and piperidines by ligand-enabled aza-Heck cyclizations and cascades of *N*-(pentafluorobenzoyloxy)carbamates. *Angew. Chem. Int. Ed.* 57 (18): 5124–5128. https://doi.org/10.1002/anie.201801109.

161 Olszewska, B., Jablonska, A., and Zawisza, A. (2018). Diastereoselective synthesis of 2-vinylpyrrolidines and 2-vinylpiperidines by the palladium-catalysed cyclization of amino-allylic carbonates containing a chiral protecting group. *Arkivoc* 2018 (5): 254–271. https://doi.org/10.24820/ark.5550190.p010.591.

162 Ma, X., Hazelden, I.R., Langer, T. et al. (2019). Enantioselective aza-Heck cyclizations of *N*-(tosyloxy)carbamates: synthesis of pyrrolidines and piperidines. *J. Am. Chem. Soc.* 141 (8): 3356–3360. https://doi.org/10.1021/jacs.8b12689.

163 Kljajic, M., Schlatzer, T., and Breinbauer, R. (2019). Synthesis of 2-pyrrolidinones by palladium-catalyzed [3+2] cycloaddition of isocyanates. *Synlett* 30 (5): 581–585. https://doi.org/10.1055/s-0037-1610692.

164 Rieckhoff, S., Frey, W., and Peters, R. (2018). Regio-, diastereo- and enantioselective synthesis of piperidines with three stereogenic centers from isoxazolinones by palladium/iridium relay catalysis. *Eur. J. Org. Chem.* 2018 (15): 1797–1805. https://doi.org/10.1002/ejoc.201800198.

165 Hu, W., Teng, F., Hu, H. et al. (2019). Pd-catalyzed C(sp^2)–H imidoylative annulation: a general approach to construct dibenzoox(di)azepines. *J. Organomet. Chem.* 84 (10): 6524–6535. https://doi.org/10.1021/acs.joc.9b00683.

166 Steeds, H.G., Knowles, J.P., Yu, W.L. et al. (2020). Rapid access to azabicyclo[3.3.1]nonanes by a tandem diverted Tsuji–Trost process. *Chem. Eur. J.* 26 (63): 14330–14334. https://doi.org/10.1002/chem.202003762.

167 Liu, Y.Z., Wang, Z., Huang, Z. et al. (2020). Palladium-catalyzed asymmetric [4+3] cyclization of trimethylenemethane: regio-, diastereo-, and enantioselective construction of benzofuro[3,2-*b*]azepine skeletons. *Angew. Chem. Int. Ed.* 59 (3): 1238–1242. https://doi.org/10.1002/anie.201909158.

168 Yeh, L.H., Wang, H.K., Pallikonda, G. et al. (2019). Palladium-catalyzed dual annulation: a method for the synthesis of norneocryptolepine. *Org. Lett.* 21 (6): 1730–1734. https://doi.org/10.1021/acs.orglett.9b00287.

169 Delost, M.D., Smith, D.T., Anderson, B.J., and Njardarson, J.T. (2018). From oxiranes to oligomers: architectures of U.S. FDA approved pharmaceuticals containing oxygen heterocycles. *J. Med. Chem.* 61 (24): 10996–11020. https://doi.org/10.1021/acs.jmedchem.8b00876.

170 Miyabe, H. (2015). Synthesis of oxygen heterocycles via aromatic C—O bond formation using arynes. *Molecules* 20 (7): 12558–12575. https://doi.org/10.3390/molecules200712558.

171 Rocaboy, R., Anastasiou, I., and Baudoin, O. (2019). Redox-neutral coupling between two C(sp^3)—H bonds enabled by 1,4-palladium shift for the synthesis of fused heterocycles. *Angew. Chem. Int. Ed.* 58 (41): 14625–14628. https://doi.org/10.1002/anie.201908460.

172 Rentería-Gómez, Á., Torres-Ochoa, R.O., Gámez-Montaño, R. et al. (2020). Palladium-catalyzed multicomponent synthesis of fully substituted alkylidene

furanones. *Org. Lett.* 22 (17): 7030–7033. https://doi.org/10.1021/acs.orglett.0c02578.

173 Phillips, D., Hewitt, J.F.M., and France, D.J. (2018). Synthesis of 3,3-disubstituted heterocycles by Pd-catalyzed arylallylation of unactivated alkenes. *ACS Omega* 3 (7): 8451–8459. https://doi.org/10.1021/acsomega.8b01021.

174 Zhang, J., Wang, J.Y., Huang, M.H. et al. (2020). Ligand-free Pd-catalyzed synthesis of 3-allylbenzofurans by merging decarboxylative allylation and nucleophilic cyclization. *J. Organomet. Chem.* 85 (11): 7036–7044. https://doi.org/10.1021/acs.joc.0c00375.

175 Du, J., Jiang, Y.J., Suo, J.J. et al. (2018). Trisubstituted alkenes with a single activator as dipolarophiles in a highly diastereo- and enantioselective [3+2] cycloaddition with vinyl epoxides under Pd-catalysis. *Chem. Commun.* 54 (93): 13143–13146. https://doi.org/10.1039/c8cc07996j.

176 Yang, J., Mo, H., Wu, H. et al. (2018). An elimination/Heck coupling/allylation cascade reaction: synthesis of 2,3-dihydrobenzofurans from allenoate adducts. *Chem. Commun.* 54 (10): 1213–1216. https://doi.org/10.1039/c7cc07435b.

177 Kołodziejczyk, A. and Chaładaj, W. (2018). Efficient and functional-group-tolerant synthesis of substituted furans through the Pd-catalyzed 5-exo-dig cyclization/coupling of γ-acetylenic β-keto esters with (hetero)aryl bromides. *Eur. J. Org. Chem.* 2018 (20): 2554–2560. https://doi.org/10.1002/ejoc.201800046.

178 Trost, B.M. and Mata, G. (2018). Enantioselective palladium-catalyzed [3+2] cycloaddition of trimethylenemethane and fluorinated ketones. *Angew. Chem. Int. Ed.* 57 (38): 12333–12337. https://doi.org/10.1002/anie.201807308.

179 Trost, B.M., Xu, S., and Sharif, E.U. (2019). New catalytic asymmetric formation of oxygen heterocycles bearing nucleoside bases at the anomeric carbon. *J. Am. Chem. Soc.* 141 (26): 10199–10204. https://doi.org/10.1021/jacs.9b06050.

180 Raj, V. and Lee, J. (2020). 2H/4H-Chromenes – a versatile biologically attractive scaffold. *Front. Chem.* 8: 1–23. https://doi.org/10.3389/fchem.2020.00623.

181 Nikolić, A.M., Živković, F., Selaković, Ž. et al. (2020). One-pot two-step synthesis of isochromene-fused CF_3-substituted pyrazoles. *Eur. J. Org. Chem.* 2020 (34): 5616–5619. https://doi.org/10.1002/ejoc.202000942.

182 Zhu, C., Liu, J., Mai, B.K. et al. (2020). Efficient stereoselective carbocyclization to *cis*-1,4-disubstituted heterocycles enabled by dual Pd/electron transfer mediator (ETM) catalysis. *J. Am. Chem. Soc.* 142 (12): 5751–5759. https://doi.org/10.1021/jacs.9b13700.

183 Manna, K., Begam, H.M., Samanta, K., and Jana, R. (2020). Overcoming the deallylation problem: palladium(II)-catalyzed chemo-, regio-, and stereoselective allylic oxidation of aryl allyl ether, amine, and amino acids. *Org. Lett.* 22 (19): 7443–7449. https://doi.org/10.1021/acs.orglett.0c02465.

184 Kumar, K.S., Rajesham, B., Kumar, N.P. et al. (2018). A ligand/additive/base-free C(sp^2)–H activation and isocyanide insertion in PEG-400: synthesis of indolizine/imidazoline-fused heterocycles. *ChemistrySelect* 3 (17): 4581–4585. https://doi.org/10.1002/slct.201800397.

185 Deichert, J.A., Mizufune, H., Patel, J.J. et al. (2020). Expedient Pd-catalyzed α-arylation towards dibenzoxepinones: pivotal Manske's ketone for the formal synthesis of cularine alkaloids. *Eur. J. Org. Chem.* 2020 (30): 4693–4697. https://doi.org/10.1002/ejoc.202000424.

186 Wang, L., Zhang, K., Wang, Y. et al. (2020). Enantioselective synthesis of isoxazolines enabled by palladium-catalyzed carboetherification of alkenyl oximes. *Angew. Chem. Int. Ed.* 59 (11): 4421–4427. https://doi.org/10.1002/anie.201912408.

187 Li, N., Sun, B., Liu, S. et al. (2020). Highly enantioselective construction of dihydrooxazines via Pd-catalyzed asymmetric carboetherification. *Org. Lett.* 22 (1): 190–193. https://doi.org/10.1021/acs.orglett.9b04123.

188 Sen, A., Takenaka, K., and Sasai, H. (2018). Enantioselective aza-Wacker-type cyclization promoted by Pd-SPRIX catalyst. *Org. Lett.* 20 (21): 6827–6831. https://doi.org/10.1021/acs.orglett.8b02946.

189 Gazzola, S., Beccalli, E.M., Borelli, T. et al. (2018). Selective 7-endo-cyclization of 3-aza-5-alkenols through oxidative Pd(II)-catalyzed olefin oxyarylation. *Synlett* 29 (4): 503–508. https://doi.org/10.1055/s-0036-1590939.

190 Xu, T., Wang, D., and Tong, X. (2019). Pd(II)-catalyzed intramolecular acetoxylative (3+2) annulation of propargylic alcohol and alkene: polycyclic oxa-heterocycle synthesis and mechanistic insight. *Org. Lett.* 21 (13): 5368–5372. https://doi.org/10.1021/acs.orglett.9b02096.

191 Pancrazzi, F., Sarti, N., Mazzeo, P.P. et al. (2020). Site-selective double and tetracyclization routes to fused polyheterocyclic structures by Pd-catalyzed carbonylation reactions. *Org. Lett.* 22 (4): 1569–1574. https://doi.org/10.1021/acs.orglett.0c00171.

192 Park, J.U., Ahn, H.I., Cho, H.J. et al. (2020). Asymmetric synthesis of N-fused 1,3-oxazolidines via Pd-catalyzed decarboxylative (3+2) cycloaddition. *Adv. Synth. Catal.* 1836–1840. https://doi.org/10.1002/adsc.201901497.

6

Biocatalytic Synthesis of Heterocycles

Alina Nastke and Harald Gröger

Bielefeld University, Chair of Industrial Organic Chemistry and Biotechnology, Faculty of Chemistry, Universitätsstr. 25, 33615 Bielefeld, Germany

6.1 Introduction

Heterocyclic chemistry is one of the most "classic" fields in synthetic organic chemistry [1–3], and many important developments date back to the nineteenth century. The resulting heterocyclic products are widely used, for example, in the field of pharmaceuticals and agrochemicals. In recent decades both the access to heterocycles by selective tailor-made chemocatalysts and the utilization of enzymes as catalyst components have gained increasing interest.

In the field of heterocyclic chemistry, biocatalysts have been applied, in particular, for the development of stereoselective approaches toward chiral heterocycles, thus making use of the excellent stereoselectivity provided by enzymes as a key feature. The versatility of enzymes as highly efficient catalysts for such a purpose has been proven by numerous examples from different fields of heterocycles, and this field of biocatalysis in the synthesis of heterocycles has also been comprehensively reviewed already in the past [4]. As will be shown later in this chapter (which has a focus in particular on more recently developed examples), in many cases the use of enzymes enabled the synthesis of the desired heterocyclic target molecules with excellent enantioselectivity while operating at environmentally friendly conditions. Furthermore, a broad range of such biocatalytic key steps have been able to be combined with other reaction within one-pot cascades, thus further improving the process economy by avoiding workup steps for intermediate isolations and contributing to a sustainable synthesis of heterocycles.

This chapter covers selected examples for the construction of three-, four-, five-, and six-membered heterocycles. As for the structure of this review, the sections have been "clustered" according to the synthetic methodologies for a specific ring size of the heterocycles.

Heterocycles: Synthesis, Catalysis, Sustainability, and Characterization, First Edition.
Edited by Teresa M.V.D. Pinho e Melo and Marta Pineiro.

6.2 Three-Membered Ring Heterocycles

6.2.1 N-Heterocycles

Due to the ring strain of the trigonal ring and the electronegativity of nitrogen, aziridines readily undergo ring opening reactions, especially in aqueous media. The fast-occurring ring cleavage of the aziridine products makes the development of new synthetic methods tedious, which is why barely any enzymatic-catalyzed synthetic strategy for aziridines is reported.

In 2015 Farwell et al. described the first enzyme-catalyzed olefine aziridination [5]. The challenging intermolecular reaction, carried out on a diverse set of styrene derivatives, was enabled by a nitrene transfer from tosyl azide to the olefinic double bond using an engineered cytochrome P450 catalyst (Scheme 6.1). The catalyst development process started with a variant of cytochrome $P450_{BM3}$, namely, $P411_{BM3}$-CIS-T438S, which was originally developed for intramolecular C–H amination and sulfide imidation of various substrates. The variant has a C400S mutation, which increases the nonnatural carbene and nitrene transfer activities found in $P450_{BM3}$ and other P450s. Active site evolution of $P411_{BM3}$-CIS-T438S could further improve the yield and enantioselectivity of the target aziridination reaction. *Escherichia coli* whole cells expressing the engineered mutant were used for the aziridination of different styrene derivatives. The products were obtained in 2–70% yield and with 81–99% ee.

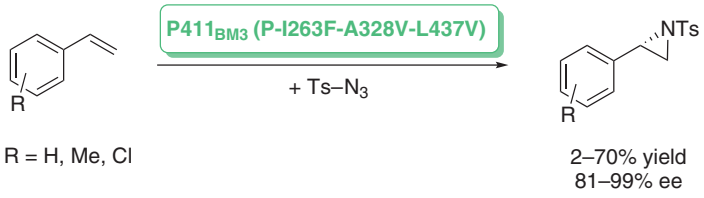

Scheme 6.1 Enantioselective aziridination of styrene derivatives with tosyl azide catalyzed by engineered $P411_{BM3}$ (P-I263F-A328V-L437V). Source: Adapted from Farewell et al. [5].

6.2.2 O-Heterocycles

The enzyme-catalyzed synthesis of oxiranes can be accomplished starting from vicinal halohydrins or from alkenes. Epoxide formation from halohydrins occurs by dehalogenation followed by intramolecular ring closure. Typically, halohydrin dehalogenases (HHDHs) are used to catalyze these kinds of reactions [6, 7]. In contrast, very different biocatalysts have been exploited for the epoxidation of alkenes. The enzymes used can be categorized into monooxygenases and peroxygenases. Among monooxygenases, a further distinction can be made between FAD-dependent monooxygenases, such as styrene monooxygenases (SMOs); heme-dependent monooxygenases, such as cytochrome P450 monooxygenases; nonheme iron-dependent monooxygenases, such as alkene and xylene monooxygenases; and peroxygenases [8, 9].

6.2.2.1 Halohydrin Dehalogenases

HHDHs catalyze intramolecular substitutions in vicinal haloalcohols to generate the corresponding epoxides. The base-catalyzed mechanism proceeds via an activated tyrosine residue in the active site of the protein scaffold. In the presence of electrophiles, HHDHs can also be used for the reverse reaction, converting a given epoxide to a β-substituted alcohol [6, 7].

Until the early 2010s, only a few different HHDHs were known. Based on their genetic sequences and bioactivity, they were classified into three phylogenetic subtypes, designated by the letters A (HheA), B (HheB), and C (HheC) [6, 10]. The recent determination of the specific sequence motif of HHDHs allowed a clear distinction of HHDHs sequences. Thus, many new enzymes have been identified as HHDHs, and four new subtypes D–G were added to the previous classification [10, 11]. Among the HHDHs, HheC has been the most studied one due to its relatively high enantioselectivity. HheC is also clearly distinguished from HheA and HheB by its substrate spectrum, which exhibits high activity toward aromatic substrates (Scheme 6.2) [12, 15]. Moreover, the HheG from *Ilumatobacter coccineus* has shown some interesting properties by accepting sterically challenging substrates [16]. Analysis of the crystal structure of this enzyme revealed a large open cleft where the active site is located, which is in sharp contrast to other HHDHs and helps to explain the specific substrate scope of HheG.

Koopmeiners et al. investigated the biocatalytic potential of the newly identified enzymes [11]. Therefore, they characterized 17 representatives from all 7 phylogenic subtypes to determine their substrate scope. They found several biocatalysts with broad substrate spectra, whereby high activities toward selected substrates were observed. The stereoselectivities of the enzymes were found to correlate with the phylogenic placing into the subtypes A–G.

Since most HHDHs show a preference for (*R*)-enantiomers, the design of (*S*)-selective HHDHs has been investigated by many researchers. The group of Zheng has intensively studied HheC and designed mutants with (*S*)-enantioselectivity. In 2015, they reported a significantly improved enantioselectivity for the asymmetric conversion of 1,3-dichloro-2-propanol. Using saturation mutagenesis, they developed the HheC double mutant $HheC_{PS}$, which generated the (*S*)-enantiomer of epichlorohydrin in 93% yield and with 92% ee [17]. Later, they used $HheC_{PS}$ immobilized on A502P resin in organic solution to convert 1,3-dichloro-2-propanol. An enhanced enantioselectivity for the (*S*)-enantiomer of >98% ee was observed with a moderate yield of 52% [18]. Furthermore, they modified the halide ion channels of $HheC_{PS}$ to generate kinetic regulations of the conversion of 1,3-dichloro-2-propanol. A series of mutants were obtained that lead to the synthesis of optically pure (*S*)-epichlorohydrin with up to 70 mM substrate concentration. However, the conversion yields tended to decrease with increasing substrate loading [19].

Seisser et al. developed a two-step cascade reaction to circumvent the lack of complementary enantioselectivities. The starting compounds of the cascade reaction were prochiral α-haloketones, which were asymmetrically reduced to the corresponding halohydrins by selected alcohol dehydrogenases (ADHs). In a second step, the corresponding epoxide was formed, catalyzed by non-selective

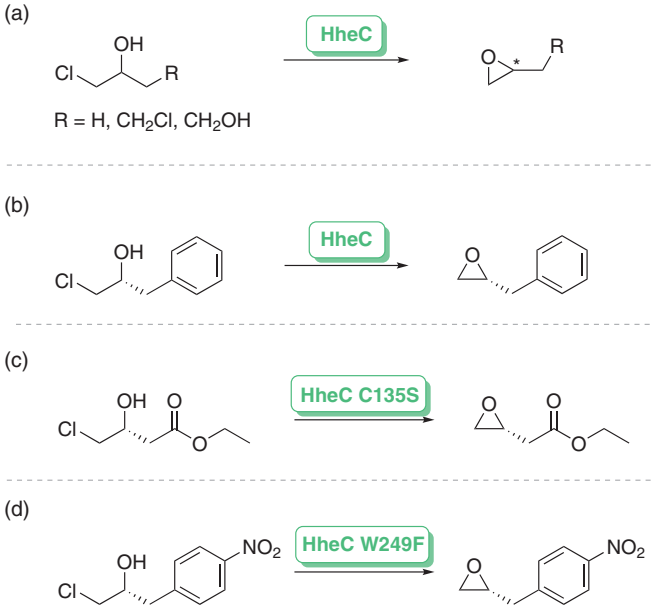

Scheme 6.2 (a) Epoxidation of differently substituted 1-chloropropan-2-ol by HheC. (b) Epoxidation of (*R*)-1-chloro-3-phenylpropan-2-ol catalyzed by HheC with preference for the (*R*)-enantiomer. Source: (a, b) Adapted from Tang et al. [12]. (c) Epoxidation of ethyl (*R*)-4-chloro-3-hydroxybutanoate catalyzed by the HheC C135S variant with preference for the (*R*)-enantiomer. Source: Adapted from Schallmey et al. [13]. (d) Epoxidation of (*R*)-1-chloro-3-(4-nitrophenyl)propan-2-ol catalyzed by HheC W249F with preference for the (*R*)-enantiomer. Source: Adapted from Tang et al. [14].

HHDHs. Since the ADH-catalyzed asymmetric reduction afforded either the (*S*)- or (*R*)-halohydrin, both corresponding epoxides were accessible with >99% ee [20].

6.2.2.2 FAD-Dependent Monooxygenases

In the category of FAD-dependent monooxygenases, SMOs are mainly used for epoxidation of alkenes. These enzymes exist predominantly as two-component constructs of a FAD-dependent styrene epoxidase (StyA) and a NADH-dependent flavin reductase (StyB), which requires NADH as a cofactor [21]. The reduced form of $FADH_2$ binds O_2 to build flavin peroxide, which then acts as oxidizing agent [22].

StyABs show excellent (*S*)-enantioselectivity for the epoxidation of styrene and styrene-related compounds. The performances of StyABs on such substrates have been intensively studied, and the reaction of selected substrates was carried out on a gram scale, yielding epoxide products with perfect enantioselectivity (Scheme 6.3) [23, 24, 26, 27].

In general, however, the epoxidation activities for substrates other than styrene turned out to be rather low. Therefore, the continuous exploration and engineering of new SMOs further enriches the diversity of this group of enzymes. The discovery of SMOs from *Pseudomonas* sp. LQ26 (StyAB2) and from *Herbaspirillum huttiense* (*Hh*MO) allowed Lin et al. to expand the substrate scope of SMOs.

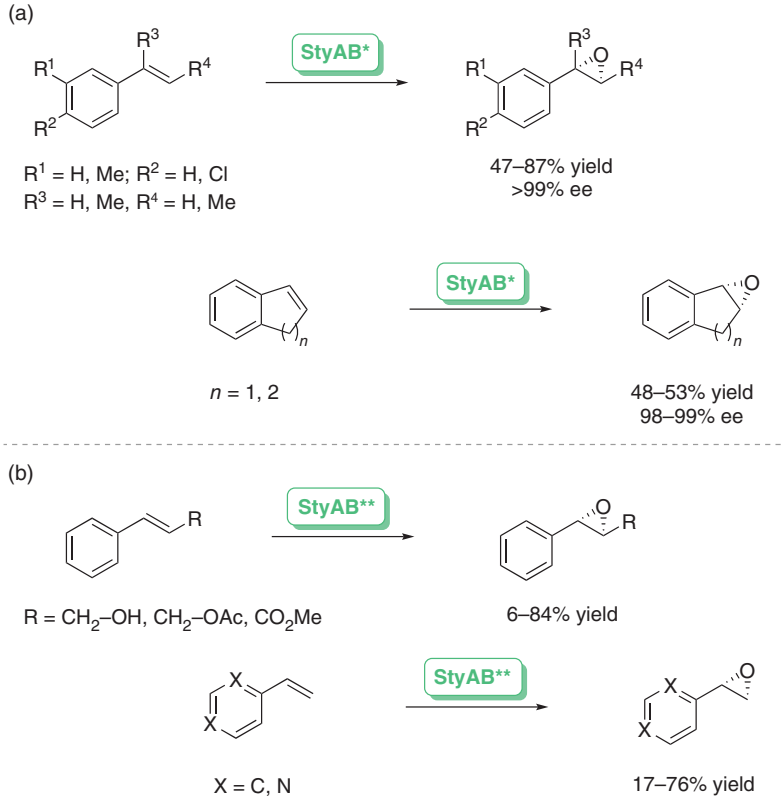

Scheme 6.3 (a) StyAB-catalyzed (*from *Pseudomonas* sp. strain VLB120) oxidation of styrene and various derivatives of styrene on a gram scale with excellent stereoselectivity (>98% ee). Source: Adapted from Refs. [23–25]. (b) StyAB-catalyzed (**from *Pseudomonas fluorescens* ST) epoxidation of different aryl, vinyl, and aryl ethenyl substrates with excellent stereoselectivity (>99% ee) and good yields. Source: Adapted from Di Gennaro et al. [26].

Pseudomonas sp. LQ26 was found to convert secondary allylic alcohols with excellent diastereo- and enantioselectivity (92–99 ee, 89–98 de), strongly favoring the (*S*)-enantiomeric substrates (kinetic resolution, Scheme 6.4a) [28]. In addition, the recently studied *Hh*MO was able to convert selected non-conjugated alkenes to the corresponding (*S*)-enantiomers with good to excellent enantioselectivity (35–99% ee) (Scheme 6.4b) [29]. Typically, the SMO-catalyzed epoxidations of non-conjugated substrates reported so far suffer from low stereoselectivities and/or low activities.

The approach of using SMOs for the epoxidation of long-chain alkenes was reported in 2014 by Toda et al. [30]. The group developed a biocatalytic process in which they investigated various straight-chain and branched terminal alkenes using the SMO from *Rhodococcus* sp. ST-10 and ADH from *Leifsonia* sp. S749. Although the biotransformations proceeded highly stereoselective (78–99% ee), only low conversion yields of up to 47% (straight-chain) and 53% (branched) were obtained.

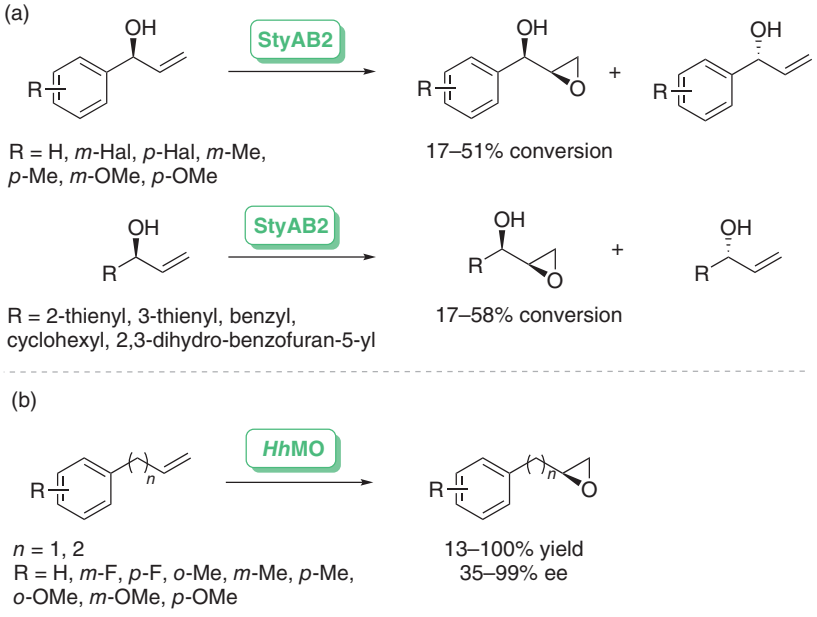

Scheme 6.4 (a) Conversion of allylic alcohols catalyzed by SMO from *Pseudomonas* sp. LQ26 with strong preference for the (*S*)-enantiomeric substrates. Source: Adapted from Lin et al. [28]. (b) Conversion of non-conjugated alkenes to the corresponding (*S*)-enantiomeric epoxide catalyzed by *Hh*MO with good to excellent enantioselectivities (35–99% ee). Source: Adapted from Lin et al. [29].

To complement (*S*)-selective SMOs, many groups have focused on finding (*R*)-selective SMOs. Recently, the group of Xiau et al. reported a clade of (*R*)-enantioselective SMOs showing activity on a relatively broad substrate scope [31]. To enhance the activity of SMOs, Corado et al. developed a chimeric SMO (Fus-SMO) obtained by genetic fusion of StyA and StyB by a flexible linker. *E. coli* cells expressing the Fus-SMO possessed about 50% higher activity for the epoxidation of different styrene derivatives compared with *E. coli* cells co-expressing StyA and StyB as independent enzymes [32].

6.2.2.3 Heme-Dependent Monooxygenases

Cytochrome P450s are heme-dependent monooxygenases that catalyze a variety of different chemical reactions. In the active site of the P450s, the heme group binds molecular oxygen and is thereby converted into the catalytically active iron(IV) oxo-heme cation radical. This oxyferryl moiety then transfers an oxygen atom to a target substrate to yield the corresponding oxygenated product [33, 34]. Hydroxylation of aliphatic substrates and epoxidation of C—C double bonds are well-known key reactions catalyzed by P450s.

Among wild-type enzymes, most P450s yield one epoxide enantiomer rather than the other. Thus, depending on the choice of the enzyme, (*S*)- or (*R*)-enantiomers are accessible. This fact is well illustrated in a report by Fruetel et al. in which styrene and *p*-chlorostyrene were converted to the corresponding epoxides by

$P450_{terp}$ from *Pseudomonas putida*, $P450_{BM3}$ from *Bacillus megaterium*, and $P450_{cam}$ from *Pseudomonas* sp. (Scheme 6.5a) [35]. Here, $P450_{terp}$ and $P450_{BM3}$ afforded the (*R*)-enantiomer with up to 82% ee and up to 46% ee, respectively, while $P450_{cam}$ afforded the (*S*)-enantiomer with up to 66% ee. However, the observed enantioselectivities can be reversed by protein engineering, as demonstrated by Li et al. using the epoxidation of *m*-chlorostyrene as an example [36]. $P450_{BM3}$, which yielded 60% ee of the (*S*)-enantiomer of *m*-chlorostyrene oxide, was inverted by inserting a single mutation into the protein scaffold, which then reversed its enantioselectivity yielding 95% ee of the (*R*)-enantiomeric product.

(a)

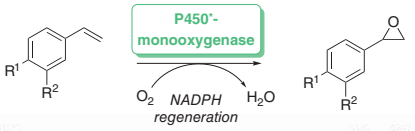

R^1	R^2	Enzyme	Enantiomer	ee (%)
H	H	$P450_{terp}$ (*Pseudomonas* sp.)	(*R*)	76
		$P450_{BM3}$ (*Bacillus megaterium*)	(*R*)	20
		$P450_{cam}$ (*Pseudomonas putida*)	(*S*)	66
Cl	H	$P450_{terp}$ (*Pseudomonas* sp.)	(*R*)	82
		$P450_{BM3}$ (*Bacillus megaterium*)	(*R*)	46
		$P450_{cam}$ (*Pseudomonas putida*)	(*S*)	48
H	Cl	$P450_{BM3}$ (*Bacillus megaterium*)	(*S*)	61
		$P450_{BM3}$ F87G (*Bacillus megaterium*)	(*R*)	95

(b)

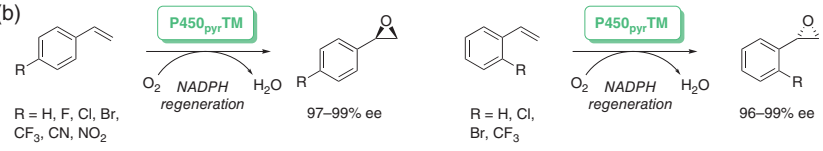

(c)

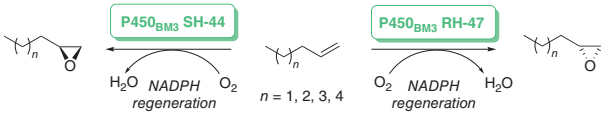

Scheme 6.5 (a) Epoxidation of styrene, *p*-chlorostyrene, and *m*-chlorostyrene catalyzed by $P450_{terp}$ from *Pseudomonas putida*, $P450_{BM3}$ from *Bacillus megaterium*, and $P450_{cam}$ from *Pseudomonas* sp. to the corresponding epoxide products. Source: Adapted from Fruetel et al. [35] and Li et al. [36]. (b) Epoxidation of several *ortho*- and *para*-substituted styrenes by triple mutant $P450_{pyr}$TM from *Sphingomonas* sp. HXN-200 with exceptional high enantioselectivities. Source: Adapted from Li et al. [37]. (c) P450-catalyzed epoxidation of long-chain terminal alkenes. Source: Adapted from Kubo et. al. [40].

Although several native and engineered P450 monooxygenases are known, their low enantioselectivities remained a challenge. Addressing this issue, Li et al. reported the variant $P450_{BM3}$ F87G, which showed a high selectivity toward the (*R*)-enantiomer. Furthermore, Li et al. engineered a triple mutant of $P450_{pyr}$ from *Sphingomonas* sp. HXN-200 that catalyzes the epoxidation of various *ortho*- and *para*-substituted styrenes with exceptional high enantioselectivities for most substrates (96–99% ee*;* Scheme 6.5b) [37]. Recently, research has increasingly focused on a deeper understanding of the mechanistic requirements of P450s

for efficient and stereoselective alkene epoxidation, which could be crucial for improving further the enantioselectivities of P450s [38, 39].

Compared with other enzymes that enable the epoxidation of alkenes, P450s can be applied to a more diverse range of substrates. In addition to styrene-related compounds, also long-chain terminal alkenes [40], fatty acids [41, 42], and natural products such as the steroid progesterone [43] or the sesquiterpenoid amorphadiene (precursor of the antimalaria drug artemisinin) [44] have been studied for P450-catalyzed epoxidations.

Denard et al. presented a tandem process in which they performed olefin metathesis with a Ru-based catalyst, followed by epoxidation of the metathesis product by $P450_{BM3}$ [45]. The process was demonstrated in a model reaction with 10-undecenoic acid and *trans*-3-hexene using a second-generation Hoveyda–Grubbs catalyst (Scheme 6.6a). The resulting cross-metathesis product, which was tridecanoic acid with an alkene moiety at the ω-2 position, was selectively epoxidized, while the self-metathesis product remained unreacted. Overall, the reaction yielded 27–48% of the epoxidated product. In addition, the cross-metathesis/epoxidation tandem reaction was applied for the conversion of 4-butenyloxyenzoic acid with *trans*-3-hexene, and the resulting epoxide was obtained in 74% yield. The enantioselectivities for both reactions, however, were rather low (38% ee for *E*-product). Later, the same group applied the cross-metathesis/epoxidation method on *Z*-stilbene and symmetrical alkenes to synthesize aryl epoxides (Scheme 6.6b) [46]. Extensive protein and reaction engineering was performed for this reaction setup. As a result, the enantioselectivity was significantly improved, obtaining *E*-aryl epoxides with up to 94% ee.

6.2.2.4 Peroxygenases

Just as the well-known P450 monooxygenases, peroxygenases rely on an oxyferryl-heme unit as the oxygenating species to catalyze oxyfunctionalization reactions. However, unlike P450 monooxygenases, peroxygenases directly use hydrogen peroxide to form the catalytical active oxyferryl moiety. In epoxidation reactions, the classical chloroperoxidase from *Caldariomyces fumago* (*Cfu*CPO) and the unspecific peroxidase from *Agrocybe aegerita* (*Aae*UPO) have been in the center of the research activities.

Although the use of *Cfu*CPO has been intensively studied [47–49], its ability to catalyze epoxidation reactions is rather poor compared with other biocatalysts. In particular, the relatively low rate of epoxidation compared with catalase activity proved to be a disadvantage. In the attempt of directed evolution of *Cfu*CPO, Rai et al. were able to find mutants with improved epoxidation activity and higher stability [50]. Nevertheless, *Aae*UPO has been shown to be a more suitable biocatalyst for epoxidation of alkenes, especially judged by the reported turnover numbers [51].

Kluge et al. described the highly efficient epoxidation activity of *Aae*UPO on styrene derivatives and cycloalkenyl benzenes (Scheme 6.7a) [52]. Styrene and its derivatives were converted in high yields in most cases (19–96%), while in the case of *cis*- and *trans*-β-methyl styrene, also excellent stereoselectivity was observed (98–99% ee). The cycloalkenyl benzenes were converted with conversion yields

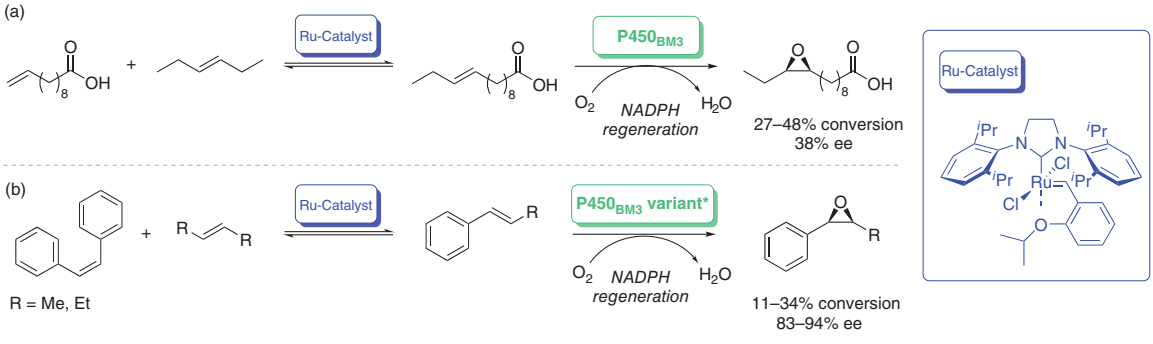

Scheme 6.6 (a) Tandem process combining cross-metathesis/epoxidation of 10-undecenoic acid and *trans*-3-hexene using a Hoveyda–Grubbs second-generation catalyst and $P450_{BM3}$. Source: Adapted from Denard et al. [45]. (b) Tandem process combining cross-metathesis/epoxidation of *Z*-stilbene and symmetrical alkenes to provide aryl epoxides using a Hoveyda–Grubbs second-generation catalyst and $P450_{BM3}$ variants RLYF or KT2. Source: Adapted from Denard et al. [46].

of 95–100%. These encouraging results could be explained by kinetic data and the catalysts tolerance to high initial H_2O_2 concentrations, leading to high total turnover numbers and space–time yields. Rauch et al. later demonstrated that the epoxidation of styrene derivatives with immobilized recombinant *Aae*UPO and *t*BuOOH as oxidant could be performed under neat reaction conditions and with high substrate concentrations of up to 360 mM [54].

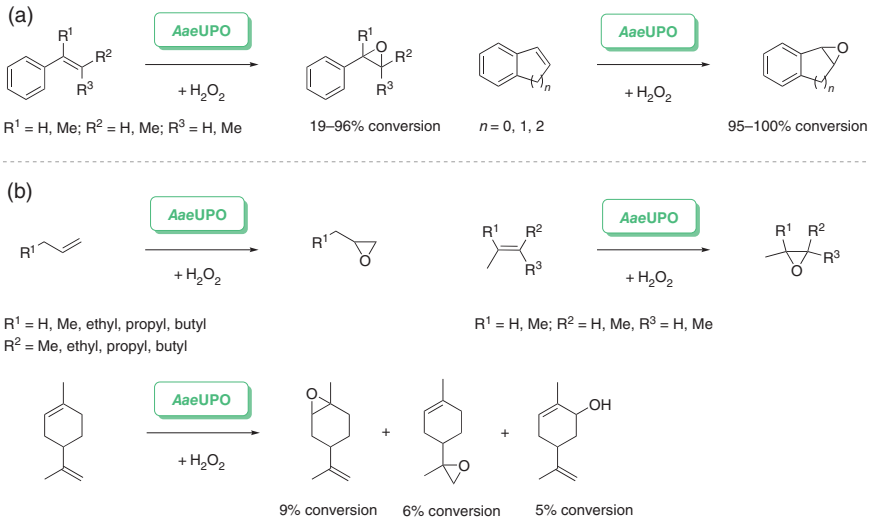

Scheme 6.7 (a) Epoxidation of styrene derivatives and cycloalkenyl benzenes catalyzed by *Aae*UPO. Source: Adapted from Kluge et al. [52]. (b) Epoxidation of linear, cyclic, and branched alkenes catalyzed by *Aae*UPO. Source: Adapted from Peter et al. [53].

In 2013 Peter et al. published their results on the epoxidation activity of linear, cyclic, and branched alkenes by *Aae*UPO (Scheme 6.7b) [53]. Branched alkenes were transformed to the corresponding epoxides with complete regioselectivity, whereas longer linear alkenes and cyclic alkenes were converted to a mixture of epoxides and allylic hydroxylation products. Although, in almost all cases the amount of epoxide product predominates, poor chemoselectivity is a major limitation with these substrates. It was furthermore shown that reactions with 1-alkenes lead to heme-alkylation, which inactivates the enzyme and results in limited conversion of these types of substrates.

The previously mentioned drawbacks hamper the use of *Aae*UPO in preparative scale, and therefore further optimization is needed. On the other hand, alternative peroxidases are emerging as oxidative catalysts for epoxidation and may be a better option. Very recently Xu et al. described the development of an unusual cofactor-independent peroxygenase based on the promiscuous peroxidase activity of the enzyme 4-oxalocrotonate tautomerase (4-OT), which accepts various hydroperoxides (*t*BuOOH and H_2O_2) to perform enantiocomplementary epoxidation of α,β-unsaturated aldehydes (citral and substituted cinnamalydehydes, Scheme 6.8) [55]. Thus, the engineered variant, namely, 4-OT-YIA, provides access to both

enantiomers of the corresponding α,β-epoxy aldehydes with good enantioselectivities (74–98% er) and high conversions (80–98%) for most substrates tested.

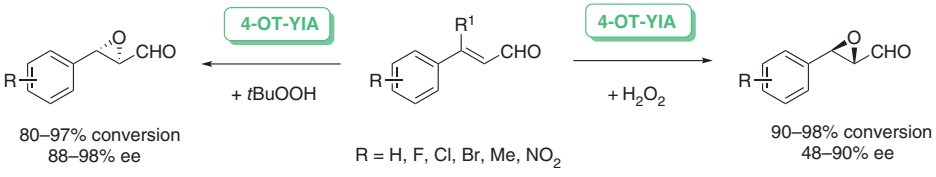

Scheme 6.8 Epoxidation of α,β-unsaturated aldehydes catalyzed by the engineered 4-oxalocrotonate tautomerase variant 4-OT-YIA with different hydroperoxides (*t*BuOOH and H_2O_2) providing access to both enantiomers of the corresponding epoxides. Source: Adapted from Xu et al. [55].

6.3 Four-Membered Ring Heterocycles

Reports of biocatalytically synthesized four-membered rings are quite uncommon. The enzymatic synthesis of β-lactams represents a rare exception in this category. β-Lactam-containing secondary metabolites are widely known for their antibacterial properties and are frequently used as antibiotics with famous examples being penicillin, monobactam, and carbapenem. The β-lactam synthetase (β-LS) of *Streptomyces clavuligerus* and the carbapenam synthetase (CarA) of *Pectobacterium carotorova* naturally catalyze the formation of β-lactam rings of clavulanic acid and (5*R*)-carbapenem-3-carboxylic acid. The structural and sequence similarities of these enzymes indicate their evolutionary origin from the class of asparagine synthetases, which convert the amino acid aspartate to asparagine [56]. Both enzymes were investigated regarding their potential as biocatalysts in organic synthesis.

Sleeman et al. evaluated the use of recombinant wild-type β-LS for the conversion of 2-methylated analogs of their natural substrate N^2-(2′-carboxyethyl)-L-arginine (CEA) to the corresponding β-lactams (Scheme 6.9a) [57]. The conversion was successfully accomplished, and it was further observed that both epimers of 2-Me-CEA appeared to be equally good substrates for β-LS.

Later, Labonte et al. engineered β-LS into a more stereoselective biocatalyst for β-lactam formation of 2-Me-CEAs (Scheme 6.9b) [58]. The aim of their research was based on the influence of the hydroxyethyl side chain naturally being in the α-position of the related β-lactams thienamycin and other examples. Therefore, they rationally designed β-LS to achieve stereoselective synthesis of the β-lactam ring bearing a simple alkyl substituent at C-2. Using a series of X-ray structures of β-LS, they were able to modify the structure of the enzyme to act on the 2-Me-CEAs and selectively form the (3*S*)-methyl-β-lactam core. The inserted mutation V446A in the β-LS scaffold created sufficient additional active site volume to achieve a 20 : 1 selectivity for (2*S*)-Me-CEA over the other substrates, with little or no loss of catalytic efficiency compared with the natural substrate.

Gerratana et al. purified recombinant CarA and used it as a catalyst for the conversion of (2*S*,5*S*)-5-carboxymethyl proline to the corresponding

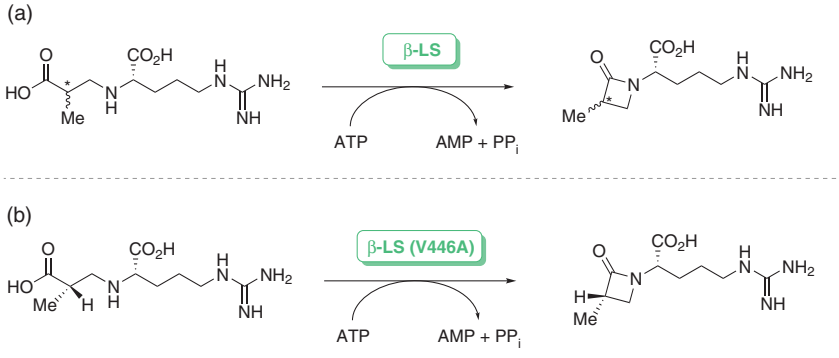

Scheme 6.9 (a) Conversion of racemic 2-Me-CEA by wild-type β-LS to the corresponding β-lactams. Source: Adapted from Sleeman et al. [57]. (b) Conversion of racemic 2-Me-CEA by the β-LS (V446A) variant with preference to the (*S*)-enantiomer to the corresponding (3*S*)-methyl β-lactam. Source: Adapted from Labonte et al. [58].

carbapenam-3-carboxylic acid (Scheme 6.10a) [59]. Various diastereomers of the natural substrate and alternative amino diacid substrates were studied for their conversion by CarA as well. The enzyme was shown to catalyze not only the formation of four-membered carbapenem derivatives but also the cyclization of linear α-amino diacids to five-, six- and seven-membered lactams.

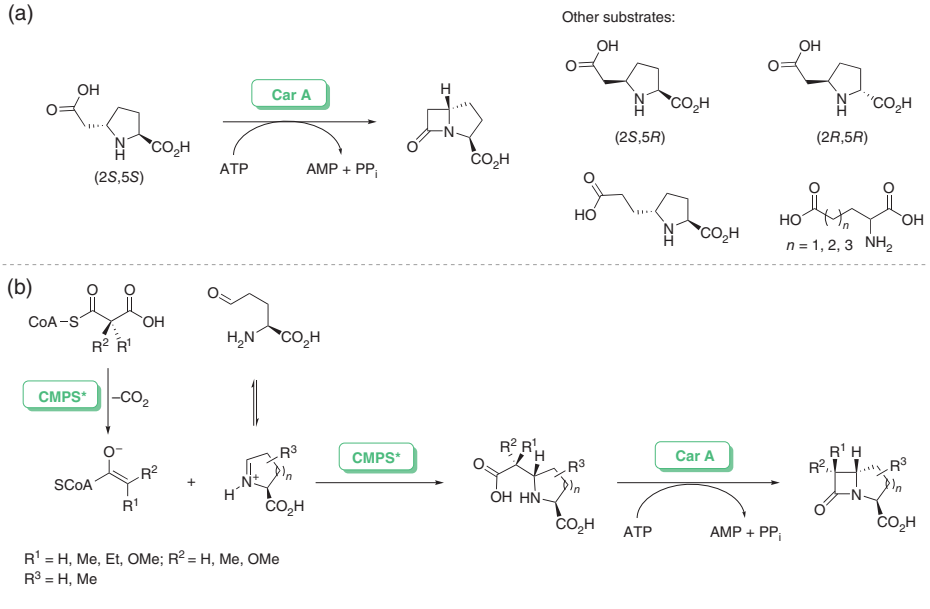

Scheme 6.10 (a) Conversion of (2*S*,5*S*)-5-carboxymethyl proline to the corresponding carbapenam catalyzed by CarA and further substrates of CarA. Source: Adapted from Gerratana et al. [59]. (b) Biocatalytic cascade using CMPS* or engineered variants of these combined with CarA form *Pectobacterium carotorova* to generate di- and tri-substituted bicyclic β-lactams. Source: Adapted from Hamed et al. [60–62].

Furthermore, Hamed et al. combined carboxymethyl synthases (CMPSs) with CarA to stereoselectively generate bi- and trisubstituted bicyclic β-lactams (Scheme 6.10b) [60–62]. For this purpose, substituted amino acid aldehydes and C-2 epimeric methylmalonyl-CoA were converted to five-, six-, or seven-membered rings by CMPSs (CarB from *Pectobacterium carotovorum* or ThnE from *Streptomyces cattleya*) or their modified variants. The resulting compounds were then transformed into the corresponding bicyclic lactams by CarA.

6.4 Five-Membered Ring Heterocycles

6.4.1 N-Heterocycles

When it comes to the synthesis of five-membered aliphatic N-heterocycles, most approaches are based on biocatalytically triggered cascades in which enzymes catalyze the formation of reactive intermediates, which in turn undergo spontaneous cyclization. Accordingly, enzyme-mediated reductive amination of diketones or keto aldehydes is a frequently described concept. Additionally, oxidative approaches starting from amino alcohols have been described. The resulting cyclic imines are subsequently reduced enzymatically or chemically to give the desired pyrrolidines (Scheme 6.11).

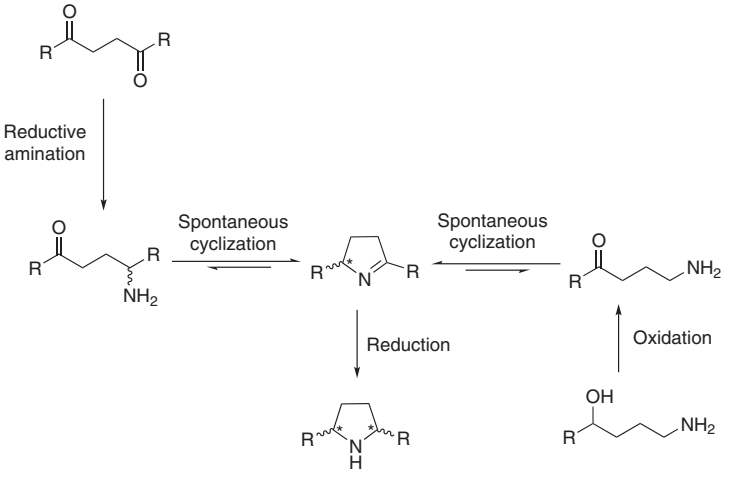

Scheme 6.11 General enzyme-mediated approaches for the synthesis of pyrrolidines.

6.4.1.1 Aliphatic Heterocycles

In accordance with the reductive strategy, the group of Turner presented different synthetic approaches to obtain substituted pyrrolidines starting from asymmetric 1,4-diketones or keto aldehydes (Scheme 6.12). In 2014, they described a chemoenzymatic cascade, in which they applied an ω-transaminase (ω-TA) and a monoamine oxidase (MAO-N) combined with $NH_3 \cdot BH_3$ to build diastereoselective pyrrolidines [63]. Herein, the (*S*)-selective transaminase ATA113 was used for the reductive

amination of different phenyl-substituted 1,4-diketones. The resulting aminoketones underwent spontaneous cyclization to the corresponding (*S*)-pyrrolines. To increase the reaction outcome, the equilibrium was shifted toward the product side by applying a combination of glucose dehydrogenase (GDH) and lactate dehydrogenase (LDH) for NAD^+-cofactor recycling. Using this strategy, the (*S*)-pyrrolines were obtained in high yields (91%) with excellent enantiomeric excess (>99% ee). The synthesis of optically pure 2,5-pyrrolidines was furthermore accomplished by the combined application of $NH_3{\cdot}BH_3$-mediated nonselective reduction of cyclic imine and MAO-N-mediated selective oxidation of only the (2*S*,5*S*)-diastereomeric amines, resulting in the accumulation of only one diastereomer. The target products were obtained in yields of up to 82% and with high diastereomeric excess (>99% de). The method was successfully implemented as an one-pot approach on a preparative scale.

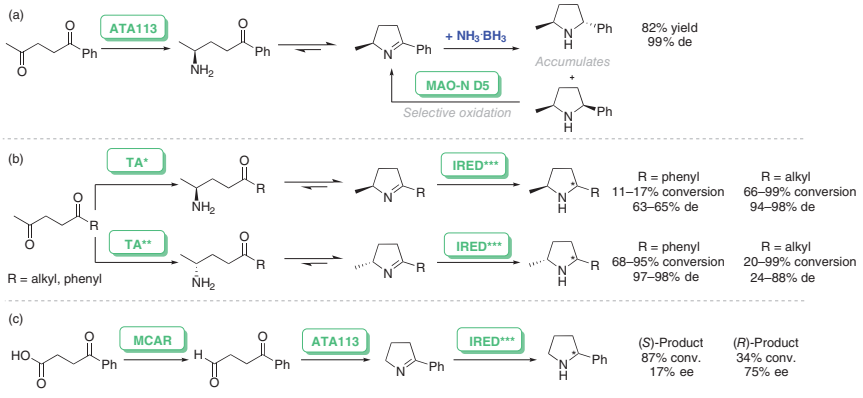

Scheme 6.12 (a) Chemoenzymatic one-pot synthesis of (2*S*,5*R*)-2-methyl-5-phenylpyrrolidine using ATA113 and the combination of $NH_3{\cdot}BH_3$/MAO-N D5. Source: Adapted from O'Reilly et al. [63]. (b) One-pot synthesis of disubstituted pyrrolidine derivatives using S-selective *ATA113 and R-selective **ATA117 in combination with ***R- or S-selective IREDs to synthesize 2-methyl-5-phenylpyrrolidine diastereomers [64] or S-selective *BmTA and R-selective **McTA in combination with ***AdRedAm to synthesize alkyl-substituted 2-methylpyrrolidines. Source: Adapted from France et al. [65]. (c) Enzymatic one-pot synthesis of 2-phenylpyrrolidines using a combination of MCAR, ATA113, and ***R- or S-selective IRED. Source: Adapted from France et al. [64].

Later, the same group proposed a similar approach for the synthesis of chiral disubstituted pyrrolidine derivatives starting from diketones (Scheme 6.12b) [64]. In this completely enzyme-catalyzed pathway, they established a two-step cascade as a one-pot approach. The first step of the cascade involved reductive amination of 1-phenylpentane-1,4-dione by the ω-TAs ATA113 or ATA117 to give the corresponding aminoketones, followed by spontaneous cyclization, which yielded the cyclic imines in (*S*)- or (*R*)-configuration with remarkably high yields (>98%). The second step of the cascade was the reduction of the imine function by imine reductases (IREDs), where the (*S*)-imine enantiomers were converted to the corresponding pyrrolidine in rather low yields with moderate de (63–65%) and

the (*R*)-imine enantiomers in modest to good yields with excellent de (97–98%). Interestingly, regardless of the IRED used, the (*R*)-enantiomer was transformed to the (2*R*,5*S*)-diastereomer with high de. In the same work a three-step one-pot approach is also presented in which chiral mono- and disubstituted pyrrolidine and piperidine derivatives were synthesized starting from keto carboxylic acids (Scheme 6.12c). The substrates were reduced to the corresponding keto aldehydes by bacterial carboxylic acid reductases (CARs) from *Mycobacterium marinum* as whole cell catalysts, while the resulting keto aldehydes were subsequentially converted to aminoketones by ATA113. The cascade showed great results for the synthesis of various piperidine derivatives with good conversion yields and mostly excellent enantiomeric excesses. However, for the synthesis of the model monosubstituted pyrrolidine derivative, the final imine reduction step showed rather poor performances ((*S*)-enantiomer, 87% conversion yield and 17% ee; (*R*)-enantiomer, 34% conversion yield and 75% ee).

In 2018 the group of Turner took up their reported two-step one-pot approach [64] and refined it to extend the substrate scope to aliphatic-substituted diketones (chain lengths of substituents C_nH_{2n+1} with $n = 3–9$ (Scheme 6.12b) [65]. By screening numerous TAs, they identified the (*S*)-selective TA of *Bacillus megaterium* (*Bm*TA) and the (*R*)-selective TA of *Mycobacterium chlorophenicum* (*Mc*TA) as efficient biocatalyst for reductive amination. The subsequent reduction step was accomplished by using the reductive aminase of *Ajellomyces dermatitidis* (*Ad*RedAm). Combined application of the two biocatalysts as a one-pot approach gave (2*R*,5*R*)-diastereomers in yields of 92–99% with moderate to good dr (84–94%) and (2*S*,5*R*)-diastereomers in yields of 95–99% with excellent dr (97–99%).

Okamoto et al. developed a hydrogen-borrowing cascade reaction to synthesize 2-phenylpyrrolidine starting from a linear amino alcohol (Scheme 6.13a) [66]. For this purpose, they combined an ADH with a self-designed artificial transfer hydrogenase (ATHase). For constructing the latter, they designed a Cp*Ir complex with a biotin moiety and 4,7-dihydroxy-1,10-phenantrolin as a bidentate ligand, which was incorporated into streptavidin. Catalytic amounts of ATHase were shown to be sufficient to catalyze the reduction of imines with high selectivity. In the cascade reaction, the substrate 4-amino-1-phenyl-butanol is firstly oxidized by an ADH, and after spontaneous cyclization, the resulting pyrroline is immediately reduced by the ATHase yielding up to 36% of 2-phenylpyrrolidin within 48 hours. The principle of hydrogen-borrowing is based on the NADPH dependency of both enzymes in opposite manner, allowing *in situ* cofactor regeneration in between the two reactions.

In 2017, Lukat et al. analyzed the biochemical conversion pathway of L-leucine to (2*S*,4*R*)-4-methylproline [68]. They demonstrated that 4-methylproline is generated upon hydroxylation of leucine, followed by oxidation to an aldehyde and ring closing formation with subsequent reduction. In addition, they conceived the crystal structure of the α-ketoglutarate-dependent leucine hydroxylase GriE and provided valuable insights into the stereospecificity of the hydroxylation step. Concurrently, Zwick and Renata exploited the hydroxylation ability of GriE and developed a chemoenzymatic cascade reaction for the synthesis of various proline derivatives (Scheme 6.13b) [67]. In their approach, they converted different four-substituted

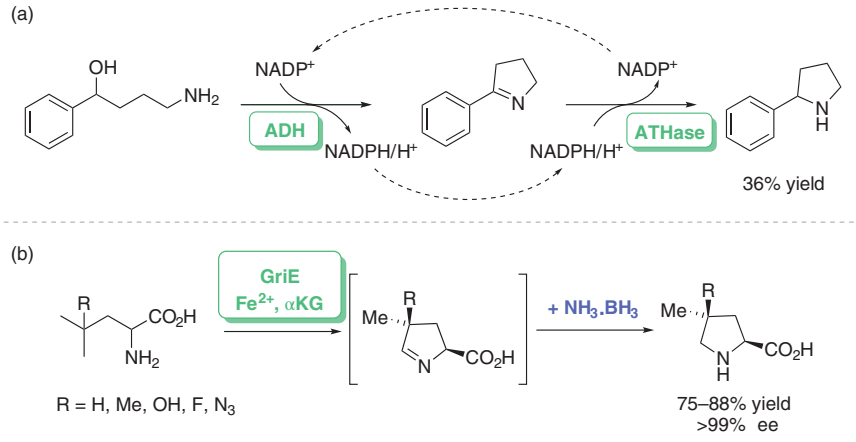

Scheme 6.13 (a) Hydrogen-borrowing cascade to synthesize 2-phenylpyrrolidine using an ADH and a self-designed ATHase. Source: Adapted from Okamato et al. [66]. (b) Chemoenzymatic one-pot approach for the synthesis of proline diastereomers. Source: Adapted from Zwick et al. [67].

leucine substrates in presence of GriE into the corresponding imines, followed by the addition of $NH_3 \cdot BH_3$ to reduce the C—N double bond. The high stereospecificity is given due to the ability of GriE to modify one of the terminal methyl groups of the substrates while accepting different substituents in the γ-position. In this way, proline diastereomers were obtained in good yields of 75–88% with complete stereocontrol.

6.4.1.2 Lactams

Both the aforementioned reductive and oxidative cyclization strategies can also be used to synthesize lactams. In the oxidative synthetic strategy, the alcoholic group of amino alcohols is usually oxidized to an aldehyde to initialize an intramolecular cyclization. A second oxidation step then leads to the formation of the desired lactone. In contrast, the reductive cyclization strategy usually starts from keto esters and initiates spontaneous cyclization by enzyme-mediated reductive amination.

The synthesis of lactams can also be accomplished using metalloenzymes. One strategy that has been used is the stereoselective oxidation of pyrroles. However, lactam synthesis by C–H activation catalyzed by artificial metalloenzymes has also been frequently reported in recent years (Scheme 6.14).

In 2015 Herter et al. engineered galactose oxidases (GOase) and combined them with molybdenum-dependent enzymes to synthesize benzofused derivatives or simple aliphatic lactams with different ring sizes (Scheme 6.15a) [69]. They identified two GOase variants as useful biocatalysts for the oxidation of amino alcohols and amino diols to form amino aldehydes, which then underwent spontaneous cyclization to cyclic imine intermediates. Interestingly, oxidation of amino alcohol substrates by $GOase_{M3-5}$ was found to be remarkably pH sensitive within the pH range of 7.0–8.5. Depending on the substrate, different pH values in this range were required to achieve complete conversion to the corresponding amino aldehydes. The cyclic imines were then converted to lactams in a one-pot process using

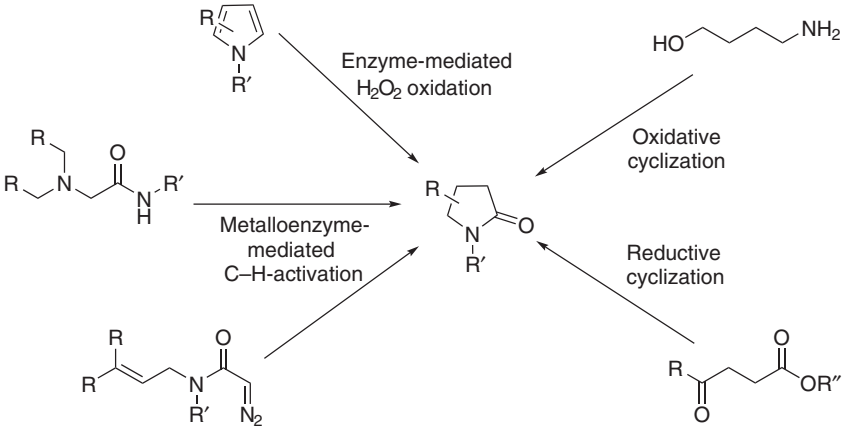

Scheme 6.14 Overview about general approaches for the synthesis of γ-lactams.

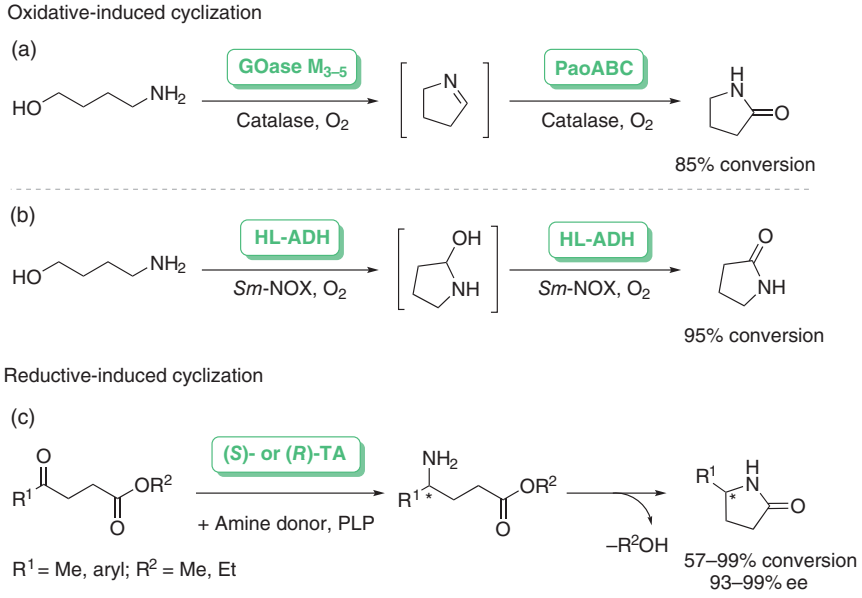

Scheme 6.15 (a) Oxidative-induced cyclization of 4-aminobutan-1-ol to synthesize γ-lactam using $GOase_{M3-5}$ and PaoABC. Source: Adapted from Herter et al. [69]. (b) One-pot approach of oxidative-induced cyclization of 4-aminobutan-1-ol to synthesize γ-lactam using HL-ADH as catalyst for two reaction steps. Source: Adapted from Huang et al. [70]. (c) Reductive-induced cyclization of β-keto ester to synthesize γ-lactam catalyzed by different (*S*)- and (*R*)-selective TAs. Source: Adapted from Mourelle-Insua et al. [71].

xanthine oxidoreductases (XORs) or periplasmic aldehyde oxidases (PaoABC). Aliphatic amino alcohols with different chain lengths were targeted substrates. When the reaction sequence was applied to 4-aminobutan-1-ol, using $GOase_{M3-5}$ and PaoABC as catalysts, pyrrolidine-2-one was obtained in 85% conversion yield. Six- and seven-membered lactams were obtained in rather low conversion yields (3–26% for six-membered lactam) or not at all (for seven-membered lactam).

Another oxidative cyclization approach for the synthesis of lactams starting from amino alcohols was presented by Huang et al. in 2018 [70]. They established an ADH-catalyzed pathway with two reaction steps, which was carried out in a one-pot process (Scheme 6.15b). Cofactor regeneration of NAD^+ was accomplished using the water-generating NADH-oxidase from *Streptococcus mutans* (*Sm*NOX). The reaction could be performed on a preparative scale, whereby the product was synthesized with 95% conversion yield. Intensive studies regarding the reaction media revealed again the relevance of pH for ring closure. Thus, the yield increased steadily with increasing pH (up to 11). Since enzyme activities were negatively affected at high pH values, an optimal range between pH 8 and 10 was determined. The approach was also applied on substrates with longer aliphatic chains. However, the yields decreased with increasing chain lengths (38% for six-membered and 14% for seven-membered lactams).

A two-step one-pot synthetic approach based on reductive amination of β-keto esters was described by Mourelle-Insua et al. in 2018 (Scheme 6.15c) [71]. In accordance with the strategy to synthesize pyrrolidines, keto esters were converted into the corresponding amino esters, which subsequently underwent spontaneous cyclization. The process was applied on different substrates bearing aliphatic as well as aromatic groups at the ketone functionality. Initial TA screening afforded both enantiomers of the five-substituted pyrrolidine-2-ones in generally good conversion yields of 57–99% and with excellent ees (>99%). Substrate concentration and temperature appeared to be the key factors in driving the reaction to high conversions. Selected substrates were converted on preparative scale biotransformations (66–90% isolated yields), demonstrating that the approach also has practical value.

The group of Ghiladi studied the ability of dehaloperoxidases (DHPs) from *Amphitrite ornata* to catalyze H_2O_2-dependent oxidation of monohaloindoles and later also pyrroles, which represent new classes of substrates for this enzyme [72, 73]. In their initial studies, 5-Br-indole was used as representative substrate, whereby the major monoxygenated products were found to be 5-Br-2-oxindole and 5-Br-3-oxindoline (Scheme 6.16a) [72]. Activity was observed for all monohaloindoles studied, regardless of the type of halogen-substituent or its position in the six-membered ring. By using isotope labeling studies, they were able to confirm that the incorporated oxygen atoms originated exclusively from H_2O_2. Furthermore, it was found that peroxygenase activity can be initiated from either the ferric or oxyferrous state with equal substrate conversion and product distribution.

Later, it was shown that the same enzyme is capable of promoting the oxidation of pyrrole to 4-pyrrolin-2-one as the sole oxidation product (Scheme 6.16b) [73]. The formation of polypyrrole is a common side reaction in the oxidative derivatization of pyrrole. It is therefore noteworthy that no polymerization of the resulting oxidation product was observed. As further substrates *N*-methylpyrrole, 2-methylpyrrole, 3-methylpyrrole, and 2,5-dimethylpyrrole were studied, and substrate oxidation was obtained for all compounds. In the oxidation of pyrrole, reactivity could be initiated from all three biologically relevant oxidation states of the catalytic globin: ferric, ferrous, and antiferrous.

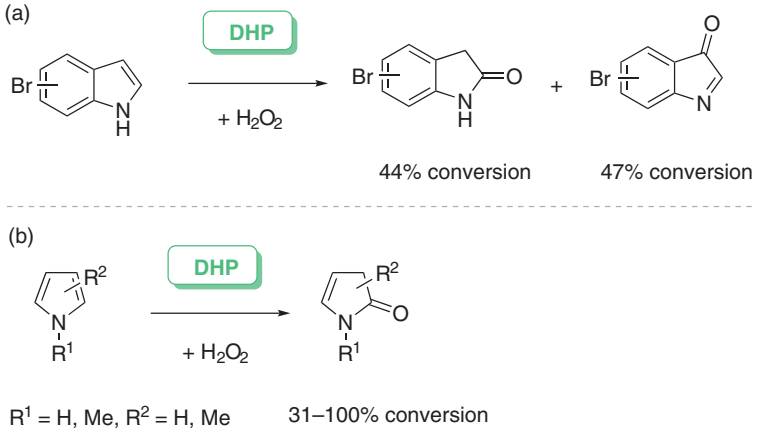

Scheme 6.16 (a) DHP-catalyzed H_2O_2-dependent oxidation of monohaloindoles, obtaining 5-Br-2-oxindole and 5-Br-3-oxindolenine as main products. Source: Adapted from Barrios et al. [72]. (b) DHP-catalyzed H_2O_2-dependent oxidation of pyrroles to obtain the 4-pyrroline-2ones as main oxidation products. Source: Adapted from McCombs et al. [73].

Ren et al. screened multiple $P450_{BM3}$ (CYP102A1) variants from *B. megaterium* with increased oxidation activity toward a number of pharmaceutical compounds [74]. Therefore, they were able to identify a $P450_{BM3}$ variant as C–H activation catalyst that enables the formation of a cyclization product of lidocaine (Scheme 6.17a). The reaction was performed on a semi-preparative scale using GDH/glucose for $NADP^+$ regeneration. The cyclic *N*,*N*-acetal product could be isolated in 95% yield. In their proposed reaction pathway, an iminium intermediate is formed either by oxidation of an aminyl-α-radical or by hydroxylation at the α-position of the N-linked ethyl group, ultimately leading to imine formation and subsequent cyclization.

Based on this result, the same group extended the substrate scope of $P450_{BM3}$ (CYP102A1) variants to the synthesis of fused bicyclic imidazolidin-4-ones/imidazolidine-4-thions and was able to establish a scalable enzymatic C–H amination process (Scheme 6.17b) [75]. Therefore, they screened selected 2-aminoacetamides in their $P450_{BM3}$ enzyme library and scaled up those reaction with high substrate conversion. Products were obtained with conversion yields ranging from 72% to 100% and isolated yields ranging from 66% to 98%, using different variants for each substrate. The substrates feature diverse properties and include aromatic amides, aliphatic amides, as well as 2-aminoacetamide derivatives with substituted tetrahydro-isoquinoline. In case of the latter ones, defined regioselectivities of C–H amination at the benzylic or non-benzylic position was observed. Thus, depending on which $P450_{BM3}$ variant was used, two different tricyclic products were obtained.

In 2020, Ren et al. developed an iron-based biocatalytic process for the synthesis of fused cyclopropane-γ-lactams (Scheme 6.17c) [76]. They designed a myoglobin-based biocatalyst that can promote the cyclization of allyl α-diazoacetamide substrates to fused bicyclic lactams. A combination of mutational landscape

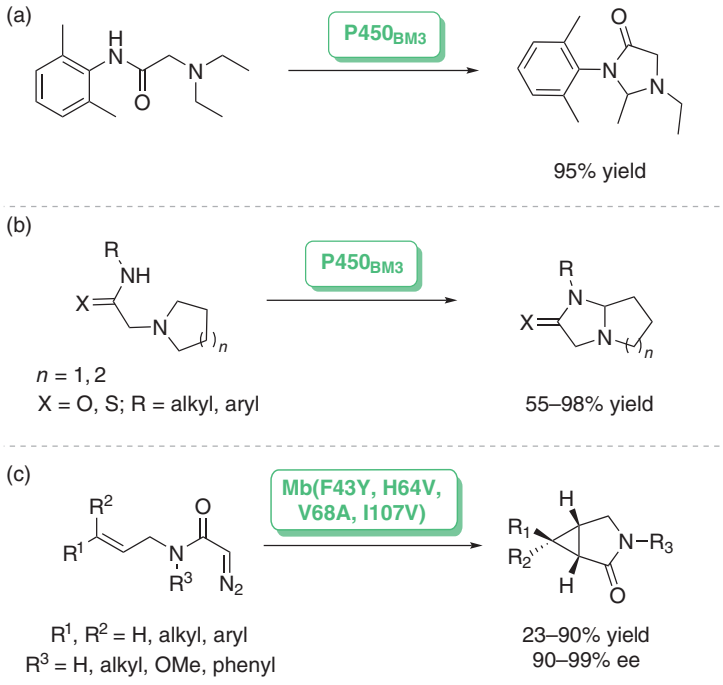

Scheme 6.17 (a) $P450_{BM3}$-catalyzed C–H activation of lidocaine, leading to the formation of the corresponding *N*,*N*-acetal product. Source: Adapted from Ren et al. [74]. (b) Synthesis of fused bicyclic imidazoline-4-ones and imidazoline-4-thions realized through $P450_{BM3}$-catalyzed C–H activation. Source: Adapted from Ren et al. [75]. (c) Synthetic strategy to generate fused cyclopropane-γ-lactams catalyzed by engineered Mb-variant. Source: Adapted from Ren et al. [76].

screening and iterative site saturation was used for engineering the myoglobin catalyst, ultimately leading to a variant with four well-considered mutations. The biocatalyst proved to be capable of converting a range of diverse allyl α-diazoacetamide substrates, mostly with moderate to excellent conversion yields (31% to >99%) while being highly enantioselective (90% to >99% ee). Substrates included diazoacetamides with aliphatic and aromatic groups on the allylic bond, as well as diazoamides with different substituents located on the amide function. It is also worth mentioning that chemical reduction of one synthesized cyclopropane-γ-lactam with $LiAlH_4$ afforded the corresponding cyclopropane-fused pyrrolidine in 82% isolated yield.

6.4.1.3 Aromatic Heterocycles

Scalacci et al. developed a chemoenzymatic concept to synthesize pyrrole derivatives from 3-pyrrolines (Scheme 6.18a) [77]. The key feature in their synthesis represents the oxidation-aromatizing activity of monoamine oxidase enzymes. As catalysts for the reaction, they used freeze-dried *E. coli* whole cells expressing monoamine oxidase from *Aspergillus niger* (MAO-N) variants D5, D9, and D11 or nicotine oxidase 6-HDNO E350L/E352D. The best conversions were obtained with

MAO-N D5, especially on N-alkylated and N-arylated substrates (up to >99% conversion). Substrates with methyl and phenyl groups in 2-, 4-, and 5-position could also be converted, albeit with lower conversion yields. The reaction was successfully implemented as chemoenzymatic cascade reaction proceeding sequentially with a ruthenium Grubbs-type catalyzed metathesis of diallylamines/-anilines.

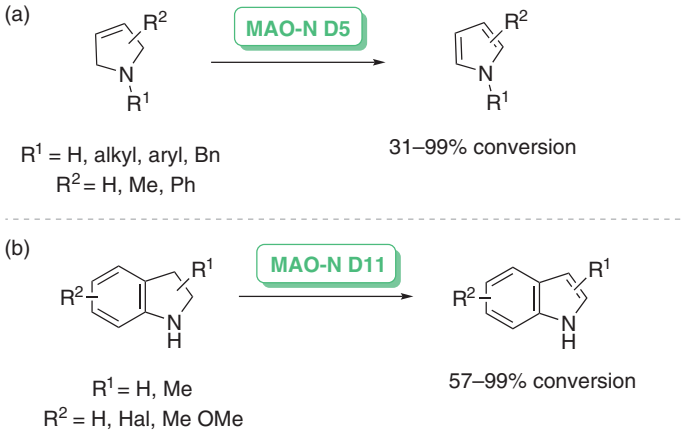

Scheme 6.18 (a) Oxidative aromatization of pyrroline derivatives to the corresponding pyrroles catalyzed by MAO-N D5. Source: Adapted from Scalacci et al. [77]. (b) Oxidative aromatization of indoline derivatives to the corresponding indoles catalyzed by MAO-N D11. Source: Adapted from Zhao et al. [78].

In 2020, the same group extended this concept of oxidative aromatization to synthesize indoles from indoline precursor molecules (Scheme 6.18b) [78]. The MAO-N D11 variant was found to be the most efficient biocatalyst for aromatization of various indoline derivatives. Substrates with small to medium-sized substituents (methyl, ethyl, phenyl, benzyl) at 2- and 3-position could be converted. N-Substituted substrates and indolines with bulky substituents could not be oxidized or showed poor conversion. Also substituents on the aromatic moiety of the indoline substrates seem to have an impact on the conversion. Especially strongly deactivating groups, such as nitro- and cyano-groups, did not lead to any conversion. Computational studies reveal that biocatalytic aromatization is mainly affected by the distribution of electrons around the indoline nitrogen as well as the α-methylene group and the ability of the substrate to align in the correct orientation to the FAD cofactor in the catalytic pocket of the enzyme.

In 2011 the group of Beifuss established an enzymatic synthetic route for the preparation of 2-aryl-1*H*-benzimidazoles using laccase from *Agaricus bisporus* (Scheme 6.19a) [79]. The desired benzimidazoles were obtained using equimolar amounts of 1,2-phenylenediamine and various aromatic aldehydes as starting materials with air acting as oxidant. The authors hypothesize that the reactions proceed via formation of a Schiff base followed by intramolecular ring closure to form *N*,*N*-acetals. Laccase-mediated oxidation of the latter leads to formation of the benzimidazoles. The reactions were performed under aerobic conditions at room

temperature either in aqueous buffer or a mixture of aqueous buffer and methanol at various ratios. The products were isolated in yields ranging from 50% to 99%.

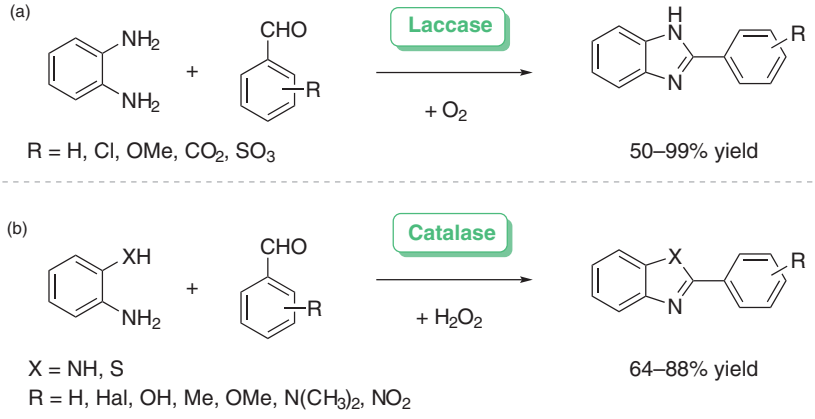

Scheme 6.19 (a) Laccase-catalyzed synthesis of 2-aryl-1*H*-benzimidazoles starting from 1,2-phenylenediamine and substituted benzaldehydes. Source: Adapted from Leutbecher et al. [79]. (b) Catalase-mediated synthesis of benzimidazoles and benzothiazoles starting from 1,2-phenylenediamine or 2-amino-thiophenol and substituted benzaldehydes. Source: Adapted from Shrivas et al. [80].

A similar approach was reported by the group of Pratap. They reported the synthesis of benzimidazoles and benzothiazoles using catalase from bovine liver (Scheme 6.19b) [80]. In this approach, 1,2-phenylenediamine or 2-aminothiophenol and benzaldehyde were treated with catalase and hydrogen peroxide in different solvents, including water and selected organic solvents. However, the best isolated yield was obtained when performing the reaction in water (84%). Furthermore, the synthetic strategy could be performed with various substituted benzaldehyde derivatives, yielding moderate amounts of isolated products (64–88%). According to their mechanistical explanation, catalase initially decomposes hydrogen peroxide to water and oxygen, whereby the latter is binding the iron center of the heme group located in the catalase scaffold. The simultaneously proceeding cyclocondensation of aldehyde and diamine is also catalyzed by catalase through activation of the aldehyde. The resulting benzimidazoline then interacts with the oxygenated heme group, leading to the desired benzimidazoles and regeneration of the native iron center.

An approach to synthesize pyrrole derivatives was reported by Xu et al. in 2018 [81]. They used TAs to selectively catalyze the amination of α-diketones to the corresponding α-amino ketones. These served as key building blocks for subsequent reaction with β-keto esters via a biocatalytic equivalent of the Knorr pyrrole synthesis (Scheme 6.20). In their initial studies, aryl-substituted α-diketones were coupled with ethyl-/methyl-β-keto esters. Therefore, the α-diketones were regioselectively aminated by ATA117 followed by spontaneous coupling with β-keto esters to afford the pyrrole derivatives in moderate to low conversions (26–78%) and isolated yields (21–48%) on a preparative scale. Upon amination of dialkyl α-diketones, the corresponding α-amino diketones tend to undergo oxidative dimerization to form

pyrazines. This side reaction could be reduced to a minimum by lowering the pH of the reaction solution to 5 and by increasing the equivalents of the β-keto esters.

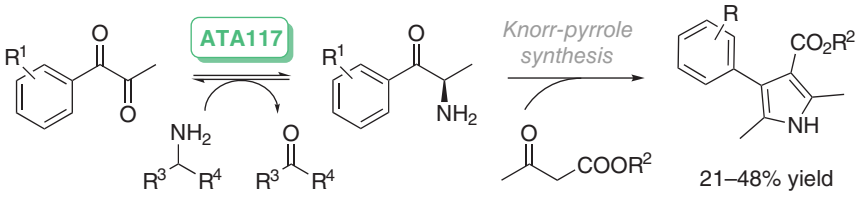

R^1 = H, Cl, OMe, CF_3
R^2 = Me, Et

Scheme 6.20 TA-catalyzed synthesis of pyrrole-derivatives via biocatalytic equivalent of the Knorr-pyrrole synthesis. Source: Adapted from Xu et al. [81].

6.4.2 O-Heterocycles

6.4.2.1 Aliphatic Heterocycles

A strategy for the synthesis of tetrahydrofurans in the form of an enzyme-triggered cascade was reported by the group of Faber [82, 83]. Their approach is based on the biocatalytic hydrolysis of 2,3-disubstituted haloalkyl epoxides with exploration of epoxide hydrolase activity, which led to the formation of vicinal diols as intermediate products. Spontaneously occurring ring closure between an alcohol group and the halogen substituent gave tetrahydrofurans in enantioconvergent manner (Scheme 6.21).

In their studies, substrates were selected in order to investigate the influence of cis- and trans-configuration of the oxirane moieties, the lengths of the haloalkyl spacer, the choice of halogen, and the length of the alkyl chain [82]. The substrates were evaluated for their biocatalyzed hydrolysis using different *Rhodococcus* and *Mycobacterium* strains. The results showed that (halomethyl)oxiranes were converted to hydroxyepoxides, while (haloethyl)oxiranes formed oxolanes exclusively. It was further found that *cis*-configurated epoxides were hydrolyzed to *anti*-(haloalkyl)diols and were ultimately giving *cis*-configurated oxolanes. Analogously, *trans*-configurated epoxides were converted into *trans*-configurated products. Therefore, the selectivity was strongly dependent on the chain lengths of the alkyl substituents – *n*-butyl derivatives were converted more selectively than ethyl derivatives. The reaction of selected substrates was repeated on a preparative scale, whereby the products were obtained in good yields (61–79%) with moderate to good ees (55–92%).

The same group applied the methodology described earlier to methylene-interrupted bis-epoxide substrates to obtain tetrahydrofurans [84, 85]. The conversion of these substrates has a much more complex product prediction, as the enzyme-catalyzed hydrolysis and spontaneously occurring cyclization proceeds according to a S_N2-mechanism, creating several possible pathways. The focus of the studies was set on a methylene-interrupted *meso*-bis-epoxide substrate, which was screened against various epoxy hydrolases with different origins. During the

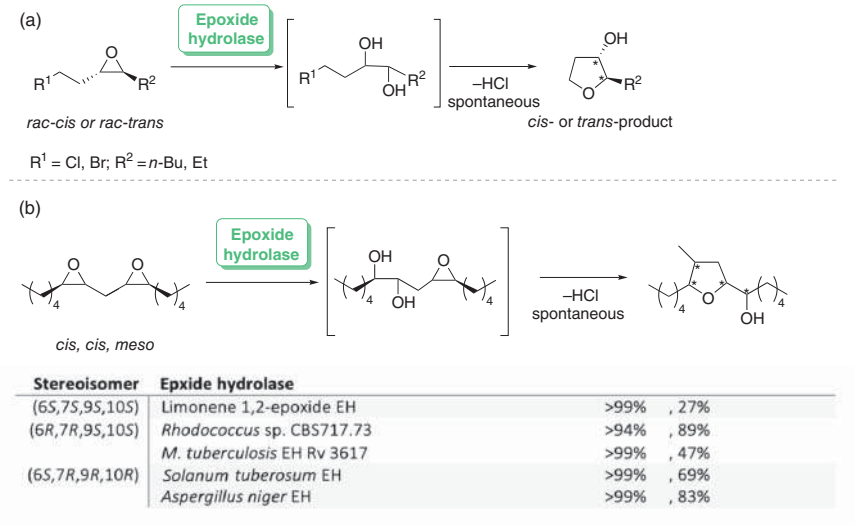

Stereoisomer	Epxide hydrolase		
(6*S*,7*S*,9*S*,10*S*)	Limonene 1,2-epoxide EH	>99%	, 27%
(6*R*,7*R*,9*S*,10*S*)	*Rhodococcus* sp. CBS717.73	>94%	, 89%
	M. tuberculosis EH Rv 3617	>99%	, 47%
(6*S*,7*R*,9*R*,10*R*)	*Solanum tuberosum* EH	>99%	, 69%
	Aspergillus niger EH	>99%	, 83%

Scheme 6.21 (a) Cascade reaction starting from 2,3-disubstituted haloalkyl epoxides to generate tetrahydrofurans catalyzed by epoxide hydrolase. Source: Adapted from Mayer et al. [82]. (b) Cascade reaction starting from methylene-interrupted bis-epoxides to generate tetrahydrofurans catalyzed by different epoxide hydrolases. Source: Adapted from Glueck et al. [84] and Ueberbecher et al. [85].

screening, several enzymes with high stereospecificity for three of the four stereoisomers were identified (up to >99% ee and up to 83% de). To explain these observations, the authors hypothesized that both steps of the hydrolysis/cyclization cascade proceed with inversion of the configuration and, thus, that the enzyme-mediated nucleophilic attack on any of the four oxirane carbon atoms would lead to a specific stereoisomer of the epoxy-diol intermediate in each case [85]. Molecular modeling studies revealed that the points of enzyme-mediated nucleophilic attack were consistent with the stereospecificities of the enzymes, whereas the stereochemical courses of cyclization were solely governed by Baldwin's rules.

In 2016, the group of Hartwig presented their approach to develop artificial heme proteins containing noble metals, more specifically iridium, instead of iron (Scheme 6.22) [86, 87]. The metal replacement created enzymes that can catalyze reactions, which are not catalyzed by native Fe enzymes or other metalloenzymes. These newly designed biocatalysts were used for C–H insertion reactions to form benzofused tetrahydrofurans. In particular, modified myoglobins containing an Ir(Me) site were prepared and further modified by directed evolution to generate mutants that form either enantiomer of the products of C–H insertion. For the preparation of the catalysts, the apo-form of eight variants of *Physeter macrocephalus* myoglobin (Myo) was expressed in *E. coli* and subsequently complemented with porphyrin factors containing various metals. Using this method, they quickly accessed 72 potential catalysts. Screening these biocatalysts for the C–H insertion of a diazoester, eight myoglobins containing Ir(Me)-PIX (PIX = porphyrin IX) formed enantioenriched benzohydrofuran in up to 50% yield. Subsequent directed

evolution of Ir(Me)-myoglobins resulted in several mutants that catalyzed the C—C bond formation of seven different substrates with selectivities of up to 84% ee and with yields up to 97% [87].

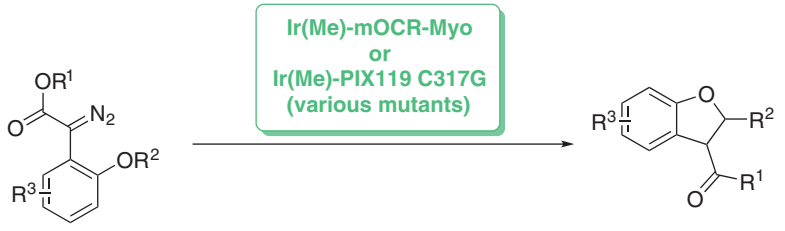

R^1 = Me, Et, Bn;
R^2 = OMe, OEt; R^3 = H, Cl, OMe

Scheme 6.22 C–H activation of diazoester to the corresponding benzohydrofurans catalyzed by the artificial metalloenzymes mutants of Ir(Me)-mOCR-Myo or Ir(Me)-PIX119 C317G. Source: Adapted from Dydio et al. [86]and Key et al. [87].

Furthermore, they applied the same strategy to design catalysts based on P450 CYP119 from *Sulfolobus solfataricus*. The resulting wild-type Ir(Me)-CYP119 and its variant C317G catalyzed the C–H insertion of a target diazoester with low rates and enantioselectivity. Directed evolution in multiple rounds supplied again various mutants that formed the desired dibenzohydrofuran at preparative scale (up to 200 mM substrate concentration) with high productivities (up to 35 000 ton) and high selectivities (up to 98% ee) [86].

Ricklefs et al. presented a biocatalyzed two-step cascade for the synthesis of phytoestrogen pinoresinol, a highly valued compound with protective activity against diverse health disorders (Scheme 6.23a) [88]. Within the presented synthetic pathway, dimerization of two coniferyl alcohol molecules led to the formation of two fused tetrahydrofuran rings, which form the core in the structure of pinoresinol. The inexpensive precursor eugenol was chosen as starting material for the cascade reaction. In the first step, coniferyl alcohol was prepared by treating eugenol with vanillyl-alcohol oxidase (VAO) from *Penicillium simplicissimum* (*Ps*VAO). The coniferyl alcohol was then oxidized by bacterial laccase, which caused dimerization by C–O and C–C coupling to give (±)-pinoresinol. However, depletion of the product was observed during the reaction, presumably caused by further laccase-catalyzed oxidation. This side reaction could be suppressed by performing the reaction in a biphasic system to directly extract the product into an organic phase. The cascade could be performed as a one-pot approach on a semi-preparative scale with 25 mM substrate concentration using *Ps*VAO in combination with laccase from *Corynebacterium glutamicum*. Although 47% of the starting material could be converted, only 13% of the racemic pinoresinol could be isolated.

Zerva et al. cloned the laccase-like multicopper oxidase (LMCO) gene from the thermophilic fungus *Thermothelomyces thermophila* (*Tt*LMCO) in *Pichia pastoris* and could successfully express it [89]. After characterizing the enzyme,

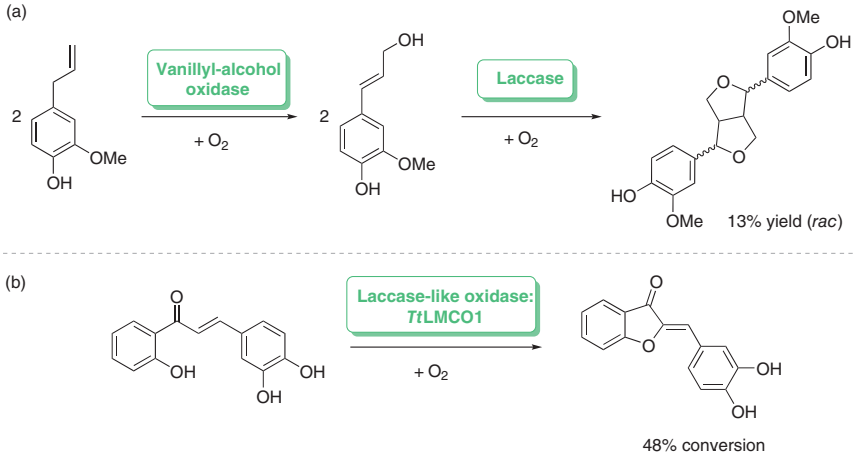

Scheme 6.23 (a) Two-step synthesis of the phytoestrogen pinoresinol by dimerization of two coniferyl alcohol molecules, catalyzed by *Ps*VAO and laccase from *Corynebacterium glutamicum*. Source: Adapted from Ricklefs et al. [88]. (b) Oxidative cyclization of 2′,3,4-trihydroxychalcone to generate 2,3-dihydroxyaurone catalyzed by *Tt*LMCO. Source: Adapted from Zerva et al. [89].

they used it to promote the oxidative cyclization of 2′,3,4-trihydroxychalcone to form 3,4-dihydroxyaurone (Scheme 6.23b). When using purified enzyme, 48% of a 4 mM substrate solution was converted to the desired product within two hours. Furthermore, the authors described an unusual substrate specifity (active against most phenolic compounds, however highest activity against ABTS and L-ascorbic acid) and a high thermostability of the enzyme ($t_{1/2}$ = 38.9 hours at 50 °C).

6.4.2.2 Lactones

For the synthesis of lactones, there are currently three major synthetic routes that have been frequently reported: Baeyer–Villiger oxidation of cyclic ketones, oxidative cyclization of diols, and reductive cyclization of γ- and δ-ketoesters [90]. However, recent reports have also described alternative synthetic strategies to access lactones. These include, for example, reports of artificial metalloenzymes that can promote the formation of diazo compounds to lactones (Scheme 6.24) [91, 92].

The enzyme-mediated preparation of lactones via Baeyer–Villiger oxidation is long-known and has been explored since the 1980s using two different enzyme classes: Baeyer–Villiger monooxygenases (BVMOs) and hydrolases.

The Baeyer–Villiger oxidation activity in BVMOs is enabled by the interaction of two cofactors: nicotinamide coenzymes (NADH or NADPH) and flavin (usually FAD). The catalytic cascade is thereby triggered by an NAD(P)H-mediated reduction of a flavin group to $FADH_2$, which further reacts with O_2 to form the catalytically active peroxoflavin species. The latter then attacks the carbonyl function of the cyclic ketones, leading to the formation of the desired lactone and water as a by-product. As observed in chemical Baeyer–Villiger reactions, the BVMO-mediated oxidation proceeds via the tetrahedral "Criegee-intermediate." While the migration of the substituents next to the ketone function is determined

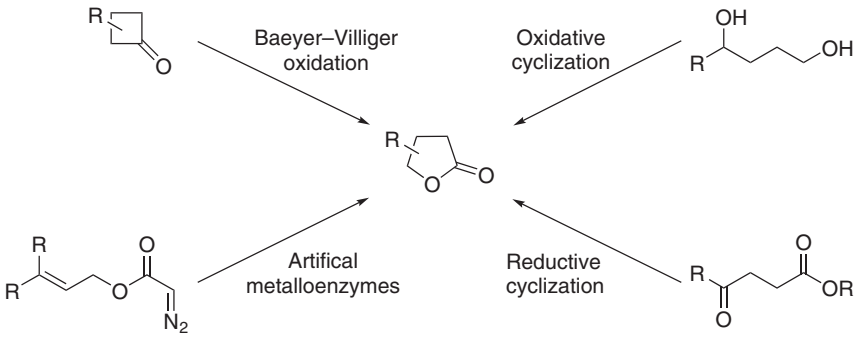

Scheme 6.24 General approaches for the enzyme-catalyzed synthesis of γ-lactones.

by their chemical reactivity, it is also influenced by the amino acid surrounding in the active site of the enzymes. Therefore, the BVMO-catalyzed Baeyer–Villiger oxidation allows access to complementary products, which usually cannot be obtained in chemically catalyzed Baeyer–Villiger reactions [90, 93].

The bicyclic-fused ketone *cis*-bicyclo[3.2.0]hept-2-en-6-one has been frequently used as substrate to demonstrate the aforementioned regiospecificity as well as enantioselectivity of BVMOs. In a report published in 1989 by the group of Furstoss, cyclohexanone monooxygenase (CHMO) from *Acinetobacter calcoaceticus* was used as a catalyst for the enantiodivergent biotransformation of racemic bicyclic-fused ketone, converting each enantiomer to a complementary lactone regioisomer (Scheme 6.25a). The (1*R*,5*S*)-enantiomer was converted to the normal lactone (chemically favored lactone formed in accordance with the migratory ability of the carbonyl group during BVMO-catalyzed oxidation), while the (1*S*,5*R*)-enantiomer was converted into the abnormal lactone (chemically unfavorable lactone formed in contradiction to the migratory ability of the carbonyl group during BVMO-catalyzed oxidation). The regioisomeric products were both obtained with excellent ee (>97%) [94]. Since these findings, the reaction has been a popular research target for studies related to BVMO. Meanwhile, using CHMO from *Saccharomyces cerevisiae* in *E. coli* whole cells, the reaction could be scaled up to an astonishing 200 l reaction volume with substrate conversion of $4.5\,g\,l^{-1}$ [98]. Other BVMOs, for example, MO14 from *Rhodococcus jostii*, exhibit high selectivity toward only one enantiomer of *cis*-bicyclo[3.2.0]hept-2-en-6-one, resulting in a kinetic resolution of the racemate. Therefore, only the (1*R*,5*S*)-enantiomer was converted into the normal lactone, while the (1*S*,5*R*)-enantiomer remained unconverted in the reaction solution (Scheme 6.25a) [95].

The practical application of CHMOs and many other BVMOs is hampered, because of their operational and thermal instability. The focus of research has therefore been set on improving the stability of certain BVMOs or on finding more robust BMVOs. As for Baeyer–Villiger oxidation of cyclobutanone, two recently discovered BVMOs have shown highly efficient performances: camphor monooxygenase (CAMO) from the ascomycete *Cylindrocarpon radicicola* ATCC 11011, which was the first recombinant BVMO reported from eukaryotic organisms

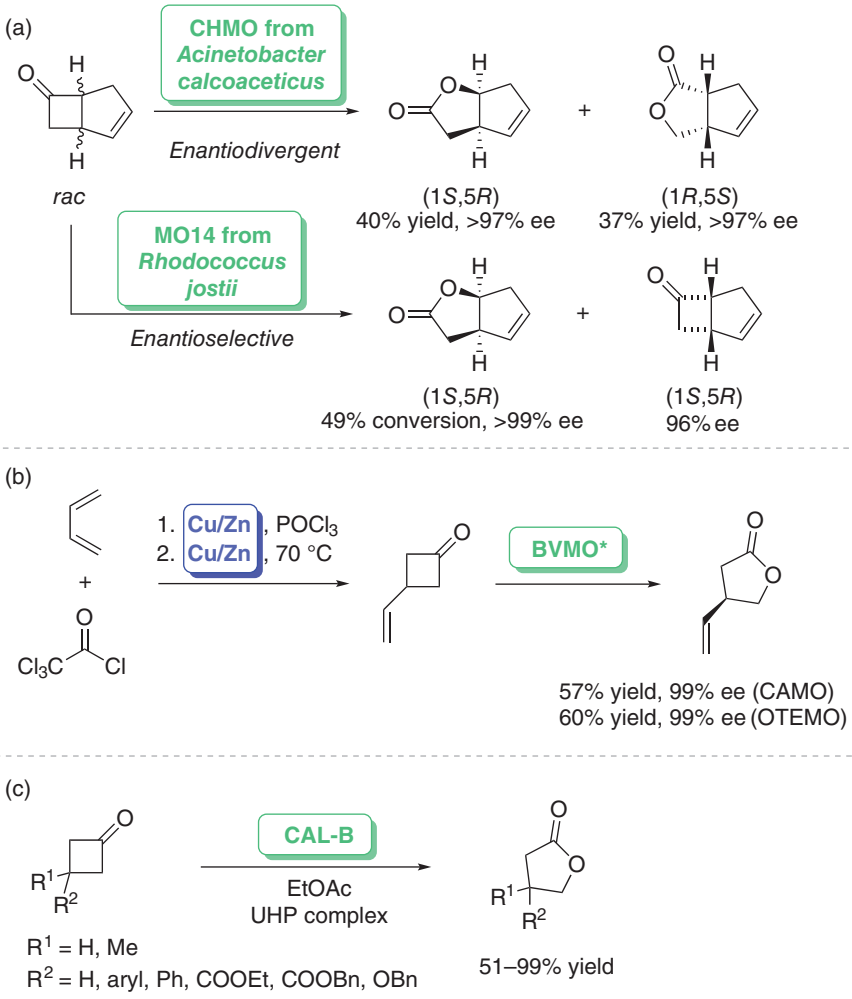

Scheme 6.25 (a) Baeyer–Villiger oxidation of the bicyclic-fused ketone cis-bicyclo[3.2.0]hept-2-en-6-one catalyzed by the CHMO from *Acinetobacter calcoaceticus* to generate two complementary lactone regioisomers and catalyzed by MO14 from *Rhodococcus jostii*, which was found to have a high selectivity toward only one enantiomer of the racemic substrate. Source: Adapted from Alphand et al. [94] and Summers et al. [95]. (b) Chemoenzymatic synthesis of the (*R*)-(−)-Taniguchi lactone using the BVMOs* CAMO or OTEMPO. Source: Adapted from Rudroff et al. [96]. (c) Synthesis of γ-butyrolactones using CAL-B according to the Baeyer–Villiger perhydrolase approach. Source: Adapted from González-Martínez et al. [97].

[99], and the recombinant 2-oxo-Δ^3–4,5,5-trimethylcyclopentenylacetyl-coenzym A monooxygenase (OTEMPO) from *P. putida* NCIMB 10007 [100]. Rudroff et al. investigated the substrate profile of these enzymes and have demonstrated their applicability in the chemoenzymatic synthesis of the (*R*)-(−)-Taniguchi lactone on a preparative scale (Scheme 6.25b) [96]. The target lactone was thereby isolated in 57% (CAMO) and 60% (OTEMPO) yields with 99% ee.

A more detailed overview of BVMOs has been provided by Fürst et al. in a review with comprehensive information on biochemical characterization, mechanistic investigation, engineering efforts, and reactivity [101].

The use of hydrolases for the Baeyer–Villiger oxidation is also known as perhydrolase approach. Mechanistically, this approach differentiates significantly from the use of BVMOs [90]. First, a carboxylic acid or ester is converted to the corresponding percarboxylic acid. This process is catalyzed by selected hydrolases that have a specific perhydrolase activity. The resulting peroxy species is then performing the actual Baeyer–Villiger oxidation. Since hydrolases are used, there is no need of expensive cofactors. However, the low stereospecificity due to the chemoenzymatic nature of these reactions is a distinct disadvantage.

González-Matínez et al. described the synthesis of γ-butyrolactones using *Candida antarctica* lipase type B (CAL-B) in combination with ethyl acetate as peracetic acid precursor and a urea-hydrogen peroxide complex as oxidizing agent (Scheme 6.25c) [97]. In their studies, several lipases were screened for the conversion of cyclobutanone. However, CAL-B proved to be the most efficient catalyst, converting 77% of the desired lactone after 24 hours. Under optimized conditions, complete conversion could be reached in the biotransformation of cyclobutanone and of many cyclobutanone derivatives (78–99% conversion yields, 51–99% isolated yields) on a preparative scale.

The oxidative cyclization of 1,4-diols to produce lactones is usually catalyzed by ADHs. Mechanistically, the process can be described in two steps. First, an alcohol group is oxidized to an aldehyde group, from which a hemiacetal forms intramolecularly. A further ADH-catalyzed oxidation completes the formation to the desired γ-lactones. Enzyme-mediated oxidative lactonization is a long-known strategy for the synthesis of lactones. Irwin and Jones already described the synthesis of δ-lactone derivatives and cyclopentane-fused γ-lactones as early as 1977 [102, 103].

Nevertheless, ever since this type of reaction was first reported, no significant increase in substrate loading has been achieved. This could be due to the spontaneous hydrolysis of the resulting lactones in aqueous environments. Kara et al. published their results of ADH-catalyzed oxidative lactonization regarding this issue (Scheme 6.26) [104]. ADH from horse liver (HL-ADH) was used as biocatalyst and laccase from *Myceliophthora thermophila* in combination with ABTS (2,2′-azinobis(3-ethylbenzthiazoline-5-sulfonic acid)) as a redox mediator for cofactor regeneration. To prevent hydrolysis of the generated lactones, they performed the reaction in a two-phase system for *in situ* product extraction into the organic phase. When using diisopropyl ether as organic solvent, the conversion of butane-1,4-diol to γ-butyrolactone was achieved with 95% conversion yield within 24 hours. Although further optimization work of this two-phase approach is required, this work represents a promising solution to the difficulty of lactone hydrolysis.

The reductive cyclization strategy has already been mentioned in connection with the synthesis of pyrroles and lactams. The synthetic approach for lactones proceeds similarly and is induced by the reduction of the keto group of keto esters. The resulting hydroxy esters are spontaneously and irreversibly cyclized to the corresponding

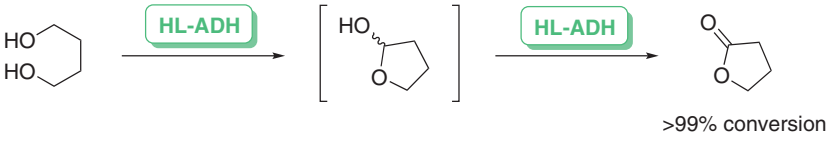

Scheme 6.26 Oxidative cyclization of 1,4-butanediol to γ-butyrolactone catalyzed by HL-ADH in combination with laccase and ABTS for cofactor regeneration. Source: Adapted from Kara et al. [104].

lactones. Most of the reported syntheses are ADH catalyzed, but other biocatalysts have also been used.

Götz et al. applied the reductive cyclization strategy to synthesize (*S*)-γ-valerolactone by using an NADH-dependent carbonyl reductase (CR) as a biocatalyst (Scheme 6.27a) [105]. Overall, they reported a chemoenzymatic route starting from levulinic acid, which was chemically esterified via an ion-exchange resin Amberlyst 15 to generate ethyl levulinate. The latter was then reduced by the (*S*)-selective CR of *Candida parapsilosis* (CP–CR) to the corresponding (*S*)-hydroxy ester. Subsequently, (*S*)-ethyl-4-hydroxypentanoate was hydrolyzed using lipase B from *Candida antarctica,* which eventually led to the formation of (*S*)-γ-valerolactone. The product was obtained in an overall yield of 90% and with >99% ee.

Díaz-Rodríguez et al. studied the ADH-mediated reductive lactonization of several keto esters to selectively synthesize γ- and δ-lactones (Scheme 6.27b) [106]. After screening a series of ADHs, they found ADH from *Rhodococcus ruber* (RR-ADH) and ADH from *Lactobacillus brevis* (LB-ADH) to be the most selective biocatalysts in the conversion of keto esters with small substituents next to the keto-function. When performing the reduction in aqueous medium with pH 9, the substrates methyl 4-oxopentanoates and ethyl 4-oxopentanoates were readily converted to γ-valerolactone with >99% ee. The conversion of the methyl ester was reproduced on a preparative scale using LB-ADH, yielding (*R*)-γ-valerolactone in 90% isolated yield and 99% ee. For keto esters with larger substituents, such as phenyl groups, ADH from *Ralstonia* sp. showed the best results for the reduction of the keto function. However, when performing the reaction in aqueous medium with pH 7.5, the hydroxy esters were formed but were not further converted into the corresponding lactones. To shift the equilibrium toward lactone formation, acidic treatment with 1 M HCl was necessary. By applying this strategy, (*R*)-γ-phenyl-γ-butyrolactone was synthesized with full conversion and with >99% ee.

A one-pot two-step cascade in which 4-oxo-pent-2-enoates derivatives were sequentially reduced by the enoate reductase (ER) YqjM, followed by different ADHs was described by Classen et al. (Scheme 6.27c) [107]. The target substrates were carrying substituents with methyl groups in α- and/or β-position. Since neither natural nor artificial enzymes with stereocomplementary activity were known for ERs at that time, stereocomplementary products were obtained by choosing the respective (*E*/*Z*)-stereoisomer as starting material. For the reduction of the ketone moiety, commercially available or generic ADH with opposite enantioselectivity

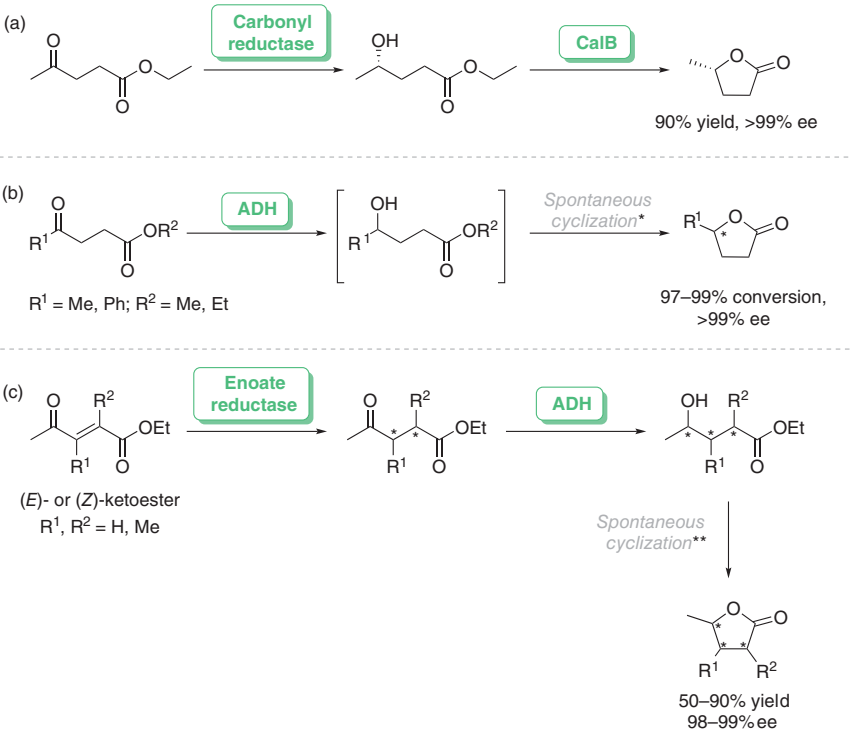

Scheme 6.27 (a) Enzymatic transformation of ethyl levulinate to (*S*)-γ-valerolactone using CP–CR and CalB. Source: Adapted from Götz et al. [105]. (b) ADH-mediated reductive lactonization of γ-keto esters to synthesize γ-lactones (*spontaneous cyclization proceeded smoothly with R^1 = Me, in case of R^1 = Ph addition of 1 M HCl was necessary to achieve lactonization). Source: Adapted from Díaz-Rodríguez et al. [106]. (c) Two-step cascade in which 4-oxo-pent-2-enoates derivatives are sequentially reduced by YqjM, followed by different ADHs to generate γ-lactones (**spontaneous cyclization proceeded smoothly with R^3 = Et, in case of R^3 = *t*Bu addition of 1 M HCl was necessary to achieve lactonization). Source: Adapted from Classen et al. [107].

were used, which generated the hydroxy compounds with excellent enantioselectivity (>99%). Ethyl ester substrates readily underwent spontaneous cyclization upon ADH reduction (50–90% yields), while *tert*-butyl ester substrates remained in a linear structure.

A completely different approach for the synthesis of lactones was developed by the group of Fasan. Similar to the previously described synthetic approach of lactams, they proposed the synthesis of lactones in 2019 [91]. An engineered myoglobin biocatalyst was thereby used to perform asymmetric intramolecular cyclopropanation of allyl diazoacetates resulting in cyclopropane-fused γ-lactones (Scheme 6.28). Through protein engineering three myoglobin variants were found to catalyze the target reactions with high enantioselectivity and in stereodivergent manner. Depending on the catalyst and substrate, moderate to excellent enantioselectivities (38–99% ee) were achieved. Using the Mb catalysts in form of whole cells, an exemplary synthesis of a key intermediate of the insecticide permethrin

was demonstrated on a gram scale, proving that their strategy is also suitable for preparative use.

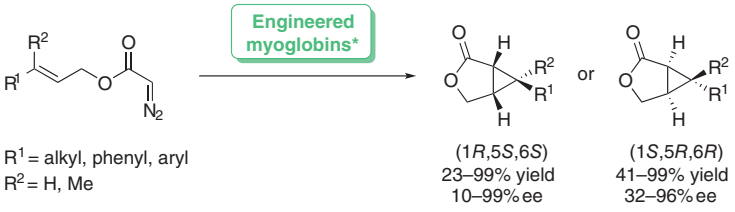

Scheme 6.28 Synthesis of cyclopropane-fused γ-lactones outgoing from allyl diazoacetates catalyzed by different engineered myoglobin catalysts (*Mb(H64V,I197S) or Mb(L29A,H64V,V68A) for the (1*R*,5*S*,6*S*) stereoisomer and Mb(F43A,H64W,V68F) for the (1*S*,5*R*,6*R*) stereoisomer). Source: Adapted from Chandgude et al. [91].

6.4.2.3 Aromatic Heterocycles

The use of laccases has been frequently reported in the synthesis of aromatic O-heterocycles. In this context, laccases were either directly or indirectly participating in the cyclization process. When thematizing laccases as direct catalysts to facilitate cyclization, laccase-catalyzed domino reactions of catechol and dicarbonyl compounds for the synthesis of benzofuran derivatives were often the center of investigations.

In 2005, Leutbecher et al. presented the laccase-mediated domino reactions of different 4-hydroxy-pyran-2-ones with catechols using molecular oxygen as the oxidating agent (Scheme 6.29a) [108]. Mechanistically, it is assumed that catechol is oxidized by laccase to the corresponding *o*-quinone, which subsequently undergoes 1,4-addition with the 4-hydroxy-pyran-2-ones. Intramolecular cyclization occurs by a second laccase-catalyzed oxidation of the resulting compound followed by intramolecular 1,4-addition. Thereby, the formation of the benzofuran derivative is accomplished. The reaction between 4-hydroxy-6-methyl-2*H*-pyran-2-one and catechol, 3-methyl catechol or 3-methoxy catechol yielded 76%, 99%, and 51%, respectively. Similar results were obtained with 4-hydroxy-2*H*-chromen-2-ones (61–99%). In these reactions, commercially available laccase from *Trametes versicolor* in acetate buffer at pH 4.37 or laccase from *A. bisporus* in acetate buffer at pH 6 was used. Shortly thereafter, the same group could extend the substrate scope of their synthetic approach, and they reported the laccase-catalyzed reaction of catechols with cyclohexane-1,3-diones, as well as with heterocyclic 1,3-dicarbonyls (pyridinones, quinolinones, thiocoumarins; Scheme 6.29b) [109, 110].

In 2007, Witayakran et al. reported an attempt, in which catechol and 1,3-dicarbonyl compounds were merged to benzofuran derivatives using laccase and the Lewis acid $Sc(OTf)_3$/SDS (Scheme 6.29c) [111]. When using solely laccase in phosphate buffer with neutral pH, 64% of the desired product was isolated. However, addition of the Lewis acid $Sc(OTf)_3$ further enhanced the 1,4-addition step and raised the yield to 74%. The addition of SDS furthermore improved the solubility of the reactants. Isolated yields ranging from 46% to 79% were obtained when catechol and 3-methyl catechol were used. Four-substituted catechols such as

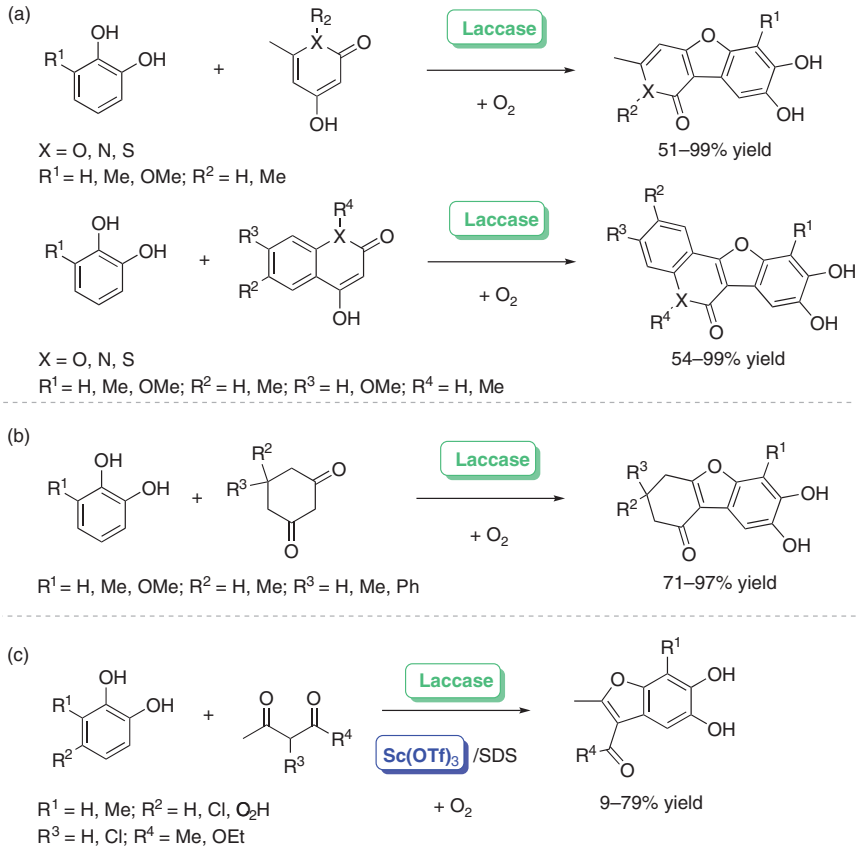

Scheme 6.29 (a) Laccase-mediated domino reaction of different 4-hydroxy-pyran-2-ones or 4-hydroxy-2*H*-chromen-2-ones with catechols to generate benzofuran derivatives. Source: Adapted from Leutbecher et al. [108] and Hajdok et al. [109]. (b) Laccase-mediated domino reaction of different cyclohexane-1,3-diones and catechols to generate benzofuran-derivatives. Source: Adapted from Hajdok et al. [110]. (c) Biocatalyzed synthesis of different benzofuran derivatives starting from catechol derivatives and 1,3-dicarbonyls catalyze by laccase in combination with the Lewis acid $Sc(OTf)_3$ and SDS. Source: Adapted from Witayakran et al. [111].

4-chlorocatechol and 3,4-dihydroxy benzoic acid gave only low isolated yields of 9% and 11%, respectively. The reactions proceeded regioselectively, and only a single stereoisomer was obtained each time.

The catalytic system of laccase/TEMPO (2,2,6,6-tetramethylpiperidinyl oxyl) for the synthesis of furans and its derivatives is an example for the indirect participation of laccase in the synthetic process. In this system, laccase acts as oxidizing agent toward TEMPO and creates the corresponding oxoammonium ion, which acts as a reducing agent on the target substrate. The reduced TEMPO species is regenerated to its original form by another oxidation by laccase.

The laccase/TEMPO-catalyzed aromatization of 2,5-dihydrofurans to furans was described by the group of Castagnolo (Scheme 6.30) [112]. The reactions

were performed in biphasic systems with NaPBS (pH 6.5) and methyl *tert*-butyl ether (MTBE) at 30 °C. By applying this synthetic strategy, a variety of furan derivatives were synthesized in moderate to high conversions (21–99%) and yields (20–72%). In general, 2-aryl substituted dihydrofurans were found to be more readily converted compared with substrates with substituents in 2- and 3-/4-position or substrates with alkyl or benzene groups in 2-position. However, they further extended their synthetic strategy for 2-aryl substituted substrates toward a chemoenzymatic cascade by combining Grubbs-catalyzed ring-closing metathesis and laccase/TEMPO-catalyzed aromatization as one-pot approach.

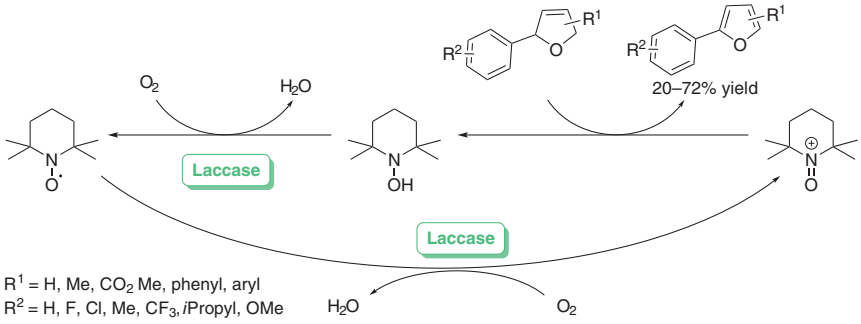

Scheme 6.30 Laccase/TEMPO-catalyzed aromatization of 2-aryl substituted 2,5-dihydrofurans to the corresponding furans. Source: Adapted from Risi et al. [112].

It is long known that allenes represent synthetically attractive building blocks that can act as acceptor for halonium ions and in consequence undergo oxidative cyclization to form heterocyclic moieties. Research for these kinds of reactions has focused on chemocatalysis. Recently, however, Naapuri et al. described an enzymatically catalyzed halocyclization of allenic alcohols and carboxylates using chloroperoxidase from *Caldariomyces fumago* to synthesize functionalized furan scaffolds (Scheme 6.31) [113]. In their reaction design, glucose oxidase (GOx) was used for controlled generation of hydrogen peroxide by reducing aerial oxygen. Subsequent oxygenation of halide salts provided reactive halonium species that attached to the allenic substrates and initiated an intramolecular cyclization process. The reactions were carried out in aqueous emulsions using the non-ionic polyethylene glycol (PEG)-based detergent Brij 35® to promote substrate solubility. Moderate to high yields (19–93%) were obtained by applying this strategy to various substrates. Peroxidase-catalyzed cyclization allowed the preparation of brominated and iodinated building blocks containing phenyl-substituents, as well as long-chain and spirocyclic alkyl-substituents. They were also able to prepare bridged bicyclic vinyl bromides. Furthermore, they could extend their strategy to a multi-enzyme cascade for the preparation of enantiomerically pure 3-bromodihydrofurans. Therefore, lipase-catalyzed desymmetrization of the allenic substrates with vinyl butyrate was performed prior to the halocyclization. As a result, the product outcome exhibited 98% ee.

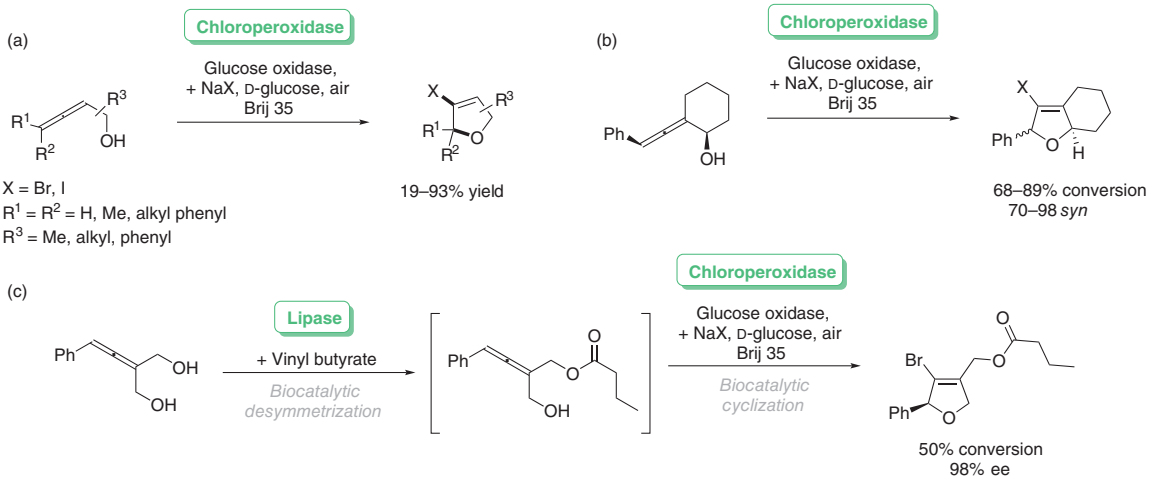

Scheme 6.31 (a) Enzymatic halocyclization of allenic substrates using chloroperoxidase, glucose oxidase, halide salts, glucose, and air. (b) Halocyclization strategy for the synthesis of bicyclic vinyl bromide. (c) Multienzyme cascade involving lipase-catalyzed desymmetrization followed by chloroperoxidase-catalyzed halocyclization. Source: Adapted from Naapuri et al. [113].

6.4.3 S-Heterocycles

Only a few reports on biocatalytic synthetic methods for generating S-containing heterocycles can be found, most of which date back to the 1990s.

In 1992, Effenberg et al. presented a stereoselective synthetic method for the preparation of different five- and six-membered thiosugars [114]. In particular, the synthesis of 5-thio-D-threo-pentulose was described, starting with the substrate 1,4-dithiane-2,5-diol. The diol is in equilibrium with the corresponding monomer 2-mercaptoacetaldehyde when dissolved in aqueous solution. By addition of dihydroxyacetone phosphate (DHAP) and rabbit muscle aldolase (RAMA), the monomeric 2-mercaptoacetaldehyde was converted in an aldol reaction to the product thiofuranose-1-phosphate, which was subsequently precipitated as a barium salt (Scheme 6.32a). The RAMA-catalyzed C–C linkage proceeded highly stereoselective, resulting in a product with C-3 in S-configuration and C-4 in *R*-configuration. In a second enzyme-catalyzed step, the phosphate ester was hydrolyzed by treatment of the thiofuranose-1-phosphate with phosphatase. The resulting 5-thio-D-threo-pentulose was found to be present in 83% as β-anomer and in 17% as α-anomer at 78% overall yield.

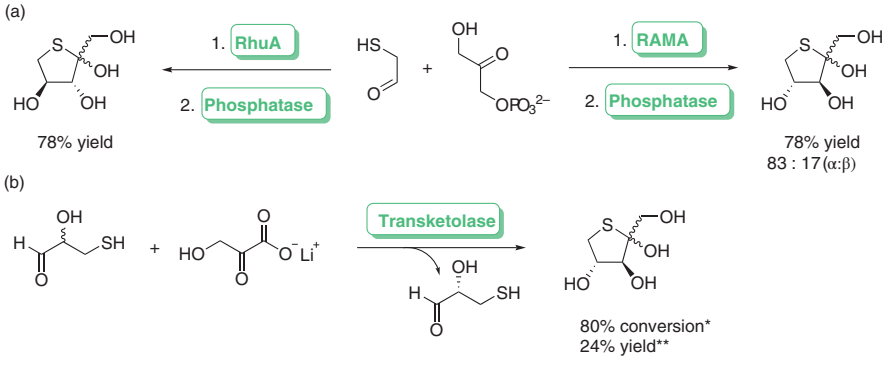

Scheme 6.32 (a) Synthesis of 5-thio-D-threo-pentulose catalyzed by RhuA in combination with acid phosphatase from sweet potato and synthesis of 5-thio-L-threo-pentulose catalyzed by RAMA in combination with acid phosphatase. Source: Adapted from Effenberger et al. [114] and Fessner et al. [115]. (b) Synthesis of 5-thio-D-threo-pentulose out of 2-hydroxy-3-mercaptopropanal and lithium hydroxypyruvate catalyzed by TK from yeast (*conversion yield in analytical scale from Effenberg et al., **isolated yield in preparative scale by Charmantry et al.). Source: Adapted from Charmantry et al. [116] and Effenberger et al. [117].

Shortly thereafter Fessner and Sinerius published their results obtained in a similar approach. They described a two-step synthesis of different sugars using the microbial rhamnulose 1-phosphate aldolase (RhuA) in combination with various phosphatases (Scheme 6.32a) [115]. Among the presented syntheses of sugars, they described the preparation of 5-thio-L-threo-pentulose with 78% isolated yield.

In 2006 Charmantry et al. reported the synthesis of 5-thio-D-threo-pentulose on a preparative scale [116]. The compound was obtained by a chemoenzymatic

route, whereby the key step was represented by the stereospecific conversion of a C—C bond, catalyzed by transketolase (TK) from yeast (Scheme 6.32b). In their synthetic route, racemic 2-hydroxy-3-mercaptopropanal was treated with TK and lithium hydroxypyruvate. Two carbon units from the pyruvate were transferred to the 2-hydroxyaldehyde in *R*-configuration, forming a new C2—C3 bond in S-configuration. The reaction was carried out with substrate concentrations of maximum 250 mM with rather low yields of up to 24%. The reaction was previously reported by Effenberg et al. in analytical scale, whereby a higher conversion of 80% was achieved [117].

6.5 Six-Membered Ring Heterocycles

6.5.1 N-Heterocycles

The application of enzymes for the preparation of six-membered aliphatic heterocycles is mainly centering on their stereoselective synthesis in order to obtain the desired products in enantiomerically and in case of more than one stereogenic center also diastereomerically pure form. Similarly to the synthesis of their five-membered counterparts, many approaches for the stereoselective synthesis of chiral six-membered aliphatic N-heterocycles are based on combining spontaneous intramolecular cyclization of an amine with a C=O-moiety under imine formation and subsequent reduction of the C=N double bond.

An overview is graphically given in Scheme 6.33 and the various concepts are briefly discussed in the following prior to describing the individual processes in detail. For the introduction of biocatalytic C=N bond reduction, two variants have mainly been studied. First, biocatalysis has been applied to introduce the chiral amine moiety of the substrate for the cyclization and, thus, cyclic imine formation step. It is noteworthy that the preparation of such chiral amine substrates for undergoing the spontaneous imine formation are based on various different and complementary enzymatic approaches, e.g. based on enzymatic transamination and C—C bond formation. As the resulting amines are already enantiomerically enriched or pure, the resulting chiral imines are also obtained. In such cases, the subsequent reduction of the imine moiety does not necessarily need to furnish a new stereogenic center and in such a case also non-selective "classic" metal hydrogenation can be conducted. Second, as an alternative approach, a prochiral cyclic imine is formed by "classic" chemical synthesis, followed by enantioselective reduction of the C=N double bond with an IRED. In this case, the subsequent imine reduction represents the stereoselective key step. Furthermore, "hybrid" processes are conceivable, which combine biocatalytic enantioselective formation of an amine bearing an additional C=O subunit, subsequent spontaneous cyclization and a further biocatalytic stereoselective step with, e.g. an IRED. Most of these syntheses address the preparation of piperidines as target heterocycles, but to some extent also aliphatic amine heterocycles with more than one nitrogen have been prepared such as piperazines.

To start with the concept of an initial stereoselective construction of an amine with a C=O moiety being suitable for subsequent spontaneous cyclization to a

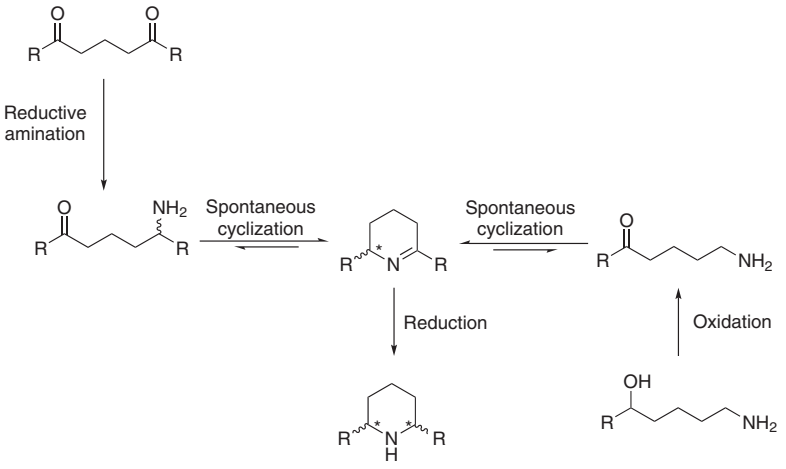

Scheme 6.33 Enantioselective synthesis of six-membered N-heterocycles comprising a reduction of an imine bond as a key step.

chiral imine and its reduction for piperidine formation, the group of Clapes applied two types of enzymatic aldol reactions for synthesizing the six-membered imine key intermediates and a representative example is shown in Scheme 6.34. In detail, an initial aldol reaction with glycine as the aldol donor and a mono-protected glyoxal furnishes, after protecting group modifications, the corresponding aldol adduct (Scheme 6.34). The aldehyde moiety in this compound can then serve as an aldol acceptor for a further aldol reaction, which then delivers the derivative bearing the needed chiral amine moiety and an additional C=O group for the subsequent cyclization to the cyclic six-membered imine. The final step consists of a "classic" hydrogenation after N-deprotection, which then delivers the desired piperidines as valuable *aza*-sugars. What makes this concept different to the other published concepts described in the following text is the fact that the chiral amine moiety is not biocatalytically formed by a reductive transformation of a C=N double bond as

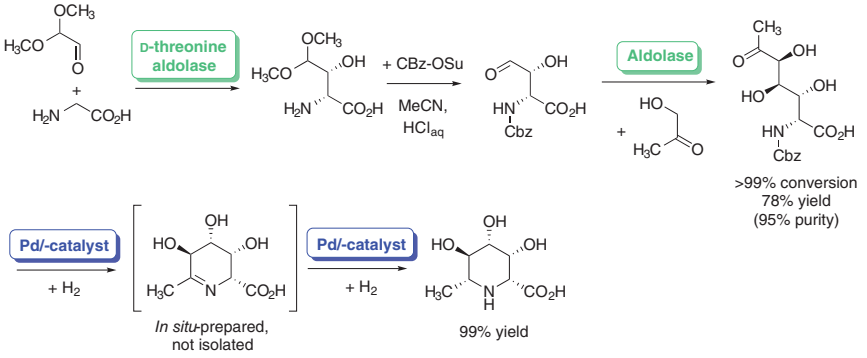

Scheme 6.34 Enantioselective multistep synthesis of six-membered N-heterocycles based on an enzymatic aldol reaction as a key step.

precursor but by an alkylation of glycine, which already bears the CH–NH_2 moiety in the prochiral initial substrate [118].

As an alternative the needed chiral amine bearing an additional C=O moiety for cyclization to the six-membered imine can be also prepared through a transaminase-catalyzed process. Such an approach has been utilized by the group of Kroutil, which enabled the synthesis of a range of piperidines. 2,5-Diketones are the starting materials, which are regio- and enantioselectively converted into the chiral amines by means of a transaminase, leading to excellent enantioselectivities of >99% ee. The formation of such amino ketones goes hand in hand with a subsequent spontaneous cyclization under formation of the six-membered imines. The formation of these heterocyclic imines is favored due to the high stability of six-membered ring systems. The final reduction step of the imine bond is then done by means of a hydrogenation with Pd/C as heterogeneous catalyst. It is noteworthy that in spite of using a non-chiral catalyst, this reduction steps is stereoselective, and the resulting piperidines with two stereogenic centers where then obtained in high yield of up to 94% and with an excellent diastereoselectivity of >99% de under these conditions [119].

Alternatively, the asymmetric step can be done enzymatically by means of IREDs, which reduce a preformed C=N-double bond of a heterocyclic imine, thus forming the desired cyclic amine moiety. The imine can be formed *in situ* and directly combined with the biocatalytic reduction step or can be preformed, e.g. in a "classic" chemical synthesis. To start with the latter approach, the reduction of six-membered heterocyclic imines with IREDs has been widely studied by several groups. It also should be added that such type of piperidine heterocycle formation has been known from the biosynthesis of the cyclic amino acid L-pipecolic acid. This approach has been demonstrated to be suitable also for organic–synthetic purpose by Yasuda et al., who applied an *N*-methyl amino acid dehydrogenase in a cascade starting from various diamino acids, which were at first oxidized to α-keto acids with an amino acid oxidase, followed by a spontaneous cyclization under formation of a cyclic amino acid. The developed recombinant *N*-methyl-L-amino acid dehydrogenase from *P. putida* then reduces such heterocyclic imines using NADPH as a cofactor. The application of this method for the synthesis of L-pipecolic acid, which led to 98% yield, 100% ee, and a product loading of 14 g l^{-1}, is shown in Scheme 6.35 [120].

Pioneering work for the reduction of the enantioselective C=N double bond of a hydrophobic six-membered heterocyclic imine (in the absence of a carboxylic acid group as a substituent) has been carried out by Mitsukura et al. for the reduction of 1-methyl-3,4-dihydroisoquinoline with 96.4% ee in the presence of an IRED from *Streptomyces* sp. as a biocatalyst [121].

The synthetic potential of this IRED from *Streptomyces* sp., which has been made accessible in a favorable recombinant form being overexpressed in *E. coli*, was explored by Turner et al. for the reduction of a broad range of six-membered heterocyclic imines. When using bi- and tricyclic imines bearing aromatic moieties as substrates at 5 mM substrate concentration, the corresponding products have been formed with >98% conversion and >98% ee. Furthermore, a monocyclic six-membered imine has been reduced at an elevated substrate concentration of

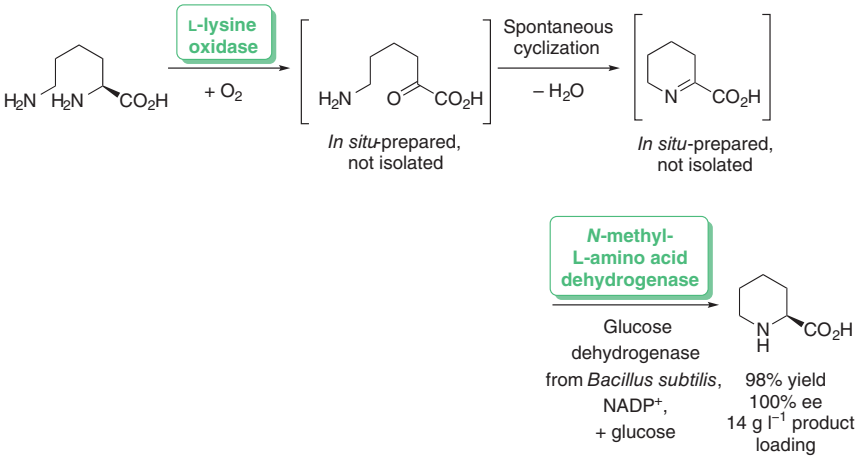

Scheme 6.35 Enantioselective synthesis of L-pipecolic acid starting from L-lysine via an enzymatic cascade.

20 mM, leading to the (*S*)-amine product also in >98% conversion and with >98% ee (Scheme 6.36) [122].

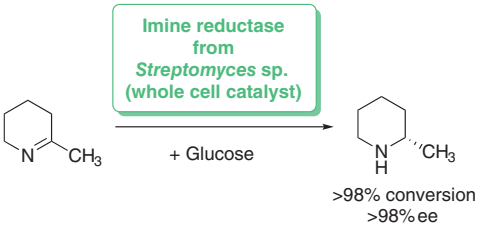

Scheme 6.36 Enantioselective reduction with an imine reductase for the formation of (*S*)-2-methylpiperidine.

The conversion of hydrophobic heterocyclic imines (in the absence of a carboxylic acid group as a substituent) was investigated in detail by Iding et al., and this study comprises the screening of numerous IREDs available in recombinant form. The screening of more than 20 IREDs revealed that also various six-membered heterocyclic imines can be successfully reduced with high to excellent enantioselectivities in many cases. After prioritization of preferred IRED biocatalysts, preparative biotransformations have been conducted. For example, in the presence of the IRED from *Streptomyces tsukubaensis*, the desired product (*R*)-2-methylpiperidine was obtained in 71% yield and with 98% ee and utilizing the IRED from *Streptomyces viridochromogenes* as a biocatalyst gave (*R*)-1-methyl-1,2,3,4-tetrahydroisoquinoline in 82% yield and with 98% ee (Scheme 6.37) [123].

Another identified biocatalyst for the reduction of six-membered imines is the IRED from *Amycolatopsis orientalis*, which has been studied by the Grogan and Turner groups. This NADPH-dependent enzyme is suitable to reduce various monocyclic and bicyclic imines. It is noteworthy that aging of the enzyme has an impact

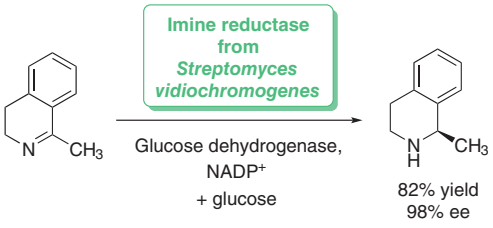

Scheme 6.37 Enantioselective reduction with an imine reductase for the formation of (*R*)-1-methyl-1,2,3,4-tetrahydroisoquinoline.

not only on activity but also on enantioselectivity. In detail it has been found that the enantiopreference is inverted when using freshly prepared and longer stored enzyme [124].

Recently, a further suitable IRED-type biocatalyst has been disclosed jointly by Pleiss and Nestl and coworkers. It is noteworthy that in this case the IRED has been designed by a rational protein engineering starting from a β-hydroxy acid dehydrogenase from *Thermocrinis albus*. This wild-type enzyme converts keto acids into the corresponding hydroxy acids, and after suitable point mutations the resulting variants are capable to tolerate six-membered cyclic imines as substrates. For example, when using the tailor-made mutant K189D/N192L/N193L/F25A/D258S in a biotransformation with *in situ* cofactor recycling with a glucose-6-phosphate dehydrogenase, the resulting chiral (*S*)-2-phenyl-piperidine was formed with 30% and 99% ee [125].

The use of IREDs have been also studied for the reduction of dihydroisoquinolines, comprising such substrates containing a bulky substituent in 1-position [126]. In 2017, the groups of Xu and Zheng reported that an IRED from *Stackebrandtia nassauensis* efficiently reduced a broad range of dihydroisoquinolines with strong variation of the substituent in 1-position, leading to the formation of the resulting tetrahydroisoquinolines with full conversion (>99%), in yields of up to 81% and with enantioselectivities of up to 99% ee when conducting the biotransformations at substrate concentrations between 5 and 100 mM.

Furthermore, research work has been done in the field of process development of IRED-catalyzed reactions. A micro-aqueous reaction environment was utilized by Maugeri and Rother for such types of biotransformations in the presence of lyophilized *E. coli* whole cells as biocatalyst formulation. A solvent screening revealed cyclopentyl methyl ether as preferred component. After process optimization, such IRED-catalyzed reductions were conducted in the micro-aqueous medium running at a substrate concentration of 20 mM, leading to conversions of up to 96% and enantioselectivities of >99%. A representative example is shown in Scheme 6.38 [127].

The process development of such type of biocatalytic reductions has been also addressed by the group of Gröger in collaboration with researchers from Hofmann-LaRoche. In detail, a recombinant *E. coli*-type whole cell catalyst has been prepared, and such cells have been directly used for the enantioselective reduction of 1-methyl-3,4-dihydroisoquinoline. For the *in situ* cofactor regeneration, a

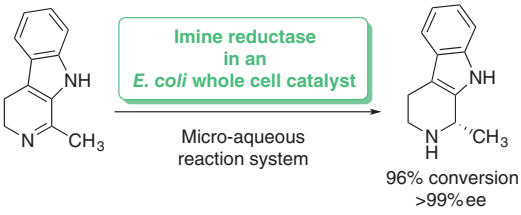

Scheme 6.38 Enantioselective reduction with an imine reductase in a micro-aqueous reaction system as reaction medium.

GDH-catalyzed oxidation of D-glucose was used, leading to high conversion and enantioselectivity of >99% ee in the presence of a biocatalyst loading of $2\,g\,l^{-1}$ up to $10\,g\,l^{-1}$ and at a substrate concentration of up to 100 mM (Scheme 6.39) [128].

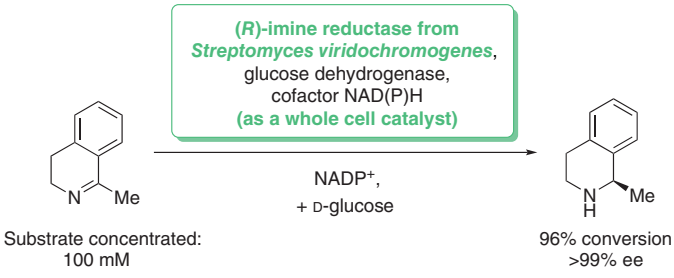

Scheme 6.39 Enantioselective reduction of 1-methyl-3,4-dihydroisoquinoline with a whole cell catalyst co-expressing an imine reductase and a glucose dehydrogenase.

A further challenge, which has been addressed in this field, has been the extension of the IRED technology to access six-membered heterocyclic amines, which contain a second heteroatom within the cyclic imine structure. The presence of such a further heteroatom can have a significant impact on the imine bond and, thus, on its reactivity. The enantioselective reduction of prochiral 2*H*-1,4-benzothiazines, which contain a sulfur atom in the imine cycle, has been reported by the Gröger group, leading to conversions of up to 96% and enantioselectivities of up to 99% ee. A selected example for the formation of both enantiomers of such a chiral sulfur-containing heterocyclic amine, which were obtained with 96% and 95% conversion and 83% and 91% ee for the (*S*)- and (*R*)-enantiomer, respectively, is shown in Scheme 6.40 [129].

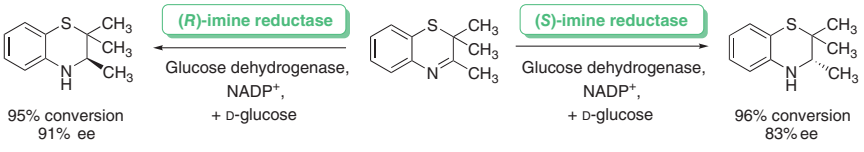

Scheme 6.40 Enantioselective reduction of a 2*H*-1,4-benzothiazine with imine reductases, leading to both amine product enantiomers.

Another chalcogen heteroatom being included in cyclic imine structures is oxygen, and one representative example of such heterocyclic imines is 1,4-benzoxazines. The corresponding reduced cyclic amines are of importance in the field of pharmaceutical intermediates and products. Various examples showing the suitability of IREDs for the reduction of these types of imines have been reported by the Gröger group, leading to conversions of >99% and enantioselectivities of up to 99% ee [130].

Such biocatalytic imine reduction steps also enable to access other six-membered heterocyclic amines bearing a further nitrogen as a heteroatom. This has been demonstrated by the group of Nestl, who reported the synthesis of a broad range of piperazines when starting from 1,2-diamines and 1,2-dicarbonyl compounds in the presence of an IRED from *Myxococcus stipitatus* as a biocatalyst [131]. The desired piperazine products were obtained with a high product formation of up to >99% and excellent enantioselectivities of up to >99% ee. A selected example is shown in Scheme 6.41.

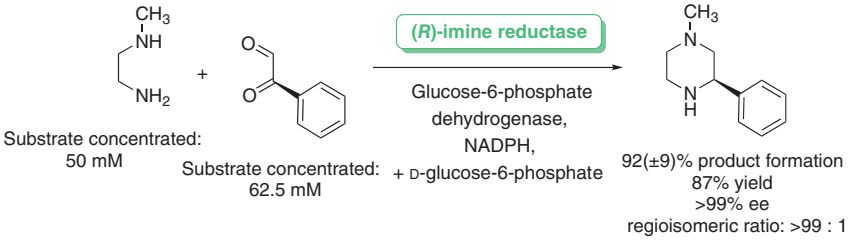

Scheme 6.41 Enantioselective syntheses of piperazines via reduction with an imine reductase from *Myxococcus stipitatus*.

Besides the identification of a broad range of IREDs being suitable for the synthesis of six-membered cyclic amines as well as the process development of such biotransformations, a further focus in recent years was on the integration of IRED-catalyzed reductions into multistep synthesis. An overview about achievements in this field of enzymatic cascades is illustrated as follows by selected examples.

In accordance with their synthetic strategy for pyrrolidines when starting from 1,4-diketones or keto aldehydes (as described earlier in Section 6.4.1.1), the group of Turner extended this concept to the analogous enantioselective biocatalytic synthesis of piperidines [64]. The synthetic concept is based on an initial synthesis of a 5-oxo aldehyde from the corresponding acid by means of reduction with a bacterial CAR from *Mycobacterium marinum*, which was used as a whole cell catalyst. A subsequent enzymatic transamination then converts the aldehyde moiety into the amine moiety, which then undergoes intramolecular cyclization with formation of the cyclic imine. Note that in spite of using a transaminase, the formed amine, and, thus, the imine are not chiral. The enantioselective step then consists of an IRED-catalyzed reduction, thus leading to piperidines with

up to 98% conversion and 98% ee. In contrast with the chemoenzymatic routes described earlier, this cascade represents a purely enzymatic cascade with a CAR, transaminase, and IRED as biocatalysts involved therein. From a synthetic diversity point of view, it is noteworthy that this purely biocatalytic cascade developed by the group of Turner (Scheme 6.42) is complementary to the chemoenzymatic cascade developed by the group of Kroutil [119], as these routes lead to the selective formation of piperidines with one and two stereogenic centers, respectively [64]. Furthermore, a cascade reaction proceeding in a whole cell was developed leading to piperidine derivatives in high yields (up to 93%) and enantiomeric excesses (up to 93% ee) [132].

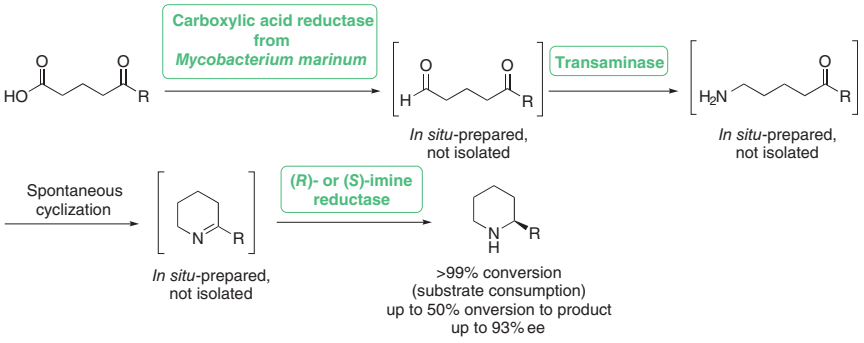

Scheme 6.42 Enantioselective enzymatic synthesis of piperidines through a cascade process.

Cascade reactions utilizing IRED and transaminase as the catalyst components for heterocycle formation have been also applied successfully for the enantioselective synthesis of dihydropyridines. Such approach has been developed by the Kroutil group who first used a transaminase for formation of the amine moiety, followed by an IRED-catalyzed imine reduction. The latter enzymatic step, in which NADPH is consumed as cofactor, has been combined with an *in situ* cofactor recycling in the presence of an ADH [133].

Besides the reduction of a C=N bond within such cascades, also enantioselective C—C bond formation can be conducted by means of enzyme catalysis [134]. In detail, an enzymatic Pictet–Spengler reaction, which was combined with enzymatic and spontaneous reaction steps to form complex multi-cyclic amine compounds in a highly enantio- and diastereoselective fashion, has been reported by the groups of Kroutil, Hailes, and Rother. The enzymatic cascade leading to the desired trisubstituted tetrahydroisoquinolines is exemplified by a representative example in Scheme 6.43: an initial enantioselective carboligation via an umpolung reaction, followed by a diastereoselective formation of the chiral amine moiety with a transaminase, and a subsequent cyclization step in the presence of a Pictet–Spenglerase enzyme. The resulting products bearing three stereogenic centers were obtained with excellent enantio- and diastereoselectivities.

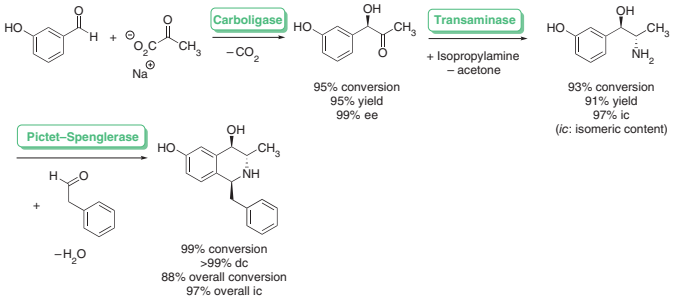

Scheme 6.43 Enantio- and diastereoselective synthesis of trisubstituted tetrahydroisoquinoline through an enzymatic cascade with a Pictet–Spenglerase.

6.5.2 O-Heterocycles

The most prominent examples of six-membered O-heterocycles are cyclic carbohydrates [135, 136], and a large number of biosynthetic approaches to these important heterocycles exist [137]. Some of them have been also applied in organic synthesis of carbohydrates using enzymes. Since the biosynthesis of carbohydrates, however, goes far beyond the scope of this book chapter, accordingly reference is made at this point to relevant literature on this subject [137].

6.6 Conclusion and Perspectives

In conclusion, biocatalysis turned out as a versatile tool for the preparation of a broad range of different heterocycles, for example, three-, four-, five- and six-membered heterocycles. A particular key feature of many of such processes are the excellent enantio- and diastereoselectivities, which can be achieved when using enzymes as catalysts. Thus, a biocatalysis toolbox is now available, which gives access to a broad range of such heterocycles in a highly stereoselective manner. Furthermore, it has been also demonstrated that such processes also proceed with high process efficiency and under environmentally friendly reaction conditions (such as low reaction temperature and aqueous reaction media), thus representing both an economical as well as sustainable access to the heterocyclic target molecules. In addition, such enzymatic reaction steps can be also combined with other reactions (for example, substrate preparation steps) toward cascade reactions. These cascade reactions further contribute to the improvement of the overall process efficiency as well as economy of biocatalytic heterocycle syntheses.

References

1 Eicher, T., Hauptmann, S., and Speicher, A. (2012). *The Chemistry of Heterocycles – Structures, Reactions, Synthesis, and Applications*, 3e. Weinheim: Wiley-VCH.

2 Joule, J.A. and Mills, K. (2010). *Heterocyclic Chemistry*, 5e. Chichester: Wiley.
3 Katritzky, A., Ramsden, C.E., Joule, J.A., and Zhdankin, V. (2010). *Handbook of Heterocyclic Chemistry*, 3e. Amsterdam: Elsevier.
4 Lechner, H., Pressnitz, D., and Kroutil, W. (2015). Biocatalysts for the formation of three- to six-membered carbo- and heterocycles. *Biotechnol. Adv.* 33 (5): 457. https://doi.org/10.1016/j.biotechadv.2015.01.012.
5 Farwell, C.C., Zhang, R.K., McIntosh, J.A. et al. (2015). Enantioselective enzyme-catalyzed aziridination enabled by active-site evolution of a cytochrome P450. *ACS Cent. Sci.* 1 (2): 89:https://doi.org/10.1021/acscentsci.5b00056.
6 Van Hylckama Vlieg, J.E.T., Tang, L., Lutje Spelberg, J.H. et al. (2001). Halohydrin dehalogenases are structurally and mechanistically related to short-chain dehydrogenases/reductases. *J. Bacteriol.* 183 (17): 5058. https://doi.org/10.1128/JB.183.17.5058-5066.2001.
7 De Jong, R.M., Tiesinga, J.J.W., Rozeboom, H.J. et al. (2003). Structure and mechanism of a bacterial haloalcohol dehalogenase: a new variation of the short-chain dehydrogenase/reductase fold without an NAD(P)H binding site. *EMBO J.* 22 (19): 4933. https://doi.org/10.1093/emboj/cdg479.
8 Lin, H., Xu, M.Y., Liu, Y., and Wu, Z.L. (2016). Biocatalytic epoxidation for green synthesis. In: *Green Biocatalysis*, 1e (ed. R.N. Patel), 351–372. Wiley.
9 Wu, S., Zhou, Y., and Li, Z. (2019). Biocatalytic selective functionalisation of alkenes via single-step and one-pot multi-step reactions. *Chem. Commun.* 55 (7): 883. https://doi.org/10.1039/c8cc07828a.
10 Schallmey, A. and Schallmey, M. (2016). Recent advances on halohydrin dehalogenases—from enzyme identification to novel biocatalytic applications. *Appl. Microbiol. Biotechnol.* 100 (18): 7827. https://doi.org/10.1007/s00253-016-7750-y.
11 Koopmeiners, J., Halmschlag, B., Schallmey, M., and Schallmey, A. (2016). Biochemical and biocatalytic characterization of 17 novel halohydrin dehalogenases. *Appl. Microbiol. Biotechnol.* 100 (17): 7517. https://doi.org/10.1007/s00253-016-7493-9.
12 Tang, L., Lutje Spelberg, J.H., Fraaije, M.W., and Janssen, D.B. (2003). Kinetic mechanism and enantioselectivity of halohydrin dehalogenase from *Agrobacterium radiobacter*. *Biochemistry* 42 (18): 5378. https://doi.org/10.1021/bi0273361.
13 Schallmey, M., Floor, R.J., Hauer, B. et al. (2013). Biocatalytic and structural properties of a highly engineered halohydrin dehalogenase. *ChemBioChem* 14 (7): 870. https://doi.org/10.1002/cbic.201300005.
14 Tang, L., Torres Pazmiño, D.E., Fraaije, M.W. et al. (2005). Improved catalytic properties of halohydrin dehalogenase by modification of the halide-binding site. *Biochemistry* 44 (17): 6609. https://doi.org/10.1021/bi047613z.
15 Drauz, K., Gröger, H., and May, O. (2012). *Enzyme Catalysis in Organic Synthesis*, 3e. Weinheim, Germany: Wiley-VCH Verlag GmbH & Co. KGaA.
16 Koopmeiners, J., Diederich, C., Solarczek, J. et al. (2017). HheG, a halohydrin dehalogenase with activity on cyclic epoxides. *ACS Catal.* 7 (10): 6877. https://doi.org/10.1021/acscatal.7b01854.

17 Xue, F., Liu, Z.Q., Wang, Y.J. et al. (2015). Efficient synthesis of (*S*)-epichlorohydrin in high yield by cascade biocatalysis with halohydrin dehalogenase and epoxide hydrolase mutants. *Catal. Commun.* 72: 147. https://doi.org/10.1016/j.catcom.2015.09.025.

18 Zhang, X.J., Shi, P.X., Deng, H.Z. et al. (2018). Biosynthesis of chiral epichlorohydrin using an immobilized halohydrin dehalogenase in aqueous and non-aqueous phase. *Bioresour. Technol.* 263: 483. https://doi.org/10.1016/j.biortech.2018.05.027.

19 Zhang, X.J., Deng, H.Z., Liu, N. et al. (2019). Molecular modification of a halohydrin dehalogenase for kinetic regulation to synthesize optically pure (*S*)-epichlorohydrin. *Bioresour. Technol.* 276: 154. https://doi.org/10.1016/j.biortech.2018.12.103.

20 Seisser, B., Lavandera, I., Faber, K. et al. (2007). Stereo-complementary two-step cascades using a two-enzyme system leading to enantiopure epoxides. *Adv. Synth. Catal.* 349 (8, 9): 1399. https://doi.org/10.1002/adsc.200700027.

21 Otto, K., Hofstetter, K., Röthlisberger, M. et al. (2004). Biochemical characterization of StyAB from *Pseudomonas* sp. strain VLB120 as a two-component flavin-diffusible monooxygenase. *J. Bacteriol.* 186 (16): 5292. https://doi.org/10.1128/JB.186.16.5292-5302.2004.

22 Kantz, A., Chin, F., Nallamothu, N. et al. (2005). Mechanism of flavin transfer and oxygen activation by the two-component flavoenzyme styrene monooxygenase. *Arch. Biochem. Biophys.* 442 (1): 102. https://doi.org/10.1016/j.abb.2005.07.020.

23 Schmid, A., Hofstetter, K., Feiten, H.J. et al. (2001). Integrated biocatalytic synthesis on gram scale: the highly enantioselective preparation of chiral oxiranes with styrene monooxygenase. *Adv. Synth. Catal.* 343 (6, 7): 732. https://doi.org/10.1002/1615-4169(200108)343:6/7<732::AID-ADSC732>3.0.CO;2-Q.

24 Kuhn, D., Kholiq, M.A., Heinzle, E. et al. (2010). Intensification and economic and ecological assessment of a biocatalytic oxyfunctionalization process. *Green Chem.* 12 (5): 815. https://doi.org/10.1039/b921896c.

25 Panke, S., Held, M., Wubbolts, M.G. et al. (2002). Pilot-scale production of (*S*)-styrene oxide from styrene by recombinant *Escherichia coli* synthesizing styrene monooxygenase. *Biotechnol. Bioeng.* 80 (1): 33. https://doi.org/10.1002/bit.10346.

26 Di Gennaro, P., Colmegna, A., Galli, E. et al. (1999). A new biocatalyst for production of optically pure aryl epoxides by styrene monooxygenase from *Pseudomonas fluorescens* ST. *Appl. Environ. Microbiol.* 65 (6): 2794. https://doi.org/10.1128/aem.65.6.2794-2797.1999.

27 Panke, S., Wubbolts, M.G., Witholt, B., and Schmid, A. (2000). Pilot-scale production of (*S*)-styrene oxide from styrene by recombinant *Escherichia coli* synthesizing styrene monooxygenase. *Biotechnol. Bioeng.* 69 (1): 91. https://doi.org/10.1002/bit.10346.

28 Lin, H., Liu, Y., and Wu, Z.L. (2011). Highly diastereo- and enantio-selective epoxidation of secondary allylic alcohols catalyzed by styrene monooxygenase. *Chem. Commun.* 47 (9): 2610. https://doi.org/10.1039/c0cc04360e.

29 Lin, H., Tang, Y., Dong, S. et al. (2020). A new monooxygenase from *Herbaspirillum huttiense* catalyzed highly enantioselective epoxidation of allylbenzenes and allylic alcohols. *Catal. Sci. Technol.* 10 (7): 2145. https://doi.org/10.1039/d0cy00081g.

30 Toda, H., Imae, R., and Itoh, N. (2014). Bioproduction of chiral epoxyalkanes using styrene monooxygenase from *Rhodococcus* sp. ST-10 (RhSMO). *Adv. Synth. Catal.* 356 (16): 3443. https://doi.org/10.1002/adsc.201400383.

31 Xiao, H., Dong, S., Liu, Y. et al. (2021). A new clade of styrene monooxygenases for (*R*)-selective epoxidation. *Catal. Sci. Technol.* 11 (6): 2195. https://doi.org/10.1039/d0cy02312d.

32 Corrado, M.L., Knaus, T., and Mutti, F.G. (2018). A chimeric styrene monooxygenase with increased efficiency in asymmetric biocatalytic epoxidation. *ChemBioChem* 19 (7): 679. https://doi.org/10.1002/cbic.201700653.

33 Egawa, T., Shimada, H., and Ishimura, Y. (1994). Evidence for compound I formation in the reaction of cytochrome-P450cam with *m*-chloroperbenzoic acid. *Biochem. Biophys. Res. Commun.* 201 (3): 1464. https://doi.org/10.1006/bbrc.1994.1868.

34 Kellner, D.G., Hung, S.C., Weiss, K.E., and Sligar, S.G. (2002). Kinetic characterization of compound I formation in the thermostable cytochrome P450 CYP119. *J. Biol. Chem.* 277 (12): 9641. https://doi.org/10.1074/jbc.C100745200.

35 Fruetel, J.A., Mackman, R.L., Peterson, J.A., and Ortiz de Montellano, P.R. (1994). Relationship of active site topology to substrate specificity for cytochrome P450(terp) (CYP108). *J. Biol. Chem.* 269 (46): 28815. https://doi.org/10.1016/s0021-9258(19)61979-4.

36 Li, Q.S., Ogawa, J., Schmid, R.D., and Shimizu, S. (2001). Residue size at position 87 of cytochrome P450 BM-3 determines its stereoselectivity in propylbenzene and 3-chlorostyrene oxidation. *FEBS Lett.* 508 (2): 249. https://doi.org/10.1016/S0014-5793(01)03074-5.

37 Li, A., Liu, J., Pham, S.Q., and Li, Z. (2013). Engineered P450pyr monooxygenase for asymmetric epoxidation of alkenes with unique and high enantioselectivity. *Chem. Commun.* 49 (98): 11572. https://doi.org/10.1039/C3CC46675B.

38 Kumar, D., Karamzadeh, B., Sastry, G.N., and De Visser, S.P. (2010). What factors influence the rate constant of substrate epoxidation by compound I of cytochrome P450 and analogous iron(IV)-oxo oxidants? *J. Am. Chem. Soc.* 132 (22): 7656. https://doi.org/10.1021/ja9106176.

39 Coleman, T., Kirk, A.M., Chao, R.R. et al. (2021). Understanding the mechanistic requirements for efficient and stereoselective alkene epoxidation by a cytochrome P450 enzyme. *ACS Catal.* 11 (4): 1995. https://doi.org/10.1021/acscatal.0c04872.

40 Kubo, T., Peters, M.W., Meinhold, P., and Arnold, F.H. (2006). Enantioselective epoxidation of terminal alkenes to (*R*)- and (*S*)-epoxides by engineered cytochromes P450 BM-3. *Chem. Eur. J.* 12 (4): 1216. https://doi.org/10.1002/chem.200500584.

41 Watanabe, Y., Laschat, S., Budde, M. et al. (2007). Oxidation of acyclic monoterpenes by P450 BM-3 monooxygenase: influence of the substrate *E*/*Z*-isomerism

on enzyme chemo- and regioselectivity. *Tetrahedron* 63 (38): 9413. https://doi.org/10.1016/j.tet.2007.06.104.

42 Lucas, D., Goulitquer, S., Marienhagen, J. et al. (2010). Stereoselective epoxidation of the last double bond of polyunsaturated fatty acids by human cytochromes P450. *J. Lipid Res.* 51 (5): 1125. https://doi.org/10.1194/jlr.M003061.

43 Jiang, D., Tu, R., Bai, P., and Wang, Q. (2013). Directed evolution of cytochrome P450 for sterol epoxidation. *Biotechnol. Lett* 35 (10): 1663. https://doi.org/10.1007/s10529-013-1254-y.

44 Dietrich, J.A., Yoshikuni, Y., Fisher, K.J. et al. (2009). A novel semi-biosynthetic route for artemisinin production using engineered substrate-promiscuous P450BM3. *ACS Chem. Biol.* 4 (4): 261. https://doi.org/10.1021/cb900006h.

45 Denard, C.A., Huang, H., Bartlett, M.J. et al. (2014). Cooperative tandem catalysis by an organometallic complex and a metalloenzyme. *Angew. Chem. Int. Ed.* 53 (2): 465. https://doi.org/10.1002/anie.201305778.

46 Denard, C.A., Bartlett, M.J., Wang, Y. et al. (2015). Development of a one-pot tandem reaction combining ruthenium-catalyzed alkene metathesis and enantioselective enzymatic oxidation to produce aryl epoxides. *ACS Catal.* 5 (6): 3817. https://doi.org/10.1021/acscatal.5b00533.

47 Colonna, S., Gaggero, N., Casella, L. et al. (1993). Enantiaselective epoxidation of styrene derivatives by chloroperoxidase catalysis. *Tetrahedron: Asymmetry* 4 (6): 1325. https://doi.org/10.1016/S0957-4166(00)80243-8.

48 Dexter, A.F., Lakner, F.J., Campbell, R.A., and Hager, L.P. (1995). Highly enantioselective epoxidation of 1,1-disubstituted alkenes catalyzed by chloroperoxidase. *J. Am. Chem. Soc.* 117 (23): 6412. https://doi.org/10.1021/ja00128a053.

49 Lakner, F.J., Cain, K.P., and Hager, L.P. (1997). Enantioselective epoxidation of ω-bromo-2-methyl-1-alkenes catalyzed by chloroperoxidase. Effect of chain length on selectivity and efficiency. *J. Am. Chem. Soc.* 119 (2): 443. https://doi.org/10.1021/ja962998x.

50 Rai, G.P., Sakai, S., Flórez, A.M. et al. (2001). Directed evolution of chloroperoxidase for improved epoxidation and chlorination catalysis. *Adv. Synth. Catal.* 343 (6–7): 638. https://doi.org/10.1002/1615-4169(200108)343:6/7<638::AID-ADSC638>3.0.CO;2-6.

51 Hobisch, M., Holtmann, D., Gomez de Santos, P. et al. (2021). Recent developments in the use of peroxygenases – exploring their high potential in selective oxyfunctionalisations. *Biotechnol. Adv.* 51: 107615. https://doi.org/10.1016/j.biotechadv.2020.107615.

52 Kluge, M., Ullrich, R., Scheibner, K., and Hofrichter, M. (2012). Stereoselective benzylic hydroxylation of alkylbenzenes and epoxidation of styrene derivatives catalyzed by the peroxygenase of *Agrocybe aegerita*. *Green Chem.* 14 (2): 440. https://doi.org/10.1039/c1gc16173c.

53 Peter, S., Kinne, M., Ullrich, R. et al. (2013). Epoxidation of linear, branched and cyclic alkenes catalyzed by unspecific peroxygenase. *Enzyme Microb. Technol.* 52 (6–7): 370. https://doi.org/10.1016/j.enzmictec.2013.02.013.

54 Rauch, M.C.R., Tieves, F., Paul, C.E. et al. (2019). Peroxygenase-catalysed epoxidation of styrene derivatives in neat reaction media. *ChemCatChem* 11 (18): 4519. https://doi.org/10.1002/cctc.201901142.

55 Xu, G., Crotti, M., Saravanan, T. et al. (2020). Enantiocomplementary epoxidation reactions catalyzed by an engineered cofactor-independent non-natural peroxygenase. *Angew. Chem.* 132 (26): 10460. https://doi.org/10.1002/ange.202001373.

56 Raber, M.L., Arnett, S.O., and Townsend, C.A. (2009). A conserved tyrosyl-glutamyl catalytic dyad in evolutionarily linked enzymes: carbapenam synthetase and β-lactam synthetase. *Biochemistry* 48 (22): 4959. https://doi.org/10.1021/bi900432n.

57 Sleeman, M.C., MacKinnon, C.H., Hewitson, K.S., and Schofield, C.J. (2002). Enzymatic synthesis of monocyclic β-lactams. *Bioorg. Med. Chem. Lett.* 12 (4): 597. https://doi.org/10.1016/S0960-894X(01)00806-X.

58 Labonte, J.W., Kudo, F., Freeman, M.F. et al. (2012). Engineering the synthetic potential of β-lactam synthetase and the importance of catalytic loop dynamics. *Med. Chem. Commun.* 3 (8): 960. https://doi.org/10.1039/c2md00305h.

59 Gerratana, B., Stapon, A., and Townsend, C.A. (2003). Inhibition and alternate substrate studies on the mechanism of carbapenam synthetase from *Erwinia carotovora*. *Biochemistry* 42 (25): 7836. https://doi.org/10.1021/bi034361d.

60 Hamed, R.B., Gomez-Castellanos, J.R., Thalhammer, A. et al. (2011). Stereoselective C—C bond formation catalysed by engineered carboxymethylproline synthases. *Nat. Chem.* 3 (5): 365. https://doi.org/10.1038/nchem.1011.

61 Hamed, R.B., Henry, L., Claridge, T.D.W., and Schofield, C.J. (2017). Stereoselective production of dimethyl-substituted carbapenams via engineered carbapenem biosynthesis enzymes. *ACS Catal.* 7 (2): 1279. https://doi.org/10.1021/acscatal.6b02509.

62 Hamed, R.B., Gomez-Castellanos, J.R., Henry, L. et al. (2019). Biocatalytic production of bicyclic β-lactams with three contiguous chiral centres using engineered crotonases. *Commun. Chem.* 2 (1): 1. https://doi.org/10.1038/s42004-018-0106-z.

63 O'Reilly, E., Iglesias, C., Ghislieri, D. et al. (2014). A regio- and stereoselective ω-transaminase/monoamine oxidase cascade for the synthesis of chiral 2,5-disubstituted pyrrolidines. *Angew. Chem. Int. Ed.* 53 (9): 2447. https://doi.org/10.1002/anie.201309208.

64 France, S.P., Hussain, S., Hill, A.M. et al. (2016). One-pot cascade synthesis of mono- and disubstituted piperidines and pyrrolidines using carboxylic acid reductase (CAR), ω-transaminase (ω-TA), and imine reductase (IRED) biocatalysts. *ACS Catal.* 6 (6): 3753. https://doi.org/10.1021/acscatal.6b00855.

65 Costa, B.Z., Galman, J.L., Slabu, I. et al. (2018). Synthesis of 2,5-disubstituted pyrrolidine alkaloids via a one-pot cascade using transaminase and reductive aminase biocatalysts. *ChemCatChem* 10 (20): 4733. https://doi.org/10.1002/cctc.201801166.

66 Okamoto, Y., Köhler, V., and Ward, T.R. (2016). An NAD(P)H-dependent artificial transfer hydrogenase for multienzymatic cascades. *J. Am. Chem. Soc.* 138 (18): 5781. https://doi.org/10.1021/jacs.6b02470.

67 Zwick, C.R. and Renata, H. (2018). Remote C–H hydroxylation by an α-ketoglutarate-dependent dioxygenase enables efficient chemoenzymatic synthesis of manzacidin C and proline analogs. *J. Am. Chem. Soc.* 140 (3): 1165. https://doi.org/10.1021/jacs.7b12918.

68 Lukat, P., Katsuyama, Y., Wenzel, S. et al. (2017). Biosynthesis of methyl-proline containing griselimycins, natural products with anti-tuberculosis activity. *Chem. Sci.* 8 (11): 7521. https://doi.org/10.1039/c7sc02622f.

69 Herter, S., McKenna, S.M., Frazer, A.R. et al. (2015). Galactose oxidase variants for the oxidation of amino alcohols in enzyme cascade synthesis. *ChemCatChem* 7 (15): 2313. https://doi.org/10.1002/cctc.201500218.

70 Huang, L., Sayoga, G.V., Hollmann, F., and Kara, S. (2018). Horse liver alcohol dehydrogenase-catalyzed oxidative lactamization of amino alcohols. *ACS Catal.* 8 (9): 8680. https://doi.org/10.1021/acscatal.8b02355.

71 Mourelle-Insua, Á., Zampieri, L.A., Lavandera, I., and Gotor-Fernández, V. (2018). Conversion of γ- and δ-keto esters into optically active lactams. Transaminases in cascade processes. *Adv. Synth. Catal.* 360 (4): 686. https://doi.org/10.1002/adsc.201701304.

72 Barrios, D.A., D'Antonio, J., McCombs, N.L. et al. (2014). Peroxygenase and oxidase activities of dehaloperoxidase-hemoglobin from *Amphitrite ornata*. *J. Am. Chem. Soc.* 136 (22): 7914. https://doi.org/10.1021/ja500293c.

73 McCombs, N.L., Smirnova, T., and Ghiladi, R.A. (2017). Oxidation of pyrrole by dehaloperoxidase-hemoglobin: chemoenzymatic synthesis of pyrrolin-2-ones. *Catal. Sci. Technol.* 7 (14): 3104. https://doi.org/10.1039/c7cy00781g.

74 Ren, X., Yorke, J.A., Taylor, E. et al. (2015). Drug oxidation by cytochrome P450BM3: metabolite synthesis and discovering new P450 reaction types. *Chem. Eur. J.* 21 (42): 15039. https://doi.org/10.1002/chem.201502020.

75 Ren, X., O'Hanlon, J.A., Morris, M. et al. (2016). Synthesis of imidazolidin-4-ones via a cytochrome P450-catalyzed intramolecular C–H amination. *ACS Catal.* 6 (10): 6833. https://doi.org/10.1021/acscatal.6b02189.

76 Ren, X., Chandgude, A.L., and Fasan, R. (2020). Highly stereoselective synthesis of fused cyclopropane-γ-lactams via biocatalytic iron-catalyzed intramolecular cyclopropanation. *ACS Catal.* 10 (3): 2308. https://doi.org/10.1021/acscatal.9b05383.

77 Scalacci, N., Black, G.W., Mattedi, G. et al. (2017). Unveiling the biocatalytic aromatizing activity of monoamine oxidases MAO-N and 6-HDNO: development of chemoenzymatic cascades for the synthesis of pyrroles. *ACS Catal.* 7 (2): 1295. https://doi.org/10.1021/acscatal.6b03081.

78 Zhao, F., Masci, D., Ferla, S. et al. (2020). Monoamine oxidase (MAO-N) biocatalyzed synthesis of indoles from indolines prepared via photocatalytic cyclization/arylative dearomatization. *ACS Catal.* 10 (11): 6414. https://doi.org/10.1021/acscatal.0c01351.

79 Leutbecher, H., Constantin, M.A., Mika, S. et al. (2011). A new laccase-catalyzed domino process and its application to the efficient synthesis of 2-aryl-1*H*-benzimidazoles. *Tetrahedron Lett.* 52 (5): 605. https://doi.org/10.1016/j.tetlet.2010.11.145.

80 Shrivas, P., Zodape, S., Wankhade, A., and Pratap, U. (2020). Facile synthesis of benzazoles through biocatalytic cyclization and dehydrogenation employing catalase in water. *Enzyme Microb. Technol.* 138: 109562: 1. https://doi.org/10.1016/j.enzmictec.2020.109562.

81 Xu, J., Green, A.P., and Turner, N.J. (2018). Chemo-enzymatic synthesis of pyrazines and pyrroles. *Angew. Chem. Int. Ed.* 57 (51): 16760. https://doi.org/10.1002/anie.201810555.

82 Mayer, S.F., Steinreiber, A., Orru, R.V.A., and Faber, K. (2001). Enzyme-triggered enantioconvergent transformation of haloalkyl epoxides. *Eur. J. Org. Chem.* 23: 4537. https://doi.org/10.1002/1099-0690(200112)2001:23<4537::AID-EJOC4537>3.0.CO;2-E.

83 Steinreiber, A., Edegger, K., Mayer, S.F., and Faber, K. (2001). Enantio- and diastereo-convergent synthesis of (2*R*,5*R*)- and (2*R*,5*S*)-pityol through enzyme-triggered ring closure. *Tetrahedron: Asymmetry* 12 (14): 2067. https://doi.org/10.1016/S0957-4166(01)00370-6.

84 Glueck, S.M., Fabian, W.M.F., Faber, K., and Mayer, S.F. (2004). Biocatalytic asymmetric rearrangement of a methylene-interrupted bis-epoxide: simultaneous control of four asymmetric centers through a biomimetic reaction cascade. *Chem. Eur. J.* 10 (14): 3467. https://doi.org/10.1002/chem.200400061.

85 Ueberbacher, B.T., Oberdorfer, G., Gruber, K., and Faber, K. (2009). Epoxide-hydrolase-initiated hydrolysis/rearrangement cascade of a methylene-interrupted bis-epoxide yields chiral THF moieties without involvement of a "cyclase". *ChemBioChem* 10 (10): 1697. https://doi.org/10.1002/cbic.200900176.

86 Dydio, P., Key, H.M., Nazarenko, A. et al. (2016). An artificial metalloenzyme with the kinetics of native enzymes. *Science* 354 (6308): 102. https://doi.org/10.1126/science.aah4427.

87 Key, H.M., Dydio, P., Clark, D.S., and Hartwig, J.F. (2016). Abiological catalysis by artificial haem proteins containing noble metals in place of iron. *Nature* 534 (7608): 534. https://doi.org/10.1038/nature17968.

88 Ricklefs, E., Girhard, M., Koschorreck, K. et al. (2015). Two-step one-pot synthesis of pinoresinol from eugenol in an enzymatic cascade. *ChemCatChem* 7 (12): 1857. https://doi.org/10.1002/cctc.201500182.

89 Zerva, A., Koutroufini, E., Kostopoulou, I. et al. (2019). A novel thermophilic laccase-like multicopper oxidase from *Thermothelomyces thermophila* and its application in the oxidative cyclization of 2′,3,4-trihydroxychalcone. *New Biotechnol.* 49: 10. https://doi.org/10.1016/j.nbt.2018.12.001.

90 Hollmann, F., Kara, S., Opperman, D.J., and Wang, Y. (2018). Biocatalytic synthesis of lactones and lactams. *Chem. Asian J.* 13 (23): 3601:https://doi.org/10.1002/asia.201801180.

91 Chandgude, A.L., Ren, X., and Fasan, R. (2019). Stereodivergent intramolecular cyclopropanation enabled by engineered carbene transferases. *J. Am. Chem. Soc.* 141 (23): 9145. https://doi.org/10.1021/jacs.9b02700.

92 Ren, X., Liu, N., Chandgude, A.L., and Fasan, R. (2020). An enzymatic platform for the highly enantioselective and stereodivergent construction of cyclopropyl-δ-lactones. *Angew. Chem. Int. Ed.* 59 (48): 21634. https://doi.org/10.1002/anie.202007953.

93 Mirza, I.A., Yachnin, B.J., Wang, S. et al. (2009). Crystal structures of cyclohexanone monooxygenase reveal complex domain movements and a sliding cofactor. *J. Am. Chem. Soc.* 131 (25): 8848. https://doi.org/10.1021/ja9010578.

94 Alphand, V., Archelas, A., and Furstoss, R. (1989). Microbial transformations 16. One-step synthesis of a pivotal prostaglandin chiral synthon via a highly enantioselective microbiological Baeyer–Villiger type reaction. *Tetrahedron Lett.* 30 (28): 3663. https://doi.org/10.1016/S0040-4039(01)80476-7.

95 Summers, B.D., Omar, M., Ronson, T.O. et al. (2015). *E. coli* cells expressing the Baeyer–Villiger monooxygenase "MO14" (ro03437) from *Rhodococcus jostii* RHA1 catalyse the gram-scale resolution of a bicyclic ketone in a fermentor. *Org. Biomol. Chem.* 13 (6): 1897. https://doi.org/10.1039/c4ob01441c.

96 Rudroff, F., Fink, M.J., Pydi, R. et al. (2017). First chemo-enzymatic synthesis of the (*R*)-Taniguchi lactone and substrate profiles of CAMO and OTEMO, two new Baeyer–Villiger monooxygenases. *Monatsh. Chem.* 148 (1): 157:https://doi.org/10.1007/s00706-016-1873-9.

97 González-Martínez, D., Rodríguez-Mata, M., Méndez-Sánchez, D. et al. (2015). Lactonization reactions through hydrolase-catalyzed peracid formation. Use of lipases for chemoenzymatic Baeyer–Villiger oxidations of cyclobutanones. *J. Mol. Catal. B: Enzym.* 114: 31. https://doi.org/10.1016/j.molcatb.2014.09.002.

98 Baldwin, C.V.F., Wohlgemuth, R., and Woodley, J.M. (2008). The first 200-L scale asymmetric Baeyer–Villiger oxidation using a whole-cell biocatalyst. *Org. Process Res. Dev.* 12 (4): 660:https://doi.org/10.1021/op800046t.

99 Leipold, F., Wardenga, R., and Bornscheuer, U.T. (2012). Cloning, expression and characterization of a eukaryotic cycloalkanone monooxygenase from *Cylindrocarpon radicicola* ATCC 11011. *Appl. Microbiol. Biotechnol.* 94 (3): 705. https://doi.org/10.1007/s00253-011-3670-z.

100 Kadow, M., Loschinski, K., Saß, S. et al. (2012). Completing the series of BVMOs involved in camphor metabolism of *Pseudomonas putida* NCIMB 10007 by identification of the two missing genes, their functional expression in *E. coli*, and biochemical characterization. *Appl. Microbiol. Biotechnol.* 96 (2): 419. https://doi.org/10.1007/s00253-011-3859-1.

101 Fürst, M.J.L.J., Gran-Scheuch, A., Aalbers, F.S., and Fraaije, M.W. (2019). Baeyer–Villiger monooxygenases: tunable oxidative biocatalysts. *ACS Catal.* 9 (12): 11207. https://doi.org/10.1021/acscatal.9b03396.

102 Irwin, A.J. and Jones, J.B. (1977). Asymmetric syntheses via enantiotopically selective horse liver alcohol dehydrogenase catalyzed oxidations of diols containing a prochiral center. *J. Am. Chem. Soc.* 99 (2): 556. https://doi.org/10.1021/ja00444a040.

103 Irwin, A.J. and Jones, J.B. (1977). Regiospecific and enantioselective horse liver alcohol dehydrogenase catalyzed oxidations of some hydroxycyclopentanes. *J. Am. Chem. Soc.* 99 (5): 1625:https://doi.org/10.1021/ja00447a057.

104 Kara, S., Spickermann, D., Schrittwieser, J.H. et al. (2013). Access to lactone building blocks via horse liver alcohol dehydrogenase-catalyzed oxidative lactonization. *ACS Catal.* 3 (11): 2436. https://doi.org/10.1021/cs400535c.

105 Götz, K., Liese, A., Ansorge-Schumacher, M., and Hilterhaus, L. (2013). A chemo-enzymatic route to synthesize (*S*)-γ-valerolactone from levulinic acid. *Appl. Microbiol. Biotechnol.* 97 (9): 3865. https://doi.org/10.1007/s00253-012-4652-5.

106 Díaz-Rodríguez, A., Borzecka, W., Lavandera, I., and Gotor, V. (2014). Stereodivergent preparation of valuable γ- or δ-hydroxy esters and lactones through one-pot cascade or tandem chemoenzymatic protocols. *ACS Catal.* 4 (2): 386. https://doi.org/10.1021/cs4010024.

107 Classen, T., Korpak, M., Schölzel, M., and Pietruszka, J. (2014). Stereoselective enzyme cascades: an efficient synthesis of chiral γ-butyrolactones. *ACS Catal.* 4 (5): 1321. https://doi.org/10.1021/cs5000262.

108 Leutbecher, H., Conrad, J., Klaiber, I., and Beifuss, U. (2005). O-Heterocycles via laccase-catalyzed domino reactions with O_2 as the oxidant. *Synlett* 20: 3126. https://doi.org/10.1055/s-2005-922748.

109 Hajdok, S., Conrad, J., Leutbecher, H. et al. (2009). The laccase-catalyzed domino reaction between catechols and heterocyclic 1,3-dicarbonyls and the unambiguous structure elucidation of the products by NMR spectroscopy and X-ray crystal structure analysis. *J. Org. Chem.* 74 (19): 7230:https://doi.org/10.1021/jo9011915.

110 Hajdok, S., Leutbecher, H., Greiner, G. et al. (2007). Laccase initiated oxidative domino reactions for the efficient synthesis of 3,4-dihydro-7,8-dihydroxy-2*H*-dibenzofuran-1-ones. *Tetrahedron Lett.* 48 (29): 5073. https://doi.org/10.1016/j.tetlet.2007.05.089.

111 Witayakran, S., Gelbaum, L., and Ragauskas, A.J. (2007). Cascade synthesis of benzofuran derivatives via laccase oxidation-Michael addition. *Tetrahedron* 63 (45): 10958. https://doi.org/10.1016/j.tet.2007.08.066.

112 Risi, C., Zhao, F., and Castagnolo, D. (2019). Chemo-enzymatic metathesis/aromatization cascades for the synthesis of furans: disclosing the aromatizing activity of laccase/TEMPO in oxygen-containing heterocycles. *ACS Catal.* 9 (8): 7264. https://doi.org/10.1021/acscatal.9b02452.

113 Naapuri, J., Rolfes, J.D., Keil, J. et al. (2017). Enzymatic halocyclization of allenic alcohols and carboxylates: a biocatalytic entry to functionalized O-heterocycles. *Green Chem.* 19 (2): 447. https://doi.org/10.1039/c6gc01926a.

114 Effenberger, F., Straub, A., and Null, V. (1992). Stereoselektive Darstellung von Thiozuckern aus achiralen Vorstufen mittels Enzymen. *Liebigs Ann. Chem.* 12: 1297. https://doi.org/10.1002/jlac.1992199201214.

115 Fessner, W.D. and Sinerius, G. (1994). Phosphoenolpyruvate as a dual purpose reagent for integrated nucleotide/nicotinamide cofactor recycling. *Bioorg. Med. Chem.* 2 (7): 639. https://doi.org/10.1016/0968-0896(94)85012-7.

116 Charmantray, F., Dellis, P., Hélaine, V. et al. (2006). Chemoenzymatic synthesis of 5-thio-D-xylopyranose. *Eur. J. Org. Chem.* 24: 5526. https://doi.org/10.1002/ejoc.200600627.

117 Effenberger, F., Null, V., and Ziegler, T. (1992). Preparation of optically pure L-2-hydroxyaldehydes with yeast transketolase. *Tetrahedron Lett.* 33 (36): 5157. https://doi.org/10.1016/S0040-4039(00)79121-0.

118 Soler, A., Garrabou, X., Hernández, K. et al. (2014). Sequential biocatalytic aldol reactions in multistep asymmetric synthesis: pipecolic acid, piperidine and pyrrolidine (homo)iminocyclitol derivatives from achiral building blocks. *Adv. Synth. Catal.* 356 (14, 15): 3007. https://doi.org/10.1002/adsc.201400453.

119 Simon, R.C., Grischek, B., Zepeck, F. et al. (2012). Regio- and stereoselective monoamination of diketones without protecting groups. *Angew. Chem.* 124 (27): 6817. https://doi.org/10.1002/anie.201202375.

120 Yasuda, M., Ueda, M., Muramatsu, H. et al. (2006). Enzymatic synthesis of cyclic amino acids by *N*-methyl-L-amino acid dehydrogenase from *Pseudomonas putida*. *Tetrahedron: Asymmetry* 17 (12): 1775. https://doi.org/10.1016/j.tetasy.2006.07.005.

121 Mitsukura, K., Kuramoto, T., Yoshida, T. et al. (2013). A NADPH-dependent (*S*)-imine reductase (SIR) from *Streptomyces* sp. GF3546 for asymmetric synthesis of optically active amines: purification, characterization, gene cloning, and expression. *Appl. Microbiol. Biotechnol.* 97 (18): 8079. https://doi.org/10.1007/s00253-012-4629-4.

122 Leipold, F., Hussain, S., Ghislieri, D., and Turner, N.J. (2013). Asymmetric reduction of cyclic imines catalyzed by a whole-cell biocatalyst containing an (*S*)-imine reductase. *ChemCatChem* 5 (12): 3505. https://doi.org/10.1002/cctc.201300539.

123 Wetzl, D., Berrera, M., Sandon, N. et al. (2015). Expanding the imine reductase toolbox by exploring the bacterial protein-sequence space. *ChemBioChem* 16 (12): 1749. https://doi.org/10.1002/cbic.201500218.

124 Aleku, G.A., Man, H., France, S.P. et al. (2016). Stereoselectivity and structural characterization of an imine reductase (IRED) from *Amycolatopsis orientalis*. *ACS Catal.* 6 (6): 3880. https://doi.org/10.1021/acscatal.6b00782.

125 Stockinger, P., Schelle, L., Schober, B. et al. (2020). Engineering of thermostable β-hydroxyacid dehydrogenase for the asymmetric reduction of imines. *ChemBioChem* 21 (24): 3511. https://doi.org/10.1002/cbic.202000526.

126 Li, H., Tian, P., Xu, J.H., and Zheng, G.W. (2017). Identification of an imine reductase for asymmetric reduction of bulky dihydroisoquinolines. *Org. Lett.* 19 (12): 3151. https://doi.org/10.1021/acs.orglett.7b01274.

127 Maugeri, Z. and Rother, D. (2016). Application of imine reductases (IREDs) in micro-aqueous reaction systems. *Adv. Synth. Catal.* 358 (17): 2745. https://doi.org/10.1002/adsc.201501154.

128 Zumbrägel, N., Wetzl, D., Iding, H., and Gröger, H. (2017). Asymmetric biocatalytic reduction of cyclic imines: design and application of a tailor-made whole-cell catalyst. *Heterocycles* 95 (2): 1261. https://doi.org/10.3987/COM-16-S(S)89.

129 Zumbrägel, N., Merten, C., Huber, S.M., and Gröger, H. (2018). Enantioselective reduction of sulfur-containing cyclic imines through biocatalysis. *Nat. Commun.* 9 (1): 1949. https://doi.org/10.1038/s41467-018-03841-5.

130 Zumbrägel, N., Machui, P., Nonnhoff, J., and Gröger, H. (2019). Enantioselective biocatalytic reduction of 2*H*-1,4-benzoxazines using imine reductases. *J. Org. Chem.* 84 (3): 1440. https://doi.org/10.1021/acs.joc.8b02867.

131 Borlinghaus, N., Gergel, S., and Nestl, B.M. (2018). Biocatalytic access to piperazines from diamines and dicarbonyls. *ACS Catal.* 8 (4): 3727. https://doi.org/10.1021/acscatal.8b00291.

132 Hepworth, L.J., France, S.P., Hussain, S. et al. (2017). Enzyme cascades in whole cells for the synthesis of chiral cyclic amines. *ACS Catal.* 7 (4): 2920. https://doi.org/10.1021/acscatal.7b00513.

133 Alvarenga, N., Payer, S.E., Petermeier, P. et al. (2020). Asymmetric synthesis of dihydropinidine enabled by concurrent multienzyme catalysis and a biocatalytic alternative to krapcho dealkoxycarbonylation. *ACS Catal.* 10 (2): 1607. https://doi.org/10.1021/acscatal.9b04611.

134 Erdmann, V., Lichman, B.R., Zhao, J. et al. (2017). Enzymatic and chemoenzymatic three-step cascades for the synthesis of stereochemically complementary trisubstituted tetrahydroisoquinolines. *Angew. Chem. Int. Ed.* 56 (41): 12503. https://doi.org/10.1002/anie.201705855.

135 Eicher, T., Hauptmann, S., and Speicher, A. (2012). Six-membered heterocycles. In: *The Chemistry of Heterocycles: Structure, Reactions, Syntheses, and Applications*, 3e, 297. Weinheim: Wiley-VCH.

136 Werz, D.B. and Vidal, S. (2014). *Modern Synthetic Methods in Carbohydrate Chemistry – From Monosaccharides to Complex Glycoconjugates*. Weinheim: Wiley-VCH.

137 Lindhorst, T.K. (2007). *Essentials of Carbohydrate Chemistry and Biochemistry*, 3e. Weinheim: Wiley-VCH.

7

Multicomponent Synthesis of Heterocycles

Carolina S. Marques[1], Elisabete P. Carreiro[1], and António P. S. Teixeira[1,2]

[1] University of Évora, Institute of Research and Advanced Training, LAQV-REQUIMTE, Rua Romão Ramalho, 59, Évora 7000-671, Portugal
[2] University of Évora, School of Health and Human Development, Department of Medical and Health Sciences, Rua Romão Ramalho, 59, Évora 7000-671, Portugal

7.1 Introduction

Although multicomponent reactions (MCRs) are as old as organic chemistry, it was with the pioneering work developed by Passerini in 1921 and Ugi in 1959 that MCRs have become pivotal protocols in the synthesis of complex and key valuable scaffolds [1]. MCRs are commonly described as convergent reactions in which three or more reagents are added to a single vessel and react to form a product that contains most of the atoms from the starting materials. Thus, they are considered as useful tools in the creation of libraries of small organic molecules using economically favored methodologies, reducing the costs associated with shorter synthetic pathways.

An upright challenge in modern drug development is to simplify synthetic routes to access complex molecules. The synthesis of heterocycles evolved from classical condensation procedures (occasionally old but gold chemistry) to MCR procedures. From the famous classic click chemistry reaction toward five-membered ring heterocycles to newer three or more membered heterocycles via MCRs, a new window of opportunities to access great molecular diversity by fine-tuning the starting materials is open for synthetic and medicinal chemists.

The limitless growth of novel MCR-based protocols forming complex and interesting heterocyclic structures has been and will continue to be a hot topic in organic chemistry, targeting the synthesis of biologically active products and high-value synthetic building blocks. Accessing high levels of molecular complexity with a minimal number of actions, in a sustainable fashion path, is a challenge that has captured the interest of the academia and industrial community.

In this sense, in this chapter, the major classes of heterocycles containing the common heteroatoms (nitrogen, oxygen, and sulfur) will be reviewed considering their synthesis by MCR protocols. Literature from 2010 until today will be covered, despite without rigid criteria. Generally, the synthesis of new heterocyclic ring formation

Heterocycles: Synthesis, Catalysis, Sustainability, and Characterization, First Edition.
Edited by Teresa M.V.D. Pinho e Melo and Marta Pineiro.

via MCR was arranged in an increasing order of the heterocyclic ring size and the increasing order of the number of heteroatoms present in the ring. Emphasis will be given to more sustainable methods, where solvent-free or green solvents protocols, catalyst-free methodologies, mild reaction conditions (such as room temperature and less energetic heating sources, microwave or ultrasonic irradiation), and short reaction times will be highlighted.

7.2 Three-Membered Ring Heterocycles

Three-membered heterocycles fit into the family of the smallest cyclic structures. Despite their massive utility as building blocks, due to their capacity to act as convenient templates for access other compounds of interest (heterocyclic units or not), they can be found in a plethora of compounds with biological relevance like natural products, agrochemicals, active pharmaceutical ingredients, macromolecules, etc. [2]. Among several described three-membered heterocyclic units, aziridines [3] (azacyclopropanes) and oxiranes [4] (epoxides or oxacyclopropanes) are the most dominant structural motifs reported in literature. The development of synthetic (and sustainable) approaches to access such important scaffolds and versatile intermediates is of utmost interest.

The synthesis of aziridines using three or more components is still considered as a challenge due to their high reactivity and consequent instability. This fact is mirrored in the scarce literature reports found on this topic. Among the few examples reported in literature concerning the use of MCRs to access aziridines, almost all of them require the use of expensive reagents, complex starting materials, multistep tedious approaches through a multicomponent strategy, or even the use of costly transition metal catalysts or organocatalysts. For instance, Che and coworkers [5, 6] developed a ruthenium porphyrin catalyzed 3-MCR of diazo compounds, nitrosoarenes, and alkynes to access functionalized aziridine-2-carboxylates, aziridine-2-phophonates, and perfluoroalkyl aziridines in good yields and diastereoselectivities. Using also a 3-MCR approach, the group of Wulff [7–9] has also been very active in the field, reporting several pioneering Brønsted acid-catalytic asymmetric aziridination reactions to obtain *cis* and *trans*-aziridines using aldehydes (aryl or alkyl), diazoesters or diazoacetamides, and a *N*-protected amine. Despite being an elegant and innovative approach, this efficient diastereo- and enantioselective transformation moves away from the concept of sustainable process, since it requires the use of low reaction temperatures, tedious sequential steps, and the use of the BOROX catalyst, prepared *in situ* from commercially available binaphthol-type organocatalysts and triphenylborate. Likewise, Bew et al. [10] reported a similar MC aza-Darzens approach using 3,3′-bis(aryl) (*S*)-BINOL *N*-triflylphosphoramides as asymmetric Brønsted acid catalyst to obtain *N*-aryl-*cis*-aziridine-carboxylate esters in good yields and high enantioselectivities. However, this transformation requires the use of *o-tert*-butoxy-aniline at −60 °C.

Examples described hereafter concerning more sustainable MC synthetic approaches to obtain interesting aziridines were reported very recently. In 2020, Li,

Chen, Xu, and coworkers reported an Ugi and novel *pseudo*-Knoevenagel cascade reaction to access *cis*-aziridinyl succinimides and *trans*-aziridines in a one-pot fashion under smooth reaction conditions [11]. Basically, using benzoyl formic acid derivatives, anilines, isocyanides, and ethyl glyoxylate, in a catalyst-free approach using MeOH as solvent at room temperature, the corresponding Ugi-4-component intermediate was obtained easily. After solvent evaporation and under microwave conditions, this crude intermediate was directly subjected to a *pseudo*-Knoevenagel condensation followed by ring expansion and intramolecular S_Ni cyclization reaction, in the presence of the adequate base and solvent. This cascade two-step one-pot reaction approach, depending on the base and solvent used in the last step, provides a collection of highly functionalized aziridine heterocycles in good yields and suitable scope (Scheme 7.1).

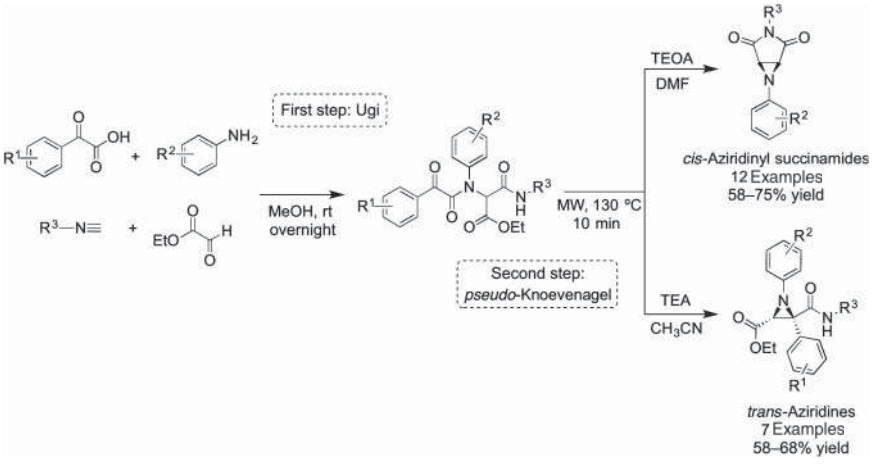

Scheme 7.1 Cascade one-pot Ugi, *pseudo*-Knoevenagel reaction for the synthesis of cis-aziridinyl succinimides and trans-aziridines in one-pot. TEOA, triethanolamine; TEA, triethylamine.

In the same year, Li et al. also reported a catalyst-free 3-MCR for the synthesis of multifunctionalized 1-arylaziridine-2-carboxylates using readily available α-diazoesters, nitrosoarenes, and alkynes (Scheme 7.2) [12]. This step-economical, highly efficient, and economically friendly synthetic approach exhibits good functional group tolerance and mild reaction conditions. A gram scale was also efficiently demonstrated, getting the desired aziridine derivatives in very good yield

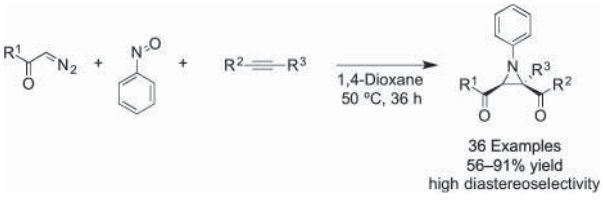

Scheme 7.2 3-MC catalyst-free approach to 1-arylaziridine-2-carboxylates.

(86–87%). The authors assumed that the mechanism involves a [3+2] cycloaddition reaction between the alkyne and a previously formed intermediate (nitrosobenzene trapped the diazo compound with consequent loss of N_2) to give an isoxazoline, which after a Baldwin rearrangement generate the desired aziridines in high diastereoselectivities (*cis* was the relative stereochemistry of the major product assigned).

Like aziridines, oxiranes are also very useful structures found in several naturally occurring compounds of biological interest and powerful synthetic intermediates. Biju and coworkers report an attractive 3-MCR involving aziridines, arynes, and aldehydes to easily access trisubstituted *N*-aryl α-amino epoxides, essential building blocks in the synthesis of amino sugars and oxygenated amino acids [13]. Based on the reaction reported by Giumanini in 1972 [14] concerning the formation of 1,4-zwitterionic intermediates by *N*-substituted aziridine derivatives and arynes, the authors use a similar approach in which 2-(trimethylsilyl)aryl triflate derivatives were employed to generate the aryne species *in situ* that subsequently reacted with N-substituted aziridines and aldehydes. This transition metal catalyst free procedure furnished the desired oxirane derivatives in moderate to good yields and high diastereoselectivity (dr = 7 : 3–9 : 1). The protocol could be easily extended to a variety of aziridines, 2-(trimethylsilyl)aryl triflate derivatives and aldehydes and also proved to be effective with *N*-substituted isatins, resulting in attractive spiroepoxy oxindole derivatives (Scheme 7.3).

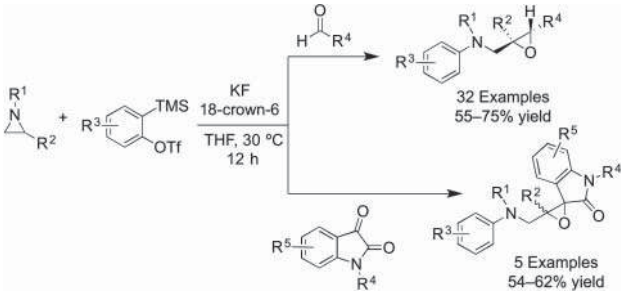

Scheme 7.3 3-MCR approach to trisubstituted *N*-aryl α-amino epoxides and spiroepoxy oxindole derivatives via the highly strained cyclic nitrogen ylide intermediates generated from aziridines and arynes.

Corrêa, Paixão, and coworkers developed an eco-friendly tandem 3-MC method to obtain epoxy-α-acyloxycarboxamides in good yields and stereoselectivities [15]. The asymmetric epoxidation catalyzed by a diarylprolinol silyl ether organocatalyst in the environmentally benign ethanol/water mixture provided the desired epoxy aldehydes, which underwent a Passerini 3-MCR with carboxylic acid derivatives and isocyanides to afford a small library of highly functionalized epoxy-α-acyloxycarboxamides (Scheme 7.4). This synthetic design displays potential for large-scale applications, and the corresponding epoxipeptidomimetics showed potent and selective inhibition profile against cathepsin L, which plays a significant role in promoting tumor progression and metastatic aggressiveness [16].

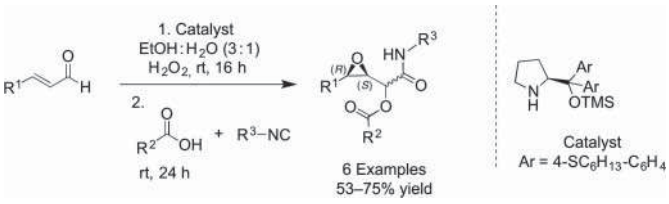

Scheme 7.4 Tandem organocatalytic epoxidation/Passerini 3-MCR toward the synthesis of epoxy-α-acyloxycarboxamides.

α-Lactams (aziridinones), important three-membered heterocycles found in several compounds with biological interest (antimicrobial and antiviral activities) and useful reactive intermediates due to their ring-opening capacity, are poorly explored regarding innovative synthetic processes. Within the scope of this chapter, only one report was found in literature considering the synthesis of monofluorinated α-lactam pseudopeptide derivatives via an unusual and unexpected 4-MC-Ugi/dehydrofluorination reaction by tuning suitable reagents using solvent-free or methanol as solvent, in mild reaction conditions (rt or 60 °C) (Scheme 7.5) [17]. The group of Cao and Qian synthesized a *gem*-difluoromethylene-containing isocyanide to use as building block in an Ugi 4-MC approach, together with amine derivatives, aldehydes, and carboxylic acids, in mild reaction conditions, in order to get α,α-difluoromethylene analogs of β-amino acids (Scheme 7.5) [18]. Intriguingly, they found out that using some substrates (R^1, R^2, and R^3 identified in Scheme 7.5), the unexpected formation of monofluorinated *pseudo*-peptides containing an α-lactam moiety was noticed, without the use of additional base in a one-pot fashion.

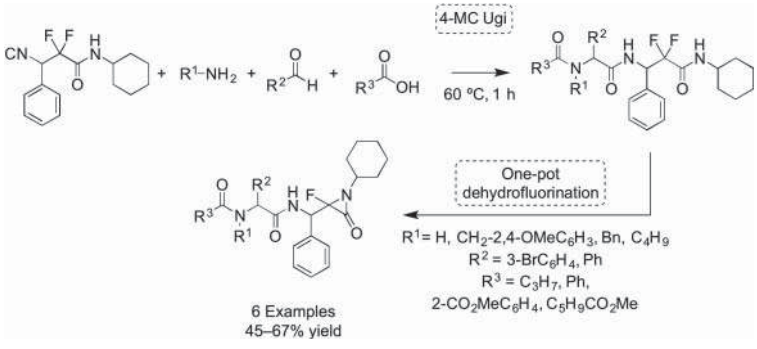

Scheme 7.5 Synthesis of monofluorinated α-lactam *pseudo*-peptides via a 4-MC-Ugi/dehydrofluorination reaction. Source: Liu et al. [17] / Springer Nature.

7.3 Four-Membered Ring Heterocycles

Contrary to α-lactams, more attention was focused on β-lactams (azetidinones), due to their extremely importance in drug discovery. Apart from their widely known antibiotic properties (penicillin's, 50% of the global antibiotics market [19]), this

structural unit can be found also in other bioactive molecules of interest [20]. Several synthetic methodologies to access these four-membered cyclic amides can be found in literature in the last two decades, but within the scope of this chapter, only MCR approaches will be addressed, emphasizing sustainable and innovative methods.

Blackie et al. described the synthesis of β-lactams by an Ugi 3-MCR from commercially available starting materials in methanol at room temperature [21]. Using β-alanine, cyclohexyl isocyanide, and several aryl substituted aldehydes, the desired β-lactams were obtained in moderate to good yield and good scope (Scheme 7.6). The racemic products were evaluated in *in vitro* assays against the chloroquine sensitive D10 strain of *Plasmodium falciparum*, showing modest micromolar range IC_{50} values concerning antimalarial activity.

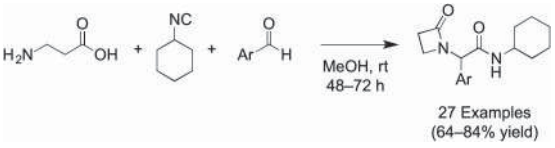

Scheme 7.6 Synthesis of novel β-lactams via an Ugi 3-MCR approach.

Using similar Ugi 3-MCR strategy, the group of Silvani reported easy access to oxindole-based β-lactams, key building blocks, using β-amino acid, isocyanide, and isatin components in a one-pot fashion (Scheme 7.7) [22]. Isatin derivatives (ketone unit) were applied as the carbonyl component, and the reaction proceeded smoothly to afford a small library of β-lactam containing 3,3-disubstituted oxindoles in moderate to good yields. When chiral β-amino acids were used, the corresponding enantiomerically pure oxindole-based β-lactams diastereoisomers were obtained (dr = 63 : 37 and 65 : 35), whose relative stereochemistry was determined by X-ray analysis. Antibacterial *in vitro* assays were performed, but the results were somehow disappointing, showing weak activity in gram-negative (*Escherichia coli* and *Pseudomonas aeruginosa*) and gram-positive (*Staphylococcus aureus* and *Streptococcus mutans*) bacteria.

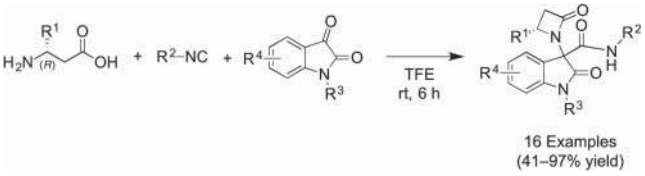

Scheme 7.7 Synthesis of β-lactam containing 3,3-disubstituted oxindoles in an Ugi 3-MCR approach. Source: Rainoldi et al. [22] / Royal Society of Chemistry.

Using the same solvent (trifluoroethanol, TFE), the group of Dömling reported the synthesis of targeted β-lactams, in an Ugi 3-MCR followed by diastereomeric separation and hydrolysis [23]. After exploiting a pharmacophore-based virtual screening platform (AnchorQuery [24]), they found that the MCRs between a specific aldehyde, substituted amino acids, and isocyanides under microwave

irradiation at 130 °C were the best conditions for the formation of the desired β-lactam Ugi adduct. Two complementary assays (fluorescence polarization and NMR-HSQC experiments) were used previously to determine the inhibitory affinities of these new scaffolds against MDM2 receptor (an important negative regulator of the p53 tumor suppressor). Concerning the fluorescence polarization binding assay, an affinity to MDM2 of 200 nM was estimated for the best compound. Years after, El Kaïm and coworkers reported the one-pot two-step synthesis of bis-β-lactam derivatives (potential biologically active and powerful synthetic intermediates) via similar microwave Ugi 3-MCR followed by a base-triggered diiodomethane cyclocondensation reaction at room temperature (Scheme 7.8) [25]. Besides demonstrating the efficiency of the Ugi reaction in the preparation of the β-lactams (nine examples, 48–73% yield), this procedure shows the robustness of the diiodomethane-based β-lactam formation (nine examples, 28–61% yield). Both were used in consecutive form, leading to fast assembling of bis-β-lactam derivatives in moderate yields (Scheme 7.8). Unfortunately, poor activity was observed against gram-positive bacteria of some of these compounds.

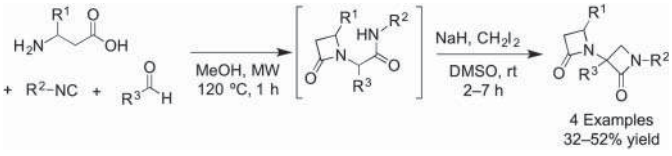

Scheme 7.8 Synthesis of bis-β-lactam derivatives via an Ugi 3-MCR followed by a diiodomethane cyclocondensation reaction, in one-pot. Source: Cheibas et al. [25] / John Wiley & Sons.

Galons, Lan, Lu, and coworkers reported the synthesis of β-lactams via an Ugi/Michael reaction cascade under mild conditions, using maleic or fumaric acid, nitrogen-containing heterocyclic aldehydes, isocyanides, and amines (Scheme 7.9) [26]. The advantage of this method is the mild conditions used and the efficiency of the protocol for generating complex nitrogen heterocyclic compounds. X-ray analysis confirmed the relative configuration of the major diastereoisomer (*cis*-conformation) and was in agreement with the DFT calculations concerning reaction mechanism and the 2D NOESY experiments. The intramolecular hydrogen bonding between the heteroatom from the aldehyde component and the amide NH group controls the chemoselectivity of the reaction, favoring the Michael addition path vs. the aza-Michael route.

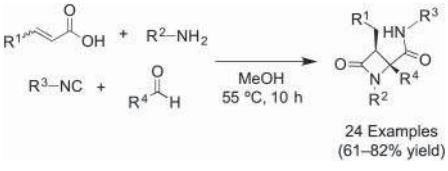

Scheme 7.9 One-pot synthesis of β-lactams by the Ugi 4-MC and Michael addition cascade reaction. Source: Gao et al. [26] / Royal Society of Chemistry.

Apart from the formation of β-lactams (azetidinones), very few reports concerning the use of MCR in the synthesis of other type of four-membered heterocycles were found in literature. Linked to the work developed within the scope of the use of tandem MCR with the effort to increase the complexity of the molecules, the group of Naskar reported an interesting tandem Petasis–Ugi MC condensation strategy to obtain aza-β-lactams [27]. Basically the tandem reaction approach begins with the formation of the hydrazine carboxylic acid salt generated via a Petasis 3-MC condensation reaction using a Boc-protected hydrazine, glyoxylic acid, and an aryl boronic acid. After Boc deprotection (with HCl) and upon evaporation of the solvent, the resulting hydrazine salt was treated directly with the aldehyde derivative and the isocyanide (Ugi) in aqueous methanol, at room temperature, providing the desired aza-β-lactams in low to moderate yields (Scheme 7.10). It was found that water was crucial to the efficiency of the reaction.

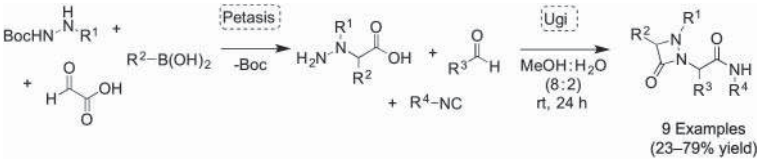

Scheme 7.10 Tandem Petasis–Ugi strategy for the synthesis of aza-β-lactams.

Shipman and coworkers highlight its interest in the synthesis of oxetanes, due to its importance regarding medicinal chemistry and their use as surrogates for common functional groups (*gem*-dimethyl or carbonyl groups) in active pharmaceutical ingredients. Beneficial effects concerning aqueous solubility, lipophilicity, and metabolic stability. are points of interest regarding this four-membered ring heterocycles. As such, they reported an interesting Passerini 3-MCR with oxetan-3-ones, carboxylic acids, and isocyanides to obtain the corresponding 3,3-disubstituted oxetanes in moderate to excellent yields in mild reaction conditions (Scheme 7.11) [28]. Good levels of diastereocontrol (dr = 4 : 1) were achieved when 2-cyclohexyloxetan-3-one was used as carbonyl component.

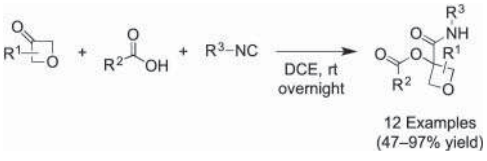

Scheme 7.11 3-MC Passerini reaction for the efficient synthesis of 3,3-disubstituted oxetanes. Source: Beasley et al. [28] / Elsevier.

7.4 Five-Membered Ring Heterocycles

Five-membered ring heterocycles are important scaffold systems found diverse natural products, biologically active molecules, and several other compounds with

different applications, such as catalysts, solvents for resins, corrosion inhibitors, or functional materials. A high diversity of systems could be found among the five-membered ring heterocycles, due to the presence of different heteroatoms, usually nitrogen, oxygen, and sulfur, and their combinations, and due to the aromatic or nonaromatic character, their partial or total hydrogenation, and their combination with other aryl or aliphatic rings. Thus, in addition to the important applications they have, these heterocycles are also valuable and versatile building blocks organic chemistry [29–33].

MCRs have been widely used to prepare diverse five-membered heterocyclic compounds through reactions that also start from very different reagents, in many different conditions. These ring systems can be constructed by distinct approaches: intramolecular cyclization, annulations, cycloadditions, and ring expansions, which add additional challenges to their synthesis [34]. In the last years, a big effort has been made to establish the synthesis of these compounds through MCR reactions under more sustainable protocols, avoiding hazardous and toxic solvents, giving preference to microwave or ultrasonic irradiation reaction conditions, etc.

7.4.1 Five-Membered Ring Heterocycles with One Heteroatom

Among five-membered ring heterocycles, pyrroles stand out due to their wide number of potential applications, biological properties, and versatility as synthetic intermediates. Its structural scaffold is found in a plethora of compounds with applications ranging from pharmaceutical agents to materials. The pyrrole ring is also present in many natural molecules, including porphyrins, globins, cytochromes, and vitamins [35–40].

In 2010, Estévez, Villacampa, and Menéndez [35] published a review with several MCR procedures for the synthesis of pyrrole derivatives. After this publication, many other heterocyclic compounds were prepared using several MCR sustainable approaches.

Bhat and Trivedi [41] prepared tetrasubstituted pyrrole derivatives through a simple and green protocol, using 1,3-dicarbonyl compounds, benzoin derivatives, and ammonium acetate, in the absence of catalyst and under solvent-free reaction conditions (Scheme 7.12). The best results were observed using 90 °C and 1.5 equiv of ammonium acetate.

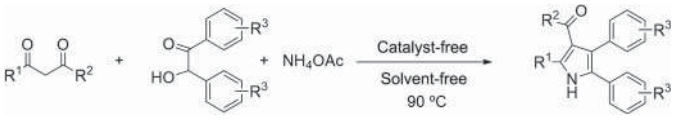

Scheme 7.12 Synthesis of tetrasubstituted pyrrole derivatives.

Tamaddon and Farahi [42] also used similar reagents to prepare tetrasubstituted pyrroles, taking the advantage of testing a silica sulfuric acid heterogeneous catalyst, under different reaction conditions (including solvent free), to afford the desired products. Sosnovskikh and coworkers [43] used 1,1,1-trifluoro-3-nitrobut-2-ene

with 1,3-dicarbonyl compounds (ethyl acetoacetate, acetylacetone, benzoylacetone) and ammonia or primary aliphatic amines on a 3-MCR approach to obtain 18 fluoride tetrasubstituted pyrrole derivatives, using ethanol as solvent.

In 2015, Zhao and coworkers [44] reported a one-pot methodology, with no solvent or catalyst, to synthesize pyrrole carboxylate derivatives via a microwave irradiation MCR, using different amines, ethyl acetoacetate, and α-bromoacetophenones. Huang, Shi, and coworkers [45] also used acetylene dicarboxylate derivatives in the preparation of polysubstituted pyrrole derivatives through a 4-MCR between an arylglyoxal, an aniline, a dialkyl but-2-ynedioate, and malononitrile under catalyst-free conditions (Scheme 7.13). The reaction can be carried out with different substituents at glyoxal's aryl group (e.g. methoxyl, methyl, chlorine, and fluorine substituents) as well as an *n*-butyl group and phenyl moiety bearing either electron-withdrawing or -donating groups (e.g. methoxyl, methyl, chlorine, bromine, fluorine, and nitro substituents) on the aniline derivative. The best results were achieved using ethanol as solvent, with yields up to 93%.

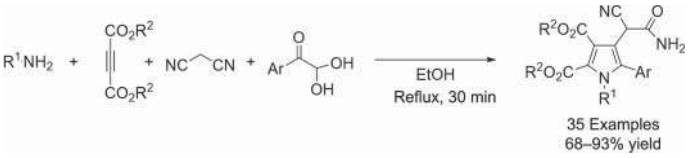

Scheme 7.13 Synthesis of tetrasubstituted pyrroles using acetylene dicarboxylate derivatives under catalyst-free conditions.

Siddiqui et al. [46] used the ionic liquid 1-butyl-3-methylimidazolium tetrafluoroborate ([bmim]BF_4) as solvent in the catalyst-free 3-MC synthesis of pyrrole derivatives carried out at room temperature (Scheme 7.14). The ionic liquid was used four times, and no loss of activity was observed. In these reactions, derivatives of phenacyl bromide, aliphatic or aromatic amines, and dimethyl or diethyl acetylene dicarboxylate (DMAD or DEAD) were used to obtain 1,2,4-trisubstituted pyrrole derivatives in excellent yields.

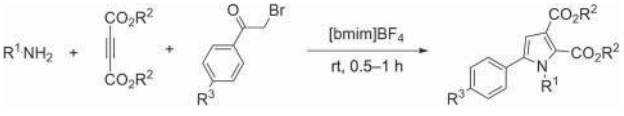

Scheme 7.14 Synthesis of substituted pyrroles using [bmim]BF_4 as solvent.

Other catalyst-free approach to pyrroles, also employing an ionic liquid as solvent, was proposed by Meshram et al. [47]. The procedure comprises a 4-MCR of amines, aldehydes, 1,3-pentanodione, and nitroalkane, using 1-*n*-butylimidazolium tetrafluoroborate ([Hbim]BF_4) as a reusable reaction medium (Scheme 7.15). Using cyclic/acyclic aliphatic amines and aromatic or heteroaromatic aldehydes, Meshram et al. were able to synthesize 29 new pyrrole derivatives with different functional groups, in a catalyst-free approach, at room temperature, in good to excellent yields.

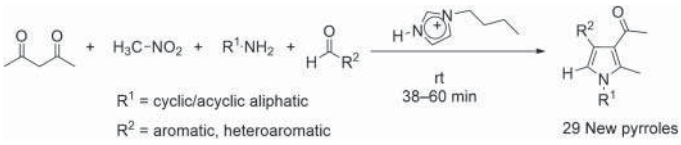

Scheme 7.15 Synthesis of new pyrroles using the ionic liquid [Hbim]BF_4 as solvent.

Zhang and coworkers [48] used nitromethane as component on the synthesis of pyrrole derivatives in a 4-MC coupling between amines, aldehydes, and 1,3-dicarbonyl compounds. Several reaction conditions were tested, including different catalysts and different solvents, but the best results have been achieved using a 50 wt% aqueous solution of gluconic acid (GAAS, a glucose derivative) as solvent (Scheme 7.16). Under these reaction conditions, using different aromatic amines and aromatic aldehydes, polysubstituted pyrroles were obtained in high yield. These environmentally friendly GAAS solution could be recycled and reused several times, with no significant loss of its activity, and good functional group tolerance was also verified.

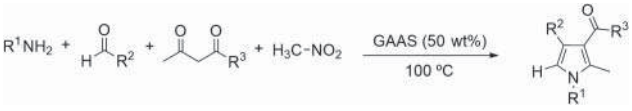

Scheme 7.16 Synthesis of new pyrroles in gluconic acid aqueous solution.

γ-Lactams also have received great attention. This structural scaffold is recognized in many natural products and is part of many molecules with biological activities; some of them are already being used as active pharmaceutical agents [49–53].

The synthesis of γ-lactams can be achieved via MCR, using a large number of different strategies. Recently, Pharande [54] and Mohammadkhani and Heravi [55] reviewed the synthesis of lactams using Ugi-4C and Ugi-3C isocyanide-based reactions, disclosing several strategies using sustainable methodologies in the construction of these lactam molecules.

Deprez and coworkers [56] prepared a series of five- and six-membered lactams via a 4-center Ugi 3-MCR under microwave irradiation and solvent-free conditions (Scheme 7.17). The use of levulinic or 5-ketohexanoic acids combined with structurally different amines and isocyanides gave five-membered or six-membered lactam rings, respectively, in shorter reaction times, in better yields comparatively to the classic synthetic approaches.

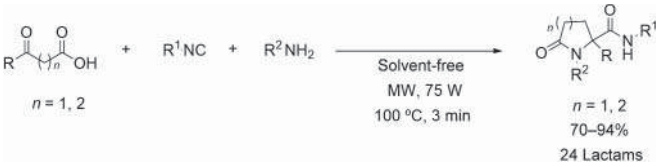

Scheme 7.17 Synthesis of five- or six-membered lactams via a 4-center Ugi-3-MCR under solvent-free and microwave irradiation conditions.

In 2016, Darehkordi et al. [57] reported the synthesis of spiro γ-lactams under mild conditions via a 4-center Ugi 3-MCR of gabapentin (an anticonvulsant), aromatic aldehydes, and cyclohexyl isocyanide. A new class of *N*-cyclohexyl-2-(3-oxo-2-azaspiro[4,5]decan-2-yl)-2-aryl acetamides were obtained in good to excellent yields and high selectivity (Scheme 7.18). Later, the same group [58] used this simple and efficient methodology to obtain *N*-cyclohexyl-3-(aryl)-3-oxo-2-(3-oxo-2-azaspiro [4,5]decan-2-yl)propanamide derivatives from gabapentin, glyoxal, and cyclohexyl isocyanide or aromatic aldehydes and *tert*-butyl isocyanide.

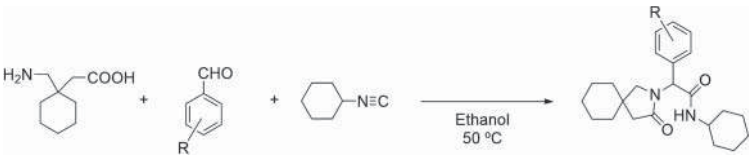

Scheme 7.18 A 4-center Ugi-3MCR to achieve spiro γ-lactam derivatives.

The unsaturated γ-lactam core is a key building block for the synthesis of amino acids and other natural products and a relevant structural system in numerous bioactive compounds, with immunosuppressive, platelet aggregation inhibitor, antitumor, and proteasome inhibitor activities [59, 60].

Komiotis and coworkers [61] synthesized a series of substituted pyrrolidinone derivatives in moderated to good yields, from sodium diethyl oxaloacetate, amines, and 3- or 4-halogenated aromatic aldehydes (Scheme 7.19). These syntheses were carried out in ethanol, under microwave irradiation, affording the desired products in moderated to good yields. Some of these compounds showed cytostatic and antiviral activities.

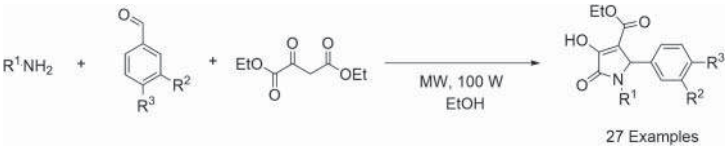

Scheme 7.19 Synthesis of substituted pyrrolidinone derivatives.

In 2014, Van der Eycken and coworkers [62] synthesized α,β-unsaturated γ-lactams via a one-pot Ugi 4-MCR, followed by carbocyclization and retro-Claisen fragmentation at 80 °C. These α,β-unsaturated γ-lactams were obtained from the reaction between propiolic acids, phenyl glyoxal, several amines, and isocyanides (Scheme 7.20). The authors demonstrated the importance of the electron-withdrawing carbonyl group next to the enolizable tertiary carbon and the Michael acceptor nature of the triple bond to trigger the 5-*endo*-dig-carbocyclization, leading to the final product. Later, the same research group [60] released a series of highly substituted α,β-unsaturated γ-lactams using a similar procedure, starting from nitrogen-containing heterocyclic aldehydes, amines, 2-alkynoic acids, and isocyanides, via a one-pot domino Ugi 4-MCR/Michael reaction procedure.

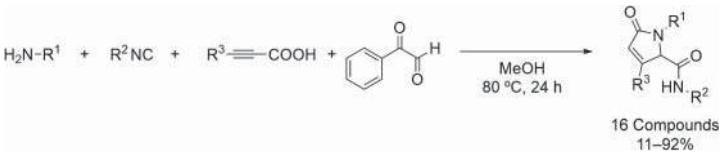

Scheme 7.20 Synthesis of α,β-unsaturated γ-lactams.

Riguet [63] prepared several chiral γ-lactams through a 4-center Ugi 3-MCR, after an enantioselective Friedel–Crafts alkylation of *N*-methylindole and 5-hydroxyfuran-2(5*H*)-one, an available renewable resource (Scheme 7.21). The Friedel–Crafts adducts were obtained in different solvents and reaction conditions, in good to excellent yields, in the presence of a chiral diphenylprolinol catalyst (the best enantiomeric ratio or diastereomeric ratio was obtained using the diphenylprolinol silyl ethers). Their reaction with aniline or benzylamine, and an isocyanide derivative, in ethanol, afforded a series of chiral products in moderated yields. The diastereoisomeric excess observed was very low, showing that the Ugi reaction was not diastereoselective, but also showed that no racemization was observed on the stereogenic center formed by the Friedel–Crafts reaction step.

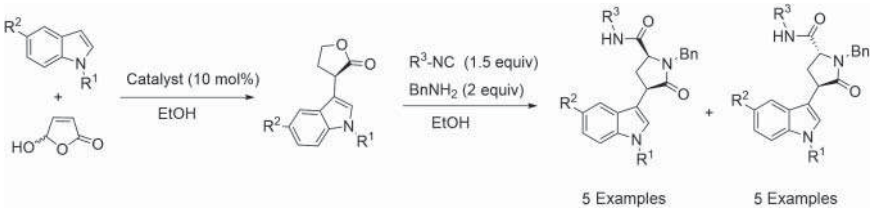

Scheme 7.21 Friedel–Crafts and Ugi reaction sequence used in the preparation of chiral γ-lactams.

In 2011, Santra and Andreana [64] disclosed the synthesis of bis-γ-lactams via an Ugi 4-CR of substituted hydroxybenzaldehydes, benzylamines, fumaric acid derivatives, and isocyanides (Scheme 7.22). These authors observed that water was the best solvent for this reaction under microwave irradiation.

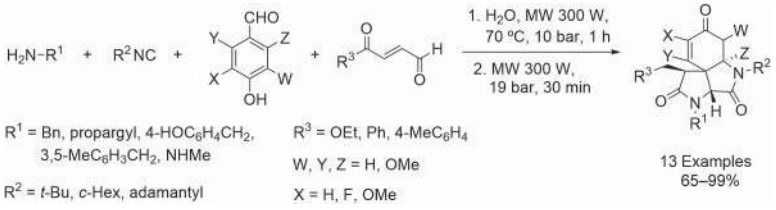

Scheme 7.22 Synthesis of bis-γ-lactams via an Ugi 4-MCR.

Spirocyclic fragments are important scaffolds in various low-molecular weight biologically active compounds. Spiroindole and spirooxindole moieties are the core of a structural scaffold found in many natural products and became a key

system of a variety of medicinal agents, with antimicrobial, anticancer, antimalarial, antiviral, antipyretic, and sodium channel blocker biological activities [30, 65–67]. Additionally, spirooxindole–pyrrolidine hybrids have deserved significant attention due to their abundant presence in natural products and to their diverse biological properties [40, 68, 69]. An impressive collection of fused N-containing five-membered heterocycles has also been prepared due to their biological and pharmaceutical relevance. Efficient, selective, and sustainable strategies, featuring high yields and shorter reaction times than conventional conditions, have been developed highlighting the importance of these compounds. These heterocyclic compounds are commonly synthesized from isatin derivatives through a 1,3-dipolar cycloaddition reaction. Other starting materials were used in these reactions to provide a high diversity of heterocyclic rings [34, 52, 70, 71].

In 2019, Nayak et al. [72] synthesized a series of 3-nitrochromene fused pyrrolidine- or piperidine-spiroindanones, through MCR reactions via 1,3-dipolar cycloaddition of several dipolarophiles with azomethine ylides generated *in situ* from proline or pipecolic acid (Scheme 7.23). This microwave-assisted protocol to afford complex structural compounds, with ethanol as solvent, led to the target compounds in higher yields, shorter reaction times, and high regio- and diastereoselectivity in comparison to conventional methods. Later that year, Nayak's group [73], using a similar MCR methodology, with different amino acids, synthesized several spiroindenoquinoxaline pyrrolidine and indanone-fused nitrochromane.

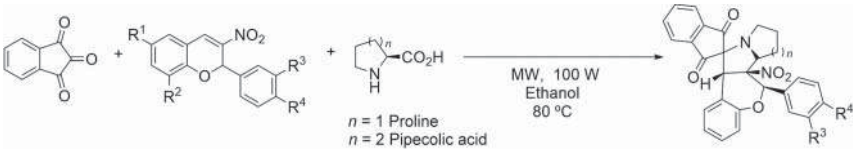

Scheme 7.23 Synthesis of 3-nitrochromane-fused pyrrolidine and piperidine spiroindanones.

Also through a 1,3-dipolar cycloaddition reaction, Kantam, Trivedi, and coworkers [74] synthesized spiroindeno[1,2-*b*]quinoxaline-11,30-pyrrolizines with AChE inhibitory activity, via a 4-MCR reaction between ninhydrin, phenylenediamine, proline, and nitrostyrene derivatives, with high regio- and stereoselectivity (Scheme 7.24). The microwave irradiation methodology provided better yields and shorter reaction time when compared to reactions carried out at refluxing ethanol.

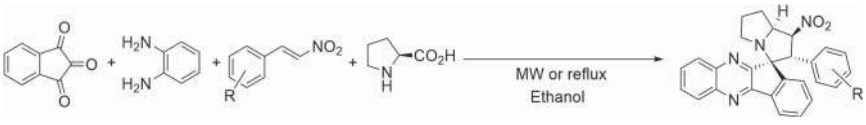

Scheme 7.24 Synthesis of spiroindeno[1,2-*b*]quinoxaline-11,30-pyrrolizines through a 4-MCR.

In 2013, Wu et al. [75] reported the synthesis of a series of regioselective spirooxindolo-pyrrolidines, pyrrolizidines, and pyrrolothiazole derivatives, by

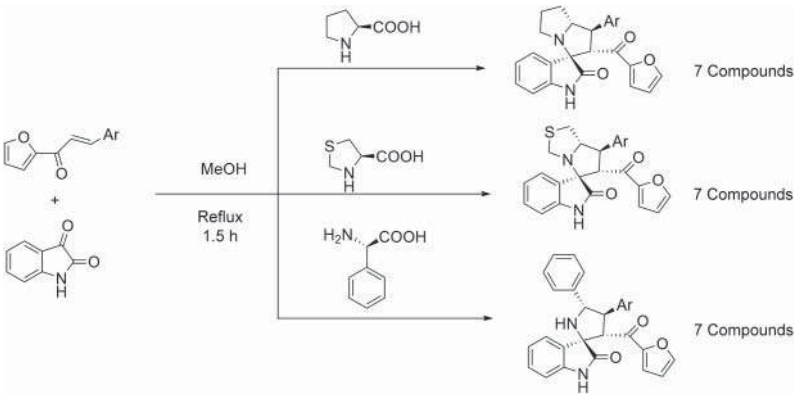

Scheme 7.25 Synthesis of spirooxindolo-pyrrolidines, pyrrolizidines, and pyrrolothiazole derivatives.

a regioselective three-component 1,3-dipolar cycloaddition reaction between α,β-unsaturated ketones with furanyl substituents, several amino acids, and unstable azomethine ylides, generated *in situ* from isatin (Scheme 7.25). The best results were achieved using methanol at reflux conditions, and the novel compounds were prepared in good yields, with high to excellent dr (up to 99 : 1). One compound showed a potent antimicrobial activity against drug-resistant bacteria, and its molecular docking studies revealed strong interactions with the active sites of lanosterol demethylase, dihydrofolate reductase, and topoisomerase II.

Wang, Wang, and Ji [76] also reported the synthesis of stereoselective polycyclic spiroindolines on a catalyst-free three-component reaction, with excellent levels of diastereoselectivity. Ethanol proved to be the best solvent to obtain the desired product from the reaction between 2-isocyanoethylindole with malononitrile and various substituted aromatic aldehydes (Scheme 7.26). The yield of the reaction was dependent on the electron-withdrawing or -donating character of the substituents at the aromatic ring of the aldehydes, with electron-withdrawing groups leading to better yields, up to 90%. In all cases, only one diastereoisomer was observed by NMR analysis. This study presents a simple and metal-free method to obtain the structural scaffold of tabersonine and akuammicine, two biologically active natural products.

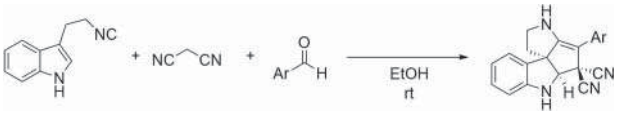

Scheme 7.26 Synthesis of polycyclic spiroindoline derivatives.

In 2016, Meshran and coworkers [69] also described the use of isatins for the preparation of spirooxindole pyrrolidines (Scheme 7.27). In this procedure, they used different isatins, β-nitrostyrenes, and benzyl amines or α-amino acids in a 3-MC 1,3-dipolar cycloaddition reaction to afford the desired products. This research group used an eco-friendly protocol, a microwave-induced procedure in an aqueous medium, to afford 21 compounds in moderate to excellent yields.

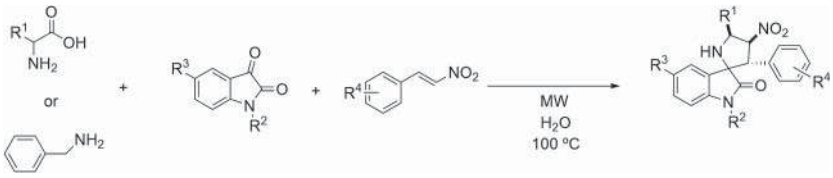

Scheme 7.27 Synthesis of spirooxindole pyrrolidines under microwave conditions.

In a recent review, Youseftabar-Miri et al. [71] reported other synthesis of spirooxindole derivatives through 1,3-dipolar cycloaddition reactions via the intermediates of azomethine ylides derived from isatins. In this publication, the author presents several examples of reactions carried out under microwave or ultrasonic irradiation, in refluxing ethanol to afford spiro-fused compounds with different heteroatoms (O, N, and S) and different rings such as pyrrolidine/pyrrolizidine (e.g. Scheme 7.28) [77–79], pyrazoline [80], triazolidine [81], and furan [82].

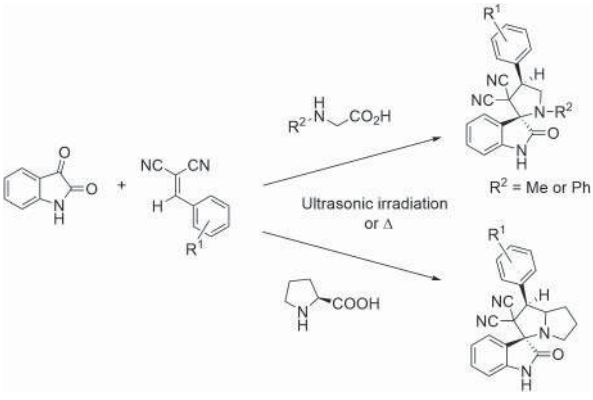

Scheme 7.28 Synthesis of spirooxindole pyrrolidine/pyrrolizidines. Source: Based on Rezaei et al. [77] and Taghizadeh et al. [78, 79].

Perumal and coworkers [83, 84] used a similar reaction in ethanol starting from isatin, thioproline, or sarcosine, and 3-(1*H*-imidazol-2-yl)-2-(1*H*-indole-3-carbonyl) acrylonitrile or 3-(1*H*-imidazol-2-yl)-2-(5-methoxy-1*H*-indole-3-carbonyl) acrylonitrile to obtain several spirooxindole–pyrrolidine or pyrrolothiazole derivatives, which showed significant activity against A549 human lung adenocarcinoma cancer cell line. Analogous compounds were synthesized by Reddy and coworkers [85] using the same methodology via a 1,3-dipolar cycloaddition reaction of azomethine ylide generated from isatin, with amino acids such as sarcosine, proline, and thioproline, and (*E*)-3-(1,3-diphenyl-1*H*-pyrazol-4-yl)-2-(1*H*-indole-3-carbonyl) acrylonitrile. In this case, the new compounds showed considerable antimicrobial activity.

Recently, Deepthi and coworkers [86] also used isatins and a heteroarylidene-malononitrile, as Nabid and coworkers [77], to react with α-amino acids, to prepare spirooxindole pyrrolidine/pyrrolizidine rings at refluxing methanol. The new

compounds exhibit potent anticancer activity by activating proapoptotic genes p53 and caspase 7.

Thiophene and its analogs have many applications, from pharmaceutical applications to functional materials, and the synthesis of their derivatives still fosters large efforts in many fields of science [40, 87, 88]. Most of the procedures reported for the synthesis of thiophene derivatives are no sustainable MCR approaches, and are outside of this chapter. One of the few sustainable MCR procedures was reported by Mantellini and coworkers [89] concerning the synthesis of a series of substituted 2,5-dihydrothiophenes by a sequential one-pot four-component reaction between primary amines, β-ketoesters, aryl isothiocyanates, and 1,2-diaza-1,3-dienes, using methanol at room temperature.

Also furans, their reduced forms and benzo analogs, are important structures in many natural products and in biologically active compounds, such as antitumor, cytotoxic, and antimicrobial agents, being also present in commercially available agrochemical, bioregulators, essential oils, cosmetics, and dyes [40, 87]. Several recent reactions were published regarding the synthesis of furans and their analogs. Rahmati and Pashmforoush [87] reviewed the preparation of several derivatives carried out using water as solvent. In the described synthetic strategies, several sustainable procedures were used, such as microwave irradiation or phase-transfer catalyst protocols.

In 2010, Ramazani et al. [90] synthesized a series of furan-2(5*H*)-imines in water, at room temperature, using alkyl isocyanides, dialkyl acetylenedicarboxylates, and phenacyl halides in good to excellent yields (Scheme 7.29). This reaction uses similar reagents used by Siddiqui's group [46] for the synthesis of pyrrole derivatives, but with the replacement of the amines by isocyanides and the use of water as solvent, instead of the ionic liquid. In the same year, Adib et al. [91] reported the synthesis of 2-{[(2-alkylimino)-1-benzofuran-3-yliden]amino}benzoic acids via a 3-MCR in water.

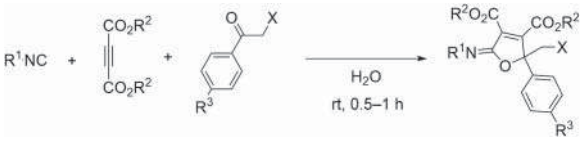

Scheme 7.29 Synthesis of furan-2(5*H*)-imines using water as solvent.

In 2011, Menéndez and coworkers [92] reported the synthesis of a series of naphtho[2,3-*b*]furan-4,9-diones using a 3-MCR approach, in water, under microwave irradiation, from 2-hydroxy-1,4-naphthoquinone, aromatic aldehydes, and a pyridinium salt in the presence of ammonium acetate.

In 2012, Alizadeh et al. [93] reported the synthesis of several propellane compounds, annulated tricyclic compounds with a Y-shaped bridgehead–bridgehead central bond, which include a dihydrofuran ring. These compounds were prepared from a 4-MCR in water at room temperature from primary amines, ninhydrin, malonitrile, and dialkyl acetylenedicarboxylates or β-ketoesters.

7.4.2 Five-Membered Ring Heterocycles with Two Heteroatoms

Five-membered heterocycles with two heteroatoms, especially those containing two nitrogen atoms or one nitrogen atom and an oxygen or a sulfur atom, have shown important biological activities, with many of them being part of structural scaffolds of commercial drugs, natural products, ionic liquids, metal-coordinating ligands, or wide-ranging advanced materials. Therefore, they have been important structural systems to consider regarding the development of molecules with biological activities, with applications on pharmaceutical, agrochemicals products, or advanced materials, as well as versatile synthons in the construction of more complex molecules. Among them, 1,2- and 1,3-azoles and their dehydro- or their fused analogs have become the most important [29, 30, 94–98].

Zohreh and Alizadeh [96, 99] synthesized several spirooxindole-pyrazolines via a catalyst-free procedure under mild conditions. Using 2 equiv of hydrazine hydrate, 1,1-bis(methylthio)-2-nitroethylene, and 2 equiv of isatin, the reaction proceeded at room temperature in ethanol, affording the desired spirooxindole-pyrazolines in high yields (60–70%), after simple purification procedures (Scheme 7.30).

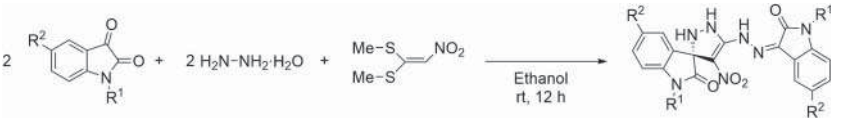

Scheme 7.30 One-pot catalyst-free synthesis of spirooxindole-pyrazolines.

In 2017, Youseftabar-Miria and Hosseinjani-Pirdehib [80] reported the synthesis of spirooxindole-pyrazole derivatives from a combination of isatins, 4-phenylurazole or phthalhydrazide, and malononitrile or ethyl cyanoacetate, in the presence of the ionic liquid [bmim]Cl acting as solvent and catalyst, which was recycled and reused. This method proved to be suitable and efficient for the synthesis of the biologically important spirooxindole-pyrazolines.

Imidazole and their reduced analogs, such as imidazolidines, are important structural scaffolds and attractive targets of pharmaceutical chemistry [87, 100].

Santeusanio and coworkers [101] developed a synthetic approach to access a family of imidazolidine-2,4-diones (hydantoins), in ethanol at room temperature, from 1,2-diaza-1,3-dienes, amines, and isocyanates (Scheme 7.31). This procedure allows the selective formation of substituted hydantoin rings, resulting from the ring closure of the initially formed asymmetric urea derivatives. The procedure also has the advantage of producing hydantoins bearing hydrazone side chains, which can be converted into other valuable functional groups that would be difficult to obtain using direct synthetic procedures.

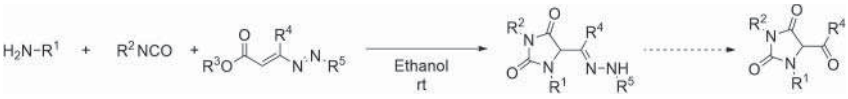

Scheme 7.31 Synthesis of hydantoins via a 3-MCR.

In 2019, Durrani and coworkers [102] reported the formation of a ring system with an imidazole ring fused with a thiadiazole ring. The synthesis of the new benzo[*d*]imidazo[2,1-*b*][1,3,4]thiadiazoles was achieved from the condensation of aromatic ketones, *N*-bromosuccinimide, and 5-(biphenyl-4-yl)-1,3,4-thiadiazol-2-amines, under microwave irradiation in PEG-400 and water as a green reaction medium (Scheme 7.32). This new eco-friendly protocol allowed the formation of the products in excellent yields (up to 98%) in minimum reaction time (<15 minutes).

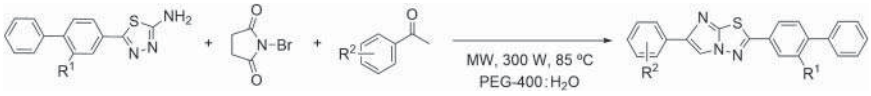

Scheme 7.32 One-pot synthesis of benzo[*d*]imidazo[2,1-*b*][1,3,4]thiadiazoles under microwave irradiation and PEG-400 in water reaction medium.

Oxazoles, isoxazoles, and their partially reduced or saturated analogs constitute the framework of several bioactive compounds, with high potential application as agrochemicals, pharmaceuticals, and functional materials [87, 103, 104]. Many procedures for their synthesis involve the use of metal catalysts, or other less or no sustainable conditions [94].

The first example of a synthesis of an isoxazole using the MCR approach emerged in 2013, with the work of Singh and coworkers [105], reporting an efficient 3-MC synthesis of 5-substituted 3-aminoisoxazoles from the reaction between β-oxo dithioesters, amines, and hydroxylamine (Scheme 7.33). Several β-oxo dithioesters and aromatic or cyclic secondary aliphatic amines were well tolerated, but the reaction using aromatic amines is slower in comparison with the reaction with aliphatic amines. A second method was described by Patel and coworkers [106] in 2017, but that procedure includes a metal catalyst and organic solvents.

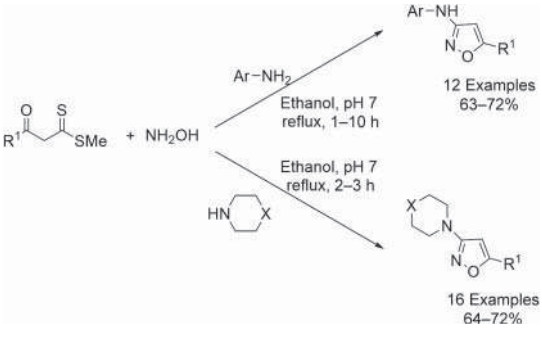

Scheme 7.33 One-pot 3-MCR in the synthesis of isoxazoles.

In the case of thiazoles and their analogs, there are recent reports of reactions of these compounds through sustainable MCR. But their synthesis usually shows better results with metal catalysts and with organic solvents.

The first thiazolidine derivatives prepared by MCR were published by Alizadeh et al. in 2009 [107]. This group described a facile and direct synthetic entry to

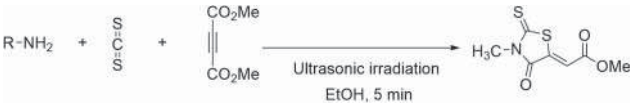

Scheme 7.34 Synthesis of methyl 4-oxo-2-thioxothiazolidin-5-ylidene acetate derivatives by ultrasonic irradiation.

rhodamine-based molecules via a 3-MCR using carbon disulfide, primary amines, and acetylenic esters under neutral conditions in water. In 2021, Alizadeh et al. [108] (Scheme 7.34) used the same reagents under a different green protocol, using ultrasonic irradiation, in ethanol, to synthesize rhodanines, which are used as key intermediates to obtain new substituted phthalimides.

In 2017, Shamsuzzaman and coworkers [109] reported the synthesis of steroidal thiazole derivatives, in ethanol, under microwave irradiation, from a 3-MCR using steroidal ketones, thiosemicarbazide, and phenacyl bromide. In 2013, Chakraborti and coworkers [110] described the synthesis of 2,3-disubstituted thiazolidin-4-ones from an equimolar mixture of benzaldehyde derivatives, anilines, and thioglycolic acid, in different solvents. The formation of the desired thiazolidin-4-ones showed a significant decrease in the yield, in solvent-free or water solvent conditions, and required a protic acid catalyst to improve the yield. Kumbhare and coworkers [111] synthesized several 2-imino-4-(trifluoromethyl)thiazolidin-4-ol derivatives from equivalent molar quantities of amines, phenyl isothiocyanate, and 3-bromo-1,1,1-trifluoropropan-2-one, at room temperature (Scheme 7.35). The reaction works without solvent or in an aqueous medium, but lower yields are observed comparatively to the use of DMF and water:DMF mixtures.

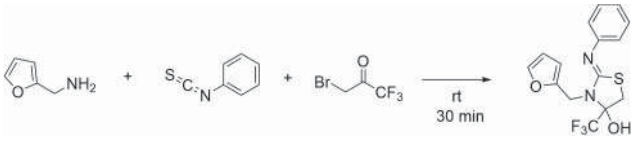

Scheme 7.35 Synthesis of 2-imino-4-(trifluoromethyl)thiazolidin-4-ol derivatives.

The limitations of several reactions in aqueous media, due to the solubility of reactants, can be surpassed by the use of aqueous micellar medium. These aqueous surfactant systems can behave as nano-reactor systems, accelerating or inhibiting a chemical reaction when compared with a pure aqueous medium. The application of micelles as reaction medium can simplify the product isolation and the catalyst recycling [112]. Tamaddon and Alizadeh [113] investigated the use of different surfactants in water for the synthesis of pyranopyrazoles, with cocamidopropyl betaine (CAPB, a biodegradable surfactant), leading to the best results. With this surfactant, in a micellar medium, at 50–60 °C for 2–18 minutes, using a 4-MCR approach with aldehydes, malononitrile, ethyl acetoacetate, and hydrazine hydrate (2 equiv), they prepared 18 pyranopirazoles in excellent yields (85–97%) (Scheme 7.36). These micellar systems showed better results than the classic ethanol–water reaction medium described by Mandha et al. [114] for the synthesis of pyranopyrazoles.

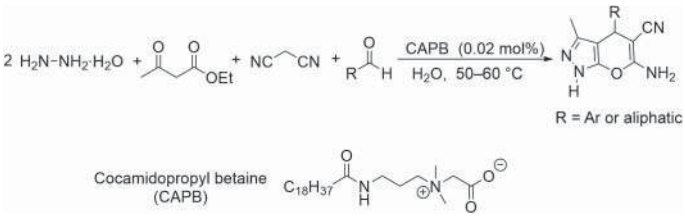

Scheme 7.36 Synthesis of pyranopyrazoles in a micellar aqueous system.

A surfactant combined catalyst, using dodecylbenzenesulfonic acid, in an aqueous medium, at room temperature, was used by Das and coworkers [115] for the synthesis of several tricyclic 4-spiropyrano[2,3-*c*]pyrazoles through a 3-MCR, from pyrazolone derivatives, cyclic ketones, and cyclic 1,3-dicarbonyls. This mild, simple, and environment-friendly synthetic methodology allowed the preparation of the expected compounds in good yields.

Dandia et al. [116] prepared spiroindole-thiazolidinone derivatives in water using the surfactant CTAB (cetyltrimethyl ammonium bromide) through a low or a high intensity ultrasonic irradiation protocol. The thiazolidinone ring of these derivatives was obtained from isatin, a pyrazolone, and 2-sulfanylpropanoic acid (Scheme 7.37), in good to excellent yields according to the sonication intensity, temperature, and reaction time. This is a simple and environmentally friendly method and avoids azeotropical removal of water, the use of organic solvents, and dehydrating agents.

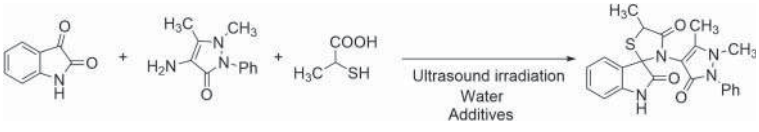

Scheme 7.37 Synthesis of spiroindole-thiazolidinone derivatives in water.

Mondal and coworkers [117] synthesized 18 thiazo[2,3-α]isoquinolin-4-ium derivatives from isoquinolines, 2-bromoacetophenones, and benzoyl isothiocyanate in a micellar system, using a mixture of Amberlite IRA 402(OH) and the cationic surfactant CTAB (Scheme 7.38). The products were synthesized in excellent yields (80–91%), but no product formation was observed in the absence of CTAB surfactant. The reaction medium was able to be recycled up to five times with slight loss of activity.

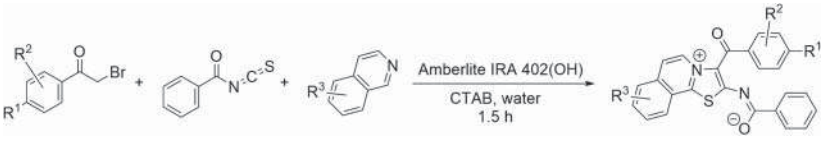

Scheme 7.38 One-pot synthesis of thiazo[2,3-α]isoquinolin-4-ium derivatives in an aqueous micellar medium.

7.4.3 Five-Membered Ring Heterocycles with Three and Four Heteroatoms

Compounds with a triazole or analog structural scaffolds continue to attract attention due to their presence on natural products and biologically active compounds, as therapeutic agents, and in several other fields of science, such as materials and catalysts, and they are also good building blocks in organic chemistry [118, 119]. Many methodologies for their synthesis have been developed, but most of them require the use of catalysts, usually metal ones, as "click chemistry" reactions, which usually involves the use of Cu catalysts for the synthesis of the triazole unit.

Recently, Ferreira and coworkers [120] reported the synthesis of 1,2,3-triazoles via a new one-pot microwave irradiation protocol using the green PEG400 solvent without a metal catalyst. The use of this solvent overcomes the solubility problems of the reagents and represents an important green advance compared with several other reports that use microwave irradiation, but the reaction is carried out in organic solvent medium.

The tetrazole moiety is also found in various bioactive and important biologic compounds and is part of pharmaceutically important molecules. Its applications include agriculture (plant growth regulators, fungicides, and herbicides), sweeteners, electrochromic electrodes, photography and photoimaging, explosives and rocket fuels, and polymers [118].

Dabiri, Bazgir, and coworkers [121] reported the synthesis of 5-substituted tetrazoles in water through a 3-MC domino Knoevenagel condensation/1,3-dipolar cycloaddition reaction of carbonyl compounds, malononitrile, and sodium azide. The procedure does not require a catalyst and the reaction proceeds in mild conditions to afford the products in good yields (up to 88%). Dömling and coworkers [122] prepared several 1,5-disubstituted tetrazolo-γ-lactams and tetrazolo-δ-lactams via a 4-MC Ugi-azide reaction using tritylamine, azidotrimethylsilane, phenylethylisonitrile, and various aldehyde esters, through a sustainable microwave irradiation procedure, to afford the tetrazole ring (Scheme 7.39). The reaction proceeds smoothly under microwave irradiation, and the use of aliphatic aldehydes afforded the best yields, up to 80%. However, the following deprotection and cyclization reaction showed some difficulties, and it was necessary to use a different non-sustainable methodology to get the lactam ring formation.

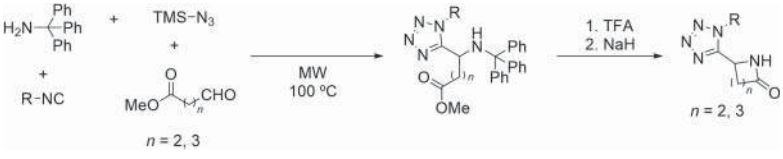

Scheme 7.39 Synthesis of 1,5-disubstituted tetrazolo-γ-lactams and tetrazolo-δ-lactams via a 4-MC Ugi-azide reaction for the synthesis of 1,5-disubstituted tetrazole ring.

Later, Dömling's group [123], on the preparation of new polycyclic bioactive compounds, used an Ugi 4-MCR to synthesize tetrazole substituted rings. These

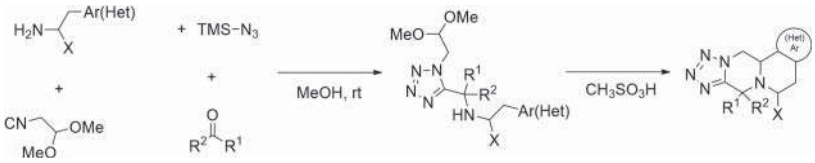

Scheme 7.40 Synthesis of polycyclic bioactive compounds via one-pot Ugi-4-MCR in the synthesis of tetrazoles.

syntheses were carried out in methanol at room temperature from different oxo components (aldehydes or ketones), diverse aryl ethyl amines, azidotrimethylsilane, and isocyanoacetaldehyde dimethylacetal (Scheme 7.40). Further cyclization reactions using metanosulfonic acid as catalyst provided the planned tricyclic derivatives with the desired pharmacophore properties.

Recently, Dömling's group [124] reported the preparation of tetrazolo indoles in two steps through a similar methodology. The first step, an Ugi 4-MCR was carried out in methanol, at room temperature, starting from substituted anilines, isocyanides, 2,2-dimethoxyacetaldehyde in aqueous solution, and $TMSN_3$, to afford the tetrazole derivatives in good to excellent yields. The second step, the formation of heterocyclic ring of the indole, was successfully carried out only in methanesulfonic acid at 70 °C, in good to excellent yields.

7.5 Six-Membered Ring Heterocycles

There is an extensive number of six-membered heterocycles with high structural diversity and complexity, which can be easily build via MCR. Undoubtedly, compounds having at least one six-membered heterocyclic unit in their scaffold have a high number of applications in medicinal chemistry, agrochemistry, and fine chemical industry. Due to the high interest in the design and development of new synthetic routes to achieve these relevant heterocycles, a vast number of MC methodologies has been described in literature. Herein, the most efficient methods for the synthesis of the main six-membered heterocycles, namely, pyridines, piperidines, quinolines, pyrans, thiopyrans, pyrimidines, dihydropyrimidinones (DHPMs), quinazolines, oxathianes, thiazinones, triazines, and thiadizines, using sustainable MCR are presented.

7.5.1 Six-Membered Ring Heterocycles with One Heteroatom

Pyridine is undoubtedly the most studied six-membered aromatic heterocycle, due its broad applications in several fields, such as natural products [125, 126], organic chemistry [127–129], medicinal chemistry [130, 131], agrochemical [132], and material science [133–135].

Considerable structural diversity of pyridine derivatives could be obtained using a wide range of MCR [136], including Hantzsch, Chichibabin, Mannich, Vilsmeier-Haack, Bohlmann-Rahtz, Krohnke, and Michael addition reactions,

among others. All these reactions could be performed under sustainable protocols, such as metal- and solvent-free conditions, under microwave irradiation, ultrasonic or visible light conditions, etc. In this chapter our aim is to report the most sustainable MCR-based protocols for the synthesis of pyridines with high structural diversity.

Ma and coworkers described a 4-component annulation affording 2,3,4,6-tetraarylpyridines from aromatic aldehydes, methyl ketones, diaryl ethanones, and ammonium acetate under catalyst- and solvent-free conditions [137]. Another sustainable methodology for the synthesis of 2-amino-4-aryl-6-substituted-pyridine-3,5-dicarbonitrile derivatives via condensation of aromatic aldehydes, malononitrile, and primary amines, without the use of solvent and catalyst, was introduced by Mahmoud and El-Sewedy [138]. These two methodologies explored a large scope of substrates, and the desired products were obtained in very good to excellent yields, with the main drawbacks being long reaction times and high temperatures. Chougala et al. reported a more advantageous protocol for the synthesis of novel 2-amino-4-(2-oxo-2*H*-chromen-4-yl)-6-arylpyridine-3-carbonitrile derivatives, which showed promising anticancer activity (Scheme 7.41). These interesting compounds were prepared via microwave-assisted 4-MCR of 4-formylcoumarin derivatives, malononitrile, aromatic ketones, and ammonium acetate, under catalyst- and solvent-free conditions [139]. The desired compounds were obtained in good to excellent yields and short reaction times. The authors also showed the advantages of using microwave technique comparatively to the traditional reflux condition, which furnished lower yields, while requiring longer reaction times (8–10 hours).

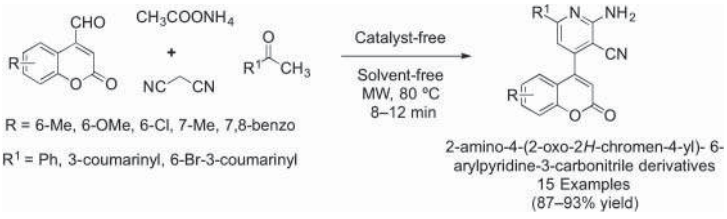

Scheme 7.41 Microwave-assisted 4-MCR to access pyridine derivatives under catalyst- and solvent-free reaction conditions.

Piperidine, a nitrogen-containing six-membered ring, is widely distributed in nature and a structural motif of synthetic alkaloids with interesting pharmacological activities [140, 141]. This heterocycle is considered a key framework for the synthesis of valuable compounds. The piperidine unit can be found in several FDA approved drugs, such as miglitol (antidiabetic), nelfinavir (antiviral), and paroxetine (antidepressant) [142]. Over the last decade, the MCR approach became pivotal to prepare substituted piperidine derivatives. Wang and coworkers reported the synthesis of polysubstituted piperidines using substituted nitrostyrenes, aromatic aldehydes, dialkyl malonates [143], or Meldrum's acid [144] and ammonium acetate, which also works as catalyst. These 4-MCRs involved a one-pot Michael

addition/nitro-Mannich/lactamization cascade sequence. Based on this approach, Egorov and coworkers described a stereoselective MCR of tetracyano-substituted piperidines from cyano olefins, malononitrile, aldehydes, and ammonium acetate [145, 146]. This methodology also enabled the direct formation of polycyano compounds from aldehydes and malononitrile [147, 148]. Recently, the same authors described two similar methodologies for the high diastereoselective MC synthesis of polysubstituted 2-piperidones, with three and four stereogenic centers, depicted in Scheme 7.42. The synthetic approach (A) is a new method for the one-pot 4-MC stereoselective synthesis of substituted 2-piperidinones, using cyano olefins (benzylidene-malononitriles and benzylidenecyanoacetates), dialkyl malonates, aromatic aldehydes, and ammonium acetate as the nitrogen source and catalyst, furnishing alkyl (±)-5,5-dicyano-2-oxo-4,6-diaryl piperidine-3-carboxylates, with three stereogenic centers, and dialkyl (±)-3-cyano-6-oxo-2,4-diarylpiperidine-3,5-dicarboxylates with four stereogenic centers as a single diastereomer [149]. Similar 4-MC stereoselective one-pot synthesis of substituted 2-piperidinones was reported (Scheme 7.42B), using aromatic aldehydes, nitriles, dialkyl malonates, and ammonium acetate or aqueous ammonia as the nitrogen source. Alkyl (3*SR*,4*RS*,6*SR*)-5,5-dicyano-2-oxo-4,6-diarylpiperidine-3-carboxylates with three stereogenic centers and dialkyl (2*SR*,3*RS*,4*RS*,5*SR*)-3-cyano-6-oxo-2,4-diaryl-piperidine-3,5-dicarboxylates with four stereogenic centers were successfully obtained as single diastereomers. When nitro-substituted aldehydes or ethyl and *n*-propyl cyanoacetates were used as starting materials, 2,4,6-triaryl-3,3,5,5-tetracyanopiperidines were obtained as side products [150].

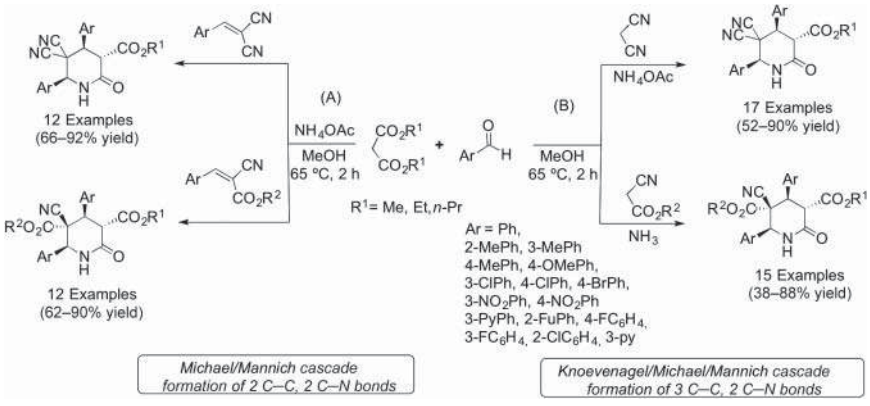

Scheme 7.42 Multicomponent stereoselective synthesis of substituted 2-piperidones.

Kazemi and coworkers reviewed the synthesis of piperidine derivatives through MCR of aromatic aldehydes, aromatic amines, and β-ketoesters (or 1,3-dicarbonylic compounds) catalyzed by several catalysts [151]. Most of the catalysts used for this reaction have several drawbacks, such as their cost, toxicity, extreme reaction temperatures, and/or long reaction times. Kangani et al. reported the pseudo-5-MCR between 2 equiv of benzaldehyde derivatives, 2 equiv of aniline,

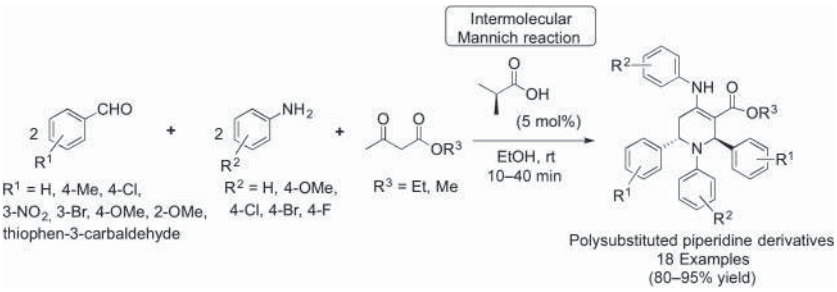

Scheme 7.43 Pseudo 5-MC synthesis of polysubstituted piperidine derivatives, catalyzed by lactic acid.

and several β-ketoesters in the presence of only 5 mol% of lactic acid, as catalyst. This reaction was carried out using ethanol as solvent, at room temperature with short reaction times furnishing the polyfunctionalized piperidine derivatives in very good yields (Scheme 7.43) [152]. Taking into account the green chemistry concept, we selected this method due to its advantages, since the catalyst used is easily accessible, inexpensive, and eco-friendly, and the reaction is carried out at room temperature in ethanol and with very attractive reaction times (<40 minutes). In addition to all these advantages, a very good subtract tolerance was noticed, with several electron-withdrawing and electron-donating substituents in the aromatic rings, which did not influence the efficiency of the reaction. The products were isolated through simple filtration techniques.

Quinolines, a benzene ring fused to pyridine ring, can be found in various natural products and in marketed drugs, e.g. ciprofloxacin (Cipro®), montelukast (Singulair®), and pitavastatin (Livalo®) [153]. Matada and coworker reported in a review some green methods and enabling technologies used for the synthesis of these scaffolds using the versatile MCR approaches [154].

Quinolines can be synthesized using MCRs under microwave irradiation [155–163] or ultrasounds [164], in aqueous medium [165], and using different catalysts, including transition metal Brønsted acids [166, 167] and magnetic catalysts [168–170]. Looking to the sustainability concept, MCRs under catalyst- or solvent-free conditions are usually more attractive. Yuvaraj et al. described the synthesis of an interesting family of isoxazolo[5,4-*b*]quinoline-fused spirooxindoles through a 3-MCR of 5-amino-3-methylisoxazole, β-diketones, and isatin derivatives, in very good to excellent yields under microwave irradiation and catalyst- and solvent-free conditions (Scheme 7.44) [171]. This methodology is advantageous as it furnished highly chemoselective products without requiring the use of any catalyst. Moreover, tedious chromatographic purification techniques were avoided regarding the isolation of the final products. This MCR involves a Knoevenagel condensation, followed by Michael addition and cyclocondensation. Using a similar approach, Mamaghani et al. reported the synthesis of pyrimido[4,5-*b*]quinoline derivatives in high yields (82–95%) and short reaction times (10–20 minutes). The 3-MCR involves 6-amino-2-(alkylthio)-pyrimidin-4(3*H*)one, 1,3-indanedione or 1,3-cyclohexadione, and aromatic aldehydes under ultrasonic irradiation and catalyst-free conditions,

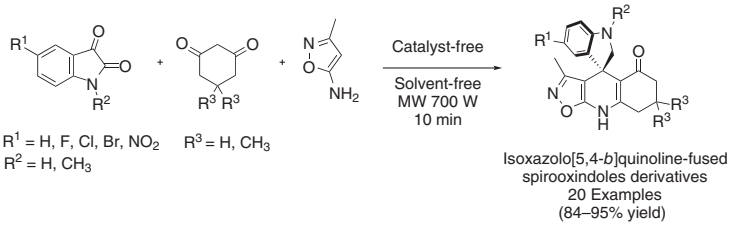

Scheme 7.44 Synthesis of isoxazolo[5,4-*b*]quinoline-fused spirooxindole derivatives under catalyst- and solvent-free conditions.

using ethylene glycol as solvent at 65 °C [164]. Another small family of substituted 1,4-dihydro-5-hydroxy-2-methyl-*N*-4-diphenylquinoline-3-carboxamide derivatives displaying interesting antibacterial and antifungal activities was synthesized through a one-pot 4-MCR using resorcinol, aromatic aldehydes, acetoacetanilide, and ammonium acetate under microwave irradiation and catalyst-free conditions, using ethanol as solvent in short reaction times [172]. Also pyrazolo-[3,4-*b*]-quinoline derivatives were synthesized in high yields and short reaction times via a microwave-assisted and catalyst-free MCR between aromatic aldehydes, dimedone, and 5-amino-3-methyl-1-phenylpyrazole at room temperature using aqueous ethanol as solvent [173].

Bhuyan et al. reported another interesting microwave-assisted one-pot 3-MC aza-Diels–Alder reaction strategy for the synthesis of complex spiroquinoline derivatives (15 examples, 75–85% yield), using 1-aminonaphthalene, aromatic aldehydes, and 5-benzylidene-1,3-dimethyl pyrimidine-2,4,6-trione under catalyst- and solvent-free conditions in short reaction times [174].

The heterocyclic pyran is a very useful subunit used commonly as building block for the synthesis of pharmacologically valuable compounds and also found in a wide range of natural products, such as coumarins, benzopyrans, sugars, flavonoids, xanthones, etc. The promising biological activities revealed by these pyran-based scaffolds unquestionably place them at the vanguard for the discovery of potential drug candidates. For that reason, great interest arises on the design of sustainable methods to obtain new compounds possessing this subunit. Zanamivir (Relenza®) is a neuraminidase inhibitor, and the first marketed drug for the flu, with this heterocycle in its structure [175].

Polysubstituted 2-amino-4*H*-pyran-3-carbonitrile derivatives are considered very important heterocyclic compounds with a wide range of interesting biological activities, such as anticancer [176] and antimicrobial [177], among others. They are also relevant intermediates for subsequent chemical transformations due to the presence of orthogonal functional groups. These interesting polysubstituted 2-amino-4*H*-pyran-3-carbonitrile derivatives could be assessed using the MCR between an aldehyde or isatin, malononitrile and β-ketoesters (or large variety of C–H activated acid compounds or phenols) with or without catalysts. Several types of catalysts can be used, including the most common acid/base, organo/organometallic, natural, nanoparticle/composite, transition metals, phase transfer, and zeolites [178]. Despite the large diversity of protocols that can be used

for the preparation of these important derivatives, most of them have disadvantages like tedious synthetic steps for catalyst preparation, use of toxic and expensive catalysts, or even hazardous solvents for the reaction or/and work up. Another important point is that most of the catalysts are not recyclable. Some methodologies for the synthesis of pyran derivatives under catalyst-free conditions and/or using enabling techniques have been reported over the last decade [114, 179–183].

Safaei et al. reported an advantageous and eco-friendly methodology using glycerol as green, biodegradable, and reusable promoting medium for the catalyst-free one-pot 3-MC synthesis of a wide diversity of 4*H*-pyran derivatives in excellent yields (Scheme 7.45). The 3-MCR between alkylmalonates, carbonyl compounds bearing a reactive α-methylene group, and aromatic aldehydes (which could be replaced by isatin derivatives or acenaphthenequinone) was successfully accomplished at 80 °C with short reaction times. Furthermore, this protocol is suitable for a broad range of substrates and for large scale synthesis maintaining its reproducibility. Also, the glycerol can be recycled and reused up to 20 times, maintaining the productivity of the reaction [184].

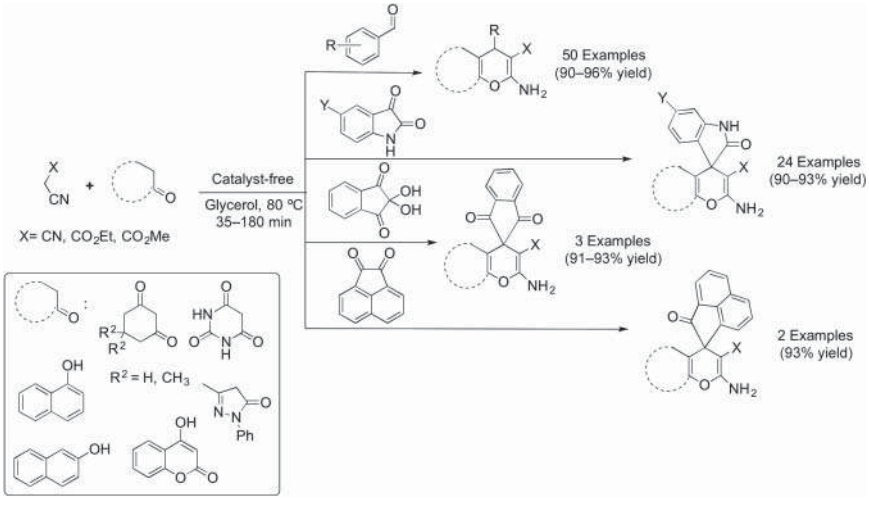

Scheme 7.45 MC synthesis of 4*H*-pyrans and spiropyrans under catalyst-free conditions.

Khan et al. developed a sustainable methodology for the synthesis of fused 4*H*-pyran derivatives via one-pot 3-MCR of 3-methyl-1-phenyl-5-pyrazolone/4-hydroxycoumarin, aromatic aldehydes, and (*E*)-*N*-methyl-1-(methylthio)-2-nitroethenamine under catalyst- and solvent-free conditions, in high temperatures (a disadvantage of this protocol) [185].

Thiopyran heterocyclic units are six-membered ring structures with a sulfur atom, where several aromaticity levels and oxidation stages can be admitted around the ring system.

Thiopyran scaffolds attract the interest of synthetic and medicinal chemists regarding their several applications in the biological, medicinal, and industrial

fields [186]. These are precursors in the synthesis of many bioactive compounds such as tetrahydrodicranenone B [187], serricornin [188], and thromboxanes [189]. Concerning the MC synthesis of this interesting scaffold, some methodologies have been described in the literature. One approach is the one-pot 3-MCR using β-oxodithioesters, aldehydes, and cyclic 1,3-diketones catalyzed by P_2O_5 under solvent-free conditions [190]. The use of malononitrile/ethyl or methyl cyanoacetate, catalyzed by 4-(dimethylamino)pyridine (DMAP), is another methodology reported [191]. Koley et al. reported an environmentally friendly method for the regioselective synthesis of 6-cycloamino-2-(methyl/benzyl)sulfanyl-3-(aroyl/hetaroyl/alkanoyl)-4-aryl-5,6-dihydro-4*H*-thiopyran derivatives via one-pot 3-MC domino coupling of β-oxodithioesters, α,β-unsaturated aldehydes, and cyclic aliphatic secondary amines at room temperature under catalyst- and solvent-free conditions in excellent yields and short reaction times (five minutes) (Scheme 7.46) [192]. These authors were the first to introduce a cyclic aliphatic secondary amine in the 6-position of the thiopyran heterocyclic ring. The reaction has a broad scope for the substrate reagents.

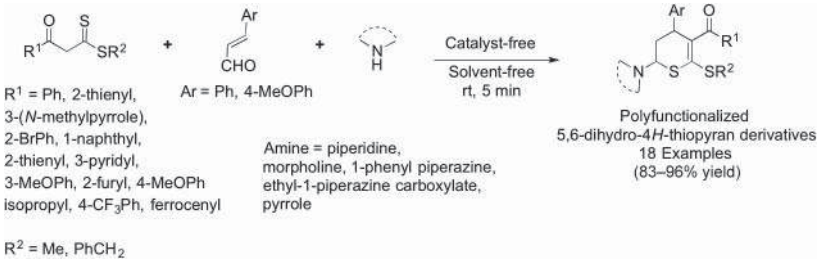

Scheme 7.46 MC synthesis of polyfunctionalized 5,6-dihydro-4*H*-thiopyran derivatives under catalyst- and solvent-free conditions.

7.5.2 Six-Membered Ring Heterocycles with Two Heteroatoms

Pyrimidine is a structural motif present in the nature and in a wide variety of marketed drugs. A remarkable sustainable MC synthesis of pyrimidines was developed by Kempes in 2015, where a dehydrogenative coupling reaction of alcohols followed by a base-mediated aldol reaction and by dehydrative amidine condensation onto the resulting enone intermediate catalyzed by an iridium–phosphine complex afforded the desired pyrimidine derivatives. Using this method, a wide diversity of 2,4,6-trisubstituted and 2,4,5,6-tetrasubstituted pyrimidines were synthesized in very good yields [193]. Despite being a robust methodology, the major drawbacks are the use of expensive metal, air-sensitive phosphine ligand and long reaction time. Kirchner and coworkers [194] and Kempes and coworker [195], independently, improved this methodology by using manganese-based catalysts; however, these approaches required the use of high temperatures. The heterogeneous catalytic version for the synthesis of pyrimidines using expensive platinum nanoparticles as catalyst was reported by Siddiki, Shimizu, and coworkers [196]. Mondal et al. used an air-stable Fe(II)-2-phenylazo-(1,10-phenanthroline) complex as catalyst for

the synthesis of various 2,4,6-trisubstituted pyrimidines under aerobic conditions, at 100 °C, via MC dehydrogenative coupling of primary and secondary alcohols with amidines. From our point of view, this methodology is more advantageous comparatively to the ones mentioned before, because it requires the use of an earth abundant and cheap metal (Fe), air-stable ligand, mild reaction conditions, and presents broad substrate scope, furnishing 41 pyrimidine derivatives in good yields (Scheme 7.47) [197].

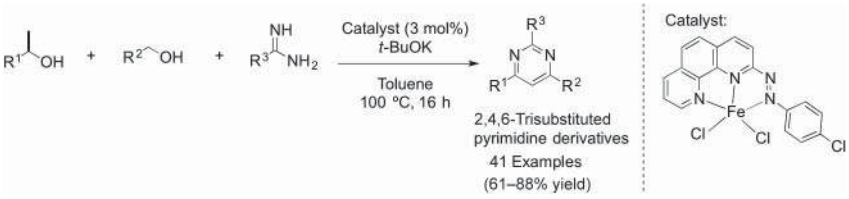

Scheme 7.47 Iron-catalyzed synthesis of 2,4,6-trisubstituted pyrimidine derivatives. Source: Mondal et al. [197] / Elsevier.

The first MC protocol for the synthesis of DHPM type frameworks was introduced by the Italian chemist Pietro Biginelli in 1893 [198]. The Biginelli reaction is a very versatile reaction, using three components (aldehydes, urea/thiourea, and active methylene compounds), which can range from commercially available building blocks to more complex synthetic structures, usually catalyzed by a Brønsted/Lewis acid in protic solvents. Due to the relevance of these heterocyclic compounds in a wide diversity of fields, from medicinal chemistry to materials chemistry (polymers, adhesives), in recent years a huge number of methodologies have been developed in order to overcome major drawbacks, such as strong acidic conditions, long reaction times, and moderated yields [199–202]. Also new sustainable and efficient synthetic procedures have emerged over the last years. Among the huge variety of homogeneous and heterogeneous catalysts developed for the synthesis of the DHPM [203, 204], we can highlight Brønsted/Lewis acids, chiral organocatalysts [205], magnetic nanocatalyst, etc. Nevertheless, some of these catalysts required long synthetic procedures and specific and expensive materials. Few methodologies have been described in the literature for the synthesis of DHPM derivatives under solvent- and catalyst-free reaction conditions [206–209] or using enabling technologies, like microwave, ball milling, and twin-screw extrusion [210–212].

Regarding the methodologies that used conventional conditions, all required high temperatures (80–110 °C) and moderate reaction times (<4 hours), and most of them are limited to aromatic aldehydes, except in the work developed by Guo et al. [208]. Interestingly, they used a large diversity of alkyl aldehydes instead of common aromatics and successfully synthesized DHPM with moderate to very good yields in two hours. These results are relevant for the synthetic routes of the bioactive compounds batzelladin A and crambescin A–C. However, catalyst- and solvent-free protocols using enabling technologies appear to be more advantageous in the sustainable chemistry point of view.

The synthesis of pure enantiomeric DHPMs is very important for the pharmaceutical industry, and in recent years some chiral organocatalysts have been established to achieve this goal [213, 214]. Barbero et al. described an environmentally friendly Biginelli protocol for the synthesis of enantiomeric pure DHPMs, using (−)-4,5-dimethyl-3,6-bis(*o*-tolyl)-1,2-benzenedisulfonimide as a chiral acid Brønsted organocatalyst for the condensation of aromatic aldehydes, urea or thiourea, and ethyl acetoacetate in the absence of solvent (Scheme 7.48). DHPMs were obtained in high yields and enantioselectivities, in short reaction times, without requiring chromatographic purification. Furthermore, this organocatalyst could be recovered and reused without loss of activity, and this protocol could be used in gram scale, which can be advantageous for the pharmaceutical industry [215].

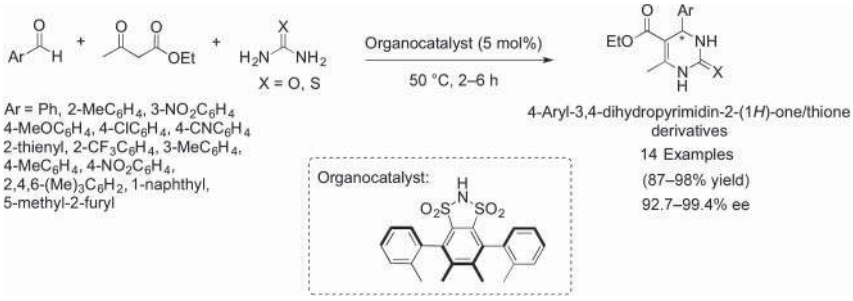

Scheme 7.48 Asymmetric synthesis of DHPM derivatives under solvent-free condition.

Quinazoline is a nitrogen containing fused heterocycle, having four isomeric forms, i.e. quinazoline, quinoxaline, cinnoline, and phthalazine, depending upon the position of the nitrogen atom in the heterocyclic ring system. There are several marketed drugs containing a quinazoline nucleus [216], such as erlotinib (Tarceva®) [217] and gefitinib (Iressa®) [218], among others. Over the recent years several MC synthetic routes have been developed, considering the sustainability concept. Quinazoline frameworks could be synthesized by a 3-MCR of aldehydes, 2-aminobenzophenones, and ammonium acetate using microwave irradiation, under catalyst- and solvent-free conditions [219], or using organic bases as catalysts [220], iodine [221], or even the ionic liquid [bmim][$FeCl_4$] [222]. Other strategies comprise the use of orthoesters [223] or methylarenes [224] instead of aldehydes to obtain the corresponding quinazoline derivatives. Metal-catalyzed formation of quinazolines via C–H activation and C–N coupling reactions was also used for the MC synthesis of quinazoline scaffolds [225–233]. Most of these methodologies are not very efficient and require high temperatures, expensive catalysts, and long reaction times while often displaying limited scope of the reaction. Zhang et al. reported an efficient, environmentally benign 3-MC protocol for the synthesis of a wide variety of 2,4-substituted quinazolines in high yields. Reaction of 2-aminoaryl ketones, aldehydes, and ammonium acetate in the absence of catalyst, under conditions of aerobic oxidation using low melting point mixtures of maltose–dimethylurea (DMU)-NH_4Cl as a new green reaction medium, affords the corresponding 2,4-substituted quinazolines (Scheme 7.49). This methodology

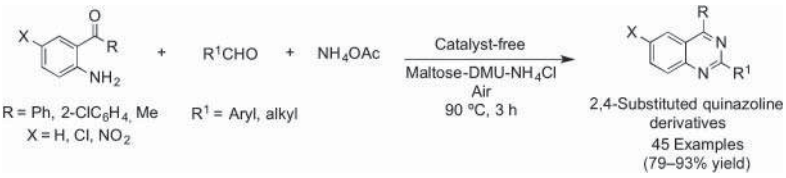

Scheme 7.49 Synthesis of 2,4-substituted quinazolines via a one-pot 3-MCR using maltose-DMU-NH_4Cl as reaction medium.

tolerates a wide range of substrates and functional groups, including aldehyde substrates possessing electron donor or acceptor groups. Another advantage of this protocol is its practicality, and it can also be used in a scale-up fashion. Furthermore, this strategy becomes very interesting for the synthesis of quinazoline derivatives with bioactive relevance, due to its inherent features, such as simple workup, moderate reaction conditions, and high yields [234].

1,4-Oxathiane is a six-membered heterocyclic unit containing one oxygen atom and one sulfur atom in opposite positions of the ring. 1,4-Oxathiane core is the main structural motif present in certain commercial systemic fungicides broadly used in agriculture. In fact, only few MC synthetic routes have been described in literature for the synthesis of 1,4-oxathiane heterocyclic compounds [235–239]. Hossaini et al. described an eco-friendly protocol for the synthesis of substituted 1,4-oxathiane-3-thione derivatives in very good yields, which consist in a 3-MCR between nitromethane, carbon disulfide, and an epoxide, catalyzed by NEt_3 in water, at 70 °C, under microwave irradiation, over two hours. Valuable advantages of this method include efficiency, scope, short reaction times, and straightforward procedure (Scheme 7.50) [235].

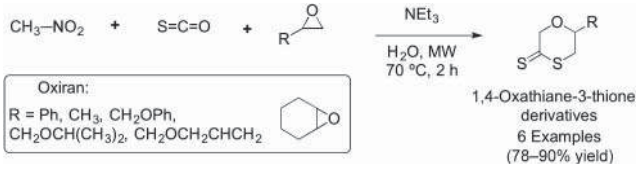

Scheme 7.50 Microwave-assisted 3-MCR catalyzed by NEt_3 under aqueous media. Source: Hossaini et al. [235] / Elsevier.

Thiazines are other six-membered heterocycles containing sulfur and nitrogen atoms, with significant relevance in the field of medicinal chemistry, although we believe that their potential concerning their pharmacological properties is neglected [240]. Some MC syntheses have been described in literature over the last years. Unfused 3,6-dihydro-2*H*-1,3-thiazine-2-thione scaffolds could be synthesized in moderate to good yields through MCR of *in situ* generated 1-azadienes with carbon disulfide [241]. Mehrabi and coworker reported a catalyst-free 4-MC synthesis of 3,6-dihydro-2*H*-1,3-thiazine-2-thione derivatives using amines, carbon disulfide, arylglyoxals, and malononitrile in aqueous ethanol, at room temperature [242]. Although the reactions previously mentioned are carried out under catalyst-free

conditions, they have some disadvantages, such as long reaction times and/or low yields of the desired products. Another interesting methodology reported by Zhuang et al. involved the reaction of cyanoacetamide with isothiocyanates and cycloketones, catalyzed by DMF in a one-pot fashion under microwave irradiation and afforded spiro-substituted 1,3-thiazine analogs in good to excellent yields [243].

Regarding environmentally benign protocols, Sharma and coworkers have developed two attractive and easy-to-perform methodologies, which have in common short reaction times, mild reaction conditions (room temperature), absence of catalyst and solvent, high regioselectivity, chromatographic-free purification, scalable synthesis, wide functional group tolerance, and high yields. In one protocol, the synthesis of 1,3-thiazin-4-ones through a domino-click reaction was achieved using commercially available substrates, just by mixing the isothiocyanate derivative and the hydrazine monohydrate, followed by the addition of diethylacetylene dicarboxylate. The substrate scope is satisfactory (12 examples), and the nature of the substituents (electron donor or acceptor) of phenylisothiocyanates did not directly affect the yield of the reaction; however the steric hindrance of some substituents blocked the formation of the products [244]. The other protocol, which is depicted in Scheme 7.51, covers the regioselective synthesis of 1,3-thiazin-4-one derivatives via a 4-MCR between isothiocyanate derivatives, hydrazine monohydrate, aldehyde derivatives, and dialkyl acetylenedicarboxylates. Good substrate scope and very good to excellent yields were obtained for the desired products [245].

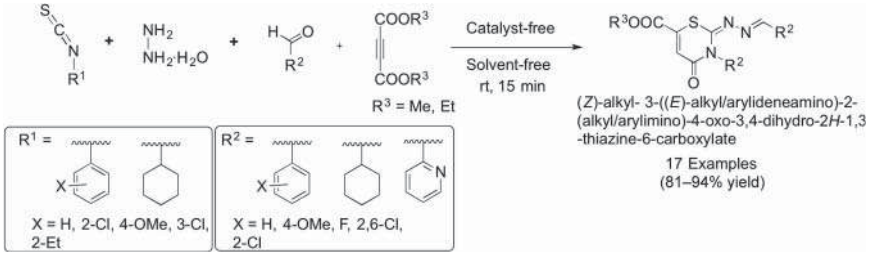

Scheme 7.51 4-MC synthesis of 1,3-thiazone derivatives.

7.5.3 Six-Membered Ring Heterocycles with Three Heteroatoms

1,3,5-Triazines are an important class of multi-N-containing heterocycles found in various pharmaceuticals, agrochemicals, and natural products [246]. In 2017, FDA approved enasidenib, an anticancer drug, possessing a 1,3,5-triazine unit [247]. Over the last years, there has been an increased interest in the development of new methodologies to expand the diversity of these class of heterocycles.

Pan et al. reported a 3-MCR of imidates, guanidines, and amides or aldehydes promoted by cesium carbonate for the synthesis of unsymmetrical 1,3,5-triazin-2-amines. This methodology has some advantages such as the absence of catalyst or additives and good scope. The drawback of the protocol is the high temperatures and long reaction times needed to reach efficiency. Using this methodology, it was possible to synthesize a family of 28 derivatives

with moderate to excellent yields [248]. Guo et al. described another method for the synthesis of unsymmetrical 1,3,5-triazine-amines that consisted in a 3-MC visible-light [3+1+2] annulation reaction of amidines, isothiocyanates, and 1,1,3,3-tetramethylguanidines, photocatalyzed by Rose Bengal, using a mixture of ethanol:dichloromethane (1 : 1) as solvent at room temperature over 12 hours (Scheme 7.52). This methodology is much more advantageous than the one reported by Pan et al., since it is tolerant to air and moisture and presents a broad substrate scope, high step economy, mild reaction conditions, and short reaction times with very good yields. In our opinion this method will have a promising application in the direct synthesis of unsymmetrical 1,3,5-triazin-2-amine drugs and pesticides [249].

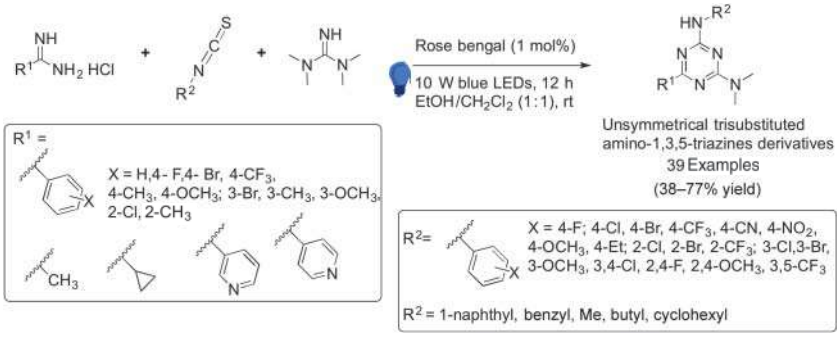

Scheme 7.52 Synthesis of unsymmetrical 1,3,5-triazine-amines through visible light-catalyzed 3-MCR.

1,3,4-Thiadiazine, a six-membered heterocyclic unit containing one sulfur atom and two nitrogen atoms in positions 1, 3, and 4, respectively, is a very important moiety present in a wide variety of compounds with pharmacological properties [250]. Moghimi et al. reported the first MCR for synthesize 1,3,4-thiadiazine derivatives, through a novel 3-MC condensation of phenylhydrazine, α-bromo aryl ketones, and aryl isothiocyanates catalyzed by NEt_3, under refluxing ethanol (Scheme 7.53A). Despite the limited scope of the reaction, this method proved to be advantageous in what concerns efficiency and easy purification of the products [251]. Later, Mishra et al. following the same strategy, developed an environmentally benign methodology consisting of the first visible light-mediated 3-MC synthesis of 1,3,4-thiadiazole derivatives. The reaction leads to the formation of C—S and C—N bonds through generation of free radical intermediates, followed by intramolecular cyclization under mild reaction conditions. The authors introduced two protocols under visible light conditions at room temperature (Scheme 7.53B): (i) catalyzed by DBU (1,8-diazabicyclo[5.4.0]undec-7-ene) in ethanol and (ii) catalyst- and solvent-free conditions. When comparing the two protocols, the method (ii) seems to be more advantageous, as it is economical and tolerates a wide range of substrates (such as electron withdrawing and donor groups), leading to good to excellent product yields, although longer reaction times must be applied [252].

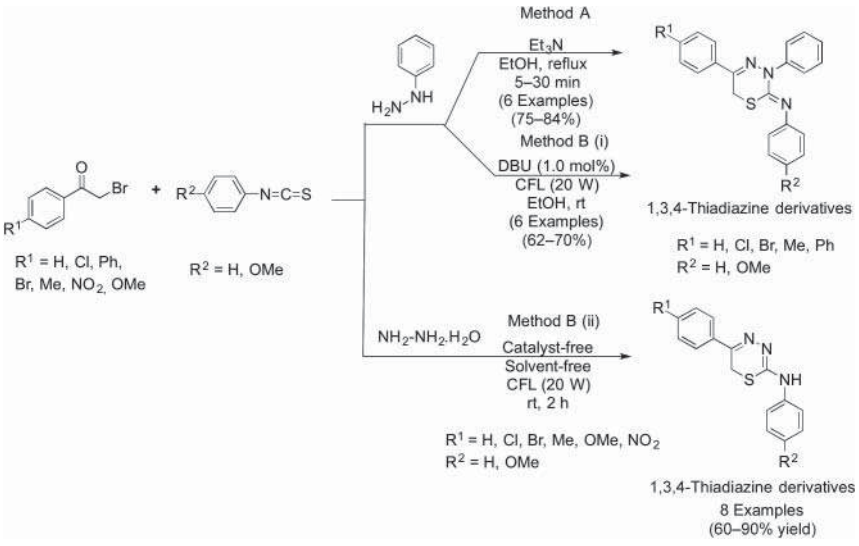

Scheme 7.53 Synthesis of 1,3,4-thiadiazine derivatives through 3-MCR.

7.6 Seven-Membered Ring Heterocycles

The chemistry of seven-membered heterocyclic compounds is less explored comparatively to that of five or six-membered ring heterocycles, although the development of powerful and efficient synthetic approaches to access large-ring heterocyclic structures is of utmost interest, since some of them have showed practical application. Caprolactam, for instance, is an azepine derivative used as an intermediate in the manufacture of nylon-6 and also in the production of films, coatings, and synthetic leather [253]. The well-known antidepressant imipramine [254] (Prazepine®) or the tranquilizer diazepam [255] (Valium®) are examples of active pharmaceutical ingredients with seven-membered heterocycle units in their scaffold. In the next paragraphs we intent to review some selected reports concerning sustainable synthetic pathways to achieve this complex and interesting units, focusing on greener methodologies.

Ghandi et al. reported a novel isocyanide-based 3-MC synthesis of benzimidazole-fused 1,4-diazepine-5-ones in moderate to very good yields [256]. The previously synthesized bifunctional 2-(2-formyl-1*H*-benzimidazol-1-yl)propionic acid was used in an Ugi 3-MCR together with amines and alkyl isocyanides, in methanol at 40 °C to access new 1,4-diazepin-5-ones (Scheme 7.54A). Few years later, Ballet and coworkers reported an Ugi 4-MCR toward dipeptides containing 4-aminotriazolo-azepinone derivatives by condensation of Boc-protected 2-amino-3-azidopropanoic acid, propargylamine, isocyanides, and aldehydes through a one-pot two-step sequence with high atom economy (Scheme 7.54B) [257].

As previously discussed, benzodiazepines are prominent units in medicinal chemistry since the discovery of chlorodiazepoxide and diazepam, and, therefore,

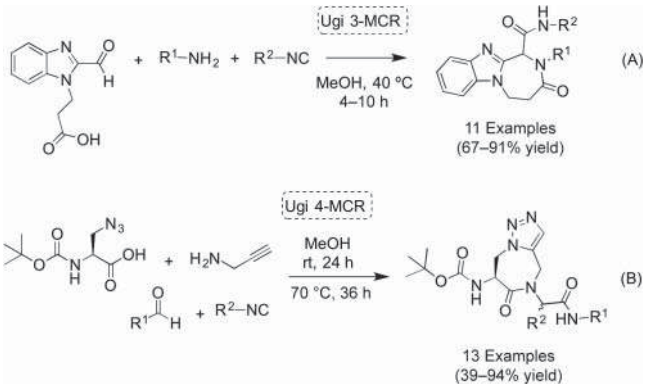

Scheme 7.54 Synthesis of complex 1,4-diazepin-5-ones via Ugi 3- or 4-MCR. Source: Barlow et al. [257] / Royal Society of Chemistry.

innovative and sustainable synthetic routes are valuable resources to access this core. The group of Foroumadi discovered a novel synthetic approach to obtain 1,2-dihydro-4*H*-benzo[*e*][1,4]diazepine-3,5-diones in mild reaction conditions [258]. Using 2-amino-N-susbtituted benzamide derivatives (easily prepared via simple reaction between isatoic anhydride and several amines in water at room temperature), arylboronic acids, and glyoxylic acid, in the presence of molecular sieves at room temperature, they could easily obtain a small library of 1,4-benzodiazepine-3,5-diones in moderate to good yields (Scheme 7.55).

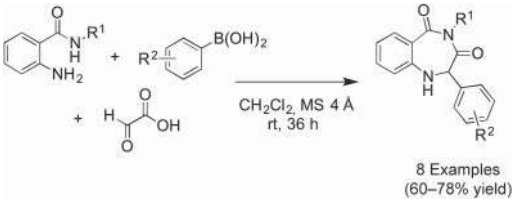

Scheme 7.55 A Petasis 3-MCR in the synthesis of 1,4-benzodiazepine-3,5-diones.

The interest in studying the synthesis of new scaffolds possessing the 1,4-thiazepine unit has been widely explored in the past but still draws some attention in modern synthetic chemistry due to the prominent biological importance of this class of heterocyclic compounds [259, 260]. Several commercially available drugs, like the cardiovascular and antiarrhythmic diltiazem [261], the antipsychotic quetiapine [262], and the angiotensin-converting enzyme inhibitor temocapril [263], have the 1,4-thiazepine unit in their framework. The group of Dandia reported a novel and environmentally benign protocol to access new spiro[indole-3,4′-pyrazolo[3,4-*e*][1,4]thiazepines] and the evaluation of their anti-hyperglycemic activity [264]. A mixture of 5-amino-3-methylpyrazole, α-mercaptoacetic acid derivatives, and isatin, or acenaphthylene-1,2-dione, or piperidinones, was used, under sonication using water as solvent, at room temperature and short reaction times to access efficiently a small family of 1,4-thiazepine

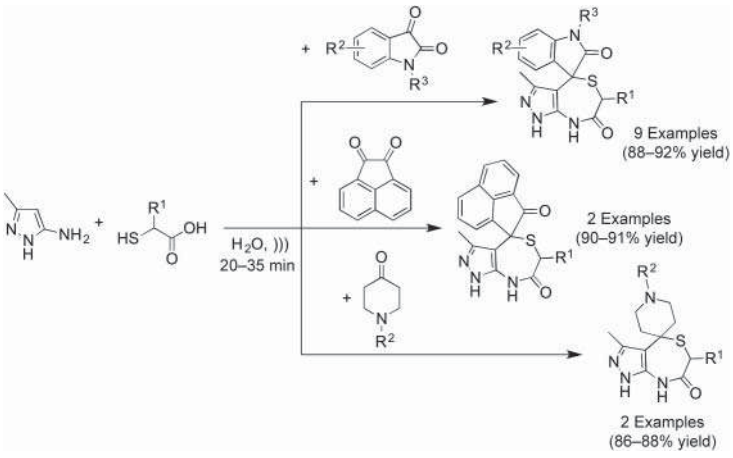

Scheme 7.56 Catalyst-free 3-MCR protocol to access spiro[indole-3,4′-pyrazolo[3,4-*e*][1,4]thiazepines] in aqueous media, under mild reaction conditions.

derivatives (Scheme 7.56). X-ray analysis confirmed the structure and relative stereochemistry of the spiro seven-membered ring system. Major advantages to point out regarding this method are the use of water as solvent and catalyst-free and the simple workup since the product was isolated by filtration alone. Only one compound showed moderate inhibition for α-amylase at 1 g concentration.

The group of Kommidi also reported an eco-friendly and attractive protocol to access thiazepine (and oxazepine) derivatives of thiazolidine-2,4-dione using a one-pot 3-MCR between substituted aromatic aldehydes, thiazolidine-2,4-dione, and 2-aminothiobenzene (or 2-aminophenol) with [bmim]BF_4, at room temperature (Scheme 7.57) [265]. After evaluation of some solvents and catalysts in this particular 3-MCR, the authors found that the ionic liquid ([bmim]BF_4) works as catalyst and solvent, affording the desired thiazepine derivatives in high yield. The high polarity and non-coordinating nature are among the advantageous features in using ionic liquids in MCR. In this case, [bmim]BF_4 increased the nucleophilic strength of one of the components, in a catalyst-free approach. This versatile protocol could be used to access the corresponding oxazepine derivatives exploiting 2-aminophenol as one component (see Scheme 7.57).

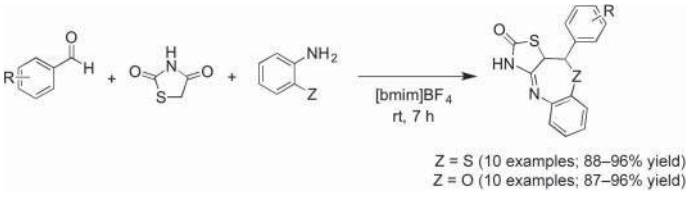

Scheme 7.57 Ionic liquid-mediated 3-MCR for the synthesis of structurally new thiazepine and oxazepine derivatives of thiazolidine 2,4-dione.

Very recently, Shaabani et al. described a method to get also biologically important bis-heterocyclic oxazepine-quinazolinone derivatives, this time using an Ugi 3-MCR approach [266]. Despite poor reaction scope (only three examples were described) in the use of 2-(2-formylphenoxy)acetic acid, 2-aminobenzamide, and isocyanide derivatives in refluxed ethanol, new structurally interesting fused oxazepine-quinazolinone heterocycles were obtained in excellent yields (Scheme 7.58). It is worth highlighting that this catalyst-free protocol uses two bifunctional starting materials and a new isocyanide-based bicyclization reaction where one C—C bond, three C—N bonds, one amine group, a benzoxazepine ring, and a quinazolinone ring are newly formed.

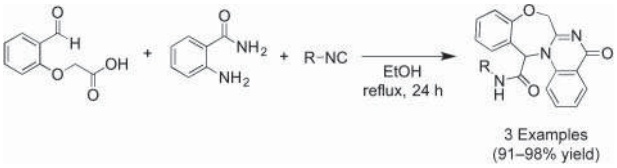

Scheme 7.58 Ugi 3-MCR protocol to get bis-heterocyclic oxazepine-quinazolinone derivatives.

ε-Lactams (2-azepanones or caprolactam) are important seven-membered ring heterocycles found in some biologically active molecules of interest, or natural products, and versatile synthetic intermediates. Foroumadi and coworkers described a green one-pot Ugi 3-MC protocol to achieve the synthesis of *N*-alkyl-2-(2-oxoazepan-1-yl)-2-arylacetamide derivatives in water in the absence of catalyst [267]. Employing 6-aminohexanoic acid, aromatic substituted aldehydes, and isocyanides using water as solvent in reflux conditions, the desired small family of ε-lactams was obtained in poor to good yields (Scheme 7.59). It was observed that the reaction does not proceed at room temperature conditions, and steric effects on the aldehyde component could play significant role concerning the efficiency of the reaction, i.e. *ortho*-methyl substituted benzaldehyde gave the lowest yield (10%).

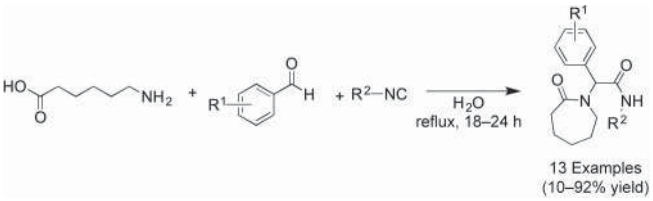

Scheme 7.59 The Ugi isocyanide-based 3-MCR in the synthesis of *N*-alkyl-2-(2-oxoazepan-1-yl)-2-arylacetamide derivatives.

Fused ε-lactams, like the dibenzo-[*c*,*e*]azepinone scaffold, are also key biaryl units present in biological molecules of interest. The γ-secretase inhibitor LY411575, synthesized by Eli Lilly [268] is an example. The group of Van der Eycken developed an efficient procedure for the generation of dibenzo-[*c*,*e*]azepinone derivatives via an intramolecular Ugi 3-MCR using bifunctionalized biaryls

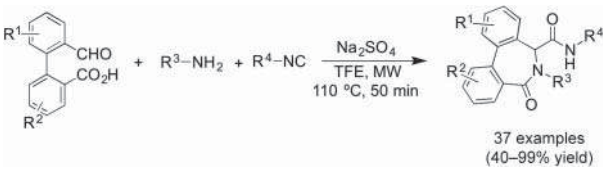

Scheme 7.60 A microwave-assisted Ugi 3-MC diastereoselective reaction to access dibenzo[*c*,*e*]azepinones. Source: Mehta et al. [269] / American Chemical Society.

(2′-formylbiphenyl-2-carboxylic acids), amines, and isocyanides in the presence of sodium sulfate in TFE under microwave irradiation at 110 °C (Scheme 7.60) [269]. The reaction tolerates different substituted groups demonstrating great scope (37 examples) in short reaction times. Moderate to excellent yields (and high diastereoselectivities) were obtained for the desired biaryl-fused ε-lactam derivatives. Despite no activity were detected against several DNA and RNA viruses in cell cultures, some compounds showed promising results concerning antiproliferative activity against two murine (leukemia L1210 and mammary carcinoma FM3A) and human (lymphocyte CEM and cervix carcinoma HeLa) tumor cell lines in the lower micromolar range.

7.7 Conclusions and Perspectives

Taking into account the examples previously given, highlighting clean, atom-, and step-efficient one-pot multicomponent synthesis for sustainable production of complex heterocyclic scaffolds, it is quite obvious that MCR chemistry has a smiling future. The increasing demand for perfect/ideal synthesis calls for the development of techniques that save time, energy, effort, and resources, decreasing the amount of waste generated in chemical reactions.

Some of the MCR-based protocols developed in recent years have great potential to be used in an industrial setting. Therefore, it is expected to observe a growing number of these protocols to be adopted by the chemical and pharmaceutical industries, as a way to meet sustainability goals. The increase in the number of MCRs is often associated with the discovery of new heterocycles; undoubtedly the area of medicinal chemistry is and will be the most privileged.

The growing number of new heterocyclic compounds achieved by MCRs makes this field of work one of the most interesting ones in recent years. Clearly the imagination will guide the future directions of the MCRs in the synthesis of heterocycles.

Acknowledgments

The authors would like to thank financial support from PT national funds (FCT/MCTES, Fundação para a Ciência e Tecnologia and Ministério da Ciência, Tecnologia e Ensino Superior) through the project UIDB/50006/2020 | UIDP/50006/2020.

References

1 Zhu, J., Wang, Q., and Wang, M.-X. (ed.) (2015). *Multicomponent Reactions in Organic Synthesis*. Weinheim, Germany: Wiley-VCH. ISBN: 978-3-527-33237-3.

2 Alvarez-Builla, J., Vaquero, J.J., and Barluenga, J. (ed.) (2011). *Modern Heterocyclic Chemistry*. Weinheim, Germany: Wiley-VCH. ISBN: 978-3-527-33201-4.

3 Singh, G.S. (2019). Chapter 4: Advances in synthesis and chemistry of aziridines. *Adv. Heterocycl. Chem.* 129: 245–335. https://doi.org/10.1016/bs.aihch.2018.12.003. ISBN 9780128174739.

4 Moschona, F., Savvopoulou, I., Tsitopoulou, M. et al. (2020). Epoxide syntheses and ring-opening reactions in drug development. *Catalysts* 10 (10): 1117. https://doi.org/10.3390/catal10101117.

5 Reddy, A.R., Zhou, C.-Y., and Che, C.-M. (2014). Ruthenium porphyrin catalyzed three-component reaction of diazo compounds, nitrosoarenes, and alkynes: an efficient approach to multifunctionalized aziridines. *Org. Lett.* 16 (4): 1048–1051. https://doi.org/10.1021/ol4035098.

6 Wu, K., Zhou, C.-Y., and Che, C.-M. (2019). Perfluoroalkyl aziridines with ruthenium porphyrin carbene intermediates. *Org. Lett.* 21 (1): 85–89. https://doi.org/10.1021/acs.orglett.8b03514.

7 Zhou, Y., Gupta, A.K., Mukherjee, M. et al. (2017). Multicomponent catalytic asymmetric synthesis of *trans*-aziridines. *J. Org. Chem.* 82 (24): 13121–13140. https://doi.org/10.1021/acs.joc.7b02184.

8 Gupta, A.K., Mukherjee, M., and Wulff, W.D. (2011). Multicomponent catalytic asymmetric aziridination of aldehydes. *Org. Lett.* 13 (21): 5866–5869. https://doi.org/10.1021/ol202472z.

9 Mukherjee, M., Zhou, Y., Dai, Y. et al. (2017). Catalyst controlled multi-component aziridinations of chiral aldehydes. *Chemistry* 23 (11): 2552–2556. https://doi.org/10.1002/chem.201605955.

10 Bew, S.P., Liddle, J., Hughes, D.L. et al. (2017). Chiral Brønsted acid-catalyzed asymmetric synthesis of *N*-aryl-cis-aziridine carboxylate esters. *Angew. Chem. Int. Ed.* 56 (19): 5322–5326. https://doi.org/10.1002/anie.201611990.

11 Lei, J., Song, G.-T., He, L.-J. et al. (2020). One-pot construction of functionalized aziridines and maleimides via a novel *pseudo*-Knoevenagel cascade reaction. *Chem. Commun.* 56 (14): 2194–2197. https://doi.org/10.1039/C9CC08220D.

12 Li, X., Feng, T., Li, D. et al. (2020). Straightforward approach toward multifunctionalized aziridines via catalyst-free three-component reactions of α-diazoesters, nitrosoarenes, and alkynes. *J. Org. Chem.* 85 (15): 9538–9547. https://doi.org/10.1021/acs.joc.0c00368.

13 Roy, T., Thangaraj, M., Gonnade, R.G., and Biju, A.T. (2016). Synthesis of functionalized amino epoxides by a three-component coupling involving aziridines, arynes and aldehydes. *Chem. Commun.* 52 (58): 9044–9047. https://doi.org/10.1039/C6CC00057F.

14 Giumanini, A.G. (1972). New deamination in a benzyne addition to *N*-benzylaziridine. *J. Org. Chem.* 37 (3): 513–514. https://doi.org/10.1021/jo00968a048.

15 Deobald, A.M., Corrêa, A.G., Rivera, D.G., and Paixão, M.W. (2012). Organocatalytic asymmetric epoxidation and tandem epoxidation/Passerini reaction under eco-friendly reaction conditions. *Org. Biomol. Chem.* 10 (38): 7681–7684. https://doi.org/10.1039/c2ob26247a.

16 Santos, D.A., Deobald, A.M., Cornelio, V.E. et al. (2017). Asymmetric synthesis and evaluation of epoxy-α-acyloxycarboxamides as selective inhibitors of cathepsin L. *Bioorg. Med. Chem.* 25 (17): 4620–4627. https://doi.org/10.1016/j.bmc.2017.06.048.

17 Liu, N., Cao, S., Wu, J. et al. (2010). A mild and efficient synthesis of monofluorinated α-lactam pseudopeptides via a novel dehydrofluorination of Ugi products. *Mol. Diversity* 14: 501–506. https://doi.org/10.1007/s11030-009-9209-x.

18 Liu, N., Cao, S., Shen, L. et al. (2009). New *gem*-difluoromethylene-containing isocyanide as a useful building block for the synthesis of difluorinated pseudopeptides via Ugi reaction. *Tetrahedron Lett.* 50 (17): 1982–1985. https://doi.org/10.1016/j.tetlet.2009.02.056.

19 Rizk, N.A., Kanafani, Z.A., Tabaja, H.Z., and Kanj, S.S. (2017). Extended infusion of beta-lactam antibiotics: optimizing therapy in critically-ill patients in the era of antimicrobial resistance. *Expert Rev. Anti. Infect. Ther.* 15 (7): 645–652. https://doi.org/10.1080/14787210.2017.1348894.

20 Saldívar-González, F.I., Lenci, E., Trabocchi, A., and Medina-Franco, J.L. (2019). Exploring the chemical space and the bioactivity profile of lactams: a chemoinformatic study. *RSC Adv.* 9 (46): 27105–27116. https://doi.org/10.1039/c9ra04841c.

21 Blackie, M.A.L., Feng, T.-S., Smith, P.J., and Chibale, K. (2016). Synthesis of novel β-lactams and in vitro evaluation against the human malaria parasite *Plasmodium falciparum*. *Arkivoc* iii: 214–235. https://doi.org/10.3998/ark.5550190.p009.465.

22 Rainoldi, G., Lesma, G., Picozzi, C. et al. (2018). One step access to oxindole-based β-lactams through Ugi four-center three-component reaction. *RSC Adv.* 8 (61): 34903–34910. https://doi.org/10.1039/c8ra08165d.

23 Shaabani, S., Neochoritis, C.G., Twarda-Clapa, A. et al. (2017). Scaffold hopping via ANCHOR.QUERY: β-lactams as potent p53-MDM2 antagonists. *MedChemComm* 8 (5): 1046–1052. https://doi.org/10.1039/C7MD00058H.

24 Koes, D.R., Dömling, A., and Camacho, C.J. (2018). AnchorQuery: rapid online virtual screening for small-molecule protein–protein interaction inhibitors. *Protein Sci.* 27 (1): 229–232. https://doi.org/10.1002/pro.3303.

25 Cheibas, C., Cordier, M., Li, Y., and Kaïm, L.E. (2019). A Ugi straightforward access to bis-β-lactam derivatives. *Eur. J. Org. Chem.* 2019 (27): 4457–4463. https://doi.org/10.1002/ejoc.201900678.

26 Gao, X., Shan, C., Chen, Z. et al. (2018). One-pot synthesis of β-lactams by the Ugi and Michael addition cascade reaction. *Org. Biomol. Chem.* 16 (33): 6096–6105. https://doi.org/10.1039/c8ob01176a.

27 Naskar, D., Roy, A., Seibel, W.L. et al. (2003). The synthesis of aza-β-lactams via tandem Petasis–Ugi multi-component condensation and 1,3-diisopropylcarbodiimide (DIC) condensation reaction. *Tetrahedron Lett.* 44 (33): 6297–6300. https://doi.org/10.1016/S0040-4039(03)01524-7.

28 Beasley, B.O., Clarkson, G.J., and Shipman, M. (2012). Passerini reactions for the efficient synthesis of 3,3-disubstituted oxetanes. *Tetrahedron Lett.* 53 (24): 2951–2953. https://doi.org/10.1016/j.tetlet.2012.03.065.

29 Joule, J.A. and Mills, K. (2010). *Heterocyclic Chemistry*, 5e. Chicester: Wiley. ISBN: 978-1-4051-9365-8.

30 Majumdar, K.C. and Chattopadhyay, S.K. (ed.) (2011). *Heterocycles in Natural Product Synthesis*. Weinheim: Wiley-VCH. ISBN: 978-3-527-32706-5.

31 Meera, G., Rohit, K.R., Saranya, S., and Anilkumar, G. (2020). Microwave assisted synthesis of five membered nitrogen heterocycles. *RSC Adv.* 10: 36031–36041. https://doi.org/10.1039/D0RA05150K.

32 Huang, J. and Yu, G. (2021). Structural engineering in polymer semiconductors with aromatic N-heterocycles. *Chem. Mater.* 33 (5): 1513–1539. https://doi.org/10.1021/acs.chemmater.0c03975.

33 Gelling, V.J., Wiest, M.M., Tallman, D.E. et al. (2001). Electroactive-conducting polymers for corrosion control: 4. Studies of poly(3-octyl pyrrole) and poly(3-octadecyl pyrrole) on aluminum 2024-T3 alloy. *Prog. Org. Coat.* 43 (1–3): 149–157. https://doi.org/10.1016/S0300-9440(01)00186-2.

34 Kaur, N. (2015). Microwave-assisted synthesis: fused five-membered N-heterocycles. *Synth. Commun.* 45 (7): 789–823. https://doi.org/10.1080/00397911.2013.824984.

35 Estévez, V., Villacampa, M., and Menéndez, J.C. (2010). Multicomponent reactions for the synthesis of pyrroles. *Chem. Soc. Rev.* 39 (11): 4402–4421. https://doi.org/10.1039/B917644F.

36 Bhardwaj, V., Gumber, D., Abbot, V. et al. (2015). Pyrrole: a resourceful small molecule in key medicinal hetero-aromatics. *RSC Adv.* 5 (20): 15233–15266. https://doi.org/10.1039/C4RA15710A.

37 Bellina, F. and Rossi, R. (2006). Synthesis and biological activity of pyrrole, pyrroline and pyrrolidine derivatives with two aryl groups on adjacent positions. *Tetrahedron* 62 (31): 7213–7256. https://doi.org/10.1016/j.tet.2006.05.024.

38 Xu, X., Chen, J., Ke, J. et al. (2021). Recent advances on pyrrole synthesis through different annulation modes. *Chin. J. Org. Chem.* 41 (1): 206–228. https://doi.org/10.6023/cjoc202005018.

39 Fan, H., Peng, J., Hamann, M.T., and Hu, J.F. (2008). Lamellarins and related pyrrole-derived alkaloids from marine organisms. *Chem. Rev.* 108 (1): 264–287. https://doi.org/10.1021/cr078199m.

40 Katritzky, E.F.V., Rees, A.R., and Scriven, C.W. (ed.) (1996). *Comprehensive Heterocyclic Chemistry II*, vol. 2. Oxford: Pergamon Press. ISBN: 9780080965185.

41 Bhat, S.I. and Trivedi, D.R. (2013). A catalyst- and solvent-free three-component reaction for the regioselective one-pot access to polyfunctionalized pyrroles. *Tetrahedron Lett.* 54 (41): 5577–5582. https://doi.org/10.1016/j.tetlet.2013.07.153.

42 Tamaddon, F. and Farahi, M. (2012). A new three-component reaction catalyzed by silica sulfuric acid: synthesis of tetrasubstituted pyrroles. *Synlett* 23 (9): 1379–1383. https://doi.org/10.1055/s-0031-1290955.

43 Korotaev, V.Y., Barkov, A.Y., Kotovich, I.V., and Sosnovskikh, V.Y. (2012). Three-component synthesis of substituted β-(trifluoromethyl)pyrroles via Grob cyclization of 1,1,1-trifluoro-3-nitrobut-2-ene with 1,3-dicarbonylic compounds and ammonia or primary amines. *J. Fluorine Chem.* 138: 42–47. https://doi.org/10.1016/j.jfluchem.2012.03.012.

44 Kan, W., Jing, T., Zhang, X. et al. (2015). Microwave-assisted one-pot synthesis of N-substituted 2-methyl-1*H*-pyrrole-3-carboxylate derivatives without catalyst and solvent. *Heterocycles* 91 (12): 2367–2376. https://doi.org/10.3987/COM-15-13340.

45 Feng, X., Wang, Q., Lin, W. et al. (2013). Highly efficient synthesis of polysubstituted pyrroles via four-component domino reaction. *Org. Lett.* 15 (10): 2542–2545. https://doi.org/10.1021/ol4010382.

46 Siddiqui, I.R., Kumar, D., and Shamim, S. (2013). Ionic liquid promoted multicomponent reaction: a good strategy for the eco-compatible synthesis of functionalized pyrroles. *J. Heterocycl. Chem.* 50 (S1): E111–E115. https://doi.org/10.1002/jhet.1085.

47 Meshram, H.M., Madhu Babu, B., Santosh Kumar, G. et al. (2013). Catalyst-free four-component protocol for the synthesis of substituted pyrroles under reusable reaction media. *Tetrahedron Lett.* 54 (19): 2296–2302. https://doi.org/10.1016/j.tetlet.2013.01.098.

48 Li, B.L., Li, P.H., Fang, X.N. et al. (2013). One-pot four-component synthesis of highly substituted pyrroles in gluconic acid aqueous solution. *Tetrahedron* 69 (34): 7011–7018. https://doi.org/10.1016/j.tet.2013.06.049.

49 Malykh, A.G. and Sadaie, M.R. (2010). Piracetam and piracetam-like drugs: from basic science to novel clinical applications to CNS disorders. *Drugs* 70 (3): 287–312. https://doi.org/10.2165/11319230-000000000-00000.

50 Lyseng-Williamson, K.A. (2011). Levetiracetam: a review of its use in epilepsy. *Drugs* 71 (4): 489–514. https://doi.org/10.2165/11204490-000000000-00000.

51 Cioc, R.C., Schaepkens van Riempst, L., Schuckman, P. et al. (2017). Ugi four-center three-component reaction as a direct approach to racetams. *Synthesis* 49 (7): 1664–1674. https://doi.org/10.1055/s-0036-1588672.

52 Kausar, N., Al Masum, A., Islam, M.M., and Das, A.R. (2017). A green synthetic approach toward the synthesis of structurally diverse spirooxindole derivative libraries under catalyst-free conditions. *Mol. Diversity* 21: 325–337. https://doi.org/10.1007/s11030-017-9728-9.

53 Royles, B.J.L. (1995). Naturally occurring tetramic acids: structure, isolation, and synthesis. *Chem. Rev.* 95 (6): 1981–2001. https://doi.org/10.1021/cr00038a009.

54 Pharande, S.G. (2021). Synthesis of lactams via isocyanide-based multicomponent reactions. *Synthesis* 53 (3): 418–446. https://doi.org/10.1055/s-0040-1706297.

55 Mohammadkhani, L. and Heravi, M.M. (2019). Synthesis of various N-heterocycles using the Ugi four-center three-component reaction. *ChemistrySelect* 4 (34): 10187–10196. https://doi.org/10.1002/slct.201902029.

56 Jida, M., Malaquin, S., Deprez-Poulain, R. et al. (2010). Synthesis of five- and six-membered lactams via solvent-free microwave Ugi reaction. *Tetrahedron Lett.* 51 (39): 5109–5111. https://doi.org/10.1016/j.tetlet.2010.07.021.

57 Darehkordi, A., Zand-Vakili, F., and Rafsanjani, A.T. (2016). A novel gabapentin based intermolecular Ugi four-center, three-component reaction for preparing *N*-cyclohexyl-2-(3-oxo-2-azaspiro[4,5]decan-2-yl)-2-aryl acetamide derivatives. *Tetrahedron Lett.* 57 (4): 498–501. https://doi.org/10.1016/j.tetlet.2015.12.079.

58 Poor, M.A., Darehkordi, A., Anary-Abbasinejad, M., and Mohammadi, M. (2018). Gabapentin-base synthesis and theoretical studies of biologically active compounds: *N*-cyclohexyl-3-oxo-2-(3-oxo-2-azaspiro[4.5]decan-2-yl)-3-arylpropanamides and *N*-(*tert*-butyl)-2-(3-oxo-2-azaspiro[4.5]decan-2-yl)-2-arylacetamide derivatives. *J. Mol. Struct.* 1152: 44–52. https://doi.org/10.1016/j.molstruc.2017.09.061.

59 Mandal, A.K., Hines, J., Kuramochi, K., and Crews, C.M. (2005). Developing microcolin A analogs as biological probes. *Bioorg. Med. Chem. Lett.* 15 (18): 4043–4047. https://doi.org/10.1016/j.bmcl.2005.06.020.

60 Li, Z., Kumar, A., Peshkov, A., and Van der Eycken, E.V. (2016). A domino Ugi/Michael approach for the synthesis of α,β-unsaturated γ-lactams. *Tetrahedron Lett.* 57 (7): 754–756. https://doi.org/10.1016/j.tetlet.2016.01.014.

61 Manta, S., Tzioumaki, N., Kollatos, N. et al. (2018). Polyfunctionalized pyrrole derivatives: easy three-component microwave-assisted synthesis, cytostatic and antiviral evaluation. *Curr. Microwave Chem.* 05 (1): 23–31. https://doi.org/10.2174/2213335605666180221155915.

62 Peshkov, A.A., Peshkov, V.A., Li, Z. et al. (2014). Assembly of a 1*H*-pyrrol-2(5*H*)-one core through a Cascade Ugi reaction/5-*endo-dig* carbocyclization/retro-Claisen fragmentation process. *Eur. J. Org. Chem.* 2014 (29): 6390–6393. https://doi.org/10.1002/ejoc.201402723.

63 Riguet, E. (2011). Enantioselective organocatalytic Friedel–Crafts alkylation reaction of indoles with 5-hydroxyfuran-2(5*H*)-one: access to chiral γ-lactones and γ-lactams via a Ugi 4-center 3-component reaction. *J. Org. Chem.* 76 (20): 8143–8150. https://doi.org/10.1021/jo201184p.

64 Santra, S. and Andreana, P.R. (2011). A bioinspired Ugi/Michael/aza-Michael cascade reaction in aqueous media: natural-product-like molecular diversity. *Angew. Chem. Int. Ed.* 50 (40): 9418–9422. https://doi.org/10.1002/anie.201103567.

65 Santos, M.M.M. (2014). Recent advances in the synthesis of biologically active spirooxindoles. *Tetrahedron* 70 (52): 9735–9757. https://doi.org/10.1016/j.tet.2014.08.005.

66 Yu, B., Yu, D.Q., and Liu, H.M. (2015). Spirooxindoles: promising scaffolds for anticancer agents. *Eur. J. Med. Chem.* 97: 673–698. https://doi.org/10.1016/j.ejmech.2014.06.056.

67 Zhou, L.M., Qu, R.Y., and Yang, G.F. (2020). An overview of spirooxindole as a promising scaffold for novel drug discovery. *Expert Opin. Drug Discovery* 15 (5): 603–625. https://doi.org/10.1080/17460441.2020.1733526.

68 Ryu, H., Seo, J., and Ko, H.M. (2018). Synthesis of spiro[oxindole-3,2′-pyrrolidine] derivatives from benzynes and azomethine ylides through 1,3-dipolar cycloaddition reactions. *J. Org. Chem.* 83 (22): 14102–14109. https://doi.org/10.1021/acs.joc.8b02117.

69 Mali, P.R., Rao, L.C., Bangade, V.M. et al. (2016). A convenient and rapid microwave-assisted synthesis of spirooxindoles in aqueous medium and their antimicrobial activities. *New J. Chem.* 40 (3): 2225–2232. https://doi.org/10.1039/C5NJ02126J.

70 Nasri, S., Bayat, M., and Mirzaei, F. (2021). Recent strategies in the synthesis of spiroindole and spirooxindole scaffolds. *Top. Curr. Chem.* 379 (4): 25. https://doi.org/10.1007/s41061-021-00337-7.

71 Youseftabar-Miri, L., Hosseinjani-Pirdehi, H., Akrami, A., and Hallajian, S. (2020). Recent investigations in the synthesis of spirooxindole derivatives by Iranian researchers. *J. Iran. Chem. Soc.* 17: 2179–2231. https://doi.org/10.1007/s13738-020-01921-2.

72 Nayak, S., Panda, P., Mohapatra, S. et al. (2019). Microwave-assisted one-pot, three-component regiospecific and stereospecific synthesis of spiro indanone pyrrolidine/piperidine fused nitrochromene derivatives through 1,3-dipolar cycloaddition reactions. *J. Heterocycl. Chem.* 56 (6): 1757–1770. https://doi.org/10.1002/jhet.3534.

73 Nayak, S., Pattanaik, P., Mohapatra, S. et al. (2019). One pot, three component synthesis of spiroindenoquinoxaline pyrrolidine fused nitrochromene derivatives following 1,3-dipolar cycloaddition. *Synth. Commun.* 49 (14): 1823–1835. https://doi.org/10.1080/00397911.2019.1606919.

74 Akondi, A.M., Mekala, S., Kantam, M.L. et al. (2017). An expedient microwave assisted regio- and stereoselective synthesis of spiroquinoxaline pyrrolizine derivatives and their AChE inhibitory activity. *New J. Chem.* 41 (2): 873–878. https://doi.org/10.1039/C6NJ02869A.

75 Wu, G., Ouyang, L., Liu, J. et al. (2013). Synthesis of novel spirooxindolo-pyrrolidines, pyrrolizidines, and pyrrolothiazoles via a regioselective three-component [3+2] cycloaddition and their preliminary antimicrobial evaluation. *Mol. Diversity* 17: 271–283. https://doi.org/10.1007/s11030-013-9432-3.

76 Wang, X., Wang, S.Y., and Ji, S.J. (2013). Isocyanide-based multicomponent reactions: catalyst-free stereoselective construction of polycyclic spiroindolines. *Org. Lett.* 15 (8): 1954–1957. https://doi.org/10.1021/ol400606c.

77 Rezaei, S.J.T., Nabid, M.R., Yari, A., and Ng, S.W. (2011). Ultrasound-promoted synthesis of novel spirooxindolo/spiroacenaphthen dicyano pyrrolidines and pyrrolizidines through regioselective azomethine ylide cycloaddition reaction. *Ultrason. Sonochem.* 18 (1): 49–53. https://doi.org/10.1016/j.ultsonch.2010.05.016.

78 Taghizadeh, M.J., Javidan, A., and Keshipour, S. (2015). Synthesis of new bis-spirooxindolopyrrolizidine(pyrrolidine) derivatives via a pseudo five-component 1,3-dipolar cycloaddition reaction. *Chem. Heterocycl. Compd.* 51: 467–471. https://doi.org/10.1007/s10593-015-1722-5.

79 Taghizadeh, M.J. and Jadidi, K. (2014). A novel synthesis of diastereomerically pure spiro-oxindolopyrrolizidines and oxindolopyrrolidines via cycloaddition reactions of azomethine ylides. *Iran. Chem. Commun.* 3: 67–72.

80 Youseftabar-Miri, L. and Hosseinjani-Pirdehi, H. (2017). An efficient approach to the synthesis of some novel heterocycles related to indoline moiety using [bmim]Cl catalysis. *Asian J. Green Chem.* 1 (2): 56–68. https://doi.org/10.22631/ajgc.2017.95721.1017.

81 Azizian, J., Morady, A.V., Soozangarzadeh, S., and Asadi, A. (2002). Synthesis of novel spiro-[3*H*-indole-3,3′-[1,2,4]triazolidine]-2-ones via azomethine imines. *Tetrahedron Lett.* 43 (52): 9721–9723. https://doi.org/10.1016/S0040-4039(02)02061-0.

82 Baharfar, R., Asghari, S., Zaheri, F., and Shariati, N. (2017). Three-component synthesis of novel spirooxindole–furan derivatives using pyridinium salts. *C.R. Chim.* 20 (4): 359–364. https://doi.org/10.1016/j.crci.2016.07.001.

83 Arun, Y., Saranraj, K., Balachandran, C., and Perumal, P.T. (2014). Novel spirooxindole–pyrrolidine compounds: synthesis, anticancer and molecular docking studies. *Eur. J. Med. Chem.* 74: 50–64. https://doi.org/10.1016/j.ejmech.2013.12.027.

84 Arun, Y., Bhaskar, G., Balachandran, C. et al. (2013). Facile one-pot synthesis of novel dispirooxindole-pyrrolidine derivatives and their antimicrobial and anticancer activity against A549 human lung adenocarcinoma cancer cell line. *Bioorg. Med. Chem. Lett.* 23 (6): 1839–1845. https://doi.org/10.1016/j.bmcl.2013.01.023.

85 Kathirvelan, D., Haribabu, J., Reddy, B.S.R. et al. (2015). Facile and diastereoselective synthesis of 3,2′-spiropyrrolidine-oxindoles derivatives, their molecular docking and antiproliferative activities. *Bioorg. Med. Chem. Lett.* 25 (2): 389–399. https://doi.org/10.1016/j.bmcl.2014.10.099.

86 Vidya, S., Priya, K., Jayasree, D.V. et al. (2019). Synthesis of heterocycle appended spiro(oxindole-3,2′-pyrrolidine) derivatives from heterocyclic ylidenes and azomethine ylide through 1,3-dipolar cycloaddition reactions. *Synth. Commun.* 49 (12): 1592–1602. https://doi.org/10.1080/00397911.2019.1605444.

87 Rahmati, A. and Pashmforoush, N. (2015). Synthesis of various heterocyclic compounds via multi-component reactions in water. *J. Iran. Chem. Soc.* 12: 993–1036. https://doi.org/10.1007/s13738-014-0562-z.

88 Ali, S.H. and Sayed, A.R. (2021). Review of the synthesis and biological activity of thiazoles. *Synth. Commun.* 51 (5): 670–700. https://doi.org/10.1080/00397911.2020.1854787.

89 Mari, G., Verboni, M., De Crescentini, L. et al. (2018). Assembly of fully substituted 2,5-dihydrothiophenes via a novel sequential multicomponent reaction. *Org. Chem. Front.* 5 (13): 2108–2114. https://doi.org/10.1039/c8qo00343b.

90 Ramazani, A., Rezaei, A., Mahyari, A.T. et al. (2010). Three-component reaction of an isocyanide and a dialkyl acetylenedicarboxylate with a phenacyl halide in the presence of water: an efficient method for the one-pot synthesis of γ-iminolactone derivatives. *Helv. Chim. Acta* 93 (10): 2033–2036. https://doi.org/10.1002/hlca.201000057.

91 Adib, M., Mahdavi, M., Bagherzadeh, S. et al. (2010). Reaction between anthranilic acids, salicylaldehydes and isocyanides in water: an efficient synthesis of 2-{[2-(alkylimino)-1-benzofuran-3-yliden]amino}benzoic acids. *Tetrahedron Lett.* 51 (1): 27–29. https://doi.org/10.1016/j.tetlet.2009.05.017.

92 Prasanna, P., Balamurugan, K., Perumal, S., and Menéndez, J.C. (2011). A facile, three-component domino protocol for the microwave-assisted synthesis of functionalized naphtho[2,3-*b*]furan-4,9-diones in water. *Green Chem.* 13 (8): 2123–2129. https://doi.org/10.1039/C0GC00952K.

93 Alizadeh, A., Rezvanian, A., and Zhu, L.G. (2012). Synthesis of heterocyclic [3.3.3]propellanes via a sequential four-component reaction. *J. Org. Chem.* 77 (9): 4385–4390. https://doi.org/10.1021/jo300457m.

94 Preeti, S.K.N. (2018). Multicomponent reactions: a sustainable tool to 1,2- and 1,3-azoles. *Org. Biomol. Chem.* 16 (47): 9084–9116. https://doi.org/10.1039/C8OB01872C.

95 Praveen, C., Nandakumar, A., Dheenkumar, P. et al. (2012). Microwave-assisted one-pot synthesis of benzothiazole and benzoxazole libraries as analgesic agents. *J. Chem. Sci.* 124: 609–624. https://doi.org/10.1007/s12039-012-0251-3.

96 Alizadeh, A. and Zohreh, N. (2012). A unique approach to catalyst-free, one-pot synthesis of spirooxindole-pyrazolines. *Synlett* 3: 428–432. https://doi.org/10.1055/s-0031-1290322.

97 Bao, Y., Wang, H., Li, Q. et al. (2012). 2,2′-Biimidazole-based conjugated polymers as a novel fluorescent sensing platform for pyrophosphate anion. *Macromolecules* 45 (8): 3394–3401. https://doi.org/10.1021/ma300361t.

98 Schmidt, A. and Dreger, A. (2011). Recent advances in the chemistry of pyrazoles. Properties, biological activities, and syntheses. *Curr. Org. Chem.* 15 (9): 1423–1463. https://doi.org/10.2174/138527211795378263.

99 Zohreh, N. and Alizadeh, A. (2013). Uncatalyzed one-pot synthesis of highly substituted pyridazines and pyrazoline-spirooxindoles via domino SN/condensation/aza-ene addition cyclization reaction sequence. *ACS Comb. Sci.* 15 (6): 278–286. https://doi.org/10.1021/co400005y.

100 Preeti, S.K.N. (2021). Metal-free multicomponent reactions: a benign access to monocyclic six-membered N-heterocycles. *Org. Biomol. Chem.* 19 (12): 2622–2657. https://doi.org/10.1039/D1OB00145K.

101 Attanasi, O.A., De Crescentini, L., Favi, G. et al. (2011). 1,3,5-Trisubstituted and 5-acyl-1,3-disubstituted hydantoin derivatives via novel sequential three-component reaction. *Org. Lett.* 13 (3): 353–355. https://doi.org/10.1021/ol102664n.

102 Wagare, D.S., Sonone, A., Farooqui, M., and Durrani, A. (2019). An efficient and green microwave-assisted one pot synthesis of imidazothiadiazoles in PEG-400 and water. *Polycyclic Aromat. Compd.* 41 (8): 1749–1754. https://doi.org/10.1080/10406638.2019.1695637.

103 Katritzky, E.F.V., Rees, A.R., and Scriven, C.W. (ed.) (1996). *Comprehensive Heterocyclic Chemistry II*, vol. 3. Oxford: Pergamon Press. ISBN: 9780080965185.

104 Patel, H.A., Ko, D., and Yavuz, C.T. (2014). Nanoporous benzoxazole networks by silylated monomers, their exceptional thermal stability, and carbon dioxide capture capacity. *Chem. Mater.* 26 (23): 6729–6733. https://doi.org/10.1021/cm503627p.

105 Samai, S., Chanda, T., Ila, H., and Singh, M.S. (2013). One-pot three-component heteroannulation of β-oxo dithioesters, amines and hydroxylamine: regioselective, facile and straightforward entry to 5-substituted 3-aminoisoxazoles. *Eur. J. Org. Chem.* 2013 (19): 4026–4031. https://doi.org/10.1002/ejoc.201300038.

106 Sau, P., Santra, S.K., Rakshit, A., and Patel, B.K. (2017). *tert*-Butyl nitrite-mediated domino synthesis of isoxazolines and isoxazoles from terminal aryl alkenes and alkynes. *J. Org. Chem.* 82 (12): 6358–6365. https://doi.org/10.1021/acs.joc.7b00946.

107 Alizadeh, A., Rostamnia, S., Zohreh, N., and Hosseinpour, R. (2009). A simple and effective approach to the synthesis of rhodanine derivatives via three-component reactions in water. *Tetrahedron Lett.* 50 (14): 1533–1535. https://doi.org/10.1016/j.tetlet.2008.12.107.

108 Alizadeh, A., Farajpour, B., Knedel, T.O., and Janiak, C. (2021). Synthesis of substituted phthalimides via ultrasound-promoted one-pot multicomponent reaction. *J. Org. Chem.* 86 (1): 574–580. https://doi.org/10.1021/acs.joc.0c02245.

109 Asif, M., Ali, A., Zafar, A. et al. (2017). Microwave-assisted one pot synthesis, characterization, biological evaluation and molecular docking studies of steroidal thiazoles. *J. Photochem. Photobiol., B* 166: 104–115. https://doi.org/10.1016/j.jphotobiol.2016.11.010.

110 Kumar, D., Sonawane, M., Pujala, B. et al. (2013). Supported protic acid-catalyzed synthesis of 2,3-disubstituted thiazolidin-4-ones: enhancement of the catalytic potential of protic acid by adsorption on solid supports. *Green Chem.* 15 (10): 2872–2884. https://doi.org/10.1039/C3GC41218K.

111 Dalmal, T., Appalanaidu, K., Kosurkar, U.B. et al. (2014). One-pot synthesis of 2-imino-4-(trifluoromethyl)thiazolidin-4-ol derivatives in a three-component reaction: application to structurally diverse scaffolds of biological interest through subsequent reactions. *Eur. J. Org. Chem.* 2014 (12): 2468–2479. https://doi.org/10.1002/ejoc.201301710.

112 Paprocki, D., Madej, A., Koszelewski, D. et al. (2018). Multicomponent reactions accelerated by aqueous micelles. *Front. Chem.* 6: 502. https://doi.org/10.3389/fchem.2018.00502.

113 Tamaddon, F. and Alizadeh, M. (2014). A four-component synthesis of dihydropyrano[2,3-*c*]pyrazoles in a new water-based worm-like micellar medium. *Tetrahedron Lett.* 55 (26): 3588–3591. https://doi.org/10.1016/j.tetlet.2014.04.122.

114 Mandha, S.R., Siliveri, S., Alla, M. et al. (2012). Eco-friendly synthesis and biological evaluation of substituted pyrano[2,3-*c*]pyrazoles. *Bioorg. Med. Chem. Lett.* 22 (16): 5272–5278. https://doi.org/10.1016/j.bmcl.2012.06.055.

115 Mukherjee, P., Paul, S., and Das, A.R. (2015). Expeditious synthesis of functionalized tricyclic 4-spiropyrano[2,3-*c*]pyrazoles in aqueous medium using

dodecylbenzenesulphonic acid as a Brønsted acid–surfactant-combined catalyst. *New J. Chem.* 39 (12): 9480–9486. https://doi.org/10.1039/C5NJ01728A.

116 Dandia, A., Singh, R., Bhaskaran, S., and Samant, S.D. (2011). Versatile three component procedure for combinatorial synthesis of biologically relevant scaffold spiro[indole-thiazolidinones] under aqueous conditions. *Green Chem.* 13 (7): 1852–1859. https://doi.org/10.1039/C0GC00863J.

117 Maity, A., Chakraborty, D., Hazra, A. et al. (2014). Novel betaines/mesoionic compounds via a simple and convenient MCR in aqueous micellar system: synthesis of thiazolo[2,3-*a*]isoquinolin-4-ium derivatives. *Tetrahedron Lett.* 55 (19): 3059–3063. https://doi.org/10.1016/j.tetlet.2014.03.122.

118 Katritzky, E.F.V., Rees, A.R., and Scriven, C.W. (ed.) (1996). *Comprehensive Heterocyclic Chemistry II*, vol. 4. Oxford: Pergamon Press. ISBN: 9780080965185.

119 Nasri, S., Bayat, M., and Kochia, K. (2021). Strategies for synthesis of 1,2,4-triazole-containing scaffolds using 3-amino-1,2,4-triazole. *Mol. Diversity* https://doi.org/10.1007/s11030-021-10197-4.

120 Alves, T.M.F., Jardim, G.A.M., and Ferreira, M.A.B. (2021). A green metal-free "one-pot" microwave assisted synthesis of 1,4-dihydrochromene triazoles. *RSC Adv.* 11 (17): 10336–10339. https://doi.org/10.1039/D1RA01169C.

121 Tisseh, Z.N., Dabiri, M., Nobahar, M. et al. (2012). Catalyst-free, aqueous and highly diastereoselective synthesis of new 5-substituted 1*H*-tetrazoles via a multi-component domino Knoevenagel condensation/1,3 dipolar cycloaddition reaction. *Tetrahedron* 68 (6): 1769–1773. https://doi.org/10.1016/j.tet.2011.12.044.

122 Boltjes, A., Liao, G.P., Zhao, T. et al. (2014). Ugi 4-CR synthesis of γ- and δ-lactams providing new access to diverse enzyme interactions, a PDB analysis. *MedChemComm* 5 (7): 949–952. https://doi.org/10.1039/C4MD00162A.

123 Patil, P., Khoury, K., Herdtweck, E., and Dömling, A. (2015). MCR synthesis of a tetracyclic tetrazole scaffold. *Bioorg. Med. Chem.* 23 (11): 2699–2715. https://doi.org/10.1016/j.bmc.2014.12.021.

124 Lei, X., Lampiri, P., Patil, P. et al. (2021). A multicomponent tetrazolo indole synthesis. *Chem. Commun.* 57 (54): 6652–6655. https://doi.org/10.1039/D1CC02384E.

125 Fu, P., Wnag, S., Hong, K. et al. (2011). Cytotoxic bipyridines from the marine-derived actinomycete *Actinoalloteichus cyanogriseus* WH1-2216-6. *J. Nat. Prod.* 74 (8): 1751–1756. https://doi.org/10.1021/np200258h.

126 Zhang, Y., Liu, Y.B., Li, Y. et al. (2013). Sesquiterpenes and alkaloids from the roots of *Alangium chinense*. *J. Nat. Prod.* 76 (6): 1058–1063. https://doi.org/10.1021/np4000747.

127 Kishbaugh, T.L.S. (2012). Chapter 6.1 – Six-membered ring systems: pyridines and benzo derivatives. *Prog. Heterocycl. Chem.* 24: 343–391. https://doi.org/10.1016/B978-0-08-096807-0.00012-9.

128 Hancock, R.D. (2013). The pyridyl group in ligand design for selective metal ion complexation and sensing. *Chem. Soc. Rev.* 42 (4): 1500–1524. https://doi.org/10.1039/C2CS35224A.

129 Zhang, L. and Jiao, L. (2017). Pyridine-catalyzed radical borylation of aryl halides. *J. Am. Chem. Soc.* 139 (2): 607–610. https://doi.org/10.1021/jacs.6b11813.

130 Baumann, M. and Baxendale, I.R. (2013). An overview of the synthetic routes to the best selling drugs containing 6-membered heterocycles. *Beilstein J. Org. Chem.* 9: 2265–2319. https://doi.org/10.3762/bjoc.9.265.

131 Trist, I.M., Nannetti, G., Tintori, C. et al. (2016). 4,6-Diphenylpyridines as promising novel anti-influenza agents targeting the PA-PB1 protein-protein interaction: structure–activity relationships exploration with the aid of molecular modeling. *J. Med. Chem.* 59 (6): 2688–2703. https://doi.org/10.1021/acs.jmedchem.5b01935.

132 Guan, A.Y., Liu, C.L., Sun, X.F. et al. (2016). Design, synthesis and insecticidal evaluation of aryloxy dihalopropene derivatives. *Bioorg. Med. Chem.* 24 (3): 342–353. https://doi.org/10.1016/j.bmc.2015.09.030.

133 Liu, W., Zheng, C.J., Wang, K. et al. (2015). Novel carbazol-pyridine-carbonitrile derivative as excellent blue thermally activated delayed fluorescence emitter for highly efficient organic light-emitting devices. *ACS Appl. Mater. Interfaces* 7 (34): 18930–18936. https://doi.org/10.1021/acsami.5b05648.

134 Liu, H., Li, J., Chen, W.C. et al. (2020). Efficient yellow thermally activated delayed fluorescent emitters based on 3,5-dicyanopyridine acceptors. *J. Phys. Chem. C* 124 (46): 25489–25498. https://doi.org/10.1021/acs.jpcc.0c08430.

135 Ye, H., Chen, D., Liu, M. et al. (2014). Pyridine-containing electron-transport materials for highly efficient blue phosphorescent OLEDs with ultralow operating voltage and reduced efficiency roll-off. *Adv. Funct. Mater.* 24 (21): 3268–3275. https://doi.org/10.1002/adfm.201303785.

136 Tenti, G., Ramos, M.T., and Menéndez, J.C. (2017). Chapter 1: Synthesis of pyridines by multicomponent reactions. In: *Multicomponent Reactions – Synthesis of Bioactive Heterocycles* (ed. K.L. Ameta and A. Dandia), 1–32. CRC Press – Taylor & Francis Group. ISBN: 9781315369754.

137 Ding, Y., Ma, R., Xiao, X.Q. et al. (2021). Sustainable four-component annulation for the synthesis of 2,3,4,6-tetraarylpyridines. *J. Org. Chem.* 86 (5): 3897–3906. https://doi.org/10.1021/acs.joc.0c02764.

138 Mahmoud, N.F.H. and El-Sewedy, A. (2018). Multicomponent reactions, solvent-free synthesis of 2-amino-4-aryl-6-substituted pyridine-3,5-dicarbonitrile derivatives, and corrosion inhibitors evaluation. *J. Chem.* 2018: 7958739: 9 pages. https://doi.org/10.1155/2018/7958739.

139 Chougala, B.M., Samundeeswari, S., Holiyachi, M. et al. (2017). Microwave synthesis of coumarinyl substituted pyridine derivatives as potent anticancer agents and molecular docking studies. *ChemistrySelect* 2 (18): 5234–5242. https://doi.org/10.1002/slct.201700358.

140 Vardanyan, R. (2017). *Piperidine-Based Drug Discovery*. Amsterdam: Elsevier Ltd. ISBN: 9780128134283.

141 Wang, W. and Hu, Y. (2012). Small molecule agents targeting the p53-MDM2 pathway for cancer therapy. *Med. Res. Rev.* 32 (6): 1159–1196. https://doi.org/10.1002/med.20236.

142 Vitaku, E., Smith, D.T., and Njardarson, J.T. (2014). Analysis of the structural diversity, substitution patterns, and frequency of nitrogen heterocycles among U.S. FDA approved pharmaceuticals. *J. Med. Chem.* 57 (24): 10257–10274. https://doi.org/10.1021/jm501100b.

143 Liu, H., Zhou, Z., Sun, Q. et al. (2012). Synthesis of polysubstituted 2-piperidinones via a Michael addition/nitro-Mannich/lactamization cascade. *ACS Comb. Sci.* 14 (6): 366–371. https://doi.org/10.1021/co300022f.

144 Li, Y., Xue, Z., Ye, W. et al. (2014). One-pot multicomponent synthesis of highly functionalized piperidines from substituted β-nitrostyrenes, meldrum's acid, aromatic aldehydes, and ammonium acetate. *ACS Comb. Sci.* 16 (3): 113–119. https://doi.org/10.1021/co4001502.

145 Vereshchagin, A.N., Karpenko, K.A., Elinson, M.N. et al. (2018). Stereoselective multicomponent synthesis of (2*RS*,6*SR*)-2,6-diaryl-3,3,5,5-tetracyanopiperidines. *Russ. Chem. Bull. Int. Ed.* 67: 1534–1537. https://doi.org/10.1007/s11172-018-2327-9.

146 Vereshchagin, A.N., Karpenko, K.A., Elinson, M.N. et al. (2018). Stereoselective one-pot synthesis of polycyanosubstituted piperidines. *Monatsh. Chem.* 149: 1979–1989. https://doi.org/10.1007/s00706-018-2187-x.

147 Vereshchagin, A.N., Karpenko, K.A., Elinson, M.N. et al. (2018). Pseudo six-component stereoselective synthesis of 2,4,6-triaryl-3,3,5,5-tetracyanopiperidines. *Mendeleev Commun.* 28 (4): 384–386. https://doi.org/10.1016/j.mencom.2018.07.014.

148 Vereshchagin, A.N., Karpenko, K.A., Elinson, M.N. et al. (2018). Four-component stereoselective synthesis of tetracyanosubstituted piperidines. *Res. Chem. Intermed.* 44: 5623–5634. https://doi.org/10.1007/s11164-018-3444-7.

149 Vereshchagin, A.N., Karpenko, K.A., Elinson, M.N. et al. (2020). Highly diastereoselective four-component synthesis of polysubstituted 2-piperidinones with three and four stereogenic centers. *Res. Chem. Intermed.* 46: 1183–1199. https://doi.org/10.1007/s11164-019-04027-4.

150 Vereshchagin, A.N., Karpenko, K.A., Elinson, M.N. et al. (2020). One-pot five-component high diastereoselective synthesis of polysubstituted 2-piperidinones from aromatic aldehydes, nitriles, dialkyl malonates and ammonium acetate. *Mol. Diversity* 24 (4): 1327–1342. https://doi.org/10.1007/s11030-019-09997-6.

151 Ardakani, L.S., Arabmarkadeh, A., and Kazemi, M. (2021). Multicomponent synthesis of highly functionalized piperidines. *Synth. Commun.* 51 (6): 856–879. https://doi.org/10.1080/00397911.2020.1861301.

152 Kangani, M., Hazeri, N., Yazdani-Elah-Abadi, A., and Maghsoodlou, M.T. (2018). Lactic acid: an efficient and green catalyst for the one-pot five-components synthesis of highly substituted piperidines. *Polycyclic Aromat. Compd.* 38 (4): 322–328. https://doi.org/10.1080/10406638.2016.1207686.

153 Nainwal, L.M., Tasneem, S., Akhtar, W. et al. (2019). Green recipes to quinoline: a review. *Eur. J. Med. Chem.* 164: 121–170. https://doi.org/10.1016/j.ejmech.2018.11.026.

154 Matada, B.S. and Yernale, N.G. (2021). The contemporary synthetic recipes to access versatile quinoline heterocycles. *Synth. Commun.* 51 (8): 1133–1159. https://doi.org/10.1080/00397911.2021.1876240.

155 Kulkarni, A. and Torok, B. (2010). Microwave-assisted multicomponent domino cyclization–aromatization: an efficient approach for the synthesis of substituted quinolones. *Green Chem.* 12 (5): 875–878. https://doi.org/10.1039/C001076F.

156 Anvar, S., Mohammadpoor-Baltork, I., Tangestaninejad, S. et al. (2012). Efficient and environmentally-benign three-component synthesis of quinolines and bis-quinolines catalyzed by recyclable potassium dodecatungstocobaltate trihydrate under microwave irradiation. *RSC Adv.* 2 (23): 8713–8720. https://doi.org/10.1039/c2ra20639k.

157 Peng, J.H., Jia, R.H., Ma, N. et al. (2013). A facile and expeditious microwave-assisted synthesis of furo[3,4-*b*]indeno[2,1-*f*]quinolin-1-one derivatives *via* multicomponent reaction. *J. Heterocycl. Chem.* 50 (4): 899–902. https://doi.org/10.1002/jhet.965.

158 Luo, Y., Sun, H., Zhang, W. et al. (2017). Triple zirconocene/Brønsted acid/CuO cooperative and relay catalysis system for tandem Mannich addition/C–C formative cyclization/oxidation. *RSC Adv.* 7 (46): 28616–28625. https://doi.org/10.1039/C7RA00870H.

159 Thigulla, Y., Kumar, T.U., Trivedi, P. et al. (2017). One-step synthesis of fused chromeno[4,3-*b*]pyrrolo[3,2-*h*]quinolin-7(1*H*)-one compounds and their anticancer activity evaluation. *ChemistrySelect* 2 (9): 2718–2721. https://doi.org/10.1002/slct.201700129.

160 Jiang, K.M., Kang, J.A., Jin, Y., and Lin, J. (2018). Synthesis of substituted 4-hydroxyalkyl-quinoline derivatives by a three-component reaction using CuCl/AuCl as sequential catalysts. *J. Org. Chem. Front.* 5 (3): 434–441. https://doi.org/10.1039/C7QO00637C.

161 Anand, N., Chanda, T., Koley, S. et al. (2015). $CuSO_4$-D-glucose, an inexpensive and eco-efficient catalytic system: direct access to diverse quinolines through modified Friedländer approach involving S_NAr/reduction/annulation cascade in one pot. *RSC Adv.* 5 (10): 7654–7660. https://doi.org/10.1039/C4RA14138E.

162 Sarode, P.B., Bahekar, S.P., and Chandak, H.S. (2016). $Zn(OTf)_2$-mediated C–H activation: an expeditious and solvent-free synthesis of aryl/alkyl substituted quinolones. *Tetrahedron Lett.* 57 (51): 5753–5756. https://doi.org/10.1016/j.tetlet.2016.10.113.

163 Mondal, R.R., Khamarui, S., and Maiti, D.K. (2016). CuBr–ZnI_2 combo-catalysis for mild Cu^{I}–Cu^{III} switching and sp^2C–H activated rapid cyclization to quinolines and their sugar-based chiral analogues: a UV–vis and XPS study. *ACS Omega* 1 (2): 251–263. https://doi.org/10.1021/acsomega.6b00185.

164 Mamaghani, M., Tabatabaeian, K., Araghi, R. et al. (2014). An efficient, clean, and catalyst-free synthesis of fused pyrimidines using sonochemistry. *Org. Chem. Int.* 2014: 1–9. https://doi.org/10.1155/2014/406869.

165 Abdolmohammadi, S. (2013). Simple route to indeno[1,2-*b*]quinoline derivatives *via* a coupling reaction catalyzed by TiO_2 nanoparticles. *Chin. Chem. Lett.* 24 (4): 318–320. https://doi.org/10.1016/j.cclet.2013.02.017.

166 Zhang, X., Xu, X., Yu, L., and Zhao, Q. (2014). Three-component reactions of aldehydes, amines, and alkynes/alkenes catalyzed by trifluoromethanesulfonic acid: an efficient route to substituted quinolines. *Asian J. Org. Chem.* 3 (3): 281–284. https://doi.org/10.1002/ajoc.201300212.

167 Yu, C., Zhang, H., Yao, C. et al. (2014). One-pot three-component synthesis of benzo[*f*]thiopyrano[3,4-*b*]quinolin-11(8*H*)-one derivatives. *J. Heterocycl. Chem.* 51 (3): 702–705. https://doi.org/10.1002/jhet.1727.

168 El-Remaily, M.A.E.A.A.A. and Hamad, H.A. (2015). Synthesis and characterization of highly stable superparamagnetic $CoFe_2O_4$ nanoparticles as a catalyst for novel synthesis of thiazolo[4,5-*b*]quinolin-9-one derivatives in aqueous medium. *J. Mol. Catal. A: Chem.* 404, 405: 148–155. https://doi.org/10.1016/j.molcata.2015.04.023.

169 Arabpoor, Z. and Shaterian, H.R. (2016). L-Leucine supported on superparamagnetic silica-encapsulated γ-Fe_2O_3 nanoparticles: design, characterization, and application as a green catalyst for highly efficient synthesis of thiazoloquinolines. *RSC Adv.* 6 (50): 44459–44468. https://doi.org/10.1039/C6RA03736D.

170 Jiang, S., Shen, M., and Sheykhahmad, F.R. (2020). Fe_3O_4@urea/HITh-SO_3H as an efficient and reusable catalyst for the solvent-free synthesis of 7-aryl-8*H*-benzo[*h*]indeno[1,2-*b*]quinoline-8-one and indeno[2′,1′:5,6]pyrido[2,3-*d*]pyrimidine derivatives. *Open Chem.* 18 (1): 648–662. https://doi.org/10.1515/chem-2020-0063.

171 Yuvaraj, P., Manivannan, K., and Reddy, B.S.R. (2015). Microwave-assisted efficient and highly chemoselective synthesis of oxazolo[5,4-*B*]quinoline-fused spirooxindoles via catalyst- and solvent-free three-component tandem Knoevenagel/Michael addition reaction. *Tetrahedron Lett.* 56 (1): 78–81. https://doi.org/10.1016/j.tetlet.2014.11.001.

172 Chidurala, P., Jetti, V., Pagadala, R. et al. (2015). A multicomponent, catalyst-free, one-pot synthesis of functionalized 1,4-dihydroquinolines and their antimicrobial studies. *J. Heterocycl. Chem.* 52 (5): 1302–1307. https://doi.org/10.1002/jhet.2230.

173 Khumalo, M.R., Maddila, S.N., Maddila, S., and Jonnalagadda, S.B. (2019). A multicomponent, facile and catalyst-free microwave-assisted protocol for the synthesis of pyrazolo-[3,4-*b*]-quinolines under green conditions. *RSC Adv.* 9 (53): 30768–30772. https://doi.org/10.1039/c9ra04604f.

174 Bhuyan, D., Sarma, R., and Prajapati, D. (2012). Microwave-assisted efficient synthesis of spiroquinoline derivatives via a catalyst- and solvent-free aza-Diels–Alder reaction. *Tetrahedron Lett.* 53 (47): 6460–6463. https://doi.org/10.1016/j.tetlet.2012.09.081.

175 Kiso, M., Kubo, S., Ozawa, M. et al. (2010). Efficacy of the new neuraminidase inhibitor CS-8958 against H5N1 influenza viruses. *PLoS Pathog.* 6 (2): e1000786. https://doi.org/10.1371/journal.ppat.1000786.

176 Kumar, D., Sharma, P., Singh, H. et al. (2017). The value of pyrans as anticancer scaffolds in medicinal chemistry. *RSC Adv.* 7 (59): 36977–36999. https://doi.org/10.1039/c7ra05441f.

177 Mungra, D.C., Patel, M.P., Rajani, D.P., and Patel, R.G. (2011). Synthesis and identification of β-aryloxyquinolines and their pyrano[3,2-*c*]chromene derivatives as a new class of antimicrobial and antituberculosis agents. *Eur. J. Med. Chem.* 46 (9): 4192–4200. https://doi.org/10.1016/j.ejmech.2011.06.022.

178 Tashrifi, Z., Mohammadi-Khanaposhtani, M., Hamedifar, H. et al. (2020). Synthesis and pharmacological properties of polysubstituted 2-amino-4*H*-pyran-3-carbonitrile derivatives. *Mol. Diversity* 24 (4): 1385–1431. https://doi.org/10.1007/s11030-019-09994-9.

179 Zonouz, A.M., Eskandari, I., and Khavasi, H.R. (2012). A green and convenient approach for the synthesis of methyl 6-amino-5-cyano-4-aryl-2,4-dihydropyrano[2,3-*c*]pyrazole-3-carboxylates via a one-pot, multi-component reaction in water. *Tetrahedron Lett.* 53 (41): 5519–5522. https://doi.org/10.1016/j.tetlet.2012.08.010.

180 Zhang, M., Fu, Q.Y., Gao, G. et al. (2017). Catalyst-free, visible-light promoted one-pot synthesis of spirooxindole-pyran derivatives in aqueous ethyl lactate. *ACS Sustainable Chem. Eng.* 5 (7): 6175–6182. https://doi.org/10.1021/acssuschem eng.7b01102.

181 Brahmachari, G. and Nurjamal, K. (2017). Facile and chemically sustainable catalyst-free synthesis of diverse 2-aryl-4-alkyl/aryl-pyrano[3,2-*c*]chromen-5(4*H*)-ones by one-pot multicomponent reactions at room temperature. *ChemistrySelect* 2 (13): 3695–3702. https://doi.org/10.1002/slct.201700687.

182 Mishra, R. and Choudhury, L.H. (2016). Catalyst-free microwave-assisted arylglyoxal-based multicomponent reactions for the synthesis of fused pyrans. *RSC Adv.* 6 (29): 24464–24469. https://doi.org/10.1039/c5ra25536h.

183 Lu, C.W., Wang, J.J., Li, F., and Yu, S.J. (2018). Efficient synthesis of 2-amino-3-cyano-4*H*-pyran derivatives via a non-catalytic one-pot three-component reaction. *Res. Chem. Intermed.* 44: 1035–1043. https://doi.org/10.1007/s11164-017-3151-9.

184 Safaei, H.R., Shekouhy, M., Rahmanpur, S., and Shirinfeshan, A. (2012). Glycerol as a biodegradable and reusable promoting medium for the catalyst-free one-pot three component synthesis of 4*H*-pyrans. *Green Chem.* 14 (6): 1696–1704. https://doi.org/10.1039/C2GC35135H.

185 Khan, M.M., Shareef, S., Saigal, and Sahoo, S.C. (2019). A catalyst- and solvent-free protocol for the sustainable synthesis of fused 4*H*-pyran derivatives. *RSC Adv.* 9 (45): 26393–26401. https://doi.org/10.1039/c9ra04370e.

186 Pathania, S., Narang, R.K., and Rawal, R.K. (2019). Role of Sulphur-heterocycles in medicinal chemistry: an update. *Eur. J. Med. Chem.* 180: 486–508. https://doi.org/10.1016/j.ejmech.2019.07.043.

187 Casy, G. and Taylor, R.J.K. (1989). The synthesis of 2,3-disubstituted cyclopentenones using the Ramberg–Baecklund reaction in conjunction with organocopper chemistry. *Tetrahedron* 45: 455–466.

188 Ward, D.E., Jheengut, V., and Beye, G.E. (2006). Thiopyran route to polypropionates: an efficient synthesis of serricornin. *J. Org. Chem.* 71 (23): 8989–8992. https://doi.org/10.1021/jo061747w.

189 (a) McDonald, B.P., Steele, R.W., Sutherland, J.K. et al. (1988). Synthetic approaches to thiathromboxanes. Part 2. Synthesis of structural isomers of thiathromboxane A2. *J. Chem. Soc., Perkin Trans.* 1: 675–679. (b) Casy, G., Lane, S., and Taylor, R.J.K. (1986). Preparation of thiathromboxane analogs and formal total synthesis of dithiathromboxane A2 based on conjugate addition reactions of thiin-4-ones. *J. Chem. Soc., Perkin Trans.* 1: 1397–1404.

190 Chowdhury, S., Nandi, G.C., Samai, S., and Singh, M.S. (2011). Regioselective synthesis of tetrahydrothiochromen-5-ones via a one-pot three-component solvent-free domino protocol. *Org. Lett.* 13 (14): 3762–3765. https://doi.org/10.1021/ol201458q.

191 Verma, R.K., Verma, G.K., Shukla, G. et al. (2012). 4-Dimethylamino pyridine-promoted one-pot three-component regioselective synthesis of highly functionalized 4*H*-thiopyrans via heteroannulation of β-oxodithioesters. *ACS Comb. Sci.* 14 (3): 224–230. https://doi.org/10.1021/co200203e.

192 Koley, S., Chowdhury, S., Chanda, T. et al. (2013). Diversity oriented catalyst-free and solvent-free one-pot MCR at room temperature: rapid and regioselective convergent approach to highly functionalized dihydro-4*H*-thiopyrans. *Tetrahedron* 69 (37): 8013–8018. https://doi.org/10.1016/j.tet.2013.07.001.

193 Deibl, N., Ament, K., and Kempe, R. (2015). A sustainable multicomponent pyrimidine synthesis. *J. Am. Chem. Soc.* 137 (40): 12804–12807. https://doi.org/10.1021/jacs.5b09510.

194 Mastalir, M., Glatz, M., Pittenauer, E. et al. (2016). Sustainable synthesis of quinolines and pyrimidines catalyzed by manganese PNP pincer complexes. *J. Am. Chem. Soc.* 138 (48): 15543–15546. https://doi.org/10.1021/jacs.6b10433.

195 Deibl, N. and Kempe, R. (2017). Manganese-catalyzed multicomponent synthesis of pyrimidines from alcohols and amidines. *Angew. Chem. Int. Ed.* 56 (6): 1663–1666; *Angew. Chem*. (2017) 129: 1685–1688. https://doi.org/10.1002/anie.201611318.

196 Poly, S.S., Siddiki, S.M.A.H., Touchy, A.S. et al. (2018). Acceptorless dehydrogenative synthesis of pyrimidines from alcohols and amidines catalyzed by supported platinum nanoparticles. *ACS Catal.* 8 (12): 11330–11341. https://doi.org/10.1021/acscatal.8b02814.

197 Mondal, R., Sinha, S., Das, S. et al. (2020). Iron catalyzed synthesis of pyrimidines under air. *Adv. Synth. Catal.* 362 (3): 594–600. https://doi.org/10.1002/adsc.201901172.

198 Biginelli, P. (1893). Aldehyde-urea derivatives of aceto- and oxaloacetic acids. *Gazz. Chim. Ital.* 23: 360–413.

199 Fatima, A., Braga, T.C., Neto, L.S. et al. (2015). A mini-review on Biginelli adducts with notable pharmacological properties. *J. Adv. Res.* 6 (3): 363–373. https://doi.org/10.1016/j.jare.2014.10.006.

200 Nagarajaiah, H., Mukhopadhyay, A., and Moorthy, J.N. (2016). Biginelli reaction: an overview. *Tetrahedron Lett.* 57 (47): 5135–5149. https://doi.org/10.1016/j.tetlet.2016.09.047.

201 Suresh, A. and Sandhu, J.S. (2012). Past, present and future of the Biginelli reaction: a critical perspective. *Arkivoc* 2012 (1): 66–133. https://doi.org/10.3998/ark.5550190.0013.103.

202 Rathwa, S.K., Vasava, M.S., Bhoi, M.N. et al. (2018). Recent advances in the synthesis of C-5-substituted analogs of 3,4-dihydropyrimidin-2-ones: a review. *Synth. Commun.* 48 (9): 963–994. https://doi.org/10.1080/00397911.2017.1423503.

203 Chopda LV, Dave PN. Recent advances in homogeneous and heterogeneous catalyst in Biginelli reaction from 2015–19: a concise review. *ChemistrySelect* 2020;5(19): 5552–5572. https://doi.org/10.1002/slct.202000742.

204 Mohammadi, B. and Behbahani, F.K. (2018). Recent developments in the synthesis and applications of dihydropyrimidin-2(1*H*)-ones and thiones. *Mol. Diversity* 22: 405–446. https://doi.org/10.1007/s11030-017-9806-z.

205 Fatima, A., Terra, B.S., Neto, L.S., and Braga, T.C. (2015). Chapter 12: organocatalyzed Biginelli reactions: a greener chemical approach for the synthesis of biologically active 3,4-dihydropyrimidin-2(1*H*)-ones/-thiones. In: *Green Synthetic Approaches for Biologically Relevant Heterocycles* (ed. G. Brahmachari), 317–337. Amsterdam: Elsevier Inc. https://doi.org/10.1016/B978-0-12-800070-0.00012-8.

206 Rao, G.B.D., Acharya, B.N., and Kaushik, M.P. (2013). An efficient synthesis of β-ketoesters via transesterification and its application in Biginelli reaction under solvent-free, catalyst-free conditions. *Tetrahedron Lett.* 54 (48): 6644–6647. https://doi.org/10.1016/j.tetlet.2013.09.130.

207 Wang, R. and Liu, Z.Q. (2012). Solvent-free and catalyst-free Biginelli reaction to synthesize ferrocenoyl dihydropyrimidine and kinetic method to express radical-scavenging ability. *J. Org. Chem.* 77 (8): 3952–3958. https://doi.org/10.1021/jo300282y.

208 Guo, Y., Tang, H., Gao, Z. et al. (2017). Solvent-free and catalyst-free Biginelli reaction to synthesize 4-alkyl-3,4-dihydropyrimidin-2-(1*H*)-ones. *ChemistrySelect* 2 (27): 8253–8255. https://doi.org/10.1002/slct.201701466.

209 Balan, B. and Bhulayan, D. (2014). A novel green synthesis of α/β-amino acid functionalized pyrimidinone peptidomimetics using triazole ligation through click-multi-component reactions. *Tetrahedron Lett.* 55 (1): 227–231. https://doi.org/10.1016/j.tetlet.2013.11.002.

210 Carvalho, R.B. and Joshi, S.V. (2019). Solvent and catalyst free synthesis of 3,4-dihydropyrimidin-2(1*H*)-ones/thiones by twin screw extrusion. *Green Chem.* 21 (8): 1921–1924. https://doi.org/10.1039/c9gc00036d.

211 M'hamed, M.O., Alshammari, A.G., and Lemine, O.M. (2016). Green high-yielding one-pot approach to Biginelli reaction under catalyst-free and solvent-free ball milling conditions. *Appl. Sci.* 6 (12): 431. https://doi.org/10.3390/app6120431.

212 Harikrishnan, P.S., Rajesh, S.M., Perumal, S., and Almansour, A.I. (2013). A microwave-mediated catalyst- and solvent-free regioselective Biginelli reaction in the synthesis of highly functionalized novel tetrahydropyrimidines. *Tetrahedron Lett.* 54 (9): 1076–1079. https://doi.org/10.1016/j.tetlet.2012.12.034.

213 Heravi, M.M., Asadi, S., and Lashkariani, B.M. (2013). Recent progress in asymmetric Biginelli reaction. *Mol. Diversity* 17: 389–407. https://doi.org/10.1007/s11030-013-9439-9.

214 Heravi, M.M., Moradi, R., Mohammadkhani, L., and Moradi, B. (2018). Current progress in asymmetric Biginelli reaction: an update. *Mol. Diversity* 22 (3): 751–767. https://doi.org/10.1007/s11030-018-9841-4.

215 Barbero, M., Cadamuro, S., and Dughera, S. (2017). A Brønsted acid catalysed enantioselective Biginelli reaction. *Green Chem.* 19 (6): 1529–1535. https://doi.org/10.1039/c6gc03274e.

216 Selvam, T.P. and Kumar, P.V. (2011). Quinazoline marketed drugs. *Res. Pharm.* 1: 1–21.

217 Raymond, E., Faivre, S., and Armand, J. (2000). Epidermal growth factor receptor tyrosine kinase as a target for anticancer therapy. *Drugs* 60: 15–23. https://doi.org/10.2165/00003495-200060001-00002.

218 Pao, W., Mille, V., Zakowski, M. et al. (2004). EGF receptor gene mutations are common in lung cancers from "never smokers" and are associated with sensitivity of tumors to gefitinib and erlotinib. *Proc. Natl. Acad. Sci. U.S.A.* 101 (36): 13306–13311. https://doi.org/10.1073/pnas.0405220101.

219 Sarma, R. and Prajapati, D. (2011). Microwave-promoted efficient synthesis of dihydroquinazolines. *Green Chem.* 13 (3): 718–722. https://doi.org/10.1039/c0gc00838a.

220 Derabli, C., Boulcina, R., Kirsch, G. et al. (2014). A DMAP-catalyzed mild and efficient synthesis of 1,2-dihydroquinazolines via a one-pot three-component protocol. *Tetrahedron Lett.* 55 (1): 200–204. https://doi.org/10.1016/j.tetlet.2013.10.157.

221 Panja, S.K., Dwivedi, N., and Saha, S. (2012). I_2-catalyzed three-component protocol for the synthesis of quinazolines. *Tetrahedron Lett.* 53 (46): 6167–6172. https://doi.org/10.1016/j.tetlet.2012.08.016.

222 Panja, S.K. and Saha, S. (2013). Recyclable, magnetic ionic liquid bmim[$FeCl_4$]-catalyzed, multicomponent, solvent-free, green synthesis of quinazolines. *RSC Adv.* 3 (34): 14495–14500. https://doi.org/10.1039/c3ra42039f.

223 Bhat, S.I., Das, U.K., and Trivedi, D.R. (2015). An efficient three-component, one-pot synthesis of quinazolines under solvent-free and catalyst-free condition. *J. Heterocycl. Chem.* 52 (4): 1253–1259. https://doi.org/10.1002/jhet.2220.

224 Zhao, D., Shen, Q., and Li, J.X. (2015). Potassium iodide-catalyzed three-component synthesis of 2-arylquinazolines via amination of benzylic C—H bonds of methylarenes. *Adv. Synth. Catal.* 357 (2, 3): 339–344. https://doi.org/10.1002/adsc.201400827.

225 Chen, J., Natte, K., Neumann, H., and Wu, X.F. (2014). A convenient palladium-catalyzed carbonylative synthesis of quinazolines from 2-aminobenzylamine and aryl bromides. *RSC Adv.* 4 (99): 56502–56505. https://doi.org/10.1039/C4RA11303A.

226 Hu, K., Zhen, Q., Gong, J. et al. (2018). Palladium-catalyzed three-component tandem process: one-pot assembly of quinazolines. *Org. Lett.* 20 (10): 3083–3087. https://doi.org/10.1021/acs.orglett. 8b01070.

227 Fan, X., Li, B., Guo, S. et al. (2014). Synthesis of quinazolines and tetrahydroquinazolines: copper-catalyzed tandem reactions of 2-bromobenzyl bromides with aldehydes and aqueous ammonia or amines. *Chem. Asian J.* 9 (3): 739–743. https://doi.org/10.1002/asia.201301296.

228 Liu, L.Y., Yan, Y.Z., Bao, Y.J., and Wang, Z.Y. (2015). Efficient synthesis of 2-arylquinazolines via copper-catalyzed dual oxidative benzylic C–H aminations of methylarenes. *Chin. Chem. Lett.* 26 (10): 1216–1220. https://doi.org/10.1016/j.cclet.2015.07.008.

229 Battula, S., Vishwakarma, R.A., and Ahmed, Q.N. (2014). Cu–benzotriazole-catalyzed electrophilic cyclization of *N*-arylimines: a methodical tandem approach to O-protected-4-hydroxyquinazolines. *RSC Adv.* 4 (72): 38375–38378. https://doi.org/10.1039/C4RA07377K.

230 Ju, J., Hua, R., and Su, J. (2012). Copper-catalyzed three-component one-pot synthesis of quinazolines. *Tetrahedron* 68 (46): 9364–9370. https://doi.org/10.1016/j.tet.2012.09.035.

231 Baghbanian, S.M. and Farhang, M. (2014). $CuFe_2O_4$ nanoparticles: a magnetically recoverable and reusable catalyst for the synthesis of quinoline and quinazoline derivatives in aqueous media. *RSC Adv.* 4 (23): 11624–11633. https://doi.org/10.1039/c3ra46119j.

232 Guo, S., Tao, L., Zhang, W. et al. (2015). Regioselective synthesis of indolo[1,2-*c*]quinazolines and 11*H*-indolo[3,2-*c*]quinolines via copper-catalyzed cascade reactions of 2-(2-bromoaryl)-1*H*-indoles with aldehydes and aqueous ammonia. *J. Org. Chem.* 80 (21): 10955–10964. https://doi.org/10.1021/acs.joc.5b02076.

233 Chen, Z., Chen, J., Liu, M. et al. (2013). Unexpected copper-catalyzed cascade synthesis of quinazoline derivatives. *J. Org. Chem.* 78 (14): 11342–11348. https://doi.org/10.1021/jo401908g.

234 Zhang, Z.H., Zhang, X.N., Mo, L.P. et al. (2012). Catalyst-free synthesis of quinazoline derivatives using low melting sugar–urea–salt mixture as a solvent. *Green Chem.* 14 (5): 1502–1506. https://doi.org/10.1039/c2gc35258c.

235 Hossaini, Z., Rostami-Charati, F., Seyfi, S., and Ghambarian, M. (2013). Multicomponent reactions for the synthesis of functionalized 1,4-oxathiane-3-thiones under microwave irradiation in water. *Chin. Chem. Lett.* 24 (5): 376–378. https://doi.org/10.1016/j.cclet.2013.03.003.

236 Samzadeh-Kermani, A. (2014). An efficient one-pot synthesis of 1,4-oxathiane and 1,4-thiomorpholine derivatives. *Synlett* 25 (13): 1839–1842. https://doi.org/10.1055/s-0034-1378277.

237 Khalaj, M. and Ghazanfarpor-Darjani, M. (2016). Regioselective synthesis of 1,4-oxathiane derivatives via multicomponent reaction. *Monatsh. Chem.* 147 (12): 2043–2049. https://doi.org/10.1007/s00706-016-1845-0.

238 Keshtegar, Z., Heydari, R., and Samzadeh-Kermani, A. (2021). Organo-catalytic synthesis of oxathians from isocyanides, isothiocyanates, and oxiranes. *J. Sulfur Chem.* 42 (1): 1–14. https://doi.org/10.1080/17415993.2020.1797742.

239 Ghazanfarpour-Darjani, M., Babapour-Kooshalshahi, M., Mousavi-Safavi, S.M. et al. (2016). Copper-catalyzed domino addition–cyclization reaction between

terminal alkynes, carbon disulfide, and oxiranes. *Synlett* 27 (02): 259–261. https://doi.org/10.1055/s-0035-1560486.

240 Badashah, S.L. and Naeem, A. (2016). Bioactive thiazine and benzothiazine derivatives: green synthesis methods and their medicinal importance. *Molecules* 21 (8): 1054. https://doi.org/10.3390/molecules21081054.

241 Kruthof, A., Ploeger, M.L., Janssen, E. et al. (2012). Multicomponent synthesis of 3,6-dihydro-2*H*-1,3-thiazine-2-thione. *Molecules* 17 (2): 1675–1685. https://doi.org/10.3390/molecules17021675.

242 Mehrabi, H. and Esfandiarpour, Z. (2015). A facile and effective procedure for the synthesis of new 1,3-thiazine-2-thione derivatives. *J. Sulfur Chem.* 36 (6): 583–590. https://doi.org/10.1080/17415993.2015.1072718.

243 Zhuang, Q.Y., Wang, X., Gao, Y. et al. (2011). Diversity-oriented synthesis of spiro-substituted 1,3-thiazine library via a one-pot, two-step, three-component reaction. *ACS Comb. Sci.* 13 (1): 84–88. https://doi.org/10.1021/co100034v.

244 Hussen, A.S., Monga, A., and Sharma, A. (2019). Regioselective synthesis of functionalized 1,3-thiazine-4-ones *via* multicomponent Click reaction approach. *ChemistrySelect* 4 (2): 650–654. https://doi.org/10.1002/slct.201803634.

245 Wadhwa, P., Hussen, A.S., and Sharma, A. (2017). A multicomponent strategy for the regioselective synthesis of [1,3]-thiazinones from an abundant feedstock: scope and structural elucidation. *Asian J. Org. Chem.* 6 (1): 88–94. https://doi.org/10.1002/ajoc.201600420.

246 (a) Shah, D.R., Modh, R.P., and Chikhalia, K.H. (2014). Privileged *s*-triazines: structure and pharmacological applications. *Future Med. Chem.* 6 (4): 463–477. https://doi.org/10.4155/FMC.13.212. (b) Sharma, A., Sheyi, R., Torre, B.G. et al. (2021). s-Triazine: a privileged structure for drug discovery and bioconjugation. *Molecules* 26 (4): 864. https://doi.org/10.3390/molecules26040864.

247 Kim, E.S. (2017). Enasidenib: first global approval. *Drugs* 77: 1705–1711. https://doi.org/10.1007/s40265-017-0813-2.

248 Pan, L., Li, Z., Ding, T. et al. (2017). Base-mediated synthesis of unsymmetrical 1,3,5-triazin-2-amines via three-component reaction of imidates, guanidines, and amides or aldehydes. *J. Org. Chem.* 82 (19): 10043–10050. https://doi.org/10.1021/acs.joc.7b01510.

249 Guo, W., Zhao, M., Du, C. et al. (2019). Visible-light-catalyzed [3+1+2] coupling annulations for the synthesis of unsymmetrical trisubstituted amino-1,3,5-triazines. *J. Org. Chem.* 84 (23): 15508–15519. https://doi.org/10.1021/acs.joc.9b02514.

250 Rodríguez, H., Suárez, M., and Albericio, F. (2012). Thiadiazines, N,N-heterocycles of biological relevance. *Molecules* 17 (7): 7612–7628. https://doi.org/10.3390/molecules17077612.

251 Moghimi, S., Shiri, M., Heravi, M.M., and Kruger, H.G. (2013). A novel and easy route to 1,3,4-thiadiazine derivatives via the three-component reaction of phenylhydrazine, α-bromo aryl ketones and aryl isothiocyanates. *Tetrahedron Lett.* 54 (46): 6215–6217. https://doi.org/10.1016/j.tetlet.2013.09.008.

252 Mishra, A., Rai, P., Singh, J., and Singh, J. (2018). A visible-light-mediated protocol: one-pot-three-component, sustainable synthesis of 1,3,4-thiadiazines. *ChemistrySelect* 3 (29): 8408–8414. https://doi.org/10.1002/slct.201801508.

253 Bhattacharjee, J., Harinath, A., Sarkar, A., and Panda, T.K. (2019). Polymerization of ε-caprolactam to nylon-6 catalyzed by barium σ-borane complex under mild condition. *ChemCatChem* 11 (15): 3366–3370. https://doi.org/10.1002/cctc.201900920.

254 Samanidou, V.F., Nika, M.K., and Papadoyannis, I.N. (2014). HPLC and its essential role in the analysis of tricyclic antidepressants in biological samples. *Recent Adv. Med. Chem.* 1: 332–380. https://doi.org/10.1016/B978-0-12-803961-8.50011-7.

255 Boddu, S.H.S. and Kumari, S. (2020). A short review on the intranasal delivery of diazepam for treating acute repetitive seizures. *Pharmaceutics* 12 (12): 1167. https://doi.org/10.3390/pharmaceutics12121167.

256 Ghandi, M., Zarezadeh, N., and Taheri, A. (2011). A novel isocyanide-based three-component synthesis of benzimidazo[1,2-*a*][1,4]diazepinones. *Tetrahedron Lett.* 52 (11): 1228–1232. https://doi.org/10.1016/j.tetlet.2011.01.073.

257 Barlow, T.M.A., Jida, M., Tourwé, D., and Ballet, S. (2014). Efficient synthesis of conformationally constrained, amino-triazoloazepinone-containing di- and tripeptides via a one-pot Ugi–Huisgen tandem reaction. *Org. Biomol. Chem.* 12 (36): 6986–6989. https://doi.org/10.1039/c4ob01381f.

258 Noushini, S., Mahdavi, M., Firoozpour, L. et al. (2015). Efficient multicomponent synthesis of 1,4-benzodiazepine-3,5-diones: a Petasis-based approach. *Tetrahedron* 71 (36): 6272–6275. https://doi.org/10.1016/j.tet.2015.06.060.

259 Dighe, N.S., Vikhe, S.B., Tambe, P.R. et al. (2015). Pharmacological and synthetic profile of benzothiazepine: a review. *Int. J. Pharm. Chem.* 5 (2): 31–39. https://doi.org/10.7439/ijpc.v5i2.1532.

260 El-Bayouki, K.A.M. (2011). Synthesis, reactions, and biological activity of 1,4-thiazepines and their fused aryl and heteroaryl derivatives: a review. *J. Sulfur Chem.* 32 (6): 623–690. https://doi.org/10.1080/17415993.2011.607165.

261 Buckley, M.M.-T., Grant, S.M., Goa, K.L. et al. (1990). Diltiazem. A reappraisal of its pharmacological properties and therapeutic use. *Drugs* 39 (5): 757–806. https://doi.org/10.2165/00003495-199039050-00009.

262 Dando, T.M. and Keating, G.M. (2005). Quetiapine: a review of its use in acute mania and depression associated with bipolar disorder. *Drugs* 65 (17): 2533–2551. https://doi.org/10.2165/00003495-200565170-00008.

263 Arakawa, M., Sasaki, M., Ohmori, M. et al. (2001). Pharmacokinetics and pharmacodynamics of temocapril during repeated dosing in elderly hypertensive patients. *Eur. J. Clin. Pharmacol.* 56 (11): 775–779. https://doi.org/10.1007/s002280000237.

264 Dandia, A., Singh, R., Joshi, J. et al. (2013). Ultrasound promoted catalyst-free and selective synthesis of spiro[indole-3,49-pyrazolo[3,4-*e*][1,4]thiazepines] in aqueous media and evaluation of their anti-hyperglycemic activity. *RSC Adv.* 3 (41): 18992–19001. https://doi.org/10.1039/c3ra43745k.

265 Kommidi, D.R., Pagadala, R., Varkolu, M. et al. (2017). New route for the synthesis of thiazolidine 2,4-dione azepine derivatives. *J. Heterocycl. Chem.* 54 (2): 1071–1076. https://doi.org/10.1002/jhet.2676.

266 Shaabani, S., Shaabani, A., Kucerakova, M., and Dusek, M. (2019). A one-pot synthesis of oxazepine-quinazolinone bis-heterocyclic scaffolds via isocyanide-based three-component reactions. *Front. Chem.* 7: 623. https://doi.org/10.3389/fchem.2019.00623.

267 Rasouli, M.A., Mahdavi, M., Ranjbar, P.R. et al. (2012). A green one-pot synthesis of *N*-alkyl-2-(2-oxoazepan-1-yl)-2-arylacetamide derivatives via an Ugi four-center, three-component reaction in water. *Tetrahedron Lett.* 53 (52): 7088–7092. https://doi.org/10.1016/j.tetlet.2012.10.075.

268 Audia, J.E., Hyslop, P.A., Nissen, J.S., et al. (2000). Biological reagents and methods for determining the mechanism in the generation of β-amyloid peptide. WO0019210A2.

269 Mehta, V.P., Modha, S.G., Ruijter, E. et al. (2011). A microwave-assisted diastereoselective multicomponent reaction to access dibenzo[*c*,*e*]azepinones: synthesis and biological evaluation. *J. Org. Chem.* 76 (8): 2828–2839. https://doi.org/10.1021/jo200251q.

8

Heterocyclic Compounds from Renewable Resources

Giuseppe Mele[1], Selma E. Mazzetto[2], and Diego Lomonaco[2]

[1] University of Salento, Department of Engineering for Innovation, Via Monteroni, 73100 Lecce, Italy
[2] Federal University of Ceará, Department of Organic and Inorganic Chemistry, Campus Pici, 60440-900 Fortaleza, Brazil

8.1 Introduction

The use of renewable feedstocks rather than depleting natural resources is one of the principles of the green chemistry. Since the interest in a bio-based economy continues to grow, platform molecules must be obtained from biomass in order to gradually overcome those supplied by fossil resources (coal, gas, and oil).

Bio-based feedstock can be differentiated into polysaccharides, lignin, proteins, and extractives (e.g. triglycerides and terpenes), being found as components within biomass in different proportions. Therefore, one of the main challenges that our society is facing is the effective and economically viable development of bio-based alternatives to traditional fossil-based products. Many efforts are being made in this sense, namely, technological development of biorefineries [1], alternative pathways for more sustainable fuels [2], and the revalorization of agro-wastes as a source of raw materials for chemical industry [3–5].

In the perspective of bio-based platforms for fine chemicals, the importance of cardanol, a low cost, largely available renewable material obtained from distillation of cashew nut shell liquid (CNSL), a well-known waste of the cashew agroindustry, has increased in recent years [6]. This will be the main focus of this chapter.

CNSL is an oil, considered as the main source of renewable phenolic lipids. It is mainly composed by anacardic acid (**1**), cardanol (**2**), cardol (**3**), and 2-methylcardol (**4**).

These phenolic compounds are very peculiar, since they have attached to the aromatic ring a long alkyl side chain containing 15 carbon, with different degrees of unsaturations (up to three double bonds) and with *cis*-configuration (Figure 8.1).

Since CNSL is obtained as a by-product of the processing of cashew kernel (*Anacardium occidentale* L.) for the food industry, CNSL may present two different basic chemical compositions depending on the extraction method: solvent-extracted or cold-pressed, giving "natural CNSL", or industrial hot-oil process, giving "technical CNSL". "Natural CNSL" represents the original composition and nature of CNSL,

Heterocycles: Synthesis, Catalysis, Sustainability, and Characterization, First Edition.
Edited by Teresa M.V.D. Pinho e Melo and Marta Pineiro.

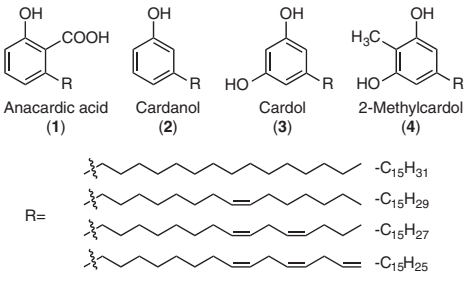

Figure 8.1 Chemical composition of CNSL.

basically composed of anacardic acids (60–70%), cardols (10–20%), cardanols (3–10%), and 2-methylcardols (2–5%), while in "technical CNSL", due to the elevated temperatures employed in the extraction procedure, anacardic acid suffers a decarboxylation, transforming into cardanol, which becomes its main constituent [7].

This chapter reviews some of the developments in the synthesis of different CNSL-based heterocycles, focusing in the main reactive sites of CNSL constituents: (i) the phenolic hydroxyl group; (ii) the aromatic ring itself, containing highly nucleophilic carbon atoms; and (iii) the unsaturations present in the 15 carbon-long alkyl side chain attached to the meta position of the phenolic ring. We also highlight some technological applications, since their use in industry is increasing each year due to the updates in legislations and policies related to chemical safety and sustainability.

Herein, an overview of the progresses of research activities related with the synthesis of functional heterocyclic systems using mainly cardanol or structural analogs (i.e. anacardic acid, cardol, methylcardol) derived from the CNSL is described. This renewable feedstock has a great potential in the field of green chemistry and design of innovative environmentally friendly materials and processes. In fact, the molecular features of cardanol allow many chemical transformations producing a large variety of fine chemicals and multifunctional heterocyclic hybrid materials. The synthetic strategies for the preparation of cardanol-based heterocycles with different ring sizes and their use as precursors of functional organic, soft, and composite materials are highlighted.

8.2 Three-, Five-, Six-, and Seven-Membered Ring Heterocycles Based on CNSL

8.2.1 Oxiranes (Epoxides)

Oxirane rings are three-membered cyclic ethers. Most commonly known as epoxides, due to their highly strained rings, this class of substances has high reactivity, which can be explored in the development of many different applications.

The main chemical process to obtain epoxides starts from alkenes, which are converted into the target compounds by treatment with peroxy acids, which act as oxygen atom donors, in a reaction named after its inventor N. Prileschajew, who

reported this protocol in 1909 [8]. Another procedure to obtain epoxy compounds involves the reaction of alcohols (aliphatic or aromatic) with epichlorohydrin, under alkaline media, through a procedure called glycidylation [9].

Nowadays, the most used epoxy in industry is the diglycidyl ether (DGEBA) obtained from glycidylation of bisphenol A (BPA), a molecule that has estrogen-like activity and may act as an endocrine disruptor, mimicking human hormones that are correlated to negative health effects [10]. Therefore, there is a growing interest in finding sustainable alternatives of BPA for the synthesis of many different products. In this context, CNSL and/or its derivatives rise as potential candidates for the effective substitution, or partial replacements, to BPA in the chemical industry.

Articles reporting the use of cardanol as starting material for the synthesis of epoxides date back to the 1980s.

Patel and coworkers reported the synthesis of cardanol-based mono- and di-epoxy derivatives and evaluated their use as reactive diluent for the polymerization of diglycidyl ether of bisphenol A (DGEBA) in the presence of different hardeners. First, the authors promoted the glycidylation of cardanol phenolic hydroxyl group using epichlorohydrin, obtaining the mono-epoxy derivative. In a second reaction, the double bonds were oxidized by using *m*-chloroperbenzoic acid (*m*CPBA), as shown in Figure 8.2 [11, 12].

An eco-friendly approach for the oxidation of cardanol's double bonds was proposed by Suresh, a peracid oxidation in which the oxidant is generated *in situ* through reaction of formic acid with aqueous hydrogen peroxide. The advantages of this protocol include the low cost of oxidants, high active oxygen content, high oxidation potential, and the formation of water as reaction by-product [13].

In a more recent approach, Palmese's group investigated the epoxidation of terminal double bond of the side chain of cardanol glycidyl ether (SCECGE) (Scheme 8.1). Due to their reduced electronegativity, compared with internal ones, terminal double bonds are not epoxidized under traditional protocols. Therefore, authors employed potassium peroxomonosulfate (Oxone®) in the presence of 1,1,1-trifluoroacetone. Authors increased the epoxy functionality of SCECGE from 2.45 to 2.65 epoxies/molecule ratio (almost 70% yield) [14].

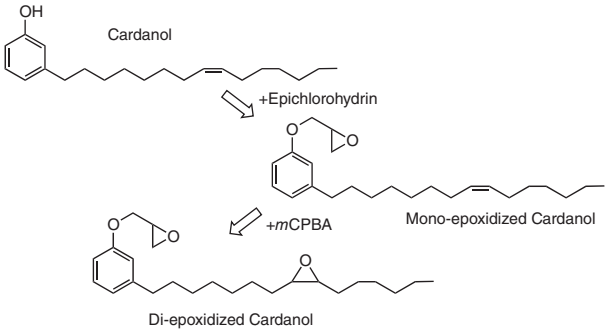

Figure 8.2 Synthetic route to cardanol-based mono- and di-epoxidized derivatives. Source: Petal et al. [11, 12].

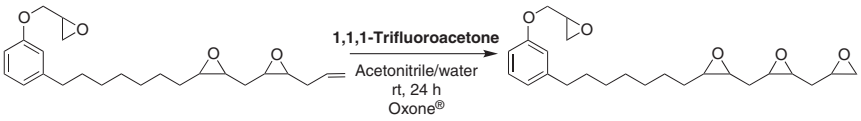

Scheme 8.1 Epoxidation of cardanol's terminal double bond.

Another interesting pathway to cardanol-based epoxy derivatives was proposed by Kim et al. who described the enzymatic epoxidation as well as the polymerization of cardanol. The epoxidation was carried out with lipase catalysis, while peroxidase catalysis was used for the polymerization of both cardanol and epoxide-containing cardanol [15].

Epoxy resins are one of the most important coating materials used in industrial fields. Due to their high chemical and physical resistance, they are mainly applied as anticorrosion coatings. A cardanol-based epoxy resin was developed by Aggarwal and coworkers using epichlorohydrin, BPA, and cardanol and was used for the production of anticorrosive paints. Results indicated that paints based on cardanol-modified resin are more durable than the commercial epoxy-based paints [16].

Coatings made from triglycidyl cardanol (TGC) resin in combination with the BPA-based epoxy were reported by Kathalewar and Sabnis. The triglycidyl derivative (TGC) was prepared from acetyl cardanol followed by modification with maleic anhydride. Then, by hydrolysis of the anhydride ring, carboxyl functional cardanol (CFC) was obtained and reacted with excess of epichlorohydrin to give the TGC resin [17].

Cardanol-based epoxides have been also used for the development of highly bio-based materials. In an innovative approach, Darroman et al. synthesized sucrose-based epoxides, starting from sorbitol and isosorbide, which were blended with cardanol epoxides and successfully produced epoxy networks with interesting properties for coating applications [18]. Bio-based epoxy foams were obtained from cardanol-derived epoxy compounds cured with vegetable oil-derived diamines, giving rigid epoxy foams with potential use as shock and thermal insulation, as also for the development of lightweight materials for industry [19].

Instead of using cardanol as starting material, Silva et al. developed novel BPA-free epoxy coatings prepared from the direct valorization of the CNSL, as shown in Scheme 8.2. This alternative resin (e-CNSL) was obtained by oxidation of double bonds using *in situ* performic acid, generated by a solvent-free methodology, and, when cured with different amine hardeners, it showed great potential for corrosion protection of steel plates [20].

A modified version of cardanol-based epoxide was also reported by Cardolite Corp. In order to obtain this novel monomer, cardanol was first phenolated through a reaction with phenol, giving a product containing two phenolic rings attached to the alkyl side chain. After the reaction with epichlorohydrin, the di-epoxidized cardanol, commercialized under the code NC-514 (Figure 8.3), was obtained. When cured with diamines or anhydrides, the novel cardanol-based epoxy coatings exhibited interesting mechanical and thermal properties [21, 22]. In another work, fully

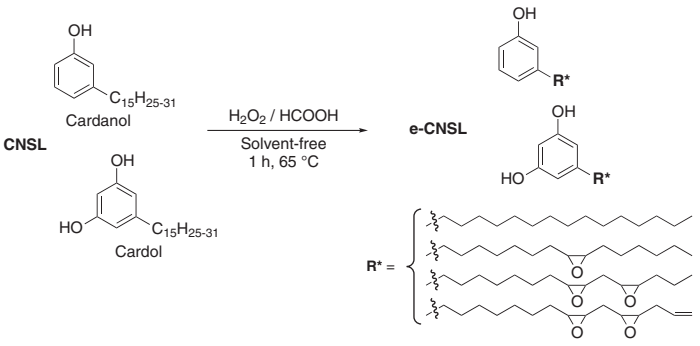

Scheme 8.2 CNSL-based epoxy resins.

Figure 8.3 Chemical structure of NC-514.

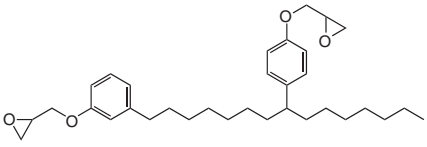

bio-based transparent films were obtained by photocuring of NC-514 with microfibrillated cellulose (MFC) [23].

Due to its unique particular chemical structure, which combines the rigidity of the aromatic ring with the flexibility of the long C-15 side chain, cardanol has been evaluated as a bio-based plasticizer, in place of the phthalate-based plasticizers, like diisononyl phthalate (DINP) and di(2-ethylhexyl)phthalate (DEHP).

To further improve the interaction with polymeric matrices, like polyvinylchloride (PVC), cardanol chemical structure was modified by simple methods. For example, Greco et al. prepared very effective plasticizers from cardanol by simply acetylating the phenolic hydroxyl group, followed by the double bond epoxidation with *m*-CPBA [24]. This novel plasticizer was successfully incorporated to PVC and PLA showing its potential in replace of other petrochemical-based products [25–27]. Fully epoxidized cardanol was also effectively used as plasticized for PVC [28].

8.2.2 Benzoxazines

In the last years, there was an increase search for the development of novel materials for high-performance applications. Among the different classes of commercially available polymers, one that have been attracting considerable attention is benzoxazine's polymeric derivatives, the polybenzoxazines.

Benzoxazines are chemically described as a benzene ring attached to an oxazine ring, a six-membered ring containing a nitrogen and oxygen heteroatoms. They are commonly synthesized through a Mannich-like condensation starting from phenol, formaldehyde, and a primary amine [29]. The use of renewable raw materials for the synthesis of benzoxazines has been widely studied in the scientific literature and has called the attention of both academia and industry due to their peculiar chemical and physical properties.

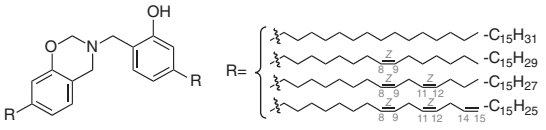

Figure 8.4 First reported cardanol-based benzoxazine monomer.

Despite being reported by Ning and Ishida in 1994 [30], only with the pioneer work developed by Calò et al. in 2007, benzoxazines started to be obtained from cardanol [31]. In this work, cardanol was reacted with formaldehyde and ammonia, producing a very peculiar benzoxazine monomer bearing two cardanol moieties (Figure 8.4). The authors also evaluated its potential as a polymeric matrix for the development of novel bio-composites using jute fiber as reinforcement, obtaining a final product with elevated bio-based content and good mechanical properties. Other bio-composite cardanol-based polybenzoxazines with different reinforcements, e.g. bamboo [32], jute [33], rice husk [34, 35], chicken feather [36], and wood flour [37], have also been explored.

Starting from individual constituents of CNSL – cardanol, cardol, and 2-methylcardol – Attanasi et al. synthesized many different mono- and bis-benzoxazines monomers (Figure 8.5) via an eco-friendly solvent-free one-pot procedure [38].

A different sustainable pathway for obtaining cardanol-based benzoxazines in high yields used a mixture of choline chloride–urea as deep eutectic solvent. This was further explored for the preparation of single-component nanovesicular systems [39]. Benzoxazines derived from cardanol with even higher bio-based contents were also synthesized, exploring the use of primary amines obtained from renewable raw materials, like furfurylamine and stearylamine [40].

A carbohydrate-based isomannide diamine was reacted with cardanol, resulting in a fully naturally sourced bifunctional benzoxazine (Figure 8.6). The incorporation of the rigid core from isomannide provided polybenzoxazines with high glass-transition temperature when compared to its aromatic diamine-based analog [41].

In a novel strategy toward highly bio-based bis-benzoxazine monomer, Puchot et al. [42] synthesized a monosubstituted cardanol-based benzoxazine, which

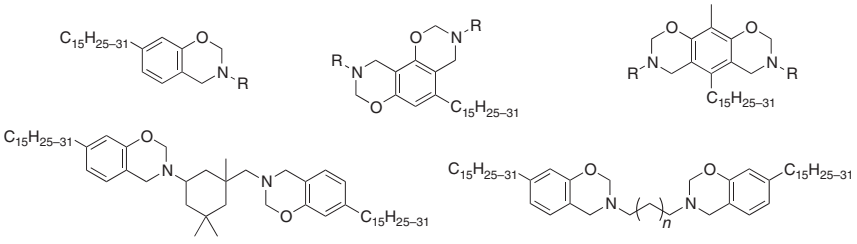

Figure 8.5 Benzoxazines monomers derived from cardanol, cardol, and methylcardol.

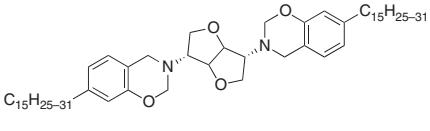

Figure 8.6 Benzoxazine monomer obtained from cardanol and isomannide.

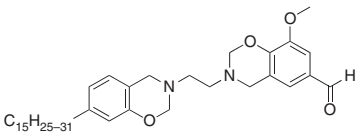

Figure 8.7 Asymmetric cardanol-based benzoxazine monomer.

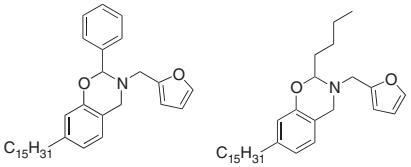

Figure 8.8 Cardanol-based 2-substituted benzoxazines.

was further coupled with vanillin, a naturally occurring aldehyde, yielding a vanillin–cardanol bis-benzoxazine (Figure 8.7). This novel asymmetric monomer exhibited lower melting temperatures than the symmetrical vanillin-based monomer, enlarging the processing window up to 126 °C.

Other naturally occurring aldehydes (valeraldehyde and benzaldehyde) were used successfully by Pereira et al. as feedstocks for cardanol-based benzoxazine synthesis (Figure 8.8). The results showed that the polymerization of 2-substituted benzoxazines presented lower activation energy values and polymerization temperatures when compared with the corresponding formaldehyde-derived benzoxazines, reinforcing the potential of benzoxazines in developing customized polymers [43].

Cardanol-based benzoxazines containing imidazole-core diamine (IDA) and pyridine-core triamine (PYTA) were synthesized by Hariharan et al. and successfully coated to cotton fabrics upon polymerization. The polybenzoxazines-coated fabrics showed highly hydrophobic water contact angles (around 160°) and were also applied to oil–water separation, showing great efficiency (96%) even with large volumes of fluid [44].

The recent development of vitrimers containing disulfide bonds made from cardanol-based polybenzoxazines was reported, for the first time, by Trejo-Machin et al. This new material was recycled, reshaped, and reprocessed, due to its fast relaxation process and low polymerization activation energy, showing also interesting healable properties [45].

Coatings based on benzoxazines are known for low water absorption, low surface free energy, and excellent dielectric properties, characteristics that play vital roles in the corrosion-resistant performance of organic coatings. An amine functional-based benzoxazine was obtained by the condensation of cardanol, paraformaldehyde, and *N*,*N*′-bis(2-aminoethyl)ethane-1,2-diamine and further modified with glycidoxypropyltrimethoxysilane (GPTMS), resulting in coatings with improved mechanical and chemical properties and enhanced protection to corrosive species [46]. In a similar approach, fully bio-based polybenzoxazines, obtained from cardanol and stearylamine, were applied as superhydrophobic anticorrosive coating, which presented outstanding anticorrosion performance during 90 days of immersion in NaCl solution, as observed by electrochemical measurement [47].

8.2.3 Cardanol-Based Lactones

Cyclocarbonylated compounds are a class of very attractive compounds due to its wide range of applications, working as building blocks of the synthesis of different new molecules, from biologically active compounds to high-performance polymers. With the increased attention to the development of novel bio-based molecules, CNSL constituents were employed as raw materials for the synthesis of interesting cyclocarbonylated derivatives.

Vasapollo and coworkers [48] reported an elegant synthetic pathway, which started by the *O*-allylation of cardanol and cardol, followed by a Claisen rearrangement reaction, affording the respective allylphenols. After a cyclocarbonylation reaction, in the presence of the homogeneous catalytic system $Pd(OAc)_2$–1,4-bis(diphenylphosphino)butane and CO/H_2 (1 : 1) and under relatively mild conditions, cardanol-based lactones and cardol-based bis-lactones were obtained in good yields (Figure 8.9, structures **a** and **b**).

A cyclocarbonylated derivative was also obtained using nitro-cardanol as starting material (Figure 8.9, compound **c**). Employing a palladium-catalyzed system, the authors reported the synthesis of a novel benzoxazolinone, a class of molecules widely used in agricultural applications [49].

Recently, Gazzotti et al. [50] reported the synthesis of a cardanol-based 1,3-dioxolan-4-one (DOX), for the synthesis of poly(lactic acid)-based copolymers. The potential of this class of monomers as an alternative to *O*-carboxyanhydrides (OCA) in the synthesis of functional polylactide-based materials was evaluated, showing good reactivity but overcoming OCA's drawbacks, such as instability and hazard starting materials (Figure 8.10).

8.2.4 Cardanol-Based Amphiphilic Heterocycles

Due to its unique chemical structure, cardanol presents a great synthetic flexibility that allows, with simple chemical modifications, to obtain structurally rich amphiphilic compounds. Its phenolic moiety can be easily modified in order to enhance the polarity of the molecule, which is the case of the combination of cardanol with sugars in hemiacetal form, resulting in aryl glycolipids (Figure 8.11), as reported by G. John and coworkers [51–53]. The authors applied this to the development of new fully bio-based glycolipids as gelators, which present the ability to gel in water and alcohol mixture or in pure organic solvents, depending on the unsaturation degree of cardanol's side chain [52].

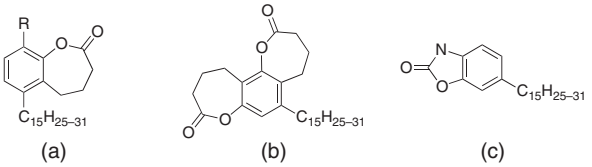

Figure 8.9 Cyclocarbonylated derivates of cardanol and cardol.

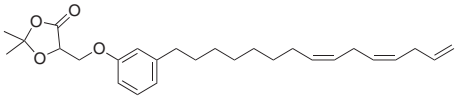

Figure 8.10 Cardanol-based 1,3-dioxolan-4-one derivative.

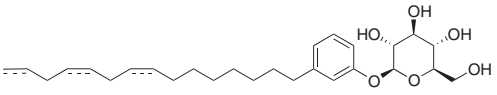

Figure 8.11 Fully bio-based glycolipids obtained from cardanol.

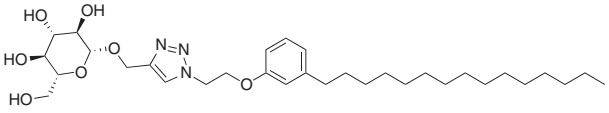

Figure 8.12 Glucose-triazole-hydrogenated cardanol conjugate.

In another approach, cardanol-based glycosides were combined and used to generate different self-assembled high-axial-ratio nanostructures (HARNs), varying from twisted ribbons and helical ribbons to nanotubes [51].

Employing a different strategy, Rao et al. synthesized cardanol-based glucose-triazole conjugate (Figure 8.12). In this case, a glucose unit was combined to cardanol via a triazole linker, resulting in a novel molecule that was used to produce four different classes of gels [54]. This glucose-triazole-hydrogenated cardanol conjugate was also applied in membrane organization and thermotropic phase transition studies [55, 56].

Amphiphilic derivatives with antioxidant activity were also synthesized from CNSL constituents. Starting from cardanol, cardol, and 2-methylcardol, Amorati and coworkers, in an interesting work, reported the synthesis of novel bio-based 4-thiaflavane antioxidants that, due to the long alkyl chain, showed potential to be used as fat stabilizers and lipid peroxidation inhibitors (Figure 8.13).

Cardanol was also employed in the synthesis of novel pyridine-based cationic surfactant (Figure 8.14) to improve single-walled carbon nanotubes (SWCNTs) dispersion in aqueous solution. Improved antibacterial activity was observed for cardanol-derived surfactants when compared to dodecylbenzene-sulfonate sodium (SDBS), confirming the great potential of cardanol in the development of eco-friendly surfactants, which may be used to expand the technological applications of SWCNT [57].

8.2.5 Fulleropyrolidines

Since the discovery of buckminsterfullerene (C_{60}) in 1985, different methodologies for fullerene functionalization were reported. One of the most common is the

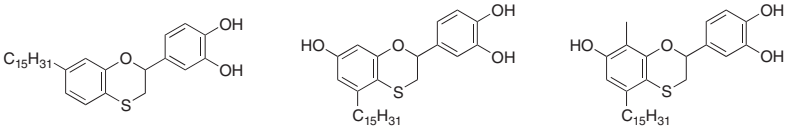

Figure 8.13 Novel cardanol-, cardol-, and methylcardol-based 4-thiaflavane antioxidants.

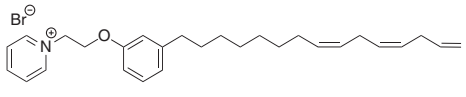

Figure 8.14 Novel cardanol-derived cationic surfactant.

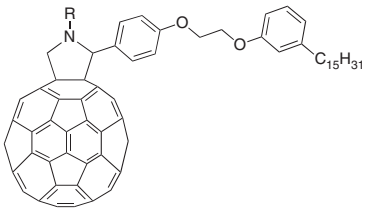

Figure 8.15 Cardanol-based fulleropyrolidine hybrids.

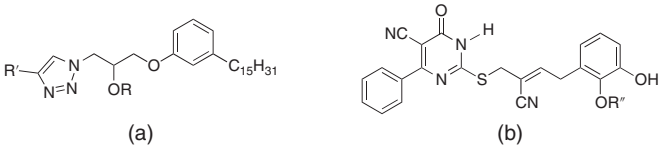

Figure 8.16 1,2,3-Triazoles and pyrimidine hybrids from cardanol.

1,3-dipolar cycloaddition of azomethine ylides, which provides an important class of derivatives, called fulleropyrolidines.

In the search of novel bio-based fullerene derivatives, cardanol-based fullerene derivatives were obtained through 1,3-dipolar addition of *in situ* generated azomethine ylides [58, 59]. The cardanol fulleropyrrolidine hybrids (Figure 8.15) showed an incredible solubility in chloroform, up to 100–300 times more than C_{60}, an important characteristic that allows easier purification, structural characterization, further chemical modifications, and scaling-up procedures.

8.2.6 Triazoles and Pyrimidine Hybrids

A variety of structurally diverse 1,2,3-triazoles [60] and pyrimidine hybrids [61], shown in Figure 8.16 and indicated as **a** and **b**, respectively, were synthesized starting from CNSL components. Some of these heterocyclic systems have exhibited anticancer properties depending on the peripheral substituent. For instance, in the case of triazoles **a**, the derivative where R′ is an acetyl group showed more pronounced cytotoxic activity than commercial drug (doxorubicin), indicating its high cancer drug potential. For compounds with the general structure **b**, the presence of propyl, butyl, pentyl, or hexyl groups in R″ conferred an increased activity against breast and liver human cancer cell lines (MCF-7 and HEP-G2, respectively).

8.3 Porphyrins and Phthalocyanines Derived from Cardanol-Based Precursors

8.3.1 Syntheses of Porphyrins (Pps) and Phthalocyanines (Pcs) from Cardanol-Based Precursors

Porphyrins (Pps) and phthalocyanines (Pcs) are considered compounds with great potential as components of molecular materials that possess unique electronic, magnetic, and photophysical properties. These classes of macro-heterocyclic

aromatic compounds are perfectly suited for their integration in light energy conversion systems. Pps and Pcs exhibit attractive physical properties, particularly very high extinction coefficients in the visible and near-IR regions, where the maximum of the solar photon flux occurs, which is necessary for efficient photon harvesting, besides a rich redox chemistry, as well as photoinduced electron transfer and semiconducting capabilities.

Cardanol, also in its hydrogenated form, was used as starting material to prepare the aldehyde precursors used for lipophilic cardanol-based metal-free and metallo-*meso*-tetraarylporphyrins [62, 63]. Selected molecular structures are reported in Scheme 8.3. These compounds exhibited good solubility in common organic solvents as well as easy manipulation and suitability for further transformation due to the presence of cardanol chains [64].

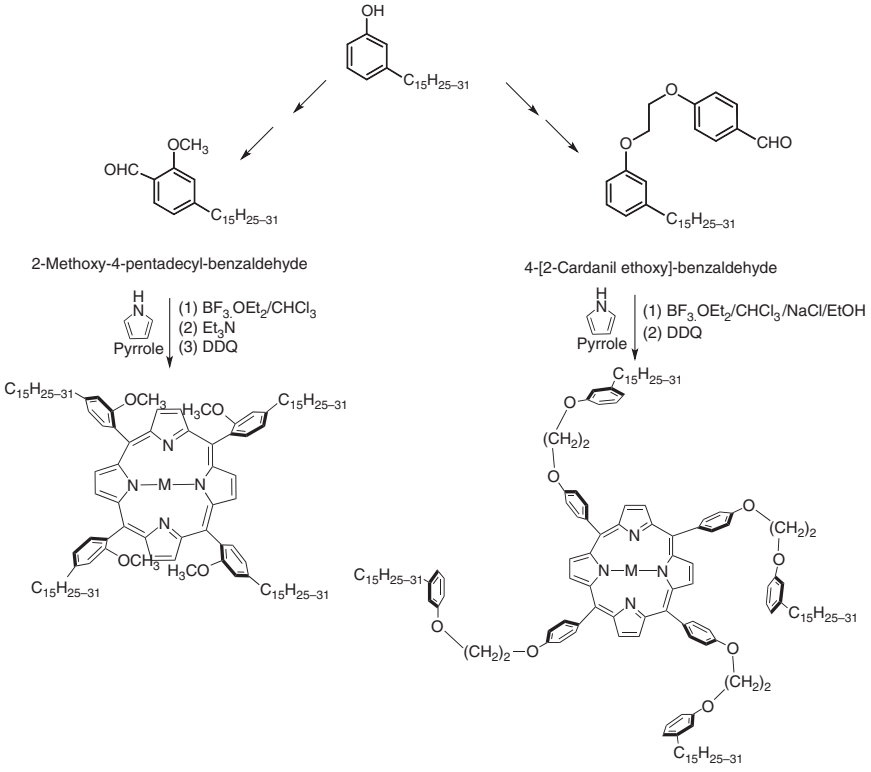

Scheme 8.3 Structures of cardanol-based porphyrins.

Phthalonitriles, having cardanol as a naturally occurring substituent, were prepared by a base-catalyzed nucleophilic aromatic nitro displacement of 4-nitrophthalonitrile. Thus, the metallo-phthalocyanines based on cardanol (Scheme 8.4) were prepared by tetramerization of cardanyl phthalonitrile precursors carried out in ethanol in the presence of selected metal salt MCl_2 (M = Cu, Zn, Pd, Ni) and 1,8-diazabicyclo[5.4.0]undec-7-ene (DBU) [65].

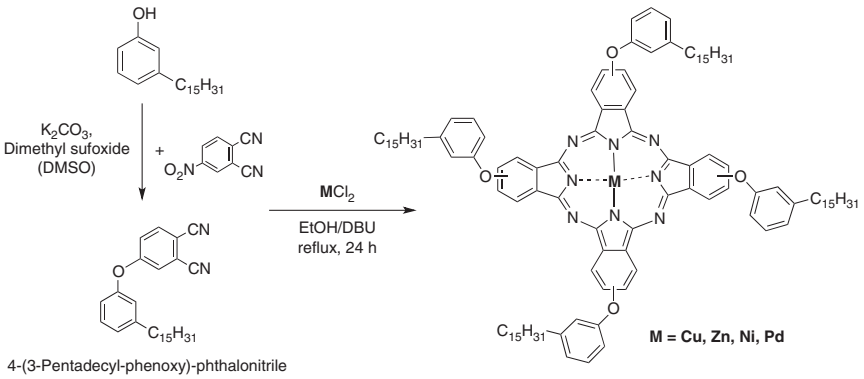

Scheme 8.4 Precursors for the preparation of cardanol-based metallo-phthalocyanines. DMSO, dimethyl sulfoxide.

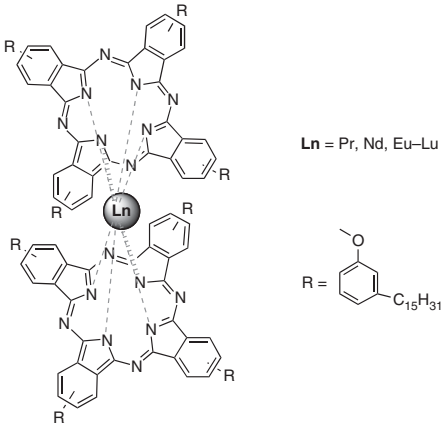

Figure 8.17 Bis-phthalocyanine lanthanides complexes peripherally substituted with pentadecylphenoxy groups. Source: Słota et al. [66].

Sandwich-type phthalocyanines containing a rare earth metal core (Pr, Nd, Eu–Lu) and the macrocycle peripherally substituted with pentadecylphenoxy groups were synthesized using a cardanol-based phthalonitrile precursor and the respective lanthanide acetate, as shown in Figure 8.17 [66].

8.3.2 Applications of Cardanol-Derived Porphyrins (Pps) and Phthalocyanines (Pcs)

The introduction of cardanol pendant into various macrocyclic frameworks such as porphyrins, phthalocyanines, and related compounds produced the enhancement of their solubility in organic solvents due to the presence of long alkyl chains. The improved processability allows the application of these functionalized macrocycles in different contexts.

8.3.2.1 Langmuir–Blodgett Films

Amphiphilic porphyrin–cardanol derivatives in Langmuir and Langmuir–Blodgett films have been applied for sensing [67] as well as fluorescent markers for diesel

fuel [63]. On the other hand, the Cu–porphyrin derived from cardanol has been used to modify the surface of a gold electrode successively and was used as an effective electrochemical sensor for nitric oxide [68].

8.3.2.2 Superparamagnetic Fluorescent Nanosystems

Functional superparamagnetic fluorescent nanosystems involving a *meso*-porphyrin with side chains derived from cardanol were assembled on Fe_3O_4 nanoparticles coated with a thin layer of oleic acid (OA). The porphyrins were anchored on the Fe_3O_4–OA nanoparticle surface by van der Waals interaction between the long alkyl chains of cardanol-derived porphyrin and the long alkyl chain of OA. This composite material proved to be stable when suspended and sonicated in different media such as water, ethanol, hexane, and dimethyl sulfoxide. The advantage of this new approach is the development of a stable nanosystem that is easy to handle, with potential applications in heterogeneous photocatalysis and as imaging agents for image contrast of cells in cancer therapies [69].

8.3.2.3 Corrosion Protection

Synthesis and characteristics of alkyd resin/metalloporphyrins (MPps), nanocomposite for corrosion protection application, have been reported. Blends of MPps (ZnPp, CuPp, and CoPp) with alkyd resin afforded the novel nanocomposite that was applied on carbon steel specimens, and the coated specimens were evaluated for their corrosion and mechanical properties in 0.5 M HCl solution. The performance of nanocomposite coatings was evaluated using potentiodynamic polarization, electrochemical impedance spectroscopy, water permeability, and pull-off adhesion measurements. The coating film capacitances were monitored with the immersion time to establish water uptake of these coating films. The incorporation of MPps significantly improved anticorrosive performance and mechanical properties of the alkyd resin, being the presence of metal atoms at the Pp core the main reason for the difference in the protection efficiency.

Effectively, MPps provided mechanical integrity to the alkyd resin due to the decreasing of the pores and increasing of its tortuosity. In particular, the ionization potential of metal ion (Zn, Cu, Co) in the MPps structure plays the main role in the difference in the protection efficiency. In fact, the electrochemical oxidation potentials of the MPps exhibited substantial variation with a change in the central metal. The ionization potentials were 9.81, 8.69, and 8.53 eV for Zn, Cu, and Co, respectively. This finding supports that the nature of central metal has some influence on the interaction between MPps molecules and the alkyd resin, which decrease steadily as metal ion progresses from Co, Cu, to Zn. Best corrosion protection of the carbon steel was found for the alkyd resin with CoPp (98.47%) [70].

8.3.2.4 Organic Light-Emitting Diodes (OLEDs)

Porphyrins derived from CNSL are promising materials to be used in organic optoelectronic devices such as emitting layers in organic light-emitting diodes (OLEDs). In particular, the *meso*-tetra-[4-(2-(3-*n*-pentadecylphenoxy)ethoxy]phenylporphyrin

(H_2Pp), obtained from hydrogenated cardanol, and its zinc (ZnPp) and copper (CuPp) complexes, were applied as emitting layers in OLEDs devices.

The energy levels of Highest Occupied Molecular Orbital (HOMO) and Lowest Unoccupied Molecular Orbital (LUMO) of the studied porphyrins were determined by cyclic voltammetry analysis to help the selection of the most appropriate materials to be used to assemble the device. H_2Pp and ZnPp presented fluorescence emission bands in the red region, from 601 to 718 nm.

The introduction of bulky substituents hinders the π–π stacking, favoring the emission in the film. Furthermore, the ZnPp complex, due to the presence of Zn(II) ions coordinated to the tetrapyrrole ring, was the strongest emitter presenting a threshold voltage of 4 V and the maximum irradiance of 10 μW cm^{-2} with a current density (J) of 15 mA cm^{-2} at 10 V. The CuPp complex proved to be a material with adequate properties for the design of OLEDs in the infrared [71].

8.3.2.5 Photodynamic Therapy

Cutaneous leishmaniasis (CL) is a tropical disease, endemic mainly in low-income countries that lack adequate basic health care. Photodynamic therapy (PDT) is a promising noninvasive and less toxic alternative for the treatment of CL.

The photodynamic effect of a new metalloporphyrin, Pd(II) *meso*-tetra[4-(2-(3-*n*-pentadecyl)phenoxy)ethoxy]phenylporphyrin (PdPp), derived from CNSL that was successfully evaluated against promastigote forms of *Leishmania braziliensis*, has been recently reported [72]. The PdPp complex has a singlet oxygen quantum yield of 0.49, favoring a type II photochemical reaction. The results of the photodynamic experiment carried out with PdPp on the promastigote forms of *Leishmania braziliensis* indicated a mortality percentage of 70% of the cells when compared to the control after exposure to blue light ($\lambda = 420$ nm). Besides this, the metalloporphyrin PdPp did not show considerable toxicity to macrophages, indicating the cell viability in the presence of the compound. Therefore, PDT with the previously mentioned metalloporphyrin derived from biomass represents an interesting therapeutic alternative for the treatment of CL, especially for patients with intolerance to the chemotherapeutic drugs currently available.

8.3.2.6 Composites Semiconductor@Sensitizer for Enhancing Photocatalytic Processes

Polycrystalline TiO_2 incorporating lipophilic cardanol-porphyrin hybrids has been used as sensitizers for the photodegradation of 4-nitrophenol (4-NP) in aqueous suspensions. The composite material obtained by impregnation of a Cu-substituted cardanol-based porphyrin onto TiO_2 (anatase phase) showed increased photoactivity in the degradation of 4-NP, confirming the importance of the lipophilicity and photostability of the sensitizer as well as the beneficial effect of Cu(II) coordinated in the core of the porphyrin [73, 74].

The synthesis, characterization, and photocatalytic activity of a new composite nanomaterials based on ZnO nanostructures impregnated by lipophilic porphyrins derived from CNSL has been reported. The photocatalytic activity

of this ZnO@cardanol porphyrin composite nanomaterial was investigated by carrying out the degradation of rhodamine B in aqueous solution, and it was demonstrated that the photoactivity of ZnO increases in the presence of the porphyrins both under visible and natural sunlight irradiation. The development of composite photocatalysts based on porphyrins derived from CNSL provides an alternative approach to eliminate efficiently toxic wastes from water under ambient conditions [75].

H_2Pp and Cu(II) Pp loaded on titanium dioxide in the anatase phase (TiO_2) were also used as a heterogeneous catalyst for the photoreduction of Cr(VI) to Cr(III) in aqueous suspensions under UV–vis light irradiation. TiO_2 impregnated with copper(II) porphyrin (TiO_2@Cu(II)Pp) was the most effective in photocatalyst reduction of toxic chromate Cr(VI) to nontoxic chromium Cr(III). An experimental design approach was carried out in order to optimize the process conditions. A full factorial design as a chemometric tool was employed to evaluate the impact on photoconversion of the modification of experimental conditions such as the catalyst amount, the concentration of Cr(VI) ions, and the pH of the medium. This multivariate approach was successfully used for fast fitting and better evaluation of significant factors affecting the experimental responses, with the advantage of reducing the number of required experiments [76].

Hybrid photocatalysts may also be used as a crucial component of diverse reaction systems designed to realize more or less complicated syntheses. Recently, the potential of novel composites based on graphitic carbon nitride, g-C_3N_4 was demonstrated in a photocatalytic synthesis of 2,5-furandicarboxyaldehyde (FDC) via oxidation of 5-hydroxymethyl-2-furfural (HMF) under natural solar irradiation. The C_3N_4 matrices were impregnated by *meso*-tetraaryl-substituted porphyrins, H_2Pp, CuPp, and ZnPp, functionalized with lipophilic 3-*n*-pentadecylphenoxyethoxy chains. The reaction was carried out in a batch photoreactor in an aqueous suspension of the hybrid catalysts (liquid–solid regime). All of the tested composites effectively prompted the conversion of HMF, and in all cases its partial oxidation product, FDC, was selectively synthetized under the appropriate process condition [77].

8.3.2.7 Photo-ignition of Carbon Nanotubes/Ferrocene/Porphyrin Under LED Irradiation

The photo-ignition process of dry multi-walled carbon nanotubes (MWCNTs) mixed with ferrocene ($FeCp_2$) powder, using a light-emitting diode (LED) as the light source, was improved by adding a cardanol-based porphyrin in powder form to the MWCNTs/$FeCp_2$ mixture. The ignition tests were carried out by employing a continuous emission and a pulsed white LED. The minimum ignition energy (MIE) of MWCNTs/$FeCp_2$ samples was determined by varying the duration of the light pulse. It was proved that ignition was obtained with a pulse duration of 110 ms and an MIE density of 266 mJ cm^{-2}. The significant reduction of the MIE value (10–40%) was ascribed to the improved photoexcitation and charge transfer properties of the porphyrin molecules when compared with results previously obtained employing a pulsed Xe lamp [78].

8.3.2.8 Intercalation of Pps into Vesicular Nanosystems

The development of soft nanomaterials by the controlled self-assembly of molecules derived from renewable sources has become a major area of interest for scientists across the world. An example of a sustainable procedure for producing cardanol-based nanodispersions, embodying a lipophilic porphyrin-cardanol hybrid, has been described. Cardanol acted as the solvent of a cardanol-porphyrin hybrid/cholesterol mixture, being the main component of the vesicular nanosystems [79].

An overview of successful applications of cardanol-based porphyrins and their metal complexes in various fields of science and technology described in Section 8.3 is presented in Figure 8.18.

8.3.2.9 Nanomaterials Based on Fe_3O_4 and Phthalocyanines Derived from CNSL

Magnetic nanomaterials made by the combination of magnetite (Fe_3O_4) nanoparticles, with the surface functionalized in sequence with OA and cardanol-derived phthalocyanines, have been prepared. The core/shell/shell morphology of the Fe_3O_4/OA/phthalocyanine nanomaterials consisted of a Fe_3O_4 core and two consecutive layers of OA and phthalocyanine molecules, the latter being derived from CNSL. The synthesis of Fe_3O_4 nanoparticles was performed via co-precipitation procedure, followed by the nanoparticle coating with OA by hydrothermal method and final anchorage of phthalocyanines on the nanostructured Fe_3O_4/OA, favored by van der Waals interactions between alkyl chains [80].

GO@Fe_3O_4/CuPc and GO@Fe_3O_4/ZnPc nanohybrid materials were also produced through a simple and effective ultrasonication method. Fe_3O_4 nanoparticles having a spinel phase with crystallize size of c. 12 nm was adhered to the surfaces of GO sheets. The magnetization curve of Fe_3O_4 and nanohybrids showed hysteresis that was slightly decreased due to the incorporation of the phthalocyanines. In the nanohybrids, dielectric measurements showed the highest dielectric constant and lower losses related to the frequency between 0.1 and 6.0 MHz. These results

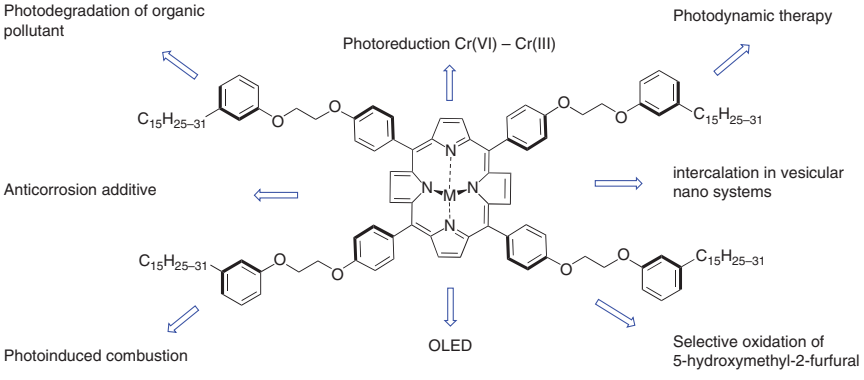

Figure 8.18 Multipurpose use of functional porphyrins based on cardanol.

showed that these nanohybrids are materials with superparamagnetic properties that are likely to be employed for dielectric–magnetic features [81].

8.4 Conclusions and Perspectives

In this chapter, several heterocycles obtained from CNSL constituents were presented. These heterocyclic compounds represent a few of the innumerous interesting molecules already derived from CNSL. Different strategies that might be implemented for the development of a more sustainable and economically feasible chemistry have been illustrated. The enormous potential of this renewable raw material is unquestionable, and the increased demand for bio-based molecules and materials in the next years will accentuate its importance in the context of more eco-friendly products and processes.

Acknowledgments

Prof. Lomonaco and Prof. Mazzetto acknowledge Brazilian agencies National Council for Scientific and Technological Development (CNPq 407291/2018-0), National Council for the Improvement of Higher Education (CAPES), and Foundation for Scientific and Technological Development of Ceara (FUNCAP) for their support.

References

1 De Bhowmick, G., Sarmah, A.K., and Sen, R. (2018). Lignocellulosic biorefinery as a model for sustainable development of biofuels and value added products. *Bioresour. Technol.* https://doi.org/10.1016/j.biortech.2017.09.163.
2 Naik, S.N., Goud, V.V., Rout, P.K., and Dalai, A.K. (2010). Production of first and second generation biofuels: a comprehensive review. *Renewable Sustainable Energy Rev.* https://doi.org/10.1016/j.rser.2009.10.003.
3 Uçkun Kiran, E., Trzcinski, A.P., and Liu, Y. (2015). Platform chemical production from food wastes using a biorefinery concept. *J. Chem. Technol. Biotechnol.* https://doi.org/10.1002/jctb.4551.
4 Coma, M., Martinez-Hernandez, E., Abeln, F. et al. (2017). Organic waste as a sustainable feedstock for platform chemicals. *Faraday Discuss.* 202: 175–195. https://doi.org/10.1039/C7FD00070G.
5 Dugmore, T.I.J., Clark, J.H., Bustamante, J. et al. (2017). Valorisation of biowastes for the production of green materials using chemical methods. *Top. Curr. Chem.* 375 (2): 46. https://doi.org/10.1007/s41061-017-0133-8.
6 Anilkumar, P. (2017). Cashew nut shell liquid: a goldfield for functional materials. In: *Cashew Nut Shell Liquid: A Goldfield for Functional Materials* (ed. P. Anilkumar). Cham: Springer https://doi.org/10.1007/978-3-319-47455-7.

7 Lomonaco, D., Mele, G., and Mazzetto, S.E. (2017). Cashew Nutshell Liquid (CNSL): from an agro-industrial waste to a sustainable alternative to petrochemical resources. In: *Cashew Nut Shell Liquid* (ed. P. Anilkumar), 19–38. Cham: Springer International Publishing https://doi.org/10.1007/978-3-319-47455-7_2.

8 Prileschajew, N. (1909). Oxydation ungesättigter Verbindungen mittels organischer Superoxyde. *Ber. Dtsch. Chem. Ges.* 42 (4): 4811–4815. https://doi.org/10.1002/cber.190904204100.

9 Nouailhas, H., Aouf, C., Le Guerneve, C. et al. (2011). Synthesis and properties of biobased epoxy resins. Part 1. Glycidylation of flavonoids by epichlorohydrin. *J. Polym. Sci., Part A: Polym. Chem.* 49 (10): 2261–2270. https://doi.org/10.1002/pola.24659.

10 Rubin, B.S. (2011). Bisphenol A: an endocrine disruptor with widespread exposure and multiple effects. *J. Steroid Biochem. Mol. Biol.* 127 (1, 2): 27–34. https://doi.org/10.1016/j.jsbmb.2011.05.002.

11 Patel, M.B., Patel, R.G., and Patel, V.S. (1988). Curing kinetics of epoxy resin using epoxidized cardanol as diluent with/without fortifier. *Thermochim. Acta* 129 (2): 277–284. https://doi.org/10.1016/0040-6031(88)87343-X.

12 Patel, M.B., Patel, R.G., and Patel, V.S. (1989). Effects of reactive diluent diepoxidized cardanol and epoxy fortifier on curing kinetics of epoxy resin. *J. Therm. Anal.* 35 (1): 47–57. https://doi.org/10.1007/BF01914263.

13 Suresh, K.I. (2013). Rigid polyurethane foams from cardanol: synthesis, structural characterization, and evaluation of polyol and foam properties. *ACS Sustainable Chem. Eng.* 1 (2): 232–242. https://doi.org/10.1021/sc300079z.

14 Kinaci, E., Can, E., La Scala, J.J., and Palmese, G.R. (2020). Epoxidation of Cardanol's terminal double bond. *Polymers* 12 (9): 2104. https://doi.org/10.3390/polym12092104.

15 Kim, Y.H., An, E.S., Park, S.Y., and Song, B.K. (2007). Enzymatic epoxidation and polymerization of cardanol obtained from a renewable resource and curing of epoxide-containing polycardanol. *J. Mol. Catal. B: Enzym.* 45 (1, 2): 39–44. https://doi.org/10.1016/j.molcatb.2006.11.004.

16 Aggarwal, L.K., Thapliyal, P.C., and Karade, S.R. (2007). Anticorrosive properties of the epoxy-cardanol resin based paints. *Prog. Org. Coat.* 59 (1): 76–80. https://doi.org/10.1016/j.porgcoat.2007.01.010.

17 Kathalewar, M. and Sabnis, A. (2014). Epoxy resin from cardanol as partial replacement of bisphenol-A-based epoxy for coating application. *J. Coat. Technol. Res.* 11 (4): 601–618. https://doi.org/10.1007/s11998-014-9570-2.

18 Darroman, E., Durand, N., Boutevin, B., and Caillol, S. (2015). New cardanol/sucrose epoxy blends for biobased coatings. *Prog. Org. Coat.* 83: 47–54. https://doi.org/10.1016/j.porgcoat.2015.02.002.

19 Dworakowska, S., Cornille, A., Bogdal, D. et al. (2015). Formulation of bio-based epoxy foams from epoxidized cardanol and vegetable oil amine. *Eur. J. Lipid Sci. Technol.* 117 (11): 1893–1902. https://doi.org/10.1002/ejlt.201500232.

20 da Silva, L.R.R., Avelino, F., Diogenes, O.B.F. et al. (2020). Development of BPA-free anticorrosive epoxy coatings from agroindustrial waste. *Prog. Org. Coat.* 139: 105449. https://doi.org/10.1016/j.porgcoat.2019.105449.

21 Jaillet, F., Darroman, E., Ratsimihety, A. et al. (2014). New biobased epoxy materials from cardanol. *Eur. J. Lipid Sci. Technol.* 116 (1): 63–73. https://doi.org/10.1002/ejlt.201300193.

22 Mora, A., Decostanzi, M., David, G., and Caillol, S. (2019). Cardanol-based epoxy monomers for high thermal properties thermosets. *Eur. J. Lipid Sci. Technol.* 121 (8): 1800421. https://doi.org/10.1002/ejlt.201800421.

23 Vacche, S.D., Vitale, A., and Bongiovanni, R. (2019). Photocuring of epoxidized cardanol for biobased composites with microfibrillated cellulose. *Molecules* 24 (21): https://doi.org/10.3390/molecules24213858.

24 Greco, A., Brunetti, D., Renna, G. et al. (2010). Plasticizer for poly(vinyl chloride) from cardanol as a renewable resource material. *Polym. Degrad. Stab.* 2169–2174. https://doi.org/10.1016/j.polymdegradstab. 2010.06.001.

25 Greco, A., Ferrari, F., and Maffezzoli, A. (2020). Compression behavior of soft PVC foams obtained by cardanol-derived plasticizer. *J. Cell. Plast.* 56 (5): 515–530. https://doi.org/10.1177/0021955X20912202.

26 Greco, A., Ferrari, F., and Maffezzoli, A. (2018). Thermal analysis of poly(lactic acid) plasticized by cardanol derivatives. *J. Therm. Anal. Calorim.* 134 (1): 559–565. https://doi.org/10.1007/s10973-018-7059-4.

27 Greco, A. and Maffezzoli, A. (2016). Cardanol derivatives as innovative bio-plasticizers for poly-(lactic acid). *Polym. Degrad. Stab.* 132: 213–219. https://doi.org/10.1016/j.polymdegradstab. 2016.02.020.

28 Chen, J., Liu, Z., Jiang, J. et al. (2015). A novel biobased plasticizer of epoxidized cardanol glycidyl ether: synthesis and application in soft poly(vinyl chloride) films. *RSC Adv.* 5 (69): 56171–56180. https://doi.org/10.1039/c5ra07096a.

29 Ishida, H. (2011). Overview and historical background of polybenzoxazine research. In: *Handbook of Benzoxazine Resins* (ed. H. Ishida and T. Agag), 3–81. Amsterdam: Elsevier https://doi.org/10.1016/B978-0-444-53790-4.00046-1.

30 Ning, X. and Ishida, H. (1994). Phenolic materials via ring-opening polymerization: synthesis and characterization of bisphenol-A based benzoxazines and their polymers. *J. Polym. Sci., Part A: Polym. Chem.* 32 (6): 1121–1129. https://doi.org/10.1002/pola.1994.080320614.

31 Calò, E., Maffezzoli, A., Mele, G. et al. (2007). Synthesis of a novel cardanol-based benzoxazine monomer and environmentally sustainable production of polymers and bio-composites. *Green Chem.* 9 (7): 754–775. https://doi.org/10.1039/b617180j.

32 Ribeiro, F.W.M., Kotzebue, L.R.V., Oliveira, J.R. et al. (2017). Thermal and mechanical analyses of biocomposites from cardanol-based polybenzoxazine and bamboo fibers. *J. Therm. Anal. Calorim.* 129 (1): 281–289. https://doi.org/10.1007/s10973-017-6191-x.

33 Rao, B.S. and Palanisamy, A. (2011). Monofunctional benzoxazine from cardanol for bio-composite applications. *React. Funct. Polym.* 71 (2): 148–154. https://doi.org/10.1016/j.reactfunctpolym.2010.11.025.

34 Krishnadevi, K., Devaraju, S., Sriharshitha, S. et al. (2020). Environmentally sustainable rice husk ash reinforced cardanol based polybenzoxazine bio-composites

for insulation applications. *Polym. Bull.* 77 (5): 2501–2520. https://doi.org/10.1007/s00289-019-02854-4.

35 Selvaraj, V., Jayanthi, K.P., and Alagar, M. (2018). Development of biocomposites from agro wastes for low dielectric applications. *J. Polym. Environ.* 26 (9): 3655–3669. https://doi.org/10.1007/s10924-018-1211-x.

36 Selvaraj, V., Jayanthi, K.P., and Alagar, M. (2019). Livestock chicken feather fiber reinforced cardanol benzoxazine-epoxy composites for low dielectric and microbial corrosion resistant applications. *Polym. Compos.* 40 (10): 4142–4153. https://doi.org/10.1002/pc.25275.

37 Agag, T., An, S.Y., and Ishida, H. (2013). 1,3-bis(benzoxazine) from cashew nut Shell oil and diaminodiphenyl methane and its composites with wood flour. *J. Appl. Polym. Sci.* 127 (4): 2710–2714. https://doi.org/10.1002/app.37584.

38 Attanasi, O.A., Behalo, M.S., Favi, G. et al. (2012). Solvent free synthesis of novel mono- and bis-benzoxazines from cashew nut shell liquid components. *Curr. Org. Chem.* 16 (21): 2613–2621. https://doi.org/10.2174/138527212804004616.

39 Behalo, M.S., Bloise, E., Mele, G. et al. (2020). Bio-based benzoxazines synthesized in a deep eutectic solvent: a greener approach toward vesicular nanosystems. *J. Heterocyclic Chem.* 57 (2): 768–773. https://doi.org/10.1002/jhet.3818.

40 Thirukumaran, P., Sathiyamoorthi, R., Shakila Parveen, A., and Sarojadevi, M. (2016). New benzoxazines from renewable resources for green composite applications. *Polym. Compos.* 37 (2): 573–582. https://doi.org/10.1002/pc.23214.

41 Amarnath, N., Shukla, S., and Lochab, B. (2019). Isomannide-derived chiral rigid fully biobased polybenzoxazines. *ACS Sustainable Chem. Eng.* 7 (22): 18700–18710. https://doi.org/10.1021/acssuschemeng.9b05305.

42 Puchot, L., Verge, P., Fouquet, T. et al. (2016). Breaking the symmetry of dibenzoxazines: a paradigm to tailor the design of bio-based thermosets. *Green Chem.* 18 (11): 3346–3353. https://doi.org/10.1039/c5gc03102h.

43 Pereira, R.C.S., Kotzebue, L.R.V., Zampieri, D. et al. (2019). Influence of natural substituents in the polymerization behavior of novel bio-based benzoxazines. *Mater. Today Commun.* 21: 100629. https://doi.org/10.1016/j.mtcomm.2019.100629.

44 Hariharan, A., Prabunathan, P., Manoj, M., and Alagar, M. (2020). Studies on heterocyclic amines based cardanol-benzoxazine for oil-water separation. *Polym. Eng. Sci.* 60 (7): 1494–1506. https://doi.org/10.1002/pen.25396.

45 Trejo-Machin, A., Puchot, L., and Verge, P. (2020). A cardanol-based polybenzoxazine vitrimer: recycling, reshaping and reversible adhesion. *Polym. Chem.* 11 (44): 7026–7034. https://doi.org/10.1039/d0py01239d.

46 Patil, D.M., Phalak, G.A., and Mhaske, S.T. (2017). Synthesis and characterization of bio-based benzoxazine oligomer from cardanol for corrosion resistance application. *J. Coat. Technol. Res.* 14 (3): 517–530. https://doi.org/10.1007/s11998-016-9892-3.

47 Cao, Y., Chen, C., Lu, X. et al. (2021). Bio-based polybenzoxazine superhydrophobic coating with active corrosion resistance for carbon steel protection. *Surf. Coat. Technol.* 405: 126569. https://doi.org/10.1016/j.surfcoat.2020.126569.

48 Amorati, R., Attanasi, O.A., El Ali, B. et al. (2002). Synthesis of new cardanol and cardol derivatives by allylation and regioselective cyclocarbonylation reactions. *Synthesis* 18: 2749–2755. https://doi.org/10.1055/s-2002-35983.

49 Attanasi, O.A., Berretta, S., Fiani, C. et al. (2006). Synthesis and reactions of nitro derivatives of hydrogenated cardanol. *Tetrahedron* 62 (25): 6113–6120. https://doi.org/10.1016/j.tet.2006.03.105.

50 Gazzotti, S., Ortenzi, M.A., Farina, H. et al. (2020). Carvacrol- and cardanol-containing 1,3-dioxolan-4-ones as comonomers for the synthesis of functional polylactide-based materials. *Macromolecules* 53 (15): 6420–6431. https://doi.org/10.1021/acs.macromol.0c01537.

51 John, G., Jung, J.H., Minamikawa, H. et al. (2002). Morphological control of helical solid bilayers in high-axial-ratio nanostructures through binary self-assembly. *Chem. Eur. J.* 8 (23): 5494–5500. https://doi.org/10.1002/1521-3765(20021202)8:23<5494::AID-CHEM5494>3.0.CO;2-P.

52 John, G., Jung, J.H., Masuda, M., and Shimizu, T. (2004). Unsaturation effect on gelation behavior of aryl glycolipids. *Langmuir* 20 (6): 2060–2065. https://doi.org/10.1021/la030177h.

53 Balachandran, V.S., Jadhav, S.R., Vemula, P.K., and John, G. (2013). Recent advances in cardanol chemistry in a nutshell: from a nut to nanomaterials. *Chem. Soc. Rev.* 42 (2): 427–438. https://doi.org/10.1039/c2cs35344j.

54 Surya Prakash Rao, H., Kamalraj, M., Swain, J., and Mishra, A.K. (2014). Characterization and phase transition study of a versatile molecular gel from a glucose-triazole-hydrogenated cardanol conjugate. RSC. *Adv.* 4 (24): 12175–12181. https://doi.org/10.1039/c3ra47540a.

55 Swain, J., Kamalraj, M., Prakash Rao, H.S., and Mishra, A.K. (2014). Thermotropic gelation induced changes in micropolarity and microviscosity of hydrogel derived from glucose-triazole-hydrogenated cardanol conjugate: a study using fluorescent molecular probe. *RSC Adv.* 4 (98): 55377–55382. https://doi.org/10.1039/c4ra08686d.

56 Swain, J., Kamalraj, M., Surya Prakash Rao, H., and Mishra, A.K. (2015). Effect of a glucose-triazole-hydrogenated cardanol conjugate on lipid bilayer membrane organization and thermotropic phase transition. *J. Mol. Struct.* 1081: 124–127. https://doi.org/10.1016/j.molstruc.2014.10.013.

57 Luo, Y., Liang, W., Ma, W. et al. (2020). Cardanol-derived cationic surfactants enabling the superior antibacterial activity of single-walled carbon nanotubes. *Nanotechnology* 31 (26): 265603. https://doi.org/10.1088/1361-6528/ab7aa4.

58 Attanasi, O.A., Del Sole, R., Filippone, P. et al. (2004). Synthesis of fullerene-cardanol derivatives. *Synlett* 5: 799–802. https://doi.org/10.1055/s-2004-820014.

59 Attanasi, O.A., Mele, G., Filippone, P. et al. (2009). Synthesis and characterization of novel cardanol based fulleropyrrolidines. *Arkivoc* 2009 (8): 69–84. https://doi.org/10.3998/ark.5550190.0010.807.

60 Braga, F.C., Ojeda, M., Perdomo, R.T. et al. (2021). Synthesis of cardanol-based 1,2,3-triazoles as potential green agents against neoplastic cells. *Sustainable Chem. Pharm.* 20: 100408. https://doi.org/10.1016/j.scp.2021.100408.

61 Reddy, T.N., Beatriz, A., da Lopes, R.S. et al. (2018). Design, synthesis and structure-activity relationship of novel phenolic based pyrimidine hybrids from Cashew Nut Shell Liquid (CNSL) components as potential antitumor agents. *Chem. Biol. Lett.* 5 (2): 41–54.

62 Attanasi, O.A., Del Sole, R., Filippone, P. et al. (2004). Synthesis of novel lipophilic porphyrin-cardanol derivatives. *J. Porphyrins Phthalocyanines* 8 (11): 1276–1284. https://doi.org/10.1142/S1088424604000635.

63 Puangmalee, S., Petsom, A., and Thamyongkit, P. (2009). A porphyrin derivative from cardanol as a diesel fluorescent marker. *Dyes Pigm.* 82 (1): 26–30. https://doi.org/10.1016/j.dyepig.2008.10.015.

64 Vasapollo, G., Mele, G., and Del Sole, R. (2011). Cardanol-based materials as natural precursors for olefin metathesis. *Molecules* 16 (8): 6871–6882. https://doi.org/10.3390/molecules16086871.

65 Attanasi, O.A., Ciccarella, G., Filippone, P. et al. (2003). Novel phthalocyanines containing cardanol derivatives. *J. Porphyrins Phthalocyanines* 7 (1): 52–57. https://doi.org/10.1142/S1088424603000082.

66 Słota, R., Dyrda, G., Hofer, M. et al. (2012). Novel lipophilic lanthanide bis-phthalocyanines functionalized by pentadecylphenoxy groups: synthesis, characterization and UV-photostability. *Molecules* 17 (9): 10738–10753. https://doi.org/10.3390/molecules170910738.

67 Sandrino, B., da Clemente, C.S., Oliveira, T.M.B.F. et al. (2013). Amphiphilic porphyrin-cardanol derivatives in Langmuir and Langmuir–Blodgett films applied for sensing. *Colloids Surf., A* 425: 68–75. https://doi.org/10.1016/j.colsurfa.2013.02.033.

68 Oliveira, T.I.S., dos Santos, V.N., Lomonaco, D. et al. (2013). Gold electrode modified with cu-porphyrin derived from cardanol as electrochemical sensor for nitric oxide. *J. Electrochem. Soc.* 160 (8): B113–B118. https://doi.org/10.1149/2.080308jes.

69 Clemente, C.S., Ribeiro, V.G.P., Sousa, J.E.A. et al. (2013). Porphyrin synthesized from cashew nut shell liquid as part of a novel superparamagnetic fluorescence nanosystem. *J. Nanopart. Res.* 15 (6): 1739. https://doi.org/10.1007/s11051-013-1739-6.

70 Deyab, M.A., Mele, G., Al-Sabagh, A.M. et al. (2017). Synthesis and characteristics of alkyd resin/M-porphyrins nanocomposite for corrosion protection application. *Prog. Org. Coat.* 105: 286–290. https://doi.org/10.1016/j.porgcoat.2017.01.008.

71 Lima, N.M.A., Avila, H.J.C., Marchiori, C.F.N. et al. (2019). Light-emitting porphyrin derivative obtained from a subproduct of the cashew nut shell liquid: a promising material for OLED applications. *Materials* 12 (7): https://doi.org/10.3390/ma12071063.

72 Lima, N.M.A., Bezerra, T.T., Almeida, M.O. et al. (2021). Photodynamic effect of palladium porphyrin derived from cashew nut shell liquid against promastigote forms of *Leishmania braziliensis*. *Photodiagn. Photodyn. Ther.* 33: 102083. https://doi.org/10.1016/j.pdpdt.2020.102083.

73 Mele, G., Del Sole, R., Vasapollo, G. et al. (2004). Polycrystalline TiO_2 impregnated with cardanol-based porphyrins for the photocatalytic degradation of 4-nitrophenol. *Green Chem.* 6 (12): 604–608. https://doi.org/10.1039/b409510c.

74 Vasapollo, G., Mele, G., Del Sole, R. et al. (2011). Use of novel cardanol-porphyrin hybrids and their TiO_2-based composites for the photodegradation of 4-nitrophenol in water. *Molecules* 16 (7): 5769–5784. https://doi.org/10.3390/molecules16075769.

75 Ribeiro, V.G.P., Marcelo, A.M.P., da Silva, K.T. et al. (2017). New ZnO@Cardanol porphyrin composite nanomaterials with enhanced photocatalytic capability under solar light irradiation. *Materials* 10 (10): https://doi.org/10.3390/ma10101114.

76 Pennetta, A., Di Masi, S., Piras, F. et al. (2020). TiO_2@lipophilic porphyrin composites: new insights into tuning the photoreduction of Cr(VI) to Cr(III) in aqueous phase. *J. Compos. Sci.* 4 (2): 82. https://doi.org/10.3390/jcs4020082.

77 García-López, E.I., Pomilla, F.R., Bloise, E. et al. (2020). C_3N_4 impregnated with porphyrins as heterogeneous photocatalysts for the selective oxidation of 5-hydroxymethyl-2-furfural under solar irradiation. *Top. Catal.* https://doi.org/10.1007/s11244-020-01293-0.

78 Visconti, P., Primiceri, P., de Fazio, R. et al. (2018). Improved photo-ignition of carbon nanotubes/ferrocene using a lipophilic porphyrin under white power LED irradiation. *Materials* 11 (1): 127. https://doi.org/10.3390/ma11010127.

79 Bloise, E., Carbone, L., Colafemmina, G. et al. (2012). First example of a lipophilic porphyrin-cardanol hybrid embedded in a cardanol-based micellar nanodispersion. *Molecules* 17 (10): 12252–12261. https://doi.org/10.3390/molecules171012252.

80 Ribeiro, M., Júnior, L., Fechine, D. et al. (2019). Nanomaterials based on Fe_3O_4 and phthalocyanines derived from cashew nut shell liquid. *Molecules* 24 (18): 3284. https://doi.org/10.3390/molecules24183284.

81 da Costa Júnior, A.E., Mota, J.P.F., Pontes, S.M.A. et al. (2017). A self-assembly of graphene oxide@Fe_3O_4/metallo-phthalocyanine nanohybrid materials: synthesis, characterization, dielectric and thermal properties. *J. Mater. Sci.* 52 (16): 9546–9557. https://doi.org/10.1007/s10853-017-1133-3.

9

Synthesis of Heterocycles in Nonconventional Bio-based Reaction Media

Anton V. Dolzhenko[1,2]

[1] *Monash University Malaysia, School of Pharmacy, Jalan Lagoon Selatan, Bandar Sunway, Selangor 47500, Malaysia*
[2] *Curtin University, Curtin Health Innovation Research Institute, School of Pharmacy and Biomedical Sciences, GPO Box U1987, Perth, Western Australia 6845, Australia*

9.1 Introduction

Organic synthesis, including the preparation of heterocyclic compounds, often requires solvents as reaction media. Quantities of solvents used in the process are usually manyfold greater than the amounts of reagents. Many classical organic solvents traditionally used as reaction media are considered nowadays as unsafe for the environment. Since most of these solvents are volatile liquids used in large volumes, their environmental impact became substantial. Further concerns are raised due to the origin of the majority of common organic solvents from nonrenewable fossil sources. For more sustainable chemistry practice, these solvents should be replaced with more environmentally friendly reaction media from renewable feedstocks, i.e. bio-based solvents, which contribute to an emerging and expanding range of green solvents [1]. Bio-based solvents are directly linked to two out of the 12 green chemistry principles [2]: the use of benign solvents and auxiliaries (principle 5) and the use of renewable feedstocks (principle 7).

Additionally, the good biodegradability of bio-based solvents and their beneficial occupational safety profile resonate well with other green chemistry principles from the design for degradation without pollutant problems to the less hazardous synthesis.

Bio-based solvents are different due to the feedstock origin and production processes, and often these processes contribute to waste prevention and reduction. Many bio-based solvents are produced from by-products of other industrial operations or use biowaste materials as feedstock. For example, glycerol is the main by-product of oily biomass transesterification in biodiesel production [3]. Limonene, directly extracted from citrus rind, is a by-product of the citrus juice industry [4]. Lactic acid, gluconic acid, levulinic acid, and Cyrene are produced by biochemical and catalytic transformations of carbohydrate-containing biomass, including waste from the agricultural and food industries. Some of these chemicals

Heterocycles: Synthesis, Catalysis, Sustainability, and Characterization, First Edition.
Edited by Teresa M.V.D. Pinho e Melo and Marta Pineiro.

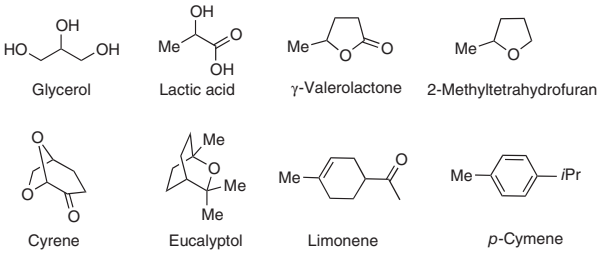

Figure 9.1 Some bio-based media for organic synthesis.

serve as platforms for further derivatization to other useful bio-based solvents, like ethyl lactate, γ-valerolactone (GVL), and 2-methyltetrahydrofuran (2-MeTHF). The interest in developing more sustainable methods for organic synthesis resulted in attempts to use these products as media for chemical reactions [5–12].

This chapter focuses on applications of bio-based media, particularly glycerol, lactic acid, GVL, 2-MeTHF, Cyrene, limonene, eucalyptol, and *p*-cymene (Figure 9.1), for the synthesis of heterocyclic compounds. The performance of these media is compared to the effectiveness of classical organic solvents.

9.2 Heterocyclizations in Glycerol

Glycerol is a common name of 1,2,3-propanetriol, a polyol ubiquitously present in nature as esterified derivatives, viz. triglycerides (fats and oils). The production of glycerol has shifted to processes utilizing biomass, and these methods have been effectively replacing the glycerol preparation from fossil resources (petroleum-derived propene). Nowadays, most of the global production of glycerol originates from biodiesel production, where glycerol is the main co-product [3, 13, 14]. Together with one ton of biodiesel, about 110 kg of crude (about 100 kg of pure), glycerol is co-produced. The success of the biodiesel industry significantly increased the market offering for glycerol: about 80% of total glycerol production comes from biodiesel manufacturing [15]. This situation reduced glycerol cost, thus making it a more available and attractive starting material for the production of valuable organic compounds [16–19]. Glycerol is a nonvolatile, nonflammable, nontoxic, recyclable, and easily biodegradable liquid possessing promising characteristics of a green solvent, which can serve as a medium for organic synthesis (Table 9.1) [20–22]. The high viscosity of glycerol, being a drawback for its applications as a reaction medium due to poor mass transfer, can be decreased by heating over 60 °C or using cosolvents (including water). The immiscibility of glycerol with nonpolar organic solvents facilitates isolation of reaction products by extraction and subsequent recovery of glycerol (often together with catalysts). The loss tangent value of 0.651 (at microwave frequency 2.45 GHz) makes glycerol an excellent medium for microwave-assisted organic synthesis [23]. Many contributions have been made utilizing glycerol as a medium for the synthesis of heterocycles as illustrated in the following text.

Table 9.1 Selected physical properties of glycerol.

Boiling point	290 °C
Flash point	177 °C (open cup)
Density, ρ	1.2613 g cm^{-3} (at 20 °C)
Viscosity, η	954 cP (at 25 °C)
Vapor pressure	1.68×10^{-4} mmHg (at 25 °C)
Solubility in water	Miscible
LogP (octanol/water)	−1.76

Source: Adapted from Díaz-Álvarez et al. [20], Jérôme [21], and García et al. [22].

9.2.1 Synthesis of Five-Membered Heterocycles in Glycerol

The Ru-catalyzed ring-closing metathesis of *N*,*N*-diallyltosylamine was effectively performed in glycerol under microwave irradiation with the quantitative conversion of the substrate to *N*-tosyldihydropyrrole (**1**) (Scheme 9.1) [24]. The catalyst and glycerol were reused in this reaction three times retaining a good activity, but the fourth run afforded only 19% of **1** due to the catalyst loss.

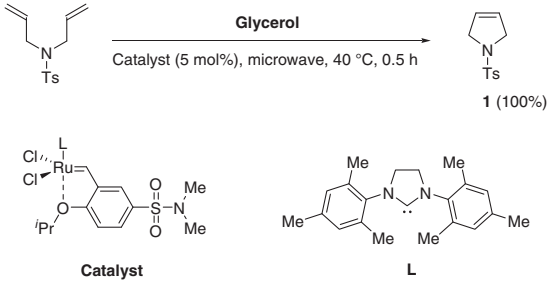

Scheme 9.1 Microwave-assisted ring-closing metathesis in glycerol.

Glycerol was suggested to play the roles of medium and reactant in the pyrrole ring annulation to 2-phenyl-3-methylquinoxaline affording **2**, which structure was confirmed by X-ray crystallographic studies (Scheme 9.2) [25].

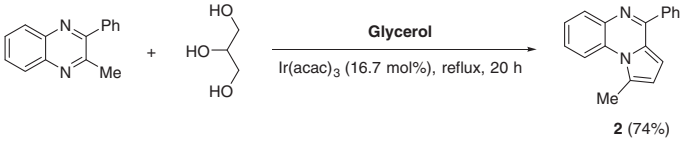

Scheme 9.2 Reaction of 2-phenyl-3-methylquinoxaline with glycerol.

In the comparative study of the efficiency of water and glycerol as media for the synthesis of 2,3-dimethylfuran (**4**) by cycloisomerization of (*Z*)-enynol **3** under the catalysis by hydrophilic Pd(II) complexes, both solvents demonstrated a good activity

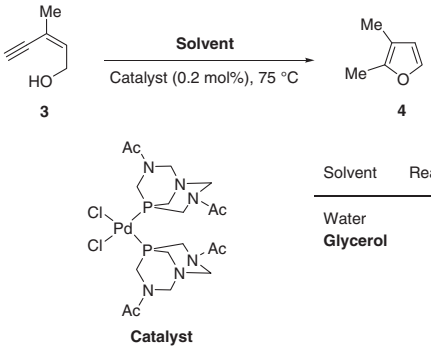

Solvent	Reaction time (min)	Yield (%)
Water	15	99
Glycerol	20	99

Scheme 9.3 Synthesis of 2,3-dimethylfuran (**4**) from (*Z*)-enynol **3**.

(Scheme 9.3) [26]. However, the reusability of the catalytic system was greater in the case of glycerol. In glycerol, the catalyst was effectively reused in 17 cycles with an excellent cumulative turnover number (TON) of 8190. The reaction was also successful with more decorated (*Z*)-enynols bearing substituents at positions 1 and 5.

Glycerol was the preferred solvent in the model reaction of α-phenylselanylacetylacetone with phenylhydrazine affording pyrazole **5** in better yield and shorter time (Scheme 9.4) [27]. This reaction was effectively performed using various α-arylselanyl-1,3-diketones and arylhydrazines.

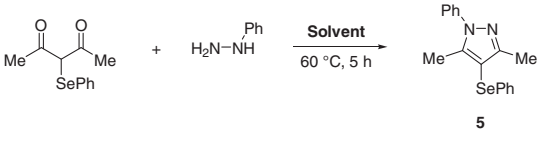

Solvent	Yield (%)
EtOH	77
Water	53
PEG-400	27
Glycerol[a]	82

[a] 3 h reaction time.

Scheme 9.4 Synthesis of 4-arylselanyl-substituted pyrazole **5**.

The synthesis of pyranopyrazole derivatives utilizing glycerol as a medium has been reported [28–30]. For example, ninhydrin reacted with hydrazone **6** affording pyrazoloisocoumarin **7** (Scheme 9.5) [28]. Glycerol was found to be more efficient in this reaction than other solvents, and the synthesis proceeded with similar efficiency when other arylhydrazones were used as substrates.

The formation of the tetrahydropyrano[2,3-*c*]pyrazole ring system was also achieved via a one-pot, two-step reaction in glycerol [29]. The reaction of arylhydrazines and β-ketoesters produced 1,3-disubstituted 5-pyrazolones, which then reacted with styrenes and paraformaldehyde to give the target compounds. This approach is exemplified by the synthesis of **8** from phenylhydrazine, ethyl benzoylacetate, α-methylstyrene, and paraformaldehyde (Scheme 9.6).

The four-component reaction of ethyl acetoacetate, hydrazine, benzaldehyde, and malononitrile resulted in the formation of pyrano[2,3-*c*]pyrazole **9** (Scheme 9.7) [30]. In this reaction, glycerol outperformed conventional organic solvents. Moreover, it

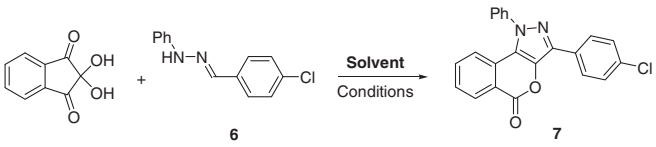

6 7

Solvent	Temperature (°C)	Time (h)	Yield (%)
EtOH	Reflux	12	0
^{n}BuOH	Reflux	12	48
GVL	Reflux	12	45
PEG-400	85	8	61
Glycerol	75	4	91

Scheme 9.5 Reaction of ninhydrin with an arylhydrazone affording a pyrazoloisocoumarin derivative.

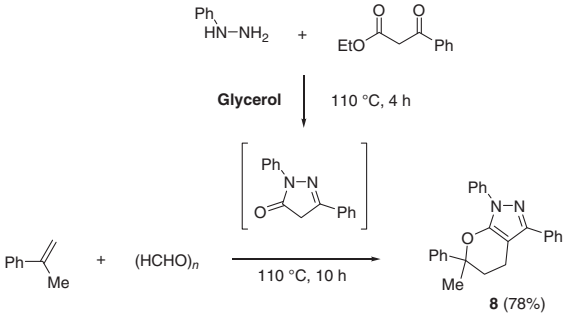

8 (78%)

Scheme 9.6 Multicomponent synthesis of a tetrahydropyrano[2,3-*c*]pyrazole in glycerol.

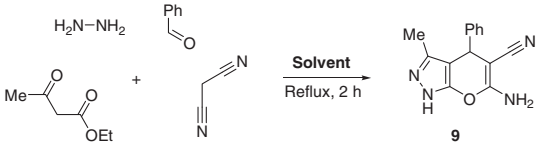

9

Solvent	Yield (%)
Chloroform	Traces
Dichloromethane (DCM)	Traces
AcOEt	Traces
MeCN	Traces
DMF	Traces
MeOH	57
EtOH	61
Water	64
PEG-400	27
Glycerol[a]	92

[a] 100 °C, 80 min.

Scheme 9.7 Four-component synthesis of the pyrano[2,3-*c*]pyrazole ring system.

was demonstrated that after extraction of **9** with ethyl acetate/hexane, the recovered glycerol could be reused in several runs with similar efficiency (87% yield after five runs). The reaction in glycerol was found to tolerate a variety of aromatic aldehydes affording analogs of **9** in comparable yield.

Glycerol demonstrated a better performance than conventional alcohol media, PEG-400, or lactic acid in the synthesis of imidazo[1,2-*a*]pyridines from 2-aminopyridine and 2-bromoacetophenone (Scheme 9.8) [31]. The yield of

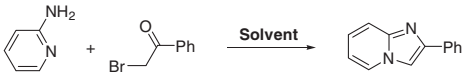

10

Solvent	Temperature (°C)	Time (h)	Yield (%)
MeOH	Reflux	6	45
EtOH	Reflux	6	40
^{n}BuOH	60	8	70
PEG-400	80	8	60
Lactic acid	60	8	65
Glycerol	60	1	90

Scheme 9.8 Synthesis of 2-phenylimidazo[1,2-*a*]pyridine (**10**).

2-phenylimidazo[1,2-*a*]pyridine (**10**) was further improved to 94% by using aqueous glycerol (glycerol : water – 4 : 1). In the reaction scaled up from 1 to 11 mmol, the yield remained high (91%). It was reported that after the reaction, glycerol could be recycled and reused in up to four cycles without significant loss of yield. The reaction was also efficient using 2-bromoacetophenones with various substituents in the aromatic ring. The imidazole-fused derivatives were also obtained using 2-amino-substituted pyridines, pyrimidine, or pyrazine as substrates.

It was reported [32] that the reaction of *o*-phenylenediamine with benzaldehyde carried out in glycerol resulted in the formation of 1-benzyl-2-phenylbenzimidazole (**11**) in good yield (Scheme 9.9). No significant loss in yield was detected when the reaction was repeated in four runs using the recovered glycerol, and only in the fifth run, the yield of **11** decreased to 85%. It was demonstrated that this reaction in glycerol was rather general and tolerated aromatic (including heterocyclic) and aliphatic aldehydes producing the corresponding analogs of **11** in similar yields.

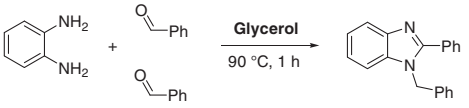

11 (91%)

Scheme 9.9 Synthesis of a benzimidazole in glycerol.

Interestingly, a similar reaction of equimolar quantities of *o*-phenylenediamine and benzaldehyde in aqueous glycerol at the same temperature was reported by another group [33] to afford 2-phenylbenzimidazole (**12**) (Scheme 9.10). The scope of this reaction was claimed to be broad: benzaldehydes, cinnamaldehyde, and heteroaryl aldehydes were well tolerated in the synthesis of 2-substituted

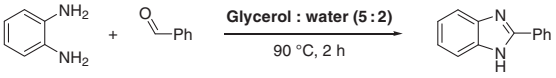

12 (75%)

Scheme 9.10 Synthesis of 2-phenylbenzimidazole (**12**) in aqueous glycerol.

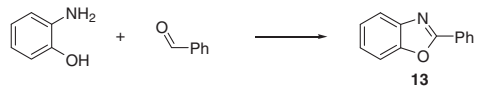

13

Solvent	Temperature (°C)	Time (min)	Yield (%)	Ref.
Glycerol : water (5 : 2)	90	240	90	33
Glycerol	110[a]	3	87	34

[a] Microwave irradiation.

Scheme 9.11 Synthesis of 2-phenylbenzoxazole (**13**) in glycerol.

benzimidazoles. Moreover, 2-substituted benzoxazoles (e.g. **13**, Scheme 9.11) were prepared under similar conditions from *o*-aminophenol and aldehydes.

In another study [34], **13** was prepared in 87% by heating *o*-aminophenol and benzaldehyde in glycerol under microwave irradiation at 110 °C for just three minutes. The microwave power was found to substantially affect the reaction outcome, and the best results were obtained at 20 W irradiation. Several aldehydes were effectively utilized in this process demonstrating a good scope of the method (Scheme 9.11).

The microwave irradiation in glycerol was also used for the efficient preparation of 2-arylbenzothiazoles from *o*-aminothiophenol and aldehydes [35]. For example, 2-phenylbenzothiazole (**14**) was obtained by this method in 92% yield (Scheme 9.12). The microwave irradiation and its power were reported to be important for the success of the reaction. The yield of **14** obtained under conventional heating for eight hours was only 56%. The best results were obtained when 180 W microwave irradiation was applied. Another study [36], however, claimed preparation of **14** in 92% yield from *o*-aminothiophenol and benzaldehyde in glycerol at ambient temperature within 30 minutes.

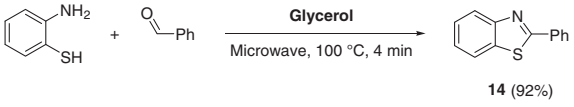

14 (92%)

Scheme 9.12 Synthesis of 2-phenylbenzothiazole (**14**) in glycerol.

The cyclization of *o*-aminothiophenol was performed by the treatment with potassium *O*-ethyldithiocarbonate in glycerol under microwave irradiation to afford benzothiazole-2-thiol (**15**) (Scheme 9.13) [37]. Several analogs of **15**, including benzoxazole-2-thiols, were prepared from *o*-amino(thio)phenols under similar conditions using glycerol or PEG-400 as media.

15 (94%)

Scheme 9.13 Synthesis of benzothiazole-2-thiol (**15**) in glycerol.

The thiazole ring closure under microwave irradiation was performed by the reaction of 2-bromoacetophenones and 2-cyanothioacetamide in glycerol

Scheme 9.14 Synthesis of a thiazole from 2-bromoacetophenone and 2-cyanothioacetamide in glycerol.

(Scheme 9.14) [38]. The reaction was more efficient and selective toward the formation of **16** when dry glycerol was used as a medium. Substituents in the benzene ring of 2-bromoacetophenone were well tolerated, allowing preparation of several analogs of **16** in generally good yields.

Glycerol was found to be an efficient solvent for the reaction of thiosemicarbazide with 2-bromoacetophenone and *p*-nitrobenzaldehyde, resulting in the thiazole ring closure and formation of hydrazone **17** (Scheme 9.15) [39]. The best results were obtained when cetyltrimethylammonium bromide (CTAB) was used as a phase transfer catalyst in glycerol. The reactions in ethanol, water, or PEG-400 were less efficient in terms of reaction time and yields. In glycerol, the reaction was successful in 1 and 10 mmol scales. It was also demonstrated that glycerol can be recovered and reused for the synthesis of **17** in five cycles with less than a 10% decrease in the yield. The reaction scope was found to be rather general, and thiosemicarbazide was converted to analogs of **17** upon the treatment with various bromoketones and aldehydes or ketones (including a series of isatins).

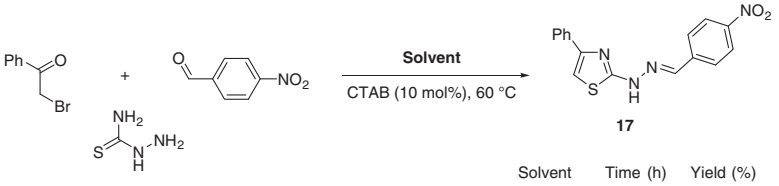

Solvent	Time (h)	Yield (%)
EtOH	6	68
Water	3	67
PEG-400	5	74
Glycerol	1	96

Scheme 9.15 Three-component synthesis of thiazoles.

9.2.2 Synthesis of Six-Membered Heterocycles in Glycerol

It was reported [40] that a diastereomeric mixture of octahydroacridines **18** can be obtained via the domino reaction of aniline with (*R*)-citronellal in glycerol (Scheme 9.16). The application of glycerol as a medium resulted in the convenient isolation of product **18**, immiscible with this solvent, by decantation. In experiments with recovered glycerol, the yield of **18** remained high (90%) even after four runs.

The four-component Hantzsch reaction was effectively performed in glycerol affording hexahydroquinoline-5-one **19** in good yield (Scheme 9.17) [41]. The method was successfully applied in the synthesis of close analogs of **19**, and

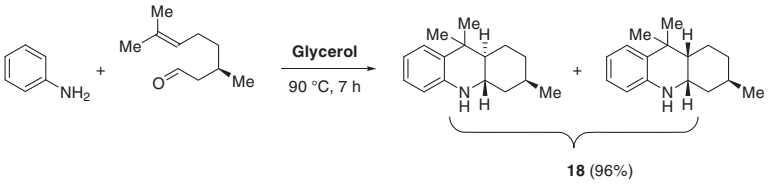

Scheme 9.16 Synthesis of octahydroacridines **18** in glycerol.

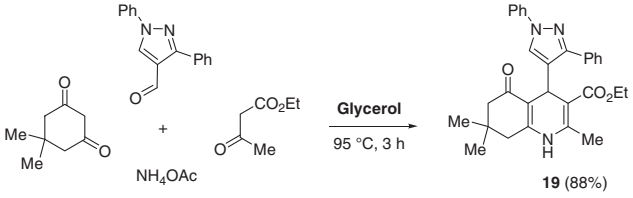

Scheme 9.17 Synthesis of a hexahydroquinoline-5-one in glycerol via Hantzsch reaction.

some of these products were found to exhibit *in vitro* activity against *Mycobacterium tuberculosis*.

Glycerol was applied as a medium for the synthesis of diverse fused pyran derivatives using various approaches for the pyran ring construction. Thus, glycerol was found to be an efficient medium for the Petasis borono–Mannich reaction of salicylaldehydes (or picolinaldehyde), arylboronic acids, and secondary amines [42]. It was suggested that glycerol activates boronic acids forming their cyclic esters. When (*E*)-styrylboronic acid was employed for this reaction, 2-phenyl-2*H*-chromene (**21**) was obtained in high yield (Scheme 9.18). The dibenzylamine acted as a catalyst via the formation of intermediate **20** in the Petasis borono–Mannich reaction. It was demonstrated that performing this reaction at 50 °C allowed insolation of **20** in 70% yield corroborating the proposed mechanistic pathway.

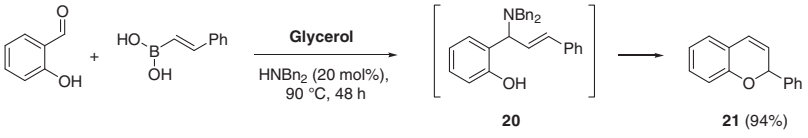

Scheme 9.18 Synthesis of 2-phenyl-2*H*-chromene (**21**) in glycerol.

It was reported that the reaction of β-naphthol and 4-fluorobenzaldehyde in the presence of acid was effectively performed using glycerol as a medium and resulted in the formation of dibenzoxanthene **22** (Scheme 9.19) [43].

The annulation of the tetrahydropyran ring was achieved via the three-component reaction of dimedone, formaldehyde, and styrene (Scheme 9.20) [44]. Proceeding via the Knoevenagel condensation and hetero-Diels–Alder reaction, the synthesis of **23** was more successful when glycerol was used as a medium, while other solvents, except acetic acid, were less efficient. Nevertheless, the isolation of **23** from acetic acid was found to be less sustainable due to the neutralization step, which required

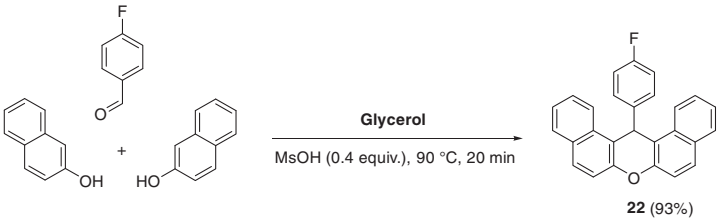

Scheme 9.19 Synthesis of a dibenzoxanthene from β-naphthol and 4-fluorobenzaldehyde in glycerol.

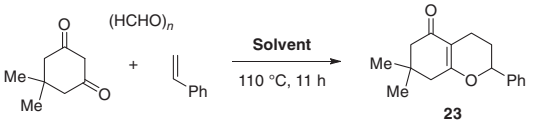

Solvent	Yield (%)
Toluene	<10
$MeNO_2$	33
AcOH	63
Water	14
Glycerol	68

Scheme 9.20 Three-component reaction of dimedone, formaldehyde, and styrene.

a substantial quantity of base. The scope of this reaction in glycerol was explored using various 1,3-cyclohexanediones and styrenes. Furthermore, three-component reactions using β-naphthol or 4-hydroxy-6-methyl-2-pyrone as substrates instead of styrene were also reported [44]. Thus, tetrahydrobenzo[*a*]xanthen-11-one **24** was obtained by heating of 1,3-cyclohexanediones, formaldehyde, and β-naphthol in glycerol at 130 °C for one hour (Scheme 9.21). Another fused pyran system **25** was prepared when dimedone, formaldehyde, and 4-hydroxy-6-methyl-2-pyrone reacted in glycerol at 90 °C (Scheme 9.22).

Glycerol substantially outperformed conventional organic solvents in the three-component reaction of dimedone, benzaldehyde, and malononitrile (Scheme 9.23) [45]. This reaction in other green media, like water, ethylene glycol, or PEG-400,

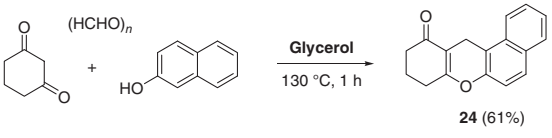

Scheme 9.21 Three-component reaction of 1,3-cyclohexanediones, formaldehyde, and β-naphthol in glycerol.

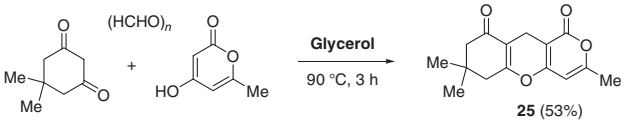

Scheme 9.22 Three-component reaction of dimedone, formaldehyde, and 4-hydroxy-6-methyl-2-pyrone in glycerol.

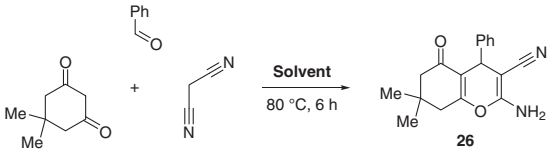

Solvent	Yield (%)
Toluene	<15
AcO^{n}Bu	<15
DMSO	<15
DMF	<15
EtOH	48
Water[a]	71
Ethylene glycol[b]	80
PEG-400[b]	83
Glycerol[c]	93

[a] 2.2 h.
[b] 1.5 h.
[c] 1 h.

Scheme 9.23 Three-component reaction of dimedone, benzaldehyde, and malononitrile.

was also less efficient than in glycerol. The reaction scope was demonstrated by successful employing of a variety of aldehydes in this reaction. Cyanoacetates behave in this three-component reaction similarly to malononitrile. Moreover, the pyran ring fusion was achieved when cyclohexanediones were replaced by α- and β-naphthols, 4-hydroxycoumarin, 5-methyl-2-phenyl-2,4-dihydro-3*H*-pyrazol-3-one, and barbituric acid as exemplified by the preparation of **27–31** (Scheme 9.24) [45]. Even greater chemical diversity was achieved when the scope of this three-component reaction in glycerol was extended to the synthesis of fused 4-spiro-substituted pyrans using isatins, acenaphthenequinone, or ninhydrin instead of aromatic aldehydes [45].

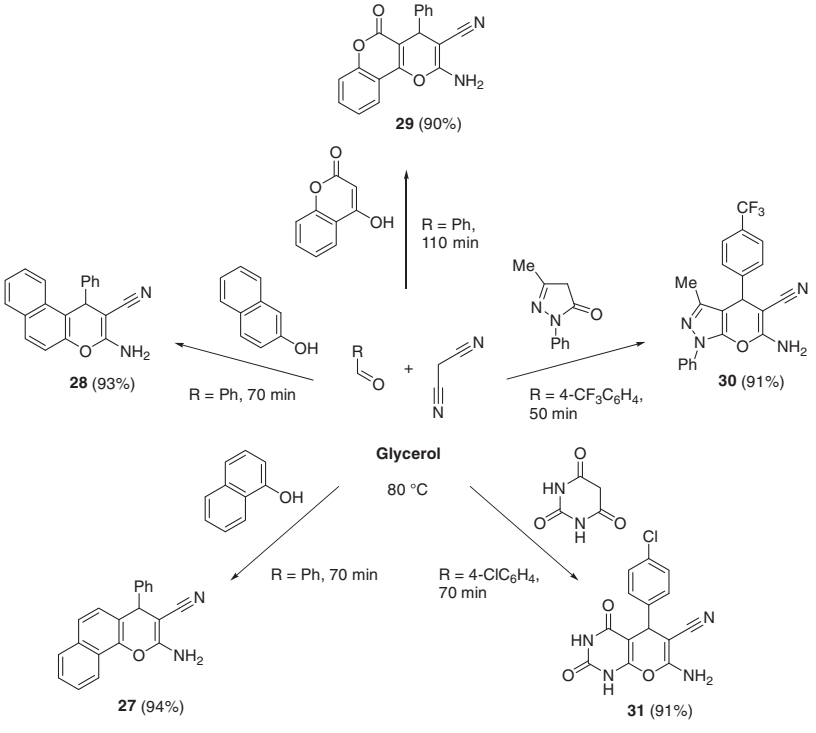

Scheme 9.24 Synthesis of 4*H*-pyran-fused derivatives via multicomponent reactions using glycerol as a medium.

Using glycerol as a medium in the domino reaction leading to heterocycle **32** (Scheme 9.25) allowed performing the reaction without additional catalyst, at the same time increasing the yield and decreasing the reaction time [46]. The reaction scope was demonstrated by the synthesis of 18 examples in similar yields.

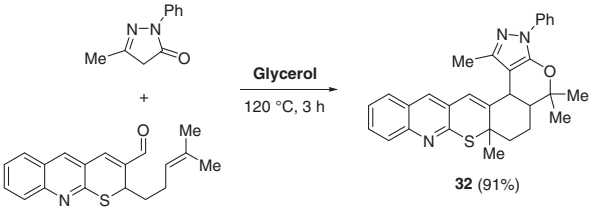

Scheme 9.25 Double ring closure in glycerol.

Glycerol was reported [33, 47] to be a suitable medium for the pyrazine ring annulation using reactions of 1,2-diamines with 1,2-diketones. For example, 2,3-diphenylquinoxaline (**33**) was obtained in the cerium(III) chloride-catalyzed reaction of *o*-phenylenediamines and benzyl (Scheme 9.26) [47]. Even though this reaction was claimed [47] to not proceed in the absence of the catalyst, another group [33] reported an effective synthesis of **33** from the same starting materials in aqueous glycerol without any catalyst (90 °C, 4 hours; 90% yield).

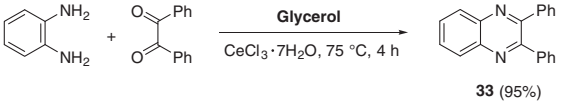

Scheme 9.26 Synthesis of 2,3-diphenylquinoxaline (**33**) in glycerol.

Under mild reaction conditions without any catalyst, the Betti reaction of β-naphthol, benzylamine, and formaldehyde in glycerol was accompanied by the oxazine ring closure affording **34** (Scheme 9.27) [43].

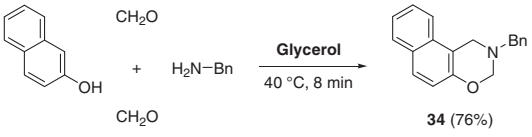

Scheme 9.27 Betti reaction with oxazine ring closure in glycerol.

9.2.3 Synthesis of Seven-Membered Heterocycles in Glycerol

The reaction of *o*-phenylenediamine with acetophenone in glycerol was reported [32] to produce 1,5-benzodiazepine **35** in excellent yield (Scheme 9.28). Structurally related benzodiazepines were successfully prepared by the treatment of *o*-phenylenediamine with other enolizable ketones under the same conditions.

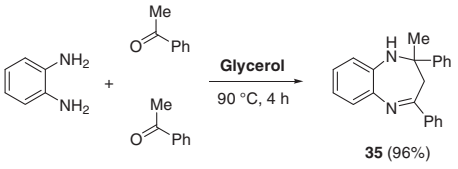

Scheme 9.28 Reaction of phenylenediamine with acetophenone in glycerol.

9.3 Heterocyclizations in Lactic Acid

Lactic acid is a common name of 2-hydroxypropanoic acid, a naturally occurring acid (typically as L-stereoisomer) biochemically derived from pyruvic acid by lactate dehydrogenase. Lactic acid is a low melting point solid miscible with water in any proportion, but not miscible with nonpolar organic solvents. The acidity of lactic acid is higher than that of acetic acid. Some physical properties of lactic acid are summarized in Table 9.2.

The industrial production of lactic acid is predominantly from renewable sources by fermentation of carbohydrates, including those from agricultural wastes of starchy and cellulosic nature. Many microorganisms (bacteria, fungi, and microalgae) have been reported [48] as good lactic acid producers, but due to the high tolerance of yeast and Lactobacillus strains to low pH, they are used by industry for fermentation of carbohydrate feedstock to lactic acid.

Lactic acid is an inexpensive, easily biodegradable, and nontoxic substance, which is recognized as a safe human food ingredient [49]. In the food industry, lactic acid is widely used as an antimicrobial agent, curing and pickling agent, flavoring agent, flavor enhancer, pH control agent, and solvent and vehicle [49]. In organic synthesis, lactic acid has also been applied as a reaction medium, though its ethyl ester is more known in this capacity [8]. Applications of lactic acids as a bio-based solvent for heterocyclic synthesis are discussed in the following text.

9.3.1 Synthesis of Five-Membered Heterocycles in Lactic Acid

Lactic acid was reported [50] to be an efficient medium for the ultrasound-promoted reduction and Knorr synthesis of pyrroles. For example, nitroso-intermediate **36**,

Table 9.2 Selected physical properties of lactic acid.

Melting point	53 °C
Boiling point	122 °C (at 15 mmHg)
Flash point	113 °C (closed cup)
Density (ρ)	1.2060 g cm^{-3} (at 21 °C)
Solubility in water	Miscible
LogP (octanol/water)	−0.72
pK_a	3.86 (at 20 °C)

prepared from ethyl acetoacetate, was effectively reduced in lactic acid and underwent cyclocondensation with ethyl acetoacetate to produce **37** in high yield (Scheme 9.29). Various combinations of 1,3-dicarbonyl compounds were well tolerated under the reaction conditions.

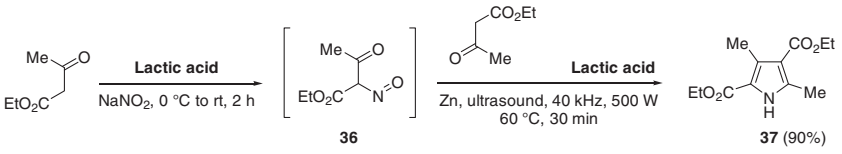

Scheme 9.29 Ultrasound-assisted synthesis of a functionalized pyrrole in lactic acid.

The four-component reaction of benzaldehyde, nitromethane, acetylacetone, and aniline in lactic acid at ambient temperature afforded pyrrole **38** in high yield (Scheme 9.30, Method A) [51]. The same reaction carried out in acetic acid under these conditions was inefficient. The yield was improved to nearly quantitative when the synthesis of **38** was performed in lactic acid using a three-component approach with β-nitrostyrene replacing benzaldehyde and nitromethane (Scheme 9.30, Method B). The scope of this method for the pyrrole ring construction was successfully extended to a variety of primary amines applied as substrates. It was demonstrated that reactions utilizing acetoacetates instead of acetylacetone were also efficient.

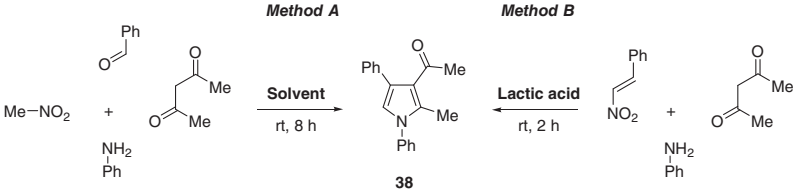

Solvent	Method	Yield (%)
AcOH	A	Traces
Lactic acid	A	90
Lactic acid	B	99

Scheme 9.30 Multicomponent syntheses of a functionalized pyrrole in lactic acid.

Another effective three-component synthesis of pyrroles in lactic acid was reported [52]. For example, the reaction of diethyl acetylenedicarboxylate, aniline, and *p*-chlorobenzaldehyde carried out under mild conditions and without additional catalyst afforded pyrrole **39** (Scheme 9.31). The synthesis of **39** performed in acetic acid instead of lactic acid was less efficient. In lactic acid, this three-component reaction was demonstrated to tolerate various anilines and benzaldehydes.

Lactic acid was found to be a good medium for the Debus–Radziszewski synthesis of imidazole **40** from benzil, ammonium acetate, and benzaldehyde (Scheme 9.32) [53]. Attempts to use catalytic quantities of lactic acid for this

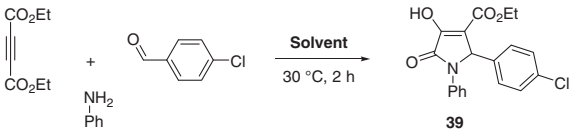

39

Solvent	Yield (%)
AcOH	33
Lactic acid	76

Scheme 9.31 Three-component synthesis of a 3-hydroxy-1*H*-pyrrol-2(5*H*)-one derivative.

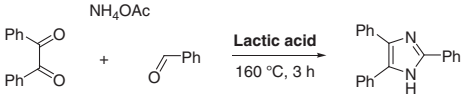

40 (90%)

Scheme 9.32 Synthesis of a functionalized imidazole via the Debus–Radziszewski reaction in lactic acid.

reaction in other solvent or under solventless conditions resulted in substantially lower yields of **40**. The reaction in lactic acid proceeded well without using any additional catalysts and tolerated a range of aromatic aldehydes.

Interestingly, the oxazole ring annulation with the formation of compound **42** took place when quinone **41** was heated with benzaldehyde and ammonium acetate in lactic acid (Scheme 9.33) [54]. The reaction proceeded chemo- and regioselectivity, and no products of the Debus–Radziszewski reaction were detected even when aniline was used instead of one of the ammonium acetate equivalents. Under the same conditions, the selective oxazole ring formation was observed in reactions of **41** with various aromatic, heterocyclic, and cinnamic aldehydes.

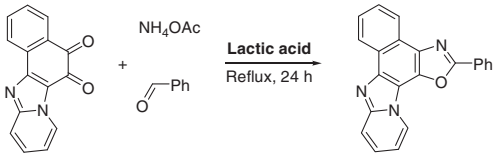

41 **42** (98%)

Scheme 9.33 Annulation of oxazole ring in lactic acid.

9.3.2 Synthesis of Six-Membered Heterocycles in Lactic Acid

Lactic acid was found to be a suitable solvent for the Friedländer quinoline synthesis without additional catalysts [52]. For example, condensation of *o*-aminoacetophenone with acetylacetone was found to be more efficient in lactic acid than in acetic acid and resulted in the formation of quinoline **43** in good yield (Scheme 9.34). This reaction of *o*-aminoacetophenone tolerated well a variety of 1,3-dicarbonyl substrates, including β-ketoesters and carbocyclic compounds.

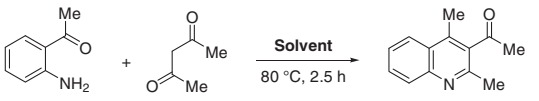

43

Solvent	Yield (%)
AcOH	85
Lactic acid	95

Scheme 9.34 Friedländer quinoline synthesis.

In the three-component reaction of sesamol, *p*-methylstyrene, and formaldehyde, lactic acid outperformed other classical and nonconventional bio-based solvents facilitating the cascade Knoevenagel/oxo Diels–Alder process affording chroman **44** (Scheme 9.35) [52]. Product **44** was separated using extraction with ethyl acetate/petroleum ether and the remaining lactic acid was reused for three cycles of the same reaction without loss of activity. The reaction was effectively scaled up from 0.65 to 10 mmol scale (71% yield). The successful tetrahydropyran ring formation in the reactions of various phenolic compounds or their analogs with formaldehyde and diverse styrenes demonstrated a good scope of this three-component reaction in lactic acid.

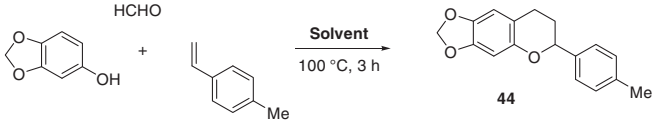

44

Solvent	Yield (%)
Toluene	< 5
MeCN	0
Dimethyl sulfoxide (DMSO)	Traces
Water	< 5
Glycerol	Traces
AcOH	25
Citric acid (aqueous 50%)	15
Gluconic acid (aqueous 50%)	< 5
Lactic acid	73

Scheme 9.35 Three-component reaction of sesamol, *p*-methylstyrene, and formaldehyde leading to a chroman derivative.

The tetrahydropyran ring formation via the Knoevenagel/oxo Diels–Alder reaction also occurred when phenolic compounds were replaced in this reaction by *N,N*-dialkylacetoacetamides [52]. In the reaction condition screening for the synthesis of **45**, lactic acid was identified as the most efficient medium (Scheme 9.36).

In the presence of aniline, salicylaldehydes reacted with diethyl acetylenedicarboxylate with the formation of substituted chromenes [52]. The reaction was particularly efficient in lactic acid. For example, chromene **46** was obtained in excellent yield from 3-methoxysalicylaldehyde and diethyl acetylenedicarboxylate when lactic acid was used as a medium, while other solvents were substantially less active (Scheme 9.37).

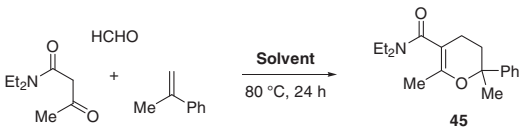

45

Solvent	Yield (%)
Toluene	0
DMSO	0
Water	0
Glycerol	0
AcOH	45
Gluconic acid (aqueous 50%)	40
Lactic acid	55

Scheme 9.36 Three-component synthesis of a tetrahydropyran derivative.

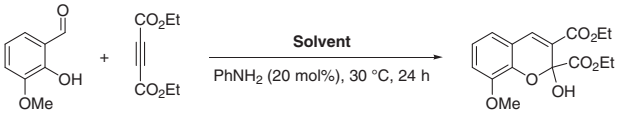

46

Solvent	Yield (%)
Glycerol	0
AcOH	32
Citric acid (aqueous 50%)	15
Gluconic acid (aqueous 50%)	6
Lactic acid	91

Scheme 9.37 Synthesis of a functionalized chromene.

The ultrasound-promoted Biginelli reaction was effectively performed in lactic acid [55]. The synthesis of dihydropyrimidinone **47** is an illustrative example of the use of this synthetic procedure (Scheme 9.38). A series of substituted pyrrole-2-carboxaldehydes were successfully involved in this reaction with acetoacetates and urea or thiourea.

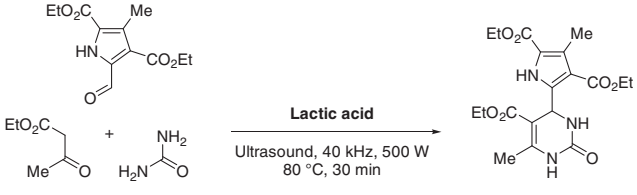

47 (84%)

Scheme 9.38 Synthesis of a pyrimidinone derivative via the Biginelli reaction.

9.4 Heterocyclizations in γ-Valerolactone

GVL is a common name of 5-methyloxolan-2-one (5-methyldihydro-2(3*H*)-furanone), which is a renewable and easily biodegradable natural product often

Table 9.3 Selected physical properties of γ-valerolactone.

Boiling point	207 °C
Flash point	96 °C (closed cup)
Density (ρ)	1.05 g cm^{-3} (at 25 °C)
Vapor pressure	26.3 mmHg (at 80 °C)
Solubility in water	Miscible
LogP (octanol/water)	−0.133

present in food. GVL is easily miscible with water and does not generate considerable vapor pressure event at elevated temperatures. Some physical properties of GVL are summarized in Table 9.3.

GVL is industrially produced by the catalytic hydrogenation of levulinic acid prepared from carbohydrate sources, including cellulose, hemicellulose, and lignocellulose-based biomass and starch-containing food waste (Scheme 9.39) [56].

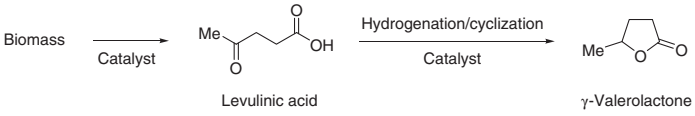

Scheme 9.39 Preparation of bio-based γ-valerolactone.

GVL is a nontoxic compound with an LD_{50} value equal to 8800 mg kg^{-1} (rats, orally). GVL is a permitted food additive used as a flavoring agent [57]. The distinct but pleasant smell of GVL also allows easy detection of leakage or spill. GVL is an efficient fuel additive and a useful green solvent for biomass processing [58, 59]. GVL can also be converted to many other high-value chemicals thus serving as a sustainable platform molecule [60]. There is a substantial interest in applications of GVL as a green solvent for organic synthesis and examples of GVL playing the role of an efficient medium for the preparation of heterocycles are discussed herein.

9.4.1 Synthesis of Five-Membered Heterocycles in γ-Valerolactone

In the study [61] focusing on the palladium-catalyzed C–H arylation of the N-substituted 1,2,3-triazoles using GVL as a medium, the intramolecular ring closure leading to the formation of 1,2,3-triazolo[1,5-*a*]isoindole **48** was reported (Scheme 9.40).

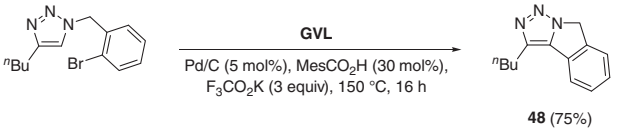

Scheme 9.40 Intramolecular C–H arylation in GVL.

In the Ru-catalyzed oxidative coupling of *o*-toluic acid with butyl acrylate, GVL was found to be a more efficient medium than other green solvents such as ethyl lactate and 2-MeTHF (Scheme 9.41) [62]. The yield of the resulting phthalide **49** was even higher (97%) when the reaction scale was increased from 1 to 5 mmol. It was found that molecular oxygen, playing the role of oxidant in the reaction, can be replaced by aqueous hydrogen peroxide using otherwise identical conditions, but the yield of **49** was lower (52%). The standard conditions based on the oxidation with molecular oxygen were effectively applied in the synthesis of phthalides using substituted benzoic acids and various alkyl acrylates.

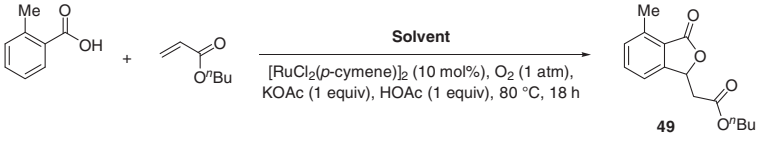

Solvent	Yield (%)
Ethyl lactate	59
2-MeTHF	81
GVL	90

Scheme 9.41 Synthesis of a phthalide via Ru-catalyzed oxidative coupling of *o*-toluic acid with butyl acrylate in green solvents.

GVL was found to be an efficient solvent for the formylation of amines with carbon dioxide in the presence of phenylsilane [63]. Outperforming classical solvents in the model formylation of *N*-methylaniline, GVL was applied as a solvent for formylation of a wide range of amines. When *o*-phenylenediamine was used as a substrate, the reaction furnished benzimidazole (**50**) and its *N*-formyl derivative **51** (Scheme 9.42). Similar reactions of *o*-aminophenol and *o*-aminothiophenol produced benzoxazole (**52**) and benzothiazole (**53**), respectively (Scheme 9.43).

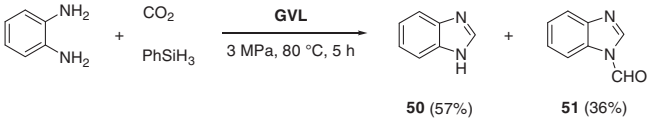

Scheme 9.42 Ring-closure formylation of *o*-phenylenediamine in GVL.

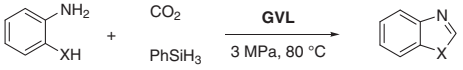

Product	X	Time (h)	Yield (%)
52	O	4	79
53	S	5	89

Scheme 9.43 Synthesis of benzoxazole (**52**) and benzothiazole (**53**) in GVL.

GVL was found to be an excellent solvent for microwave-promoted reactions, which benefit from the good microwave absorption and heating profiles of GVL.

Moreover, using GVL as a medium for the palladium-catalyzed reactions allowed to avoid hotspot formation under microwave irradiation [64].

The hydrogen transfer synthesis of benzimidazoles was effectively performed from *o*-phenylenediamines and aliphatic amines under microwave irradiation using crotononitrile as the hydrogen acceptor and GVL as the reaction medium [64]. In the model reaction of *o*-phenylenediamine and triethylamine, GVL afforded greater conversion than toluene (Scheme 9.44) and allowed isolation of 2-methylbenzimidazole (**54**) in 80% yield. Moreover, it was demonstrated that the catalyst loading could be reduced to 2.5 mol%, achieving the same conversion and similar isolated yield. This reaction was effectively performed using a variety of amines and was also successful when substituted *o*-phenylenediamines were used as substrates. The arching phenomenon, typical for microwave-assisted reactions catalyzed by Pd/C, was not observed when the reaction was performed in GVL.

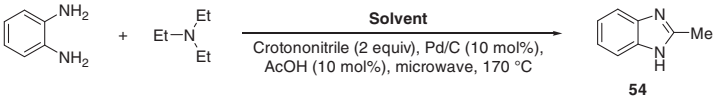

54

Solvent	Reaction time (min)	Conversion (%)	Yield (%)
Toluene	90	73	nr[a]
GVL	20	90	80
GVL[b]	20	90	78

[a] Not reported.
[b] 2.5 mol% of Pd/C were used.

Scheme 9.44 Hydrogen transfer palladium-catalyzed synthesis of 2-methylbenzimidazole (**54**).

9.4.2 Synthesis of Six-Membered Heterocycles in γ-Valerolactone

GVL was found to be a suitable solvent for the construction of the pyridine ring [65]. In the synthesis of isoquinoline **55** using the model reaction of acetophenone oxime and diphenylacetylene under the rhodium(III) catalysis, GVL was more effective than typical organic solvents (Scheme 9.45). The method tolerated various substituents in oximes, which were successfully involved in the reaction with diphenylacetylene or 1,4-diaryldiacetylenes.

The three-component reaction of isatin, malononitrile, and 4-hydroxycoumarin was effectively performed in GVL affording **56** in excellent yield without requiring the addition of catalysts (Scheme 9.46) [66]. The reaction was not efficient when carried out in other solvents. Upon heating at 80 °C in GVL, 16 analogs of **56** were prepared in consistently good yields (91–96%) using the reaction of (un)substituted isatin, malononitrile (or ethyl cyanoacetate as its equivalent), and 4-hydroxycoumarin. It should be noted that a similar multicomponent reaction was successfully performed under photocatalytic conditions in ethyl lactate, another bio-based solvent [67].

The four-component synthesis of 3-arylquinazolin-4-ones was efficiently performed under microwave irradiation [68]. For example, the reaction of *o*-iodoaniline,

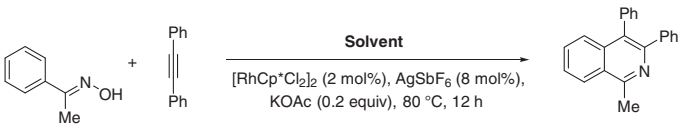

55

Solvent	Yield (%)
1,2-Dichloroethane (DCE)	60
THF	36
MeCN	46
DMF	58
DMSO	15
Water	20
GVL	88

Scheme 9.45 Rh-catalyzed synthesis of isoquinolines from *N*-hydroxyoximes and alkynes.

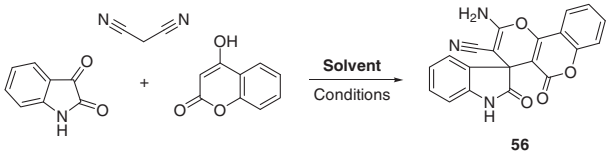

56

Solvent	Temperature (°C)	Time (h)	Yield (%)
MeOH	64	10	Traces
Water	100	10	Traces
MeCN	82	10	Traces
THF	66	10	Traces
DMSO	100	10	Traces
AcOH	100	10	28
GVL	80	0.5	95

Scheme 9.46 Three-component pyran ring annulation.

aniline, trimethyl orthoformate, and carbon monoxide, performed under the catalysis by the β-cyclodextrin cross-linked palladium, resulted in the formation of 3-phenylquinazolin-4-one (**57**) in excellent yield (Scheme 9.47). A variety of aromatic (except highly deactivated *o*-chloroaniline) and aliphatic amines were successfully used in this type of quinazolin-4-one synthesis. The 4-chloro- or 4-cyano-substitution of *o*-iodoaniline was also tolerated. For all reactions, GVL was compared with acetonitrile, which outperformed other conventional solvents in the optimization experiments. The reaction was found to be consistently more efficient

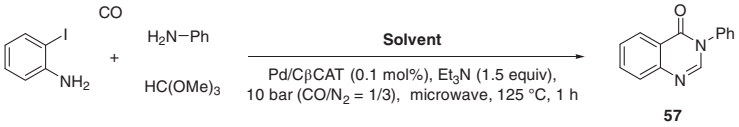

57

Solvent	Yield (%)
MeCN	94
GVL	97

Scheme 9.47 Multicomponent microwave-promoted synthesis of 3-phenylquinazolin-4-one (**57**).

in GVL than in acetonitrile for all substrates. It was demonstrated that the catalyst and GVL can be recovered and reused over several runs with minimal impact on the yield, thus further contributing to the sustainability of the process.

Using GVL as a medium for palladium-catalyzed reactions benefits from the minimal palladium leaching in this solvent. The previously described microwave-induced four-component reaction in GVL was incorporated into the synthetic protocol leading to 3-arylquinazolin-4-one **58** [69]. The procedure combined a direct arylation of 2-methylthiophene with *p*-nitrobromobenzene, a subsequent catalytic reduction of the nitro group, and the four-component reaction of the resulting aniline with *o*-iodoaniline, trimethyl orthoformate, and carbon monoxide affording **58** (Scheme 9.48). Unfortunately, the yield of **58** of this one-pot method was not reported, but in the independent microwave-assisted four-component reaction using potassium acetate as a base and otherwise identical conditions, **58** was obtained in 88% yield.

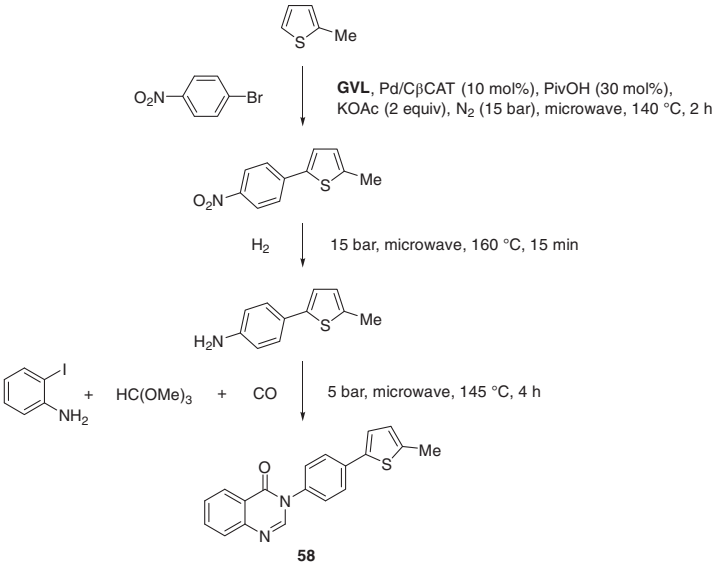

Scheme 9.48 One-pot microwave-promoted synthesis of a 3-arylquinazolin-4-one in GVL.

9.5 Heterocyclizations in 2-Methyltetrahydrofuran

2-MeTHF is a bio-based cyclic ether. In general, 2-MeTHF possesses properties similar to that of its conventional analog tetrahydrofuran (THF), which is typically obtained from nonrenewable sources. Like THF, 2-MeTHF is a strong Lewis base with an extraordinary coordinating potential toward metals [70]. However, in addition to a renewable character, 2-MeTHF possesses other properties making it a more sustainable and operationally convenient solvent than THF. Unlike THF, 2-MeTHF is only partially miscible in water and forms an azeotrope with water allowing a convenient solvent separation by distillation [71]. 2-MeTHF is more

Table 9.4 Selected physical properties of 2-MeTHF.

Boiling point	80 °C
Flash point	−10 °C (closed cup)
Density, ρ	0.8552 g cm^{-3} (at 20 °C)
Vapor pressure	102 mmHg (at 20 °C)
Solubility in water	14 g per 100 g at (at 20 °C)
LogP (octanol/water)	1.35

stable than THF in the presence of strong bases or acids [71]. The volatility of 2-MeTHF is also lower than that of THF. Some physical properties of 2-MeTHF are summarized in Table 9.4.

2-MeTHF is industrially produced from lignocellulose biomass via the catalytic hydrogenation of levulinic acid or furfural with or without isolation of intermediate GVL or furfuryl alcohol (Scheme 9.49) [72–74].

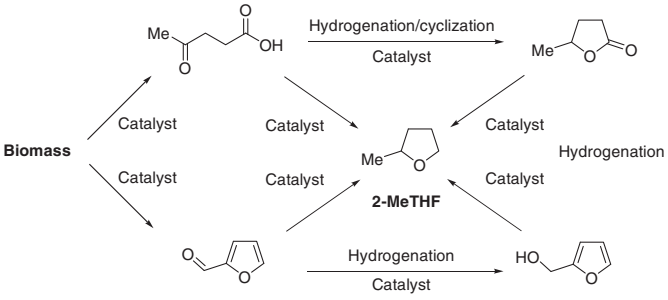

Scheme 9.49 Preparation of bio-based 2-methyltetrahydrofuran. Source: Adapted from Liu et al. [72], Obregón et al. [73, 74].

The production of 1 kg of bio-based 2-MeTHF is associated with 0.191 kg of overall and 0.150 kg of CO_2 life cycle emissions, which are nearly 30 times lower than those for THF [75]. 2-MeTHF demonstrated substantially lower toxicity than THF possessing LC_{50} value twofold greater than that of THF. No evidence of genotoxicity and mutagenicity was observed for 2-MeTHF [76]. These are properties of a green solvent attracting attention to 2-MeTHF as an alternative to conventional solvents, particularly THF, in organic synthesis [5]. Many metallorganic reactions found benefits in applying 2-MeTHF as a medium due to its good stability and coordinating properties [70, 77]. 2-MeTHF also demonstrated efficiency in several heterocyclization reactions as exemplified in the following text.

9.5.1 Synthesis of Five-Membered Heterocycles in 2-Methyltetrahydrofuran

A sustainable one-pot method for the synthesis of substituted pyrroles was developed via Michael addition of primary amines to ketal-functionalized β-nitroacrylates followed by cyclization–aromatization reactions under the

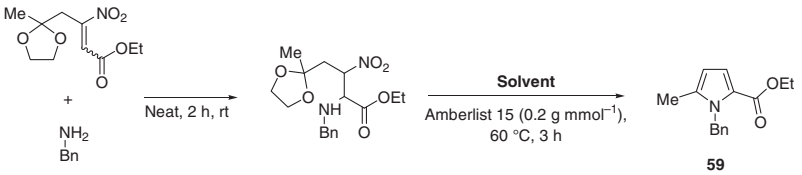

Solvent	Yield (%)
DCM	42
AcOEt	48
Cyclopentyl methyl ether (CPME)	55
2-MeTHF	68

Scheme 9.50 Amberlist 15-catalyzed synthesis of a functionalized pyrrole.

Amberlist 15 catalysis [78]. In the model reaction, 2-MeTHF was demonstrated to be a more efficient medium than other solvents (Scheme 9.50). Several analogs of **59** were successfully prepared using this Amberlist 15-catalyzed reaction in 2-MeTHF, and the method was further transferred to the flow synthesis using an Amberlist 15-packed column and 2-MeTHF as a carrier.

The palladium(II)-catalyzed synthesis of 2-aroylbenzofurans was efficiently carried out using 2-MeTHF as a medium [79]. In the model reaction, 2-MeTHF outperformed conventional organic solvents affording heterocycle **60** in good yield (Scheme 9.51). Using 2-MeTHF as a medium, this reaction was performed with a variety of substrates having well-tolerating substituents in the aromatic rings. Moreover, the scope of this tandem addition/cyclization reaction in 2-MeTHF was successfully extended for the synthesis of 2-aroyl-3-phenylindoles from the *N*-cyanomethyl substituted 2-aminobenzophenone and arylboronic acids.

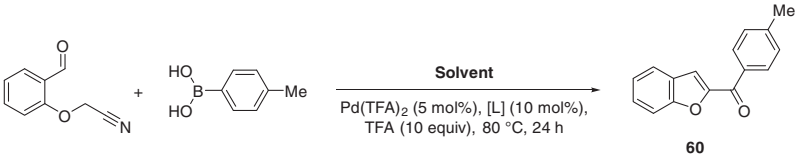

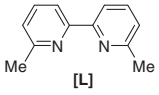

Solvent	Yield (%)
Toluene	43
DMF	73
EtOH	37
Water	46
1,4-Dioxane	74
THF	84
2-MeTHF	92

Scheme 9.51 Palladium-catalyzed synthesis of a 2-aroylbenzofuran.

The synthesis of 2-alkylamino substituted heterocycles (imidazolines, benzimidazoles, quinazolines, and related systems) was effectively performed using the palladium(II)-catalyzed aerobic oxidative isocyanide insertion into the corresponding bisnucleophile substrates [80]. For this reaction, 2-MeTHF was found to be a more suitable medium than conventional organic solvents. Among numerous

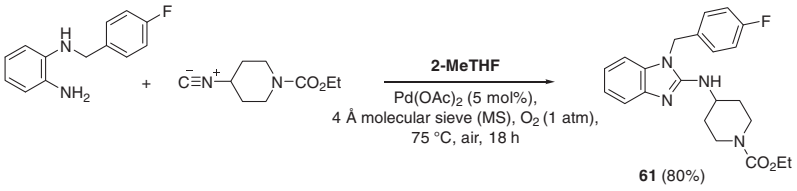

Scheme 9.52 Synthesis of a functionalized benzimidazole in 2-MeTHF.

examples, this method was illustrated by the synthesis of benzimidazole **61** (Scheme 9.52), which is a synthetic precursor of antihistaminic drugs astemizole and norastemizole.

9.5.2 Synthesis of Six-Membered Heterocycles in 2-Methyltetrahydrofuran

The nickel(II)-catalyzed reaction of homophthalonitrile with phenylboronic acid produced 1-amino-3-phenylisoquinoline (**62**) in greater yield when 2-MeTHF was used as a medium (Scheme 9.53) [81]. The conventional organic solvents were less efficient reaction media for carrying out this heterocyclization. The reaction in 2-MeTHF tolerated various substituents in substrates. Similarly, 2-MeTHF was found to be a good solvent (much more effective than THF) for the synthesis of 3-phenylisoquinolin-1(2*H*)-one (**63**) (Scheme 9.54) [81]. The reaction was compatible with various arylboronic acids. Analogs of **63** with alkyl groups in position 4 were also prepared using this method.

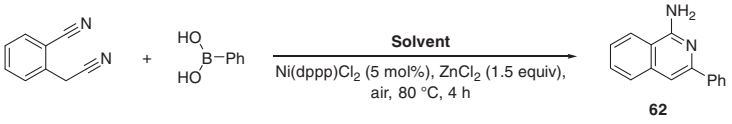

Solvent	Yield (%)
Toluene	38
DMF	8
Acetone	48
Water	27
1,4-Dioxane	42
THF	72
2-MeTHF	89

Scheme 9.53 Nickel-catalyzed synthesis of 1-amino-3-phenylisoquinoline (**62**).

The annulation reaction of 4-aminocoumarin leading to pyridine-fused derivatives was performed by the treatment with α-phenylacetylenyl nitrostyrene in the presence of copper(II) acetate under aerobic conditions in 2-MeTHF (Scheme 9.55) [82]. The resulting pyridocoumarin **64** and its analogs prepared by the same method were explored for targeting CAG repeat RNA, which are associated with Huntington's disease and spinocerebellar ataxia. Some compounds demonstrated a good level of activity and selectivity.

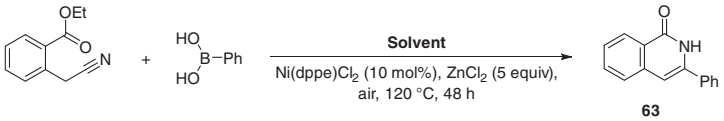

63

Solvent	Yield (%)
MeOH	19
Water	0
THF	45
2-MeTHF	81

Scheme 9.54 Nickel-catalyzed synthesis of 3-phenylisoquinolin-1(2*H*)-one (**63**).

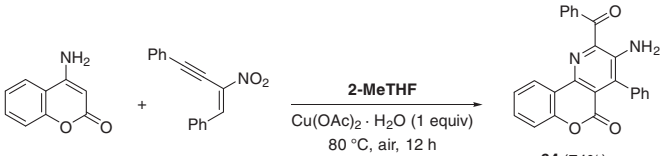

64 (74%)

Scheme 9.55 Synthesis of a pyridocoumarin derivative in 2-MeTHF.

In the synthesis of 2-phenylquinazolin-4(3*H*)-one (**65**) by the domino cross-coupling reaction of *o*-iodobenzoic acid and benzamidine catalyzed by the copper–glucose system, 2-MeTHF was a more efficient medium than many conventional organic solvents and was equipotent with *N,N*-dimethylformamide (DMF) (Scheme 9.56) [83]. Similar reactions of benzamidine with less reactive *o*-bromo- or *o*-chlorobenzoic acids were successful only at higher temperatures: 60 °C, 81% yield and 80 °C, 62% yield, respectively. The reaction scope exploration confirmed that 2-MeTHF was a suitable medium for the ring-closure cross-coupling of various *o*-halobenzoic acids with benzamidines or aliphatic amidines.

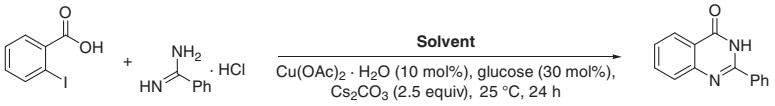

65

Solvent	Yield (%)
^{i}PrOH	63
MeCN	69
DMF	91
DMSO	71
Water	Traces
Toluene	Traces
Dioxane	12
2-MeTHF	91

Scheme 9.56 Synthesis of 2-phenylquinazolin-4(3*H*)-one (**65**).

It was reported [84] that 2-MeTHF outperformed common organic solvents as a medium for the synthesis of 2-phenyl-3,1-benzoxazin-4-one (**66**) using cyclocarbonylation of *o*-iodoaniline under the heterogeneous catalysis of

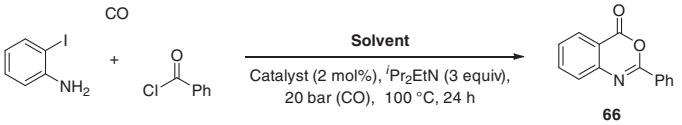

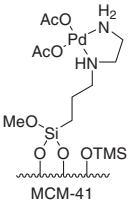

Solvent	Yield (%)
MeCN	56
NMP	73
DMF	84
DMSO	62
Toluene	69
Dioxane	71
THF	95
2-MeTHF	97

Scheme 9.57 Synthesis of 2-phenyl-3,1-benzoxazin-4-one (**66**).

2-aminoethylamino-modified MCM-41-anchored palladium acetate complex (Scheme 9.57). Under the optimized conditions, *o*-iodoaniline, carbon monoxide, and benzoyl chloride afforded **66** in high yield (94%) even after reusing the catalyst in eight reaction cycles. The palladium leaching in this cyclocarbonylation was negligible. The reaction was effective with various acid chlorides and tolerated well substituents in the aromatic ring of *o*-iodoaniline.

9.6 Heterocyclizations in Miscellaneous Unconventional Bio-based Media

Continuous attempts to find more sustainable and efficient solvents for chemical transformations resulted in more emerging bio-based media for organic synthesis. Some of these solvents were found to be suitable for heterocyclizations replacing conventional non-sustainable solvents.

Cyrene is the trade name of dihydrolevoglucosenone, which serves as a dipolar, aprotic, high boiling point liquid derived from cellulose-containing biomass [85]. These characteristics, together with sustainable nature, low toxicity, and biodegradability, make Cyrene a good alternative to conventional dipolar solvents like DMF and NMP in organic synthesis, including synthesis of some heterocyclic compounds [86]. Cyrene was as efficient as DMF in the Sonogashira coupling with the subsequent Cacchi-type cyclization affording indole **67** (Scheme 9.58) [87].

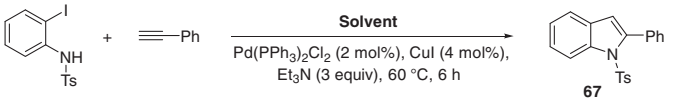

Solvent	Yield (%)
DMF	91
Cyrene	90

Scheme 9.58 Synthesis of indole **67** in Cyrene vs. DMF.

This tandem reaction in Cyrene was successfully performed using various terminal alkynes and amino-substituted aryl iodides. When *o*-iodophenol was employed as a substrate for a similar reaction with phenylacetylene, 2-phenylbenzofuran (**68**) was obtained in good yield (Scheme 9.59).

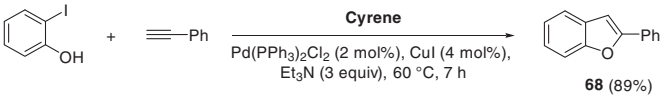

Scheme 9.59 Synthesis of 2-phenylbenzofuran (**68**) in Cyrene.

Bio-based solvents eucalyptol and limonene, derived, respectively, from eucalyptus leaf [88, 89] and citrus fruit peel [90, 91] essential oils, were used as solvents for the reaction of 2-aminopyridine with 2-bromoacetophenone to prepare 2-phenylimidazo[1,2-*a*]pyridine (**10**) (Scheme 9.60) [92]. Eucalyptol was also suitable for the Pd-catalyzed arylation of **10** with aryl bromides, which was also effectively performed in a one-pot manner. However, attempts of the same arylation in limonene were not successful.

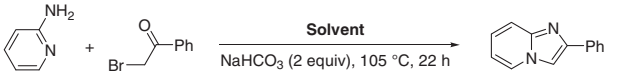

Solvent	Yield (%)
Eucalyptol	83
Limonene	84

Scheme 9.60 Reaction of 2-aminopyridine and 2-bromoacetophenone in eucalyptol and limonene.

Eucalyptol was an excellent solvent for the one-pot metal-free azidation-click reaction sequence in the synthesis of triazole **69** (Scheme 9.61) [93]. However, the superior performance of eucalyptol over other ethereal solvents or toluene was not consistent when other similar substrates were employed for the reaction.

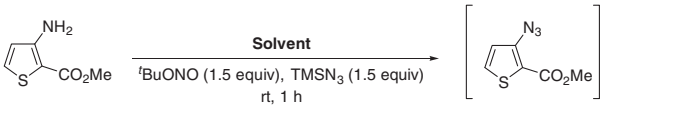

Solvent	Yield (%)
Toluene	92
CPME	74
2-MeTHF	71
Eucalyptol	95

Scheme 9.61 Metal-free click synthesis of a triazole derivative.

In the multicomponent synthesis of pyridine **70**, eucalyptol outperformed methanol under catalyst-free conditions (Scheme 9.62) [94]. This reaction in eucalyptol was carried out using malononitrile and various cyclic amines and aldehydes affording desired analogs of **70** in comparable yields.

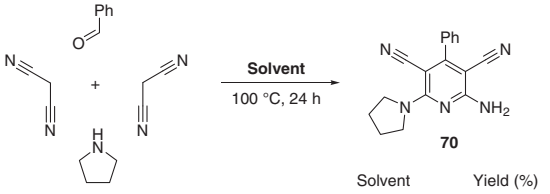

Solvent	Yield (%)
MeOH	43
Eucalyptol	54

Scheme 9.62 Multicomponent synthesis of a penta-substituted pyridine in methanol and eucalyptol.

The one-pot Buchwald–Hartwig coupling and the subsequent pyrimidine ring closure were achieved when hetero-fused analogs of methyl anthranilate were treated with 2-bromopyridines in eucalyptol [95]. For example, this palladium-catalyzed reaction was efficiently applied in the synthesis of polyfused heterocycle **71** (Scheme 9.63). Attempts to perform similar reactions using 2-bromoquinoline did not result in the pyrimidine ring closure. Instead, they led either to the recovery of starting materials or to the isolation of Buchwald–Hartwig coupling products.

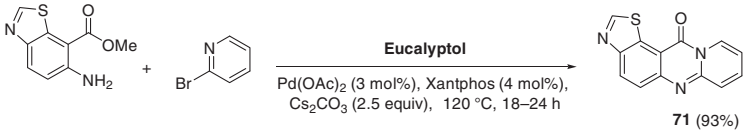

Scheme 9.63 Buchwald–Hartwig coupling and pyrimidine ring closure in eucalyptol.

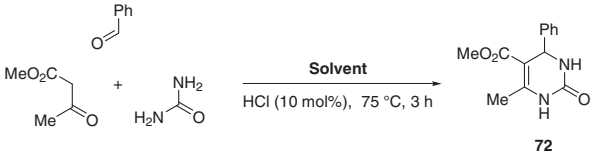

Solvent	Yield (%)
DCE	44
AcOEt	51
DMF	37
EtOH	56
^{t}BuOH	55
Ethylene glycol	38
AcOH	35
Toluene	59
***p*-Cymene**	66

Scheme 9.64 Solvent effect on the Biginelli reaction.

An interesting study [96] on the influence of solvents on the efficiency of the classic hydrochloric acid-catalyzed Biginelli reaction revealed that bio-based solvent *p*-cymene outperformed other solvents under identical conditions (Scheme 9.64). The reaction productivity was found to strongly depend on the keto-enol tautomerization equilibrium for starting methyl acetoacetate in different media. The yield of dihydropyrimidinone **72** was higher in less polar *p*-cymene, which promoted the equilibrium shift more toward the enol form.

9.7 Conclusion and Perspectives

Bio-based media have demonstrated great potential on the way toward more sustainable heterocyclic synthesis. Together with relatively more explored bio-based media, such as glycerol, lactic acid, GVL, and 2-MeTHF, other solvents, namely, Cyrene, limonene, eucalyptol, and *p*-cymene are finding their niche in the heterocyclization reactions. Different physicochemical properties of these media allow finding suitable replacements for conventional fossil-based organic solvents. Moreover, it has been demonstrated that for many methods developed for the synthesis of heterocycles, bio-based media are more efficient than conventional organic solvents.

Derived from renewable sources, bio-based media represent the future of organic chemistry, where these media will become the first choice in the method optimization. To bring this more sustainable future closer, more contributions evaluating applications of bio-based media and expanding the variety of renewable solvents are needed.

Acknowledgments

The funding by the Ministry of Higher Education, Malaysia, under the Fundamental Research Grant Scheme (Grant no. FRGS/1/2020/STG04/MUSM/02/2) is acknowledged.

References

1 Clarke, C.J., Tu, W.-C., Levers, O. et al. (2018). Green and sustainable solvents in chemical processes. *Chem. Rev.* 118 (2): 747–800. https://doi.org/10.1021/acs.chemrev.7b00571.

2 Erythropel, H.C., Zimmerman, J.B., de Winter, T.M. et al. (2018). The Green ChemisTREE: 20 years after taking root with the 12 principles. *Green Chem.* 20 (9): 1929–1961. https://doi.org/10.1039/C8GC00482J.

3 Tan, H.W., Abdul Aziz, A.R., and Aroua, M.K. (2013). Glycerol production and its applications as a raw material: a review. *Renew. Sustain. Energy Rev.* 27: 118–127. https://doi.org/10.1016/j.rser.2013.06.035.

4 Ciriminna, R., Lomeli-Rodriguez, M., Demma Carà, P. et al. (2014). Limonene: a versatile chemical of the bioeconomy. *Chem. Commun.* 50 (97): 15288–15296. https://doi.org/10.1039/C4CC06147K.

5 Pace, V., Hoyos, P., Castoldi, L. et al. (2012). 2-Methyltetrahydrofuran (2-MeTHF): a biomass-derived solvent with broad application in organic chemistry. *ChemSusChem.* 5 (8): 1369–1379. https://doi.org/10.1002/cssc.201100780.

6 Vaccaro, L., Santoro, S., Curini, M., and Lanari, D. (2017). The emerging use of γ-valerolactone as a green solvent. *Chem. Today.* 35 (2): 46–48.

7 Camp, J.E. (2018). Bio-available solvent Cyrene: synthesis, derivatization, and applications. *ChemSusChem.* 11 (18): 3048–3055. https://doi.org/10.1002/cssc.201801420.

8 Dolzhenko, A.V. (2020). Ethyl lactate and its aqueous solutions as sustainable media for organic synthesis. *Sustain. Chem. Pharm.* 18: 100322. https://doi.org/10.1016/j.scp.2020.100322.

9 Lim, H.Y. and Dolzhenko, A.V. (2021). Gluconic acid aqueous solution: a bio-based catalytic medium for organic synthesis. *Sustain. Chem. Pharm.* 21: 100443. https://doi.org/10.1016/j.scp.2021.100443.

10 Santoro, S., Ferlin, F., Luciani, L. et al. (2017). Biomass-derived solvents as effective media for cross-coupling reactions and C–H functionalization processes. *Green Chem.* 19 (7): 1601–1612. https://doi.org/10.1039/C7GC00067G.

11 Sydnes, M.O. (2019). Green bio-based solvents in C–C cross-coupling reactions. *Curr. Green Chem.* 6 (2): 96–104. https://doi.org/10.2174/2213346106666190411151447.

12 Gandeepan, P., Kaplaneris, N., Santoro, S. et al. (2019). Biomass-derived solvents for sustainable transition metal-catalyzed C–H activation. *ACS Sustain. Chem. Eng.* 7 (9): 8023–8040. https://doi.org/10.1021/acssuschemeng.9b00226.

13 Yang, F., Hanna, M.A., and Sun, R. (2012). Value-added uses for crude glycerol – a byproduct of biodiesel production. *Biotechnol. Biofuels.* 5 (1): 13. https://doi.org/10.1186/1754-6834-5-13.

14 Quispe, C.A.G., Coronado, C.J.R., and Carvalho, J.A. Jr., (2013). Glycerol: production, consumption, prices, characterization and new trends in combustion. *Renew. Sustain. Energy Rev.* 27: 475–493. https://doi.org/10.1016/j.rser.2013.06.017.

15 Ciriminna, R., Pina, C.D., Rossi, M., and Pagliaro, M. (2014). Understanding the glycerol market. *Eur. J. Lipid Sci. Technol.* 116 (10): 1432–1439. https://doi.org/10.1002/ejlt.201400229.

16 Kaur, J., Sarma, A.K., Jha, M.K., and Gera, P. (2020). Valorisation of crude glycerol to value-added products: perspectives of process technology, economics and environmental issues. *Biotechnol. Rep.* 27: e00487. https://doi.org/10.1016/j.btre.2020.e00487.

17 Zhou, C.H., Zhao, H., Tong, D.S. et al. (2013). Recent advances in catalytic conversion of glycerol. *Catal. Rev.* 55 (4): 369–453. https://doi.org/10.1080/01614940.2013.816610.

18 Gholami, Z., Abdullah, A.Z., and Lee, K.-T. (2014). Dealing with the surplus of glycerol production from biodiesel industry through catalytic upgrading to polyglycerols and other value-added products. *Renew. Sustain. Energy Rev.* 39: 327–341. https://doi.org/10.1016/j.rser.2014.07.092.

19 Karimi Estahbanati, M.R., Feilizadeh, M., Attar, F., and Iliuta, M.C. (2020). Current developments and future trends in photocatalytic glycerol valorization: photocatalyst development. *Ind. Eng. Chem. Res.* 59 (52): 22330–22352. https://doi.org/10.1021/acs.iecr.0c04765.

20 Díaz-Álvarez, A.E., Francos, J., Lastra-Barreira, B. et al. (2011). Glycerol and derived solvents: new sustainable reaction media for organic synthesis. *Chem. Commun.* 47 (22): 6208–6227. https://doi.org/10.1039/C1CC10620A.

21 Gu, Y. and Jérôme, F. (2010). Glycerol as a sustainable solvent for green chemistry. *Green Chem.* 12 (7): 1127–1138. https://doi.org/10.1039/C001628D.

22 García, J.I., García-Marín, H., and Pires, E. (2014). Glycerol based solvents: synthesis, properties and applications. *Green Chem.* 16 (3): 1007–1033. https://doi.org/10.1039/C3GC41857J.

23 Cintas, P., Tagliapietra, S., Calcio Gaudino, E. et al. (2014). Glycerol: a solvent and a building block of choice for microwave and ultrasound irradiation procedures. *Green Chem.* 16 (3): 1056–1065. https://doi.org/10.1039/C3GC41955J.

24 Bakhrou, N., Lamaty, F., Martinez, J., and Colacino, E. (2010). Ring-closing metathesis in glycerol under microwave activation. *Tetrahedron Lett.* 51 (30): 3935–3937. https://doi.org/10.1016/j.tetlet.2010.05.101.

25 Ammermann, S., Hrib, C., Jones, P.G. et al. (2012). Pyrrolo[1,2-*a*]quinoxalines: novel synthesis via annulation of 2-alkylquinoxalines. *Org. Lett.* 14 (19): 5090–5093. https://doi.org/10.1021/ol302348v.

26 Francos, J. and Cadierno, V. (2010). Palladium-catalyzed cycloisomerization of (*Z*)-enynols into furans using green solvents: glycerol vs. water. *Green Chem.* 12 (9): 1552–1555. https://doi.org/10.1039/C0GC00169D.

27 Nascimento, J.E.R., Oliveira DHd, Abib, P.B. et al. (2015). Synthesis of 4-arylselanylpyrazoles through cyclocondensation reaction using glycerol as solvent. *J. Braz. Chem. Soc.* 26: 1533–1541. https://doi.org/10.5935/0103-5053.20150127.

28 Yadav, V.B., Rai, P., Sagir, H. et al. (2017). Catalyst-free synthesis for pyrazole-fused isocoumarins in recyclable and biodegradable reaction medium. *ChemistrySelect* 2 (27): 8320–8325. https://doi.org/10.1002/slct.201700976.

29 Tan, J.-N., Li, M., and Gu, Y. (2010). Multicomponent reactions of 1,3-disubstituted 5-pyrazolones and formaldehyde in environmentally benign solvent systems and their variations with more fundamental substrates. *Green Chem.* 12 (5): 908–914. https://doi.org/10.1039/B924699A.

30 Vekariya, R.H. and Patel, H.D. (2016). Glycerol mediated green and one-pot synthesis of 6-amino-1,4-dihydropyrano[2,3-*c*]-pyrazole-5-carbonitriles under catalyst free conditions. *Ind. J. Chem.* 55B (8): 999–1006.

31 Tufail, F., Singh, S., Saquib, M. et al. (2017). Catalyst-free, glycerol-assisted facile approach to imidazole-fused nitrogen-bridgehead heterocycles. *ChemistrySelect* 2 (21): 6082–6089. https://doi.org/10.1002/slct.201700557.

32 Radatz, C.S., Silva, R.B., Perin, G. et al. (2011). Catalyst-free synthesis of benzodiazepines and benzimidazoles using glycerol as recyclable solvent. *Tetrahedron Lett.* 52 (32): 4132–4136. https://doi.org/10.1016/j.tetlet.2011.05.142.

33 Bachhav, H.M., Bhagat, S.B., and Telvekar, V.N. (2011). Efficient protocol for the synthesis of quinoxaline, benzoxazole and benzimidazole derivatives using glycerol as green solvent. *Tetrahedron Lett.* 52 (43): 5697–5701. https://doi.org/10.1016/j.tetlet.2011.08.105.

34 Lei, J., Luo, L., Fu, W., and Zhou, W. (2017). Microwave-assisted synthesis of benzoxazoles in glycerol. *Chin. J. Appl. Chem.* 34 (3): 324–329. https://doi.org/10.11944/j.issn.1000-0518.2017.03.160243.

35 Zhang, X.-Z., Zhou, W.-J., Yang, M. et al. (2012). Microwave-assisted synthesis of benzothiazole derivatives using glycerol as green solvent. *J. Chem. Res.* 36 (8): 489–491. https://doi.org/10.3184/174751912x13400085970187.

36 Sadek, K.U., Mekheimer, R.A., Hameed, A.M.A. et al. (2012). Green and highly efficient synthesis of 2-arylbenzothiazoles using glycerol without catalyst at ambient temperature. *Molecules* 17 (5): 6011–6019. https://doi.org/10.3390/molecules17056011.

37 Deligeorgiev, T.G., Kaloyanova, S.S., Lesev, N.Y., and Vaquero, J.J. (2011). An environmentally benign procedure for the synthesis of substituted 2-thiobenzothiazoles, 2-thiobenzoxazoles, 2-thiobenzimidazoles, and 1,3-oxazolopyridine-2-thiols. *Monatsh. Chem.* 142 (9): 895–899. https://doi.org/10.1007/s00706-011-0551-1.

38 Deligeorgiev, T., Kaloyanova, S., Lesev, N. et al. (2011). An environmentally benign synthesis of 2-cyanomethyl-4-phenylthiazoles under focused microwave irradiation. *Green Sustain. Chem.* 1 (4): 170–175. https://doi.org/10.4236/gsc.2011.14026.

39 Tiwari, J., Singh, S., Tufail, F. et al. (2018). Glycerol micellar catalysis: an efficient multicomponent-tandem green synthetic approach to biologically important 2,4-disubstituted thiazole derivatives. *ChemistrySelect* 3 (41): 11634–11642. https://doi.org/10.1002/slct.201802511.

40 Nascimento, J.E.R., Barcellos, A.M., Sachini, M. et al. (2011). Catalyst-free synthesis of octahydroacridines using glycerol as recyclable solvent. *Tetrahedron Lett.* 52 (20): 2571–2574. https://doi.org/10.1016/j.tetlet.2011.03.045.

41 Jamale, D.K., Undare, S.S., Valekar, N.J. et al. (2019). Glycerol mediated synthesis, biological evaluation, and molecular docking study of 4-(1*H*-pyrazol-4-yl)-polyhydroquinolines as potent antitubercular agents. *J. Heterocycl. Chem.* 56 (2): 608–618. https://doi.org/10.1002/jhet.3438.

42 Rosholm, T., Gois, P.M.P., Franzen, R., and Candeias, N.R. (2015). Glycerol as an efficient medium for the Petasis borono–Mannich reaction. *ChemistryOpen* 4 (1): 39–46. https://doi.org/10.1002/open.201402066.

43 Ganesan, S.S., Rajendran, N., Sundarakumar, S.I. et al. (2013). β-Naphthol in glycerol: a versatile pair for efficient and convenient synthesis of aminonaphthols, naphtho-1,3-oxazines, and benzoxanthenes. *Synthesis* 45 (11): 1564–1568. https://doi.org/10.1055/s-0033-1338430.

44 Li, M., Chen, C., He, F., and Gu, Y. (2010). Multicomponent reactions of 1,3-cyclohexanediones and formaldehyde in glycerol: stabilization of paraformaldehyde in glycerol resulted from using dimedone as substrate. *Adv. Synth. Catal.* 352 (2, 3): 519–530. https://doi.org/10.1002/adsc.200900770.

45 Safaei, H.R., Shekouhy, M., Rahmanpur, S., and Shirinfeshan, A. (2012). Glycerol as a biodegradable and reusable promoting medium for the catalyst-free one-pot three component synthesis of 4*H*-pyrans. *Green Chem.* 14 (6): 1696–1704. https://doi.org/10.1039/C2GC35135H.

46 Parmar, N.J., Barad, H.A., Labana, B.M. et al. (2013). A glycerol mediated domino reaction: an efficient, green synthesis of polyheterocycles incorporating a new thiochromeno[2,3-*b*]quinoline unit. *RSC Adv.* 3 (43): 20719–20725. https://doi.org/10.1039/C3RA43205J.

47 Narsaiah, A.V. and Kumar, J.K. (2012). Glycerin and $CeCl_3 \cdot 7H_2O$: a new and efficient recyclable reaction medium for the synthesis of quinoxalines. *Synth. Commun.* 42 (6): 883–892. https://doi.org/10.1080/00397911.2010.533050.

48 Abdel-Rahman, M.A., Tashiro, Y., and Sonomoto, K. (2013). Recent advances in lactic acid production by microbial fermentation processes. *Biotechnol. Adv.* 31 (6): 877–902. https://doi.org/10.1016/j.biotechadv.2013.04.002.

49 Lactic acid. (2020). *Code of Federal Regulations*. FDA, United States, Title 21, Vol. 3, 184.1061. https://www.accessdata.fda.gov/scripts/cdrh/cfdocs/cfcfr/CFRSearch.cfm?fr=184.1061 (accessed 10 December 2021).

50 Wang, S.-F., Guo, C.-L., Cui, K.-k. et al. (2015). Lactic acid as an invaluable green solvent for ultrasound-assisted scalable synthesis of pyrrole derivatives. *Ultrason. Sonochem.* 26: 81–86. https://doi.org/10.1016/j.ultsonch.2015.01.002.

51 Akbaslar, D., Giray, E.S., and Algul, O. (2021). Revisit to the synthesis of 1,2,3,4-tetrasubstituted pyrrole derivatives in lactic acid media as a green solvent and catalyst. *Mol. Divers.* 25 (4): 2321–2338. https://doi.org/10.1007/s11030-020-10122-1.

52 Yang, J., Tan, J.-N., and Gu, Y. (2012). Lactic acid as an invaluable bio-based solvent for organic reactions. *Green Chem.* 14 (12): 3304–3317. https://doi.org/10.1039/C2GC36083G.

53 Sonar, J., Pardeshi, S., Dokhe, S. et al. (2019). An efficient method for the synthesis of 2,4,5-trisubstituted imidazoles using lactic acid as promoter. *SN Appl. Sci.* 1 (9): 1045. https://doi.org/10.1007/s42452-019-0935-0.

54 Balijapalli, U., Thiyagarajan, M.D., Manickam, S., and Sathiyanarayanan, K.I. (2016). Synthesis of T-shaped oxazolonaphthoimidazo[1,2-*a*]pyridines using lactic acid as bio-based green solvent: an insight into photophysical studies. *ChemistrySelect* 1 (11): 2900–2908. https://doi.org/10.1002/slct.201600585.

55 Li, Y.-H., Wang, L-t., Wang, Z. et al. (2016). Ultrasound-assisted synthesis of novel pyrrole dihydropyrimidinones in lactic acid. *ChemistrySelect* 1 (21): 6855–6858. https://doi.org/10.1002/slct.201601438.

56 Dutta, S., Yu, I.K.M., Tsang, D.C.W. et al. (2019). Green synthesis of gamma-valerolactone (GVL) through hydrogenation of biomass-derived levulinic acid using non-noble metal catalysts: a critical review. *Chem. Eng. J.* 372: 992–1006. https://doi.org/10.1016/j.cej.2019.04.199.

57 Gamma-Valerolactone. (1998). In JECFA Specifications for Flavourings. The Joint Food and Agriculture Organization of the United Nations and the World Health Organization Expert Committee on Food Additives (JECFA), Session 51, 220. http://www.fao.org/food/food-safety-quality/scientific-advice/jecfa/jecfa-flav/details/en/c/458 (accessed 10 December 2021).

58 Tang, X., Zeng, X., Li, Z. et al. (2014). Production of γ-valerolactone from lignocellulosic biomass for sustainable fuels and chemicals supply. *Renew. Sustain. Energy Rev.* 40: 608–620. https://doi.org/10.1016/j.rser.2014.07.209.

59 Xu, R., Liu, K., Du, H. et al. (2020). Falling leaves return to their roots: a review on the preparation of γ-valerolactone from lignocellulose and its application in the conversion of lignocellulose. *ChemSusChem* 13 (24): 6461–6476. https://doi.org/10.1002/cssc.202002008.

60 Alonso, D.M., Wettstein, S.G., and Dumesic, J.A. (2013). Gamma-valerolactone, a sustainable platform molecule derived from lignocellulosic biomass. *Green Chem.* 15 (3): 584–595. https://doi.org/10.1039/C3GC37065H.

61 Tian, X., Yang, F., Rasina, D. et al. (2016). C–H arylations of 1,2,3-triazoles by reusable heterogeneous palladium catalysts in biomass-derived γ-valerolactone. *Chem. Commun.* 52 (63): 9777–9780. https://doi.org/10.1039/C6CC03468C.

62 Bechtoldt, A., Baumert, M.E., Vaccaro, L., and Ackermann, L. (2018). Ruthenium(II) oxidase catalysis for C–H alkenylations in biomass-derived γ-valerolactone. *Green Chem.* 20 (2): 398–402. https://doi.org/10.1039/C7GC03353B.

63 Song, J., Zhou, B., Liu, H. et al. (2016). Biomass-derived γ-valerolactone as an efficient solvent and catalyst for the transformation of CO_2 to formamides. *Green Chem.* 18 (14): 3956–3961. https://doi.org/10.1039/C6GC01455K.

64 Petricci, E., Risi, C., Ferlin, F. et al. (2018). Avoiding hot-spots in microwave-assisted Pd/C catalysed reactions by using the biomass derived solvent γ-valerolactone. *Sci. Rep.* 8 (1): 10571. https://doi.org/10.1038/s41598-018-28458-y.

65 Jiang, K.-C., Wang, L., Chen, Q. et al. (2021). Rh(III)–catalyzed synthesis of isoquinolines from *N*-hydroxyoximes and alkynes in γ-valerolactone. *Synth. Commun.* 51 (1): 94–102. https://doi.org/10.1080/00397911.2020.1819326.

66 Diwan, F. and Farooqui, M. (2018). γ-Valerolactone as a promising bio-compatible media for one-pot synthesis of spiro[indoline-3,4'-pyrano[3,2-*c*]chromene] derivatives. *J. Heterocycl. Chem.* 55 (12): 2817–2822. https://doi.org/10.1002/jhet.3351.

67 Zhang, M., Fu, Q.-Y., Gao, G. et al. (2017). Catalyst-free, visible-light promoted one-pot synthesis of spirooxindole-pyran derivatives in aqueous ethyl lactate. *ACS Sustain. Chem. Eng.* 5 (7): 6175–6182. https://doi.org/10.1021/acssuschemeng.7b01102.

68 Calcio Gaudino, E., Tagliapietra, S., Palmisano, G. et al. (2017). Microwave-assisted, green synthesis of 4(3*H*)-quinazolinones under CO pressure in γ-valerolactone and reusable Pd/β-cyclodextrin cross-linked catalyst. *ACS Sustain. Chem. Eng.* 5 (10): 9233–9243. https://doi.org/10.1021/acssuschemeng.7b02193.

69 Tabasso, S., Calcio Gaudino, E., Acciardo, E. et al. (2020). Microwave-assisted protocol for green functionalization of thiophenes with a Pd/β-cyclodextrin cross-linked nanocatalyst. *Front. Chem.* 8: 253. https://doi.org/10.3389/fchem.2020.00253.

70 Monticelli, S., Castoldi, L., Murgia, I. et al. (2017). Recent advancements on the use of 2-methyltetrahydrofuran in organometallic chemistry. *Monatsh. Chem.* 148 (1): 37–48. https://doi.org/10.1007/s00706-016-1879-3.

71 Aul, R. and Comanita, B. (2007). A green alternative to THF. *Manuf. Chem.* 78 (5): 33–34.

72 Liu, P., Sun, L., Jia, X. et al. (2020). Efficient one-pot conversion of furfural into 2-methyltetrahydrofuran using non-precious metal catalysts. *Mol. Catal.* 490: 110951. https://doi.org/10.1016/j.mcat.2020.110951.

73 Obregón, I., Gandarias, I., Ocio, A. et al. (2017). Structure-activity relationships of Ni–Cu/Al_2O_3 catalysts for γ-valerolactone conversion to 2-methyltetrahydrofuran. *Appl. Catal. B.* 210: 328–341. https://doi.org/10.1016/j.apcatb.2017.04.006.

74 Obregón, I., Gandarias, I., Miletić, N. et al. (2015). One-pot 2-methyltetrahydrofuran production from levulinic acid in green solvents using Ni–Cu/Al_2O_3 catalysts. *ChemSusChem* 8 (20): 3483–3488. https://doi.org/10.1002/cssc.201500671.

75 Slater, C.S., Savelski, M.J., Hitchcock, D., and Cavanagh, E.J. (2016). Environmental analysis of the life cycle emissions of 2-methyl tetrahydrofuran solvent manufactured from renewable resources. *J. Environ. Sci. Heal. A.* 51 (6): 487–494. https://doi.org/10.1080/10934529.2015.1128719.

76 Antonucci, V., Coleman, J., Ferry, J.B. et al. (2011). Toxicological assessment of 2-methyltetrahydrofuran and cyclopentyl methyl ether in support of their use in pharmaceutical chemical process development. *Org. Process Res. Dev.* 15 (4): 939–941. https://doi.org/10.1021/op100303c.

77 Aycock, D.F. (2007). Solvent applications of 2-methyltetrahydrofuran in organometallic and biphasic reactions. *Org. Process Res. Dev.* 11 (1): 156–159. https://doi.org/10.1021/op060155c.

78 Palmieri, A., Gabrielli, S., Parlapiano, M., and Ballini, R. (2015). One-pot synthesis of alkyl pyrrole-2-carboxylates starting from β-nitroacrylates and primary amines. *RSC Adv.* 5 (6): 4210–4213. https://doi.org/10.1039/C4RA13094D.

79 Gong, J., Hu, K., Shao, Y. et al. (2020). Tandem addition/cyclization for synthesis of 2-aroyl benzofurans and 2-aroyl indoles by carbopalladation of nitriles. *Org. Biomol. Chem.* 18 (3): 488–494. https://doi.org/10.1039/C9OB02408E.

80 Vlaar, T., Cioc, R.C., Mampuys, P. et al. (2012). Sustainable synthesis of diverse privileged heterocycles by palladium-catalyzed aerobic oxidative isocyanide insertion. *Angew. Chem. Int. Ed.* 51 (52): 13058–13061. https://doi.org/10.1002/anie.201207410.

81 Zhen, Q., Chen, L., Qi, L. et al. (2020). Nickel-catalyzed tandem reaction of functionalized arylacetonitriles with arylboronic acids in 2-MeTHF: eco-friendly synthesis of aminoisoquinolines and isoquinolones. *Chem. Asian J.* 15 (1): 106–111. https://doi.org/10.1002/asia.201901442.

82 Khan, E., Biswas, S., Mishra, S.K. et al. (2019). Rationally designed small molecules targeting toxic CAG repeat RNA that causes Huntington's disease (HD) and spinocerebellar ataxia (SCAs). *Biochimie* 163: 21–32. https://doi.org/10.1016/j.biochi.2019.05.001.

83 Dubey, A.V. and Kumar, A.V. (2018). Cu(II)–glucose: sustainable catalyst for the synthesis of quinazolinones in a biomass-derived solvent 2-methyl THF and application for the synthesis of diproqualone. *ACS Sustain. Chem. Eng.* 6 (11): 14283–14291. https://doi.org/10.1021/acssuschemeng.8b02940.

84 Hao, W., Xu, Z., Zhou, Z., and Cai, M. (2020). Recyclable heterogeneous palladium-catalyzed cyclocarbonylation of 2-iodoanilines with acyl chlorides in the biomass-derived solvent 2-methyltetrahydrofuran. *J. Org. Chem.* 85 (13): 8522–8532. https://doi.org/10.1021/acs.joc.0c00887.

85 Sherwood, J., De Bruyn, M., Constantinou, A. et al. (2014). Dihydrolevoglucosenone (Cyrene) as a bio-based alternative for dipolar aprotic solvents. *Chem. Commun.* 50 (68): 9650–9652. https://doi.org/10.1039/C4CC04133J.

86 Kong, D. and Dolzhenko, A.V. (2022). Cyrene: A bio-based sustainable solvent for organic synthesis. *Sustain. Chem. Pharm.* 25: 100591. https://doi.org/10.1016/j.scp.2021.100591.

87 Wilson, K.L., Kennedy, A.R., Murray, J. et al. (2016). Scope and limitations of a DMF bio-alternative within Sonogashira cross-coupling and Cacchi-type annulation. *Beilstein J. Org. Chem.* 12: 2005–2011. https://doi.org/10.3762/bjoc.12.187.

88 García, C., Montero, G., Coronado, M.A. et al. (2017). Valorization of eucalyptus leaves by essential oil extraction as an added value product in Mexico. *Waste Biomass Valor.* 8 (4): 1187–1197. https://doi.org/10.1007/s12649-016-9695-x.

89 Babu, G.D.K. and Singh, B. (2009). Simulation of *Eucalyptus cinerea* oil distillation: a study on optimization of 1,8-cineole production. *Biochem. Eng. J.* 44 (2): 226–231. https://doi.org/10.1016/j.bej.2008.12.012.

90 John, I., Muthukumar, K., and Arunagiri, A. (2017). A review on the potential of citrus waste for D-limonene, pectin, and bioethanol production. *Int. J. Green Energy* 14 (7): 599–612. https://doi.org/10.1080/15435075.2017.1307753.

91 Battista, F., Remelli, G., Zanzoni, S., and Bolzonella, D. (2020). Valorization of residual orange peels: limonene recovery, volatile fatty acids, and biogas production. *ACS Sustain. Chem. Eng.* 8 (17): 6834–6843. https://doi.org/10.1021/acssuschemeng.0c01735.

92 Campos, J.F., Scherrmann, M.-C., and Berteina-Raboin, S. (2019). Eucalyptol: a new solvent for the synthesis of heterocycles containing oxygen, sulfur and nitrogen. *Green Chem.* 21 (6): 1531–1539. https://doi.org/10.1039/C8GC04016H.

93 Campos, J.F., Cailler, M., Claudel, R. et al. (2021). Demonstration of green solvent performance on O,S,N-heterocycles synthesis: metal-free click chemistry and Buchwald-Hartwig coupling. *Molecules* 26 (4): 1074. https://doi.org/10.3390/molecules26041074.

94 Campos, J.F., Ferreira, V., and Berteina-Raboin, S. (2021). Eucalyptol: a bio-based solvent for the synthesis of O,S,N-heterocycles. application to Hiyama coupling,

cyanation, and multicomponent reactions. *Catalysts* 11 (2): 222. https://doi.org/10.3390/catal11020222.

95 Campos, J.F., Pacheco-Benichou, A., Fruit, C. et al. (2020). Synthesis of benzo-fused 11*H*-pyrido[2,1-*b*]quinazolin-11-ones by a Buchwald–Hartwig coupling/pyridine dearomatization sequence in eucalyptol. *Synthesis* 52 (20): 3071–3076. https://doi.org/10.1055/s-0040-1707158.

96 Clark, J.H., Macquarrie, D.J., and Sherwood, J. (2013). The combined role of catalysis and solvent effects on the Biginelli reaction: improving efficiency and sustainability. *Chem. Eur. J.* 19 (16): 5174–5182. https://doi.org/10.1002/chem.201204396.

10

Mechanochemistry in Heterocyclic Synthesis

Vjekoslav Štrukil and Davor Margetić

Ruđer Bošković Institute, Laboratory for Physical Organic Chemistry, Division of Organic Chemistry and Biochemistry, Bijenička cesta 54, Zagreb 10000, Croatia

10.1 Introduction

During the last two decades, mechanochemistry has emerged as a powerful tool in synthetic chemistry, providing opportunities for more efficient and clean preparation of chemical species ranging from inorganic structures to small organic molecules, supramolecular assemblies, and polymers [1–3]. Particularly noticeable advancements have been made in the area of organic synthesis where solid-state mechanochemical milling enabled access not only to many known molecules in excellent yields and high selectivities but also to compounds difficult to make or isolate, which are normally regarded as reactive intermediates in solution environment. Specific activation modes, characteristic for solid-state milling reactions, eliminate the effects of bulk solvent on the chemical reactivity, creating possibilities for reaction discovery and methodology development in conjunction with conventional activation through metal, organo, and photocatalysis [4–7]. It is therefore not surprising that the International Union for Pure and Applied Chemistry (IUPAC) has listed mechanochemistry as one of the 10 innovations with a potential to change the world [8].

The main feature of mechanochemical reactions, i.e. the ones induced by energy transformation from mechanical into chemical, is that they take place in the solid state. As such, they do not require the presence of bulk solvents, resulting in more efficient, faster, and cleaner chemical transformations. Solvent-free (or neat) milling is complemented with the liquid-assisted grinding (LAG) approach where only a catalytic amount of a liquid phase is added to the mixture to enhance reaction kinetics and facilitate product recovery [9]. Such reactions are traditionally performed by hand in mortars using a pestle or more conveniently in electrical laboratory instruments called ball mills. Depending on the mechanism of ball milling, several types of mills are in use, with mixer and planetary ball mills being the most common (Figure 10.1). While mixer mills operate on the principle of high-speed horizontal vibrations, which usually reach frequencies up to 35 Hz, reaction vessels in planetary

Heterocycles: Synthesis, Catalysis, Sustainability, and Characterization, First Edition.
Edited by Teresa M.V.D. Pinho e Melo and Marta Pineiro.

Figure 10.1 Laboratory instrumentation in mechanochemistry research: (a) mortar and pestle, (b) mixer ball mill, and (c) planetary ball mill.

ball mills spin around the central axis, as well as their own with a frequency up to 800 rpm, in a motion reminiscent of planetary trajectories around the sun.

Mechanochemical reactions are carried out in vessels or jars made of materials as diverse as stainless steel, tungsten carbide, zirconia, teflon, polymethylmethacrylate, or even duran glass. The jars are charged with preweighted reactants alongside one or more grinding balls of different diameter and mass. In the case of LAG reactions, the required volume of a liquid phase is also added via a syringe or pipette. The jars are finally mounted on the ball mill and shaken/spun for a certain period of time. Upon completion of the milling process, crude reaction mixtures are worked up and products isolated and characterized (Figure 10.2). Recently, solid-state analytical techniques have been developed for real-time *in situ* monitoring of mechanochemical reactions, revealing some of the mechanistic aspects of milling processes [10–12]. Mixer and planetary ball mills can process relatively small amount of material (up to several hundred grams) and are not intended for scale-up purposes. On the other hand, twin-screw extruders allow for the continuous mode of operation and far greater amounts of materials to be processed [13].

As ubiquitous constituents of natural products, pharmaceuticals, and a plethora of other molecules with pronounced biological effects such as agrochemicals, heterocyclic compounds have played a pivotal role in the development of synthetic organic chemistry over the past two centuries.

Numerous cases of mechanochemical derivatization of heterocyclic cores have already been described in the literature and still continue to attract much attention among synthetic chemists [4]. This chapter, however, will focus exclusively on the

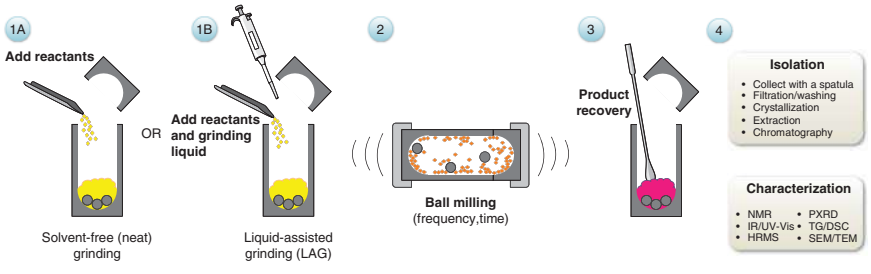

Figure 10.2 Typical steps involved in setting up and analysis of mechanochemical reactions.

most representative or recent examples where mechanochemical milling has been used to construct heterocyclic molecules from their noncyclic precursors, systematically arranged in the order of increasing ring size and the type of heteroatoms involved.

10.2 Mechanosynthesis of N-Heterocycles

10.2.1 Five-Membered Ring Heterocycles

Kaupp et al. investigated the synthesis of several pyrrole derivatives, as typical representatives of aromatic five-membered heterocycles, under ball milling conditions starting from enamine esters **1** and *trans*-1,2-dibenzoylethene **2** in stoichiometric ratio [14]. Solid-state reactions were run for three hours in a 10 ml stainless steel jar with two balls (6.5 g) and temperatures from −20 to 25 °C, depending on the substrate reactivity. In the complex cascade of four distinct reactions, the last step required elimination of water and was carried out by heating the solid mixture at 80 °C, to afford highly substituted pyrroles **3** in quantitative yields without the need for further purification (Scheme 10.1). When 3-(phenylamino)cyclohex-2-enone was used, an indole-type derivative **4** was quantitatively obtained. The same reactions in methanol or xylene solution under reflux gave only moderate yields (46–81%).

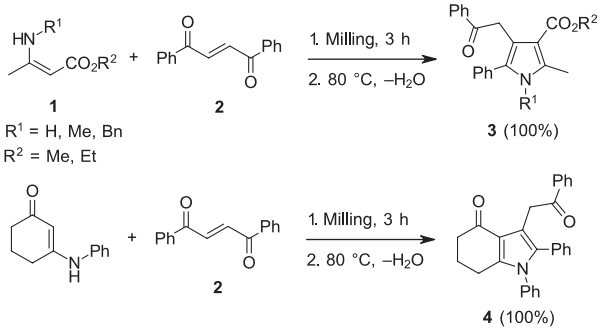

Scheme 10.1 Mechanosynthesis of substituted pyrroles from enamine esters and *trans*-1,2-dibenzoylethene.

A one-pot multicomponent mechanochemical version of the Hantzsch pyrrole synthesis was reported by Menéndez and coworkers [15]. The reaction sequence started by *p*-toluenesulfonic acid (*p*-TsOH)-catalyzed *N*-iodosuccinimide-promoted iodination of ketone substrates **5**. After one hour milling at 20 Hz in zirconium oxide media (25 ml jar and a single 20 mm ball), a mixture of primary amine, β-dicarbonyl compound, 5 mol% cerium(IV) ammonium nitrate (CAN), and 1 equiv of silver nitrate was added to the α-iodoketone intermediate, and milling continued for another one hour. This procedure led to a broad scope of polysubstituted pyrroles **6** in 60–97% isolated yields, tolerating various functional groups on the nitrogen atom

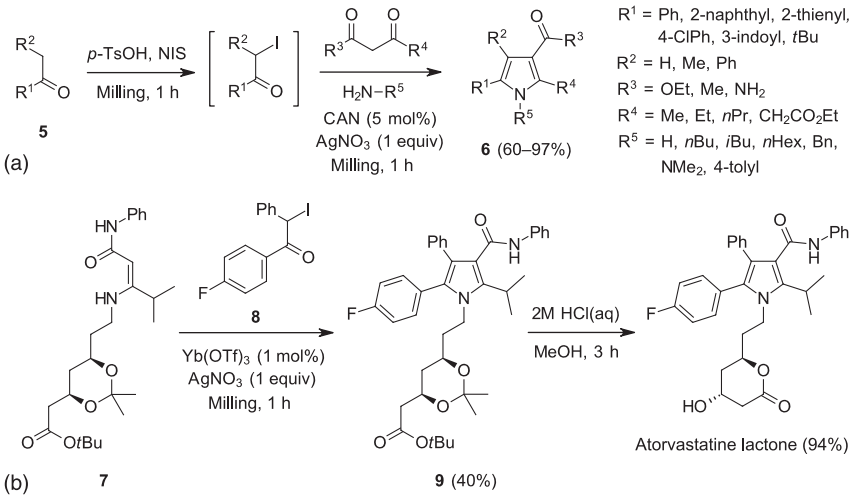

Scheme 10.2 (a) Mechanochemical Hantzsch pyrrole synthesis. (b) Ball milling in the construction of the pyrrole core in atorvastatine lactone.

and C2–C5 positions (Scheme 10.2a). In a later study, the scope was even further extended to cyclic ketones, allowing the synthesis of fused pyrroles with indole, homoindole, benzo[*g*]indole, and indeno[1,2-*b*]pyrrole frameworks in 40–97% [16]. Mechanochemical construction of the pyrrole core in the top-selling antihyperlipidemic drug atorvastatine was also accomplished by the same group [17]. Although the CAN-catalyzed formation of enaminone **7** precursor failed and yterbium triflate had to be used in ethanol solution at 40 °C in the first step, the subsequent mechanochemical coupling of α-iodoarylketone **8** with **7** in the presence of silver nitrate afforded **9** in 40% yield overall. In the final step, **9** underwent hydrolytic deprotection and lactonization to atorvastatine lactone in excellent 94% yield (Scheme 10.2b).

Mechanochemical approach in the iodine-catalyzed pyrrole synthesis was extensively studied by several groups. For example, Xu et al. described a solid-state transformation of a mixture of β-nitrostyrene and β-enaminones or β-enamine esters (1.2 equiv) into polysubstituted pyrroles **10** [18]. Under optimized conditions (20 minutes milling at 30 Hz), 20 mol% of iodine was necessary to ensure high isolated yields (75–94%). A cyclohexane-fused pyrrole derivative **11** was prepared in 72% yield with 3-(phenylamino)cyclohex-2-enone as the reactant (Scheme 10.3a). Without iodine, no pyrrole was formed. In comparison with enaminones, enamine esters were generally more reactive, while a strong electron-withdrawing substituent such as NO_2-group in the β-nitrostyrene component resulted in lower yields. Different aromatic and alkyl functionalities on the nitrogen atom were also tolerated.

The Wang's group explored the potential of solid-state ball milling for a one-pot sequential multicomponent synthesis of 2,3-dihydropyrroles and pyrroles from amines, alkyne esters, and chalcones [19]. Due to importance of both classes of these simple heterocycles, synthetic efforts were focused on the use of I_2/PhI(OAc)$_2$

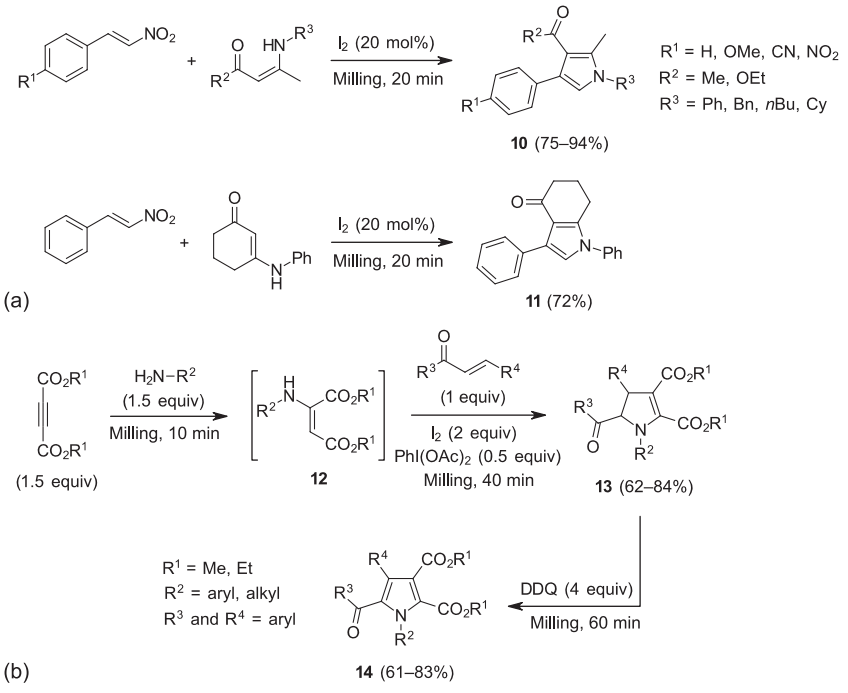

Scheme 10.3 (a) Mechanochemical I_2-catalyzed pyrrole synthesis from β-nitrostyrene. (b) I_2/PhI(OAc)$_2$-promoted synthesis of 2,3-dihydropyrroles and their dehydrogenative aromatization with DDQ to pyrroles under ball milling conditions.

system in combination with readily available starting materials. In the first step, grinding jars were loaded with a mixture of amine (0.3 mmol, 1.5 equiv) and alkyne ester (0.3 mmol, 1.5 equiv) and milled for 10 minutes at 30 Hz until enamine intermediates **12** were quantitatively formed. Next, chalcone (0.2 mmol, 1 equiv), iodine (0.4 mmol, 2 equiv), and PhI(OAc)$_2$ (0.1 mmol, 0.5 equiv) were added and milling continued for 40 minutes, leading to a series of 2,3-dihydropyrroles **13** in 62–84% isolated yield (Scheme 10.3b). The optimized conditions proved general as substituted anilines and alkyl amines, diethyl or dimethyl acetylene dicarboxylate, and chalcones with electron-donating or withdrawing substituents all reacted well. Analogous reactions in different solvents gave poor yields after 12–24 hours at temperatures from 50 to 80 °C, while in an experiment where all reactants were added at once, the 2,3-dihydropyrrole product was isolated in only 18%, with unreacted chalcone and other by-products remaining. The coupling constant of 4.0 Hz in ^{1}H-NMR spectra indicated the trans-configuration of protons on the dihydropyrrole moiety in all products.

The mechanochemical sequence was completed in the third step with the addition of 4 equiv of 2,3-dichloro-5,6-dicyano-1,4-benzoquinone (DDQ) to the reaction mixture containing the 2,3-dihydropyrrole products. After ball milling for 60 minutes, dehydrogenative aromatization took place affording polysubstituted pyrroles **14** in 61–83%.

Xu and Zhang recently reported an extension of this method to prepare 2,3-dihydropyrroles from substituted chalcones and 4-arylamino- or 4-alkylaminopent-3-en-2-one under mechanochemical LAG conditions [20]. They found that small amount of acetonitrile as the grinding liquid facilitated the iodine-promoted cyclization to 2,3-dihydropyrrole scaffold, resulting in 65–85% after 30 minutes of ball milling.

The same group reported earlier an example of mechanochemical manganese(III) acetate-mediated radical cyclization approach for the synthesis of *N*-substituted 2,5-dimethyl-3,4-dicarboxylate and 3,4-diphenylpyrroles [21]. Interestingly, among several oxidants, including Cu(II), Co(II), Mn(II), and Ag(I) acetates; I_2; and $PhI(OAc)_2$, only Mn(III) acetate exhibited superior chemoselectivity and led to clean reaction providing the pyrrole product in 95% yield. In all other cases, as well as in THF, toluene, and acetic acid solution, the formation of enamine ester was the preferred pathway with no or only traces of pyrrole. Under optimized conditions, ethyl or isobutyl acetoacetate (2 equiv) was milled with the corresponding aromatic or alkyl amine (1 equiv) and $Mn(OAc)_3$ (2 equiv) for 60 minutes at 30 Hz to afford *N*-substituted 2,5-dimethyl-3,4-dicarboxylate pyrroles **15** in 59–93%. Replacing acetoacetates with 2-phenylacetaldehyde enabled a mild and rapid solvent-free mechanochemical synthesis of *N*-substituted 3,4-diphenylpyrroles **16** in good to excellent yields (Scheme 10.4).

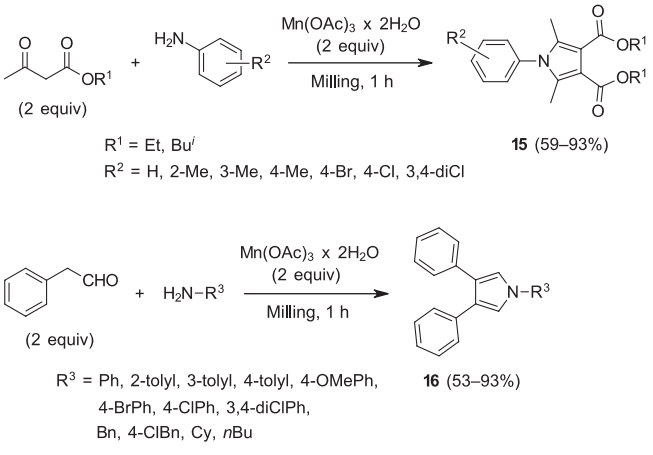

Scheme 10.4 Manganese(III) acetate-mediated radical mechanosynthesis of pyrrole derivatives.

Mechanochemical synthesis of indoles, as benzene-fused pyrrole derivatives, was first documented by Stolle et al. Their approach was based on a solvent-free intramolecular hydroamination of 2-alkynylanilines promoted by Lewis acids [22]. Using a planetary ball mill and hardened steel media, optimization study was performed on the model cyclization of 2-phenylethynylaniline to 2-phenyl-1*H*-indole **17** (R = Ph), which identified zinc bromide in stoichiometric amount as the best Lewis acid. Sodium chloride was used as an inert milling auxiliary to prevent

eutectic formation during high-energy milling. The selectivity of the reaction and the indole yield could be kept at high levels at lower rotational frequency (200 rpm), however, at the expense of prolonged milling time (eight hours). Besides phenyl derivative, 4-tolyl, 2-pyridyl, *n*-octyl, and trimethylsilyl analogs were employed affording indoles in 71–82% isolated yield (Scheme 10.5a). With shorter reaction time (45 minutes) and higher rotational frequency (800 rpm), the yields dropped to 59–72%. According to the proposed mechanism, $ZnBr_2$ forms a π-adduct with the alkyne substrate, followed by its rearrangement to a σ-complex and protodemetalation to the indole product.

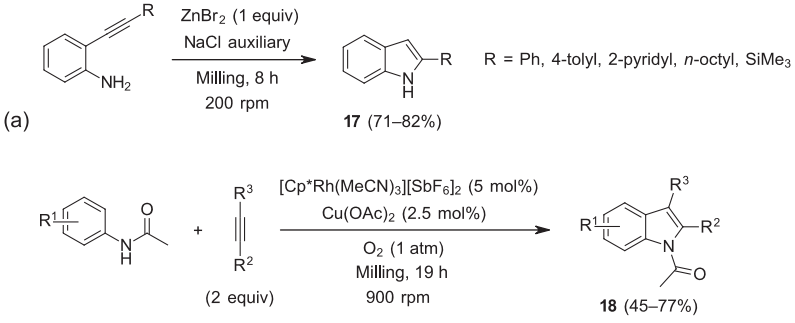

Scheme 10.5 (a) $ZnBr_2$-promoted intramolecular hydroamination of 2-alkynylanilines to indoles achieved by ball milling. (b) Mechanochemical synthesis of indoles by rhodium-catalyzed C–H activation of acetanilides.

Another interesting strategy for the construction of indole heterocyclic core relies on the rhodium-catalyzed C–H activation of acetanilides. Bolm et al. showed that ball milling enabled a solvent-free transformation of a 1 : 2 mixture of substituted acetanilides and acetylenes to indoles **18** in the presence of 5 mol% of rhodium(III) catalyst $[Cp^*Rh(MeCN)_3][SbF_6]_2$ (Cp^* = pentamethylcyclopentadienyl), catalytic quantity of copper(II) acetate as a redox modulator (2.5 mol%), and molecular oxygen as the terminal oxidant [23]. High-energy milling was carried out in zirconium oxide media at rotational frequency of 900 rpm for c. 19 hours (15 cycles of 60 minutes milling + 15 minutes cooling breaks). Different *ortho*-, *meta*-, and *para*-substituted acetanilides and aromatic acetylenes reacted well with 45–77% isolated yields, whereas dipropylacetylene gave *N*-acetyl-2,3-dipropylindole in only 9% yield (Scheme 10.5b). The directing acetyl group in *N*-acetyl-2,3-diphenylindole, important for the coordination of the rhodium catalyst, could also be removed mechanochemically in excellent 90% yield using potassium hydroxide (2 equiv) after one hour milling at 600 rpm.

The ability of molecular iodine to promote heterocyclizations was further explored by Wang et al. for the synthesis of racemic 3,2′-pyrrolinyl spirooxindoles via a tandem addition/cyclization sequence [24]. Solid-state ball milling of alkylidene oxindoles (0.2 mmol, 1 equiv) with enamine esters (0.4 mmol, 2 equiv), iodine (0.2 mmol,

1 equiv), and diazabicyclo[2.2.2]octane hexahydrate base (DABCO·6H_2O, 0.1 mmol, 0.5 equiv) for one hour in the presence of silica as the grinding auxiliary led to a range of highly substituted spirooxindoles **19** in 48–83% yield after chromatography workup (Scheme 10.6a). Besides broad functional group tolerance, NMR spectroscopy confirmed excellent diastereoselectivity of the reaction, which was in most cases ≥99 : 1.

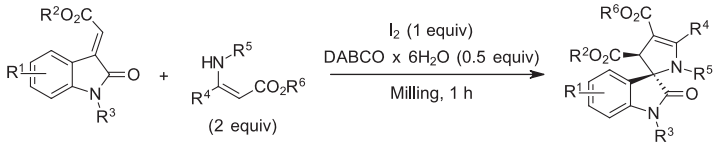

R^1 = H, 2-Me, 4-Me, 2,4-diMe, 4-OMe, 4-Cl, 4-Br
R^2 = Et
R^3 = H, Me, Ac, COEt, COAr
R^4 = Me, Et, *i*Pr, Ph
R^5 = aryl, alkyl
(a) R^6 = Me, Et, *n*Pr, *t*Bu

19 (48–83%)

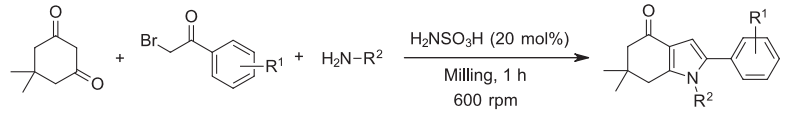

R^1 = H, 4-OMe, 4-Cl, 4-CN
R^2 = aryl, alkyl
(b)

20 (84–98%)

Scheme 10.6 (a) Iodine-catalyzed ball milling synthesis of spirooxindoles reported by Wang et al. (b) Multicomponent mechanosynthesis of 4-oxo-tetrahydroindoles.

Lambat et al. reported an interesting multicomponent reaction performed in the solid state, leading to the synthesis of 4-oxo-tetrahydroindoles **20** [25]. Using a planetary ball mill equipped with steel media, a stoichiometric mixture of dimedone, substituted phenacyl bromide, and aniline, in the presence of 20 mol% of sulfamic acid (H_2NSO_3H) catalyst, was subjected to milling at 600 rpm for one hour. After extraction with ethanol and acetone, followed by recrystallization, excellent isolated yields (84–98%) of aromatic tetrahydroindoles **20** were obtained (Scheme 10.6b).

Ball milling was also utilized for the solvent-free synthesis of benzimidazoles. Starting from 1,2-phenylenediamine, substituted benzaldehydes (2 equiv), and iron(III) chloride hexahydrate as the Lewis acid (25 mol%), Jin et al. showed that 1,2-disubstituted benzimidazoles **21** could be prepared in excellent yields up to 96% [26]. The reactions were performed in a 50 ml teflon jar with five agate balls at 400 rpm frequency for two hours. To keep the crude reaction mixture in powdered form, sodium chloride was used as an inert grinding auxiliary (Scheme 10.7). The same approach was pursued by Jang and coworkers, who employed recyclable zinc oxide nanoparticles as the catalyst (0.5 mol%) instead of $FeCl_3$·6H_2O in a high-yielding synthesis of benzimidazoles, as well as benzothiazoles (from 2-aminothiophenol) and benzoxazoles (from 2-aminophenol) [27].

Tandem aza-Michael addition/cyclization as a strategy to access heterocycles in a solvent-free manner was exploited by Su and coworkers [28]. In their work, chalcones were reacted with *N*-arylhydrazines and sodium hydrogensulfate

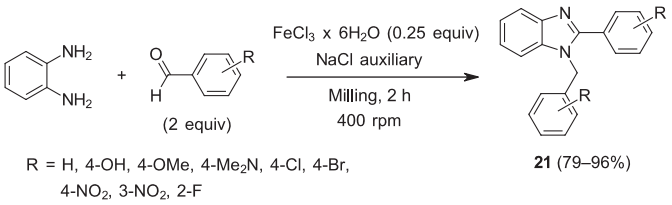

Scheme 10.7 Ball milling synthesis of benzimidazoles catalyzed by $FeCl_3 \cdot 6H_2O$.

monohydrate in 1 : 2 : 0.2 molar ratio to produce 1,3,5-triaryl-2-pyrazolines **22** in excellent yields by solid-state ball milling after only 5–15 minutes (Scheme 10.8a). Silica was used as the grinding auxiliary, and the excess *N*-arylhydrazine was separated by chromatography and reused in several cycles without significant loss of yield.

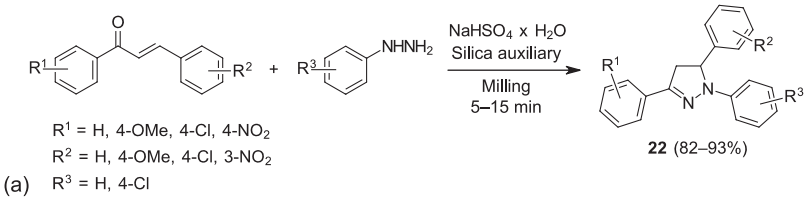

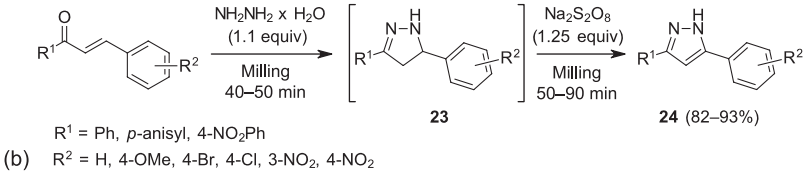

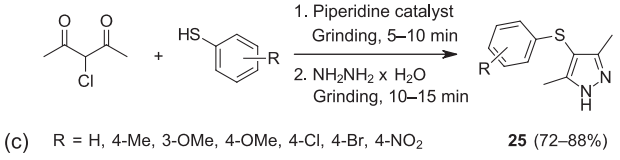

Scheme 10.8 (a) Aza-Michael/cyclization sequence in the mechanochemical synthesis of pyrazolines. (b) $Na_2S_2O_8$-catalyzed oxidation of pyrazolines to 1*H*-pyrazoles. (c) Solid-state synthesis of 3,5-dimethyl-4-(arylsulfanyl)pyrazoles by manual grinding.

Working along the same lines, the Zhang's group went a step further to mechanochemically convert pyrazolines **23** (without isolation) into 1*H*-pyrazoles **24**. This was achieved in the presence of sodium persulfate $Na_2S_2O_8$ (1.2 equiv) oxidant after 50–90 minutes of milling at 30 Hz [29]. High efficiency was retained with a series of chalcones and hydrazine monohydrate as reactants, affording aryl-substituted 1*H*-pyrazoles **24** in 82–93% (Scheme 10.8b).

Saeed demonstrated that solid-state heterocyclic reactions could also be efficiently carried out by using simple apparatus such as mortar and pestle [30]. In the first step, an equimolar mixture of 3-chloro-2,4-pentanedione and substituted thiophenols was manually ground in the presence of a catalytic amount of

piperidine base for 5–10 minutes. To the semisolid mixture, hydrazine monohydrate (1 equiv) was added, and grinding continued for another 10–15 minutes (Scheme 10.8c). The crude mixture was suspended in ethyl acetate and filtered; the filtrate concentrated and the product recrystallized from ethanol. In this way, 3,5-dimethyl-4-(arylsulfanyl)pyrazoles **25** were isolated in 72–88% yield.

Bicyclic pyrazolidinones possessing the 5-oxo-1,5,6,7-tetrahydropyrazolo[1,2-*a*]pyrazole core were successfully prepared by ball milling [31]. Using catalytic copper(I) acetate (10 mol%), calcium fluoride additive (20 mol%), and silica auxiliary, the 1,3-dipolar cycloaddition reaction between azomethine imines (1.2 equiv) and terminal alkynes (1 equiv) proceeded smoothly with pyrazolidinone **26** yields up to 96% after milling at 20 Hz in six 10-minute cycles with five minutes cooling breaks (Scheme 10.9). The milling pause was found to be crucial for reaction efficiency since overheating significantly lowered the yield in an experiment without the cooling breaks. The process was also carried out on gram scale affording 5-oxo-1-phenyl-1,5,6,7-tetrahydropyrazolo[1,2-*a*]pyrazole-2-carboxylate in excellent 83% (1.128 g).

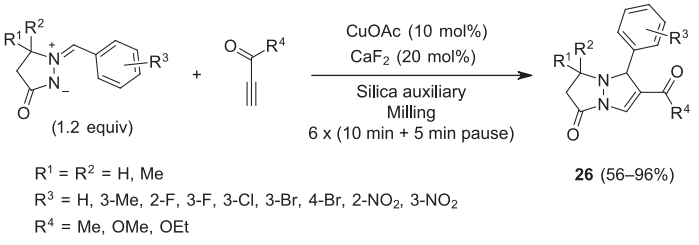

Scheme 10.9 Mechanochemical synthesis of pyrazolidinones via CaF_2-promoted CuOAc-catalyzed 1,3-dipolar cycloaddition.

Browne and coworkers prepared a series of difluorinated pyrazolones in a one-pot two-step mechanochemical process [32]. First, *N*-phenylhydrazine was ball milled with ethyl benzoylacetate (1 equiv) and acetic acid catalyst (0.5 equiv) in the presence of sodium chloride additive. The role of NaCl was to provide an environment where effective mixing and energy transfer could be realized, as both reactants were in the liquid state. After 40 minutes of milling at 30 Hz, 92% isolated yield of 2,5-diphenyl-2,4-dihydro-3*H*-pyrazol-3-one was recorded in the model reaction. Next, the difluorination step using Selectfluor (2 equiv) was optimized on the isolated diphenylpyrazolone **27** and was shown to proceed in quantitative yield with a combination of NaCl and sodium carbonate base (1.25 equiv) after 60 minutes of milling. Integration of these two compatible mechanochemical steps into a one-pot sequential procedure enabled the synthesis of aromatic difluorinated pyrazolones **28** in 37–83% (Scheme 10.10), where electron-withdrawing substituents (e.g. *para*-CF_3) significantly reduced the yield, presumably by retarding the initial pyrazolone formation.

Heterocyclic five-membered spiro derivatives were accessed from alkyl- or arylidenes and amidines as described by the Wang's group [33]. *N*-iodosuccinimide (NIS)

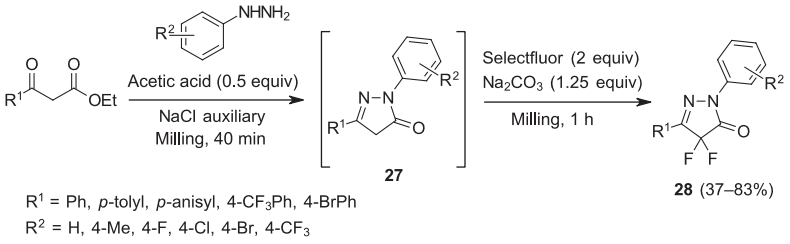

Scheme 10.10 Mechanochemical *in situ* generation of aromatic pyrazolones and subsequent difluorination using Selectfluor.

was used to promote a cascade reaction comprised of Michael-type addition between an alkene substrate and an amidine nucleophile, α-iodination of the intermediate adduct, and cyclization into the spiroimidazolines **29** with elimination of iodide. Milling was performed in stainless steel media for just 20 minutes at 30 Hz and with alkene : amidine : NIS = 1 : 1.5 : 1.2 ratio resulted in excellent isolated yields up to 94% (Scheme 10.11a). In the case of 1,3-dimethylbarbituric acid-derived alkenes, the yields were also very good (67–92%). This rapid and mild mechanochemical approach, which displayed a broad functional group tolerance, was also feasible for high-yielding gram-scale synthesis of spiroimidazolines.

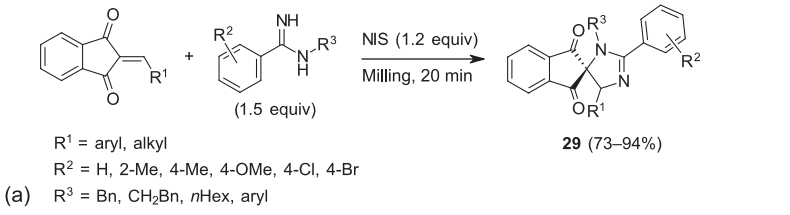

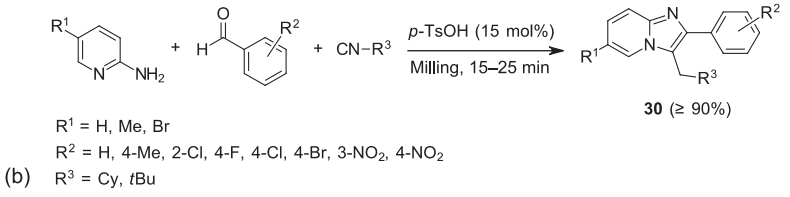

Scheme 10.11 (a) NIS-promoted mechanosynthesis of spiroimidazolines. (b) Multicomponent solvent-free ball milling synthesis of imidazo[1,2-*a*]pyridines.

Due to their importance as structural components in many pharmaceutically relevant molecules, the synthesis of imidazo[1,2-*a*]pyridines has been targeted by many groups. Maleki et al. employed solvent-free mechanochemical methodology to construct their heterocyclic core starting from 2-aminopyridines, aromatic aldehydes, and isocyanides in stoichiometric ratio with 15 mol% of *p*-TsOH [34]. This multicomponent reaction proceeded with remarkable efficiency, affording substituted 3-aminoimidazo[1,2-*a*]pyridines **30** in ≥90% yields after simple aqueous workup and recrystallization from hot water (Scheme 10.11b).

In the first application of ball milling for the synthesis of 1,2,3-triazoles, Stolle and coworkers reported a mechanochemical 1,3-dipolar cycloaddition between azides and alkynes, also known as the Huisgen or "click" reaction [35]. The 1,4-disubstituted 1*H*-1,2,3-triazoles **31** readily formed (typically >90%) in the presence of copper acetate catalyst (5 mol%) and fused quartz sand auxiliary after only 10 minutes of milling in zirconium oxide media at 800 rpm (Scheme 10.12a). The optimal alkyne : azide ratio was found to be 1.1 : 1, while sodium ascorbate (5 mol%) could be used with less reactive substrates. The mechanochemical "click" protocol was next used to prepare triazoles from bis- and tris-alkynylbenzenes and propargyl-functionalized polystyrene.

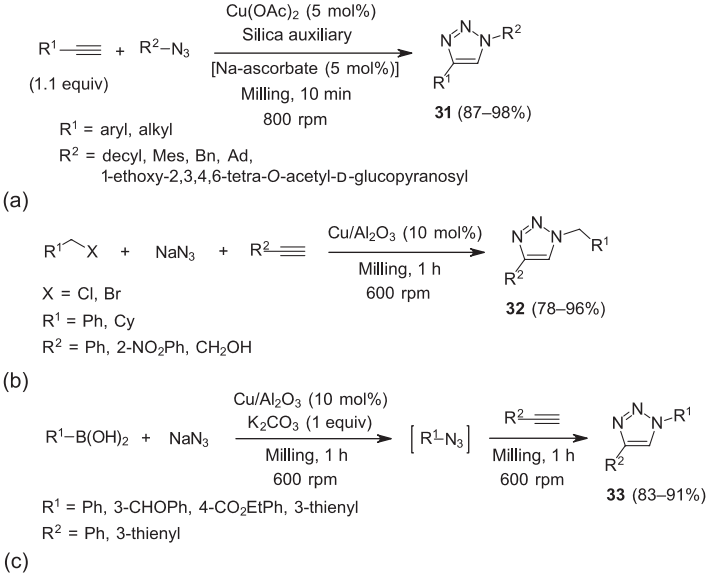

Scheme 10.12 (a) Huisgen 1,3-dipolar cycloaddition reaction catalyzed by copper acetate under ball milling conditions. Cu/Al_2O_3-catalyzed mechanosynthesis of triazoles from (b) alkyl halides and (c) aryl boronic acids.

Ranu et al. developed a modified version of the mechanochemical "click" reaction with two major improvements: the copper(II) sulfate catalyst was supported on alumina (Cu/Al_2O_3), which enabled easier recovery and recycling, and hazardous shock-sensitive organic azides were formed *in situ* [36]. Starting from an equimolar mixture of alkyl halides, sodium azide, and alkynes, in the presence of 10 mol% Cu/Al_2O_3, milling at 600 rpm for one hour gave 1*H*-1,2,3,-triazoles **32** in excellent 78–96% (Scheme 10.12b). However, this approach did not work for aromatic halides. Instead, aryl boronic acids were milled with NaN_3 for one hour in the first step, which required the addition of potassium carbonate base (1 equiv), followed by the 1,3-dipolar cycloaddition with an alkyne to afford aromatic 1,2,3-triazoles **33** in 83–91% after one hour (Scheme 10.12c).

The use of copper salts in the solid-state Huisgen reaction can be completely avoided, as nicely shown by Mack and coworkers who performed this reaction

by milling alkynes with azides in a copper jar charged with copper balls for 15 minutes [37]. In this way, the milling media itself acted as the catalyst, giving 1,2,3-triazole products in high yields.

10.2.2 Six-Membered Ring Heterocycles

The construction of pyridine heterocyclic core has not been extensively studied under ball milling conditions. Pyridine-fused coumarins were prepared by a solvent-free method in a catalytic three-component reaction between 3-aminocoumarins **34** (1 equiv), aromatic aldehydes (1.2 equiv), and phenylacetylene (1 equiv), as demonstrated by Kausar et al. [38]. They found that neither copper nor zinc catalyst alone could promote the process comprised of C—C/C—N bond formation and C(sp^2)–H activation of the coumarin substrate. However, a combination of copper(I) iodide (7 mol%) and zinc acetate (9 mol%) in CuI/$Zn(OAc)_2$ combo system successfully led to a series of chromeno[3,4-*b*]pyridines **35** in 80–95% after ball milling in stainless steel media at 30 Hz for 35–90 minutes (Scheme 10.13a).

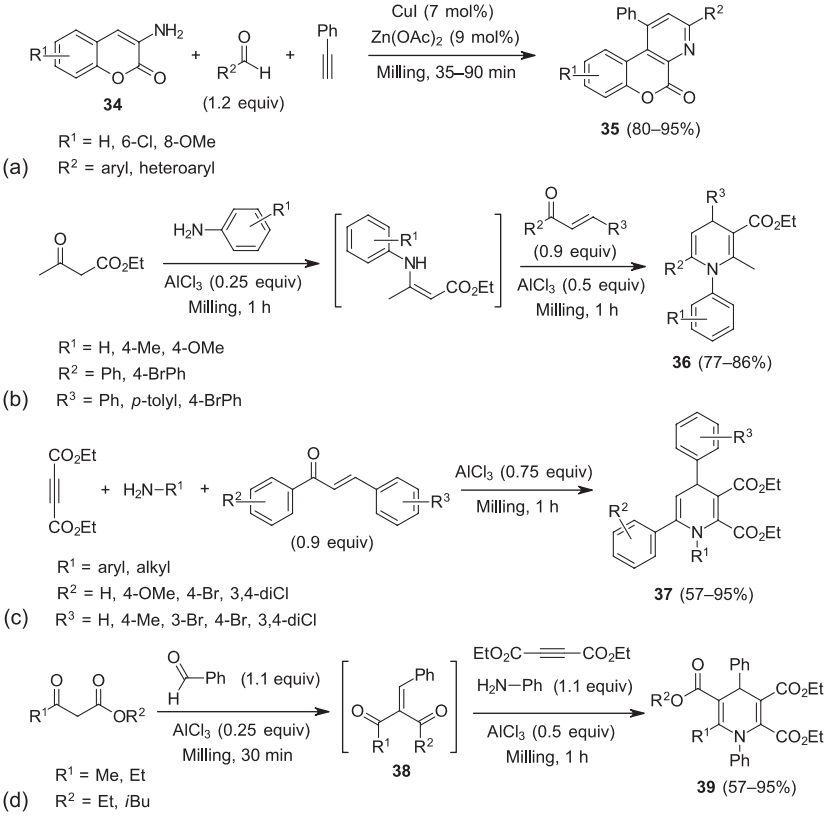

Scheme 10.13 (a) CuI/$Zn(OAc)_2$-catalyzed mechanosynthesis of chromeno[3,4-*b*]pyridines. (b–d) Mechanochemical $AlCl_3$-promoted synthesis of polysubstituted 1,4-dihydropyridines.

Zhang's group was also engaged in the development of mechanochemical dihydropyridine synthesis [39]. In their extensive work on the application of aluminum chloride ($AlCl_3$) to promote cyclization of various β-keto derivatives with *in situ* generated enamines, successful mechanochemical synthesis of 1,4-dihydropyridines was described. In the case of chalcones, enamines were first prepared by milling anilines and ethyl acetoacetate for 30 minutes at 30 Hz and were used without isolation in the second step. The reaction required $AlCl_3$ (0.75 equiv) and one hour milling to afford pentasubstituted dihydropyridines **36** in 77–86%. When enamines were prepared from amines and diethylacetylene dicarboxylate, a one-pot multicomponent procedure with a very broad substrate scope worked well, furnishing dihydropyridines **37** in 57–95% after one hour of milling in the presence of 0.75 equiv $AlCl_3$. Additionally, *in situ* generated α,β-unsaturated ketone **38** from benzaldehyde and β-ketoesters (the Knoevenagel reaction), in combination with aniline and diethylacetylene dicarboxylate, gave fully substituted dihydropyridines **39** in excellent yields (Scheme 10.13b–d).

Functionalized quinolines were recently prepared in the solid state by manual grinding in a mortar and pestle. Sarkar et al. developed a synthetic strategy to access quinoline heterocyclic core from *ortho*-enyne substituted anilines **40** in an iodine-mediated oxidative annulation [40]. Enyne substrates **40** were easily available in a single step via a tandem Heck–Sonogashira reaction in DMF, employing 2-iodoanilines and trimethylsilylacetylene as reactants. The best performance of the cyclization reaction was achieved by solvent-free manual grinding in air for two hours using 1.2 equiv of iodine (Scheme 10.14). As a result, a set of 2-iodomethylquinolines **41**, bearing electron-donating and withdrawing substituents, were prepared in good to excellent yields (65–89%). Iodo-functionalized quinolines could be further manipulated in, e.g. redox, cross-coupling, or nucleophilic substitution reactions.

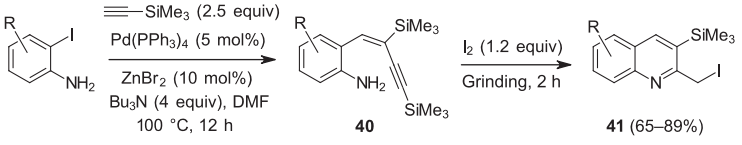

R = H, 2-Me, 4-Me, 3-OMe, 2,4-diMe, 4-*n*Bu,
4-F, 4-Cl, 4-Br, 4-CF_3, 4-CN, 4-NO_2, 4-COMe, 4-CO_2Me

Scheme 10.14 I_2-mediated oxidative annulation of *ortho*-enyne substituted anilines in the solid state via manual grinding.

Solvent-free synthesis of structurally related tetrahydroquinolines, commonly found in many natural products, has also been investigated. Most notably, the classical approach via Povarov cyclization was exploited by Zhang and Li who resorted to hetero-Diels–Alder reaction as a tool to construct the tetrahydroquinoline core [41]. In the course of optimization study, the authors found that strong Lewis acids such as $ZnCl_2$, $AlCl_3$, $FeCl_3$, and $BF_3{\cdot}OEt_2$ strongly promoted the hetero-Diels–Alder reaction between styrene and *in situ* formed imines **42**. Imines were prepared

in the first step by milling an equimolar mixture of substituted anilines and benzaldehydes for 30–90 minutes at 30 Hz and were subsequently used without isolation since the conversions were quantitative. In the second step, styrene and environmentally friendly $FeCl_3$ catalyst (25 mol%) were added and milling continued for 90 minutes to afford *cis*-2,4-diaryl-1,2,3,4-tetrahydroquinolines **43** in high 71–91% yield (Scheme 10.15). Remarkably, this mechanochemical Povarov reaction is highly diastereoselective with exclusive formation of *cis*-(2e,4e) isomers, as established by ^1H NMR and single crystal X-ray diffraction analyses.

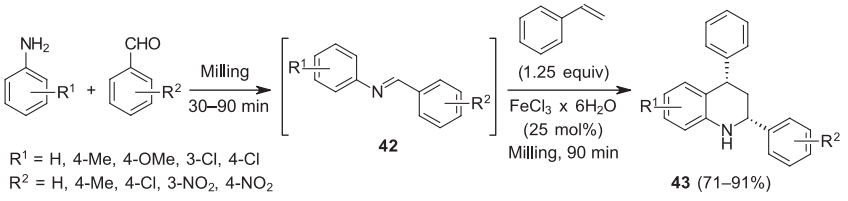

Scheme 10.15 Synthesis of tetrahydroquinolines via mechanochemical $FeCl_3$-catalyzed hetero-Diels–Alder reaction.

A highly efficient coupling reaction between 1,2-diamines and 1,2-diketones leading to quinoxaline heterocycles could be accomplished via solid-state milling. Several groups reported on this type of transformation [4]; for example, Carlier et al. prepared a series of dibenzo[*a*,*c*]phenazines **44** by this route [42]. Starting from phenanthrene-9,10-dione and aromatic 1,2-diamines, milling at 50 Hz for four hours furnished substituted quinoxalines in almost quantitative yields (Scheme 10.16a). With 2,3-diaminopyridine reactant, dibenzo[*f*,*h*]pyrido[3,2-*b*]quinoxaline (X = N) was isolated in 88%.

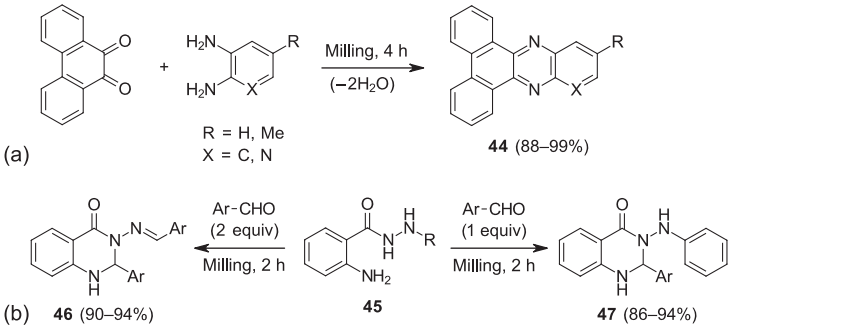

Scheme 10.16 (a) Solid-state synthesis of quinoxalines by condensation of 1,2-diamines with 1,2-diketones. (b) Synthesis of quinazolinones via a ball milling strategy.

Fülöp investigated a mechanochemical approach for the synthesis of quinazolinones **46** by coupling anthranilhydrazide **45** (R = H) with 2 equiv of aromatic aldehydes [43]. After ball milling for two hours at 25 Hz in a stainless steel jar with two zirconium oxide balls (to avoid iron contamination from wear),

quinazolinones **46** were isolated in yields greater than 90%. In the case of 2-amino-*N*′-phenylbenzohydrazide **45** (R = Ph), a stoichiometric reaction with aldehydes furnished excellent yields of quinazolines **47** again, except for 2-naphthyl and 4-biphenyl aldehydes, which gave only moderate 42% and 30% yield, respectively. The same group reported a ball milling synthesis of spirocyclic quinazolinones in near-quantitative yields from anthranilamide and cyclic ketones in 1 : 1 ratio, catalyzed by molecular iodine (5 mol%) under the same reaction conditions (Scheme 10.16b) [44].

Mechanochemical multicomponent reactions have been recognized as a very effective way to access a variety of heterocyclic compounds [45], e.g. the Biginelli reaction of aromatic aldehydes, active methylene derivatives (e.g. malononitrile and β-dicarbonyls), and (thio)ureas affords dihydropyrimidinone compounds (Scheme 10.17). When an equimolar mixture of *para*-substituted benzaldehydes, malononitrile, and (thio)ureas was milled for 40 minutes [46], 5-cyanopyrimidine derivatives **48** were isolated in 92–96% yield in the oxo-series (X = O) and in 95–98% yield in the case of the sulfur analogs (X = S). An interesting example of a mechanochemical Biginelli reaction was also reported by Mal and coworkers [47].

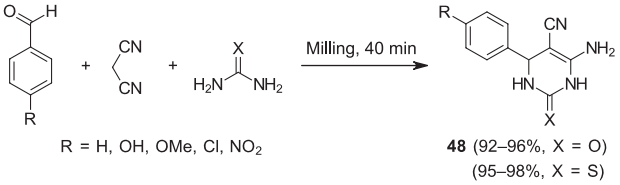

Scheme 10.17 Mechanochemical Biginelli reaction.

10.2.3 Porphyrins

The challenging high-yielding synthesis of porphyrins by cyclocondensation of pyrrole and aldehydes to porphyrinogens, followed by their oxidation, still represents one of the persisting problems in heterocyclic chemistry. Hence, it is not surprising that solvent-free ball milling, as a methodology that offers significant improvements over conventional solution synthesis, has been investigated in this sense.

The first report on the use of solvent-free approach for the synthesis of porphyrins came from the Hamilton's group [48]. Initial studies performed in a mortar and pestle revealed that pyrrole and benzaldehyde (1 : 1 ratio), in the presence of *p*-TsOH catalyst (4 mol%), failed to give tetraphenylporphyrin **50** (TPP, R = Ph) as evidenced by the absence of Soret band at 417 nm in the UV–vis spectrum of the reaction mixture. When the crude pink powder was left in air for two weeks, only 3% of TPP was detected, presumably due to reversibility of the condensation reaction and the presence of several reduced porphyrin forms in the mixture. The reaction was then carried out under ball milling conditions (stainless steel media, 25 Hz, 20–40 minutes), and the resulting pink powder containing porphyrinogen **49** immediately dissolved in chloroform along with DDQ (3 equiv) for oxidation. After two hours stirring and chromatographic purification, 27.9%

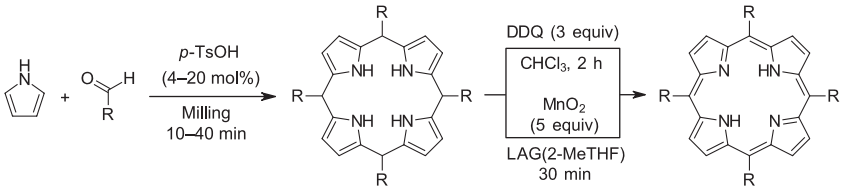

Scheme 10.18 Mechanochemical synthesis of meso-substituted porphyrins.

of TPP was isolated, comparable to solution protocols. Other benzaldehydes also performed well, affording the porphyrin derivatives **50** in 2.7–32.7%, depending on the substituent (Scheme 10.18). The combination of solvent-free pyrrole-aldehyde condensation with DDQ oxidation in chloroform was recently extended to the synthesis of *meso*-tetrakis(2,4,6-trimethylphenyl)porphyrin **50** (R = Mes) in 5.1% after 10 minutes of milling at 25 Hz, followed by one month solution oxidation [49].

In a slightly modified procedure, Pineiro and coworkers recently reported the use of manganese(IV) oxide (MnO_2) as an oxidant in the mechanochemical porphyrin synthesis [50]. In a model reaction, pyrrole and *para*-anisaldehyde were milled with *p*-TsOH (20 mol%) for 30 minutes, followed by DDQ oxidation in chloroform solution for two hours, resulting in 6% of *meso*-tetrakis(*p*-anisyl)porphyrin **50** (R = *p*-anisyl). When MnO_2 (5 equiv) was employed in the solvent-free second step, 3% of the porphyrin was isolated. However, LAG approach with 2-methyltetrahydrofuran (0.2 ml) as the grinding liquid increased the yield to 10%. This two-step procedure was more efficient than one-step reaction where 3% and 5% were obtained in the solvent-free, i.e. LAG experiment. In comparison with microwave heating at 200 °C or stirring at room temperature, the two-step LAG mechanosynthesis ranked best based on the *E*-factor sustainability parameter, providing porphyrins in 7–27% isolated yields (Scheme 10.18).

10.3 Mechanosynthesis of O-, S-, and Other Heterocycles

10.3.1 Three-Membered Ring Heterocycles

Examples of three-membered heterocyclic rings prepared by milling are rare. Two-step mechanochemical epoxidation of a diol was carried out in zirconium oxide media [51]. The α-, β-, and γ-cyclodextrins (CDs) **51** were subjected to *O*-tosylation of vicinal diols with *N*-tosylimidazole (TsIm) in the presence of an inorganic base (KOH). The transformation was facile and proceeded in very short time. In subsequent reaction, mono-2-tosyl-CDs **52** were subjected to ball

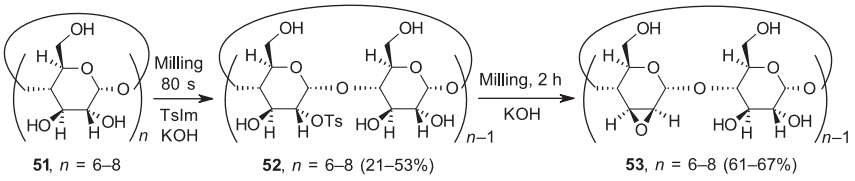

Scheme 10.19 Mechanochemical epoxidation of cyclodextrins.

milling in the presence of KOH, with mono-epoxide-CDs **53** obtained in high yields (Scheme 10.19).

10.3.2 Five-Membered Ring Heterocycles

Series of benzo[*b*]furans **54** was prepared by a mechanochemical electrophilic cyclization of *ortho*-alkynylanisoles with 1 equiv of iodine [52]. Various substituents were tested, and it was shown that electron-donating groups disfavor this 5-*endo-dig* cyclization. Moderate to high yields of products were obtained after milling for one hour at 15 Hz frequency (Scheme 10.20a).

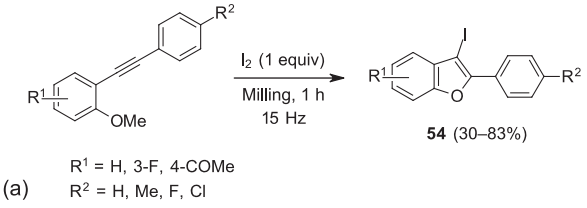

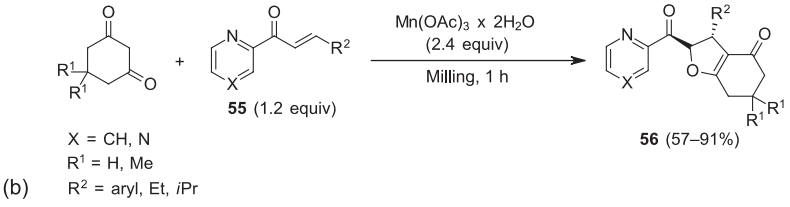

Scheme 10.20 (a) Preparation of benzofurans via ball milling. (b) Manganese(III)-promoted synthesis of dihydrofurans.

Wang discovered that manganese(III) acetate dihydrate was found to be the reagent of choice for synthesis of various dihydrofuran derivatives under ball milling conditions [53]. Thus, when 1,3-cyclohexadienones were reacted with 1-(pyridin-2-yl)-enones (1.2 equiv) **55** in the presence of $Mn(OAc)_3 \cdot 2H_2O$ (2.4 equiv), *trans*-2-acyl-3-aryl/alkyl-benzofuranones **56** were obtained in high yields as single diastereomers (Scheme 10.20b). The advantage of mechanosynthesis over the solution reaction is demonstrated as the solution conditions for model system provided complex reaction mixture.

Thiophenes were also synthesized in ball mill by the Gewald reaction [54]. Multicomponent reaction of ketones, ethyl cyanoacetate, and elemental sulfur in the

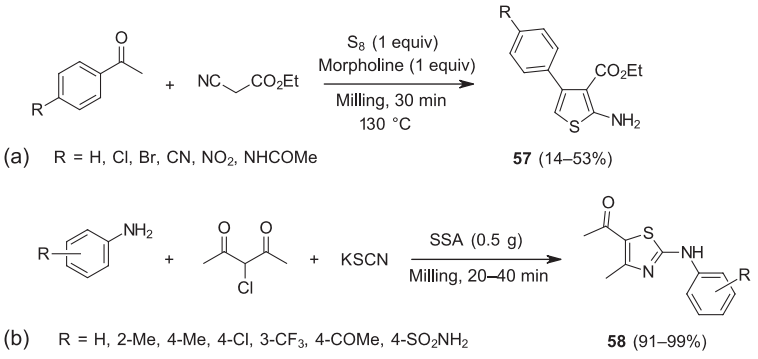

Scheme 10.21 Mechanochemical synthesis of (a) thiophenes and (b) 2-acetylthiazoles.

presence of morpholine provided polysubstituted 2-aminothiophenes **57** in 12–41% after milling for 24 hours. However, heating of milling vessel at 130 °C was necessary to increase the rate of reaction and the yield to 14–53% (Scheme 10.21a).

Multicomponent reaction involving aromatic amines, 3-chloro-2,4-pentanedione, and potassium thiocyanate with silica sulfuric acid (SSA) was developed for an efficient synthesis of substituted thiazoles by ball milling [55]. Using stainless steel media (50 ml jar and two 12 mm balls), 2-acetylthiazoles **58** were prepared in excellent 91–99% yield (Scheme 10.21b). Here, SSA had a dual role of solid catalyst and milling auxiliary, since both reactants were liquids. Additionally, SSA could be recycled for several runs without loss of its catalytic activity.

1,3-Dipolar cycloadditions represent a powerful route to five-membered heterocycles possessing two heteroatoms. For instance, Chakraborty described the use of 1,3-dipoles such as *N*-methyl-C-(2-furyl)nitrone **59** in a highly efficient mechanochemical synthesis of isoxalines [56]. When nitrone **59**, obtained in 84% yield by milling furfural, *N*-methylhydroxylamine hydrochloride, and sodium bicarbonate for one hour at 30 Hz, was ball milled with electron-deficient alkyne dipolarophiles, isoxazolines **60** were isolated. In a similar manner, from the cycloaddition of **59** with maleimides, acting as activated alkenes, isoxazolidines **61** were obtained in very high yield and diastereomeric excess (Scheme 10.22).

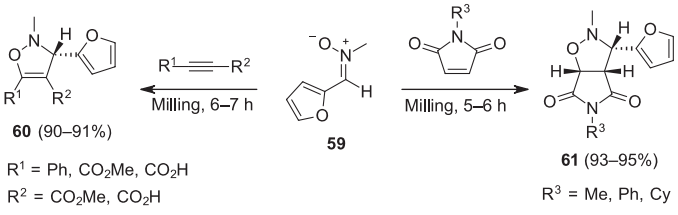

Scheme 10.22 Solvent-free synthesis of isoxazolidines and isoxazolines.

Simple ball milling technique for the synthesis of boronic esters was reported by Schnürch et al. [57]. Mechanochemical reaction of equal amounts of 2,2-dimethylpropan-1,3-diol or pinacol with different boronic acids for one hour

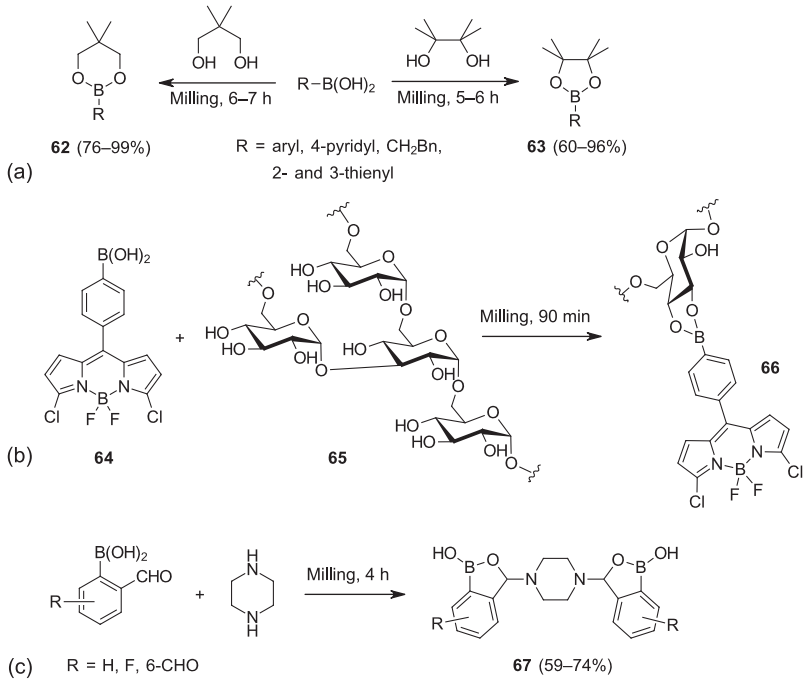

Scheme 10.23 (a) Mechanosynthesis of boronic esters. (b) Conjugation of dextran with a BODIPY dye via solvent-free ball milling. (c) Solid-state synthesis of bis(benzoxaboroles).

afforded boronic esters **62** and **63** (Scheme 10.23a). Excellent purity and high yields of boronic acid esters demonstrate high efficiency of mechanochemical conditions and their advantage over classical solution chemistry in terms of shorter time and the avoidance of solvents. Reaction could be easily scaled up by 20-fold. Besides simple diols, boronic ester of structurally more complex substrates could be easily prepared mechanochemically [58]. By milling BODIPY-derived boronic acid **64** with dextran **65** for 90 minutes, boronic ester-functionalized polymer **66** was obtained in better yields compared with derivatization in solution (Scheme 10.23b).

Adamczyk-Wozniak and coworkers reported on the solvent-free synthesis of antifungal bis(benzoxaboroles) [59]. When piperazine (1 equiv) was ball milled for four hours with a variety of boronic acid aldehydes (2 equiv), bis(benzoxaboroles) **67** were successfully prepared (Scheme 10.23c). Obtained yields were high and in most cases exceeded the yields from solution synthesis.

Mechanochemistry was also employed for the synthesis of substituted isoxazoles, as shown by the Wang's group [60]. Ball milling of *N*-hydroxybenzimidoyl chlorides and enamine substrates provided in short time the corresponding isoxazoles **68** (Scheme 10.24). Yields of this condensation reaction are dependent on the electronic nature of substituents on the reactants, where electron-withdrawing groups R^1 and particularly *N*-phenyl substituent in the enamine (R^4 = Ph) reduced the efficiency.

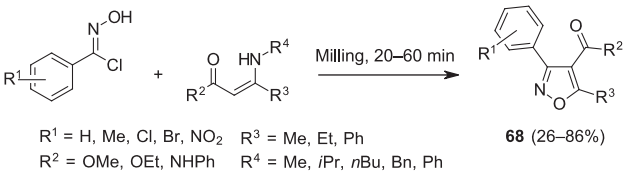

Scheme 10.24 Mechanochemical synthesis of isoxazoles.

10.3.3 Six-Membered Ring Heterocycles

A multicomponent reaction of equimolar amounts of phenol or *ortho*-allylphenol, paraformaldehyde, and a primary amine (aromatic, benzylic, or allylic) in a planetary ball mill was described by Cravotto, Colacino and coworkers [61]. The method was based on utilizing "parallel mechanochemistry" approach, where a special modification of the planetary jar adapter enabled up to 12 simultaneous reactions to be carried out in 2 ml glass vials containing glass or inox beads (1–3 mm diameter) as milling media. After four hours of milling at 550 rpm, a library of 3,4-dihydro-2*H*-benzo[*e*][1,3]oxazines **69** was prepared (Scheme 10.25a). This one-pot cascade reaction, comprising condensation and Mannich base ring closure reactions, proceeds in modest to high yields.

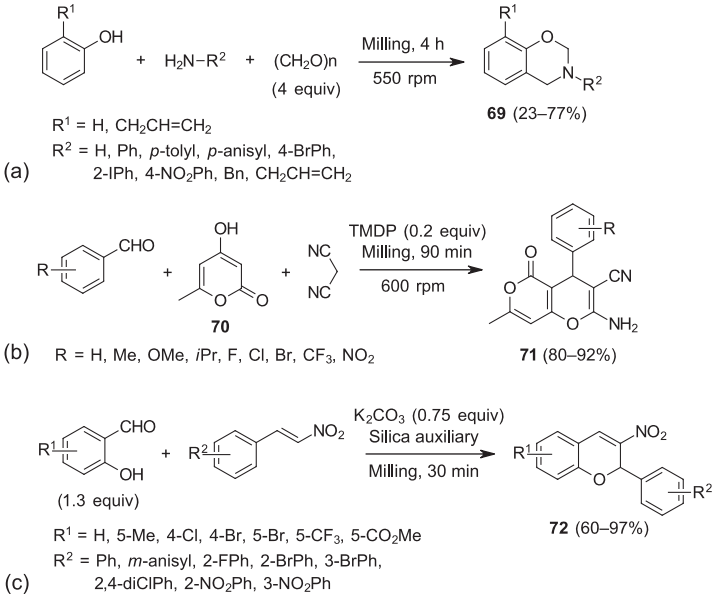

Scheme 10.25 (a) Parallel mechanosynthesis of oxazines. (b) Solid-state synthesis of pyrano[4,3-*b*]pyrans. (c) Ball milling synthesis of 2*H*-chromenes.

Pyrano[4,3-*b*]pyrans were accessed by a one-pot multicomponent reaction between aromatic aldehydes, 4-hydroxy-6-methyl-2-pyrone **70**, and malononitrile in a planetary ball mill [62]. Mechanistically, this transformation consisted of the

Knoevenagel reaction, followed by Michael addition, and 6-*exo-dig* cyclization in a reaction catalyzed by 4,4′-trimethylenedipiperidine (TMDP, 20 mol%). Solid-state condensations of different aldehydes were completed at ambient temperature, in much shorter times than in classical solution conditions, which required heating and in higher yields of pyrans **71**, typically greater than 80% in all experiments (Scheme 10.25b).

Cascade oxa-Michael–Henry reaction of salicylaldehyde derivatives with β-nitrostyrenes was carried out with in the presence of potassium carbonate base (0.75 equiv) and silica as the milling auxiliary [63]. After 30 minutes of milling (in two 15 minutes cycles), both electron-rich and electron-deficient salicylaldehydes provided 2*H*-chromenes **72** in good to excellent yields (Scheme 10.25c). The protocol could be scaled up to 2 g quantity of the product (R^1 = H, R^2 = Ph) with 80% isolated yield.

Su demonstrated that mechanochemical cyclodehydration of 1,3-propanediones could serve as another synthetic approach to flavones [64]. A solid-state reaction of 1-(2-hydroxyphenyl)-3-aryl-1,3-propanediones to produce flavones **73** was accomplished in the presence of 0.2 equiv of potassium bisulfate (Scheme 10.26) and silica gel as the milling auxiliary after only 5–15 minutes of ball milling. A series of flavone derivatives **73** was obtained in very high yields, while $KHSO_4$/silica support could be reused for several times with minimal loss of yields.

Scheme 10.26 Mechanosynthesis of flavones via $KHSO_4$-catalyzed cyclodehydration.

Oxidative rearrangement of furfuryl alcohols by Achmatowicz reaction was found to proceed well in a ball mill with *meta*-chloroperoxybenzoic acid (*m*-CPBA) as an oxidant [65]. As a result, 6-hydroxy-2*H*-pyran-3(6*H*)-ones **75** could be prepared from furfuryl alcohols **74**. Solid-state reaction employing *m*-CPBA was carried out with quartz sand in agate beaker and balls. Solvent-free synthesis was completed by simple dilution of reaction mixture with water and filtration to afford **75** in 63–95% (Scheme 10.27a).

Šebesta investigated an oxa-Diels–Alder reaction of α,β-unsaturated ketones with aldehydes, as a route to substituted pyranones under nonclassical conditions [66]. In the case of ball milling protocol, the best results were obtained with five-fold excess of the enone reactant. For a successful reaction, pyrrolidine catalyst (30 mol%) and benzoic acid cocatalyst had to be used, leading to 51–75% of pyranone derivatives **76** after three cycles of 90-minute milling (Scheme 10.27b). The efficiency of the mechanochemical procedure was better than under classical conditions, which required several days for completion.

Kaupp and coworkers extensively studied solid-state reactions involving ninhydrin, including ones promoted by ball milling [67]. For example, an efficient

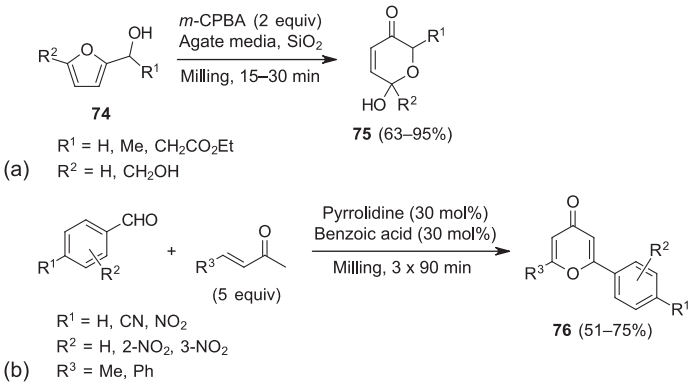

Scheme 10.27 (a) Achmatowicz rearrangement of furfuryl alcohols. (b) Oxa-Diels–Alder reaction under ball milling conditions.

solvent-free protocol was developed for the preparation of 10*a*-hydroxyindeno[2,1-*b*] benz[1,4]thiazin-11(10*aH*)-one (**77**) (Scheme 10.28a). The synthetic procedure, comprised of three cascade reactions (substitution, cyclization, and elimination), involved ball milling of 2-aminothiophenol hydrochloride with ninhydrin in a 1 : 1 ratio for one hour. The product, in the form of a chloride salt, was triturated with saturated $NaHCO_3$ solution, washed with water, and dried to afford pure **77** in 99%.

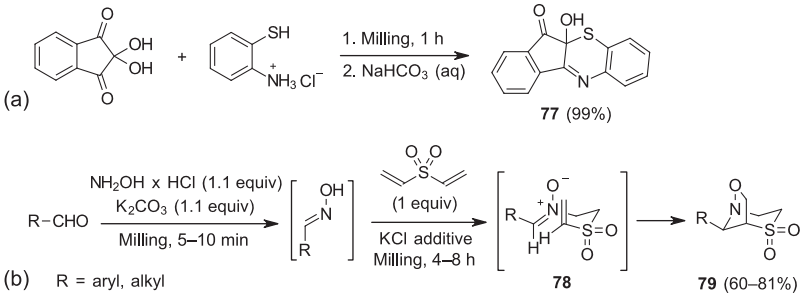

Scheme 10.28 (a) Condensation of ninhydrin and 2-aminothiophenol. (b) Two-step solid-state synthesis of bicyclic dioxides.

An interesting example of mechanochemical synthesis of N,O,S-containing heterobicyclic scaffold was reported by Chatterjee, Banerjee and coworkers [68]. Bridged aza-sulfones **79** were prepared by a two-step mechanochemical procedure. The first step included brief milling (5–10 minutes) of aldehydes with hydroxylamine hydrochloride (1.1 equiv) in the presence of potassium carbonate base (1.1 equiv) for an *in situ* generation of aldoximes. Addition of potassium chloride as solid additive and divinyl sulfone (1 equiv) to the crude mixture was followed by prolonged milling (four to eight hours). Michael addition produced the intermediate nitrone **78**, and its 1,3-dipolar cycloaddition afforded 7-oxa-4-thia-1-aza-bicyclo[3.2.1]octane-4,4-dioxides **79** in 60–81% isolated yields (Scheme 10.28b).

As already shown for five-membered boronate esters, synthesis of six-membered analogs proved equally successful via ball milling. Severin and coworkers applied mechanosynthesis to prepare three-dimensional cages possessing boronate ester linkers [69]. When 1,3,5-tris(aminomethyl)-2,4,6-triethylbenzene (**80**) was ball milled with pentaerythritol and 4-formylphenylboronic acid for one hour, cage **81** was obtained in very high yield (94%). Here, the two reactions of imine and boronate ester formation were carried in one-pot one-step manner (Scheme 10.29a). This multicomponent [6+3+2] condensation reaction also worked well for the longer spacer, 4-(4-formylphenyl)phenylboronic acid, which afforded larger cage **82**. Superiority of this ball milling procedure over classical solution reaction is demonstrated by significantly lower yields in ethanol (56% and 40% yield, for **81** and **82**, respectively).

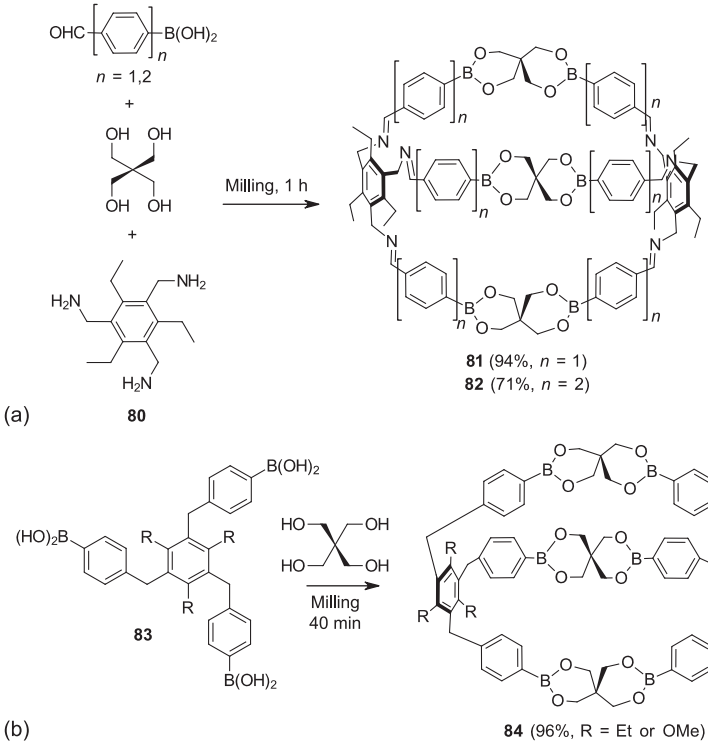

Scheme 10.29 Mechanochemical synthesis of boronate ester 3D cages developed in the research groups of (a) Severin and (b) Wang.

Somewhat simpler synthetic [3+2] condensation approach to boronic ester cages was reported by Wang and coworkers [70]. In this case, pentaerythritol was coupled directly with tris-boronic acids **83** by milling for 40 minutes. Cage compounds **84** (R = Et or OMe) were obtained essentially pure in near-quantitative yields (96%); thus further purification was not necessary (Scheme 10.29b).

10.3.4 Eight-Membered Ring Heterocycles

Severin also engaged in the solid-state synthesis of borasiloxanes [71]. In an initial experiment, condensation of di-*tert*-butylsilanediol and 4-formylphenylboronic acid afforded an eight-membered dialdehyde **85** in 65% (toluene reflux) and 75% yield (ball milling), respectively. The dialdehyde **85** was subsequently used in imine condensation with diamine linkers, leading to 33% of macrocycle **86** (R = 4,4′-bis(methylene)biphenyl) in benzene and 50% of macrocycle **87** (R = *trans*-(1*R*,2*R*)-1,2-cyclohexyl) in dichloromethane solutions. Borasiloxane-containing macrocycles were also prepared by a mechanochemical three-component [6+6+3] condensation starting from 4-formylphenylboronic acid, di-*tert*-butylsilanediol, and diamine. After 90 minutes of milling at 30 Hz, 85% of **86** and 65% of **87** were isolated (Scheme 10.30). For comparison, a one-step solution synthesis of **86** gave only 20% yield. In both cases, mechanochemical milling outperformed classical preparation of macrocycles in boiling organic solvents.

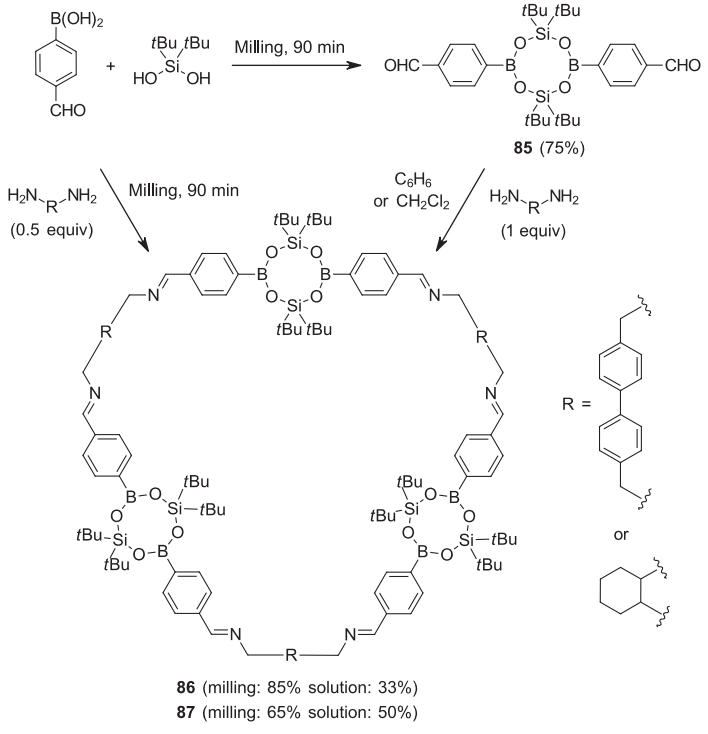

Scheme 10.30 Synthesis of macrocycles incorporating eight-membered borasiloxanes.

10.4 Conclusions and Perspectives

The examples of mechanochemical synthesis of heterocycles, selected in this chapter, represent only a fraction of available literature data on this topic. The high

efficiency of solid-state reactions under ball milling conditions has been exploited in environmentally friendly heterocyclic synthesis, rendering the use of bulk solvents obsolete in the synthesis steps, while near-quantitative yields in many cases obviate the need for purification and additional consumption of solvents. Considering the impact mechanochemistry has made across all fields of modern chemistry, its further application in heterocycles will surely lead to new developments and discoveries.

References

1 Friščić, T., Mottillo, C., and Titi, H.M. (2020). Mechanochemistry for synthesis. *Angew. Chem. Int. Ed.* 59 (3): 1018–1029. https://doi.org/10.1002/anie.201906755.

2 Friščić, T. (2012). Supramolecular concepts and new techniques in mechanochemistry: cocrystals, cages, rotaxanes, open metal–organic frameworks. *Chem. Soc. Rev.* 41: 3493–3510. https://doi.org/10.1039/C2CS15332G.

3 Boswell, B.R., Mansson, C.M.F., Cox, J.M. et al. (2021). Mechanochemical synthesis of an elusive fluorinated polyacetylene. *Nat. Chem.* 13: 41–46. https://doi.org/10.1038/s41557-020-00608-8.

4 Margetić, D. and Štrukil, V. (2016). *Mechanochemical Organic Synthesis*. Elsevier.

5 Tan, D. and Friščić, T. (2018). Mechanochemistry for organic chemists: an update. *Eur. J. Org. Chem.* 2018 (1): 18–33. https://doi.org/10.1002/ejoc.201700961.

6 Andersen, J. and Mack, J. (2018). Mechanochemistry and organic synthesis: from mystical to practical. *Green Chem.* 20: 1435–1443. https://doi.org/10.1039/C7GC03797J.

7 Štrukil, V. (2018). Mechanochemical organic synthesis: the art of making chemistry green. *Synlett* 29 (10): 1281–1288. https://doi.org/10.1055/s-0036-1591868.

8 Gomollón-Bel, F. (2019). Ten chemical innovations that will change our world: IUPAC identifies emerging technologies in chemistry with potential to make our planet more sustainable. *Chem. Int.* 41 (2): 12–17. https://doi.org/10.1515/ci-2019-0203.

9 Friščić, T., Childs, S.L., Rizvi, S.A.A., and Jones, W. (2009). The role of solvent in mechanochemical and sonochemical cocrystal formation: a solubility-based approach for predicting cocrystallisation outcome. *CrystEngComm* 11: 418–426. https://doi.org/10.1039/B815174A.

10 Friščić, T., Halasz, I., Beldon, P.J. et al. (2013). Real-time and in situ monitoring of mechanochemical milling reactions. *Nat. Chem.* 5: 66–73. https://doi.org/10.1038/nchem.1505.

11 Halasz, I., Puškarić, A., Kimber, S.A.J. et al. (2013). Real-time in situ powder X-ray diffraction monitoring of mechanochemical synthesis of pharmaceutical cocrystals. *Angew. Chem. Int. Ed.* 52 (44): 11538–11541. https://doi.org/10.1002/anie.201305928.

12 Užarević, K., Halasz, I., and Friščić, T. (2015). Real-time and in situ monitoring of mechanochemical reactions: a new playground for all chemists. *J. Phys. Chem. Lett.* 6 (20): 4129–4140. https://doi.org/10.1021/acs.jpclett.5b01837.

13 Crawford, D.E., Miskimmin, C.K.G., Albadarin, A.B. et al. (2017). Organic synthesis by Twin Screw Extrusion (TSE): continuous, scalable and solvent-free. *Green Chem.* 19: 1507–1518. https://doi.org/10.1039/C6GC03413F.

14 Kaupp, G., Schmeyers, J., Kuse, A., and Atfeh, A. (1999). Cascade reactions in quantitative solid-state syntheses. *Angew. Chem. Int. Ed.* 38 (19): 2896–2899. https://doi.org/10.1002/(SICI)1521-3773(19991004)38:19<2896::AID-ANIE2896>3.0.CO;2-3.

15 Estévez, V., Villacampa, M., and Menéndez, J.C. (2013). Three-component access to pyrroles promoted by the CAN–silver nitrate system under high-speed vibration milling conditions: a generalization of the Hantzsch pyrrole synthesis. *Chem. Commun.* 49: 591–593. https://doi.org/10.1039/C2CC38099D.

16 Estévez, V., Sridharan, V., Sabaté, S. et al. (2016). Three-component synthesis of pyrrole-related nitrogen heterocycles by a Hantzsch-type process: comparison between conventional and high-speed vibration milling conditions. *Asian J. Org. Chem.* 5 (5): 652–662. https://doi.org/10.1002/ajoc.201600061.

17 Estévez, V., Villacampa, M., and Menéndez, J.C. (2014). Concise synthesis of atorvastatin lactone under high-speed vibration milling conditions. *Org. Chem. Front.* 1: 458–463. https://doi.org/10.1039/C4QO00052H.

18 Xu, H., Li, Y., Xing, M. et al. (2015). Synthesis of pyrroles from β-enamines and nitroolefins catalyzed by I_2 under high-speed vibration milling (HSVM). *Chem. Lett.* 44 (4): 574–576. https://doi.org/10.1246/cl.141102.

19 Xu, H., Liu, H.W., Chen, K., and Wang, G.W. (2018). One-pot multicomponent mechanosynthesis of polysubstituted *trans*-2,3-dihydropyrroles and pyrroles from amines, alkyne esters, and chalcones. *J. Org. Chem.* 83 (11): 6035–6049. https://doi.org/10.1021/acs.joc.8b00665.

20 Weng, M.Y., Xu, H., Chen, H., and Zhang, Z. (2021). Liquid-assisted mechanosynthesis of *trans*-2,3-dihydropyrroles from chalcones and enaminones. *Heterocycles* 102 (1): 114–121. https://doi.org/10.3987/COM-20-14365.

21 Zeng, J.C., Xu, H., Yu, F., and Zhang, Z. (2017). Manganese(III) acetate mediated synthesis of polysubstituted pyrroles under solvent-free ball milling. *Tetrahedron Lett.* 58 (7): 674–678. https://doi.org/10.1016/j.tetlet.2017.01.016.

22 Zille, M., Stolle, A., Wild, A., and Schubert, U.S. (2014). $ZnBr_2$-mediated synthesis of indoles in a ball mill by intramolecular hydroamination of 2-alkynylanilines. *RSC Adv.* 4: 13126–13133. https://doi.org/10.1039/C4RA00715H.

23 Hermann, G.N., Jung, C.L., and Bolm, C. (2017). Mechanochemical indole synthesis by rhodium-catalysed oxidative coupling of acetanilides and alkynes under solventless conditions in a ball mill. *Green Chem.* 19: 2520–2523. https://doi.org/10.1039/C7GC00499K.

24 Xu, H., Liu, H.W., Lin, H.S., and Wang, G.W. (2017). Solvent-free iodine-promoted synthesis of 3,20-pyrrolinyl spirooxindoles from alkylidene oxindoles and enamino esters under ball-milling conditions. *Chem. Commun.* 53: 12477–12480. https://doi.org/10.1039/c7cc08306h.

25 Lambat, T.L., Abdala, A.A., Mahmood, S. et al. (2019). Sulfamic acid promoted one-pot multicomponent reaction: a facile synthesis of 4-oxo-tetrahydroindoles

under ball milling conditions. *RSC Adv.* 9: 39735–39742. https://doi.org/10.1039/c9ra08478a.

26 Jin, M., Song, G., Li, Z. et al. (2014). Efficient synthesis of 2-aryl-1-arylmethyl-1*H*-benzimidazoles in ball mill without solvent. *J. Heterocycl. Chem.* 51 (6): 1838–1843. https://doi.org/10.1002/jhet.1113.

27 Sharma, H., Singh, N., and Jang, D.O. (2014). A ball-milling strategy for the synthesis of benzothiazole, benzimidazole and benzoxazole derivatives under solvent-free conditions. *Green Chem.* 16: 4922–4930. https://doi.org/10.1039/C4GC01142B.

28 Zhu, X., Li, Z., Jin, C. et al. (2009). Mechanically activated synthesis of 1,3,5-triaryl-2-pyrazolines by high speed ball milling. *Green Chem.* 11: 163–165. https://doi.org/10.1039/B816788E.

29 Zhang, Z., Tan, Y.J., Wang, C.S., and Wu, H.H. (2014). One-pot synthesis of 3,5-diphenyl-1*H*-pyrazoles from chalcones and hydrazine under mechanochemical ball milling. *Heterocycles* 89 (1): 103–112. https://doi.org/10.3987/COM-13-12867.

30 Saeed, A. and Channar, P.A. (2017). A green mechanochemical synthesis of new 3,5-dimethyl-4-(arylsulfanyl)pyrazoles. *J. Heterocycl. Chem.* 54 (1): 780–783. https://doi.org/10.1002/jhet.2528.

31 Chen, X., Jia, C., Cao, L. et al. (2015). Solvent-free 1,3-dipolar cycloaddition of azomethine imines with terminal alkynes promoted by calcium fluoride under the ball milling condition. *Chem. Res. Chin. Univ.* 31: 543–548. https://doi.org/10.1007/s40242-015-4480-0.

32 Howard, J.L., Nicholson, W., Sagatov, Y., and Browne, D.L. (2017). One-pot multistep mechanochemical synthesis of fluorinated pyrazolones. *Beilstein J. Org. Chem.* 13: 1950–1956. https://doi.org/10.3762/bjoc.13.189.

33 Xu, H., Chen, K., Liu, H.W., and Wang, G.W. (2018). Solvent-free *N*-iodosuccinimide-promoted synthesis of spiroimidazolines from alkenes and amidines under ball-milling conditions. *Org. Chem. Front.* 5: 2864–2869. https://doi.org/10.1039/c8qo00723c.

34 Maleki, A., Javanshir, S., and Naimabadi, M. (2014). Facile synthesis of imidazo[1,2-*a*]pyridines via a one-pot three-component reaction under solvent-free mechanochemical ball-milling conditions. *RSC Adv.* 4: 30229–30232. https://doi.org/10.1039/c3ra43221a.

35 Thorwirth, R., Stolle, A., Ondruschka, B. et al. (2011). Fast, ligand- and solvent-free copper-catalyzed click reactions in a ball mill. *Chem. Commun.* 47: 4370–4372. https://doi.org/10.1039/c0cc05657j.

36 Mukherjee, N., Ahammed, S., Bhadra, S., and Ranu, B.C. (2013). Solvent-free one-pot synthesis of 1,2,3-triazole derivatives by the 'Click' reaction of alkyl halides or aryl boronic acids, sodium azide and terminal alkynes over a Cu/Al_2O_3 surface under ball-milling. *Green Chem.* 15: 389–397. https://doi.org/10.1039/c2gc36521a.

37 Cook, T.L., Walker, J.A., and Mack, J. (2013). Scratching the catalytic surface of mechanochemistry: a multi-component CuAAC reaction using a copper reaction vial. *Green Chem.* 15: 617–619. https://doi.org/10.1039/c3gc36720g.

38 Kausar, N. and Das, A.R. (2017). CuI–$Zn(OAc)_2$ catalyzed $C(sp^2)$–H activation for the synthesis of pyridocoumarins through an uncommon Cu^{I}–Cu^{III} switching mechanism: a fast, solvent-free, combo-catalytic, ball milling approach. *Tetrahedron Lett.* 58 (26): 2602–2607. https://doi.org/10.1016/j.tetlet.2017.05.074.

39 Zeng, J.C., Yu, F., Asiri, A.M. et al. (2017). $AlCl_3$-promoted cyclization of β-keto derivatives with in situ generated enamines under solvent-free high speed ball milling: an efficient one-pot access to polysubstituted 1,4-dihydropyridines. *Heterocycles* 94 (11): 2054–2064. https://doi.org/10.3987/COM-17-13801.

40 Halder, A., Maiti, D., and Sarkar, S.D. (2020). Mechanochemical synthesis of functionalized quinolines by iodine mediated oxidative annulation. *Chem. Asian J.* 15 (5): 577–580. https://doi.org/10.1002/asia.201901758.

41 Tan, Y.J., Zhang, Z., Wang, F.J. et al. (2014). Mechanochemical milling promoted solvent-free imino Diels–Alder reaction catalyzed by $FeCl_3$: diastereoselective synthesis of *cis*-2,4-diphenyl-1,2,3,4-tetrahydroquinolines. *RSC Adv.* 4: 35635–35638. https://doi.org/10.1039/c4ra05252h.

42 Carlier, L., Baron, M., Chamayou, A., and Couarraze, G. (2011). Use of co-grinding as a solvent-free solid state method to synthesize dibenzophenazines. *Tetrahedron Lett.* 52 (36): 4686–4689. https://doi.org/10.1016/j.tetlet.2011.07.003.

43 Magyar, T., Miklós, F., Lázár, L., and Fülöp, F. (2015). Application of a ball milling technique for the condensation of anthranilic hydrazides with aromatic aldehydes towards 4-quianzolinone derivatives. *Chem. Heterocycl. Comp.* 50: 1464–1470. https://doi.org/10.1007/s10593-014-1611-3.

44 Miklós, F., Hum, V., and Fülöp, F. (2014). Eco-friendly syntheses of 2,2-disubstituted- and 2-spiroquinazolinones. *Arkivoc* 2014 (6): 25–37. https://doi.org/10.3998/ark.5550190.p008.717.

45 Leonardi, M., Villacampa, M., and Menéndez, J.C. (2018). Multicomponent mechanochemical synthesis. *Chem. Sci.* 9: 2042–2064. https://doi.org/10.1039/C7SC05370C.

46 M'hamed, M.O. and Alduaij, O.K. (2014). An efficient one-pot synthesis of new 2-thioxo and 2-oxo-pyrimidine-5-carbonitriles in ball-milling under solvent-free and catalyst-free conditions. *Phosphorus Sulfur Silicon Relat. Elem.* 189 (2): 235–241. https://doi.org/10.1080/10426507.2013.818995.

47 Sahoo, P.K., Bose, A., and Mal, P. (2015). Solvent-free ball-milling Biginelli reaction by subcomponent synthesis. *Eur. J. Org. Chem.* 2015 (32): 6994–6998. https://doi.org/10.1002/ejoc.201501039.

48 Shy, H., Mackin, P., Orvieto, A.S. et al. (2014). The two-step mechanochemical synthesis of porphyrins. *Faraday Discuss.* 170: 59–69. https://doi.org/10.1039/c3fd00140g.

49 Su, Q. and Hamilton, T.D. (2019). Extending mechanochemical porphyrin synthesis to bulkier aromatics: tetramesitylporphyrin. *Beilstein J. Org. Chem.* 15: 1149–1153. https://doi.org/10.3762/bjoc.15.111.

50 Gomes, C., Peixoto, M., and Pineiro, M. (2019). Porphyrin synthesis using mechanochemistry: sustainability assessment. *J. Porphyrins Phthalocyanines* 23 (7, 8): 889–897. https://doi.org/10.1142/S1088424619500755.

51 Menuel, S., Doumert, B., Saitzek, S. et al. (2015). Selective secondary face modification of cyclodextrins by mechanosynthesis. *J. Org. Chem.* 80 (12): 6259–6266. https://doi.org/10.1021/acs.joc.5b00697.

52 Mantovani, A.C., Hernández, J.G., and Bolm, C. (2018). Synthesis of 3-iodobenzofurans by electrophilic cyclization under solventless conditions in a ball mill. *Eur. J. Org. Chem.* 2018 (20, 21): 2458–2461. https://doi.org/10.1002/ejoc.201800027.

53 Wang, G.W., Dong, Y.W., Wu, P. et al. (2008). Unexpected solvent-free cycloadditions of 1,3-cyclohexanediones to 1-(pyridin-2-yl)-enones mediated by manganese(III) acetate in a ball mill. *J. Org. Chem.* 73 (18): 7088–7095. https://doi.org/10.1021/jo800870z.

54 Shearouse, W.C., Shumba, M.Z., and Mack, J. (2014). A solvent-free, one-step, one-pot Gewald reaction for alkyl-aryl ketones via mechanochemistry. *Appl. Sci.* 4 (2): 171–179. https://doi.org/10.3390/app4020171.

55 Bogami, A.S., Saleh, T.S., and Al-Shareef, A.H. (2020). Mechanochemical synthesis of 5-acetylthiazole: a step toward green and sustainable chemistry. *J. Heterocycl. Chem.* 57 (10): 3605–3611. https://doi.org/10.1002/jhet.4079.

56 Chakraborty, B. (2020). Solvent-free synthesis and 1,3-dipolar cycloaddition reactions of *N*-methyl-C-(2-furyl) nitrone in a ball mill and anticancer activities of the new cycloadducts. *J. Heterocycl. Chem.* 57 (1): 477–485. https://doi.org/10.1002/jhet.3804.

57 Schnürch, M., Holzweber, M., Mihovilovic, M.D., and Stanetty, P. (2007). A facile and green synthetic route to boronic acid esters utilizing mechanochemistry. *Green Chem.* 9: 139–145. https://doi.org/10.1039/B611424E.

58 Andreozzi, P., Tamberi, L., Tasca, E. et al. (2020). The B & B approach: ball-milling conjugation of dextran with phenylboronic acid (PBA)-functionalized BODIPY. *Beilstein J. Org. Chem.* 16: 2272–2281. https://doi.org/10.3762/bjoc.16.188.

59 Borys, K.M., Wieczorek, D., Tarkowska, M. et al. (2020). Mechanochemical synthesis of antifungal bis(benzoxaboroles). *RSC Adv.* 10: 37187–37193. https://doi.org/10.1039/D0RA07767D.

60 Xu, H., Fan, G.P., Liu, Z., and Wang, G.W. (2018). Catalyst- and solvent-free mechanochemical synthesis of isoxazoles from *N*-hydroxybenzimidoyl chlorides and enamino carbonyl compounds. *Tetrahedron* 74 (45): 6607–6611. https://doi.org/10.1016/j.tet.2018.09.044.

61 Martina, K., Rotolo, L., Porcheddu, A. et al. (2018). High throughput mechanochemistry: application to parallel synthesis of benzoxazines. *Chem. Commun.* 54: 551–554. https://doi.org/10.1039/C7CC07758K.

62 Khaligh, N.G., Mihankhah, T., and Johan, M.R. (2019). 4,4′-Trimethylenedipiperidine (TMDP): an efficient organocatalyst for the mechanosynthesis of pyrano[4,3-*b*]pyrans under solid-state conditions. *Polycyclic Aromat. Compd.* 40 (5): 1606–1615. https://doi.org/10.1080/10406638.2018.1564679.

63 Liu, S.X., Jia, C.M., Yao, B.Y. et al. (2016). Cascade oxa-Michael–Henry reaction of salicylaldehydes with nitrostyrenes via ball milling: a solvent-free synthesis of

3-nitro-2*H*-chromenes. *Synthesis* 48 (3): 407–412. https://doi.org/10.1055/s-0035-1560964.

64 Zhu, X., Li, Z., Shu, Q. et al. (2009). Mechanically activated solid-state synthesis of flavones by high-speed ball milling. *Synth. Commun.* 39 (23): 4199–4211. https://doi.org/10.1080/00397910902898551.

65 Falenczyk, C., Pölloth, B., Hilgers, P., and König, B. (2014). Mechanochemically initiated Achmatowicz rearrangement. *Synth. Commun.* 45 (3): 348–354. https://doi.org/10.1080/00397911.2014.963624.

66 Mojzesová, M., Mečiarová, M., Marti, R., and Šebesta, R. (2015). Organocatalytic oxa-Diels–Alder reaction of α,β-unsaturated ketones under non-classical conditions. *New J. Chem.* 39: 2573–2579. https://doi.org/10.1039/C4NJ02361G.

67 Kaupp, G., Naimi-Jamal, M.R., and Schmeyers, J. (2002). Quantitative reaction cascades of ninhydrin in the solid state. *Chem. Eur. J.* 8 (3): 594–600. https://doi.org/10.1002/1521-3765(20020201)8:3<594::AID-CHEM594>3.0.CO;2-5.

68 Bhutia, Z.T., Das, A., Biswas, M. et al. (2018). 7-Oxa-4-thia-1-aza-bicyclo[3.2.1] octane 4,4-dioxides: mechanochemical synthesis by tandem Michael addition-1,3-dipolar cycloaddition of aldoximes and evaluation of antibacterial activities. *Eur. J. Org. Chem.* 2018 (4): 506–514. https://doi.org/10.1002/ejoc.201701511.

69 Içli, B., Christinat, N., Tönnemann, J. et al. (2009). Synthesis of molecular nanostructures by multicomponent condensation reactions in a ball mill. *J. Am. Chem. Soc.* 131 (9): 3154–3155. https://doi.org/10.1021/ja809279s.

70 Li, H.G., Li, L., Xu, H., and Wang, G.W. (2018). Mechanochemical synthesis and properties of boronic ester cage compounds. *Curr. Org. Chem.* 22 (9): 923–929. https://doi.org/10.2174/1385272821666171106151700.

71 Pascu, M., Ruggi, A., Scopelliti, R., and Severin, K. (2013). Synthesis of borasiloxane-based macrocycles by multicomponent condensation reactions in solution or in a ball mill. *Chem. Commun.* 49: 45–47. https://doi.org/10.1039/C2CC37538A.

11

Flow Chemistry: Sequential Flow Processes for the Synthesis of Heterocycles

Pedro Brandão[1,2], Marta Pineiro[1], and Teresa M.V.D. Pinho e Melo[1]

[1] *University of Coimbra, Coimbra Chemistry Centre (CQC) and Department of Chemistry, Rua Larga, 3004-535 Coimbra, Portugal*
[2] *University of Évora, LAQV-REQUIMTE, Rua Romão Ramalho, 59, 7000 Évora, Portugal*

11.1 Introduction

The challenges in modern organic chemistry go from the discovery of new entities based on increasing knowledge of reaction mechanisms to the embracing of sustainability issues in laboratory and industry scales. The inherent characteristics of flow chemistry setups, including increase of surface-to-volume ratio, intensification of heat and mass transfer phenomena (particularly important in exothermic reactions), critical control over concentration, use of high diluted solutions (important for stoichiometrically controlled reactions, as well as intramolecular reactions), the opportunity to use different activation modes (such as photon and electron activation, allowing to explore new reaction mechanisms), safety, and reproducibility, open the way to new compounds in a sustainable manner. Furthermore, scale-up production is easily enabled under flow conditions, as flow devices are compact and can be reconfigured according to the output needed. The possibility of combining flow methodologies with artificial intelligence and robotics is another advantage [1–4].

With the current environmental concerns, displayed by society and regulatory authorities, both academia and industrial organic chemists turned their attention to the sustainability and eco-friendliness of continuous manufacturing, the flow chemistry. The opportunity to establish continuous flow processes, which allow new reactions that cannot be performed under conventional conditions, high reproducibility, and control of the several stages in a time-efficient manner, combined with improved safety and less margin for human error, is highly beneficial [5–7].

From the synthetic chemistry point of view, the modular nature of most flow chemistry systems is one of the main advantages. The opportunity to couple different reactors, in-line purification methods, and addition of reactants at different stages makes continuous manufacturing a very versatile process. Another desirable feature is the different catalytic processes that can be promoted under

Heterocycles: Synthesis, Catalysis, Sustainability, and Characterization, First Edition.
Edited by Teresa M.V.D. Pinho e Melo and Marta Pineiro.

continuous flow. These technologies can be applied using homogeneous and heterogeneous catalytic systems including photocatalytic, biocatalytic, and enantioselective catalytic systems. The variety of chemical transformations currently being explored under continuous flow systems will provide an endless source of possibilities and increase the value of these methodologies in years to come [8–11].

The sustainability of flow chemistry processes was recognized by the CHEM21 project [12], by awarding a green flag for continuous flow reactions, in opposition to an amber flag for those performed under batch conditions [13]. The green nature of flow processes is of major relevance, as it provides gains in multiple stages of chemical development, from small-scale laboratory productions to kilogram-scale and full-scale manufacturing, leading to considerable improvements in both chemical optimization and process intensification and therefore corresponding to the synergy between synthetic chemistry and chemical engineering [14].

In recent years, the development and application of continuous flow systems in the synthesis of molecules bearing heterocycles, crucial scaffolds in organic chemistry and particularly relevant in the search of bioactive compounds [15], was object of a giant leap. It is probably the most revolutionary tool in the field of organic synthesis, by completely replacing the classic glassware and instrumentation to fully automated laboratories, enabling chemists to focus their attention in work planning and design [16–20].

In this chapter, we aim to highlight the most recent developments in heterocyclic synthesis using sequential or consecutive continuous flow systems, providing important examples of high-value molecules currently being prepared using these methodologies, in both academic and industrial contexts. Often called reaction telescoping, as more than one chemical transformation occurs without isolation of intermediates, multistep/sequential/consecutive flow systems allow in-line purification and introduction of required reagents at any given point of the flow setup [1, 21]. Nevertheless, one-step syntheses of emblematic heterocycles are also included.

11.2 Flow Synthesis of Heterocycles

11.2.1 Three-Membered Ring Heterocycles

Three-membered heterocycles, namely, oxiranes and aziridines (or their unsaturated counterparts, azirines), are very relevant building blocks for synthetic chemists [22]. Due to their inherent ring strain, three-membered heterocycles display high chemical reactivity and therefore are susceptible to a variety of electrophiles and nucleophiles, which has been known and exploited for the construction of various compounds, including several active pharmaceutical ingredients (APIs).

Epichlorohydrin and glycidol, two important oxiranes used as synthetic precursors to relevant APIs bearing β-amino alcohol moieties (e.g. propranolol, alprenolol, and naftopidil) [23], were synthesized under flow conditions from bio-based glycerol through sequential hydrochlorination/dichlorination process. Using pimelic acid as the catalyst, glycerol was converted into 1,3-dichloro-2-propanol

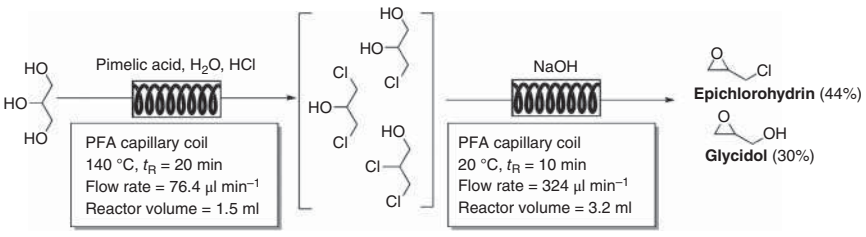

Scheme 11.1 Synthesis of glycidol and epichlorohydrin, important APIs synthetic intermediates, using a multistep flow system.

that was transformed *in situ* into a mixture of glycidol and epichlorohydrin (2,3) (Scheme 11.1), separable by an in-line membrane separation system.

The Neber reaction of activated oximes is a well-established synthetic pathway to 2*H*-azirines [24]. Using continuous flow techniques, 2*H*-azirines can also be prepared from oxime precursors via Neber reaction. Mesylation of the oxime by reaction with MsCl in the presence of Et_3N at 40 °C in a tubular flow coil, followed by base-promoted cyclization at room temperature in a glass column filled with silica supported pyridine ($PySiO_2$) and silica gel (SiO_2), gave the target three-membered heterocycles. The diaryl-2*H*-azirines prepared (isolated yield after in-line purification up to 87%) were converted into aziridines bearing nitrile and trifluoromethyl substituents through a continuous flow procedure. The nitrile derivatives were prepared, in good yield and good *cis*-diastereoselectivity (dr > 19 : 1), by mixing a solution of the 2*H*-azirine in acetonitrile with sodium cyanide in a tubular reactor coil at room temperature for five minutes. Following the preparation of 2*H*-azirines, the sequential reaction with trimethyl(trifluoromethyl)silane in a fluoride monolith maintained at 50 °C followed by a tubular flow coil (10 ml volume, 50 °C, five minutes residence time) allowed the synthesis of trifluoromethyl-substituted aziridines as pure *cis* diastereoisomers (Scheme 11.2) [25].

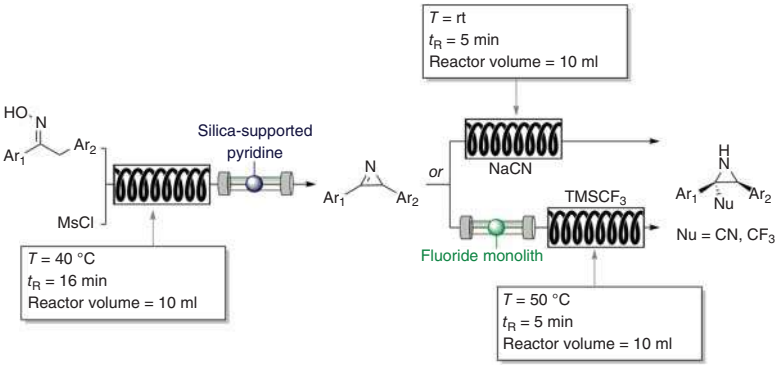

Scheme 11.2 Sequential Neber rearrangement and nucleophilic addition to prepare 2*H*-azirines and aziridines.

Fused aziridines were also prepared under flow conditions and further derivatized through nucleophilic opening of immobilized aziridines, illustrating the

utility of flow chemistry as a tool for functionalization through consecutive reactions. Zakrzewski et al. used 3,3,5,5-tetramethylmorpholin-2-one as starting material and promoted a palladium-catalyzed C(sp^3)–H activation to afford 2,2,6-trimethyl-4-oxa-1-azabicyclo[4.1.0]heptan-5-one. In-line purification techniques, including a QuadraSil AP® (Pd scavenger) and a catch–release Isolute SCX-3 gel® (amine scavenger), were carried out to achieve the product in high yield and high purity. The aziridine, while on the SCX-3 column, is immobilized by sulfonic acid protonation, which makes it susceptible to ring opening via nucleophilic attack when a nucleophile (water, methanol, or hydrazoic acid generated *in situ* from trimethylsilyl azide, $TMSN_3$) is pumped through the resulting column. This synthetic procedure afforded the derivatized products in good yields. The use of a solid-state support significantly facilitated the reaction procedure giving the final products in good yields, minimized the number of purification steps, and shortened the reaction time (Scheme 11.3) [26].

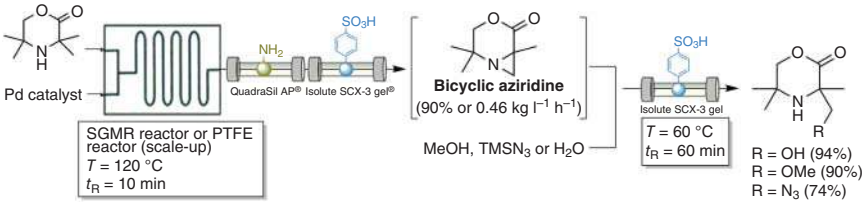

Scheme 11.3 Sequential C–H activation for the synthesis of fused aziridines and nucleophilic ring opening.

11.2.2 Four-Membered Ring Heterocycles

Flow setups combined with microwave, photochemical synthesis, or conventional heating have been used for the synthesis of β-lactams. The β-lactam ring, part of the structure of penicillins [27, 28], was synthesized using the Wolff–Staudinger cascade reaction. The formal [2+2] cycloaddition of *in situ* generated ketenes with imines was performed under continuous flow at high temperature (185 °C), using microwave irradiation, with the final heterocycles being prepared in moderate to very good yields (30–85%) and stereoselectivities [29].

The flow preparation of a β-lactam synthetic intermediate of the stimulant drug methylphenidate hydrochloride (Ritalin®) has been recently reported by Gérardy et al. exploring two flow methodologies. The quantitative conversion of the tosylhydrazone to the β-lactam intermediate of this drug was obtained using a conventional flow thermolysis within five minutes residence time at 180 °C, whereas using a photolysis flow setup almost quantitative conversions were obtained within one hour of reaction and operating at temperature below 40 °C (Scheme 11.4) [30].

11.2.3 Five-Membered Ring Heterocycles

Five-membered ring heterocycles play a major role in organic chemistry as they possess a plethora of applications. Among them, pyrrole is an iconic structure,

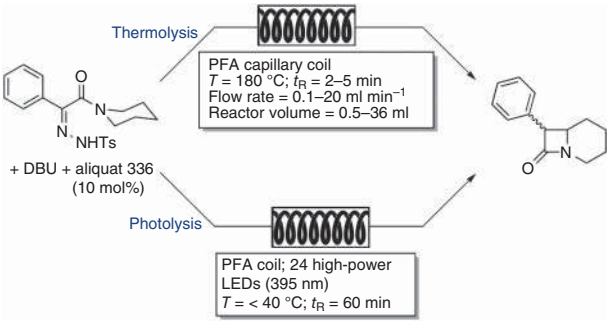

Scheme 11.4 Synthesis of a β-lactam synthetic intermediate of Ritalin®, using flow thermolysis or photolysis.

widespread in nature, and in many pharmacologically active agents. Hantzsch [31] and Paal–Knorr [32, 33] pyrrole syntheses are classical methodologies used for the synthesis of this heterocycle. These one-pot reactions were successfully performed under flow conditions; however, due to its nature, there is no need for sequential setups.

The Hantzsch pyrrole synthesis, involving the reaction of β-ketoesters with ammonia (or primary amines) and α-haloketones, was successfully performed under continuous flow conditions to synthesize pyrrole-3-carboxylic acids from commercially available *tert*-butyl acetoacetates, amines, and 2-bromoketones, followed by deprotection of the carbocyclic acid with *in situ* generated HBr. Pyrroles were obtained in good yields using *N,N*-diisopropylethylamine (DIEA) as catalyst and *N,N*-dimethylformamide (DMF) as solvent and introducing the reactant solutions in a preheated microreactor at 200 °C and 5.0 bar, with a flow rate of 62.5 µl min^{-1}, with a total reaction time of eight minutes. Scale-up of the synthesis of 1-benzyl-2-methyl-5-phenyl-1*H*-pyrrole-3-carboxylic acid under the established flow conditions allowed to obtain 850 mg (63% yield) of the compound in 2.5 hours (Scheme 11.5) [34].

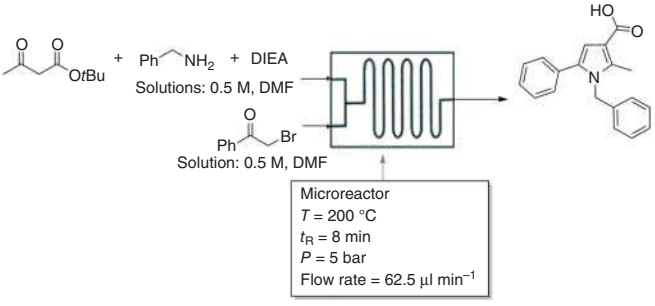

Scheme 11.5 Synthesis of 1-benzyl-2-methyl-5-phenyl-1*H*-pyrrole-3-carboxylic acid via Hantzsch synthesis under flow conditions.

Nieuwland et al. described a facile approach to optimize and perform pyrrole synthesis via Paal–Knorr cyclocondensation using flow chemistry. This reaction

has industrial relevance, even though it requires thermal control, since it is highly exothermic, which makes it an excellent candidate to be performed under flow conditions [35]. Using 2,5-hexanedione and ethanolamine or ethylamine in amine : diketone ratio of 5 : 1 or 10 : 1, respectively, the pyrrole was obtained quantitatively after 100 s at 20 °C. In order to quench the excess of primary amine used in the reaction, acetone was added through a third stream, leading to the formation of the corresponding imine as a secondary product. This step was included to allow a better determination of the optimal reactional conditions via offline gas chromatography–mass spectrometry (GC–MS) analysis. Scale-up in continuous flow using a microstructured flow reactor allowed the production of a pyrrole derivative at a rate of 55.8 g h^{-1}, (Scheme 11.6) [35]. The same type of reaction was later explored by Cranwell et al., but this time using a gas-phase reactant (ammonia). The variety of scaffolds achieved with this methodology was very diverse, with the yield appearing to be dependent on the steric hindrance [36].

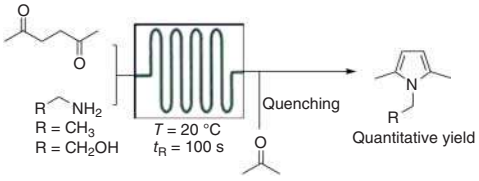

Scheme 11.6 Paal–Knorr synthesis of pyrrole.

The Fischer indole synthesis is a widely applied strategy to obtain indole derivatives using flow processes. Kappe and coworkers achieve the synthesis of tetrahydrocarbazole in 90% yield, at 200 °C (t_R of three minutes) in a 16 ml stainless steel coil affording 25 g of tetrahydrocarbazole within 1 h [37]. Using a monomodal microwave synthesizer heated at 150 °C, coupled to an high performance liquid chromatography (HPLC) system, allowing a t_R of four minutes, Bagley et al. achieved the synthesis of tetrahydrocarbazole in 90% yield [38, 39]. Increasing the reaction temperature to 240 °C and using a single-mode microwave applicator, developed to perform reactions under flow conditions as it generates a uniform electromagnetic field within its resonant cavity, tetrahydrocarbazole was produced at a rate of 115 g h^{-1} [39]. The same heterocycle was obtained effectively using an ethylene tetrafluoroethylene (ETFE) tubing packed with Amberlite IR 120 H (100 mg) and sealed with cotton wool at 90 °C within a residence time of five minutes [40]. The same reaction conditions were applied for the synthesis of pyrido[2,3-*a*]carbazole derivatives (40–90% yield) from phenylhydrazines and 5-oxodecahydroquinoline via the Fischer indole synthesis (Scheme 11.7a) [40].

The sustainability associated with the flow process was increased using an ionic liquid as recyclable solvent for the synthesis of 3-methylindole. The Fischer indole synthesis was performed in high yields, with the initial generation of phenylhydrazone from phenylhydrazine and propanal, followed by cyclization catalyzed

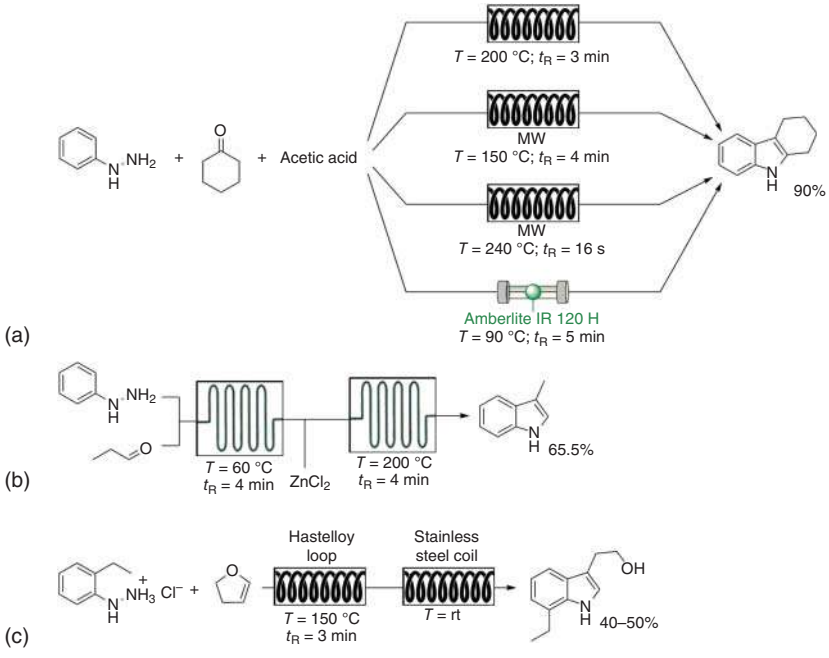

Scheme 11.7 Fischer indole synthesis under flow conditions.

by $ZnCl_2$ in 1-ethyl-3-methylimidazolium tetrafluoroborate ([EMIM][BF_4]) at 200 °C for four minutes. The ionic liquid used as solvent was successfully recycled four times in the flow reaction without any significant loss of activity (Scheme 11.7b) [41].

7-Ethyltryptophol, a very important synthetic intermediate for the synthesis of the API etodolac, was prepared using flow Fischer reaction and available starting materials, ethylphenylhydrazine hydrochloride and dihydrofuran, catalyzed by HCl in methanol/H_2O (2 : 1) at 150 °C within a short residence time (three minutes). This can be considered an efficient transformation (40–50% yield) since it is a more challenging reaction system, which is able to form several side products (Scheme 11.7c) [42].

As an example of the application of flow processes in the synthesis of compounds with an indole core, we highlight one example reported by Baumann et al. on the total flow synthesis of an auxin mimic-based herbicide (Scheme 11.8) [43]. A total of four steps were established in order to achieve the final product (80% overall yield), bearing an indole core and an oxadiazole core. The synthesis of these heterocycles was achieved through reduction of the nitrobenzene derivative and intramolecular cyclization using a Thales Nano H-cube® system, operating in full hydrogen mode (internal pressure 15 bar) with the flow rate of 1.3 ml min^{-1} and acetic acid as catalyst (10 mol%), which allowed quantitative conversion into the desired indole. This translates to an output of 3.7 g of product/h in 93% of isolated yield. The condensation of the indole-3-carboxylate with hydrazine and the reaction of the formed acyl hydrazine with triphosgene in a heated (55 °C) flow coil led to the synthesis

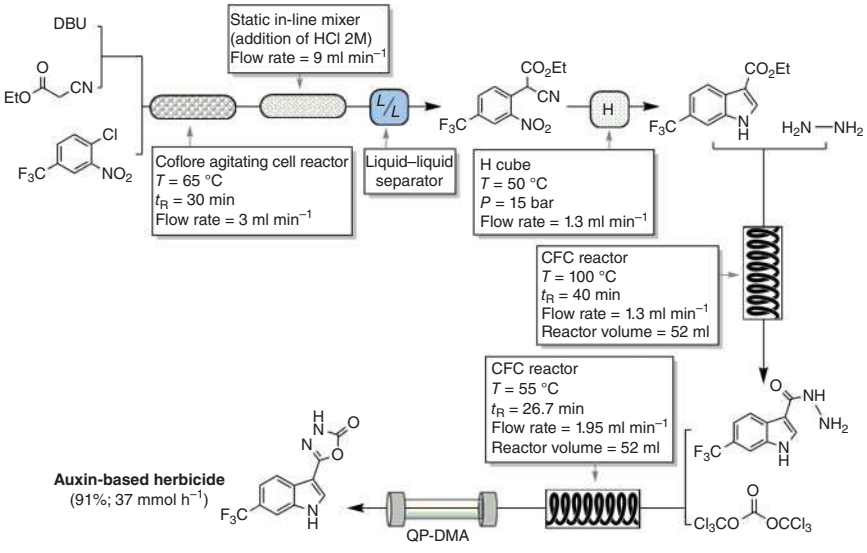

Scheme 11.8 Synthesis of an auxin-based herbicide bearing the indole and the oxadiazole cores using flow chemistry.

of 3*H*-[1,3,4]oxadiazol-2-one unit, which after purification by passage through a scavenging cartridge of QP-DMA (*N*,*N*-dimethylbenzylamine polystyrene) yielded the desired product in 91% of isolated yield.

The γ-lactam ring (pyrrolidin-2-one) is present in several synthetic and natural biologically active compounds [44]. Tsubogo et al. reported the asymmetric catalytic synthesis of (*R*)- and (*S*)-rolipram and derivatives under heterogeneous conditions using commercially available starting materials. Briefly, they promoted a multistep flow synthetic procedure, applying heterogeneous catalysts, without the need to isolate intermediates or by-products throughout the process. Aldehyde and nitromethane were converted into the nitroalkene with >90% yield, in the presence of a base (silica-supported amine and crushed anhydrous calcium chloride). The asymmetric 1,4-addition of malonate to the obtained nitroalkene was performed using a chiral polymer-supported (PS) calcium catalyst (PS-(*S*)-pybox-calcium chloride, where pybox is pyridinebisoxazoline) affording the γ-nitro ester intermediate in 84% yield with 94% enantiomeric excess. The reduction of the γ-nitro ester using a polysilane-supported palladium/carbon (Pd/DMPSi-C, where DMPSi is dimethylpolysilane) catalyst, followed by cyclization, afforded selectively the pyrrolidone in 74% yield with 94% enantiomeric excess (Scheme 11.9). The hydrolysis and decarboxylation of the ester group to obtain rolipram (50% yield, 96% ee) were also achieved under flow conditions using *o*-xylene and water as solvent through silica-supported carboxylic acid and Celite [45].

Imidazopyridines are another example of bicyclic heterocycles with great interest for medicinal chemists [46–49]. As an application of flow processes in drug discovery, focus will be given to the work developed by Guetzoyan et al. [50] on the synthesis of γ-aminobutyric acid ($GABA_A$) agonists – $GABA_A$ receptor is the therapeutic

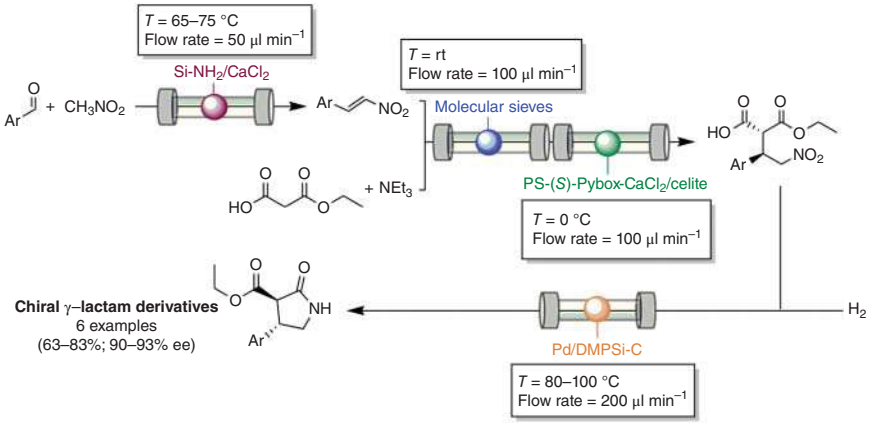

Scheme 11.9 Flow sequential synthesis of chiral γ-amino acid derivatives with γ-lactam moiety.

target for benzodiazepines, general anesthetics, and barbiturates [51, 52]. Two commercially available drugs were obtained – zolpidem, a sedative/hypnotic drug, and alpidem, an anxiolytic drug – as well as 20 other imidazo[1,2-*a*]pyridines. In addition to the total synthesis by flow processes, in-line evaluation of the binding affinity of the compounds to human serum albumin (HSA) by frontal affinity chromatography was also performed, as an example of an interface development between synthesis and bioassays, setting a starting point for an automated drug discovery platform. The heterocycle-forming synthetic step is shown in Scheme 11.10. The unsaturated ketone, obtained by the acid-catalyzed condensation between ethyl glyoxylate and acetophenone in reactors packed with polymer-supported sulfonic acid resin (QP-SA) at 120 °C, was further transformed into the ketimine derivative by reaction with an aminopyridine derivative in the $MgSO_4$ packed column at 50 °C. The subsequent 5-exo cyclization step was carried out in the convection flow coil (CFC) reactor

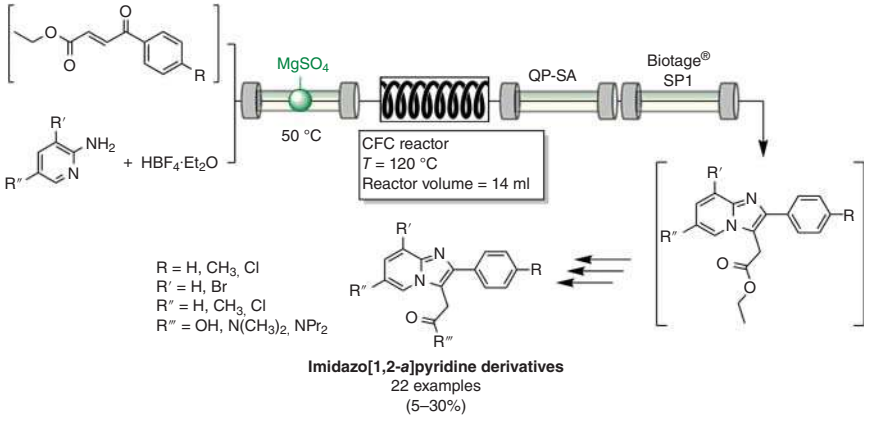

Scheme 11.10 Flow multistep synthesis of $GABA_A$ agonists with imidazopyridine scaffold.

heated at 120 °C. The Quadrapure-sulfonic acid resin (QP-SA) column allowing the retention of unreacted aminopyridine (scavenger) and the Biotage® SP1 column performed in-line chromatographic purification [50].

One of the most remarkable examples of flow chemistry applied to drug development is the synthesis of prexasertib. Prexasertib is a checkpoint kinase inhibitor drug with dual activity, toward Chk1 and Chk2, which work as key regulators in cellular DNA damage response pathways. Preclinical trials showed the promising antitumor activity of prexasertib, which was selected to pursue its development in clinical trials [53–59].

To ensure the production of a safe and high-quality drug for human use, Cole et al. developed a seven-step synthetic route for large-scale production of prexasertib (24 kg). The last four steps were performed under continuous flow conditions, the condensation of a nitrile with a hydrazine to form a pyrazole derivative, followed by a S_NAr reaction between the pyrazole derivative and a pyrazine, amine deprotection, and salt formation (Scheme 11.11). Using this continuous flow process, prexasertib was prepared in kilogram-scale, identifying several advantages compared with more conventional methodologies, such as better yield and impurity rejection, efficient solvent stripping with enhanced performance in terms of product stability, elimination of isolation steps, increased quality assurance, and the possibility of using online process analytical technology and process automation [60].

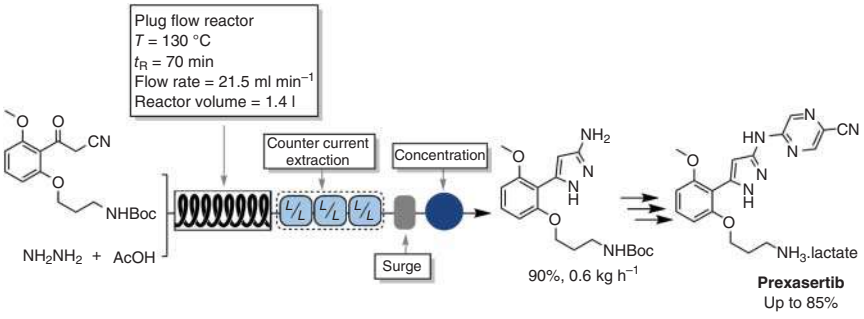

Scheme 11.11 Heterocycle-forming step on prexasertib preparation under flow conditions.

In respect to five-membered ring heterocycles bearing three nitrogen atoms, triazoles are an interesting class of heterocyclic compounds with a broad spectrum of bioactivities, efficiently obtained using "click" reactions [61–65]. Beyond the synthesis of the triazole, "click" chemistry has been applied in a multitude of synthetic strategies [66] and also for the synthesis of cyclic peptoids [67]. The multicomponent Ugi reaction can be applied in the synthesis of peptoid-like molecules, by exploring the click copper-catalyzed strategy for macrocyclization. In the synthesis of cyclic peptoids, for example, the peptoid backbone cyclization was considered as the most challenging aspect in the synthesis of intramolecular cycloaddition reaction between an azide moiety and an alkyne moiety. Indeed, Kappe et al. reported the synthesis

of cyclic peptoid molecules following this synthetic approach under flow conditions (Scheme 11.12).

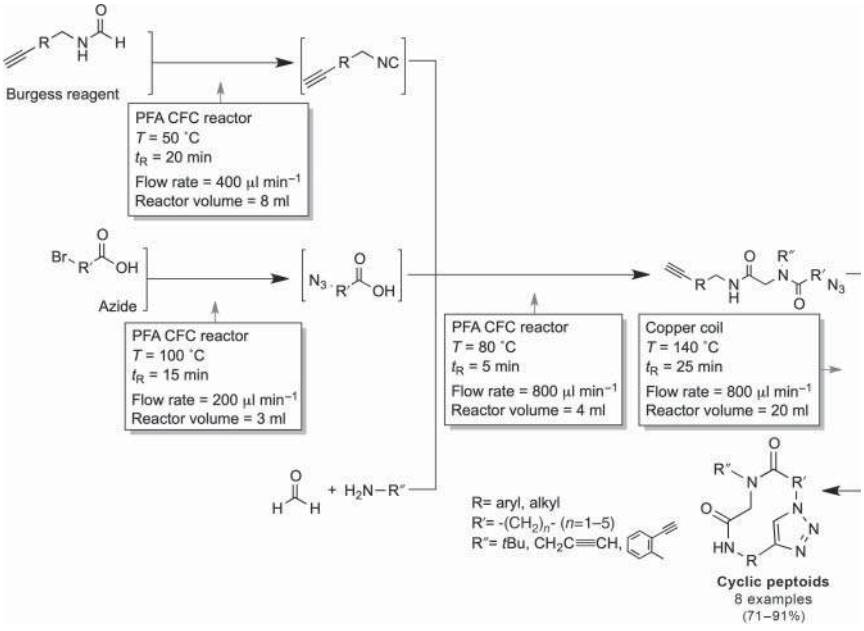

Scheme 11.12 Flow chemistry for the synthesis of cyclic peptoids via Ugi reaction followed by copper-catalyzed click intramolecular cycloaddition.

Formamide in acetonitrile was mixed with the Burgess reagent (also in MeCN) and passed through a perfluoroalkoxy (PFA) coil at 50 °C to afford the isocyanide, which was mixed with a solution of the azide prepared by reaction of 2-bromoacetic acid dissolved in acetonitrile with tetrabutylammonium azide in a PFA coil at 100 °C. Paraformaldehyde and *tert*-butylamine were constantly pumped with a flow rate and mixed with the output of the isocyanide generation and the azide formation in a cross shaped mixing device. The reaction was performed in a PFA coil tube at 80 °C to yield the Ugi product in 80% yield without further purification and avoiding the handling of potentially toxic and/or explosive intermediates. The copper-catalyzed azide–alkyne cycloaddition was performed by heating the resulting solution in a copper coil at 140 °C [68].

The continuous flow synthesis of rufinamide, an antiepileptic drug with a broad spectrum of efficacy and high tolerability [69], has caught the attention of several groups working in the field of flow chemistry [70, 71]. Borukhova et al. described the synthesis of a rufinamide precursor under flow conditions, using 2,6-difluorobenzyl alcohol as the starting material. The alcohol is converted *in situ* into 2,6-difluorobenzyl chloride by reacting with hydrogen chloride gas. Water is generated as the sole by-product jointly with the immediate consumption of the synthesized 2,6-difluorobenzyl azide in the 1,3-dipolar cycloaddition to yield triazole, which minimizes the risk associated with the detonation of

organic azides, improving the sustainability of the overall process. The use of (*E*)-methyl-3-methoxyacrylate as dipolarophile in the cycloaddition step is a safer and cheaper alternative to the corresponding alkyne dipolarophile (for example, propiolamide would lead to the formation of the rufinamide precursor) [72]. Scheme 11.13 summarizes the synthesis of this important antiepileptic drug.

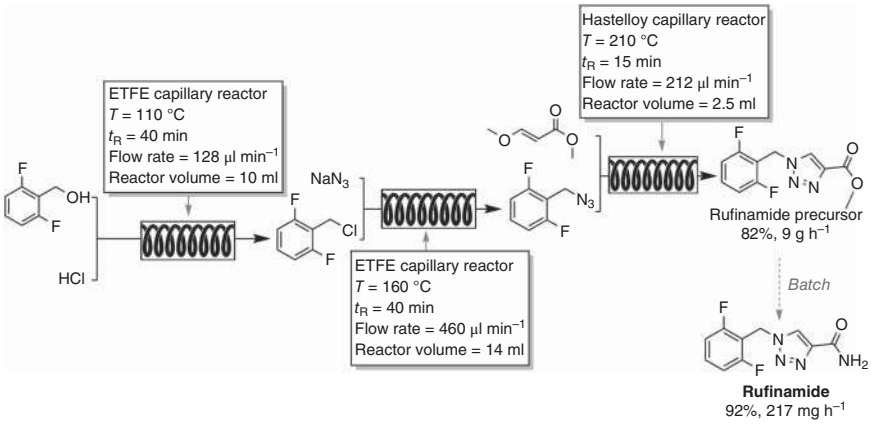

Scheme 11.13 Flow synthesis of antiepileptic drug rufinamide.

Five-membered cyclic carbonates can be produced from epoxides and one-carbon synthons. Phosgene, traditionally used for this purpose, has been replaced by less hazardous carbon dioxide [73]. The reaction of carbon dioxide and epoxides is an efficient approach for the production of cyclic carbonates and is one of the few industrially relevant reactions utilizing carbon dioxide [74].

Sathe et al. used olefins as substrates for oxidative carboxylation reaction under flow conditions (Scheme 11.14). Hydrogen peroxide was applied as the oxidative agent and methyltrioxorhenium (MTO) as the catalyst for the epoxidation reaction,

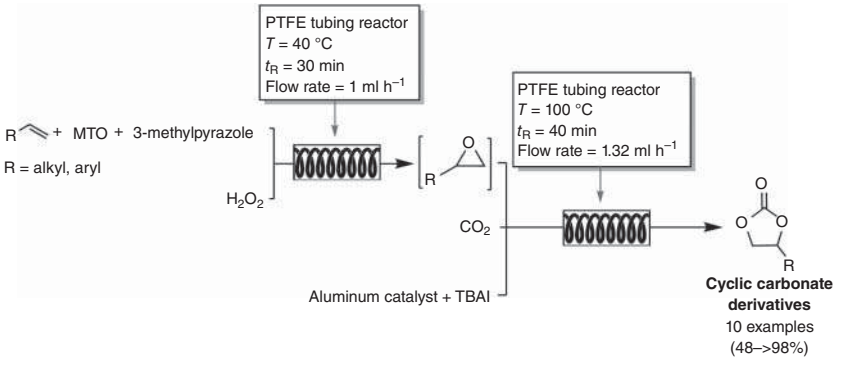

Scheme 11.14 Synthesis of cyclic carbonate derivatives from olefins via two-step oxidative carboxylation using a flow setup.

associated with an N-donor ligand (3-methylpyrazole). For the epoxide carboxylation step, an amino trisphenolate complexed aluminum catalyst, with tetrabutylammonium iodide (TBAI) cocatalyst, was selected. Using 2 mol% catalyst loading in the presence of 10 mol% TBAI in a stainless steel tubing packed with sand heated at 100 °C, complete conversion of styrene oxide to styrene carbonate was observed in 40 minutes. Between the two reactors, a membrane-based separator was placed, in order to remove the unreacted hydrogen peroxide, since it would be unfavorable for the carboxylation step. The epoxidation and carboxylation of substituted styrenes and aliphatic olefins was achieved in overall yield between 56% and 91%; however, the process was unsuccessful for the transformation of internal olefins [75].

Oxazole and oxazoline-containing products are also versatile molecules, namely, for natural product synthesis, and have caught attention due to their presence in several products with interesting biological activities [76–78]. Siphonazoles, a new class of natural products of bacterial origin, first reported at the beginning of this century, present an unusual feature – the presence of two oxazole moieties [79, 80]. A multistep flow procedure was developed to prepare the *O*-methyl siphonazole, and the steps leading to the synthesis of the functionalized oxazole are depicted in Scheme 11.15 [81].

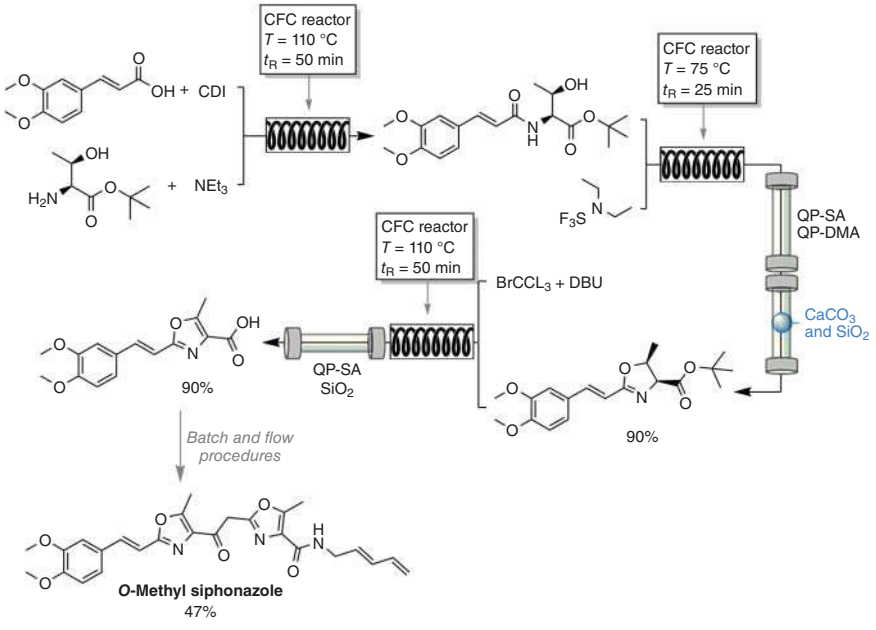

Scheme 11.15 Synthesis of an oxazole synthetic intermediate of *O*-methyl siphonazole under flow conditions.

The *in situ* coupling of dimethoxycinnamic acid, activated by carbonyldiimidazole (CDI), with threonine *tert*-butyl ester hydrochloride was carried out at 110 °C for 50 minutes, followed by the addition of diethylaminosulfur trifluoride (DAST),

leading to the cyclodehydration of the amide intermediate, at 75 °C for 25 minutes, affording the oxazoline in high yield. A set of heterogeneous scavengers [sulfonic acid (QP-SA), to remove Et_3N, imidazole, and residual threonine *tert*-butyl ester; a tertiary amine (QP-DMA) to remove acid residues; $CaCO_3$ and SiO_2 for fluorinated reactants and residues] were used in the in-line purification of the oxazoline prior to the oxidation to the corresponding oxazole, using a mixture of $BrCCl_3$ and 1,8-diazabicyclo(5.4.0)undec-7-ene (DBU) at 110 °C for 50 minutes. The flow sequence afforded the oxazole carboxylic acid in multigram quantities without the need to perform any traditional workup or purification steps.

1,2,4-Oxadiazoles, used in medicinal chemistry as bioisosteres of amide and ester functional groups, were prepared in a single continuous flow chemistry procedure. Using commercially available hydroxylamine, nitriles, carboxylic acids, and aminopyridines as starting materials, 1,2,4-oxadiazoles and imidazo[1,2-*a*]pyridin-2-yl-1,2,4-oxadiazoles were prepared via intramolecular cyclodehydration. The combination of 1-ethyl-3-(3-dimethylaminopropyl)carbodiimide (EDC)/HOBt/DIEA (1 : 1 : 1) provided the best conditions for complete conversion of benzoic acids to the corresponding 1,2,4-oxadiazole derivative through the reaction with amidooximes previously formed by the reaction of hydroxylamine and alkyl or aryl nitriles. The general approach to obtain the oxadiazole derivatives is depicted in Scheme 11.16 [82].

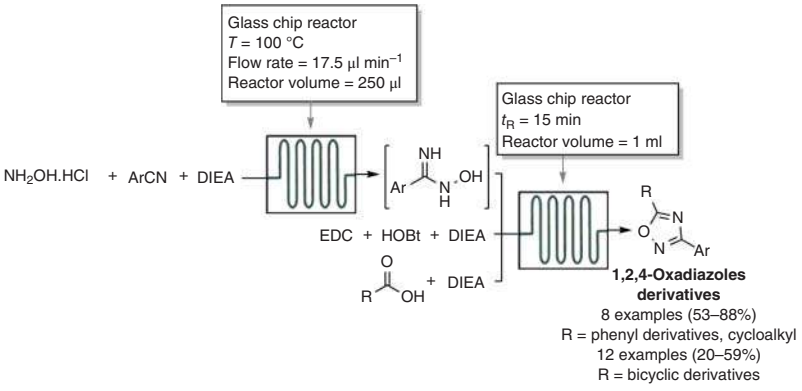

Scheme 11.16 Synthesis of 1,2,4-oxadiazole derivatives using multistep flow chemistry.

11.2.4 Six-Membered Ring Heterocycles

Six-membered heterocyclic ring systems constitute a very relevant class of compounds in the field of organic and medicinal chemistry, being present in multiple commercialized drugs. Among some of the most recent examples, we highlight the flow synthesis of an enantiomeric pure dihydropyridinone derivative – (3*R*,4*R*)-3,4,6-triphenyl-1-tosyl-3,4-dihydropyridin-2(1*H*)-one – using an immobilized chiral benzotetramisole (PS-supported BTM) analog as the organocatalyst. Briefly, the catalyst-free reaction of phenylacetic acid and pivaloyl chloride yields the phenylacetic anhydride, which through domino

Michael addition/cyclization reaction with a chalcone-type tosylimine led to the desired product in high yield (70%) and excellent enantiomeric excess (>99%) (Scheme 11.17). An in-line control (Fourier-transform infrared spectroscopy [FTIR] analysis) and a workup procedure (liquid–liquid separator) were also included in the flow setup [83].

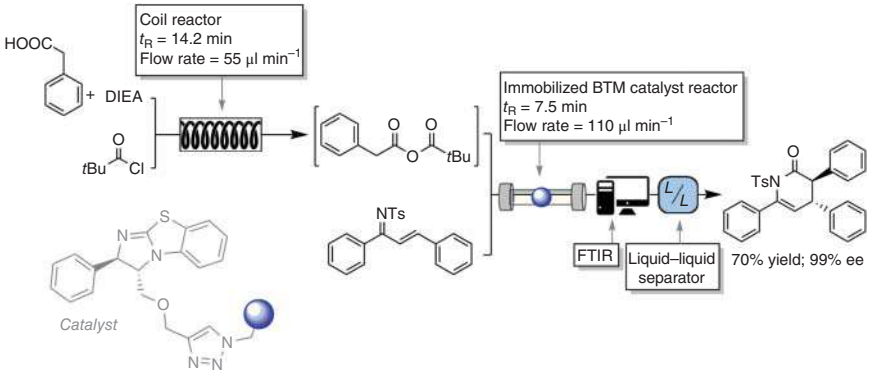

Scheme 11.17 Flow synthesis of a dihydropyridinone derivative with in-line analysis and workup.

Another relevant heterocyclic core is quinoxaline, a bicyclic moiety consisting of a benzene ring fused with a pyrazine ring, displaying a wide plethora of bioactivities, as extensively reviewed in the literature [84–86]. The multistep flow synthesis of quinoxaline derivatives in a safe manner has been reported by Martin et al. The setup allowed the reactions to occur without requiring the isolation of diazoketone intermediates, potentially explosive compounds, as well as to minimize operators exposure to phenylenediamine intermediates [87], an important feature as these compounds are classified as carcinogenic [88, 89]. Further, in-line purification was also carried out under the described methodology, by using a QP-TU pad (polymer-supported thiourea – metal scavenger), a PS-TsCl (polymer-supported tosylchloride) or PS-TsNCO (polymer-supported isocyanate – scavenger of unreacted diamine and reduced quinoxaline derivatives), and a PS-Ts-$NHNH_2$ (polymer-supported tosylhydrazine – a scavenger for the residual diazoketone), with the final quinoxaline derivatives being obtained in variable yields (21–96%) (Scheme 11.18) [87].

Ingham et al. described a very interesting flow setup, using a monolith-supported synthetic procedure to prepare 2-aminopyrimidine derivatives, by a "catch–react–release" methodology. This approach consists of immobilizing one of the reagents on a solid support, which is then exposed to different conditions. Briefly, immobilized thiouronium chloride reacts with different enaminones in the presence of DIEA – cyclization step ("catch"). Next, the formed heterocycle reacts with *meta*-chloroperoxybenzoic acid (*m*-CPBA), in a monolith oxidative activation. As the last step, the oxidized heterocycle reacts with amine derivatives in the presence of DIEA, leading to an amine displacement of 2-aminopyrimidine

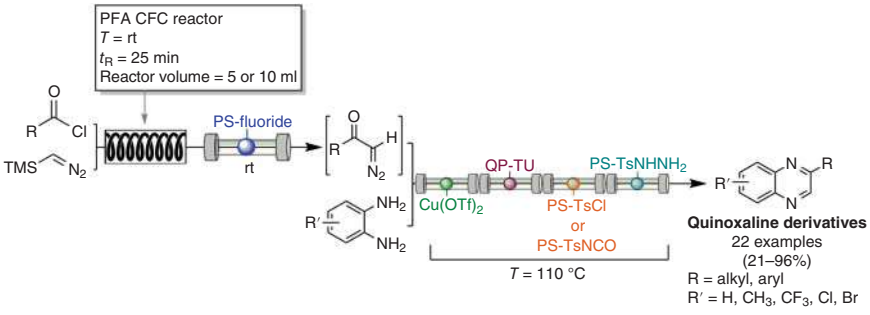

Scheme 11.18 Multistep flow synthesis of quinoxaline derivatives.

derivatives ("release" step) (Scheme 11.19) [90]. Using the described procedure *N*-(2-methyl-5-nitrophenyl)-4-(pyridin-3-yl)pyrimidin-2-amine, a known precursor in the synthesis of tyrosine kinase inhibitor Imatinib [91] was obtained in 48% yield, overcoming problems associated with the low solubility of some intermediates.

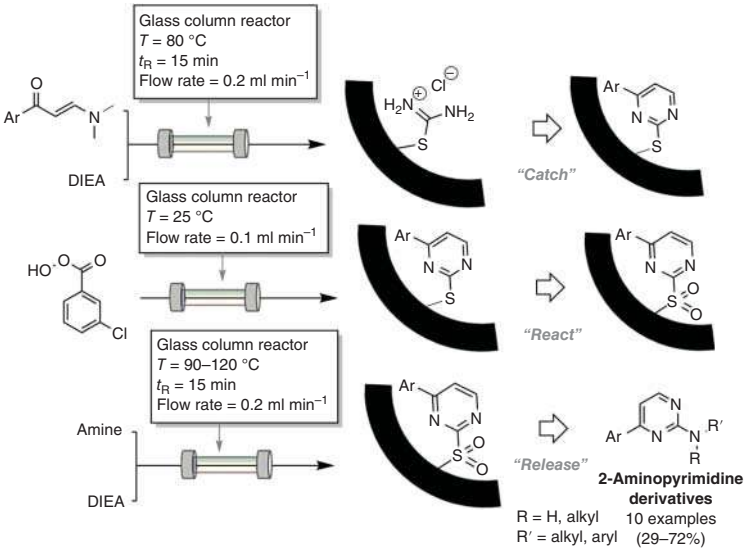

Scheme 11.19 "Catch-react-release" flow procedure for the synthesis of 2-aminopyrimidine derivatives.

Filipponi et al. prepared a library of dihydropyridazine-3-carboxylic acid derivatives using sequential flow chemistry. Dynamically mixed tubular (DMT) reactors were employed in two of the synthetic steps. This type of reactor allows overcoming of a serious drawback of conventional flow systems, as they enable reactions to proceed even when solids are formed. Briefly, different anilines react with $NaNO_2$ affording a diazonium salt intermediate, which further reacts with a pyranone derivative to give a hydrazone intermediate. In the last step, requiring the presence of a base (K_2CO_3) and with a temperature increment, the hydrazone cyclizes

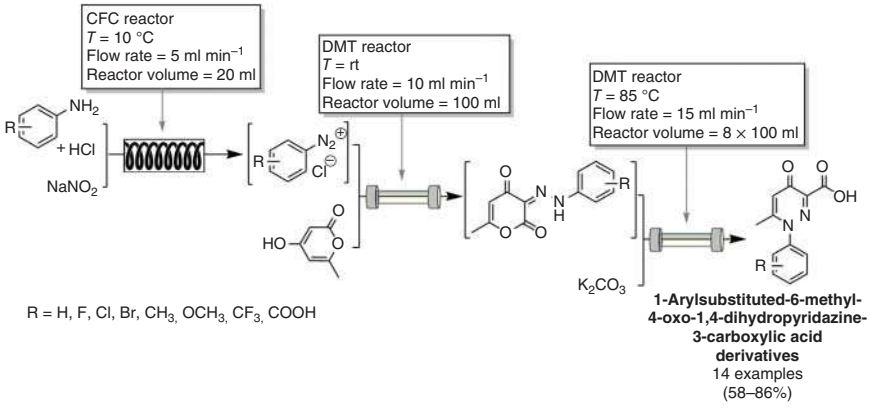

Scheme 11.20 Multistep flow chemistry using DMT reactors. Source: Adapted from Filipponi and Baxendale [92] and Filipponi et al. [93].

to the final product (Scheme 11.20) [92, 93]. Using this continuous process, the *p*-bromophenyl derivative was obtained with productivity over $9.6\,g\,h^{-1}$, with high purity, avoiding the safety problems usually associated with the diazonium salts. This family of compounds is relevant in drug discovery, as they are known for interacting with bromodomain containing proteins, a druggable target with increasing interest in pharmacology [94, 95].

Thioquinazolinone derivatives were prepared via a multistep flow process by Kim et al., through the generation of two organolithium intermediates, putting into evidence the safety inherent to flow chemistry. The full process takes place at room temperature, without isolation of any of the intermediates and with high efficacy, since compounds are prepared quickly (up to 10 s) in very high yields (75–98%). Briefly, *o*-bromophenyl-isothiocyanate reacts with *n*BuLi, affording 2-isothiocyanatophenyl lithium intermediates, which further react with a phenyl isocyanate, achieving a lithium thiolate intermediate. The final step consists in the reaction of this last intermediate with functionalized benzyl bromide to attain the desired thioquinazolinone derivates (Scheme 11.21) [96].

The multistep flow synthesis of six-membered ring heterocycles bearing oxygen atoms has been less explored. Nevertheless, the synthesis of pyranonaphthoquinone derivatives under sequential flow reactions was reported by Osorio-Planes et al., using a heterogeneous catalytic system consisting of a chiral squaramide immobilized in polystyrene. The continuous flow setup consists of two sequential steps (Michael reaction and a cyclization step), performed at room temperature. The heterogeneous chiral organocatalyst enabled high enantioselective Michael reaction, and the final products were achieved in high yield and enantioselectivity (Scheme 11.22) [97].

Artemisinin, a natural product with outstanding relevance in the field of medicinal chemistry as it presents a strong antimalarial activity, has been a synthetic challenge for organic chemists. Its complex framework, with multiple rings, includes two heterocycles, which are crucial for its biological activity – a

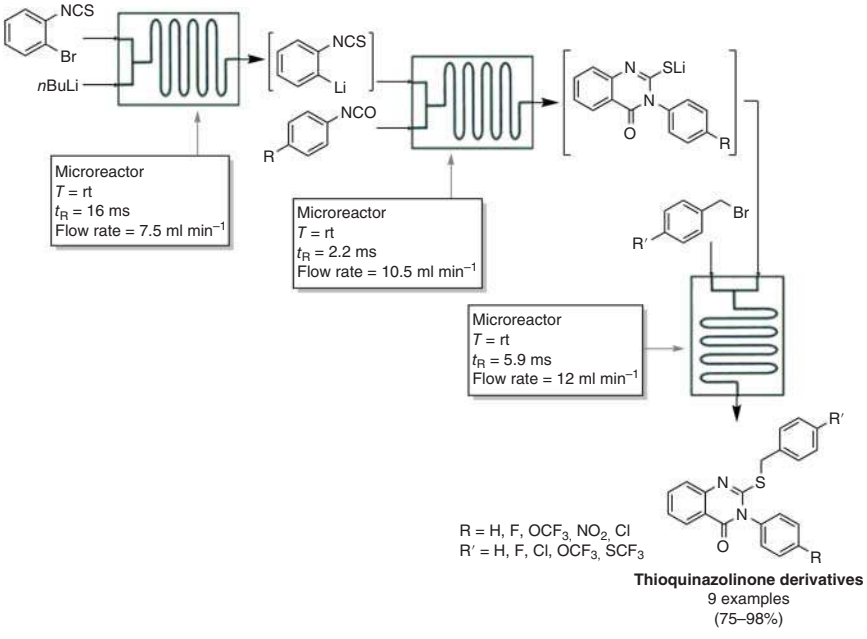

Scheme 11.21 Flow multistep synthesis of thioquinazolinone derivatives, using organolithium intermediates.

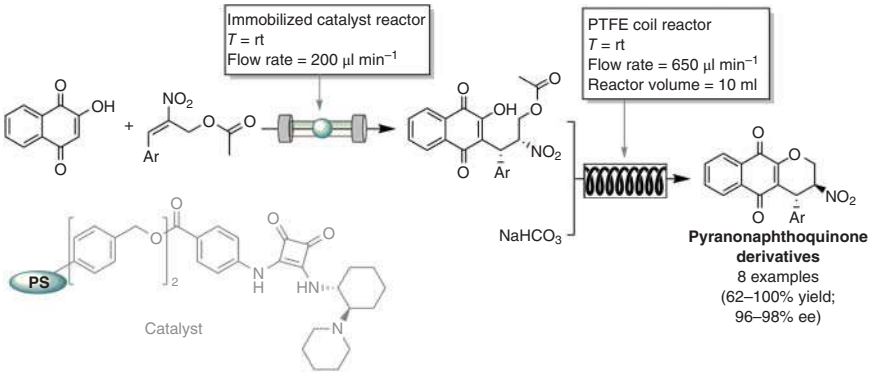

Scheme 11.22 Flow enantioselective multistep synthesis of pyranonaphthoquinone derivatives.

six-membered lactone and a cyclic endoperoxide [98]. Artemisinic acid is the usual starting material for the synthesis of artemisin, since it is easier to extract from natural sources or through biotechnological processes. It was used by Lévesque et al. to prepare artemisinin (200 g day^{-1}) in a continuous flow photochemical setup (Scheme 11.23), using tetraphenylporphyrin as photosensitizer. In the first step, photooxidation of dihydroartemisinic acid generates the corresponding tertiary allylic hydroperoxide intermediates, which are protonated in the presence of an acid, leading to the migration of the allylic group and the formation of the

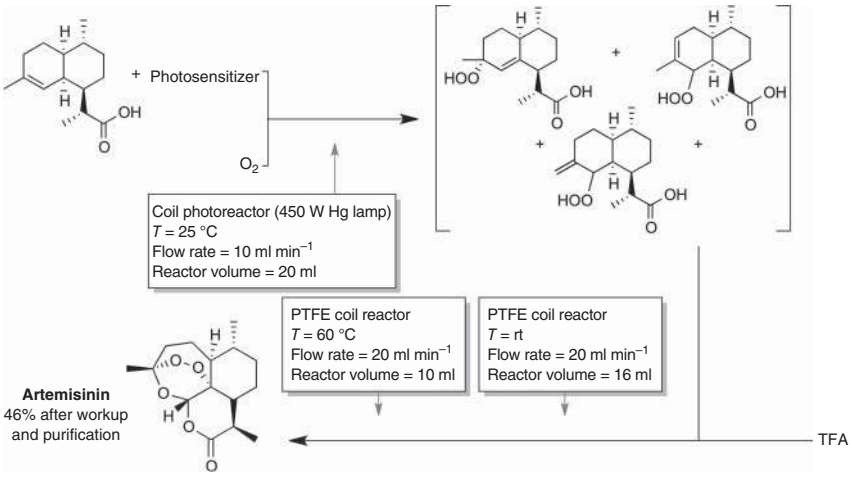

Scheme 11.23 Synthesis of artemisinin from dihydroartemisinic acid under flow conditions.

corresponding hemiketal, which is converted into an enol intermediate, key for the final formation of artemisinin [99].

At this point, we would like to highlight one recent example of flow chemistry applied to the synthesis of six-membered ring heterocycles bearing different types of heteroatoms. The synthesis of 6-amino-2,2,7-trifluoro-4*H*-benzo-[1,4]-oxazin-3-one, through a three-step nitration/hydrogenation/cyclization synthetic route is summarized in Scheme 11.24. One of the main advantages of this sequential approach is to avoid operator handling of labile and explosive synthetic intermediates [100]. Naturally occurring benzoxazinones have been considered useful lead compounds for new herbicide development, namely, due to environmental, toxicological, and economic impact of synthetic herbicides [101, 102].

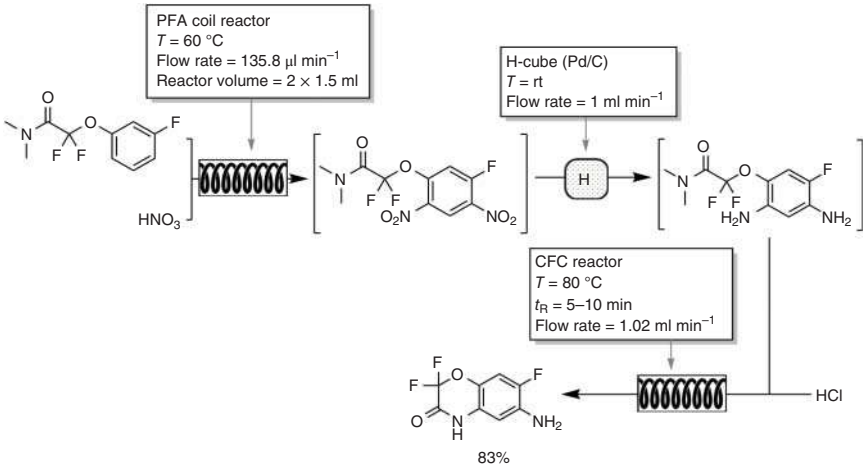

Scheme 11.24 Multistep flow synthesis of a benzoxazinone herbicide.

11.2.5 Seven-Membered Ring Heterocycles

Hartwig et al. reported the multistep flow synthesis of an important benzodiazepine, olanzapine, used in clinical practice as an antipsychotic drug. Briefly, a Buchwald–Hartwig reaction was performed between 1-iodo-2-nitrobenzene and one aminothiazole. Further, nitro group reduction and acid-promoted cyclization occurs to afford the seven-membered ring heterocycle, which after thermal condensation with *N*-methylpiperazine affords the API (Scheme 11.25) [103].

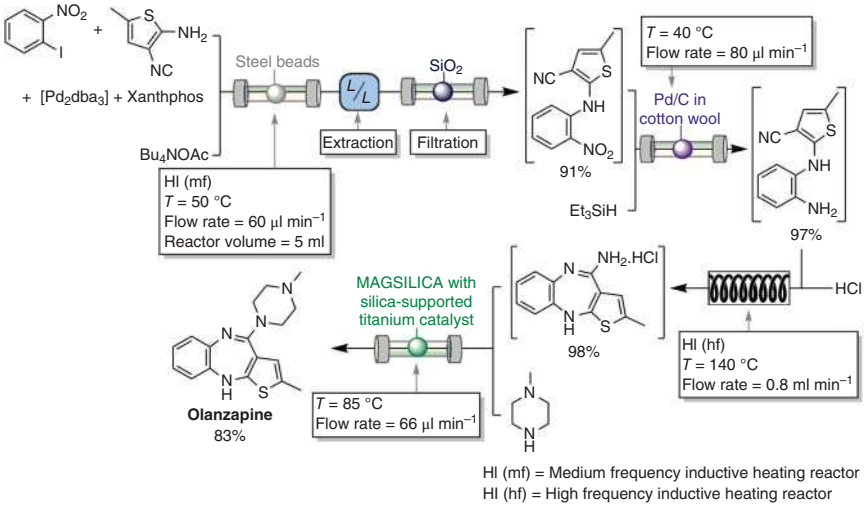

Scheme 11.25 Flow multistep synthesis of olanzapine (Zyprexa®).

Recently, the use of a multistep flow setup for the synthesis of another API – diazepam – was reported as a sustainable process. Although other examples were previously reported in the literature concerning the flow synthesis of this drug [104], Bédard et al. reduced the E-factor for this synthesis by fourfold (from

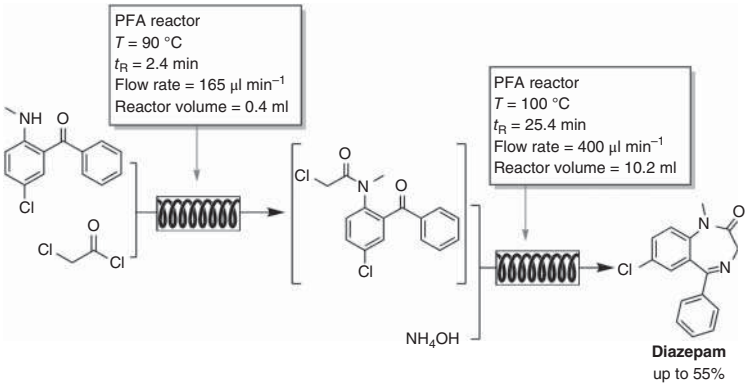

Scheme 11.26 Flow multistep synthesis of diazepam (Valium®).

36 to 4). This cutback was accomplished by a multifactorial approach, but the replacement of ethyl acetate by 2-methyltetrahydrofuran was a key player for this significant reduction. Diazepam was produced by an amidation reaction (between benzophenone and chloroacetyl chloride) followed by cyclization (Scheme 11.26) [105].

11.3 Conclusions and Perspectives

In the past few decades, continuous flow organic synthesis went from an unexplored technique, based on "do-it-yourself" systems, to one of the most revolutionary tools for organic chemists, changing the face of many research laboratories from typical glassware and batch procedures to fully automatized processes. The scaffold diversity attained using continuous flow apparatus, in the field of heterocyclic compounds synthesis, makes this technique a versatile and valuable approach for academia and industry, for the preparation of high-value products, such as fine chemicals, APIs, and natural products.

The possibility to perform sequential reaction steps in a closed flow system enhances the possibilities to perform complex, and even unexplored, chemical transformations in an efficient, safe, profitable, and scalable manner. While process intensification is already one of the main advantages of applying continuous flow systems, the future of flow chemistry, especially in drug discovery settings, will likely be oriented to increase new molecules output, integrating multicomponent and multistep synthesis, purification, and in-process control, accelerating the overall hit identification and drug discovery process.

Acknowledgments

P. Brandão acknowledges FCT for the PhD grant PD/BD/128490/2017–CATSUS FCT-PhD Program. CQC was supported by the Portuguese Agency for Scientific Research, "Fundação para a Ciência e a Tecnologia" (FCT) through projects UIDB/00313/2020 and UIDP/00313/2020, cofounded by COMPETE2020-UE. LAQV-REQUIMTE was financed by the FEDER Funds through the Operational Competitiveness Factors Program – COMPETE and by National Funds through FCT within the scope of the projects UIDB/50006/2020 and UIDB/04423/2020.

References

1 Britton, J. and Raston, C.L. (2017). Multi-step continuous-flow synthesis. *Chem. Soc. Rev.* 46 (5): 1250–1271. https://doi.org/10.1039/C6CS00830E.

2 Luis, S.V. and Garcia-Verdugo, E. (2010). *Chemical Reactions and Processes under Flow Conditions* (ed. J.H. Clark and G.A. Kraus). UK: RSCPublishing https://doi.org/10.1039/9781847559739.

3 Guidi, M., Seeberger, P.H., and Gilmore, K. (2020). How to approach flow chemistry. *Chem. Soc. Rev.* 49 (24): 8910–8932. https://doi.org/10.1039/C9CS00832B.

4 Hardwick, T. and Ahmed, N. (2020). Digitising chemical synthesis in automated and robotic flow. *Chem. Sci.* 11 (44): 11973–11988. https://doi.org/10.1039/D0SC04250A.

5 Rogers, L. and Jensen, K.F. (2019). Continuous manufacturing – the green chemistry promise? *Green Chem.* 21 (13): 3481–3498. https://doi.org/10.1039/C9GC00773C.

6 Vaccaro, L., Lanari, D., Marrocchi, A., and Strappaveccia, G. (2014). Flow approaches towards sustainability. *Green Chem.* 16 (8): 3680–3704. https://doi.org/10.1039/C4GC00410H.

7 Vaccaro, L. (2017). *Sustainable Flow Chemistry – Methods and Applications*. Weinheim, Germany: Wiley-VCH.

8 Noël, T. and Luque, R. (2020). *Accounts on Sustainable Flow Chemistry* (ed. T. Noël and R. Luque), 29–65. Springer International Publishing.

9 Sambiagio, C. and Noël, T. (2020). Flow photochemistry: shine some light on those tubes! *Trends Chem.* 2 (2): 92–106. https://doi.org/10.1016/j.trechm.2019.09.003.

10 Yu, T., Ding, Z., Nie, W. et al. (2020). Recent advances in continuous-flow enantioselective catalysis. *Chem. Eur. J.* 26 (26): 5729–5747. https://doi.org/10.1002/chem.201905151.

11 Britton, J., Majumdar, S., and Weiss, G.A. (2018). Continuous flow biocatalysis. *Chem. Soc. Rev.* 47 (15): 5891–5918. https://doi.org/10.1039/C7CS00906B.

12 Summerton, L., Taylor, R.J., and Clark, J.H. (2016). Promoting the uptake of green and sustainable methodologies in pharmaceutical synthesis: CHEM21 education and training initiatives. *Sustainable Chem. Pharm.* 4: 67–76. https://doi.org/10.1016/j.scp.2016.09.003.

13 McElroy, C.R., Constantinou, A., Jones, L.C. et al. (2015). Towards a holistic approach to metrics for the 21st century pharmaceutical industry. *Green Chem.* 17 (5): 3111–3121. https://doi.org/10.1039/C5GC00340G.

14 Baxendale, I.R. (2013). The integration of flow reactors into synthetic organic chemistry. *J. Chem. Technol. Biotechnol.* 88 (4): 519–552. https://doi.org/10.1002/jctb.4012.

15 Taylor, A.P., Robinson, R.P., Fobian, Y.M. et al. (2016). Modern advances in heterocyclic chemistry in drug discovery. *Org. Biomol. Chem.* 14 (28): 6611–6637. https://doi.org/10.1039/C6OB00936K.

16 Plutschack, M.B., Pieber, B., Gilmore, K., and Seeberger, P.H. (2017). The Hitchhiker's guide to flow chemistry. *Chem. Rev.* 117 (18): 11796–11893. https://doi.org/10.1021/acs.chemrev.7b00183.

17 Sharma, U.K. and Van der Eycken, E.V. (2018). *Flow Chemistry for the Synthesis of Heterocycles* (ed. B. Maes, J. Cossy and S. Polanc). Springer.

18 Brandão, P., Pineiro, M., and Pinho e Melo, T.M.V.D. (2019). Flow chemistry: towards a more sustainable heterocyclic synthesis. *Eur. J. Org. Chem.* 2019 (43): 7188–7217. https://doi.org/10.1002/ejoc.201901335.

19 Colombo, M. and Peretto, I. (2008). Chemistry strategies in early drug discovery: an overview of recent trends. *Drug Discovery Today* 13 (15): 677–684. https://doi.org/10.1016/j.drudis.2008.03.007.

20 Baumann, M. (2018). Integrating continuous flow synthesis with in-line analysis and data generation. *Org. Biomol. Chem.* 16 (33): 5946–5954. https://doi.org/10.1039/C8OB01437J.

21 Britton, J. and Jamison, T.F. (2017). The assembly and use of continuous flow systems for chemical synthesis. *Nat. Protoc.* 12: 2423. https://doi.org/10.1038/nprot.2017.102.

22 Ji Ram, V., Sethi, A., Nath, M., and Pratap, R. (2019). Chapter 3: Three-membered ring heterocycles. In: *The Chemistry of Heterocycles* (ed. V. Ji Ram, A. Sethi, M. Nath and R. Pratap), 19–92. Elsevier.

23 Morodo, R., Gérardy, R., Petit, G., and Monbaliu, J.-C.M. (2019). Continuous flow upgrading of glycerol toward oxiranes and active pharmaceutical ingredients thereof. *Green Chem.* 21 (16): 4422–4433. https://doi.org/10.1039/C9GC01819K.

24 Tarannum, S., Chauhan, N., and Ghorai, M.K. (2020). *Aziridines and 2H-Azirines – Monocyclic. Reference Module in Chemistry, Molecular Sciences and Chemical Engineering*. Elsevier.

25 Baumann, M. and Baxendale, I.R. (2016). Continuous-flow synthesis of 2*H*-azirines and their diastereoselective transformation to aziridines. *Synlett* 27 (01): 159–163. https://doi.org/10.1055/s-0035-1560391.

26 Zakrzewski, J., Smalley, A.P., Kabeshov, M.A. et al. (2016). Continuous-flow synthesis and derivatization of aziridines through palladium-catalyzed C(sp^3)–H activation. *Angew. Chem. Int. Ed.* 55 (31): 8878–8883. https://doi.org/10.1002/anie.201602483.

27 Pitts, C.R. and Lectka, T. (2014). Chemical synthesis of β-lactams: asymmetric catalysis and other recent advances. *Chem. Rev.* 114 (16): 7930–7953. https://doi.org/10.1021/cr4005549.

28 Kamath, A. and Ojima, I. (2012). Advances in the chemistry of β-lactam and its medicinal applications. *Tetrahedron* 68 (52): 10640–10664. https://doi.org/10.1016/j.tet.2012.07.090.

29 Musio, B., Mariani, F., Śliwiński, E.P. et al. (2016). Combination of enabling technologies to improve and describe the stereoselectivity of Wolff–Staudinger cascade reaction. *Synthesis* 48 (20): 3515–3526. https://doi.org/10.1055/s-0035-1562579.

30 Gérardy, R., Winter, M., Vizza, A., and Monbaliu, J.-C.M. (2017). Assessing inter- and intramolecular continuous-flow strategies towards methylphenidate (ritalin) hydrochloride. *React. Chem. Eng.* 2 (2): 149–158. https://doi.org/10.1039/C6RE00184J.

31 Hantzsch, A. (1890). Neue bildungsweise von pyrrolderivaten. *Ber. Dtsch. Chem. Ges.* 23 (1): 1474–1476. https://doi.org/10.1002/cber.189002301243.

32 Knorr, L. (1885). Einwirkung des diacetbernsteinsäureesters auf ammoniak und primäre aminbasen. *Ber. Dtsch. Chem. Ges.* 18 (1): 299–311. https://doi.org/10.1002/cber.18850180154.

33 Paal, C. (1885). Synthese von thiophen- und pyrrolderivaten. *Ber. Dtsch. Chem. Ges.* 18 (1): 367–371. https://doi.org/10.1002/cber.18850180290.

34 Herath, A. and Cosford, N.D.P. (2010). One-step continuous flow synthesis of highly substituted pyrrole-3-carboxylic acid derivatives via in situ hydrolysis of *tert*-butyl esters. *Org. Lett.* 12 (22): 5182–5185. https://doi.org/10.1021/ol102216x.

35 Nieuwland, P.J., Segers, R., Koch, K. et al. (2011). Fast scale-up using microreactors: pyrrole synthesis from micro to production scale. *Org. Process Res. Dev.* 15 (4): 783–787. https://doi.org/10.1021/op100338z.

36 Cranwell, P.B., O'Brien, M., Browne, D.L. et al. (2012). Flow synthesis using gaseous ammonia in a teflon AF-2400 tube-in-tube reactor: Paal–Knorr pyrrole formation and gas concentration measurement by inline flow titration. *Org. Biomol. Chem.* 10 (30): 5774–5779. https://doi.org/10.1039/C2OB25407G.

37 Razzaq, T., Glasnov, T.N., and Kappe, C.O. (2009). Continuous-flow microreactor chemistry under high-temperature/pressure conditions. *Eur. J. Org. Chem.* 2009 (9): 1321–1325. https://doi.org/10.1002/ejoc.200900077.

38 Bagley, M.C., Jenkins, R.L., Lubinu, M.C. et al. (2005). A simple continuous flow microwave reactor. *J. Organomet. Chem.* 70 (17): 7003–7006. https://doi.org/10.1021/jo0510235.

39 Yokozawa, S., Ohneda, N., Muramatsu, K. et al. (2015). Development of a highly efficient single-mode microwave applicator with a resonant cavity and its application to continuous flow syntheses. *RSC Adv.* 5 (14): 10204–10210. https://doi.org/10.1039/C4RA12428F.

40 Bosch, C., López-Lledó, P., Bonjoch, J. et al. (2016). Fischer indole reaction in batch and flow employing a sulfonic acid resin: synthesis of pyrido[2,3-*a*]carbazoles. *J. Flow Chem.* 6 (3): 240–243. https://doi.org/10.1556/1846.2016.00016.

41 Yu, J., Xu, J., Yu, Z. et al. (2017). A continuous-flow fischer indole synthesis of 3-methylindole in an ionic liquid. *J. Flow Chem.* 7 (2): 33–36. https://doi.org/10.1556/1846.2017.00004.

42 Gutmann, B., Gottsponer, M., Elsner, P. et al. (2013). On the Fischer indole synthesis of 7-ethyltryptophol – mechanistic and process intensification studies under continuous flow conditions. *Org. Process Res. Dev.* 17 (2): 294–302. https://doi.org/10.1021/op300363s.

43 Baumann, M., Baxendale, I.R., and Deplante, F. (2017). A concise flow synthesis of indole-3-carboxylic ester and its derivatisation to an auxin mimic. *Beilstein J. Org. Chem.* 13: 2549–2560. https://doi.org/10.3762/bjoc.13.251.

44 Caruano, J., Muccioli, G.G., and Robiette, R. (2016). Biologically active [gamma]-lactams: synthesis and natural sources. *Org. Biomol. Chem.* 14 (43): 10134–10156. https://doi.org/10.1039/C6OB01349J.

45 Tsubogo, T., Oyamada, H., and Kobayashi, S. (2015). Multistep continuous-flow synthesis of (R)- and (S)-rolipram using heterogeneous catalysts. *Nature* 520: 329. https://doi.org/10.1038/nature14343.

46 Cecile, E.-G. and Alain, G. (2007). Recent progress in the pharmacology of imidazo[1,2-*a*]pyridines. *Mini Rev. Med. Chem.* 7 (9): 888–899. https://doi.org/10.1038/nature14343.

47 Bagdi, A.K., Santra, S., Monir, K., and Hajra, A. (2015). Synthesis of imidazo[1,2-*a*]pyridines: a decade update. *Chem. Commun.* 51 (9): 1555–1575. https://doi.org/10.1039/C4CC08495K.

48 Tara, L.S.K. (2016). Pyridines and imidazopyridines with medicinal significance. *Curr. Top. Med. Chem.* 16 (28): 3274–3302. https://doi.org/10.2174/1568026616666160506145141.

49 Krause, M., Foks, H., and Gobis, K. (2017). Pharmacological potential and synthetic approaches of imidazo[4,5-*b*]pyridine and imidazo[4,5-*c*]pyridine derivatives. *Molecules* 22 (3): 399. https://doi.org/10.3390/molecules22030399.

50 Guetzoyan, L., Nikbin, N., Baxendale, I.R., and Ley, S.V. (2013). Flow chemistry synthesis of zolpidem, alpidem and other $GABA_A$ agonists and their biological evaluation through the use of in-line frontal affinity chromatography. *Chem. Sci.* 4 (2): 764–769. https://doi.org/10.1039/C2SC21850J.

51 Whiting, P.J. (2003). GABA-A receptor subtypes in the brain: a paradigm for CNS drug discovery? *Drug Discovery Today* 8 (10): 445–450. https://doi.org/10.1016/s1359-6446(03)02703-x.

52 Rudolph, U. and Knoflach, F. (2011). Beyond classical benzodiazepines: novel therapeutic potential of $GABA_A$ receptor subtypes. *Nat. Rev. Drug Discovery* 10: 685. https://doi.org/10.1038/nrd3502.

53 King, C., Diaz, H.B., McNeely, S. et al. (2015). LY2606368 causes replication catastrophe and antitumor effects through CHK1-dependent mechanisms. *Mol. Cancer Ther.* 14 (9): 2004–2013. https://doi.org/10.1158/1535-7163.MCT-14-1037.

54 Rorà, A.G.L.D., Iacobucci, I., Imbrogno, E. et al. (2016). Prexasertib, a Chk1/Chk2 inhibitor, increases the effectiveness of conventional therapy in B-/T- cell progenitor acute lymphoblastic leukemia. *Oncotarget* 7 (33): 53377–53391. https://doi.org/10.18632/oncotarget.10535.

55 Lowery, C.D., VanWye, A.B., Dowless, M. et al. (2017). The checkpoint kinase 1 inhibitor prexasertib induces regression of preclinical models of human neuroblastoma. *Clin. Cancer Res.* 23 (15): 4354–4363. https://doi.org/10.1158/1078-0432.CCR-16-2876.

56 Yang, E.S., Zeng, L., Beggs, R. et al. (2017). Combining Chk1/2 inhibition with cetuximab and radiation enhances in vitro and in vivo cytotoxicity in head and neck squamous cell carcinoma. *Int. J. Rad. Oncol. Biol. Phys.* 99 (2, Suppl): S148–S149. https://doi.org/10.1158/1535-7163.MCT-16-0352.

57 For more information, please check the data for the following clinical trials: NCT01115790; NCT02124148; NCT02203513; NCT02514603; NCT02555644; NCT02735980; NCT02649764; NCT02860780; NCT02778126; NCT02873975; NCT02808650; NCT03057145; NCT03414047. Available on https://www.clinicaltrials.gov (accessed 04 February 2020).

58 Hong, D., Infante, J., Janku, F. et al. (2016). Phase I study of LY2606368, a checkpoint kinase 1 inhibitor, in patients with advanced cancer. *J. Clin. Oncol.* 34 (15): 1764–1771. https://doi.org/10.1200/JCO.2015.64.5788.

59 Lee, J.-M., Nair, J., Zimmer, A. et al. (2018). Prexasertib, a cell cycle checkpoint kinase 1 and 2 inhibitor, in BRCA wild-type recurrent high-grade serous

ovarian cancer: a first-in-class proof-of-concept phase 2 study. *Lancet Oncol.* 19 (2): 207–215. https://doi.org/10.1016/S1470-2045(18)30009-3.

60 Cole, K.P., Groh, J.M., Johnson, M.D. et al. (2017). Kilogram-scale prexasertib monolactate monohydrate synthesis under continuous-flow CGMP conditions. *Science* 356 (6343): 1144–1150. https://doi.org/10.1126/science.aan0745.

61 Sathish Kumar, S.P. and Kavitha, H. (2013). Synthesis and biological applications of triazole derivatives – a review. *Mini Rev. Org. Chem.* 10 (1): 40–65. https://doi.org/10.2174/1570193X11310010004.

62 Zhou, Ch and Wang, Y. (2012). Recent researches in triazole compounds as medicinal drugs. *Curr. Med. Chem.* 19 (2): 239–280. https://doi.org/10.2174/092986712803414213.

63 Otvos, S.B. and Fulop, F. (2015). Flow chemistry as a versatile tool for the synthesis of triazoles. *Catal. Sci. Technol.* 5 (11): 4926–4941. https://doi.org/10.1039/C5CY00523J.

64 Ali, A.A. (2020). 1,2,3-Triazoles: synthesis and biological application. In: *Azoles – Synthesis, Properties, Applications and Perspectives* (ed. A. Kuznetsov). IntechOpen https://doi.org/10.5772/intechopen.92692.

65 Totobenazara, J. and Burke, A.J. (2015). New click-chemistry methods for 1,2,3-triazoles synthesis: recent advances and applications. *Tetrahedron Lett.* 56 (22): 2853–2859. https://doi.org/10.1016/j.tetlet.2015.03.136.

66 Bao, J. and Tranmer, G.K. (2015). The utilization of copper flow reactors in organic synthesis. *Chem. Commun.* 51 (15): 3037–3044. https://doi.org/10.1039/C4CC09221J.

67 Shin, S.B.Y., Yoo, B., Todaro, L.J., and Kirshenbaum, K. (2007). Cyclic peptoids. *J. Am. Chem. Soc.* 129 (11): 3218–3225. https://doi.org/10.1021/ja066960o.

68 Salvador, C.E.M., Pieber, B., Neu, P.M. et al. (2015). A sequential Ugi multicomponent/Cu-catalyzed azide–alkyne cycloaddition approach for the continuous flow generation of cyclic peptoids. *J. Organomet. Chem.* 80 (9): 4590–4602. https://doi.org/10.1021/acs.joc.5b00445.

69 Wheless, J.W. and Vazquez, B. (2010). Rufinamide: a novel broad-spectrum antiepileptic drug. *Epilepsy Curr.* 10 (1): 1–6. https://doi.org/10.1111/j.1535-7511.2009.01336.x.

70 Zhang, P., Russell, M.G., and Jamison, T.F. (2014). Continuous flow total synthesis of rufinamide. *Org. Process Res. Dev.* 18 (11): 1567–1570. https://doi.org/10.1021/op500166n.

71 Borukhova, S., Noël, T., Metten, B. et al. (2013). Solvent- and catalyst-free huisgen cycloaddition to rufinamide in flow with a greener, less expensive dipolarophile. *ChemSusChem* 6 (12): 2220–2225. https://doi.org/10.1002/cssc.201300684.

72 Borukhova, S., Noël, T., Metten, B. et al. (2016). From alcohol to 1,2,3-triazole via a multi-step continuous-flow synthesis of a rufinamide precursor. *Green Chem.* 18 (18): 4947–4953. https://doi.org/10.1039/C6GC01133K.

73 Omae, I. (2012). Recent developments in carbon dioxide utilization for the production of organic chemicals. *Coord. Chem. Rev.* 256 (13): 1384–1405. https://doi.org/10.1016/j.ccr.2012.03.017.

74 Fukuoka, S., Kawamura, M., Komiya, K. et al. (2003). A novel non-phosgene polycarbonate production process using by-product CO_2 as starting material. *Green Chem.* 5 (5): 497–507. https://doi.org/10.1039/B304963A.

75 Sathe, A.A., Nambiar, A.M.K., and Rioux, R.M. (2017). Synthesis of cyclic organic carbonates via catalytic oxidative carboxylation of olefins in flow reactors. *Catal. Sci. Technol.* 7 (1): 84–89. https://doi.org/10.1039/C6CY01974A.

76 Tilvi, S.S. and Singh, K. (2016). Synthesis of oxazole, oxazoline and isoxazoline derived marine natural products: a review. *Curr. Org. Chem.* 20 (8): 898–929. https://doi.org/10.2174/1385272819666150804000046.

77 Jin, Z. (2011). Muscarine, imidazole, oxazole, and thiazole alkaloids. *Nat. Prod. Rep.* 28 (6): 1143–1191. https://doi.org/10.1039/b718045b.

78 Kakkar, S. and Narasimhan, B. (2019). A comprehensive review on biological activities of oxazole derivatives. *BCM Chem.* 13: 16. https://doi.org/10.1186/s13065-019-0531-9.

79 Nett, M., Erol, Ö., Kehraus, S. et al. (2006). Siphonazole, an unusual metabolite from *Herpetosiphon* sp. *Angew. Chem. Int. Ed.* 45 (23): 3863–3867. https://doi.org/10.1002/anie.200504525.

80 Linder, J., Blake, A.J., and Moody, C.J. (2008). Total synthesis of siphonazole and its *O*-methyl derivative, structurally unusual bis-oxazole natural products. *Org. Biomol. Chem.* 6 (21): 3908–3916. https://doi.org/10.1039/B810855B.

81 Baumann, M., Baxendale, I.R., Brasholz, M. et al. (2011). An integrated flow and batch-based approach for the synthesis of *O*-methyl siphonazole. *Synlett* 2011 (10): 1375–1380. https://doi.org/10.1055/s-0030-1260573.

82 Herath, A. and Cosford, N.D.P. (2017). Continuous-flow synthesis of highly functionalized imidazo-oxadiazoles facilitated by microfluidic extraction. *Beilstein J. Org. Chem.* 13: 239–246. https://doi.org/10.3762/bjoc.13.26.

83 Izquierdo, J. and Pericàs, M.A. (2016). A recyclable, immobilized analogue of benzotetramisole for catalytic enantioselective domino Michael addition/cyclization reactions in batch and flow. *ACS Catal.* 6 (1): 348–356. https://doi.org/10.1021/acscatal.5b02121.

84 Pereira, J.A., Pessoa, A.M., Cordeiro, M.N.D.S. et al. (2015). Quinoxaline, its derivatives and applications: a state of the art review. *Eur. J. Med. Chem.* 97: 664–672. https://doi.org/10.1016/j.ejmech.2014.06.058.

85 Ajani, O.O. (2014). Present status of quinoxaline motifs: excellent pathfinders in therapeutic medicine. *Eur. J. Med. Chem.* 85: 688–715. https://doi.org/10.1016/j.ejmech.2014.08.034.

86 Tariq, S., Somakala, K., and Amir, M. (2018). Quinoxaline: an insight into the recent pharmacological advances. *Eur. J. Med. Chem.* 143: 542–557. https://doi.org/10.1016/j.ejmech.2017.11.064.

87 Martin, L.J., Marzinzik, A.L., Ley, S.V., and Baxendale, I.R. (2011). Safe and reliable synthesis of diazoketones and quinoxalines in a continuous flow reactor. *Org. Lett.* 13 (2): 320–333. https://doi.org/10.1021/ol1027927.

88 Milman, H.A. and Peterson, C. (1984). Apparent correlation between structure and carcinogenicity of phenylenediamines and related compounds. *Environ. Health Perspect.* 56: 261–273. https://doi.org/10.1289/ehp.8456261.

89 Ames, B.N., Kammen, H.O., and Yamasaki, E. (1975). Hair dyes are mutagenic: identification of a variety of mutagenic ingredients. *Proc. Natl. Acad. Sci. USA* 72 (6): 2423–2427. https://doi.org/10.1073/pnas.72.6.2423.

90 Ingham, R.J., Riva, E., Nikbin, N. et al. (2012). A "Catch–React–Release" method for the flow synthesis of 2-aminopyrimidines and preparation of the imatinib base. *Org. Lett.* 14 (15): 3920–3923. https://doi.org/10.1021/ol301673q.

91 Liu, Y.-F., Wang, C.-L., Bai, Y.-J. et al. (2008). A facile total synthesis of Imatinib base and its analogues. *Org. Process Res. Dev.* 12 (3): 490–495. https://doi.org/10.1021/op700270n.

92 Filipponi, P. and Baxendale, I.R. (2016). The generation of a library of bromodomain-containing protein modulators expedited by continuous flow synthesis. *Eur. J. Org. Chem.* 2016 (11): 2000–2012. https://doi.org/10.1002/ejoc.201600222.

93 Filipponi, P., Gioiello, A., and Baxendale, I.R. (2016). Controlled flow precipitation as a valuable tool for synthesis. *Org. Process Res. Dev.* 20 (2): 371–375. https://doi.org/10.1021/acs.oprd.5b00331.

94 Fujisawa, T. and Filippakopoulos, P. (2017). Functions of bromodomain-containing proteins and their roles in homeostasis and cancer. *Nat. Rev. Mol. Cell Biol.* 18: 246. https://doi.org/10.1038/nrm.2016.143.

95 Sanchez, R., Meslamani, J., and Zhou, M.-M. (2014). The bromodomain: from epigenome reader to druggable target. *Biochim. Biophys. Acta, Gene Regul. Mech.* 1839 (8): 676–685. https://doi.org/10.1016/j.bbagrm.2014.03.011.

96 Kim, H., Lee, H.-J., and Kim, D.-P. (2015). Integrated one-flow synthesis of heterocyclic thioquinazolinones through serial microreactions with two organolithium intermediates. *Angew. Chem. Int. Ed.* 54: 1877–1880. https://doi.org/10.1002/anie.201410062.

97 Osorio-Planes, L., Rodríguez-Escrich, C., and Pericàs, M.A. (2016). Removing the superfluous: a supported squaramide catalyst with a minimalistic linker applied to the enantioselective flow synthesis of pyranonaphthoquinones. *Catal. Sci. Technol.* 6 (13): 4686–4689. https://doi.org/10.1039/C6CY00473C.

98 Li, Y. (2012). Qinghaosu (artemisinin): chemistry and pharmacology. *Acta Pharmacol. Sin.* 33 (9): 1141–1146. https://doi.org/10.1038/aps.2012.104.

99 Lévesque, F. and Seeberger, P.H. (2012). Continuous-flow synthesis of the anti-malaria drug artemisinin. *Angew. Chem. Int. Ed.* 51 (7): 1706–1709. https://doi.org/10.1002/anie.201107446.

100 Cantillo, D., Wolf, B., Goetz, R., and Kappe, C.O. (2017). Continuous flow synthesis of a key 1,4-benzoxazinone intermediate via a nitration/hydrogenation/cyclization sequence. *Org. Process Res. Dev.* 21 (1): 125–132. https://doi.org/10.1021/acs.oprd.6b00409.

101 Macias, F.A., Marin, D., Oliveros-Bastidas, A., and Molinillo, J.M.G. (2009). Rediscovering the bioactivity and ecological role of 1,4-benzoxazinones. *Nat. Prod. Rep.* 26 (4): 478–489. https://doi.org/10.1039/b700682a.

102 Flamini, G. (2012). Chapter 13: Natural herbicides as a safer and more environmentally friendly approach to weed control: a review of the literature since

2000. In: *Studies in Natural Products Chemistry*, vol. 38 (ed. R. Attaur), 353–396. Elsevier https://doi.org/10.1016/B978-0-444-59530-0.00013-7.

103 Hartwig, J., Ceylan, S., Kupracz, L. et al. (2013). Heating under high-frequency inductive conditions: application to the continuous synthesis of the Neuroleptic olanzapine (Zyprexa). *Angew. Chem. Int. Ed.* 52 (37): 9813–9817. https://doi.org/10.1002/anie.201302239.

104 Adamo, A., Beingessner, R.L., Behnam, M. et al. (2016). On-demand continuous-flow production of pharmaceuticals in a compact, reconfigurable system. *Science* 352 (6281): 61–67. https://doi.org/10.1126/science.aaf1337.

105 Bédard, A.-C., Longstreet, A.R., Britton, J. et al. (2017). Minimizing E-factor in the continuous-flow synthesis of diazepam and atropine. *Bioorg. Med. Chem.* 25 (23): 6233–6241. https://doi.org/10.1016/j.bmc.2017.02.002.

12

Matrix Isolation in Heterocyclic Chemistry

José P. L. Roque, Cláudio M. Nunes, and Rui Fausto

University of Coimbra, Coimbra Chemistry Centre – Institute of Molecular Sciences (CQC-IMS), Department of Chemistry, Rua Larga, Coimbra 3004-535, Portugal

12.1 Introduction

The matrix isolation method has been used as a research tool in organic chemistry since the beginning of the 1970s. It was proposed first in 1954, almost simultaneously by George Pimentel (Berkeley, CA) and George Porter (Cambridge, UK) [1, 2], but it only became popular among the organic chemistry community after publication of the papers by Lin and Krantz [3], Chapman et al. [4], and Pong and Shirk [5], all of them describing the photochemistry of α-pyrone as a precursor of cyclobutadiene, whose existence was, at the time, still under discussion. Upon ultraviolet (UV) irradiation, matrix-isolated α-pyrone (**1**) was found to undergo fast photoequilibration with its isomeric open ring aldehyde-ketene **2**, as well as a slower ring closure isomerization to a bicyclo β-lactone **3** followed by CO_2 elimination to generate cyclobutadiene (**4**) (Figure 12.1).

Isolation of molecules in a cryogenic matrix provides ideal conditions for structural studies when conjugated with a structure-sensitive probing technique, like infrared (IR) spectroscopy. But the technique has also an enormous potential for studies of chemical reactivity, which has been explored since its debut as a privileged experimental tool in organic chemistry, in particular to study light-induced processes.

In a matrix isolation experiment, molecules are trapped from the gas phase into an environment of a solidified inert gas (in general a frozen noble gas) at temperatures close to absolute zero. Under these conditions, chemical processes with an activation barrier larger than a few kJ mol^{-1} are virtually quenched, except if they occur via the quantum mechanical tunneling (QMT) mechanism [7]. This opens the gate to the direct study of unstable intermediates, otherwise inaccessible to experimentation, thus allowing for detailed mechanistic investigations.

In addition, the matrix being a solid, rigidity prevents diffusion of the sample, and, as a consequence, molecular fragments resulting from different precursor molecules in general do not recombine. Such feature is commonly known as "cage effect" and

Heterocycles: Synthesis, Catalysis, Sustainability, and Characterization, First Edition.
Edited by Teresa M.V.D. Pinho e Melo and Marta Pineiro.

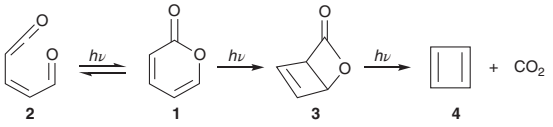

Figure 12.1 α-Pyrone photochemical reaction pathways: fast photoequilibration with the isomeric aldehyde-ketene and slow ring closure to its Dewar isomer (bicyclo β-lactone). The aldehyde-ketene is produced as a mixture of several conformers. The bicyclo β-lactone isomer releases CO_2, giving rise to cyclobutadiene [3–6].

simplifies extraordinarily the mechanistic studies. On the other hand, recombination of species produced from the same molecule is a highly probable event. This, however, can be controlled appropriately in most cases by judicious choice of the experimental conditions (e.g. matrix host, temperature).

In situ irradiation and/or matrix annealing at a given temperature allow for introduction of energy in a molecule in a controlled way, defining the range of possible chemical transformations of the isolated species. UV and visible irradiation may lead either to bond-breaking/bond-forming processes or conformational isomerizations (or to the two types of processes in simultaneous), while irradiation at the longer IR wavelengths most of times can only give rise to conformational changes, though we have recently reported an example of a bond-breaking/bond-forming reaction induced by IR light (the bidirectional hydroxyl-thiol tautomerization of thiotropolone [8], which will be described in details later in Section 12.5). On the other hand, thermal processes are limited to processes with very low energy barriers (of only a few kJ mol^{-1}), since the matrices start to lose their properties at still considerably low temperatures (the maximum work temperatures for argon and xenon matrices, for example, are ca. 40 and 70 K, respectively, above which the matrices start to sublimate extensively).

In general, heterocycles are prone to react photochemically, frequently exhibiting competitive reaction pathways. The use of narrowband selective irradiation allows to select a given species formed along the reaction and makes it generate a specific product while keeping other species present in the matrix unreactive. Such possibility has been used successfully to shed light on mechanistic details of reactions undergone by heterocyclic compounds to an unprecedented level, with the detection and characterization of the reactivity of a large number and types of intermediates that are highly reactive under other experimental conditions.

Another relevant area of application of matrix isolation in heterocyclic chemistry is the study of tunneling-driven reactions. Since at the very low-temperature conditions of a matrix isolation experiment most of the thermal processes are suppressed, the direct observation of tunneling becomes accessible to experimentation. The use of matrix isolation to address QMT has been recently revitalized by observation of several fascinating examples of the very rare heavy-atom tunneling phenomenon in heterocyclic compounds [7, 9, 10]. Indeed, the QMT of atoms (both of hydrogen atom and of heavy atoms) has newly been recognized to be more important to chemical reactivity than it was previously assumed, with recent studies demonstrating that the impact of QMT on chemical reactivity can be so relevant that it can even control

how reactions proceed, i.e. a chemical process can take place exclusively by tunneling, leading to a product whose reaction path faces a barrier higher than those related with other *a priori* possible products, thus superseding kinetic control and breaking the transition state theory (TST) rules [11].

In the next sections, several illustrative cases of application of the matrix isolation method for the investigation of the structure and reactivity of a variety of heterocyclic compounds will be presented. We will concentrate on our own recent investigations and focus on selected examples of different types of reactivity: thermal, photochemical, and tunneling-driven. In the case of the photochemical reactions, examples of both IR and UV–visible triggered processes will be provided.

We shall here mention a previous publication dedicated to the use of matrix isolation in heterocyclic chemistry, which can be considered complementary to the present chapter regarding some aspects. In that publication [12], written upon invitation from one of the editors of this book (T.M.V. Pinho e Melo), one of the authors of the present chapter (R. Fausto), together with his coworkers I. Reva and A. Gómez-Zavaglia, described the use of the technique in the investigation of some of the most important families of heterocyclic compounds (which were grouped according to their ring size, from three- to six-membered ring compounds), by providing examples of relevant studies that had then been recently published in the specialized literature. To the best of our knowledge, no other publication addressing this subject in a comprehensive way has been reported since then. We also invite the readers that may be interested to look in deeper details to the relevance of the QMT in organic chemistry reactivity to look to our recent publication on the subject appearing in the book *Tunnelling in Molecules: Nuclear Quantum Effects from Bio to Physical Chemistry,* edited by J. Kästner and S. Kozuch and published by the Royal Society of Chemistry [7]. For those that may want to further explore the capabilities and technical details of the matrix isolation method, we shall recommend the books on the subject authored or edited by Meyer [13], Andrews and Moskovits [14], Barnes et al. [15], Dunkin [16], Fausto [17], and Khriachtchev [18], as well as the review by Frija et al. [19], where strategies for *in situ* preparation of rare organic molecules resulting from UV–visible irradiation of matrix-isolated tetrazole precursors are addressed in great detail, and the special issue of the *Journal of Molecular Structure* (Elsevier) edited by Nunes et al., on the structure, spectroscopy, and chemistry of organic reactive species [20].

12.2 Structural Characterization

Matrix isolation IR spectroscopy is an extremely powerful research tool to structurally characterize heterocyclic compounds. An interesting example has been reported by Breda et al. [21], where the isomeric diazines, pyrazine, pyrimidine, and pyridazine (Figure 12.2) were investigated. The compounds were isolated in argon matrices and their IR spectra assigned with the help of vibrational calculations performed based on electronic structure calculations undertaken at the DFT(B3LYP)/6-311++G(d,p) level of theory.

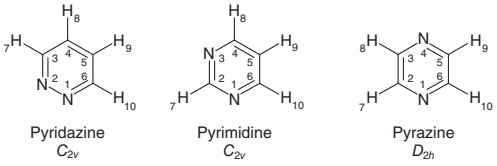

Figure 12.2 Pyridazine, pyrimidine, and pyrazine. The symmetry point groups of the molecules are indicated in the figure. Source: Reprinted from Breda et al. [21]. Copyright 2006, with permission from Elsevier.

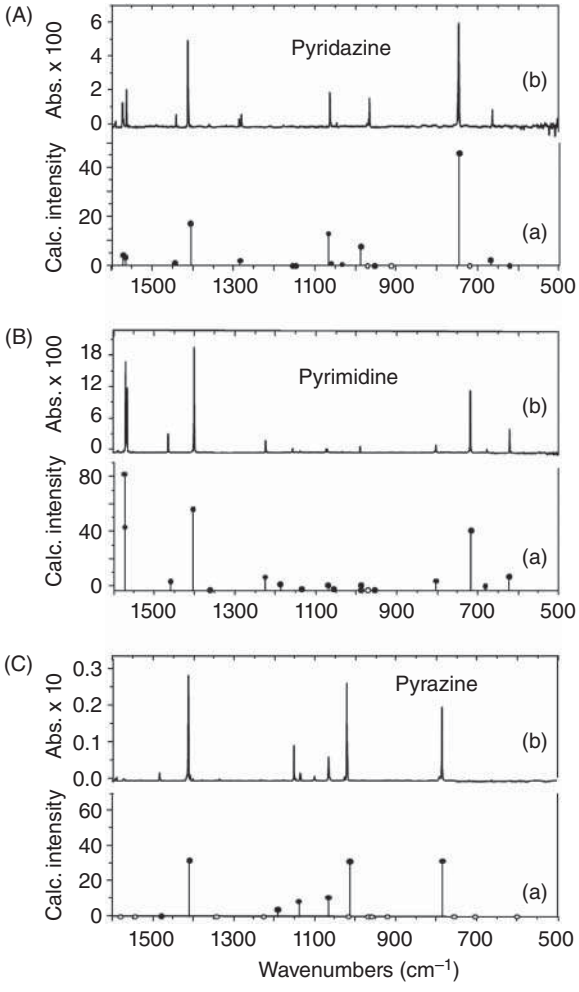

Figure 12.3 B3LYP/6-311++G(d,p) calculated infrared spectrum of pyridazine, pyrimidine, and pyrazine (a) and the observed infrared spectra of the compounds isolated in solid argon at 10 K (b). In the calculated spectra, open circles indicate the positions of the IR inactive modes. Calculated frequencies are scaled by a single factor 0.978; calculated intensities are in km mol^{-1}. Calc., calculated; Abs., absorbance. Source: Adapted from Breda et al. [21]. Copyright 2006, with permission from Elsevier.

The first interesting fact to note is that, in spite of being isomers, the studied diazines have IR spectra under matrix isolation conditions that differ very much from each other (Figure 12.3). This is particularly notorious for pyrazine, since the symmetry of the molecule is different (D_{2h} vs. C_{2v} for the other two compounds) leading to a smaller number of active IR modes in this molecule (12 vs. 22 in pyrimidine and 20 in pyridazine), but the spectra of pyrimidine and pyridazine are also significantly distinct.

Spectra/structure correlations can be extracted from the vibrational data, in particular regarding the degree of aromaticity exhibited by the three molecules. The relative values of the CC stretching frequencies are a good indicator of the degree of aromaticity, since they correlate with the bond lengths. The ν(C4C5) stretching vibration in pyridazine has the highest frequency (1572.9 cm^{-1}) among all CC stretching vibrations in the studied diazines, while the average frequency of the stretching modes associated with the C3C4 and C5C6 bonds in the same molecule is the smallest one (1243.4 cm^{-1}). Both in pyrazine and pyrimidine, the average ν(CC) frequency values ($\approx$1320 cm^{-1}) are in between the two extreme values observed for the CC vibrations in pyridazine. The observed ν(C4C5) frequency (1572.9 cm^{-1}) is typical of a CC bond with a large double bond character, indicating a high degree of π-electron localization in the pyridazine ring and allowing to conclude that in this molecule the contribution of the canonic form where the C4C5 bond corresponds to a double bond is considerably more important than the alternative canonic form where this bond corresponds to a single bond. This conclusion is reinforced also by the small vibrational frequency of the ν(N1N2) mode in pyridazine (967.3 cm^{-1}), which is typical of a single bond. Contrarily to what happens in pyridazine, the π-electron systems in both pyrazine and pyrimidine rings are strongly delocalized over all heavy atoms.

In the described investigation [21], the authors were also able to observe the UV-induced photoisomerization of pyrazine into pyrimidine (Figure 12.4), suggesting that the mechanism for the phototransformation most probably involves intermediacy of a benzvalene-like transient species generated from the prefulvene diradical, which is believed to be a primary photoproduct in the photochemistry of pyrazine (and also of benzene) [22–25].

Another interesting example of a structural characterization by matrix isolation IR spectroscopy that was used to confirm the chemical identity of the reaction product has been reported by Lopes et al. [26]. This is an interesting case where the technique was shown to surpass the most commonly used NMR and mass spectrometry analyses.

The investigation appeared following a series of studies on the thermolysis of 2-benzoyl-2-halo-2*H*-azirine-3-carboxylates **5** (Figure 12.5) [27]. These compounds were found to undergo ring expansion giving products in high yield, which were first identified as being 4-haloisoxazoles **6**. Both ^{1}H NMR and mass spectrometry measurements gave results compatible with formation of isoxazoles [27]. In addition, it is known that thermolysis of 2*H*-azirines usually takes place by cleavage of the N—C single bond, resulting in a transient vinyl nitrene that can subsequently evolve to the corresponding isoxazole. This reaction is essentially the reverse of the cyclization of vinyl nitrenes commonly used to prepare 2*H*-azirines [28]. Nevertheless, the reactivity pattern of 2*H*-azirine derivatives is in fact difficult to establish *a priori*, since it is significantly dependent on the nature of the substituents. For example, methyl 2-chloro-3-methyl-2*H*-azirine-2-carboxylate and methyl 3-methyl-2*H*-azirine-2-carboxylate isolated in argon matrices were found to undergo both C—C and N—C bond cleavages, leading to production of nitrile ylides or methylated ketene imines, respectively [29–31]. 2*H*-Azirines bearing an aromatic

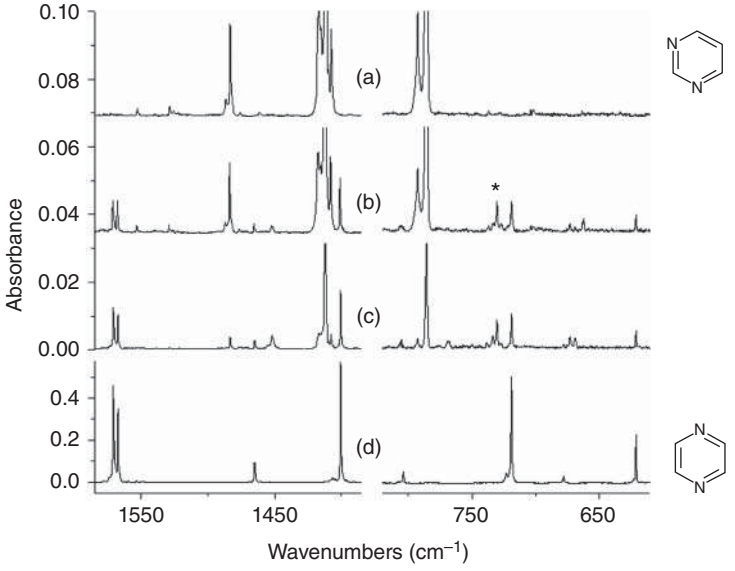

Figure 12.4 Fragments of the infrared spectra of pyrazine isolated in an Ar matrix: (a) recorded after deposition of the matrix; (b) recorded after three hours of irradiation with high pressure mercury lamp fitted with a cutoff filter transmitting light with $\lambda > 270$ nm; (c) recorded (in a separate experiment) after 20 minutes of irradiation with a pulsed excimer laser $\lambda = 308$ nm; (d) corresponding fragments of the spectrum of pyrimidine isolated in an Ar matrix. The asterisk indicates the band (at 730 cm^{-1}) that should be assigned to the bending vibration of the HCN photoproduct. Source: Adapted from Breda et al. [21]. Copyright 2006, with permission from Elsevier.

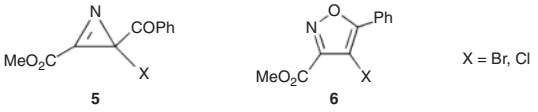

Figure 12.5 2-Benzoyl-2-halo-2*H*-azirine-3-carboxylates and suggested products of thermolysis, 4-haloisoxazoles.

substituent at C2 [32, 33] were also found to undergo competitive C—C and N—C bond cleavages, with the tendency toward the N—C bond cleavage increasing with the electron-withdrawing ability of the ring substituents.

In their study, Lopes et al. [26] demonstrated that the matrix isolation IR spectrum of the product of thermolysis of methyl 2-benzoyl-2-chloro-2*H*-azirine-3-carboxylate (**7**) corresponds to that of oxazole **8** (methyl 4-chloro-5-phenyl-1,3-oxazole-2-carboxylate) and not to that of the initially postulated product, its isomeric isoxazole **9** (methyl 4-chloro-5-phenylisoxazole-3-carboxylate) (Figure 12.6). The two isomers (**8** and **9**) give rise to similar ^{1}H and ^{13}C NMR spectra and similar patterns of fragmentation in mass spectrometry experiments, while their matrix isolation IR spectra are very much distinct, thus allowing for their easy differentiation (Figure 12.7).

The formation of oxazole **8** from the 2*H*-azirine **7** can be explained considering the thermal cleavage of the C—C bond of the azirine to give nitrile ylide **10** followed by recyclization. Interestingly, since the oxazole is obtained in high yield (98%)

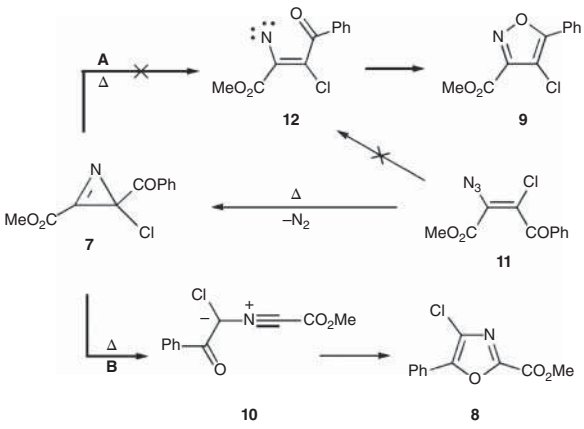

Figure 12.6 General mechanism for thermolysis of 2-benzoyl-2-chloro-2*H*-azirine-3-carboxylate (**7**), prepared from the corresponding chloroazidoalkene **11**. **A** and **B** correspond to the two *a priori* possible reaction pathways, associated respectively to the C—N and C—C bond cleavages of the azirine ring. Source: Adapted from Lopes et al. [26]. Copyright 2009, with permission from Elsevier.

[27], this means that, for the type of molecules investigated, the C—C bond cleavage strongly dominates over the N—C one. Furthermore, the unequivocal identification by matrix isolation IR spectroscopy of oxazole **8** as the single reaction product of thermolysis of **7** leads also to the conclusion that the formation of the 2*H*-azirine ring from its precursor haloazidoalkene **11** must take place via a concerted process. Otherwise the formation of the putative vinyl nitrene intermediate **12** should lead to formation of the isoxazole **9**.

In conclusion, the matrix isolation IR spectroscopy studies doubtlessly established that the thermolysis of 2-benzoyl-2-halo-2*H*-azirine-3-carboxylates leads to oxazoles and not, as initially suggested [27], to isoxazoles.

Another interesting study where matrix isolation IR spectroscopy was shown to be instrumental to identify the structural nature of the compound under investigation was reported by Reva et al. [34], which deals with the identification of the most stable tautomer of maleic hydrazide and its preferred conformer in the gas phase. The matrix isolation experimental studies were complemented by a series of quantum chemical calculations.

The electronic energies for the different tautomers of maleic hydrazide (and their conformational states) were obtained at the QCISD level of theory (Table 12.1), which predicted the oxo-hydroxy conformer **13a** as the most stable form of the compound. The oxo-hydroxy conformer **13b** as well as the dihydroxy forms **14a**, **14b**, and **14c** were predicted to be higher in energy by 23.1, 20.3, 47.7, and 76.3 kJ mol^{-1}, respectively, while the dioxo tautomer **15** was predicted to have a relative energy of 21.0 kJ mol^{-1}.

The IR spectrum of maleic hydrazide isolated in an Ar matrix was found to exhibit characteristic bands due to the stretching vibrations of the OH, NH, and C=O groups, respectively at 3588, 3441, and 1708/1707/1699 cm^{-1}. The presence

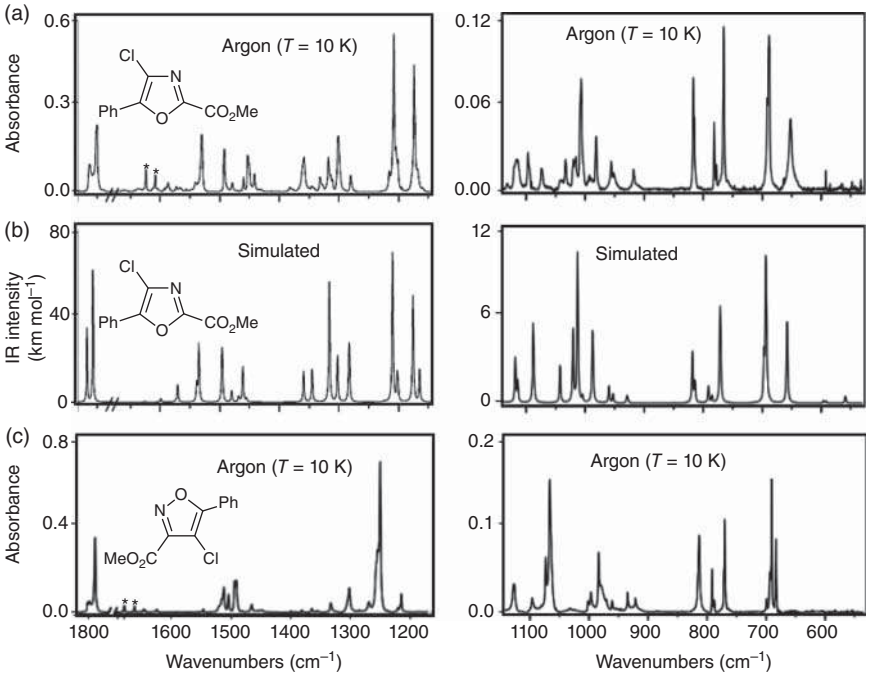

Figure 12.7 (a): Infrared spectrum of the product of thermolysis of the azirine **7** in an argon matrix, in the 1800–1145 and 1100–550 cm^{-1} regions. (b): Simulated IR spectrum of isoxazole **8** (in the same spectral regions) based on the DFT(B3LYP)6-311++G(d,p) calculated wavenumbers – scaled by 0.9817 – and intensities for the two lowest energy conformers of isoxazole **8** weighted by their expected populations in the gas phase at 323 K (temperature of deposition of the matrix of the product of thermolysis of the azirine **7**). (c): Spectrum of matrix isolated isoxazol **9**. Bands marked with an asterisk are due to monomeric water impurity. Source: Adapted from Lopes et al. [26]. Copyright 2009, with permission from Elsevier.

Table 12.1 Relative energies (ΔE, kJ mol^{-1}) of the isomeric forms of maleic hydrazide obtained using the electronic energies calculated at the QCISD/6-31++G(d,p) level and zero-point corrections obtained at the DFT(B3LYP)/6-31++G(d,p) level.

	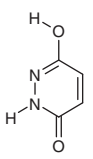 13a	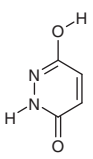 13b	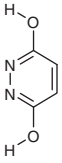 14a	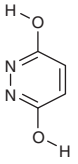 14b	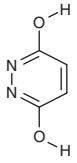 14c	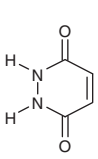 15
	Oxo-hydroxy			**Dihydroxy**		**Dioxo**
Symmetry	C_s	C_s	C_{2v}	C_s	C_{2v}	C_2
ΔE	0.0	23.1	20.3	47.7	76.3	21.0

Source: Adapted from Reva et al. [34]. Copyright 2012, with permission from Elsevier.

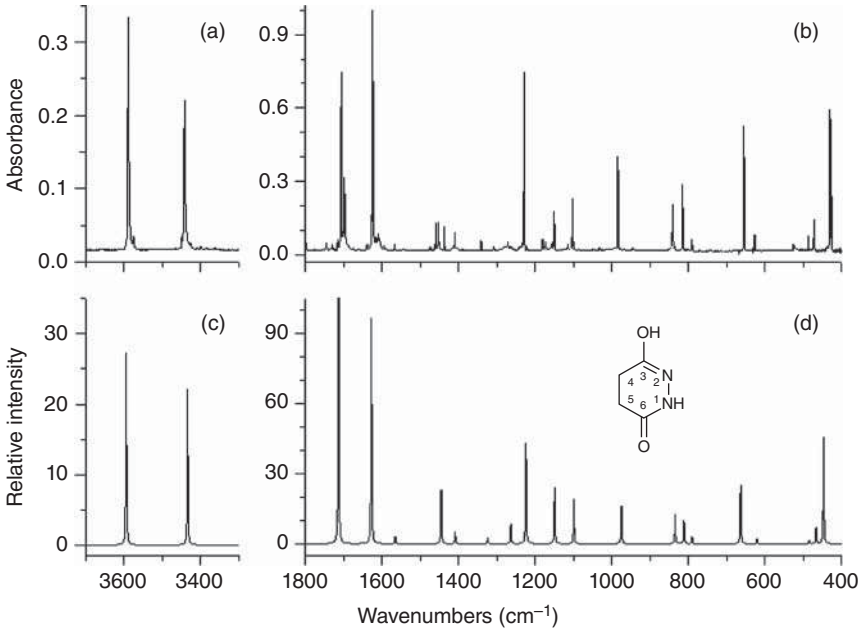

Figure 12.8 Top panels (a, b): Experimental IR spectrum of maleic hydrazide isolated in an argon matrix at 15 K. Bottom panels (c, d): Theoretical IR spectrum of maleic hydrazide isomer **13a** calculated at the DFT(B3LYP)/6-31++G(d,p) level and scaled by 0.950 (c) and 0.975 (d). Source: Adapted from Reva et al. [34]. Copyright 2012, with permission from Elsevier.

of these characteristic bands indicates that the molecules of the compound exist in the matrix (and in the gas phase from where they were trapped in the cryogenic medium) as the oxo-hydroxy conformer **13a**. This conclusion is strongly supported by the good general agreement between the experimental IR spectrum and the spectrum theoretically predicted for **13a** (Figure 12.8), which demonstrates that **13a** is in fact the only species present in the matrix.

Why is it so that the oxo-hydroxy form **13a** is by far the most stable form of maleic hydrazide, while uracil, which is an isomer of maleic hydrazide with switched positions of one pair of NH and C=O groups, is known [35] to exist exclusively in the dioxo tautomeric form? The key structural feature to understand the high stability of structure **13a** is the presence of two vicinal nitrogen atoms in the pyridazine ring of the maleic hydrazide molecule. The same hybridization at these two nitrogen atoms is strongly destabilizing to the system [36]: in the dihydroxy tautomer **14**, energy rises due to repulsion of lone electron pairs at the nitrogen atoms, while in the dioxo tautomer **15**, repulsion of the positively loaded hydrogen atoms of the two NH groups strongly destabilizes the system. Only in the oxo-hydroxy **13**, the destabilizing repulsive effects (described above) are replaced by an energy-lowering, attractive interaction between the hydrogen atom of the NH group and the lone electron pair of the other nitrogen atom. Conformer **13a** is more stable than **13b** because in the first case two stabilizing interactions, of O–H…N and N–H…O types, exist, while

in **13b** the stabilizing O–H…N interaction is replaced by the destabilizing H–O…N repulsion.

A type of systems for which matrix isolation IR spectroscopy has been used very successfully to structural elucidation comprehends heterocyclic molecules bearing hydroxyl or methoxyl ring substituents. These molecules most often have conformers whose structures differ only in the orientation of the substituent relatively to the molecular framework and that possess very similar energies. Also, frequently in these cases, the vibrational spectra of the individual conformers are very much similar. The high spectral resolution achieved under matrix isolation conditions then becomes instrumental for structure characterization.

Methoxy-substituted indoles in position C5 or C6 have been studied by Lopes Jesus et al. [37, 38]. Both molecules possess two conformers differing in the orientation of the methoxyl substituent, whose energies have been estimated theoretically to be within 4 kJ mol^{-1} (Figure 12.9).

The IR spectra of compounds isolated in noble gas matrices recorded immediately after isolation are represented in Figures 12.10 and 12.11. For 5-methoxyindole, a theoretical IR spectrum of the gas-phase conformational mixture at 298.15 K, built based on the results of B3LYP/6-311++G(d,p) harmonic vibrational calculations carried out for the two conformers, with the IR intensities calculated for each one of them scaled by the respective gas-phase Boltzmann population estimated at the same level of theory (80% *anti*; 20% *syn*), shows a very good agreement with the experimental spectrum (see Figure 12.10), indicating that both conformers are present in the matrix and also that their energy difference shall be very close to the predicted one. The experimental confirmation of the higher stability of the *anti* conformer was obtained by annealing the matrix up to 40 K, which resulted in

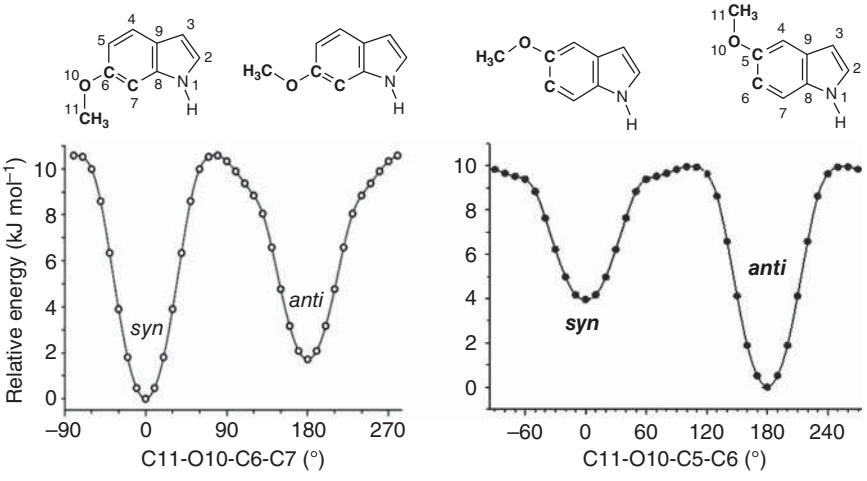

Figure 12.9 DFT(B3LYP)/6-311++G(d,p) calculated potential energy profiles for internal rotation of the methoxyl substituent in 6-methoxyindole (left) and 5-methoxyindole (right). Source: Adapted from Lopes Jesus et al. [37], with permission from AIP publishing; Adapted with permission from Lopes Jesus et al. [38]. Copyright 2017, American Chemical Society.

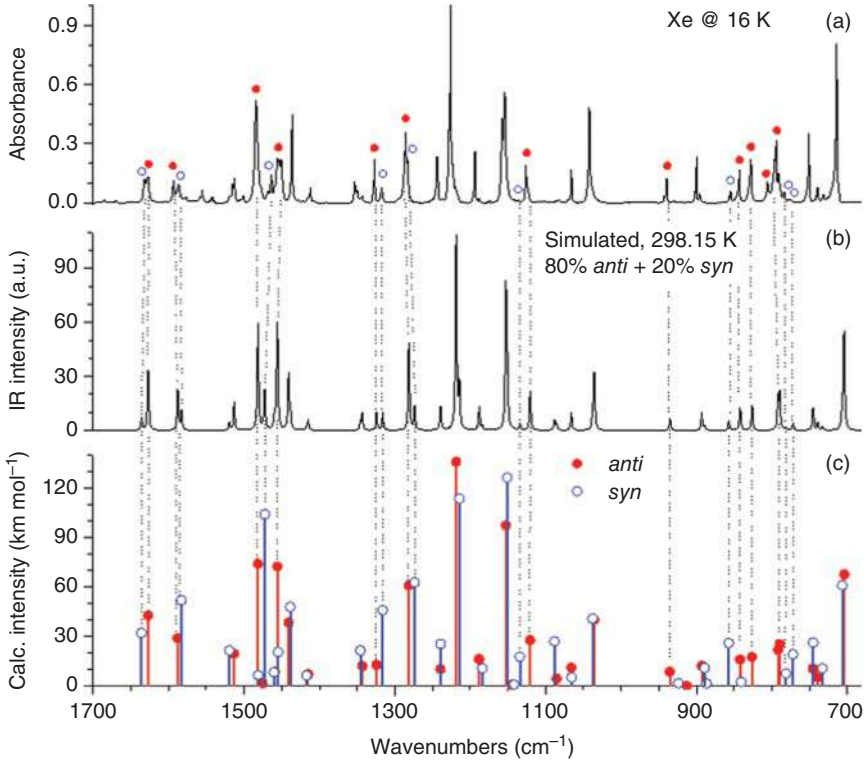

Figure 12.10 Top panel (a): Experimental IR spectrum of 5-methoxyindole recorded immediately after isolating the compound in a low-temperature xenon matrix at 16 K. Middle panel (b): Simulated IR spectrum of the gas-phase conformational mixture at 298.15 K, weighted by the calculated Boltzmann populations at 298.15 K for the conformers (80% *anti* + 20% *syn*). Bottom panel (c): Individual stick spectra calculated for the *anti* (closed red circles) and *syn* (open blue circles) conformers at the B3LYP/6 311++G(d,p) level. Source: Adapted with permission from Lopes Jesus et al. [38]. Copyright 2017, American Chemical Society.

conversion of the higher energy *syn* conformer into the most stable *anti* form, as shown in Figure 12.12.

For 6-methoxyindole, the IR spectra of the as-deposited matrices (argon; xenon) also clearly reveal presence of both *anti* and *syn* conformers (see Figure 12.11). The performed annealing experiments confirmed that in this molecule the *syn* conformer corresponds to the most stable form, as predicted by the calculations. Indeed, during the annealing experiments (xenon matrix), when the sample temperature reached 34 K, the intensity of the bands assigned to the *anti* conformer started to decrease, and concomitantly the bands ascribed to the *syn* form increased (Figure 12.13), which is an irrefutable evidence for occurrence of the *anti* → *syn* relaxation, thus confirming that *syn* is in fact the most stable conformer.

For both molecules, the relative stability of the conformers could be explained by determining the orbital stabilization interaction energies according to the natural bond orbital (NBO) theory [39]. These results revealed that the most significant

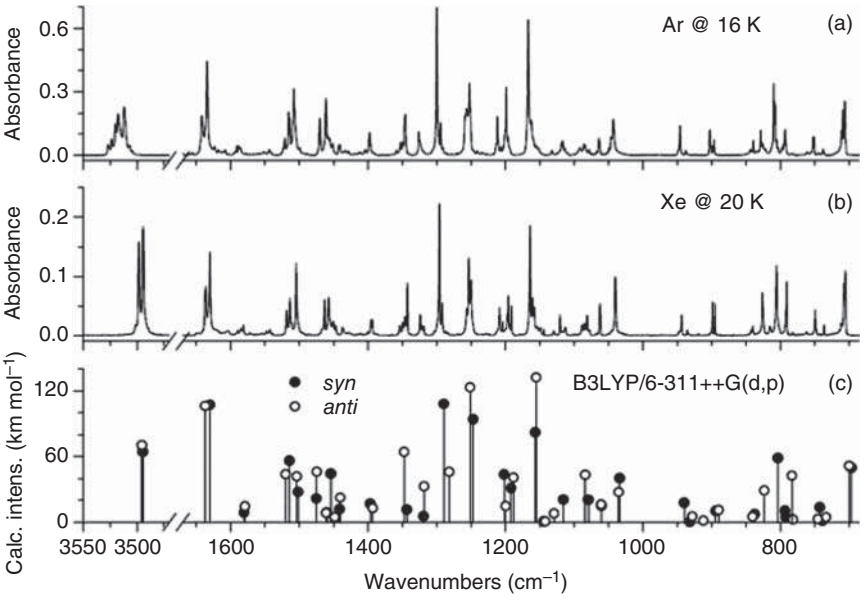

Figure 12.11 Top and middle panels: Experimental IR spectrum of 6-methoxyindole isolated in an argon matrix at 16 K (a) or a xenon matrix at 20 K (b). Bottom panel (c): Theoretical spectra of the *syn* and *anti* conformers calculated at the B3LYP/6-311++G(d,p) level. Source: Adapted from Lopes Jesus et al. [37], with permission from AIP publishing.

stabilizing effect comes from the Lp2(O10) → π*(C6C7), in 5-methoxyindole, or Lp2(O10) → π*(C4C5), in 6-methoxyindole, conjugative interactions.

12.3 UV-Induced Photochemical Reactivity

In the present section, illustrative examples on the UV-induced reactivity of heterocycles isolated in cryogenic matrices will be pinpointed. Special emphasis will be given on the capture of reactive intermediates, or elusive products, which allowed the establishment of mechanistic proposals or supported previous hypothesis.

The UV-induced photochemistry of heterocyclic compounds has been typically understood in terms of the chemistry of their π*←π or π*←*n* electronic excited states [40, 41]. However, this paradigm was shifted in 2002, when Sobolewski et al. showed that dark σ*←π states featuring a dissociative character along a hydroxyl (OH) or azine (NH) group must also be taken into account [42]. Once populated, either by direct excitation from the ground electronic state or by interconversion from a π*←π state, these dark states can quickly relax back to their ground state, through a conical intersection, or follow its dissociative path and lose the labile hydrogen atom from the OH/NH groups. These predictions were later confirmed by photofragment translational spectroscopy studies on UV-induced indole molecules in supersonic jets, in which it was possible to detect fast and slow detached hydrogen atoms [43, 44]. The co-fragment of the detached hydrogen atoms should be a radical species (the indolyl

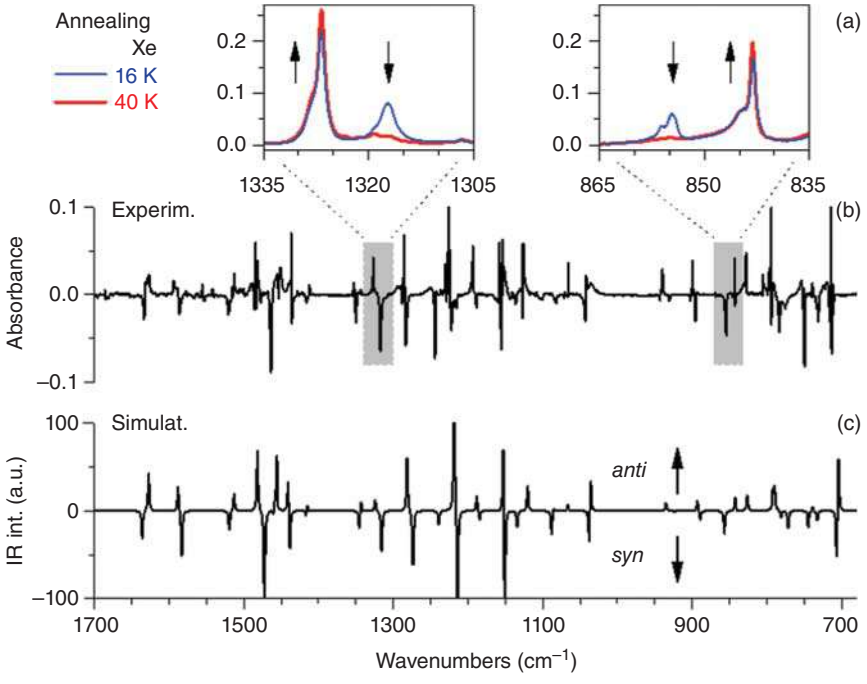

Figure 12.12 Top panels (a): Fragments of the IR spectra of the as-deposited matrix of 5-methoxy-indole, at 16 K, and the same sample after annealing to 40 K. Middle panel (b): Experimental difference spectrum (40 K *minus* 16 K). Bottom panel (c): Simulated B3LYP/6-311++G(d,p) difference spectrum. Source: Adapted with permission from Lopes Jesus et al. [38]. Copyright 2017, American Chemical Society.

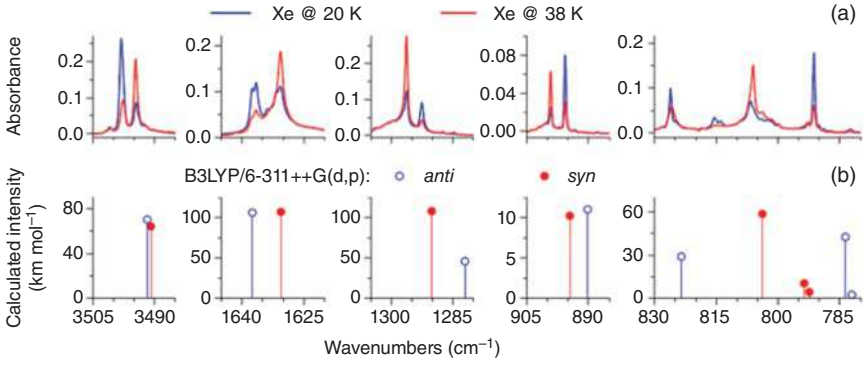

Figure 12.13 Top panels (a): Selected spectral regions illustrating the changes taking place after annealing of 6-methoxyindole isolated in a Xe matrix from 20 K (red) to 38 K (blue). Middle panels (b): Theoretical spectra of *syn* (open circles) and *anti* (closed circles) conformers of 6-methoxyindole calculated at the B3LYP/6-311++G(d,p) level of theory. Source: Adapted from Lopes Jesus et al. [37], with permission from AIP publishing.

radical, for instance) and, to further support Sobolewski's hypothesis, such radicals species should be captured and experimentally characterized. The matrix isolation technique was originally conceived for this exact goal (capture of free radicals) [1, 2, 45] and thus appeared as a promising technique to address this question. This was indeed the motivation behind the study of the photochemistry of matrix-isolated indole reported recently by Reva et al. [46].

Deposition of indole with a large excess of either argon or neon at 15 or 5 K, respectively, and monitorization by IR spectroscopy reveal the sole presence in the matrices of the 1*H*-indole tautomeric form. This was particularly evident by the intense and characteristic ν(NH) stretching and γ(NH) rocking bands found at 3523 and 395 cm^{-1} in argon and at 3522 and 390 cm^{-1} in neon matrices, respectively. Irradiations of the matrices with broadband light ($\lambda > 270$ nm) led to the consumption of 1*H*-indole and formation of both the indolyl radical and the 3*H*-indole tautomer (Figure 12.14). The 1*H*-indole → 3*H*-indole tautomerization was interpreted as resulting from the recombination of the photodetached H-atom and indolyl radical formed initially. Studies on the gas-phase photochemistry of indole showed that the H-atom dissociation occurs to an extent that does not allow its back recombination with the indolyl radical [43]. However, as mentioned earlier, in matrix isolation conditions, the two photofragments are confined inside

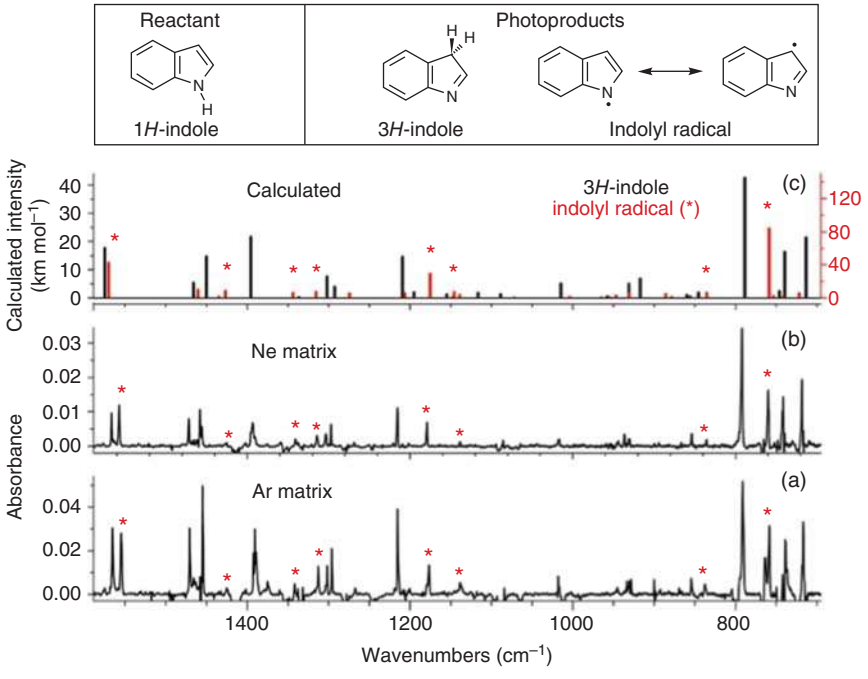

Figure 12.14 The top panel shows the structures of the different species. Bottom panels: Infrared spectra of photoproducts generated upon UV ($\lambda > 270$ nm) irradiation of indole monomers isolated in Ar (a) and Ne (b) matrices, compared with the calculated spectra of 3*H*-indole (black) and indolyl radical (red) (c). Source: Adapted from Ref. [46], with permission from AIP publishing.

the same matrix site (cage effect) and, therefore, are most likely to recombine. Such a mechanism of phototautomeric reactions has recently been designated as photoinduced dissociation association (PIDA) and follows the Sobolewski's hypothesis [42, 47].

A detailed theoretical analysis of the electronic structure of the indolyl radical was carried out by NBO analysis. The indolyl radical is a doublet species with one unpaired electron. However, the unpaired electron is not located at the N1 position from where the H-atom has been detached (as one could intuitively expect), but otherwise it is delocalized along the entire structure. The natural spin density calculations provided a picture of where it is most likely to find this electron, in this case, at the C3 center (+0.538; Figure 12.15), which shall justify the tendency for the recombination at this position and formation of 3*H*-indole.

The formation of the 3*H*-tautomer together with radical species is a common trend in the photochemistry of indole derivatives isolated in cryogenic matrices and has been observed also, for instance, for 3-formylindole [46], 4-, 5- and 6-methoxyindoles [48, 49], and even in the case of 7-azaindole [50]. It is worth mentioning that in the latter case, the 7*H*-azaindole tautomer has been identified as a photoproduct of 7-azaindole isolated in an argon matrix, but not for this compound isolated in a hydrogen (n-H_2) matrix. In fact, it seems that phototautomeric reactions occurring by the PIDA mechanism are highly dependent on the matrix host, since some materials are more prone to restrict the radical and the H-atom inside the same cage than others [51]. Globally, the results that emerge from these studies support the earlier predictions by Sobolewski and coworkers and are consistent with the results obtained by photofragment translational spectroscopy.

Photoreactivity of cytosine has also been the subject of recent investigations using matrix isolation. Cytosine is a biologically relevant compound whose photochemistry is mainly governed by reactions involving hydrogen atoms. Spectroscopic studies on cytosine in the gas phase showed the existence of multiple cytosine tautomers. However, its exact number is still somewhat controversial [52]. While the identification of the amino-oxo (**AO**) isomer and the amino-hydroxy (**AH**) form is consistent through the use of several spectroscopic techniques [52–56], experimental evidence

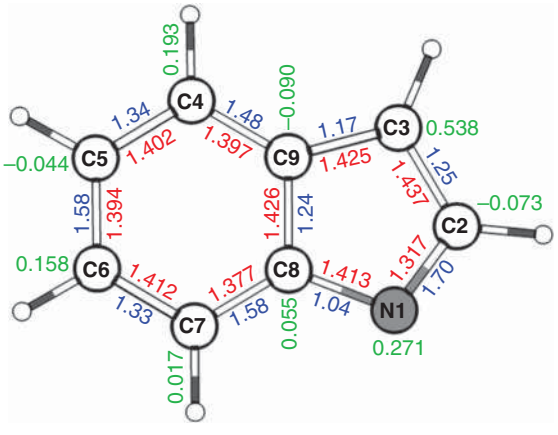

Figure 12.15 Optimized C–C and N–C distances in Å (red), natural bond orders (blue), and natural spin densities (green) calculated for the indolyl radical at the B3LYP/6-311 ++G(d,p) level. Source: Adapted from Reva et al. [46], with permission from AIP publishing.

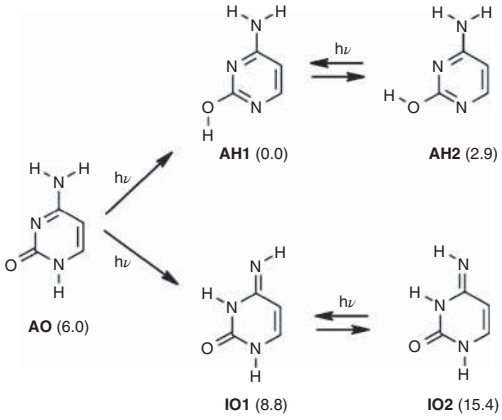

Figure 12.16 UV-induced hydrogen-atom-transfer processes converting the amino-oxo tautomer of cytosine into the amino-hydroxy and imino-oxo forms. The numeric values shown in parentheses are the relative energies of the different forms expressed in kJ mol^{-1}. Source: Adapted from Lapinski et al. [57], with permission from the PCCP Owner Societies.

for the imino-oxo (**IO**) form has been very scarce and preliminary [52, 55]. Recently, Lapinski et al. were able to successfully bring further support to the characterization of the elusive cytosine **IO** tautomer, in a photochemical study of the matrix-isolated compound where tunable monochromatic radiation was used as excitation source. This approach not only provided the IR spectra separation of the three major cytosine tautomers (**AO**, **AH**, and **IO**) but also allowed to distinguish the vibrational signatures of the two possible isomeric forms of the tautomers **AH** (conformers **AH1** and **AH2**) and **IO** (*E* and *Z* isomers **IO1** and **IO2**) (Figure 12.16) [57].

According to quantum mechanical computations on the relative stability of cytosine isomers (see Figure 12.16) [57, 58], one could expect **AH1** and **AH2** to dominate in the gas-phase, **AO** and **IO1** to have minor populations, and **IO2** to be present only in a trace amount. Deposition of cytosine vapors with a large excess of argon results in a matrix containing a mixture of cytosine isomers, whose exact nature could be identified through a series of photochemical experiments resulting in the separation of the IR signatures of the different isomers.

Upon irradiations at $\lambda = 314–312$ nm, the change in the intensity of a low- and of a very low-intensity set of bands in the IR spectrum was observed, while the most intense set of bands remained unchanged. The reactive sets were assigned to **IO1** (consumed) and to **IO2** (produced), based on the comparison of the experimental data with the calculated IR spectra for the whole set of isomers shown in Figure 12.16. The observed reaction involves the $E \rightarrow Z$ isomerization of the imino group in the **IO** tautomer, which typically takes place due to a conical intersection between the S_1 and S_0 electronic states at the geometry where the hydrogen atom is nearly perpendicular to the C=N bond [59]. Interestingly, the depletion of **IO1** was never absolute, indicating that a photostationary state between the two **IO** isomers was established, although dependent on the wavelength of irradiation.

Remarkably, the hypsochromic shift of the source of irradiation by 1 nm, to $\lambda = 311$ nm, drastically changed the outcome of the photochemistry. At this wavelength, the IR bands ascribable to the **AO** form quickly lost their intensity and the bands due to all **IO1**, **IO2**, **AH1**, and **AH2** forms increased (Figure 12.17).

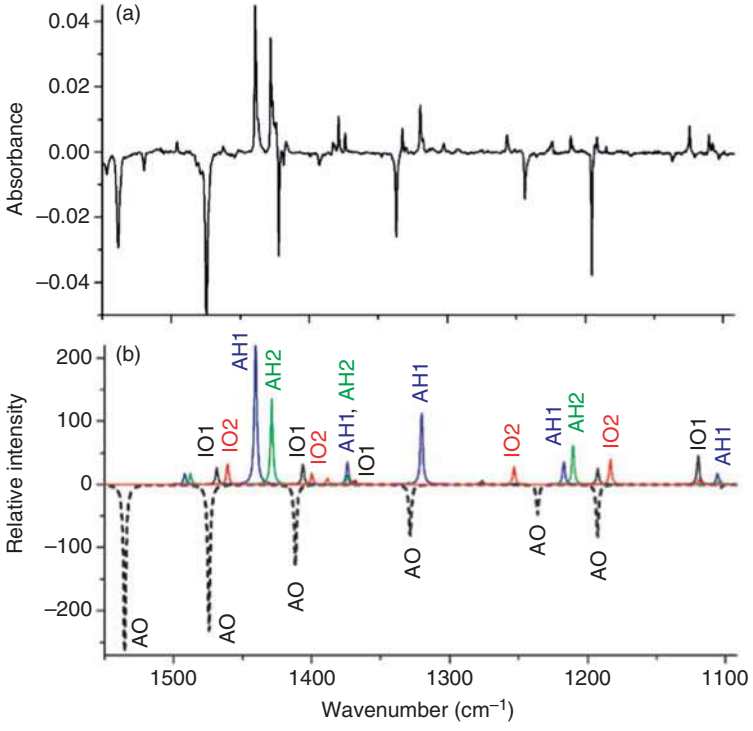

Figure 12.17 Phototransformation of the **AO** tautomer of matrix-isolated cytosine into the **AH1**, **AH2**, **IO1**, and **IO2** forms. (a) Subtraction result: experimental spectrum recorded after UV irradiation at 311 nm *minus* that recorded after the previous UV irradiation at 312 nm; (b) DFT(B3LYP)/6-31++G(d,p) simulated spectra for **AH1** (blue), **AH2** (green), **IO1** (black solid line), **IO2** (red), and **AO** (black dashed line) isomers of cytosine. Intensities in the theoretical spectra have the following weights: 2 for **AH1**; 1 for **AH2**, **IO1**, and **IO2**; and −5 for **AO**. Source: Adapted from Lapinski et al. [57], with permission from the PCCP Owner Societies.

It was suggested that not all photoproducts are necessarily the result of a primary reaction, but most likely are due to an initial oxo-hydroxy (**AO→AH1**) or amino-imino (**AO→IO1**) isomerization, followed by partial conversions to **AH2** and **IO2** by rotation around the C—O or C=N bonds, respectively. The initial consumption of the **AO** isomer might also take place along the repulsive πσ* states, following the common trend of heterocyclic compounds containing azine (NH) [42] or amine (NH_2) [60] groups. Analogous photoreactions were also found for cytosine derivatives isolated in cryogenic matrices, namely, 1-methyl-, 5-methyl-, and 5-fluoro-cytosine [61, 62].

In a final stage of irradiation (at $\lambda = 300$ nm), the **AO** isomer was totally consumed, and the matrix was left with **AH** and **IO** isomers. At the **IO1**/**IO2** photostationary state resulting from those irradiations, **IO2** was left in a majority amount. However, subsequent irradiations at $\lambda = 311$ nm disturbed the equilibrium and were found to lead to **IO1** at the cost of **IO2**, proving the photo reversibility of the **IO1↔IO2** reaction and providing a clear picture of the IR spectrum of each isomer (Figure 12.18).

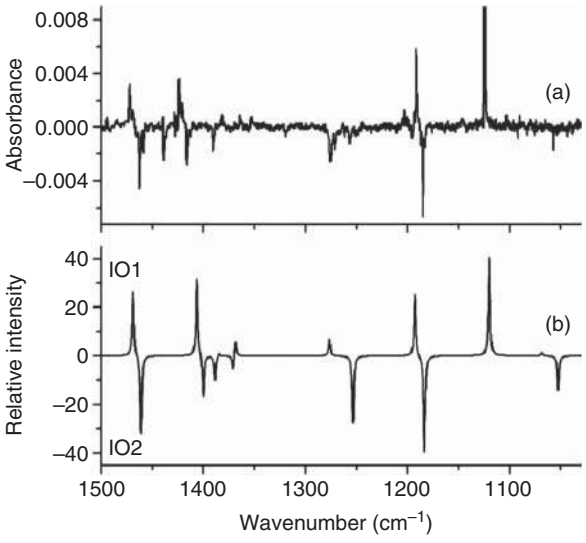

Figure 12.18 Identification of **IO1** and **IO2** imino–oxo isomers of cytosine: (a) difference spectrum, obtained by subtraction of the spectrum recorded after UV ($\lambda = 300$ nm) irradiation from the spectrum recorded after the subsequent UV ($\lambda = 311$ nm) irradiation; (b) subtraction result: spectrum theoretically simulated for the **IO1** form *minus* the spectrum simulated for **IO2**. Source: Adapted from Lapinski et al. [57], with permission from the PCCP Owner Societies.

Concomitantly to the main reactions mentioned earlier, the consumption of **AO** also led to the appearance of a low-intensity and structured band in the 2300–2230 cm^{-1} region, ascribable to the antisymmetric stretching of an isocyanate group. The amount of this isocyanate photoproduct in the matrix, which results from the cytosine ring opening, must be low, since the IR band corresponding to this type of vibration is characterized by their usual very high intensity (usually larger than 1000 km mol^{-1}) [63]. Controlled interconversion between **AH1** and **AH2** forms could also be successfully attained in the described study [57]. However, this was achieved by the use of narrowband IR irradiations and will be discussed in detail in Section 12.5, which focuses on IR-induced processes.

Although it has been proven to be fundamental for a better understanding of the photochemistry of heterocycles, the model proposed by Sobolewski and coworkers is obviously not applicable for compounds that do not have any XH group (X = O, N, NH). In that case, it is often seen that the photochemistry is centered on the cleavage of bonds formed by the ring heteroatoms. The photochemical behavior of the tetrazole moiety, a five-membered aromatic heterocyclic ring, is a good example.

Tetrazoles possess a very rich photochemistry, although strongly dependent on the ring substituents. Our group has been engaged in the study of the photochemistry of tetrazoles for many years. Here, our attention will be mainly focused in a recent case study, which will serve as an illustrative example [64]. For those interested in a more comprehensive analysis on the photochemistry of matrix-isolated tetrazoles, we encourage the reading of the reviews that can be found elsewhere [19, 65].

Tetrazoles may exist in multiple tautomeric forms, depending on the ring substituents and the environment conditions. In the crystalline phase, the parent tetrazole (**16**) (see Figure 12.19) was found to exist exclusively in its 1*H*-form, whereas in the gas phase, it was found to exist in its most stable 2*H*-form [67]. Early studies on the photochemistry of matrix-isolated tetrazole (**16**) were conducted by Maier et al. in 1996 and showed that 2*H*-tetrazole was the tautomer trapped in argon

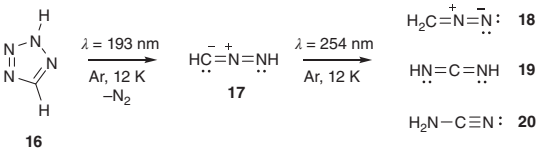

Figure 12.19 Summary of the experimental observations for the photochemistry of tetrazole **16** isolated in a low-temperature argon matrix at 12 K [66].

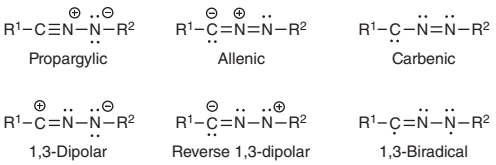

Figure 12.20 Different resonance forms that can represent the structure of a nitrile imine. Source: Adapted from Nunes et al. [64], with permission from John Wiley and Sons. Copyright 2020 WILEY-VCH Verlag GmbH & Co. KGaA, Weinheim.

at 12 K [66]. Thereafter, irradiation of the matrix at 193 nm induced N_2 elimination and production of nitrile imine (**17**), diazomethane (**18**), carbodiimide (**19**), and cyanamide (**20**) (plus an HCN…NH complex). The nitrile imine (**17**) was assigned as the primary photoproduct, since its bands were observed to grow up promptly in the first minutes of irradiation and, after 10 minutes, seen to start reducing of intensity. Subsequent irradiations of the matrix, with a low-pressure mercury lamp coupled to a vycor filter ($\lambda = 254$ nm), consumed the totality of **17** and produced the remaining photoproducts **18**–**20** (Figure 12.19).

These were very interesting results, not only because the detection of **17**, a species that for long remained elusive (despite the elusiveness of nitrile imine **17** until that point in time, Huisgen et al. had shown, in 1959, the formation of substituted nitrile imines as key intermediates in the thermolysis of 2,5-disubstituted tetrazoles [68]), was finally successful, but mostly because it opened doors for the detailed characterization of other nitrile imines, molecules that are of major practical application as reactants in 1,3-dipolar cycloaddition reactions [69, 70]. The nitrile imines are in fact very intriguing species, because they may be described as a combination of multiple resonance structures (Figure 12.20), whose relative importance differs depending on its substituents. In 2012, Bégué et al. have characterized a series of nitrile imines, produced by either thermolysis or photolysis of tetrazoles [71]. They concluded that nitrile imines owning ν_{as}(CNN) modes with IR absorptions above 2200 cm^{-1} are described as essentially propargylic structures (for example, diphenyl nitrile imine PhCNNPh), whereas those with IR absorptions below 2200 cm^{-1} are predominantly of allenic character (e.g. the parent nitrile imine (**17**), HCNNH, or *C*-phenyl nitrile imine PhCNNH). Moreover, it was also suggested that electronegative substituents with lone-pair donating groups, such as F, NR_2, or OR (R = alkyl), should stabilize the carbenic structure of nitrile imines [72]. On the light of these predictions, we have investigated the photochemistry of matrix-isolated 5-aminotetrazole on a quest for experimental evidence of existence of carbenic nitrile imines [64].

Similarly to the studies on the simplest tetrazole (**16**), only the 2*H*-form of 5-aminotetrazole (**21**) (Figure 12.21) was found in an argon matrix at 15 K.

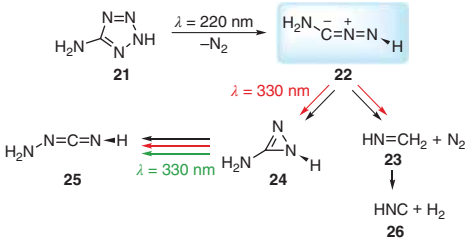

Figure 12.21 Summary of experimental observations in the UV-induced photochemistry of 5-amino-2*H*-tetrazole (**21**) isolated in an argon matrix: Generation of *C*-amino nitrile imine (**22**) and its photochemical transformation into **25** via **24** and decomposition to **23**. The colors of the arrows are related to different wavelengths and irradiation stages: $\lambda = 220$ nm (black), $\lambda = 330$ nm first stage (red), and $\lambda = 330$ nm second stage (green). Source: Adapted from Nunes et al. [64], with permission from John Wiley and Sons. Copyright 2020 WILEY-VCH Verlag GmbH & Co. KGaA, Weinheim.

Irradiation of the matrix at $\lambda = 220$ nm during 120 seconds consumed roughly 50% of the tetrazole to yield *C*-amino nitrile imine (**22**) as primary photoproduct. After the initial 120 seconds, the IR bands assigned to **22** in the spectra of the irradiated matrix stopped growing, while many others continue to increase in intensity. These bands could be assigned to methylene imine (**23**), 3-amino-1*H*-diazirine (**24**), 1-aminocarbodiimide (**25**), and hydrogen isocyanide (**26**), which were identified as secondary photoproducts. Subsequent irradiations performed at $\lambda = 330$ nm, a wavelength at which **21** does not absorb, consumed the primary product **22** and populated photoproducts **23**–**25**, as monitored by IR spectroscopy (Figure 12.22).

The reactivity of **22** must follow two distinct paths: (i) cyclic rearrangement to the 3-membered ring **24** and (ii) C—N bond cleavage to yield the decomposition photoproduct **23** and N_2. 1-Aminocarbodiimide (**25**) is not a direct product of **22**, but rather produced at the cost of **24**. In fact, upon the total consumption of **22**, additional irradiations at 330 nm led to the selective conversion of **24** into **25**. Intermediacy of an 1*H*-diazirine in the conversion of a nitrile imine to the corresponding carbodiimide isomeric species was initially observed in the study of the photochemistry of matrix-isolated 5-methyltetrazole [73]. Furthermore, 1*H*-diazirines had also been previously identified as photoproducts of tetrazole derivatives by Gómez-Zavaglia et al. in their pioneering photochemistry studies of matrix-isolated 5-methoxy-1-phenyl-1*H*-tetrazole [74]. Additional studies on this topic, in particular dealing with the photochemistry of 1- and 2-methyl-5-aminotetrazoles, can be found elsewhere [75].

Unlike many other nitrile imines, the ν_{as}(CNN) mode of **22** was observed below 2000 cm^{-1} (at c. 1998 cm^{-1}). This feature triggered a detailed theoretical characterization of this species, carried out using natural resonance theory (NRT) calculations. It was found that for **22** the weight of the carbenic resonance structure amounts to 20%, contrasting to the 0% amount in the parent nitrile imine (**17**) and *C*-methyl nitrile imine [64].

Another type of molecules whose UV-induced photochemistry is initiated by the cleavage of a bond containing a heteroatom is the isoxazole family of compounds.

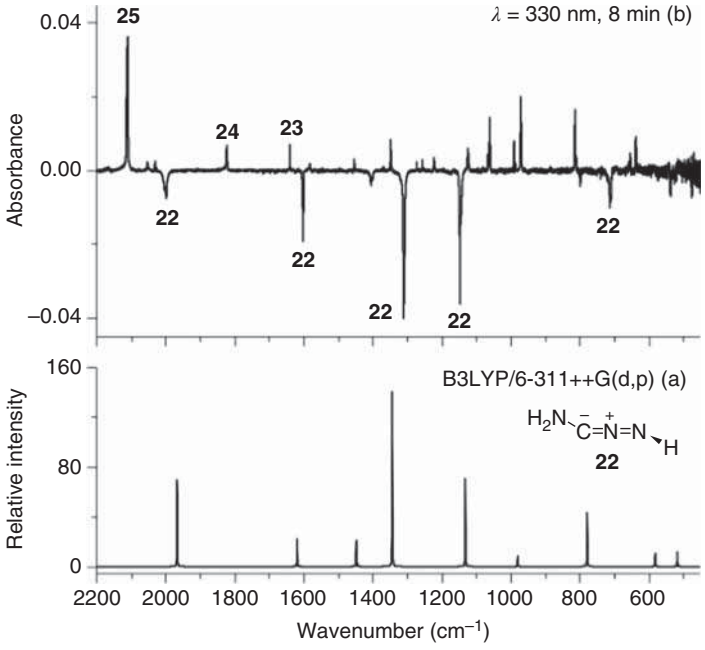

Figure 12.22 (a) IR spectrum of *C*-amino nitrile imine (**22**) simulated at the B3LYP/6-311++G(d,p) level of theory. (b) Experimental difference IR spectrum showing changes after irradiation at $\lambda = 330$ nm (8 minutes, 35 mW) in an argon matrix (subsequent to the initial irradiation of **21** at $\lambda = 220$ nm; see Figure 12.21). The negative bands are due to the consumed photoproduct **22**. The positive bands are due to photoproducts **23**–**25**. Source: Adapted from Nunes et al. [64], with permission from John Wiley and Sons. Copyright 2020, WILEY-VCH Verlag GmbH & Co. KGaA, Weinheim.

The photochemical study of isoxazole derivatives has received significant attention from the scientific community for a long time. It has been demonstrated that the main reactive channel involves the isoxazole → oxazole isomerization, mediated by a 2*H*-azirine intermediate [76–78]. However, only recently experimental results on the photochemistry of unsubstituted isoxazole (**27**) isolated in cryogenic matrices were reported [79].

Monomeric isoxazole (**27**) (Figure 12.23) isolated in an argon matrix at 15 K was found to react slowly by narrowband irradiation at $\lambda = 238$ nm. The initial 70 minutes of irradiation consumed 10% of **27** and led exclusively to its photodecomposition, yielding ketene (**28**) and hydrogen cyanide (**29**). Irradiations of the matrix at shorter wavelength, $\lambda = 221$ nm, not only led to enhance the reaction kinetics (10% of **27** was consumed in only one minute) but also led to the appearance of multiple new bands in the IR spectrum (Figure 12.24). The new photoproducts were assigned as 2-formyl-2*H*-azirine (**30**), 3-formylketenimine (**31**), 3-hydroxypropenenitrile (**32**), imidoylketene (**33**), and 3-oxopropanenitrile (**34**). Photoproducts **30** and **31** were formed in a first stage as the primary photoproducts of isoxazole, since the bands assigned to this species reached their maxima intensity in the first minutes of irradiation (unlike the others). It was argued that vinylnitrene

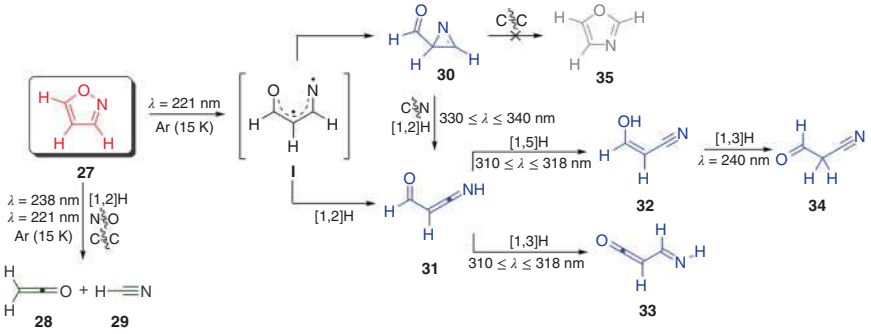

Figure 12.23 Summary of experimental observations and the mechanistic proposal for the UV-induced photochemistry pathways of isoxazole (**27**) isolated in a low-temperature argon matrix. Structures given in blue possess different conformers (for simplicity not shown in the figure). Source: Adapted with permission from Nunes et al. [79]. Copyright 2017, American Chemical Society.

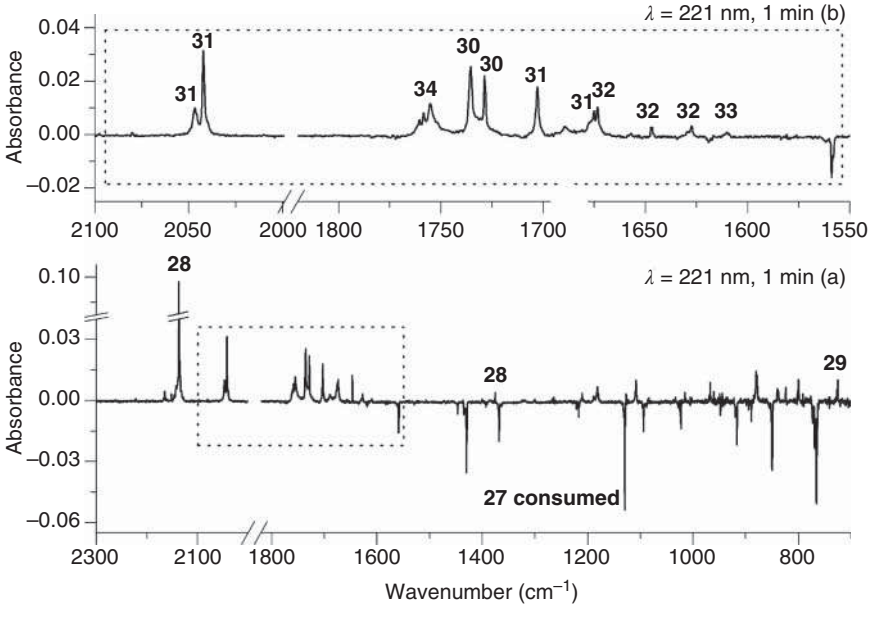

Figure 12.24 (a) Experimental difference IR spectrum: spectrum obtained after UV-laser irradiation at $\lambda = 221$ nm (one minute) of isoxazole (**27**) in argon matrix *minus* the spectrum of the sample before irradiation (as deposited matrix). Positive labeled bands are due to ketene (**28**) and hydrogen cyanide (**29**). (b) Expanded view, corresponding to the dashed rectangle in frame (a), showing only the 2100–2000 and 1800–1600 cm^{-1} regions, where the most intense bands due to photoisomerization products (labels **30** to **34**) appear (see text). Source: Adapted with permission from Nunes et al. [79]. Copyright 2012, American Chemical Society.

I must intermediate their formation. Indeed, the formation of 2-formyl-2*H*-azirine (**30**) must be intermediated by the singlet-state vinylnitrene **I**, which is the first species to be formed upon the cleavage of the isoxazole N—O bond. The singlet-state **I** has a 1,3-diradical character, and its isomerization to **30** only requires the closure of the N–C–C angle. On the other hand, 3-formylketenimine (**31**) should be formed by an [1,2]-H-shift reaction in the ground electronic triplet-state **I**. The vinylnitrene **I** plays a pivotal role in the theoretical models proposed to explain the reactivity of isoxazoles, as will be shown in Section 12.4 [80].

In a second stage of irradiation, the photoproducts were consumed by irradiations above 240 nm, where isoxazole (**27**) does not absorb. Irradiations in the 340–330 nm wavelength range led to the conversion of the primary product **30** into **31**, through the cleavage of the C—N bond in **30**, followed by an [1,2]-H-shift reaction. Note that 2-formyl-2*H*-azirine (**30**) contains two distinct conformers, differing in the orientation of the aldehyde group relatively to the ring. In the *anti*-conformation, the aldehyde H-atom faces the N-atom of the ring, and facilitates the H migration from *anti*-**30** to anti-**31**. Subsequent irradiations in the 318–310 nm wavelength range induced a very interesting pair of conformer-selective reactions: the *anti*-**31** conformer reacted through a [1,3]-H-shift and was converted to *anti*-(*E*)-**33**, whereas the *syn*-**31** conformer (less stable then its *anti* counterpart by 4–5 kJ mol^{-1}) reacted through a [1,5]-H-shift to yield *syn*-(*Z*)-**32**. The spatial proximity between the H-donor (OH or CH) and the H-acceptor (C=O or C=N) in conformers *anti*-**31** and *syn*-**31**, respectively, is the reason for the preferential reaction path for each conformer. Finally, 3-hydroxypropenenitrile (**32**) was consumed by irradiation at $\lambda = 240$ nm and isomerized by a [1,5]-H-shift to 3-oxopropanenitrile (**34**). Surprisingly, throughout the entire experiment, there were no signs of the formation of oxazole **35**.

In the view of the obtained results for isoxazole (**27**), which deviated from the common trends reported for other isoxazoles (i.e. formation of the corresponding oxazoles as final products), an interest arose to study 3,5-dimethylisoxazole (**36**) [81]. The motivation behind this study was that the unsaturation of positions 3 and 5 of the isoxazole ring could be expected to suppress most of the H-shift reactions observed for the primary photoproducts of the parent isoxazole (**27**). Matrix-isolated **36** (argon, 15 K) was irradiated at $\lambda = 222$ nm during one minute, which led to the consumption of ∼2% of the compound and production of 2-acetyl-3-methyl-2*H*-azirine (**37**) and 3-acetyl-*N*-methylketenimine (**38**) as primary photoproducts (Figure 12.25).

In this first stage of irradiation, the primary photoproducts are analogous to those formed in the study performed on the parent isoxazole (**27**) [79], and their formation must be intermediated by the vinylnitrene **II**. However, the second stage of reactivity of isoxazole **36** was found to be drastically different from that of isoxazole (**27**). An extended irradiation of the matrix (80 minutes) consumed roughly 46% of **36** and produced, in addition to the primary photoproducts **37** and **38**, the reactive intermediary 1-methyl-3-acetylnitrile ylide (**39**), through a C—C bond cleavage of **37**. Additional irradiations at $\lambda = 340$ nm resulted in the transformation of **39** into the final product 2,5-dimethyloxazole (**40**) (see Figure 12.25), which was also found to be present in the matrix after prolonged irradiation at only $\lambda = 222$ nm.

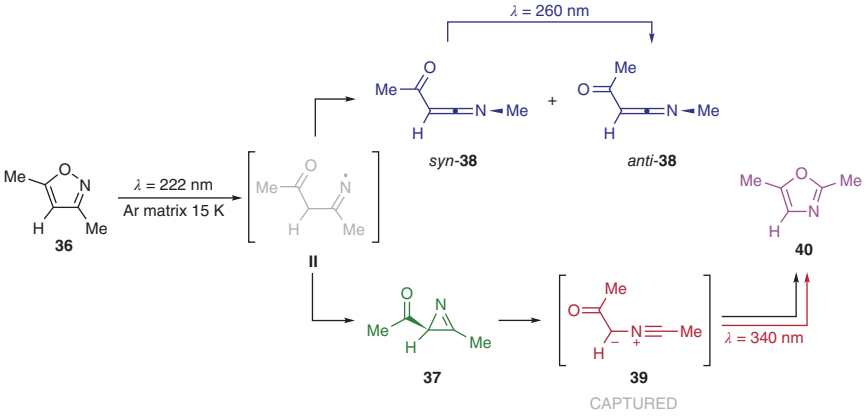

Figure 12.25 Summary of the experimental observations and the mechanism for photochemistry of 3,5-dimethylisoxazole (**36**) isolated in a low-temperature argon matrix. Source: Adapted with permission from Ref. [81]. Copyright 2013, American Chemical Society.

The nitrile ylide **39** may exist in two conformational states (*syn* or *anti*), according to the relative orientation of the nitrile ylide and carbonyl groups. Both conformers might have been produced by the UV irradiation of **37**. However, only the *anti*-**39** conformer survived in the matrix and could be experimentally characterized. In the *syn*-**39** conformer, the nitrile ylide and the carbonyl groups are properly aligned for an intramolecular 1,5-electrocyclization to **40**. Computations on the potential energy surface of this system revealed that *syn*-**39** connects with **40** through a 10 kJ mol^{-1} barrier. This barrier can be easily surmounted, especially since *syn*-**39** is produced by UV irradiation and left in a vibrational excited state, which makes its capture virtually impossible. On the other hand, there is no direct path that connects *anti*-**39** to oxazole **40,** and this reaction must go across the *syn*-**39** conformer. Therefore, the effective barrier for the *anti*-**39** → **40** reaction corresponds to that of the conformational isomerization of **39** (*anti*-**39** → *syn*-**39**) and amounts for 54.5 kJ mol^{-1} (Figure 12.26). Such a high energy barrier cannot be overcome under the matrix isolation conditions and enabled the capture of *anti*-**39**. As a consequence of these results, the theoretically formulated hypothesis [80] that a nitrile ylide should intermediate the isoxazole–oxazole photoisomerization received experimental confirmation.

12.4 Thermal Reactivity

In the present section, thermally activated reactions of heterocyclic compound studied by matrix isolation IR spectroscopy will be considered. The chosen examples are reactions involving isoxazoles, whose photoinduced reactions were also considered in Section 12.3.

As it has already been pointed out, the chemistry of isoxazoles is very rich, due to the simultaneous feature of aromaticity and the presence of a weak N—O bond.

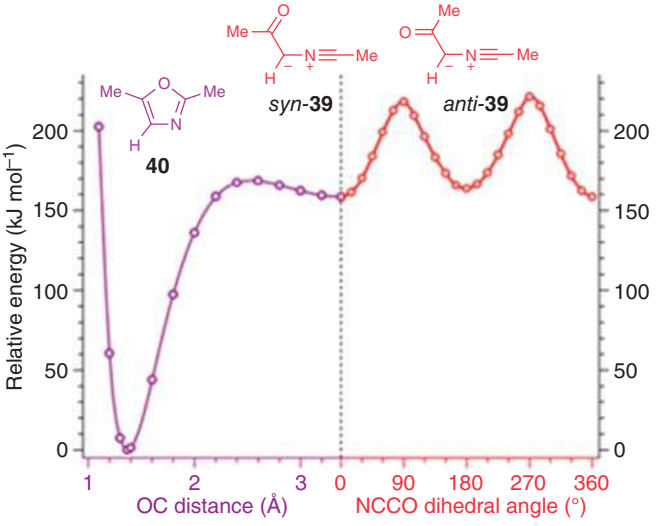

Figure 12.26 Relaxed potential energy profiles for (right, red) the intramolecular rotation of the acetyl group in nitrile ylide **39** around the NCCO dihedral angle and (left, purple) the ring contraction from nitrile ylide *syn*-**39** to 2,5-dimethyloxazole (**40**) as a function of the OC distance. The energy of **40** was chosen as the relative zero. Both scans were carried out at the B3LYP/6-311++G(d,p) level of theory. Source: Adapted with permission from Nunes et al. [81]. Copyright 2013, American Chemical Society.

For long, studies have been reported that focused on the thermal reactivity of this family of heterocycles. As a common fact, it has been shown that 2*H*-azirines are formed in the initial stages of the thermolysis of isoxazoles. However, the final products depend on the substituents present at positions 3 (R^3) and 5 (R^5) of the ring. For instance, the flash vacuum pyrolysis (FVP) of isoxazoles with $R^3 = H$ preferably leads to the formation of nitrile species, which involve H-shift reactions [82, 83], whereas the FVP of isoxazoles with $R^3 \neq H$ produces the corresponding oxazoles [84, 85]. Recently, we have revisited the pyrolysis of isoxazoles using the high-pressure pulsed pyrolysis method coupled to matrix isolation [80]. In pulsed pyrolysis, a pre-mixture of a noble gas and the compound to investigate passes through a heated SiC tube, and the activation occurs by collision of the molecules of the targeted compound with the noble gas molecules, thus avoiding possible side reactions that could be catalyzed by the walls of the pyrolysis tube. The proposed mechanistic interpretation for the thermolysis of isoxazole was supported by high-level quantum mechanical electronic structure calculations [80].

The pyrolysate of isoxazole (**27**) and Ar mixture (~1 : 1000) was deposited onto a cryogenic substrate at 15 K and probed by IR spectroscopy. Bands assigned to pyrolysis products began to appear at the temperature of 600 °C (Figure 12.27). At 800 °C, the most intense bands observed in the spectrum were already due to pyrolysis products. One immediate remark on the IR spectrum of the pyrolysate is the absorption at 2138 cm^{-1}, the characteristic vibrational mode of carbon monoxide (CO). Another characteristic band was found in the 2100–2000 cm^{-1}

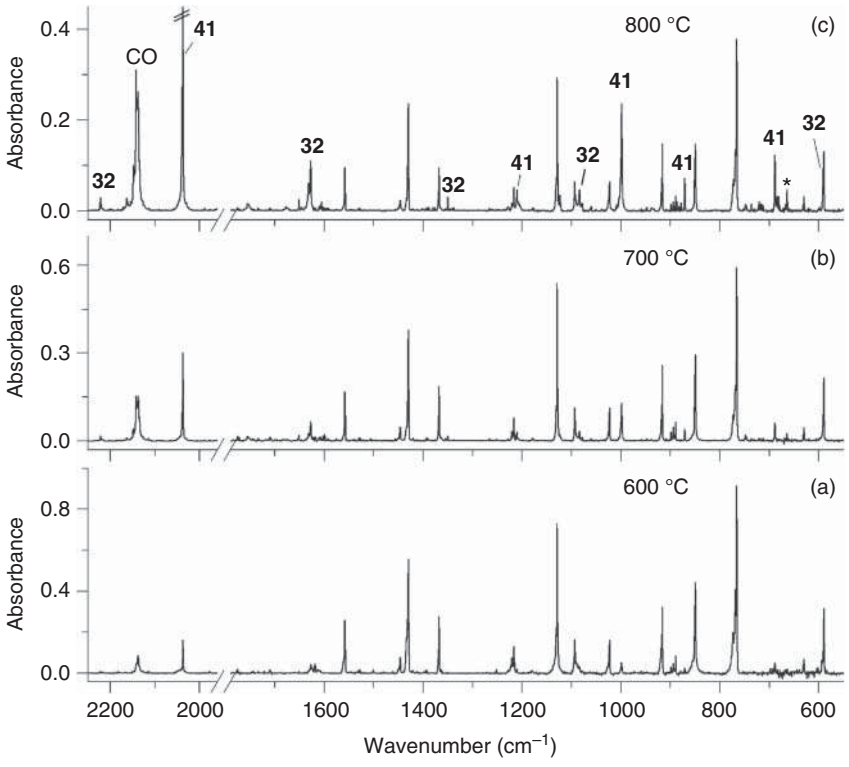

Figure 12.27 Experimental IR spectra of products of pulsed pyrolysis of isoxazole (**27**) trapped in argon matrices at 15 K. The temperature of the SiC tube was at (a) 600, (b) 700, and (c) 800 °C. The new major bands in the spectrum (c) are assigned to **32** and **41**. The band marked with an asterisk is due to an impurity from the pyrolysis system. Source: Reprinted with permission from Nunes et al. [80]. Copyright 2011, American Chemical Society.

range and assigned to the ν_{as}(NCC) mode of a ketenimine group. However, the lack of observation of any band in the ν_{as}(C=O) region excludes 3-formylketenimine (**31**) (see Figure 12.23), a found photoproduct of isoxazole [79], as the possible responsible for the band observed in the 2100–2000 cm^{-1} region. In turn this band was assigned to the ν_{as}(NCC) mode of the parent ketenimine (**41**), which must be formed alongside with CO (Figure 12.28). Additionally, a new primary product of isoxazole's thermolysis was identified, the 3-hydroxypropenenitrile (**32**) (which was also observed as secondary photoproduct in the photolysis of **27** [79]; see also Figure 12.23). 3-Hydroxypropenenitrile (**32**) may exist in four distinct conformations, but only the most stable *syn*-(*Z*)-**32** was found in the matrix, which suggest that this species is formed in a stereospecific fashion. At the end of the pyrolysis at 800 °C, the matrix was irradiated at $\lambda = 240$ nm until a photostationary state was reached. At that point, the bands previously assigned to *syn*-(*Z*)-**32** decreased in intensity and new bands emerged in the spectrum, corresponding to the isomeric *syn*-(*E*)-**32** and *anti*-(*E*)-**32** species.

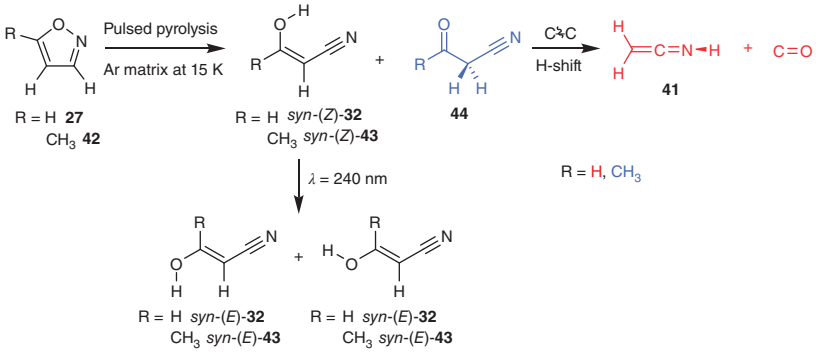

Figure 12.28 Summary of observations from the pulsed pyrolysis of isoxazole (**27**) (R = H) and 5-methylisoxazole (**42**) (R = CH_3). Detection of an oxo-nitrile **44** (blue) was only found in the pyrolysis of **42**, whereas decomposition (red) to ketenimine (**41**) and carbon monoxide was only observed in the pyrolysis of **27** [80].

A similar study was undertaken on 5-methylisoxazole (**42**) [80], to evaluate the influence of $R^5 \neq H$ on the pyrolysis of isoxazoles. The pyrolysis of **42** led to the formation of 3-hydroxybutanenitrile *syn-(Z)*-**43**, which, like the equivalent nitrile species resulting from the pyrolysis of the parent isoxazole (**27**) (i.e. 3-hydroxypropenenitrile (**32**)), was found to photoisomerize to conformers *syn*-(*E*)-**43** and *anti*-(*E*)-**43** upon UV irradiation. However, no signs of carbon monoxide and methyl-ketenimine could be found in the spectra of the pyrolysate of **42**. The path for decomposition seems indeed to be blocked by the presence of the methyl group in the position 5 of the ring, because in order to be possible this reaction would require a migration of the methyl group, which is a very improbable process in a cryogenic solid matrix. Instead, the IR signature of 3-oxobutanenitrile (**44**) was found. It might also be that 3-oxopropanenitrile (**34**) is formed during pyrolysis of unsubstituted isoxazole **27** but promptly decomposes to form CO and ketenimine, since in that case the H-shift is likely to occur.

Finally, the pyrolysis of 3,5-dimethylisoxazole (**36**) at 600 °C yielded 2-acetyl-3-methyl-2*H*-azirine (**37**) and 2,5-dimethyloxazole (**40**). At higher temperatures, **40** continued to be produced at the cost of **37** (Figure 12.29). These results agree with the earlier studies on the thermolysis of **36** by Murature et al. [84]. In a similar picture to that found for the photochemistry of isoxazoles **27** and **36** (see Section 12.3), the dimethyl derivative was found to yield oxazole as final product, whereas the unsubstituted isoxazole underwent H-shift reactions to open-ring products.

In an attempt to shed light on the experimental results, a theoretical investigation was held by state-of-the-art quantum chemistry computations. The first step in isoxazoles thermolysis is unquestionably the cleavage of the N—O bond, which should in principle produce vinyl nitrene intermediates. However, the detection of these species has not yet been successful, and earlier theoretical calculations on the thermolysis of isoxazoles failed to recognize its pivotal role [86]. The reason for such failure was the misperception that the lowest singlet state of vinyl nitrenes would be of closed-shell nature. In fact, their lowest singlet state has actually been shown

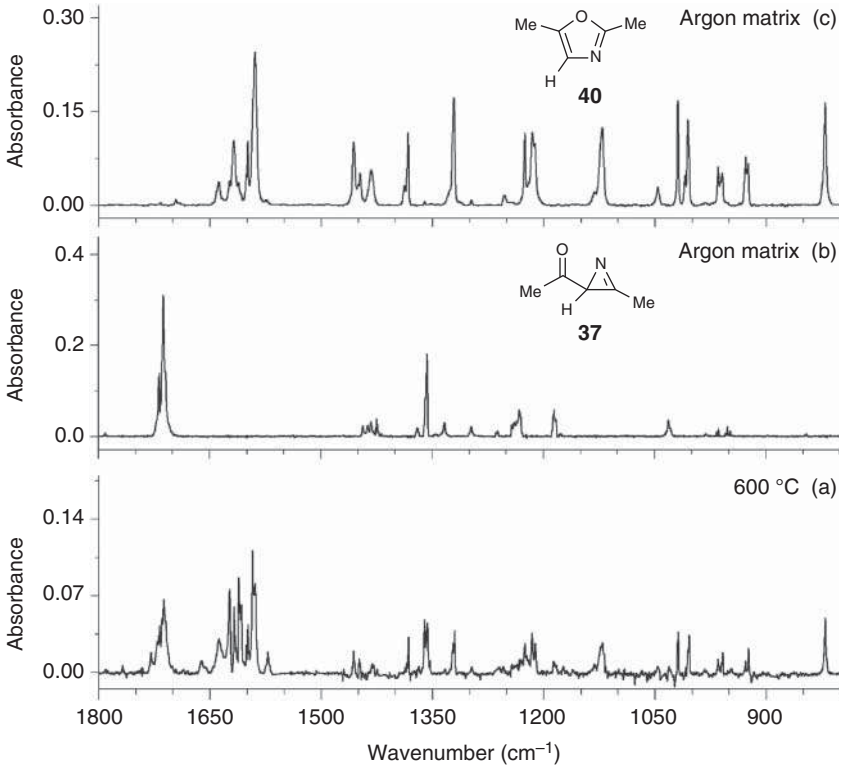

Figure 12.29 (a) Experimental IR spectrum of products of pulsed pyrolysis of 3,5-dimethylisoxazole (**36**) (600 °C), trapped in an argon matrix at 15 K. The absorptions due to the reagent were eliminated. (b, c) Experimental IR spectra of 2-acetyl-3-methyl-2*H*-azirine (**37**) (b) and 2,5-dimethyloxazole (**40**) (c) isolated in argon matrices at 15 K in separate experiments. Source: Adapted with permission from Nunes et al. [80]. Copyright 2011, American Chemical Society.

to be of open-shell nature [87], and, therefore, any single-determinant method fails to correctly describe it. The reinvestigation on this topic by Nunes et al. [80] using multiconfigurational complete active space self-consistent field (CASSCF) methods showed that open-shell vinyl nitrenes are indeed minima, although almost barrierless regarding their decay to 2*H*-azirines. Moreover, it was found that vinyl nitrene **I** could be produced at the cost of isoxazole (**27**) by surmounting a barrier of roughly 50 kcal mol^{-1}. Then, the transition states for the candidate reactions departing either from vinyl nitrene **I** or 2-formyl-2*H*-azirine (**30**) were searched. Remarkably, the lowest energy barrier (49 kcal mol^{-1}) reaction found resulted to be that leading to the formation of 3-hydroxypropenenitrile (**32**), at the cost of vinyl nitrene **I**. This was indeed the first product to be seen during the pyrolysis of isoxazole (**27**). Further computations were carried to rationalize the formation of secondary products, namely, ketenimine (**41**) and CO in the case of isoxazole (**27**) and 2,5-dimethyloxazole (**40**) in the case of 3,5-dimethylisoxazole (**36**). In the end, a general picture of isoxazole thermolysis, with an open-shell vinyl nitrene as the pivotal intermediate for all subsequent

transformations, was presented that fully supports the experimental observations and, in particular, explains the reasons for the observed selective transformations.

12.5 IR-Induced Processes

As already mentioned, the low temperature of the cryogenic matrices suppresses thermal conversions, providing, in this way, ideal conditions to investigate conformational isomerization processes, which are in general characterized by relatively low-energy barriers. IR vibrational excitation in conjugation with the matrix isolation technique has in fact been successfully used for more than two decades to manipulate in a very precise and selective way molecular conformations of different types of organic compounds [88–90]. The idea behind this approach is to use frequency-tunable narrowband IR light to deposit energy in a vibrational state of a molecular system. If subsequent energy dissipation by intramolecular vibrational energy redistribution (IVR) is partially channeled to a torsional reaction coordinate, conformational isomerization might be activated [90]. This methodology has been proved to be extremely selective, since vibrational energy can be specifically deposited in a chosen molecular species, in a particular conformation, and in a particular environment (which can result from different accommodations of the molecule in the cryogenic matrix; matrix sites) [88–90].

In this section, we will describe a few examples of IR-induced conformational isomerizations taking place in heterocyclic systems, focusing on recent advances achieved in our group. We will also mention recent pioneer results demonstrating that the previously mentioned approach can also be developed as a promising way to induce and control bond-breaking/bond-forming reactions.

In order to deposit energy into a torsional reactive coordinate so that it takes the molecule to a state above the torsional barrier or close to its top, vibrational excitation is typically carried out at first XH (X = O or N) stretching overtones with significant enough absorption cross section [88, 90]. This is nicely illustrated in the work carried out by Lapinski et al. on cytosine [91].

As mentioned in Section 12.3, the two amino-hydroxy conformers of cytosine, **AH1** and **AH2**, differing by the rotation of the hydroxy group, are the most stable forms of the monomeric compound under matrix isolation conditions (Figure 12.30). Their energy difference is 1–3 kJ mol^{-1} in favor of **AH1**. The amino-oxo (**AO**) and imino-oxo (**IO**) tautomeric forms are less stable by 4–6 and ≥8 kJ mol^{-1}, respectively [57, 58, 92, 93].

As it could be expected, **AH1** and **AH2** forms of cytosine dominate in a freshly deposited low-temperature matrix. Selective and reversible interconversion between these two forms was successfully achieved upon narrowband (0.2 cm^{-1}) IR irradiation [57, 91]. Vibrational excitation of the first OH stretching overtone of **AH1** conformer at 7013 cm^{-1} leads to its conversion into **AH2**, whereas vibrational excitation of the first OH stretching overtone of **AH2** conformer at 7034 cm^{-1} leads to its conversion into **AH1** (Figure 12.31). The population of **AH1** and **AH2** conformers was experimentally transferred many times using irradiation cycles (7013 and

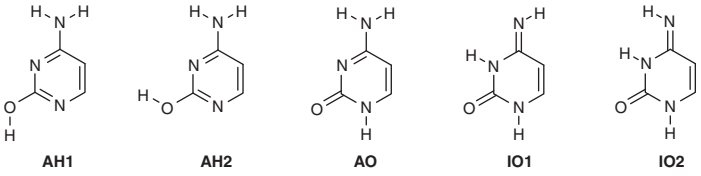

Figure 12.30 Most relevant forms of cytosine monomers ordered from left to right by their thermodynamic stability.

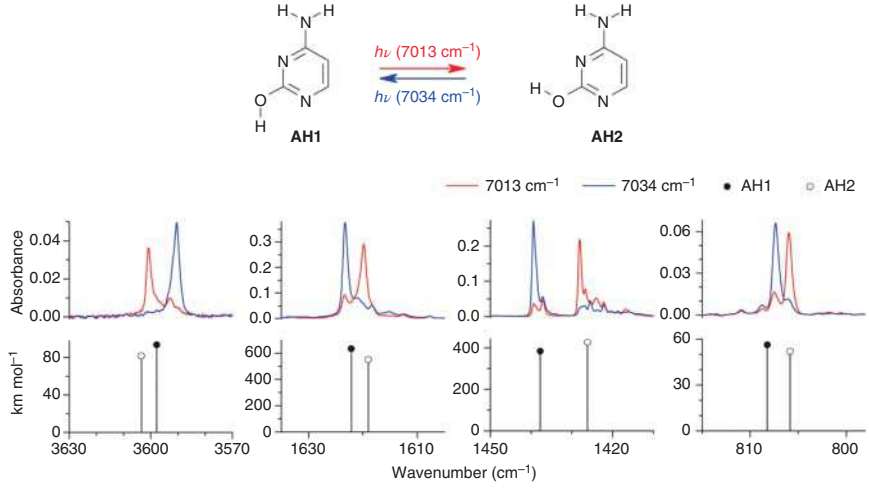

Figure 12.31 The effects of narrowband IR irradiations. Fragments of the IR spectra of cytosine isolated in an argon matrix: (red) after irradiation at 7013 cm^{-1}; (blue) after irradiation at 7034 cm^{-1}; compared to the IR spectra computed for **AH1** and **AH2** at the B3LYP/6-31++G(d,p) level of theory. Source: Adapted from Lapinski et al. [91], with permission from the PCCP Owner Societies.

7034 cm^{-1}) without any loss of the total amount and without affecting the population of **AO** and **IO** tautomeric forms present in the matrix in smaller amounts.

After shifting the population in favor of **AH2** or **AH1** by narrowband IR irradiation, it was found that broadband IR radiation from the globar source of the FTIR spectrometer affects the population of these conformers [94]. In fact, independently of the initial **AH1** : **AH2** ratio, the exposure of the matrix sample to the IR spectrometer radiation induces changes toward a photostationary state where the **AH1** : **AH2** ratio is approximately 1 : 1. Experiments with IR bandpass filters led to the interpretation that excitations at the fundamental OH and NH stretching vibrations also induce mutual conversion between **AH1** and **AH2** conformers. These excitations provide ~40 kJ mol^{-1}, which is enough to induce the conformational isomerizations, since the higher barrier for the **AH1** : **AH2** interconversion was estimated as ~30 kJ mol^{-1}. Therefore, having access to narrowband IR light in the mid-IR region, one should also be able to attain control of **AH1** and **AH2** relative populations by irradiations at the frequencies of their fundamental OH stretching modes.

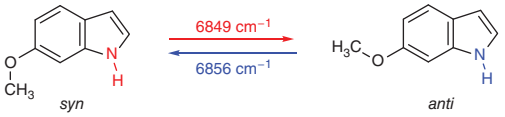

Figure 12.32 Conformational switching of 6-methoxyindole (**6MOI**) promoted by vibrational excitation of the remote NH bond at its first stretching overtone frequency.

In experiments carried out on 5-methylcytosine and 5-fluorocytosine [62], it was analogously demonstrated that the corresponding amino-hydroxy conformers, **AH1** and **AH2**, can be selectively and reversibly interconverted upon narrowband IR irradiation at the frequencies of their first OH stretching overtones. Conformational manipulation by IR vibrational excitation was demonstrated as well as for other heterocyclic compounds having an OH fragment, such as 9-methylguanine [95], thiazole-2-carboxylic acid [96], and tetrazole-5-carboxylic acid [97].

An important breakthrough on this methodology was made by our group in 2015 by demonstrating that reversible interconversion between two conformational states can be achieved by selective vibrational excitation of a bond remotely located in relation to the conformational isomerization coordinate (Figure 12.32) [98].

6-Methoxyindole (**6MOI**) was used as molecular model. This molecule can adopt two conformations, *syn* and *anti*, where the methoxy fragment (OCH_3) points to the same or to the opposite direction of the NH group, respectively. Their energy difference is 2–3 kJ mol^{-1} in favor of the *syn* conformer, the energy barrier separating the two conformers being ~9 kJ mol^{-1}. According to the relative energy of the conformers, in a freshly deposited cryogenic matrix, a *syn* : *anti* population ratio ~65 : 35 was observed. Distinctive NH stretching vibrations were measured for these conformers: in a xenon matrix at 30 K, *syn*-**6MOI** shows the ν(NH) at 3494.5 cm^{-1} and the 2ν(NH) at 6849.3 cm^{-1}, whereas *anti*-**6MOI** shows the ν(NH) at 3498.0 cm^{-1} and the 2ν(NH) at 6855.6 cm^{-1}. Narrowband IR irradiation tuned at 6849 cm^{-1} for 30 minutes was then found to promote a large-scale *syn* → *anti* isomerization, as evidenced by the difference IR spectrum shown in Figure 12.33a (spectrum obtained after irradiation *minus* spectrum of the as-deposited matrix). The comparison of this spectrum with the B3LYP/6-311++G(d,p) computed IR spectra of the two conformers (Figure 12.33b) undoubtedly allows assigning the bands that decrease of intensity to the *syn* conformer and those that concomitantly increase to the *anti* conformer. Subsequent irradiation tuned at 6856 cm^{-1} was found to promote the inverse *anti* → *syn* isomerization, as evidenced by the corresponding difference IR spectrum (Figure 12.33c), which mirrors that previously described. Remarkably, these results prove the possibility of efficient intramolecular vibrational relaxation to carry the energy deposited in the NH stretching bond into a distant reactive C–O torsional mode to induce conformational switching of the methoxy group.

Conformational isomerizations induced by vibrational excitation of a remote bond relatively to the fragment that changes its orientation were also reported for matrix-isolated 2-thiocytosine [99] and 5-hydroxy-2-hydroxymethyl-4*H*-pyran-4-one (kojic acid) [100] (Figure 12.34).

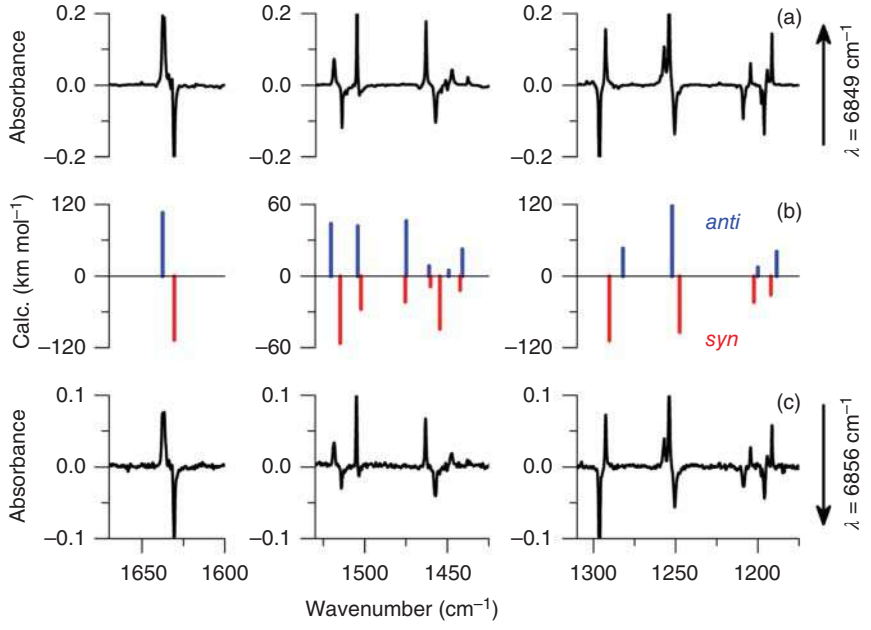

Figure 12.33 Fragments of experimental (Xe, 30 K) and theoretical IR spectra of **6MOI** in the fingerprint region showing the effect of the IR irradiations: (a) experimental spectrum registered after irradiation at 6849 cm^{-1} minus that obtained before any irradiation; (c) experimental spectrum registered before any irradiation at 6856 cm^{-1} minus that obtained after irradiation at this frequency. Arrows indicate the direction of the bands growing upon irradiation; (b) IR spectra of the *anti* (upward bars, blue) and *syn* (downward bars, red) **6MOI** conformers computed at the B3LYP/6-311++G(d,p) level of theory. Source: Reprinted with permission from Lopes Jesus et al. [98]. Copyright 2015, American Chemical Society.

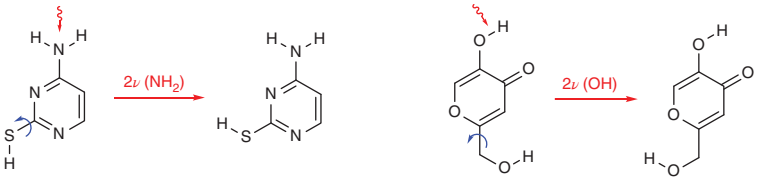

Figure 12.34 Conformational isomerization by vibrational excitation of a remote bond reported for matrix-isolated 2-thiocytosine and kojic acid.

We have further extended the concept of remote vibrational antenna, by introducing the concept of interchangeable remote vibrational antennas. Specifically, it was demonstrated that the conformation of an aldehyde (–CHO) fragment attached to a 2*H*-azirine ring can be controlled by excitation of interchangeable NH_2 or OH vibrational antennas attached to the opposite position of the ring (Figure 12.35) [101].

Computations for 3-amino-2-formyl-2*H*-azirine (**45**) and 3-hydroxy-2-formyl-2*H*-azirine (**46**) show that both molecules possess two conformers concerning the orientation of the aldehyde group, i.e. weather the C=O is *syn*-periplanar (**45A** and **46A**) or *anti*-periplanar (**45B** and **46B**) relative to the three-membered ring. For both

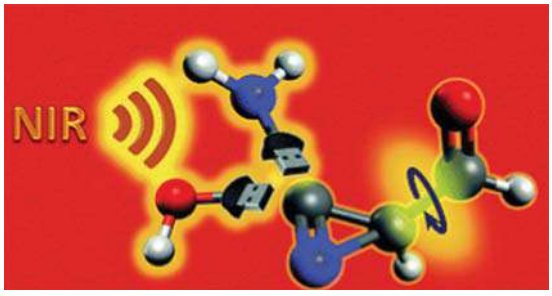

Figure 12.35 Conformational control over an aldehyde fragment of a 2*H*-azirine by selective vibrational excitation of interchangeable NH_2 and OH remote antennas. Source: Lopes Jesus et al. [101]/with permission of Royal Society of Chemistry.

molecules their energy difference is 6–7 kJ mol^{-1} in favor of the conformer **B**, which is separated from the conformer **A** by an energy barrier of ~17 kJ mol^{-1}. Upon generation of 2*H*-azirines **45** and **46**, by UV irradiation of the corresponding isoxazole precursors isolated in argon matrixes at 15 K, both conformers **A** and **B** were identified by IR spectroscopy. Particularly relevant was the identification of six bands of **45** (three for each, **45A** and **45B**) in the near-IR 7100–6700 cm^{-1} range, ascribed to the first overtones of the antisymmetric [$2\nu(NH_2)_a$] and symmetric [$2\nu(NH_2)_s$]

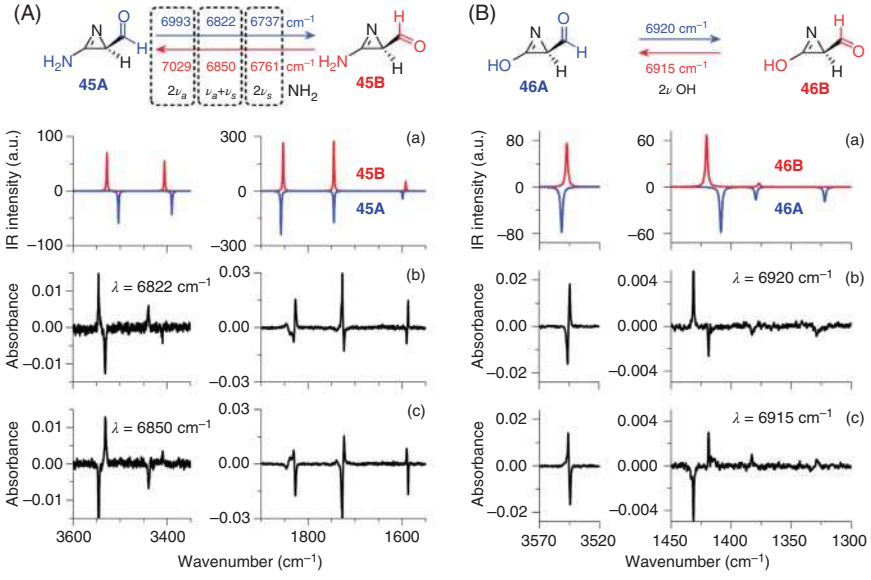

Figure 12.36 Conformational interconversions of a remove aldehyde induced by selective narrowband IR irradiation of the NH_2 antenna of **45** (A) and OH antenna of **46** (B). Left panel: (a) Computed IR spectra for **45A** (blue, intensities multiplied by −1) and **45B** (red) at the B3LYP/6311++G(d,p) level of theory; IR spectral changes resulting from irradiation of **45** isolated in an Ar matrix at 15 K, (b) at 6822 cm^{-1} and (c) at 6850 cm^{-1}. Right panel: Computed IR spectra for **46A** (blue, intensities multiplied by −1) and **46B** (red) at the B3LYP/6-311++G(d,p) level of theory; IR spectral changes resulting from irradiation of **46** isolated in an Ar matrix at 15 K, (b) at 6920 cm^{-1}, and (c) at 6915 cm^{-1}. In both panels, the positive bands grow upon IR irradiations. Source: Adapted from Lopes Jesus et al. [101], with permission from the Royal Society of Chemistry.

stretching vibrations and to the combination band [$\nu(NH_2)_a + \nu(NH_2)_s$]. In the case of **46**, a doublet band was identified covering the 6927–6910 cm^{-1} range, which was ascribed to the first overtone of the OH stretching vibrations [2ν(OH)] of **46A** and **46B**. The two aldehyde conformers of **45** and **46** (**A** and **B**) were then manipulated bidirectionally and reversibly by narrowband IR irradiation tuned at the identified frequencies of the NH_2 and OH vibrational antennas (Figure 12.36).

Finally, two examples reported by us demonstrate that vibrational excitation can also be used to induce and control bond-breaking/bond-forming reactions.

The first example was the discovery that broadband IR radiation induces electrocyclic ring expansion of benzazirine **47** to a cyclic ketenimine **48** (Figure 12.37) [102]. As it will be addressed in more detail in Section 12.6, we observed that upon generation of **47** in an argon matrix at 10 K, it undergoes spontaneous ring-expansion tunneling to cyclic ketenimine **48**. The process was measured to take place with a half-life time of $t_{1/2} \sim 260$ hours both under dark conditions or when the sample was kept permanently exposed to the IR light source of the spectrometer with a cutoff filter transmitting only below 2200 cm^{-1}. However, when the sample was kept permanently exposed to the IR light source of the spectrometer without any filter, the ring expansion was found to take place with a $t_{1/2} \sim 13$ hours, which clearly provides evidences of an IR-induced process. In a recent study not yet published, we were also able to demonstrate that by introducing appropriate substituents on the benzazirine **47**, the spontaneous tunneling can be suppressed, and exploitation of the use of a

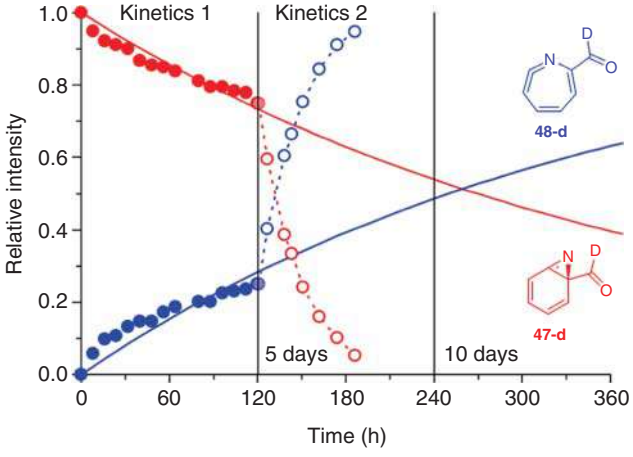

Figure 12.37 Kinetics of rearrangement of benzazirine **47**-d to cyclic ketenimine **48**-d in an argon matrix at 10 K. Kinetics 1 (initial five days, left): rearrangement of **47**-d [solid red circles, consumption] into **48**-d [solid blue circles, production] with the sample kept in the dark, except when the spectra were recorded, the sample was then protected by an infrared long-pass cutoff filter transmitting only below 2200 cm^{-1}. Kinetics 2 (after five days in the dark, right): rearrangement of **47**-d [empty red circles, consumption] into **48**-d [empty blue circles, production] with the sample permanently exposed to the IR light source of the FTIR spectrometer. Source: Adapted with permission from Nunes et al. [102]. Copyright 2017, American Chemical Society.

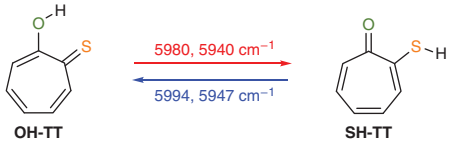

Figure 12.38 Bidirectional tautomerization in thiotropolone induced by vibrational excitation.

remote OH vibrational antenna to selectively trigger ring expansion to ketenimine **48** can be achieved.

The second example was the demonstration that bidirectional tautomerization of thiotropolone (**49**) can be achieved by vibrational excitation (Figure 12.38) [8]. Narrowband IR irradiations of the hydroxy-tautomer of thiotropolone (**OH-TT**) isolated in an argon matrix at the frequency of its first CH stretching overtone or combination modes lead to its conversion into the thiol-tautomer (**SH-TT**). The irradiations of the thiol-tautomer at the frequency of its first CH stretching overtone or combination modes lead to the reverse tautomerization.

These two unprecedented examples open prospects for new advances on IR vibrational excitation as a promising approach for gaining exceptional control of chemical reactions, in ways that cannot be attained via thermal or electronic excitations.

12.6 Tunneling in Heterocyclic Chemistry

QMT is a fascinating phenomenon that allows particles to penetrate through potential energy barriers regardless of insufficient thermal energy to surmount them [103]. In this way, QMT breaks the classic TST, commonly used by the organic chemistry community to rationalize molecular transformations [104, 105]. An interesting consequence is that a QMT reaction can lead to a product whose reaction path faces a higher barrier (compared to other *a priori* possible processes) and whose formation is then not expected on the basis of classic TST [106]. Such discovery led to the emerging of tunneling control as the third paradigm in chemical reactivity, next to the kinetic and thermodynamic control [11, 107].

For a chemical reaction under ordinary laboratory conditions, the existence of QMT contribution can be assessed indirectly by the observation of nonlinear Arrhenius plots or abnormal kinetic isotopic effects and typically results in an increase of the reaction rate compared to the expectations based on the classical TST [108]. On the other hand, under cryogenic conditions (e.g. 3–10 K), thermal activated rates are negligible for systems having barrier as low as 1 kcal mol^{-1} (~4 kJ mol^{-1}), and the occurrence of a chemical reaction can only be due to QMT from the vibrational ground state [7]. The rates of the reactions governed by QMT are usually temperature independent and, if occurring on the timescale of seconds to days, they can be directly observed using steady-state spectroscopic techniques [7].

In a simplified manner, the tunneling probability (P) depends linearly on the width of the barrier (w) and on the square root of both the moving mass (m) and the height of the barrier ($\Delta E^{\ddagger}$) (Eq. (12.1)) [109]. Therefore, QMT is expected to be particularly relevant for reactions involving the motion of light particles, like an electron, a

hydrogen atom, or a proton [109]. Although heavy atoms, such as carbon, have been assumed to behave classically for long, recent discoveries suggest that heavy-atom QMT can actually occur through very narrow and moderated to small energy barriers [7, 110, 111].

$$P \sim e^{-xw\sqrt{\Delta E^{\ddagger} m/\mathrm{h}}} \tag{12.1}$$

In this section, we will highlight examples described by our group regarding QMT reactions directly observed by matrix isolation spectroscopy. These comprise tunneling-driven chemical processes ranging from conformational isomerizations to H-atom and heavy-atom bond-breaking/bond-forming reactions, in which a heterocyclic compound is either a precursor, a reactant, or a product.

The story of our investigations on the photochemistry of 1,2-benzisoxazoles began with the goal of generating vinyl nitrenes [112–114] and ended up being the starting point for a series of discoveries on QMT-driven reactions.

UV irradiation of parent 1,2-benzisoxazole (**50**) was found to lead to 2-cyanophenol (**53**) via *spiro*-2*H*-azirine **51** and ketenimine **52** intermediates (Figure 12.39) [112]. Although in polar solvents the irradiation of **50** affords mainly 1,3-benzoxazole (**54**) [116], no trace of this species was observed in argon and nitrogen matrices [112]. UV irradiation of **54** was found to lead to 2-isocyanophenol (**55**), which was characterized as a kinetically unstable species that rearranges back to **54** upon thermal annealing or by UV irradiation (Figure 12.39) [115]. Intriguing, at that time, **53** and **55** in nitrogen matrices were generated in the *anti*-OH (**53a** and **55a**) and *syn*-OH (**53s** and **55s**) conformations, whereas in argon matrices only in the *syn*-OH (**53s** and **55s**) conformation [112, 115, 117].

In further investigations, it was discovered that keeping 2-cyanophenol (**53**) or 2-isocyanophenol (**55**) in a nitrogen matrix at 10 K, in the dark, resulted in a decrease of the population of the less stable **53a** or **55a** conformer and a concomitant increase of the population of the most stable **53s** or **55s** form [115, 117]. Fitting the kinetic data to a single-exponential equation, rate constants of $\sim 2.8 \times 10^{-4}$ and $\sim 3.2 \times 10^{-4}$ s^{-1} [corresponding to half-life times ($t_{1/2}$) of ~40 and ~36 minutes]

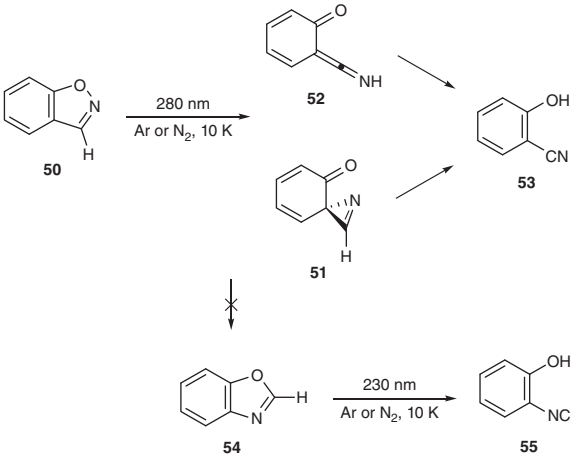

Figure 12.39 Photochemistry of 1,2-benzisoxazole (**50**) and 1,3-benzoxazole (**54**) in cryogenic matrices leads to 2-cyanophenol (**53**) and 2-isocyanophenol (**55**), respectively [112, 115].

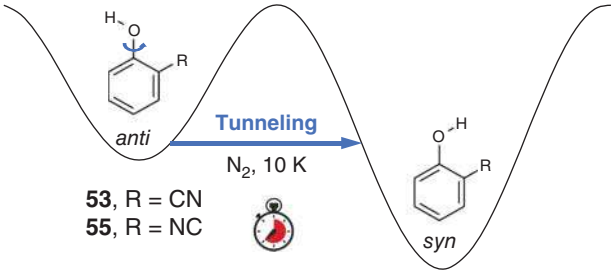

Figure 12.40 Conformational isomerization tunneling (*anti*-OH → *syn*-OH) of 2-cyanophenol (**53**) and 2-isocyanophenol (**55**) isolated in nitrogen matrices at 10 K [115, 117].

were estimated for the spontaneous **53a** → **53s** and **55a** → **55s** conformational isomerizations, respectively. These transformations cannot take place over the barrier [~12 and ~11 kJ mol^{-1}, respectively, at the B3LYP/6-311++G(d,p) level] due to the absence of enough thermal energy at such low temperatures and, therefore, should be governed by tunneling (Figure 12.40) [115, 117]. That was unequivocally confirmed upon increasing the temperature by a factor of 2 (from 10 to 20 K) and observing a negligible effect on the conformational isomerization rate constants.

The lack of detection of the **53a** and **55a** conformers in argon matrices was attributed to the occurrence of a much faster conformational isomerization by tunneling [115, 117]. This behavior has been reported for simple carboxylic acids having conformers differing by the OH rotation. For example, the OH isomerization tunneling of the higher energy conformers of formic and acetic acids was found to be approximately 55 and 600 times faster in argon matrices than in nitrogen matrices [118]. Apparently, this effect is due to the increased stability of the higher energy conformers in a nitrogen matrix as a result of the formation of specific OH$\cdots$N$_2$ interactions, which is associated with the fact that N$_2$ molecules have a permanent quadrupole moment and noble gas atoms do not [118].

Isomerization tunneling of higher energy conformers differing by an OH rotation were also observed for heterocyclic compounds such as 2-furoic acid [119], tetrazole-5-acetic acid [97], 2-hydroxy-3-nitropyridine [120], cytosine [94], and cytosine derivatives [62]. Indeed, isomerization tunneling seems to be a ubiquitous phenomenon on the conformational dynamic of monomeric molecules having an OH fragment.

The photochemistry of 2,1-benzisoxazole (**56**) was also investigated as a possible gateway to nitrenes. Irradiation of **56** in an argon matrix was shown to lead to the concomitant formation of several products, making their identification problematic. However, we discovered that one of the products, formed in trace amount, disappeared spontaneously when the sample was kept in the dark. This allowed us to record its spectral signature and identify it as the triplet 2-formylphenyl nitrene (*anti*-^{3}**58**). Nitrene *anti*-^{3}**58** was also generated via photolysis of 2-formyphenylazide (**57**) isolated in Ar, Kr, and Xe matrices and characterized by IR, UV–vis, and electron paramagnetic resonance (EPR) spectroscopies (Figure 12.41) [121].

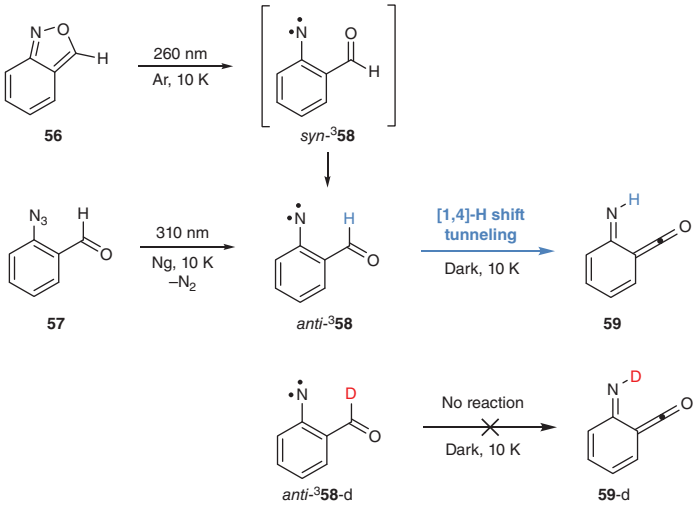

Figure 12.41 Summary of experimental observation regarding [1,4]-H-shift tunneling from triplet nitrene *anti*-^{3}**58** to imino-ketene **59** in cryogenic matrices at 10 K.

Upon its generation in matrices at 10 K, *anti*-^{3}**58** spontaneously rearranges in the dark to imino-ketene **59** (Figure 12.42). The kinetics of this transformation was monitored in an argon matrix, and a rate constant of $\sim 3 \times 10^{-5}$ s^{-1} ($t_{1/2} \sim 5.8$ hours) was measured, which implies a barrier of only ~0.8 kJ mol^{-1}, if determined using the classical TST. The existence of such low barrier is inconceivable, which suggests that the reaction proceeds via tunneling. Unequivocal evidences for [1,4]-H-shift tunneling from *anti*-^{3}**58** to **59** was provided by experiments with the deuterated derivative *anti*-^{3}**58**-d, which shows no conversion to **59**-d (see Figure 12.41) [121].

It is plausible that *anti*-^{3}**58** undergoes [1,4]-H-shift tunneling on the triplet surface to ^{3}**59**, followed by intersystem crossing (ISC) to singlet ground state **59**. Computations at different levels of theory on this triplet surface estimate a reaction barrier around c. 82 kJ mol^{-1}, which precludes any contribution from a classical thermal over-the-barrier process. B3LYP/6-311++G(d,p) computations provide a barrier with a height of 72.8 kJ mol^{-1} and a width of 1.3–1.4 Å. The tunneling probabilities of the H and D atoms penetration through such barrier were assessed based on the Wentzel–Kramers–Brillouin (WKB) approximation, which provided half-lives times on the order of tens-of-minutes/hours and 10^5 years, respectively, in agreement with the experimental observations [121]. This example constituted the first direct experiment evidence of a tunneling reaction involving a nitrene species.

In subsequent investigations, it was found that irradiation of protium or deuterated triplet 2-formylphenylnitrene (^{3}**58**) with visible light (530 nm) generates benzazirine **60**. Interestingly, in this way, we then discovered the heavy-atom tunneling reaction involving the spontaneous ring expansion of **60** into its isomeric cyclic ketenimine **61** (Figure 12.43) [102]. In an argon matrix at 10 K, the reaction takes place with a rate constant of $\sim 7.4 \times 10^{-7}$ s^{-1} ($t_{1/2} \sim 260$ hours), despite a reaction

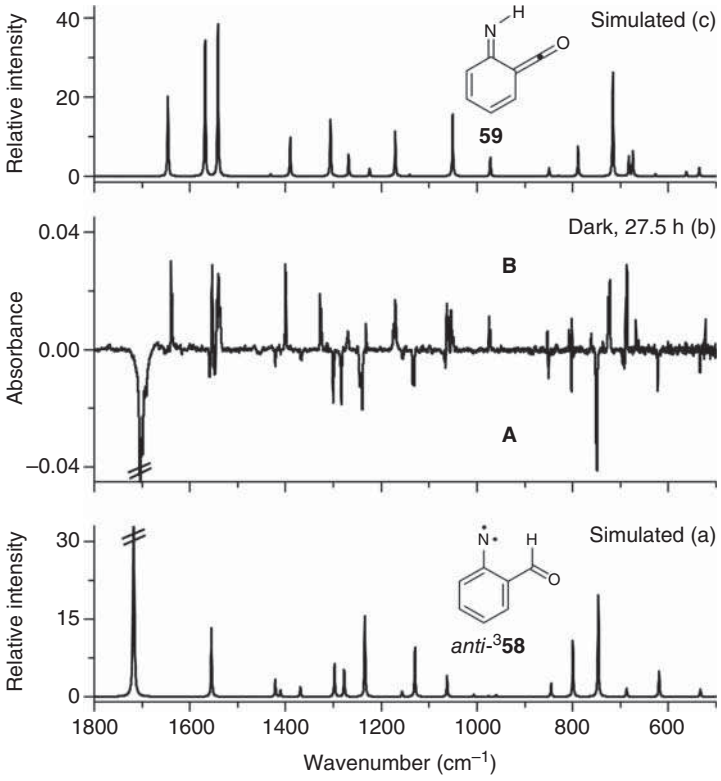

Figure 12.42 (a) B3LYP/6-311++G(d,p) computed IR spectrum of imino-ketene **59**. (b) Spontaneous changes in the IR spectrum upon keeping the sample for 27.5 hours in the dark, after UV irradiation (308 nm) of 2-formylphenylazide (**57**) isolated in Ar matrix at 10 K. (c) B3LYP/6-311++G(d,p) computed IR spectrum of triplet nitrene *anti*-^{3}**58**. Source: Adapted with permission from Nunes et al. [121]. Copyright 2016, American Chemical Society.

barrier of 31.4 kJ mol^{-1} estimated at the CCSD(T)//M06-2X level of theory. Solid evidence for the occurrence of the heavy-atom tunneling process was provided by the observation of the almost invariance of the reaction rate ($\sim 8.9 \times 10^{-7}$ s^{-1} at 20 K) upon increasing the temperate by a factor of 2. Computed rate constants without (1.8×10^{-177} s^{-1}) and with tunneling (3.5×10^{-5} s^{-1}) consideration (using canonical variational transition state theory [CVT] and small curvature tunneling [SCT]) confirmed that the observed spontaneous process can only occurs by heavy-atom tunneling [102].

McMahon, Sander, and coworkers reported heavy-atom tunneling in other benzazirine derivatives by matrix isolation spectroscopy (Figure 12.44) [122, 123]. They found that the type, position, and conformation of a substituent can enormously influence the tunneling probability of benzazirines ring expansion to cyclic ketenimines. While some substituents provide the right tunneling rates for observations by steady-state spectroscopy, others make tunneling rates too slow or too fast for detection. In the cases where the tunneling rate is too fast, the molecular system

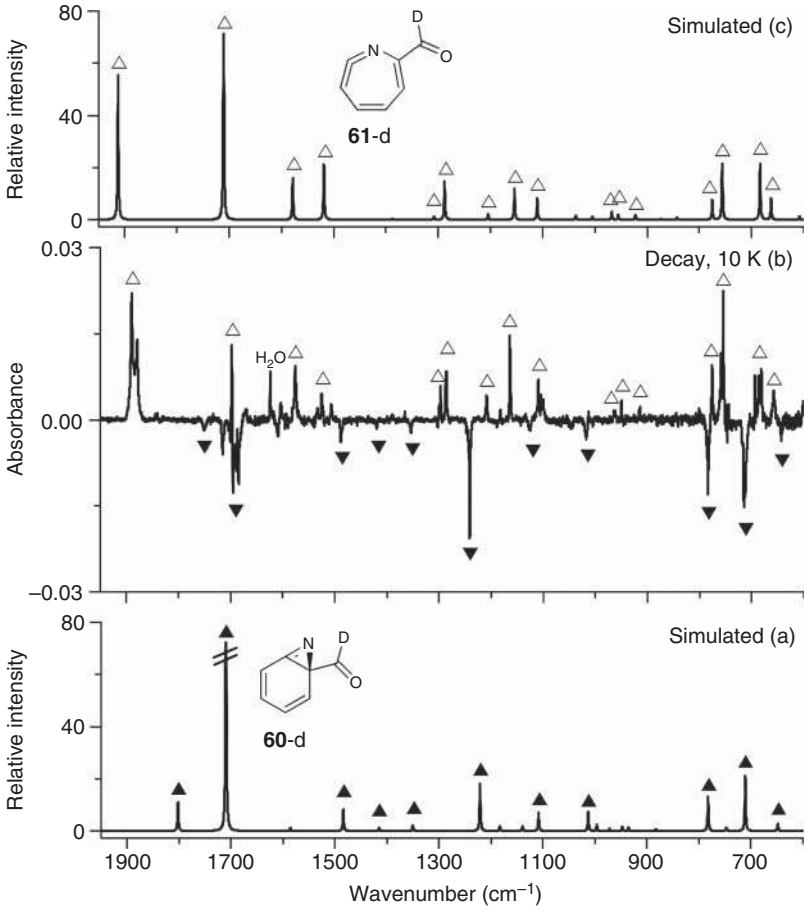

Figure 12.43 (a) B3LYP/6-311++G(d,p) computed IR spectrum of benzazirine **60-**d. (b) Spontaneous changes in the IR spectrum upon keeping the sample in an argon matrix at 10 K for three days, after irradiation (530 nm) of 2-formylphenynitrene ^{3}**58-**d. (c) B3LYP/6-311++G(d,p) computed IR spectrum of cyclic ketenimine **61-**d. Source: Adapted with permission from Nunes et al. [102]. Copyright 2017, American Chemical Society.

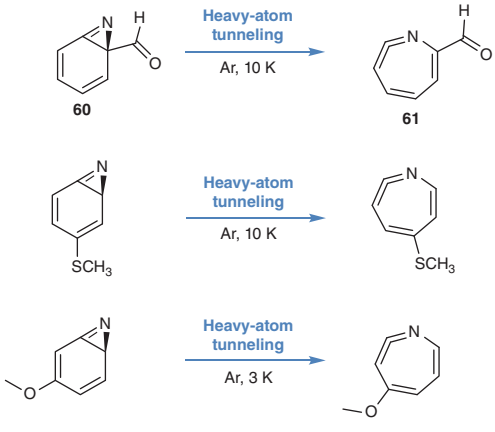

Figure 12.44 Heavy-atom tunneling ring expansion of benzazirine derivatives to cyclic ketenimines, directly observed by matrix isolation steady-state spectroscopy [102, 122, 123].

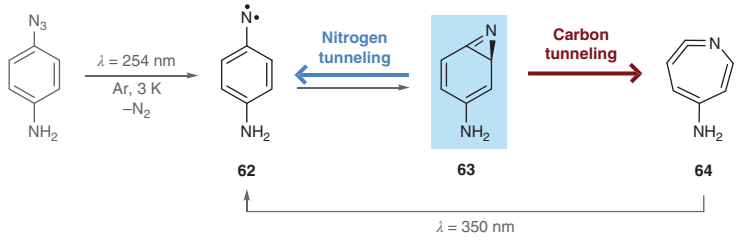

Figure 12.45 Summary of the UV-induced reactions and the observed competitive tunneling ring open versus ring expansion of benzazirine **63** to triplet nitrene ^{3}**62** and cyclic ketenimine **64**, respectively.

is characterized as having quantum tunneling instability, and, therefore, although having a structure corresponding to a local minimum on the PES, it is not a stable observable molecule even at cryogenic temperatures [124].

Remarkably, we have recently discovered that tunneling reactions can even be competitive and, thereby, determine the selectivity outcome of a reaction that cannot be predicted based of the classic TST model. Upon the generation of 4-amino-2*H*-benzazirine (**63**) in an argon matrix at 3 K, it was found that this compound spontaneous decay in the dark to concomitantly yield two different products, the triplet nitrene ^{3}**62** and the cyclic ketenimine **64** (Figures 12.45) [9]. Following the process by IR spectroscopy (Figure 12.46), the detail identification of **63** was established with the support of its B3LYP/6-311+G(2d,p) computed IR spectrum, whereas the identification of ^{3}**62** and **64** was performed based on the IR signature of these two species, which were obtained upon selective conversion of **64** to ^{3}**62** by irradiation at 350 nm. A rate constant of $\sim 5.5 \times 10^{-5}$ s^{-1} ($t_{1/2} \sim 210$ minutes) and a product ratio ^{3}**62** : **64** of 15 : 85 was measured. Increasing the absolute temperature by a factor up to five (up to 18 K) barely produced any change in both the rate constant and the product ratio, confirming that the decay of **63** and the formation of ^{3}**62** and **64** were not due to thermal over-the-barrier processes but to two independent and competitive heavy-atom tunneling reactions [9].

The ring opening of **63** should lead to an open-shell singlet (OSS) ^{1}**62**, which then relaxes fast by ISC to triplet ground state ^{3}**62**. For that process, computations at NEVPT2(8,8)//CASSCF(8,8) multiconfigurational level predict an energy barrier of ~10 kJ mol^{-1} [9]. For the ring expansion of **63** to **64**, computations at CCSD(T)//B3LYP level predict an energy barrier of ~30 kJ mol^{-1}. These barriers are clearly prohibitive for a thermal activated process to take place at the experimental cryogenic temperatures. Moreover, the major product **64** faces a higher energy barrier than the minor product ^{3}**62**, which cannot be explained based on the classical TST. The computed tunneling probabilities through these barriers, applying the WKB formalism, predict the existence of two competitive tunneling reactions in accordance with the experimental observations. The ring opening **63** → ^{1}**62** is predominantly a case of nitrogen-atom tunneling, since the nitrogen atom in the three-membered ring is the heavy atom having by far the largest displacement. On the other hand, the ring expansion **63** → **64** is predominantly a case of carbon-atom

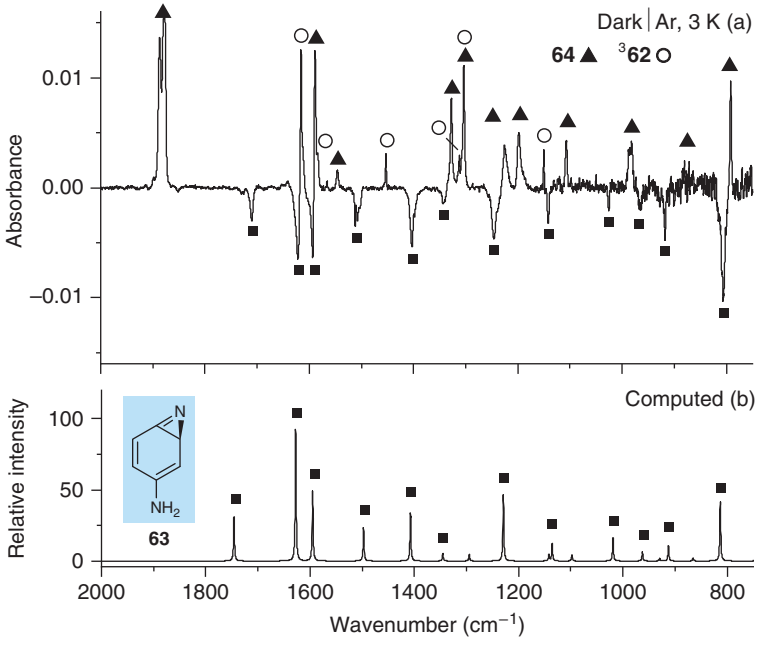

Figure 12.46 (a) Experimental difference IR spectrum showing changes after keeping the sample at 3 K (argon matrix) in the dark for 24 hours, subsequent to depletion of nitrene ^{3}**62** at 435 nm. The downward bands are due to the consumption of **63**. The upward bands arise from the formation of both ^{3}**62** and **64**. (b) B3LYP/6-311+G(2d,p) computed IR spectrum of benzazirine **63**. Source: Adapted with permission from Nunes et al. [9]. Copyright 2019, American Chemical Society.

tunneling, since the two carbon atoms in the three-membered ring are clearly the heavy atoms with the largest displacements [9].

Our most recent (2020) example of heavy-atom tunneling was discovered in continuation of our studies with 2-formylphenyl nitrenes. The precursor 2-formyl-3-fuorophenylazide (**65**) was designed to achieve stabilization of the *syn*-aldehyde conformation; the fluorine atom acts as a hydrogen bond acceptor for aldehyde hydrogen [10]. That conformational tuning provided access to triplet *syn*-2-formylphenyl nitrene ^{3}**66** via UV irradiation of **65** isolated in argon matrix (Figure 12.47). Triplet nitrene ^{3}**66** was then observed to spontaneously cyclize in the dark to 2,1-benzisoxazole **67**. The kinetics of the process was followed by IR spectroscopy, and a rate constant of $\sim 1.4 \times 10^{-3}$ s^{-1} ($t_{1/2} \sim 8$ minutes) was measured at 10, 15, and 20 K. The fast and temperature-independent cyclization of ^{3}**66** to **67** at extremely low temperatures provided strong arguments for the occurrence of a heavy-atom tunneling process. Computations indicated that ^{3}**67** is much more energetic than ^{3}**66**, preluding the possibility of a tunneling event on the triplet surface (which followed by ISC would give singlet ground state **67**). A minimum energy crossing point was located at ~50 kJ mol^{-1} (MRMP(10,10)//CASSCF(10,10) level) connecting the triplet surface of ^{3}**66** and the singlet surface of **67** (Figure 12.48). Calculations based on non-adiabatic models [10] estimated rate constants in fair

Figure 12.47 Summary of experimental observation regarding heavy-atom tunneling cyclization of triplet nitrene ^{3}**66** to 2,1-benzisoxazole **67** in argon matrix at 10 K.

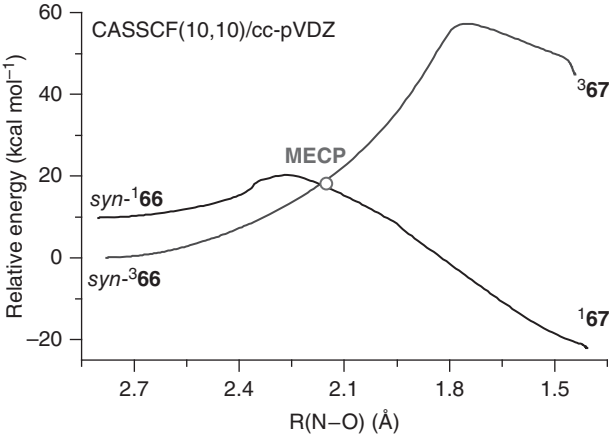

Figure 12.48 Intrinsic reaction coordinate (IRC) path for the cyclization of ^{3}**66** to **67** on the singlet (gray) and triplet (black) surfaces computed the CASSCF/cc-pVDZ level of theory as a function of the N…O distance (Å). The minimum energy crossing point (MECP) is shown in an open circle. To include dynamic correlations, single point energies were subsequently computed at MRMR level of theory. Source: Adapted from Nunes et al. [10], with permission from John Wiley and Sons. Copyright 2020, WILEY-VCH Verlag GmbH & Co. KGaA, Weinheim.

agreement with experimental values, providing evidence for a mechanism of heavy-atom tunneling from ^{3}**66** to **67** through crossing triplet and singlet potential energy surfaces. Another feature that makes this heavy-atom tunneling reaction distinctive is the considerable displacement of the oxygen atom along the process, which puts a new limit for the heavier atom that can significantly participate in a tunneling reaction under low-temperature matrix isolation conditions.

Finally, we are aware of only two additional examples of tunneling directly observed by matrix isolation spectroscopy in the context of heterocyclic chemistry. One of such examples was reported by Gerbig and Schreiner demonstrating that ketene **69**, prepared by irradiation of *o*-nitrobenzaldehyde (**68**), rearranges spontaneously to isoxazolone **70** via tunneling, at temperatures as low as 3 K (Figure 12.49a) [106]. Interestingly, based on computations performed at the CCSD(T)//MP2 level, **70** is neither thermodynamically nor kinetically favored, because the pathway to the energetically more stable product **71** has a lower energy barrier. Therefore, **70** constitutes an intriguing tunneling product. The other example was reported by Schleif et al. [125], who showed that the equilibrium between benzene oxide (**72**) and oxepin (**73**) is governed by heavy-atom tunneling

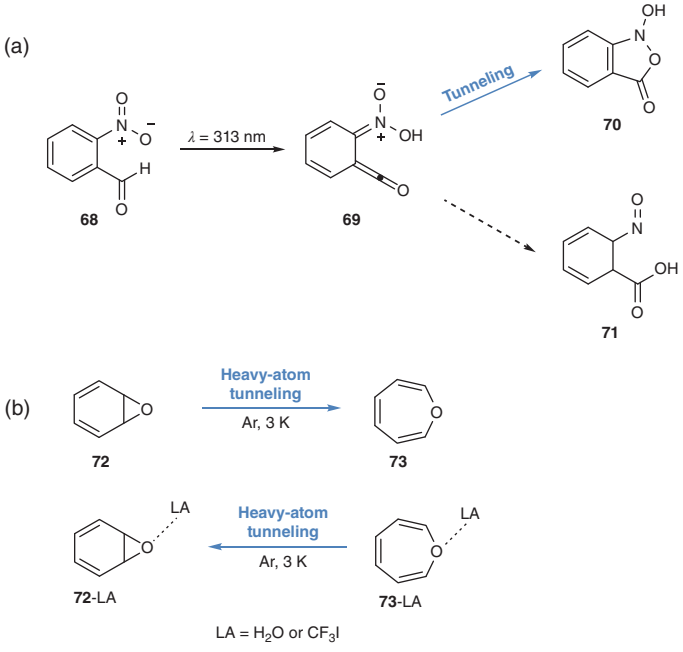

Figure 12.49 Additional examples of tunneling directly observed by matrix isolation spectroscopy: (a) the rearrangement of ketene **69** to isoxazolone **70**; (b) the transformation between benzene oxide (**72**) and oxepin (**73**).

(Figure 12.49b). In argon matrices at 3 K, **72** rearranges to **73** by tunneling, which conciliates well with results from CCSD(T) computations that estimate **73** to be more stable by 3.8 kJ mol^{-1}. When the matrix is doped with H_2O or CF_3I (LA), the **73**…**LA** complexes formed upon annealing rearrange by tunneling to **72**…**LA**, which conciliates also well with computations that estimate the non-covalent complexes **72**…**LA** to be more stable than the **73**…**LA** species by 2.5–3.8 kJ mol^{-1} [125].

12.7 Conclusion and Perspectives

As discussed in this chapter, matrix isolation has given major contributions to the field of heterocyclic chemistry since its debut in the 1950s. Noteworthy, as mentioned in the Introduction section, it was its application to a heterocyclic reaction (the photochemistry of α-pyrone [3–5]) that made it popular among the organic chemists community.

Recent developments in the technique, as well as in the auxiliary instrumentation (particularly in lasers, but also the appearance of more sensitive detectors for IR spectrometers), have allowed matrix isolation to be used, nowadays, to extract detailed mechanistic insights on reactions involving heterocyclic compounds in an unprecedented way. In particular, when narrowband light is used, excitation of a

given reactant or intermediate can be performed in a very selective way. This gives access, frequently, to the possibility to follow individual steps of the reaction, one at a time, in an exclusive way. Besides, the cage effect most of the time simplifies extraordinarily the chemical processes, precluding undesired reactions involving recombination of fragments initially produced from different molecules, so that unimolecular chemistry is easily accessible.

The examples we provided in this chapter illustrate clearly the potential of the technique when combined with IR spectroscopy to address both photochemical reactions (either resulting from UV–vis or IR excitation) and thermal processes. We also showed that tunneling-driven reactions can also be followed *directly* under matrix isolation conditions, and this possibility has opened a new field of research in this area. In this domain, recent studies like those described in this chapter have demonstrated that QMT is in fact more relevant in organic chemistry than it has been considered hitherto. Moreover, other detection techniques can also be used together with matrix isolation, and these may considerably expand the range of application of the method in the field of heterocyclic chemistry (and in organic chemistry in general), like EPR, for the detection of radicals and other species with unshared electrons, or Raman spectroscopy, including resonance Raman, which may open an entirely new field of studies on systems where more complex species play a major role.

Acknowledgments

The authors thank the Portuguese Science Foundation (*Fundação para a Ciência e a Tecnologia* (FCT)), Lisbon (Portugal), for the financial support through Projects PTDC/QUI-QFI/1880/2020, POCI-01-0145-FEDER-028973, UIDB/QUI/0313/2020, and UIDP/QUI/0313/2020, also co-funded by FEDER (via Portugal 2020-POCI) or by COMPETE-UE. C.M. Nunes and J.P.L. Roque also acknowledge FCT for an Auxiliary Researcher grant and a PhD (2020.04467.BD) grant, respectively. We also thank all members of the Laboratory of Molecular Cryospectroscopy and Biospectroscopy (LMCB) of the Coimbra Chemistry Centre (present and past) as well as our coauthors from other research laboratories who participated in the studies mentioned in this chapter.

References

1 Whittle, E., Dows, D.A., and Pimentel, G.C. (1954). *J. Chem. Phys.* 22: 1943–1944. https://doi.org/10.1063/1.1739957.

2 Norman, I. and Porter, G. (1954). *Nature* 174: 508–509. https://doi.org/10.1038/174508a0.

3 Lin, C.Y. and Krantz, A. (1972). *J. Chem. Soc. Chem. Commun.* 1111–1112. https://doi.org/10.1039/C39720001111.

4 Chapman, O.L., McIntosh, C.L., and Pacansky, J. (1973). *J. Am. Chem. Soc.* 95 (1): 244–246. https://doi.org/10.1021/ja00782a047.

5 Pong, R.G.S. and Shirk, J.S. (1973). *J. Am. Chem. Soc.* 95 (1): 248–249. https://doi.org/10.1021/ja00782a049.

6 Breda, S., Reva, I., Lapinski, L., and Fausto, R. (2004). *Phys. Chem. Chem. Phys.* 6 (5): 929–937. https://doi.org/10.1039/B309660B.

7 Nunes, C.M., Reva, I., and Fausto, R. (2021). Direct observation of tunneling reactions by matrix isolation spectroscopy. In: *Tunnelling in Molecules: Nuclear Quantum Effects from Bio to Physical Chemistry*, Theoretical and Computational Chemistry Series, N° 18, Chapter 1 (ed. J. Kästner and S. Kozuck), 1–60. London, UK: Royal Society of Chemistry.

8 Nunes, C.M., Pereira, N.A.M., Reva, I. et al. (2020). *J. Phys. Chem. Lett.* 11 (19): 8034–8039. https://doi.org/10.1021/acs.jpclett.0c02272.

9 Nunes, C.M., Eckhardt, A.K., Reva, I. et al. (2019). *J. Am. Chem. Soc.* 141 (36): 14340–14348. https://doi.org/10.1021/jacs.9b06869.

10 Nunes, C.M., Viegas, L.P., Wood, S.A. et al. (2020). *Angew. Chem. Int. Ed.* 59 (40): 17622–17627. https://doi.org/10.1002/anie.202006640.

11 Schreiner, P.R. (2017). *J. Am. Chem. Soc.* 139 (43): 15276–15283. https://doi.org/10.1021/jacs.7b06035.

12 Fausto, R., Reva, I.D., and Gómez-Zavaglia, A. (2007). Matrix isolation spectroscopy in heterocyclic chemistry. In: *Recent Research Developments in Heterocyclic Chemistry* (ed. T.M.V.D. Pinho e Melo and A.M.'.A. Rocha Gonsalves). Kerala, India: Research Signpost, Chapter 7.

13 Meyer, B. (1971). *Low Temperature Spectroscopy*. New York, USA: American Elsevier Publishers Company.

14 Andrews, L. and Moskovits, M. (1989). *Chemistry and Physics of Matrix Isolated Species*. Amsterdam, Holland: Elsevier.

15 Barnes, A., Orville-Thomas, W.J., Gaufrès, R., and Müller, A. (1981). *Matrix Isolation Spectroscopy*. London, UK: Springer.

16 Dunkin, I.R. (1998). *Matrix Isolation Techniques: A Practical Approach*. Oxford, UK: Oxford University Press.

17 Fausto, R. (1996). *Low Temperature Molecular Spectroscopy*, NATO-ASI Series C483. Amsterdam, Holland: Kluwer.

18 Khriachtchev, L. (2011). *Physics and Chemistry at Low Temperatures*. New York, USA: Jenny Stanford Publishing.

19 Frija, L.M.T., Cristiano, M.L.S., Gómez-Zavaglia, A. et al. (2014). *J. Photochem. Photobiol. C: Photochem. Rev.* 18: 71–90. https://doi.org/10.1016/j.jphotochemrev.2013.09.001.

20 Nunes, C.M., Gudmundsdottir, A.D., and Fausto, R. Special Issue: Structure, Spectroscopy and Chemistry of Reactive Species (2018). *J. Mol. Struct.* 1172.

21 Breda, S., Reva, I.D., Lapinski, L. et al. (2006). *J. Mol. Struct.* 786 (2–3): 193–206. https://doi.org/10.1016/j.molstruc.2005.09.010.

22 Lobastov, V.A., Srinivasan, R., Goodson, B.M. et al. (2001). *J. Phys. Chem. A* 105 (50): 11159–11164. https://doi.org/10.1021/jp013705b.

23 Kanamaru, N. (1998). *Bull. Chem. Soc. Jpn.* 71 (10): 2299–2308. https://doi.org/10.1246/bcsj.71.2299.

24 Domcke, W., Sobolewski, A.L., and Woywod, C. (1993). *Chem. Phys. Lett.* 203 (2–3): 220–226. https://doi.org/10.1016/0009-2614(93)86391-Z.

25 Sobolewski, A.L., Woywod, C., and Domcke, W. (1993). *J. Chem. Phys.* 98 (7): 5627–5641. https://doi.org/10.1063/1.464907.

26 Lopes, S., Nunes, C.M., Fausto, R., and Pinho e Melo, T.M.V.D. (2009). *J. Mol. Struct.* 919 (1–3): 47–53. https://doi.org/10.1016/j.molstruc.2008.08.014.

27 Pinho e Melo, T.M.V.D., Lopes, C.S.J., Rocha Gonsalves, A.M.'.A., and Storr, R.C. (2002). *Synthesis* 5: 605–608. https://doi.org/10.1055/s-2002-23542.

28 Palacios, F., Retana, A.M.O., Marigorta, E.M., and Santos, J.M. (2001). *Eur. J. Org. Chem.* 2001 (13): 2401–2414. https://doi.org/10.1002/1099-0690(200107)2001:13<2401::AID-EJOC2401>3.0.CO;2-U.

29 Gómez-Zavaglia, A., Kaczor, A., Cardoso, A.L. et al. (2006). *J. Phys. Chem. A* 110 (26): 8081–8092. https://doi.org/10.1021/jp062094q.

30 Kaczor, A., Gómez-Zavaglia, A., Cardoso, A.L. et al. (2006). *J. Phys. Chem. A* 110 (37): 10742–10749. https://doi.org/10.1021/jp064049o.

31 Gómez-Zavaglia, A., Kaczor, A., Cardoso, A.L. et al. (2007). *J. Mol. Struct.* 834–836: 262–269. https://doi.org/10.1016/jmolstruc.2006.12.027.

32 Inui, H. and Murata, S. (2002). *Chem. Phys. Lett.* 359 (3–4): 267–272. https://doi.org/10.1016/S0009-2614(02)00708-X.

33 Inui, H. and Murata, S. (2005). *J. Am. Chem. Soc.* 127 (8): 2628–2636. https://doi.org/10.1021/ja040109x.

34 Reva, I., Almeida, B.J.A.N., Lapinski, L., and Fausto, R. (2012). *J. Mol. Struct.* 1025: 74–83. https://doi.org/10.1016/j.molstruc.2011.11.051.

35 Piacenza, M. and Grimme, S. (2004). *J. Comput. Chem.* 25 (1): 83–89. https://doi.org/10.1002/jcc.10365.

36 Taft, R.W., Anvia, F., Taagepera, M. et al. (1986). *J. Am. Chem. Soc.* 108 (12): 3237–3239. https://doi.org/10.1021/ja00272a013.

37 Lopes Jesus, A.J., Reva, I., Araujo-Andrade, C., and Fausto, R. (2006). *J. Chem. Phys.* 144 (12): 124306. https://doi.org/10.1063/1.4944528.

38 Lopes Jesus, A.J., Fausto, R., and Reva, I. (2017). *J. Phys. Chem. A* 121 (18): 3372–3382. https://doi.org/10.1021/acs.jpca.7b01713.

39 Weinhold, F. and Landis, C.R. (2005). *Valency and Bonding: A Natural Bond Orbital Donor–Acceptor Perspective*. New York, USA: Cambridge University Press.

40 Reid, S.T. (1970). *Adv. Heterocycl. Chem.* 11: 1–121. https://doi.org/10.1016/S0065-2725(08)60774-6.

41 Klán, P. and Wirz, J. (2009). *Photochemistry of Organic Compounds: From Concepts to Practice*. Chichester, UK: Wiley.

42 Sobolewski, A.L., Domcke, W., Dedonder-Lardeux, C., and Jouvet, C. (2002). *Phys. Chem. Chem. Phys.* 4 (7): 1093–1100. https://doi.org/10.1039/B110941N.

43 Lin, M.F., Tseng, C.M., Lee, Y.T., and Ni, C.K. (2005). *J. Chem. Phys.* 123 (12): 124303. https://doi.org/10.1063/1.2009736.

44 Nix, M.G.D., Devine, A.L., Cronin, B., and Ashfold, M.N.R. (2006). *Phys. Chem. Chem. Phys.* 8 (22): 2610–2618. https://doi.org/10.1039/B603499C.

45 Orville-Thomas, W.J. (1981). *The history of matrix isolation spectroscopy*. In: *Matrix Isolation Spectroscopy* (ed. A.J. Barnes, W.J. Orville-Thomas, A. Müller and R. Gaufrès), 1–11. London, UK: Springer.

46 Reva, I., Lapinski, L., Lopes Jesus, A.J., and Nowak, M.J. (2017). *J. Chem. Phys.* 147 (19): 194304. https://doi.org/10.1063/1.5003326.

47 Chmura, B., Rode, M.F., Sobolewski, A.L. et al. (2008). *J. Phys. Chem. A* 112 (51): 13655–13661. https://doi.org/10.1021/jp8070986.

48 Lopes Jesus, A.J., Reva, I., and Fausto, R. (2017). *J. Photochem. Photobiol. A Chem.* 336: 123–130. https://doi.org/10.1016/j.jphotochem.2016.12.024.

49 Lopes Jesus, A.J., Rosado, M.T.S., Fausto, R., and Reva, I. (2020). *Phys. Chem. Chem. Phys.* 22 (40): 22943–22955. https://doi.org/10.1039/D0CP04354K.

50 Nowak, M.J., Reva, I., Rostkowska, H., and Lapinski, L. (2017). *Phys. Chem. Chem. Phys.* 19 (18): 11447–11454. https://doi.org/10.1039/C7CP01363A.

51 Lapinski, L., Nowak, M.J., and Rostkowska, H. (2017). *J. Chem. Phys.* 146 (9): 094306. https://doi.org/10.1063/1.4977604.

52 Feyer, V., Plekan, O., Richter, R. et al. (2009). *J. Phys. Chem. A* 113 (19): 5736–5742. https://doi.org/10.1021/jp900998a.

53 Szczesniak, M., Kwiatkowski, J.S., Szczepaniak, K. et al. (1988). *J. Am. Chem. Soc.* 110 (25): 8319–8330. https://doi.org/10.1021/ja00233a006.

54 Nowak, M.J., Lapinski, L., and Fulara, J. (1989). *Spectrochim. Acta, Part A* 45 (2): 229–242. https://doi.org/10.1016/0584-8539(89)80129-1.

55 Brown, R.D., Godfrey, P.D., McNaughton, D., and Pierlot, A.P. (1989). *J. Am. Chem. Soc.* 111 (6): 2308–2310. https://doi.org/10.1021/ja00188a058.

56 Nir, E., Müller, M., Grace, L.I., and De Vries, M.S. (2002). *Chem. Phys. Lett.* 355 (1–2): 59–64. https://doi.org/10.1016/S0009-2614(02)00180-X.

57 Lapinski, L., Reva, I., Nowak, M.J., and Fausto, R. (2011). *Phys. Chem. Chem. Phys.* 13 (20): 9676–9684. https://doi.org/10.1039/C0CP02812F.

58 Trygubenko, S.A., Bogdan, T.V., Rueda, M. et al. (2002). *Phys. Chem. Chem. Phys.* 4 (17): 4192–4203. https://doi.org/10.1039/B202156K.

59 Ruiz, D.S., Cembran, A., Garavelli, M. et al. (2002). *Photochem. Photobiol.* 76 (6): 622–633. https://doi.org/10.1562/0031-8655(2002)076<0622:SOTCID>2.0.CO;2.

60 King, G.A., Oliver, T.A.A., and MNR, A. (2010). *J. Chem. Phys.* 132 (21): 214307. https://doi.org/10.1063/1.3427544.

61 Reva, I., Nowak, M.J., Lapinski, L., and Fausto, R. (2012). *J. Phys. Chem. B* 116 (19): 5703–5710. https://doi.org/10.1021/jp302375u.

62 Lapinski, L., Reva, I., Rostkowska, H. et al. (2014). *J. Phys. Chem. B* 118 (11): 2831–2841. https://doi.org/10.1021/jp411423c.

63 Lapinski, L., Rostkowska, H., Khvorostov, A. et al. (2003). *J. Phys. Chem. A* 107 (31): 5913–5919. https://doi.org/10.1021/jp035155i.

64 Nunes, C.M., Reva, I., Rosado, M.T.S., and Fausto, R. (2015). *Eur. J. Org. Chem.* 2015 (34): 7484–7493. https://doi.org/10.1002/ejoc.201501153.

65 Gómez-Zavaglia, A., Reva, I.D., Frija, L.M.T. et al. (2008). Photochemistry of tetrazole derivatives in cryogenic rare gas matrices. In: *Photochemistry Research Progress* (ed. A. Sánchez and S.J. Gutierrez), 295–324. New York, USA: Nova Science Publishers.

66 Maier, G., Eckwert, J., Bothur, A. et al. (1996). *Liebigs Ann.* 1996 (7): 1041–1053. https://doi.org/10.1002/jlac.199619960704.

67 Bugalho, S.C.S., Maçôas, E.M.S., Cristiano, M.L.S., and Fausto, R. (2001). *Phys. Chem. Chem. Phys.* 3 (17): 3541–3547. https://doi.org/10.1039/B103344C.

68 Huisgen, R., Seidel, M., Sauer, J. et al. (1959). *J. Org. Chem.* 24 (6): 892–893. https://doi.org/10.1021/jo01088a034.

69 Tasdelen, M.A. and Yagci, Y. (2013). *Angew. Chem. Int. Ed.* 52 (23): 5930–5938. https://doi.org/10.1002/anie.201208741.

70 Lim, R.K.V. and Lin, Q. (2011). *Acc. Chem. Res.* 44 (9): 828–839. https://doi.org/10.1021/ar200021p.

71 Bégué, D., Qiao, G.G., and Wentrup, C. (2012). *J. Am. Chem. Soc.* 134 (11): 5339–5350. https://doi.org/10.1021/ja2118442.

72 Bégué, D. and Wentrup, C. (2014). *J. Org. Chem.* 79 (3): 1418–1426. https://doi.org/10.1021/jo402875c.

73 Nunes, C.M., Araujo-Andrade, C., Fausto, R., and Reva, I. (2014). *J. Org. Chem.* 79 (8): 3641–3646. https://doi.org/10.1021/jo402744f.

74 Gómez-Zavaglia, A., Reva, I.D., Frija, L. et al. (2006). *J. Photochem. Photobiol. A Chem.* 180 (1–2): 175–183. https://doi.org/10.1016/j.jphotochem.2005.10.012.

75 Ismael, A., Fausto, R., and Cristiano, M.L.S. (2016). *J. Org. Chem.* 81 (23): 11656–11663. https://doi.org/10.1021/acs.joc.6b02023.

76 Ullman, E.F. and Singh, B. (1966). *J. Am. Chem. Soc.* 88 (8): 1844–1845. https://doi.org/10.1021/ja00960a066.

77 Sauers, R.R. and Van Arnum, S.D. (1987). *Tetrahedron Lett.* 28 (47): 5797–5800. https://doi.org/10.1016/S0040-4039(01)81056-X.

78 Pavlik, J.W., Martin, H.S.T., Lambert, K.A. et al. (2005). *J. Heterocyclic Chem.* 42 (2): 273–281. https://doi.org/10.1002/jhet.5570420215.

79 Nunes, C.M., Reva, I., Pinho e Melo, T.M.V.D., and Fausto, R. (2012). *J. Org. Chem.* 77 (19): 8723–8732. https://doi.org/10.1021/jo301699z.

80 Nunes, C.M., Reva, I., Pinho Melo, T.M.V.D. et al. (2011). *J. Am. Chem. Soc.* 133 (46): 18911–18923. https://doi.org/10.1021/ja207717k.

81 Nunes, C.M., Reva, I., and Fausto, R. (2013). *J. Org. Chem.* 78 (21): 10657–10665. https://doi.org/10.1021/jo4015672.

82 Pérez, J.D., Yranzo, G.I., and Wunderlin, D.A. (1982). *J. Org. Chem.* 47 (6): 982–984. https://doi.org/10.1021/jo00345a017.

83 Pérez, J.D. and Wunderlin, D.A. (1986). *Int. J. Chem. Kinet.* 18 (12): 1333–1340. https://doi.org/10.1002/kin.550181205.

84 Murature, D.A., Pérez, J.D., De Bertorello, M.M., and Bertorello, H.E. (1976). *An. Asoc. Quim. Argent.* 64: 337.

85 Pérez, J.D., de Diaz, R.G., and Yranzo, G.I. (1981). *J. Org. Chem.* 46 (17): 3505–3508. https://doi.org/10.1021/jo00330a025.

86 Tanaka, H., Osamura, Y., Matsushita, T., and Nishimoto, K. (1981). *Bull. Chem. Soc. Jpn.* 54 (5): 1293–1298. https://doi.org/10.1246/bcsj.54.1293.

87 Parasuk, V. and Cramer, C.J. (1996). *Chem. Phys. Lett.* 260 (1–2): 7–14. https://doi.org/10.1016/0009-2614(96)0865-2.

88 Nunes, C.M., Reva, I., and Fausto, R. (2019). *Phys. Chem. Chem. Phys.* 21 (45): 24993–25001. https://doi.org/10.1039/C9CP05070A.

89 Góbi, S., Reva, I., Csonka, I.P. et al. (2019). *Phys. Chem. Chem. Phys.* 21 (45): 24935–24949. https://doi.org/10.1039/C9CP05370K.

90 Fausto, R., Khriachtchev, L., and Hamm, P. (2010). Conformational changes in cryogenic matrices. In: *Physics and Chemistry at Low Temperatures* (ed. L. Khriachtchev), 51–84. New York, USA: Jenny Stanford Publishing.

91 Lapinski, L., Nowak, M.J., Reva, I. et al. (2010). *Phys. Chem. Chem. Phys.* 12 (33): 9615–9618. https://doi.org/10.1039/C0CP00177E.

92 Fogarasi, G. (2002). *J. Phys. Chem. A* 106 (7): 1381–1390. https://doi.org/10.1021/jp013067.

93 Wolken, J.K., Yao, C., Tureček, F. et al. (2007). *Int. J. Mass Spectrom.* 267 (1–3): 30–42. https://doi.org/10.1016/j.ijms.2007.02.016.

94 Reva, I., Nowak, M.J., Lapinski, L., and Fausto, R. (2012). *J. Chem. Phys.* 136 (6): 064511. https://doi.org/10.1063/1.3683217.

95 Nowak, M.J., Reva, I., Lopes Jesus, A.J. et al. (2019). *Phys. Chem. Chem. Phys.* 21 (41): 22857–22868. https://doi.org/10.1039/C9CP04487F.

96 Halasa, A., Reva, I., Lapinski, L. et al. (2016). *J. Phys. Chem. A* 120 (13): 2078–2088. https://doi.org/10.1021/acs.jpca.5b11615.

97 Araujo-Andrade, C., Reva, I., and Fausto, R. (2014). *J. Chem. Phys.* 140 (6): 064306. https://doi.org/10.1063/1.4864119.

98 Lopes Jesus, A.J., Reva, I., Araujo-Andrade, C., and Fausto, R. (2015). *J. Am. Chem. Soc.* 137 (45): 14240–14243. https://doi.org/10.1021/jacs.5b08588.

99 Halasa, A., Lapinski, L., Rostkowska, H., and Nowak, M.J. (2015). *J. Phys. Chem. A* 119 (35): 9262–9271. https://doi.org/10.1021/acs.jpca.5b06221.

100 Halasa, A., Reva, I., Lapinski, L. et al. (2016). *J. Phys. Chem. A* 120 (17): 2647–2656. https://doi.org/10.1021/acs.jpca.6b01275.

101 Lopes Jesus, A.J., Nunes, C., Fausto, R., and Reva, I. (2018). *Chem. Commun.* 54 (38): 4778–4781. https://doi.org/10.1039/C8CC01052H.

102 Nunes, C.M., Reva, I., Kozuch, S. et al. (2017). *J. Am. Chem. Soc.* 139 (48): 17649–17659. https://doi.org/10.1021/jacs.7b10495.

103 Kästner, J. and Kozuch, S. (2021). *Tunnelling in Molecules*, Theoretical and Computational Chemistry Series, N° 18. London, UK: The Royal Society of Chemistry.

104 Carey, F.A. and Sundberg, R.J. (2000). *Advance Organic Chemistry Part A: Structure and Mechanisms*. New York, USA: Kluwer Academics/Plenum Publishers.

105 Schreiner, P.R. (2020). *Trends Chem.* 2 (11): 984–989. https://doi.org/10.1016/j.trechm.2020.08.006.

106 Gerbig, D. and Schreiner, P.R. (2017). *Angew. Chem. Int. Ed.* 56 (32): 9445–9448. https://doi.org/10.1002/anie.201705140.

107 Schreiner, P.R., Reisenauer, H.P., Ley, D. et al. (2011). *Science* 332 (6035): 1300–1303. https://doi.org/10.1126/science.1203761.
108 Greer, E.M., Kwon, K., Greer, A., and Doubleday, C. (2016). *Tetrahedron* 72 (47): 7357–7373. https://doi.org/10.1016/j.tet.2016.09.029.
109 Bell, R.P. (1980). *The Tunnel Effect in Chemistry*. Boston, USA: Springer.
110 Borden, W.T. (2016). *WIREs Comput. Mol. Sci.* 6 (1): 20–46. https://doi.org/10.1002/wcms.1235.
111 Castro, C. and Karney, W.L. (2020). *Angew. Chem. Int. Ed.* 59 (22): 8355–8366. https://doi.org/10.1002/anie.201914943.
112 Nunes, C.M., Pinto, S.M.V., Reva, I., and Fausto, R. (2016). *Eur. J. Org. Chem.* 2016 (24): 4152–4158. https://doi.org/10.1002/ejoc.201600668.
113 Nunes, C.M., Pinto, S.M.V., Reva, I., and Fausto, R. (2016). *Tetrahedron Lett.* 57 (46): 5038–5041. https://doi.org/10.1016/j.tetlet.2016.09.098.
114 Nunes, C.M., Pinto, S.M.V., Reva, I. et al. (2018). *J. Mol. Struct.* 1172: 33–41. https://doi.org/10.1016/j.molstruc.2017.11.009.
115 Lopes Jesus, A.J., Reva, I., Nunes, C.M. et al. (2020). *Chem. Phys. Lett.* 747: 137069. https://doi.org/10.1016/j.cplett.2019.137069.
116 Ferris, J.P. and Antonucci, F.R. (1974). *J. Am. Chem. Soc.* 96 (7): 2010–2014. https://doi.org/10.1021/ja00814a005.
117 Lopes Jesus, A.J., Nunes, C.M., Reva, I. et al. (2019). *J. Phys. Chem. A* 123 (20): 4396–4405. https://doi.org/10.1021/acs.jpca.9b01382.
118 Lopes, S., Domanskaya, A.V., Fausto, R. et al. (2010). *J. Chem. Phys.* 133 (14): 144507. https://doi.org/10.1063/1.3484943.
119 Halasa, A., Lapinski, L., Reva, I. et al. (2015). *J. Phys. Chem. A* 119 (6): 1037–1047. https://doi.org/10.1021/jp512302s.
120 Nagaya, M. and Nakata, M. (2007). *J. Phys. Chem. A* 111 (28): 6256–6262. https://doi.org/10.1021/jp0726687.
121 Nunes, C.M., Knezz, S.N., Reva, I. et al. (2016). *J. Am. Chem. Soc.* 138 (47): 15287–15290. https://doi.org/10.1021/jacs.6b07368.
122 Inui, H., Sawada, K., Oishi, S. et al. (2013). *J. Am. Chem. Soc.* 135 (28): 10246–10249. https://doi.org/10.1021/ja404172s.
123 Schleif, T., Mieres-Perez, J., Henkel, S. et al. (2019). *J. Org. Chem.* 84 (24): 16013–16018. https://doi.org/10.1021/joc.9b02482.
124 Amlani, H., Frenklah, A., and Kozuch, S. (2021). Tunnelling instability in molecular systems. An exercise in computational chemistry prediction power. In: *Tunnelling in Molecules: Nuclear Quantum Effects from Bio to Physical Chemistry*, Theoretical and Computational Chemistry Series, N° 18, Chapter 2 (ed. J. Kästner and S. Kozuck), 61–87. London, UK: Royal Society of Chemistry.
125 Schleif, T., Merini, M.P., and Sander, W. (2020). *Angew. Chem. Int. Ed.* 59 (46): 20318–20322. https://doi.org/10.1002/anie.202010452.

13

NMR Structural Characterization of Oxygen Heterocyclic Compounds

Ricardo A.L.S. Santos, Diana C.G.A. Pinto, and Artur M.S. Silva

University of Aveiro, Associated Laboratory for Green Chemistry (LAQV) of the Network of Chemistry and Technology (REQUIMTE) and Department of Chemistry, Campus de Santiago, 3810-193 Aveiro, Portugal

13.1 Introduction

Heterocyclic compounds are a huge portion of organic chemicals that have attracted a lot of attention in the last decades, with an unaccountable number of reviews, articles, and scientific papers produced each year. Every day, new heterocycles are synthesized or extracted from natural sources. Therefore, a good elucidation of their structures is mandatory. Nuclear magnetic resonance (NMR) is unrivaled by any other analytical method since it gives information on the local magnetic field around atomic nuclei and can provide exhaustive information on the chemical structure. The local magnetic field of the nucleus is directly influenced by features of the molecular structure such as constitution, configuration, conformation, and intermolecular interactions, among others.

NMR spectroscopy is based on the spin transition of nuclei of the different chemical elements and isotopes when their spin is not null, under the influence of a strong magnetic field. First, radiofrequency pulses are irradiated toward the sample, which induces its magnetization, and then the spin relaxation is recorded, producing signals with characteristic frequencies. Those frequencies are reported as chemical shifts (δ) and are related to a unique chemical structure.

The most common unidimensional NMR analyses are ^{1}H and ^{13}C, although other elements can also be analyzed. For heterocycles, considerably useful are the resonances of nitrogen (^{14}N or ^{15}N), oxygen (^{17}O), phosphorus (^{31}P), sulfur (^{33}S), and fluorine (^{19}F). It is important to remember that the relaxation of the oxygen and sulfur isotopes is quadrupolar due to their higher spin, which increases the bandwidth of the signals and limits its usage to small molecules with only a few of those heteroatoms.

Besides the chemical shifts, other information can be obtained from NMR spectra. For example, the spin relaxation is accompanied by coupling (J) with surrounding nuclei, so the main signal is split into smaller ones. By the splitting pattern, it is possible to recognize the neighboring nuclei. In addition, a special technique increases the

Heterocycles: Synthesis, Catalysis, Sustainability, and Characterization, First Edition.
Edited by Teresa M.V.D. Pinho e Melo and Marta Pineiro.

neighboring nuclei's signal intensity, called the nuclear Overhauser effect (NOE). This involves not only the bonded nuclei but also the ones that are near spatially.

Unfortunately, many compounds present many overlapping signals. In those cases, multidimensional analysis is required. For example, ^{1}H–^{1}H COSY (COrrelated SpectroscopY) has the unidimensional ^{1}H NMR spectrum of the compound on both axes. The couplings appear as a contour map, so close protons' correlation is easier to determine. Hydrogen–carbon bonds can be deduced from, for example, heteronuclear single quantum coherence (HSQC) spectrum. This bidimensional technique has the ^{1}H spectrum on one axis and the ^{13}C spectrum in the other, leaving the coupling between directly bonded nuclei in the graphic area. For long-range ^{1}H–^{13}C coupling, the correlation can be extracted from heteronuclear multiple bond correlation (HMBC) spectrum.

For the chemical structure elucidation of organic compounds based on NMR spectra, previous knowledge of the characteristic frequency signals of the compound's family is recommended because most of the time, changes are small and follow specific behaviors. For example, the inclusion of electron-withdrawing groups is related to the increase of the chemical shift. In contrast, the opposite is also true for electron-donating substituents, which diminishes it. Therefore, in the following sections, the NMR data of the main O-heterocycles will be visited. The focus will be on O-heterocycles since there is already a comprehensive chapter on *N*-heterocycles [1]. In addition, our group has developed considerable research on phenolic compounds, including chromones.

13.2 Three-Membered Heterocyclic Compounds

The simplest O-heterocycles are oxirane (**1**) and oxirene (**2**) (Figure 13.1). Oxirane structures are common, mainly obtained via epoxidation of alkenes, a synthetic strategy used in the epoxidation of fatty acids or in the synthesis of epoxy resins [2, 3]. Therefore, there are many NMR characterizations of those compounds in the literature of either hydrogen, carbon, or oxygen isotopes. On the other hand, oxirenes are considered intermediates of peroxyacid alkyne oxidation, being further oxidized or converted into ketenes and ketones (Table 13.1) [4].

Oxirane itself presents a single peak in ^{1}H, ^{13}C, and ^{17}O NMR spectra. Its protons have a chemical shift of 2.54 ppm [5], which is more deshielded than those of cyclopropane (δ 0.22 ppm) and aziridine (δ 1.48 ppm) [1]. Carbons also follow that trend, reaching δ 40.8 ppm [6]. The inductive effect of oxygen is conspicuous, claiming the compound's electronic density to itself. As a result, the signal in the ^{17}O NMR spectrum is moved upfield (−49 ppm) [7].

Figure 13.1 Three-membered O-heterocycles: oxirane (**1**), oxirene (**2**), and dioxirane (**3**).

Table 13.1 ^{1}H, ^{13}C, and ^{17}O NMR chemical shifts and coupling constants of some oxirane derivatives, in selected solvents.

Compound/ substituent	^{1}H (δ, ppm) (J, Hz)	^{13}C (δ, ppm)	^{17}O (δ, ppm)	Solvent	References
1	2.54	—	—	Neat	[5–7]
	—	40.8	—	$CDCl_3$ (50%)	
	—	—	−49	$CDCl_3$	
1a 2-Methyl	2.98 (H-2) 2.43 (H-3 *trans*) 2.74 (H-3 *cis*)	48.2 (C-2) 47.9 (C-3)	−16	$CDCl_3$	[7, 10, 11]
1b 2,2-Dimethyl	2.61	—	10	$CDCl_3$	[6, 7, 12]
	—	53.9 (C-2) 54.5 (C-3)	—	$CDCl_3$ (50%)	
1c (2*R*,3*S*)-2,3-Dimethyl	—	—	14	$CDCl_3$	[6, 7]
	—	52.4	—	$CDCl_3$ (50%)	
1d (2*R*,3*R*)-2,3-Dimethyl	—	—	17	$CDCl_3$	[6, 7]
	—	55.2	—	$CDCl_3$ (50%)	
1e 2,2,3,3-Tetramethyl	—	—	57	$CDCl_3$	[6, 7]
	—	61.7	—	$CDCl_3$ (50%)	
1f 2-Phenyl	—	51.6 (C-2) 50.6 (C-3)	−6	$CDCl_3$	[7, 13]
1g 2-Methyl-2-phenyl	2.77 (H-3 *cis*) 2.92 (H-3 *trans*) (J 5.5 Hz)	56.3 (C-2) 56.6 (C-3)	—	$CDCl_3$	[13–15]
1h (2*R*,3*S*)-3-Methyl-2-phenyl	3.91 (H-2) 3.20 (H-3) (J 4.19 Hz)	—	—	CCl_4	[16]
1i (2*R*,3*R*)-3-Methyl-2-phenyl	3.58 (H-2) 2.98 (H-3) (J 2.00 Hz)	—	—	CCl_4	[17]
1j 2-Heptyl	—	52.2–52.3 (C-2) 46.9–47.1 (C-3)	—	$CDCl_3$	[13, 14]
1k 2-Styryl	—	52.6 (C-2) 49.1 (C-3)	—	$CDCl_3$	[13]

Table 13.1 (Continued)

Compound/ substituent	^{1}H (δ, ppm) (J, Hz)	^{13}C (δ, ppm)	^{17}O (δ, ppm)	Solvent	References
1l 2-Spiro cyclohexane	—	59.3 (C-2) 54.4 (C-3)	—	$CDCl_3$	[13]
1m 2-Chloro	4.95 (H-2) 2.88 (H-3 *trans*) 2.81 (H-3 *cis*) (J_{gem} 4.7 Hz J_{cis} 1.42 Hz J_{trans} 2.68 Hz)	—	—	Neat	[18]
1n 2-Formyl	3.36 (H-2) 3.17 (H-*trans*) 3.10 (H-*cis*) (J_{gem} 5.54 Hz J_{cis} 4.87 Hz J_{trans} 2.09 Hz)	—	—	Neat	[19]
1o 2-Cyano	3.51 (H-2) 3.01 (H-3 *trans*) 3.12 (H-3 *cis*) (J_{gem} 5.53 Hz J_{cis} 4.23 Hz J_{trans} 2.51 Hz)	—	—	Neat	[20]
1p Fullerene epoxide	—	90.2	—	Benzene-d_6	[8]

Source: Modified from Stille et al. [4].

The addition of substituents to oxirane often increases the chemical shift of the core oxygen and carbons, being the substituted carbon the most affected. Iwamura et al. reported a series of oxirane derivatives ^{17}O NMR data [7]. In their study, the 2-methyloxirane (**1a**) (Figure 13.2) observed an increment of the chemical shift to −16 ppm, whereas, with the phenyl substituted oxirane **1f**, it changed even further to −6 ppm. The addition of other methyl groups to the ring had an additive result in the chemical shifts. With two methyl groups, it ranged from 10 ppm in 2,2-dimethyloxirane (**1b**) to 17 ppm in (2*R*,3*R*)-2,3-dimethyloxirane (**1d**), and with four methyl groups, the chemical shift reached 57 ppm (oxirane **1e**).

In ^{13}C NMR, the slope is not so steep. The chemical shift of the substituted carbon of compound **1a** is observed at nearly δ 48 ppm (Figure 13.3), with two methyl groups, and **1d** showed the signal around δ 55 ppm and **1e** at δ 61.7 ppm. Again, the phenyl group has a higher impact than the methyl, as the oxirane **1f** (δ around

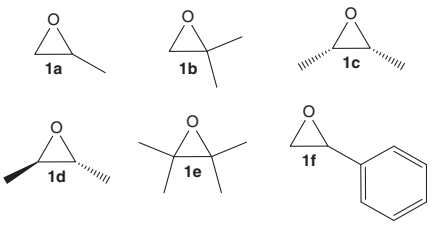

Figure 13.2 Derivatives of oxirane: 2-methyloxirane (**1a**), 2,2-dimethyloxirane (**1b**), (2*R*,3*S*)-2,3-dimethyloxirane (**1c**), (2*R*,3*R*)-2,3-dimethyloxirane (**1d**), 2,2,3,3-tetramethyloxirane (**1e**), and 2-phenyloxirane (**1f**).

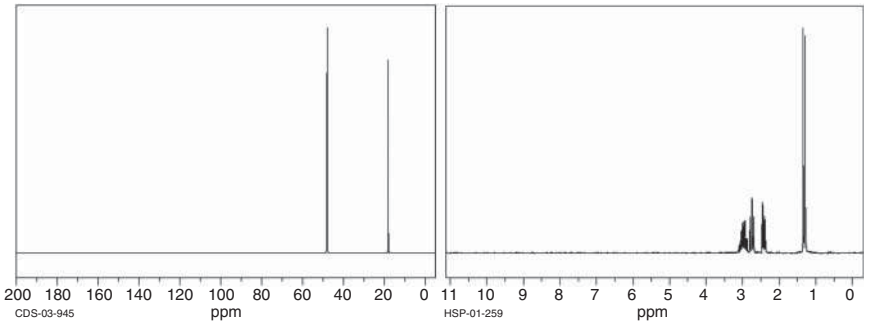

Figure 13.3 2-Methyloxirane (**1a**) ^{13}C and ^{1}H NMR spectra. Source: SDBSWeb: https://sdbs.db.aist.go.jp. National Institute of Advanced Industrial Science and Technology, accessed 05 December 2021.

51 ppm) surpassed the δ of **1a**. ^{13}C NMR spectra analysis of many more compounds can be found in the list compiled by Davies and Whitham in 1975 [6]. A unique oxirane derivative synthesized later is the fullerene epoxide, which shows a peak at 90.2 ppm corresponding to the oxirane's carbons and the other signals between 140 and 146 ppm [8].

In ^{1}H NMR, differences between substituents are even smaller. For 2-methyloxirane (**1a**), the highest frequency corresponds to H-2 (δ 2.98 ppm), which is the one bonded to the substituted carbon (Figure 13.3). The double doublet signal (dd) also encloses the signals for H-3, with the proton in a *trans*-configuration relative to the methyl group having the smaller resonance frequency. The steric hindrance of the methyl substituent can be responsible for the observed pattern. The coupling constants are usually small, being 6 Hz for *geminal* protons, 4 Hz for *cis*, and 2 Hz for *trans*, approximately, as can be seen in the entries for compounds **1g**, **1h**, and **1i** (Table 13.1 and Figure 13.4).

From the Advanced Industrial Science and Technology's (AIST) Spectral Database for Organic Compounds [9], information regarding the effect of oxirane's electron-withdrawing substituents can be found. For example, the chemical shift of H-2 is determined by the nature of the substituent, ranging from 3.36 ppm in 2-formyloxirane (**1n**) and 3.51 ppm in 2-cyanooxirane (**1o**) to 4.95 ppm in 2-chlorooxirane (**1m**). Meanwhile, the H-3 keeps a lower chemical shift around 3 ppm.

The works of Villa et al. and Benassi et al. have compared the effect of substitution on the aromatic ring of (2*R*,3*S*)- and (2*R*,3*R*)-3-methyl-2-phenyloxiranes, (**1h**)

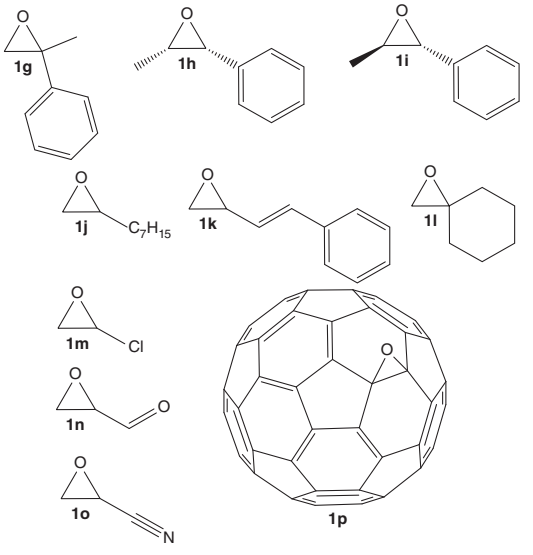

Figure 13.4 Derivatives of oxirane **1**: 2-methyl-2-phenyloxirane (**1g**), (2*R*,3*S*)-3-methyl-2-phenyloxirane (**1h**), (2*R*,3*R*)-3-methyl-2-phenyloxirane (**1i**), 2-heptyloxirane (**1j**), 2-styryloxirane (**1k**), spiro[cyclohexane-1,2′-oxirane] (**1l**), 2-chlorooxirane (**1m**), 2-formyloxirane (**1n**), and 2-cyanooxirane (**1o**).

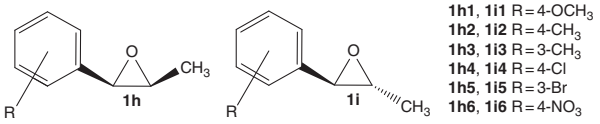

Figure 13.5 Derivatives of (2*R*,3*S*)-3-methyl-2-phenyloxirane (**1h**) and (2*R*,3*R*)-3-methyl-2-phenyloxirane (**1i**). Source: Modified from Benassi et al. [17].

and (**1i**), respectively (Table 13.2 and Figure 13.5) [16, 17]. H-2 is always the most deshielded of the two oxirane ring protons. The phenyl group has a more significant impact than the methyl group. In addition, the chemical shifts are both higher for the *cis*-isomer, along with the coupling constants.

Relatively to the substituents on the phenyl ring, electron-donating groups such as methyl, methoxy, and methylthio decrease the chemical shifts of the oxirane protons. Their opposites, electron-withdrawing groups such as cyano and nitro groups, increase those frequencies, as expected. The haloderivatives **1i4** and **1i5** show different behavior. While in the apolar solvent CCl_4, their frequencies resemble those of the unsubstituted compound **1i**. In the polar solvents, acetone-d_6 and DMSO-d_6, they are shifted to higher frequencies since those solvents act as Lewis bases, withdrawing electrons from the compounds. In general, chemical shifts increase in the solvent order: CCl_4, acetone-d_6, and DMSO-d_6.

Three-membered rings, dioxirane derivatives **3** (Figures 13.1 and 13.6), have been used for oxidation processes of other molecules, and some NMR spectra have also been published [21], as can be seen in Table 13.3. The ^{17}O NMR of two derivatives, [3,3-dimethyldioxirane (**3a**) and 3-methyl-3-(trifluoromethyl)dioxirane (**3b**)], present a signal with δ around 300 ppm. For **3b**, the ^{13}C NMR of the dioxirane ring's carbon resonates at δ 97.3 ppm.

Table 13.2 ^{1}H NMR chemical shifts of (2*R*,3*S*)- (**1h**) and (2*R*,3*R*)-3-methyl-2-phenyloxirane (**1i**) derivatives, in selected solvents.

Compound/ substituent	H-2	H-3	*J*, Hz	Solvent	References
1h H	3.91	3.20	4.19	CCl_4	[16]
1h1 4-OCH_3	3.84	3.14	3.98	CCl_4	[16]
1h2 3,4-CH_3	3.82	3.13	4.12	CCl_4	[16]
1h3 3-CH_3	3.85	3.16	4.11	CCl_4	[16]
1h4 3-CN	3.97	3.28	4.11	CCl_4	[16]
1h5 4-CN	3.98	3.30	4.17	CCl_4	[16]
1h6 4-SCH_3	3.85	3.17	4.08	CCl_4	[16]
1i H	3.40	2.83	1.93	CCl_4	[17]
	3.58	2.98	2.00	$(CH_3)_2CO$-d_6	
	3.60	3.03	2.06	DMSO-d_6	
1i1 4-OCH_3	3.35	2.82	1.96	CCl_4	[17]
	3.51	2.98	2.01	$(CH_3)_2CO$-d_6	
	3.59	3.07	2.05	DMSO-d_6	
1i2 4-CH_3	3.36	2.81	1.90	CCl_4	[17]
	3.52	2.96	2.03	$(CH_3)_2CO$-d_6	
	3.60	3.05	2.08	DMSO-d_6	
1i3 3-CH_3	3.36	2.82	1.82	CCl_4	[17]
	3.53	2.96	1.98	$(CH_3)_2CO$-d_6	
	3.61	3.05	2.04	DMSO-d_6	
1i4 4-Cl	3.40	2.82	1.89	CCl_4	[17]
	3.62	2.99	2.03	$(CH_3)_2CO$-d_6	
	3.70	3.07	2.04	DMSO-d_6	
1i5 3-Br	3.39	2.83	1.70	CCl_4	[17]
	3.63	3.00	2.02	$(CH_3)_2CO$-d_6	
	3.71	3.085	1.97	DMSO-d_6	
1i6 4-NO_2	3.81	3.07	1.88	$(CH_3)_2CO$-d_6	[17]
	3.90	3.14	1.98	DMSO-d_6	

Source: Modified from Villa et al. [16].

13.3 Four-Membered Heterocyclic Compounds

The oxetane derivatives (Figure 13.7) are not as common as oxiranes. In nature, they are often present as β-lactones, which are oxetan-2-ones. Along with oxetan-3-ones, their impact in medicinal chemistry in the synthesis of active compounds is very relevant [22–24].

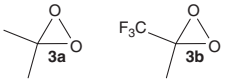

Figure 13.6 Structures of 3,3-dimethyldioxirane (**3a**) and 3-methyl-3-(trifluoromethyl) dioxirane (**3b**).

Table 13.3 ^{13}C and ^{17}O NMR chemical shifts of dioxirane derivatives, in acetone-d_6.

Compound/substituent	^{13}C (δ, ppm)	^{17}O (δ, ppm)	References
3a 3,3-Dimethyl	—	302	[21]
3b 3-Methyl-3-(trifluoromethyl)	97.3	297	[21]

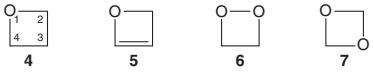

Figure 13.7 Four-membered O-heterocycles: oxetane (**4**), 2*H*-oxete (**5**), 1,2-dioxetane (**6**), and 1,3-dioxetane (**7**).

In the NMR spectra, the coupling pattern of oxetane derivatives does not follow simple multiplicities. The chemical structure of oxetane is near planar [25], so the tiny nonplanarity may present some additional peak split. This fact is evident in the ^{1}H NMR spectrum of oxetane (**4**) from AIST's spectral database [26]. The deshielded H-2 are not a triplet anymore, despite the two neighboring protons, and for the H-3, a complex multiplicity appears.

In terms of shielding, H-2 and C-2 nuclei present higher chemical shifts than H-3 and C-3, respectively, because of the electronegativity of oxygen. The H-2 signal appears at δ 4.75 ppm and H-3 at δ 2.70 ppm, while C-2 shows its peak at δ 72.6 ppm and C-3 at δ 22.6 ppm (Table 13.4).

In the case of 2-methyloxetane (**4a**) (Figure 13.8), all protons of the heterocycle are nonequivalent, resulting in five different signals. The most deshielded is H-2, whose resonance frequency surpasses its homologous in oxetane (δ 4.84 ppm). Then H-4 chemical shifts appears around 4.4 ppm. Finally, H-3 keeps the lowest values, with $\delta \sim 2.4$ ppm, which are also lower than the corresponding ones in oxetane. Thus, the nuclei in *trans*-configuration relatively to methyl group are shifted downfield compared with those in a *cis*-configuration.

In terms of coupling constants, J_{gem} has negative values in the range −10 to −5 Hz. J_{cis} and J_{trans} of neighboring protons range between 5 and 9 Hz, with higher values for the *cis*-configuration. J_4 coupling is negligible.

When there is an aromatic substituent instead of a 2-methyl group (taking 2-(2-chlorophenyl)oxetane (**4b**) as an example), H-2 becomes more deshielded, and H-4 seems to be shifted upfield (the solvents used in the analysis of compounds **4**,

Table 13.4 ^{1}H and ^{13}C NMR chemical shifts and coupling constants of some oxetane derivatives.

Compound/substituent	^{1}H (δ, ppm) (J, Hz)	^{13}C (δ, ppm)	Solvent	References
4	4.75 (H-2) 2.70 (H-3)	72.6 (C-2) 22.6 (C-3)	$CDCl_3$	[26, 30]
4a 2-Methyl	4.84 (H-2) 2.64 (H-3 *trans*) 2.24 (H-3 *cis*) 4.49 (H-4 *trans*) 4.37 (H-4 *cis*) (J_{gem} −10 to −5 Hz $J_{cis,trans}$ 5–9 Hz)	—	CCl_4	[31]
4b 2-(*o*-Chlorophenyl)	5.90 (H-2) 2.69 (H-3 *trans*) 2.11 (H-3 *cis*) 4.40 (H-4 *trans*) 4.21 (H-4 *cis*)	—	Benzene-d_6	[32]
4c 3,3-Bis (chloromethyl)	4.45	76.6 (C-2) 45.7 (C-3)	$CDCl_3$	[33, 34]
4d 4-Methyl-2-oxo	3.56 (H-3 *trans*) 3.08 (H-3 *cis*) 4.70 (H-4)	168.4 (C-2) 44.4 (C-3) 68.1 (C-4)	$CDCl_3$	[35, 36]
4e 4-Methylidene-2-oxo	3.90	165.2 (C-2) 42.4 (C-3) 147.7 (C-4)	$CDCl_3$	[37, 38]
4f 4-(Dichloromethyl)-2-oxo	3.50 (H-3) 4.60 (H-4)	—	$CDCl_3$	[27]
4g (1′*S*,2*S*)-2-(1′-Chloro-1′-phenylmethyl)-3-oxo	5.75 (H-2) 5.27 (H-4) (J_{gem} 14.7 Hz J_{cis} 3.4 Hz J_{trans} 1.5 Hz)	—	$CDCl_3$	[28]
4h 3,3-Dimethyl-2,4-dioxo	—	59.2 (C-3) 169.1 (C-2)	Reaction mixture (−30 °C)	[29]

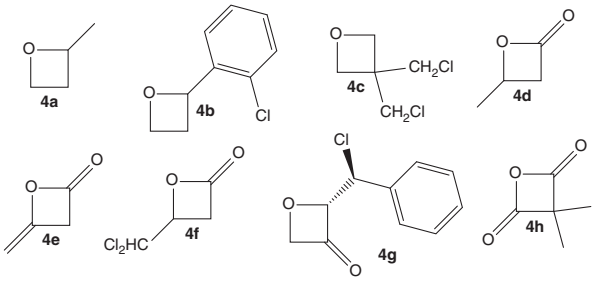

Figure 13.8 Derivatives of oxetane (**4**): 2-methyloxetane (**4a**), 2-(2-chlorophenyl)oxetane (**4b**), 3,3-bis(chloromethyl)oxetane (**4c**), 4-methyloxetan-2-one (**4d**), 4-methylideneoxetan-2-one (**4e**), 4-(dichloromethyl)oxetan-2-one (**4f**), (1′*S*,2*S*)-2-(1-chloro-1-phenylmethyl) oxetan-3-one (**4g**), and 3,3-dimethyloxetane-2,4-dione (**4h**).

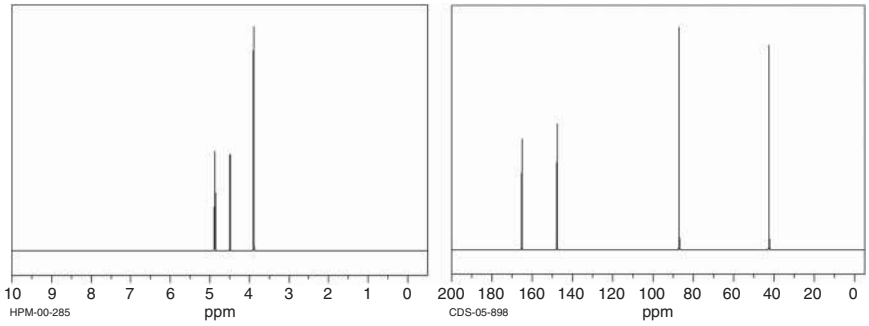

Figure 13.9 4-Methylideneoxetan-2-one (**4e**) ^{1}H and ^{13}C NMR spectra. Source: SDBSWeb: https://sdbs.db.aist.go.jp. National Institute of Advanced Industrial Science and Technology, accessed 05 December 2021.

4a, and **4b** [Table 13.4] are different, which makes comparisons more difficult to make).

As mentioned before, oxetanones are an important subdivision of these compounds' family. 4-Methyloxetan-2-one (**4d**), also known as β-butyrolactone, presents signals at δ 4.70 ppm for H-4 (similarly to oxetane) and at δ 3.56 and 3.08 ppm, for H-3. The *trans*-proton relative to the methyl group appears at the higher frequency, hence following the trend noticed before. If the methyl group is replaced by a methylidene (4-methylideneoxetan-2-one (**4e**), also named diketene), the H-3 signal shifts downfield to δ 3.90 ppm (Figure 13.9).

Wynberg and Staring prepared a series of chloro-4-alkyloxetan-2-ones and analyzed their ^{1}H NMR spectra. 4-(Dichloromethyl)oxetan-2-one (**4f**) is the simplest example they studied, and the chemical shifts presented are δ 4.60 and 3.50 ppm for H-4 and H-3, respectively [27]. Results are considerably similar to those of **4d**.

Thijs et al. studied the synthesis of oxetan-3-ones from α,β-epoxydiazomethyl ketones [28]. All the chemical shifts of the protons of the oxetan-3-one rings appear below δ 5 ppm. *Geminal* coupling constants present values of 14.5–15.3 Hz, whereas J_4 was 3.5–4.0 Hz for *cis*-configuration and 0–1.5 Hz for *trans*-configuration. In terms of ^{13}C NMR, the resonance frequencies of oxetane (**4**) were already

mentioned. In 3,3-bis(dichloromethyl)oxetane (**4c**), the heavily substituted carbon becomes more deshielded, reaching δ 45.7 ppm, whereas C-2 is narrowly shifted downfield to δ 76.6 ppm when compared with **4**.

In oxetan-2-ones, carbonyl peaks appear above δ 165 ppm, and the resonance of the α-carbon changes to a chemical shift between 40 and 50 ppm. Relatively to C-4, its chemical shift appears at 68.1 ppm in **4d**, but the methylidene group of **4e** increments its shift to δ 147.7 ppm (Figure 13.9) due to the inductive effect of the sp^2 carbon. In malonyl anhydride **4h**, the carbonyl carbon appears at δ 169.1 ppm, and the α-carbon is shifted downfield to δ 59.2 ppm [29].

^{17}O NMR spectra of oxetane heterocycles are not found in literature.

The oxetes are usually unstable at room temperature, with half-life times reported to be less than one day, being converted to enones. They are also susceptible to air oxidation. Nevertheless, some NMR spectra have been obtained [39].

The ^{1}H-NMR spectrum of 2*H*-oxete (**5**) in $CDCl_3$ (Figure 13.7) shows peaks at δ 6.74, 5.77, and 5.27 ppm (Table 13.5). Thus, the most shielded protons are from methylene, under the influence of electronegative oxygen. Additionally, the double bond anisotropy results in higher frequencies for the other protons, where H-4 is the most deshielded due to the proximity of the oxygen.

In 2*H*-3-phenyloxete (**5a**) (Figure 13.10), both proton frequencies increase. The H-2 reaches δ 5.50 ppm. The other proton chemical shift is coincident with the multiplet signal of the five phenyl protons, around δ 6.74 ppm. For the ^{13}C NMR in $CDCl_3$, the methylene carbon is the most shielded, with chemical shift at δ 80.4 ppm, and C-4 is the most deshielded, observed at δ 149.3 ppm. The remaining carbons have their chemical shifts from 122 to 130 ppm, mixed with the aromatic carbons' signals [39].

Table 13.5 ^{1}H and ^{13}C NMR chemical shifts of 2*H*-oxete derivatives, in $CDCl_3$.

Compound/substituent	^{1}H (δ, ppm)	^{13}C (δ, ppm)	Solvent	References
5	6.74 (H-4) 5.77 (H-3) 5.27 (H-2)	—	$CDCl_3$	[39]
5a 3-Phenyl	7.40–7.00 (H-4) 5.50 (H-2)	149.3 (C-4) 122–130 (C-3) 80.4 (C-2)	$CDCl_3$	[39]
5b 4-(Chloromethyl)-2,3-bis(methoxy methanoyl)-4-phenyl	—	149.6 (C-4) 123.0 (C-3) 85.6 (C-2)	$CDCl_3$	[40]
5c 2-Ethanoyl-2-methylbenzo[*c*]	—	164.7 (C-4) 132.7 (C-3) 103.2 (C-2)	$CDCl_3$ (−35 °C)	[41]

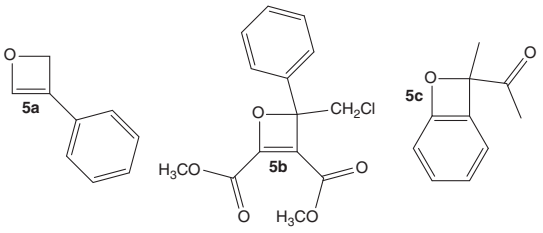

Figure 13.10 Derivatives of 2*H*-oxete (**5**): 3-phenyl-2*H*-oxete (**5a**), dimethyl 4-(chloromethyl)-4-phenyl-2*H*-oxete-2,3-dicarboxylate (**5b**), and 2-acetyl-2-methylbenzoxete (**5c**).

Asghari and Habibi have synthesized four highly substituted 2*H*-oxetes from the reaction between alkynes and ketones, catalyzed by triphenylphosphine [40]. Because of the substituents, no ring protons are present in the heterocycle. In the ^{13}C NMR, the chemical shift of C-2 ranged from δ 85 to δ 90 ppm. The olefinic carbon signals were identified at δ 123–124 ppm for C-3 and δ 149.6 ppm for C-4. Dimethyl 4-(chloromethyl)-4-phenyl-2*H* oxete-2,3-dicarboxylate (**5b**) (Figure 13.10) is one of the four compounds studied.

A different type of compounds is 2*H*-benzoxetes. Adam et al. prepared 12 derivatives, with different substituents in the aromatic ring, with the simplest example being 2-ethanoyl-2-methyl-2*H*-benzoxete (**5c**) [41]. In this case, all carbon signals are shifted downfield when compared with 2*H*-oxete. Thus, the C-2 increased to δ 103.2 ppm, the C-3 to δ 132.7 ppm, and the most deshielded C-4 to δ 164.7 ppm. It is important to remark that the change in the C-2 resonance frequency should be attributed mainly to the substituents on that carbon and less to the benzene ring, which in the case of **5c** is the ethanoyl group.

The four-membered heterocycles with two oxygens in the ring are 1,2-dioxetane (**6**) and 1,3-dioxetane (**7**) (Figure 13.7). The former is obtained after mild oxidation of alkenes with molecular oxygen at low temperatures. It is used as a chemiluminescent, and it can explode upon warming [42, 43].

The ^{1}H NMR spectra of 1,2-dioxetanes stabilized with ethoxy substituents, **6a** and **6b** in Figure 13.11, show peaks at δ 5.89–5.91 ppm (Table 13.6) [43]. However, these heterocycles are often highly substituted, so the ^{13}C NMR is used to make their identification. The carbons from the dioxetane ring of 3,3,4,4-tetraphenyl-1,2-dioxetane (**6c**) resonate at δ 97.8 [42].

Other 1,2-dioxetanes were studied by Schaap's group, compounds **6d**–**6f**, [44–47]. When oxygen atoms are attached to the dioxirane ring, the chemical shift of the heterocycle carbons increases to δ 110.0–112.3 ppm. The spiroadamantyl ring preserves the corresponding carbon signal at δ 95.6–96.8 ppm.

One last compound of the 1,2-dioxetane family herein reported is the 1,2-dioxetanedione (**6g**), identified as an intermediate of oxalyl chloride peroxidation. The spectrum of the enriched ^{13}C compound showed a peak at δ 154.5 ppm [48].

The 1,3-dioxetanes (**7**) (Figure 13.7) are supposed to be more stable than 1,2-dioxetanes by molecular orbitals calculations, but no NMR results were found in the literature [49].

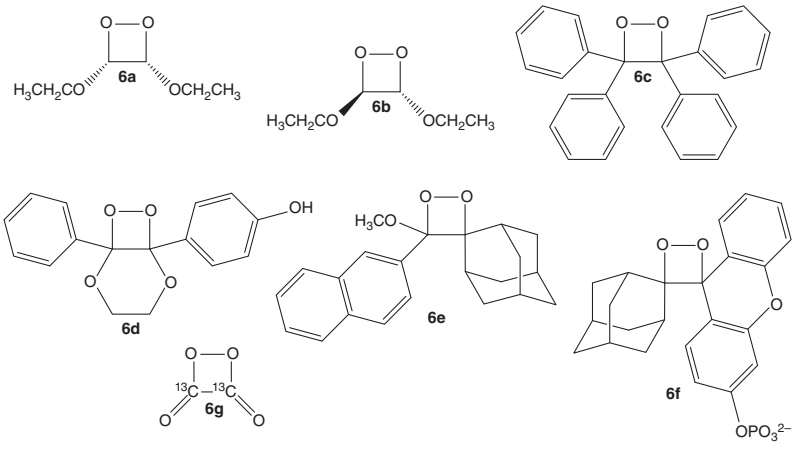

Figure 13.11 Derivatives of 1,2-dioxetane (**6**): (3*S*,4*R*)-3,4-diethoxy-1,2-dioxetane (**6a**), (3*S*,4*S*)-3,4-diethoxy-1,2-dioxetane (**6b**), 3,3,4,4-tetraphenyl-1,2-dioxetane (**6c**), 2a-(4-hydroxyphenyl)-6a-phenyl-1,2,3,6-tetraoxobicyclo[4.2.0]octane (**6d**), spiro [adamantane-1,3′-[4]methoxy[4]naphthyl[1,2]dioxetane] (**6e**), dispiro[adamantane-1,4′-[1,2]dioxetane-3′,9″-[6]phosphatidyl[9*H*]xanthene] (**6f**), and 1,2-dioxetane-3,4-dione-3,4-$^{13}C_2$ (**6g**).

Table 13.6 ^{1}H and ^{13}C NMR chemical shifts of 1,2-dioxetane derivatives.

Compound/ substituent	^{1}H (δ, ppm)	^{13}C (δ, ppm)	Solvent	References
6a (3*S*,4*R*)-3,4-Diethoxy	5.91	—	Reaction mixture (−78 °C)	[43]
6b (3*S*,4*S*)-3,4-Diethoxy	5.89	—	Reaction mixture (−78 °C)	[43]
6c 3,3,4,4-Tetraphenyl	—	97.8	$CDCl_3$	[42]
6d 3,4-(Ethane-1,2-dioxy)-3-(4-hydroxyphenyl)-4-phenyl	—	109.8 110.0	$CDCl_3$	[44]
6e 3,3-(Bicyclo[3.3.1] nonane-2,5-diyl)-4-methoxy-4-napht-2-yl	—	95.6 (C-3) 112.3 (C-4)	Unknown	[45]
6f 4,4-(Bicyclo[3.3.1] nonane-2,5-diyl)-3,3-(2-phenoxy-4-phosphatidylphen-1,2′-diyl)	—	96.8 (C-4) 84.4 (C-3)	$CDCl_3$	[47]
6g 3,4-Dioxa-3,4-$^{13}C_2$	—	154.5	Reaction mixture (−80 °C)	[48]

13.4 Five-Membered Heterocyclic Compounds

The oxolane (**8**) (Figure 13.12), commonly named tetrahydrofuran (THF), is a solvent frequently used in the laboratory in organometallic synthesis, where it can also act as a ligand, and in the production of polymers [50]. In addition, its stable pentagonal structure is ubiquitous in nature, for example, in many sugars.

Two signals define the characterization of the oxolane ring through ^{1}H NMR, the H-2,5 at δ 3.73 ppm and the H-3,4 at δ 1.84 ppm. The expected coupling constants are in the range 6–8 Hz, as illustrated by the NMR data of compound **8a** presented in Table 13.7 (Figure 13.13). In the ^{13}C NMR spectrum, the shielded carbons appear at δ 25.8 ppm, while those bonded to the oxygen are at δ 68.0 ppm [51–53].

The methyl group at C-2 increases the spectra complexity since all protons of the heterocycle experience unique electronic fields. The H-2 is shifted downfield to δ 3.94 ppm. The H-3 are split into two signals, with the hydrogen in position *trans* relatively to the methyl group having a higher chemical shift (δ 1.99 ppm) and the *cis* in a lower chemical shift (δ 1.41 ppm). These results are characteristic of an envelope conformation, where the equatorial proton (*trans*) is under great hindrance from the methyl group. Protons H-4 resonance is at δ 1.89 ppm, and the unshielded H-5 appears at δ 3.89 and 3.70 ppm, with the axial proton nearer the electronegative oxygen.

With two chlorine atoms, the signals of (2*S*,3*S*)-2,3-dichlorooxolane (**8c**) (Figure 13.13) protons moved downfield in the ^{1}H NMR spectrum scale (Figure 13.14). First, the H-2 appears at δ 6.23 ppm. In addition, highly deshielded are H-3, at δ 4.64 ppm, and the two H-5 at δ 4.44 and 4.25 ppm. The H-4 is the most shielded, below δ 3 ppm. The protons on the same side of the chloro atoms' pentagonal plane are always more deshielded than their counterpart. *Geminal* coupling achieves values around −15 Hz.

Looking at the other examples in Table 13.7, from **8e** to **8i**, a general trend can be identified. Protons next to the oxygen H-2,5 tend to give signals around δ 4 ppm, being shifted downfield with bigger or more electronegative substituents. The other protons barely reach δ 2 ppm in most cases. However, in the highly substituted **8h** and **8i**, their values almost reach δ 3 ppm (the 4-phenyl substituent in **8h** being a decisive factor). In the γ-butyrolactone (**8g**), all chemical shifts are also moved downfield compared with the oxolane nucleus **8**. In ^{13}C NMR, the presence of substituents often increases the resonance frequency. The carbons in compound **8a**, bonded to the oxygen have their chemical shifts at δ 75.3 and 67.8 ppm (C-2 and C-5, respectively), and the other carbons appear at δ 33.3 and 26.0 ppm (C-3 and C-4, respectively).

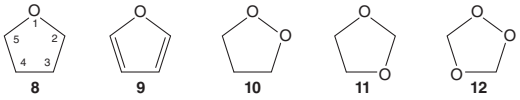

Figure 13.12 Five-membered O-heterocycles: oxolane (**8**), furan (**9**), 1,2-dioxolane (**10**), 1,3-dioxolane (**11**), and 1,2,4-trioxolane (**12**).

Table 13.7 ^{1}H and ^{13}C NMR chemical shifts and coupling constants of oxolane derivatives, in $CDCl_3$.

Compound/substituent	^{1}H (δ, ppm) (J, Hz)	^{13}C (δ, ppm)	References
8	3.73 (H-2) 1.84 (H-3)	68.0 (C-2) 25.8 (C-3)	[51, 52]
8a 2-Methyl	3.94 (H-2) 1.41 (H-3 *cis*) 1.99 (H-3 *trans*) 1.89 (H-4) 3.89 (H-5 *cis*) 3.70 (H-5 *trans*) ($J_{cis,trans}$ 6–8 Hz)	75.3 (C-2) 33.3 (C-3) 26.0 (C-4) 67.8 (C-5)	[53, 54]
8b 3-Methyl	—	74.9 (C-2) 33.7 (C-3) 34.3 (C-4) 68.0 (C-5)	[55]
8c (2*S*,3*S*)-2,3-Dichloro	6.23 (H-2) 4.64 (H-3) 2.81 (H-4 *cis*) 2.26 (H-4 *trans*) 4.44 (H-5 *cis*) 4.25 (H-5 *trans*) (J_{gem} −15 Hz)	99.8 (C-2) 63.9 (C-3) 31.9 (C-4) 68.7 (C-5)	[56, 57]
8d (2*R*,5*S*)-2,5-Dimethoxy	—	106.2 (C-2) 31.1 (C-3)	[58]
8e 2-(Bromomethyl)	4.13 (H-2) 3.86 (H-5) 1.49–2.32 (H-3,4)	78.2 (C-2) 30.4 (C-3) 25.9 (C-4) 68.8 (C-5)	[59, 60]
8f 2-(2-Ethoxy-2-oxoethyl)	4.25 (H-2) 2.05 (H-3 *cis*) 1.60 (H-3 *trans*) 1.91 (H-4) 4.00 (H-5)	75.4 (C-2) 31.3 (C-3) 25.7 (C-4) 68.0 (C-5)	[61, 62]
8g 2-Oxo	2.48 (H-3) 2.28 (H-4) 4.35 (H-5)	178.0 (C-2) 27.8 (C-3) 22.2 (C-4) 68.7 (C-5)	[63, 64]
8h 5-Methyl-2,2-bis (methoxymethanoyl)-4-phenyl	4.21 (H-5) 2.94–3.03 (H-3,4) ($J_{4,5}$ 9.7 Hz)	86.0 (C-2) 42.7 (C-3) 52.8 (C-4) 85.0 (C-5)	[65]
8i 5-Methyl-2,2-bis (methoxymethanoyl)-5-phenyl	2.14–2.62 (H-3,4)	—	[65]

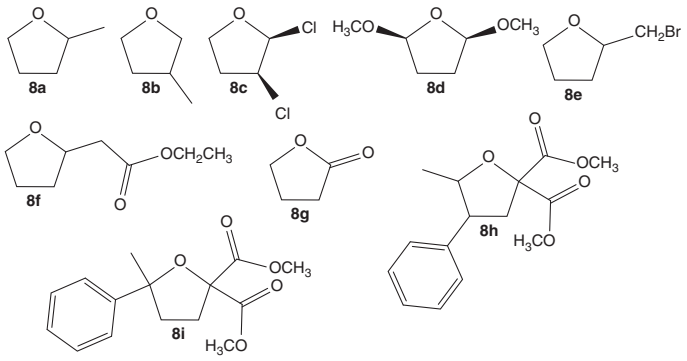

Figure 13.13 Derivatives of oxolane (**8**): 2-methyloxolane (**8a**), 3-methyloxolane (**8b**), (2*S*,3*S*)-2,3-dichlorooxolane (**8c**), (2*R*,5*S*)-2,5-dimethoxyoxolane (**8d**), 2-(bromomethyl) oxolane (**8e**), ethyl oxolan-2-ylethanoate (**8f**), oxolan-2-one (**8g**), dimethyl 5-methyl-4-phenyloxolane-2,2-dicarboxylate (**8h**), and dimethyl 5-methyl-5-phenyloxolane-2,2-dicarboxylate (**8i**).

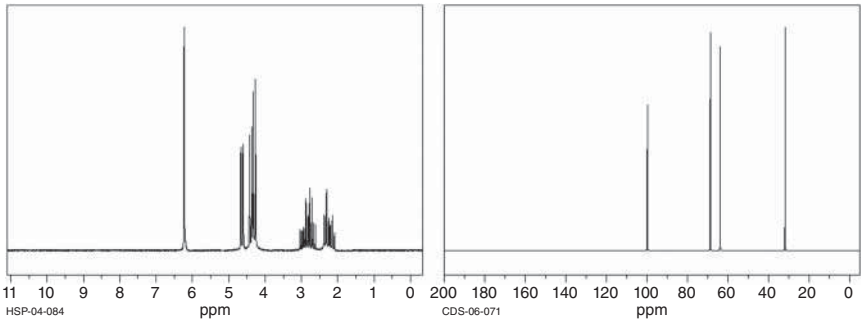

Figure 13.14 (2*S*,3*S*)-2,3-Dichlorooxolane (**8c**) ^{1}H and ^{13}C NMR spectra. Source: SDBSWeb: https://sdbs.db.aist.go.jp. National Institute of Advanced Industrial Science and Technology, accessed 05 December 2021.

When the methyl group is at C-3, compound **8b**, the chemical shifts are similar, except for C-4, which now appears at δ 34.3 ppm.

(2*S*,3*S*)-2,3-Dichlorooxolane (**8c**) is more deshielded at C-2 and C-3, whose chemical shifts are δ 99.8 and 63.9 ppm, respectively (Figure 13.14). The same occurs in (2*R*,5*S*)-2,5-dimethoxyoxolane (**8d**), as the C-2 (and C-5) is shifted downfield to δ 106.2 ppm. This trend is followed in the spectra of compounds **8e** and **8f**, but in γ-butyrolactone (**8g**), a disparity is observed. Carbon C-2 is deshielded due to the electronegativity of both oxygens, resulting in a chemical shift typical of carbonyls at δ 178.0 ppm. The resonance frequencies increase in the highly substituted oxolane derivative **8h**, particularly for C-3 and C-4. The 4-phenyl substituent makes the C-4 reach δ 52.8 ppm.

Monosaccharides (Figure 13.15) can be present in nature in many conformations or configurations, one of them having the oxolane (furanose) ring. Wu and Vuorinen studied the kinetic conformation exchange for D-ribulose and D-xylulose in 1990,

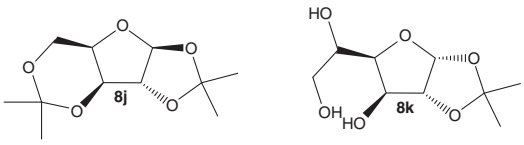

Figure 13.15 Monosaccharides derivatives of oxolane (**8**): 1,2 : 3,5-di-*O*-isopropylidene-α-D-xylofuranose (**8j**) and 1,2-*O*-isopropylidene-D-glucofuranose (**8k**).

Table 13.8 ^{1}H and ^{13}C NMR chemical shifts of two furanoses.

Compound/ substituent	^{1}H (δ, ppm)	^{13}C (δ, ppm)	Solvent	References
8j	6.00 (H-2)	105.3 (C-2)	$CDCl_3$	[67, 68]
	4.52 (H-3)	84.7 (C-3)		
	4.29 (H-4)	73.3 (C-4)		
	4.10 (H-5)	71.7 (C-5)		
8k	5.78 (H-2)	104.4 (C-2)	DMSO-d_6	[69, 70]
	4.37 (H-3)	84.6 (C-3)		
	4.03 (H-4)	73.3 (C-4)		
	3.83 (H-5)	80.0 (C-5)		

using NMR techniques [66]. The signals used for assessment were the chemical shift of C-2 in the ^{13}C-NMR because it appears around δ 214 ppm for the open-chain form and at much lower chemical shift for the furanose anomers. In the case of α-ribulofuranose, it appears at δ 104.0 ppm, while for the β-anomer, the chemical shift is δ 107.0 ppm. For the xylulofuranose, chemical shifts of δ 107.2 and 104.4 ppm have been registered for the α- and β-anomers, respectively. The other carbons of monosaccharides often appear between δ 70 and 85 ppm (Table 13.8). In the ^{1}H NMR spectra, the H-2 is the most deshielded (δ below 6 ppm) due to the neighboring oxygen atoms. The other protons are more shielded and range between δ 3.8 and 4.5 ppm, where it seems to decrease following the order H-3, H-4, and H-5.

Furan (**9**) (Figure 13.12) is an aromatic heterocycle with a completely different NMR profile. All its signals are shifted downfield as a consequence of the aromaticity. The H-2,5 resonates at δ 7.43 ppm and the other protons at δ 6.38 ppm. The ^{13}C NMR spectrum has two peaks, one at δ 142.6 ppm (C-2) and the other at δ 109.5 ppm (C-3) (Table 13.9).

The substitution with methyl group at C-2, compound **9a** (Figure 13.16), has a shielding effect, which is the opposite of the previously discussed cases. The chemical shift of H-5 shifts to δ 7.25 ppm, the H-4 resonates at δ 6.23 ppm, and the H-3 resonance frequency is even lower (δ 5.93 ppm). As for the coupling constants, $J_{3,4}$ is the highest (3.2 Hz), and $J_{4,5}$ is 1.7–1.8 Hz. Sometimes, long-range coupling is visible, with $J_{3,5}$ below 1 Hz.

When the methyl group is at C-3, compound **9b** (Figure 13.16), the H-4 chemical shift decreases even further to δ 6.21 ppm, the H-5 gets slightly deshielded

Table 13.9 ^{1}H and ^{13}C NMR chemical shifts and coupling constants of furan derivatives.

Compound/substituent	^{1}H (δ, ppm) (J, Hz)	^{13}C (δ, ppm)	Solvent	References
9	7.44 (H-2) 6.38 (H-3)	142.6 (C-2) 109.5 (C-3)	$CDCl_3$	[71, 72]
9a 2-Methyl	5.93 (H-3) 6.23 (H-4) 7.25 (H-5) $J_{3,4}$ 3.2 Hz $J_{4,5}$ 1.8 Hz	152.2 (C-2) 105.5 (C-3) 110.4 (C-4) 140.8 (C-5)	$CDCl_3$	[73, 74]
9b 3-Methyl	7.17 (H-2) 6.21 (H-4) 7.30 (H-5)	139.3 (C-2) 119.8 (C-3) 112.2 (C-4) 139.5 (C-5)	$CDCl_3$	[75, 76]
9c 2,5-Dimethyl	5.81	150.2 (C-2) 106.0 (C-3)	$CDCl_3$	[77, 78]
9d 2-Methanoyl	7.30 (H-3) 6.63 (H-4) 7.73 (H-5) $J_{3,4}$ 3.6 Hz $J_{4,5}$ 1.7 Hz	153.1 (C-2) 121.6 (C-3) 112.8 (C-4) 148.3 (C-5)	$CDCl_3$	[79, 80]
9e 2-(Hydroxymethanoyl)	7.35 (H-3) 6.57 (H-4) 7.66 (H-5)	147.5 (C-2) 120.2 (C-3) 112.3 (C-4) 143.9 (C-5)	$CDCl_3$	[81, 82]
9f 2-Nitro	7.51 (H-3) 6.85 (H-4) 7.89 (H-5) $J_{3,5}$ 0.98 Hz	—	Acetone-d_6	[83]

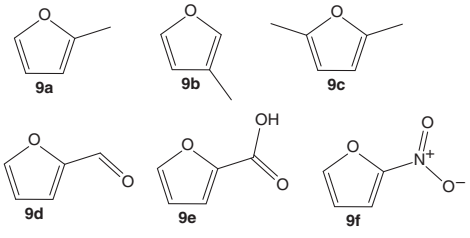

Figure 13.16 Derivatives of furan (**8**): 2-methylfuran (**9a**), 3-methylfuran (**9b**), 2,5-dimethylfuran (**9c**), furan-2-carbaldehyde (**9d**), furan-2-carboxylic acid (**9e**), and 2-nitrofuran (**9f**).

(δ 7.30 ppm), and the H-2 signal appears at δ 7.17 ppm. Finally, with two methyl groups, as in 2,5-dimethylfuran (**9c**), the chemical shifts of the protons at the heterocycle appears upfield at δ 5.81 ppm.

If electron-withdrawing groups are present in the chemical structure, the opposite is true regarding the chemical shifts. In summary, they are shifted downfield. Furfural (**9d**) has the most deshielded H-5 of all derivatives, followed by H-3 (Figure 13.16). Both are deshielded by the electron-withdrawing ability of the carbonyl group via conjugation, besides the inductive effect of the ring oxygen on H-5. Though not significantly affected by the furan–carbonyl conjugation, the chemical shift of H-4 is more deshielded than its homologous in furan. In the spectrum of 2-furoic acid (**9e**), similar effects of the carboxylic group on the chemical shifts of the ring protons can be observed. In the 2-nitrofuran (**9f**) spectrum, the H-4 signal appears at δ 6.85 ppm, and the other ones are shifted further downfield to δ 7.51 and 7.89 ppm for H-3 and H-5, respectively (Figure 13.16).

In ^{13}C NMR, the methyl substituents deshield the carbons to which they are bonded, while the rest have unpredictable variations. Therefore, in 2-methylfuran (**9a**), the C-2 resonates at δ 152.2 ppm, and in 3-methylfuran (**9b**), the C-3 resonates at δ 119.8 ppm. In the case of derivatives having methyl substituents at both C-2 and C-5, compound **9c** (Figure 13.16) both appear at δ 150.2 ppm. With the carbonyl and the carboxylic moieties attached to C-2 in compounds **9d** and **9e**, respectively, the C-2 itself is shifted downfield to δ 153.1 and 147.5 ppm. Also shifted downfield are C-3 and C-5 due to the furan–carbonyl group conjugation. Carbon C-3 appears above δ 120 ppm, and C-5 at δ 148.3 ppm (in **9d**) and δ 143.9 ppm (in **9e**). The C-4 signal appears around δ 112 ppm.

Benzofurans are a subclass of furans also present in nature [84]. The principal compounds have the structure of benzofuran (**9g**), isobenzofuran (**9i**), or dibenzofuran (**9j**). The flavonoid aurone (**9h**) has a benzofuranone scaffold, as can be seen in Figure 13.17.

As expected, the resonance frequencies for the furan ring in benzofurans are higher than those of furans (Table 13.10). In the ^{1}H NMR spectra of compound **9g**,

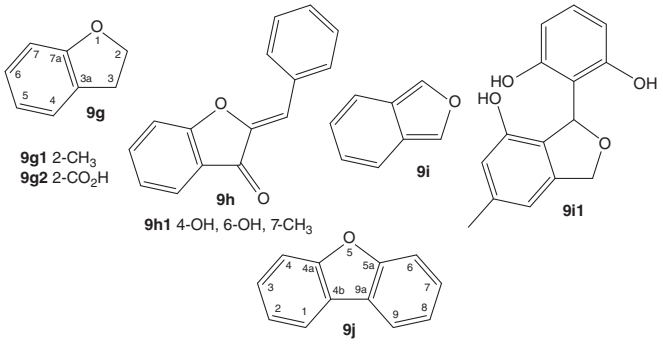

Figure 13.17 Benzofurans and some derivatives: benzofuran (**9g**), aurone (**9h**), isobenzofuran (**9i**), 1,3-dihydro-1-(2,6-dihydroxyphenyl)-7-hydroxy-5-methylbenzofuran (**9i1**), and dibenzofuran (**9j**).

Table 13.10 ^{1}H and ^{13}C NMR chemical shifts and coupling constants of benzofurans derivatives.

Compound/substituent	^{1}H (δ, ppm) (J, Hz)	^{13}C (δ, ppm)	Solvent	References
9g Benzo[*d*]	7.54 (H-2) 6.69 (H-3)	144.9 (C-2) 106.5 (C-3) 127.5 (C-3a) 155.0 (C-7a)	$CDCl_3$	[85, 86]
9g1 2-Methylbenzo[*d*]	6.36	155.4 (C-2) 102.6 (C-3) 129.2 (C-3a) 154.8 (C-7a)	$CDCl_3$	[87, 88]
9g2 2-(Hydroxymethanoyl) benzo[*d*]	7.72	146.2 (C-2) 113.4 (C-3) 126.9 (C-3a) 155.0 (C-7a)	DMSO-d_6	[89, 90]
9h1 (Z)-2-Benzylidene-4,6-dihydroxy-7-methylbenzo[*d*]	—	148.0 (C-2) 179.5 (C-3) 102.1 (C-3a) 156.0 (C-7a)	DMSO-d_6	[91]
9j Dibenzo[*b*,*d*]	—	156.2 (C-4a) 124.2 (C-4b)	$CDCl_3$	[92, 93]
9i1 1,3-Dihydro-1-(2,6-dihydroxyphenyl)-7-hydroxy-5-methylbenzo[*c*]	6.79 (H-1) 5.01 (H-3 *cis*) 5.33 (H-3 *trans*) (J_{gem} 11.3 Hz $J_{1,3}$ 2.7 Hz)	79.9 (C-1) 74.4 (C-3) 142.5 (C-3a) 124.8 (C-7a)	Unknown	[84]

the H-3 appear at δ 6.69 ppm. The other proton's signal is mixed with the aromatic multiplets at δ 7.54 ppm. With a 2-methyl substituent, **9g1**, the chemical shift of H-3 decreases to δ 6.36 ppm, whereas with a 2-carboxylic group, **9g2**, it increases to δ 7.72 ppm.

In the isobenzofuran derivative **9i1**, the H-1 appears downfield at δ 6.79 ppm. H-3 are nonequivalent, and the H-3 *cis* to H-1 has a chemical shift of δ 5.01 ppm, and its geminal proton, which is *trans* to H-1 appears at δ 5.33 ppm. The geminal coupling constant frequency is 11.3 Hz, and the long-range coupling between the H-1 and the H-3 on the same side of the ring has a value of 2.7 Hz.

In the ^{13}C NMR of these derivatives, the C-7a (or C-4a in the case of dibenzofuran (**9j**)) is the most deshielded, frequently with a chemical shift around δ 155 ppm, as in the case of compound **9g**. The other carbon common to the benzene and the furan rings often ranges between δ 124 and 129 ppm. However, the two hydroxy groups at ortho- and para-positions shield it to δ 102.1 ppm in compound **9h1**.

Table 13.11 ^{1}H and ^{13}C NMR chemical shifts of 1,2-dioxolane derivatives, in $CDCl_3$.

Compound/substituent	^{1}H (δ, ppm)	^{13}C (δ, ppm)	Solvent
10a 3-Ethoxy	5.32 (H-3) 2.59 (H-4 *cis*) 2.76 (H-4 *trans*) 4.24 (H-5 *cis*) 3.94 (H-5 *trans*)	101.7 (C-3) 42.5 (C-4) 68.0 (C-5)	[94]
10b 3,3-Dimethoxy	2.52 (H-4) 4.24 (H-5)	123.3 (C-3) 39.0 (C-4) 71.6 (C-5)	[95]
10c 3-Ethanoyloxy	6.56 (H-3) 2.75 (H-4 *cis*) 2.96 (H-4 *trans*) 4.31 (H-5 *cis*) 4.09 (H-5 *trans*)	95.0 (C-3) 42.3 (C-4) 68.0 (C-5)	[95]

The C-2 and C-3 chemical shifts of benzofuran derivatives resemble furan, with negligent variances. The C-3 appears at δ 179.5 ppm only in aurone (**9h**) due to the carbon sp^2 hybridization and the inductive effect of carbonyl's oxygen, and the values are also different for compound **9i1**. In this last compound, the hybridization is the same as oxolane, so the δ 79.9 ppm for C-1 and δ 74.4 ppm for C-3 are not unexpected.

The 1,2-dioxolanes (**10**) (Figures 13.12 and 13.18) can be produced by ozonolysis of alkenes, as reported by Keul et al. [94]. Very few examples of NMR spectra of these heterocycles can be found in the literature (Table 13.11). As expected, H-3 and H-5 are the most deshielded. In the case of 3-ethoxy-1,2-dioxolane (**10a**), the H-3 signal appears at δ 5.32 ppm, while the two H-5 appear at δ 4.24 and 3.94 ppm, *cis*- and *trans*-relatively to the substituent, respectively. The two H-4 *cis*- and *trans*-relatively to the ethoxy substituent appear at δ 2.59 and 2.76 ppm. When there are two alkoxy groups at C-3, **10b**, H-4 and H-5 appear in the ^{1}H NMR spectrum, as doublets, with the same chemical shift. When an acetyloxy group is present, compound **10c** (Figure 13.18), all the protons are shifted downfield compared to the ethoxy substituent. The H-3 has the most significant difference, with a resonance frequency at δ 6.56 ppm, while in the chemical shift of the other protons, the changes are minimal (<0.20 ppm).

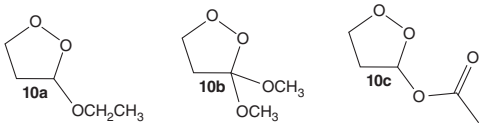

Figure 13.18 Derivatives of 1,2-dioxolane (**10**): 3-ethoxy-1,2-dioxolane (**10a**), 3,3-dimethoxy-1,2-dioxolane (**10b**), and 1,2-dioxolan-3-yl ethanoate (**10c**).

Table 13.12 ^{1}H and ^{13}C NMR chemical shifts of 1,3-dioxolane derivatives.

Compound/substituent	^{1}H (δ, ppm)	^{13}C (δ, ppm)	Solvent	References
11	4.90 (H-2) 3.88 (H-4)	95.1 (C-2) 64.6 (C-4)	$CDCl_3$	[98, 99]
11a 2-Methyl	4.98 (H-2) 3.97 (H-4 *cis*) 3.86 (H-4 *trans*)	101.6 (C-2) 64.9 (C-4)	$CDCl_3$	[100, 101]
11b 2-Benzyl	5.04 (H-2) 3.78 (H-4 *cis*) 3.88 (H-4 *trans*)	104.6 (C-2) 64.9 (C-3)	$CDCl_3$	[102, 103]
11c 2-Methoxy	5.74 (H-2) 4.08 (H-4 *cis*) 3.96 (H-4 *trans*)	116.0 (C-2) 64.1 (C-3)	$CDCl_3$	[104, 105]
11d 2-(Chloromethyl)	5.16 (H-2) 3.96 (H-4 *cis*) 4.05 (H-4 *trans*)	102.6 (C-2) 65.6 (C-3)	$CDCl_3$	[106, 107]
11e (*R*)-4-(Methoxymethyl)-2-oxo	4.80 (H-4) 4.50 (H-5 *cis*) 4.38 (H-5 *trans*)	154.9 (C-2) 75.0 (C-4) 71.5 (C-5)	$CDCl_3$	[108, 109]
11f	5.02 (H-2) 3.66 (H-4 *cis*) 3.46 (H-4 *trans*)	—	Benzene-d_6	[110]

In the ^{13}C NMR spectra of 1,2-dioxolanes (**10**), the C-4 has a signal around δ 40 ppm, and the unsubstituted C-5 is approximately at δ 70 ppm. In the compounds presented in Table 13.11, the C-3 chemical shift varies with the substituent. For example, it appears at δ 101.7 ppm when there is one alkoxy substituent at this position and δ 123.3 ppm when two alkoxy substituents are linked to C-3. A smaller chemical shift was observed in the case of compound **10c** (δ 95.0 ppm).

The 1,3-dioxolane (**11**) (Figure 13.12) derivatives have attracted academic interest for their use in the production of new polymers and liquid crystals [96, 97]. Therefore, knowing their resonance frequencies is mandatory for a good characterization of those materials (see Table 13.12).

The 1,3-dioxolane (**11**) (Figure 13.12) presents two singlets in the ^{1}H NMR spectrum, with chemical shifts of δ 4.90 ppm for H-2 and δ 3.88 ppm for H-4. In the ^{13}C NMR spectrum, the C-2 appears at δ 95.14 ppm, and the other two carbons appear at δ 64.6 ppm since they are equivalent. When a methyl group is attached to C-2, **11a**, the chemical shifts of both H-2 and C-2 are shifted downfield. The other protons' signals are split into two doublets because of the different chemical environments on each side of the ring. Hence, the H-2 resonance frequency is δ 4.98 ppm,

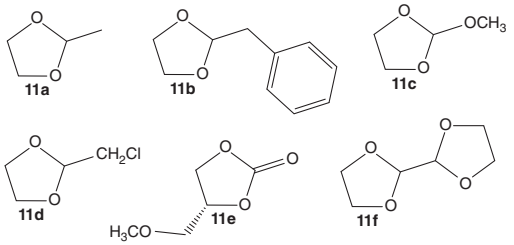

Figure 13.19 Derivatives of 1,3-dioxolane (**11**): 2-methyl-1,3-dioxolane (**11a**), 2-benzyl-1,3-dioxolane (**11b**), 2-methoxy-1,3-dioxolane **(11c)**, 2-(chloromethyl)-1,3-dioxolane (**11d**), (*R*)-4-(methoxymethyl)-1,3-dioxolan-2-one (**11e**), and 2,2′-bis(1,3-dioxolane) (**11f**).

and the other two signals in ^{1}H NMR are δ 3.97 and 3.86 ppm for the *cis*- and the *trans*-protons, respectively (Figure 13.19).

For other substituents such as 2-benzyl, 2-methoxy, and 2-(chloromethyl) (compounds **11b**, **11c**, and **11d**), it was reasonable to expect the same trend. However, unexpectedly, the results published in AIST's database [9] report higher chemical shifts for the *trans*-protons in **11b** and **11d** than for their *cis*-protons. Therefore, caution is recommended in profiling these signals, and nuclear overhauser effect spectroscopy (NOESY) analysis should be carried out to properly assign them. The H-2 signals appear at δ 5.04, 5.74, and 5.16 ppm for **11b**, **11c**, and **11d**, respectively, the most deshielded being **11c** due to the inductive effect of the three oxygen atoms.

For the 2,2′-bis-1,3-dioxolane (**11f**), the H-2 signal appears at δ 5.02 ppm, while the H-4 signals are at δ 3.66 and 3.46 ppm (*cis* and *trans*, respectively). The slightly lower chemical shift of H-4, when compared with 1,3-dioxolane, may be due to the different solvent used in each case (last column of Table 13.12).

In compound **11e**, the carbonyl at C-2 has an impact on H-4 and H-5 chemical shifts. They now appear upfield, at δ 4.80 ppm for H-4 and around δ 4.4 ppm for H-5, the *cis*-protons being more deshielded than the *trans*.

In the ^{13}C NMR, the resonance frequency of C-2 for the 2-methyl-1,3-dioxolane (**11a**) appears at δ 101.6 ppm, while the C-4 appears at δ 64.9 ppm. For the other 2-substituents, the benzyl in compound **11b** and the methoxy in compound **11c**, the C-4 practically does not change, ranging between δ 64 and 66 ppm. The C-2 shows more variance, with δ 102.6 ppm in **11d** and δ 116.0 ppm if there is a 2-methoxy substituent. The spectrum of compound **11e** presents a signal at δ 154.9 ppm from the carbonyl's resonance, and two other more shielded signals at δ 75.0 and 71.5 ppm. The first belongs to C-4, which has the methoxymethyl group, and the other to C-5.

1,2,4-Trioxolanes (**12**), often called ozonides (Figures 13.12 and 13.20) are produced by alkene ozonolysis [95, 111]. The NMR of the reference compound (1,2,4-trioxolane (**12**)) cannot be found in the literature. Only the spectra of some derivatives and some generic fatty esters were described (Table 13.13). Despite the lack of experimental data, the chemical shifts of 1,2,4-trioxolane can be estimated by comparison with data from similar compounds. In both ^{1}H and ^{13}C NMR, only one peak is expected. In the first case, the chemical shift should be near δ 5 ppm,

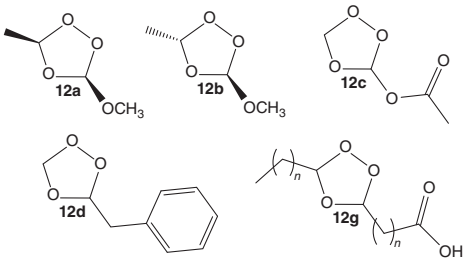

Figure 13.20 Derivatives of 1,2,4-trioxolane (**12**): *cis*-3-methoxy-5-methyl-1,2,4-trioxolane (**12a**), *trans*-3-methoxy-5-methyl-1,2,4-trioxolane (**12b**), 1,2,4-trioxolan-2-yl ethanoate (**12c**), 3-benzyl-1,2,4-trioxolane (**12d**), and ω-(5-alkyl-1,2,4-trioxolan-3-yl) alkanoic acid (**12g**).

Table 13.13 ^{1}H and ^{13}C NMR chemical shifts of 1,2,4-trioxolane derivatives, in $CDCl_3$.

Compound/substituent	^{1}H (δ, ppm)	^{13}C (δ, ppm)	References
12a *cis*-3-Methoxy-5-methyl	6.02 (H-3) 5.26 (H-5)	112.7 (C-3) 101.3 (C-5)	[95]
12b *trans*-3-Methoxy-5-methyl	6.02 (H-3) 5.67 (H-5)	113.2 (C-3) 101.6 (C-5)	[95]
12c 3-Ethanoyloxy	7.14 (H-3) 5.56 (H-5 *cis*) 4.97 (H-5 *trans*)	—	[95]
12d 3-Benzyl	5.39 (H-3) 5.18 (H-5 *cis*) 5.09 (H-5 *trans*)	103.5 (C-3) 94.1 (C-5)	[112]
12g Fatty derivatives	5.12–5.19	104.1–104.5	[111, 113]

similar to the most deshielded proton of the unsubstituted position in compound **12c** (the H-2 from 1,3-dioxolane (**11**), which has two oxygen atoms nearby, appears at δ 4.90 ppm). In the ^{13}C NMR spectrum, the signal should be around δ 95 ppm, similar to C-5 in 3-benzyl-1,2,4-trioxolane (**12d**) and C-2 of 1,3-dioxolane (**11**).

Wojciechowski et al. have analyzed the resonance frequencies of some simple 1,2,4-trioxolane derivatives synthesized by them [95]. *cis*-3-Methoxy-5-methyl-1,2,4-trioxolane (**12a**) showed a singlet at δ 6.02 ppm (H-3) and a quartet at δ 5.26 ppm (H-5) due to the coupling with the methyl protons. The *trans*-isomer presented a signal at δ 6.02 ppm (H-3), and a signal for H-5 shifted downfield to δ 5.67 ppm. In the ^{13}C NMR spectra, the most deshielded carbon (C-2) appeared at δ 112.7 and 113.2 ppm, and the C-5 at δ 101.31 and 101.6 ppm, for the *cis*- and *trans*-isomers, respectively. Overall, **12b** had higher resonance frequencies than **12a**.

Lower chemical shifts are observed in the 3-benzyl-1,2,4-trioxolane (**12d**) spectrum. The H-3 signals appear at δ 5.39 ppm and the others slightly above δ 5 ppm, with the *cis*-proton more deshielded. The spectrum of **12c**, with a 3-ethanoyloxy

substituent, has three signals. The H-5 appear at δ 5.56 and 4.97 ppm for *cis* and *trans*, respectively. The H-3 is shifted downfield to δ 7.14 ppm.

In the ^{13}C NMR, the 3-methoxy group causes the corresponding carbon to present a chemical shift at δ 112.7–113.2 ppm (**12a** and **12b**), and the C-5 appears at δ 101.3–101.6 ppm. In the case of **12d**, the most deshielded carbon (C-3) is at δ 103.5 ppm, while the other one has a lower resonance frequency (δ 94.1 ppm).

The chemical environment of the 1,2,4-trioxolane core produced by ozonolysis of many fatty acids is quite similar. Resonance frequencies are reported in the range δ 5.12–5.19 ppm for its protons and between δ 104.1 and 104.5 ppm for the carbons [111, 113].

13.5 Six-Membered Heterocyclic Compounds

The oxane (**13**) (Figure 13.21), more commonly known as tetrahydropyran (THP), is the simplest six-membered O-heterocycle. The resonance frequencies are not so different from oxolane (**8**) (Figure 13.12), but there are extra signals for the new atoms. The peaks that appear at δ 3.65 ppm correspond to four protons (H-2 and H-6), and the multiplet at δ 1.59 ppm is due to the resonance of all the other protons. In the ^{13}C NMR spectrum, it is possible to distinguish C-3/C-5 and C-4, at δ 27.0 and 23.9 ppm, respectively. The deshielded carbon C-2 and C-6 resonate at δ 68.8 ppm.

When there are substituents in the ring, the two chair conformations become inequivalent, so the equatorial and axial positions' chemical shifts are different. Furthermore, in asymmetrically substituted derivatives, the presence of stereogenic centers implies that the two protons of the nearby methylene groups become inequivalent. From the results collected in Table 13.14, it is possible to conclude that there is a trend for more deshielded equatorial protons than axials. For example, 2-(hydroxymethyl)oxane (**13b**) (Figure 13.22) presents signals at δ 4.01 and 3.46 ppm, which correspond to H-6. The first proton is in the equatorial position and the second in the axial position; i.e. the first is on the same side of the plane as the substituent (*cis*) and the other one on the opposite side (*trans*). Then, the H-2 proton is at δ 3.42 ppm, and the rest of the chemical shifts are upshield. While proton H-3 has been differentiated into δ 1.86 and 1.32 ppm for the equatorial and axial positions, others (H-4 and H-5) are in the range δ 1.45–1.64 ppm. With a 2-(bromomethyl) substituent **13c**, almost all the resonance frequencies are slightly shifted downfield (around $\Delta\delta$ 0.1 ppm).

3-Methyloxane (**13d**) has two different signals for H-2 (Figure 13.23). The equatorial appears at δ 3.80 ppm and the axial at δ 2.98 ppm. The axial H-3 is more deshielded than in the previous compounds, with a chemical shift at δ 1.68 ppm. In the H-4, there is also a significant difference in the resonance frequencies between

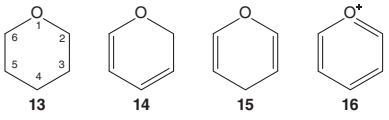

Figure 13.21 Six-membered O-heterocycles with only one oxygen: oxane (**13**), 2*H*-pyran (**14**), 4*H*-pyran (**15**), and pyrylium (**16**).

Table 13.14 ^{1}H and ^{13}C NMR chemical shifts of oxane derivatives, in $CDCl_3$.

Compound/substituent	^{1}H (δ, ppm)	^{13}C (δ, ppm)	References
13	3.65 (H-2) 1.59 (H-3,4)	68.8 (C-2) 27.0 (C-3) 23.9 (C-4)	[115, 116]
13a 2-Methyl	—	73.9 (C-2) 33.9 (C-3) 23.8 (C-4) 26.1 (C-5) 68.5 (C-6)	[117]
13b 2-(Hydroxymethyl)	3.42 (H-2) 1.32 (H-3 *cis*) 1.86 (H-3 *trans*) 1.45–1.64 (H-4,5) 4.01 (H-6 *cis*) 3.46 (H-6 *trans*)	78.5 (C-2) 26.0 (C-3) 23.0 (C-4) 27.5 (C-5) 68.3 (C-6)	[118, 119]
13c 2-(Bromomethyl)	3.50 (H-2) 1.36 (H-3 *cis*) 1.74 (H-3 *trans*) 1.48–1.63 (H-4) 1.48–1.63 (H-5 *cis*) 1.88 (H-5 *trans*) 4.04 (H-6 *cis*) 3.48 (H-6 *trans*)	76.9 (C-2) 30.2 (C-3) 23.1 (C-4) 25.7 (C-5) 68.6 (C-6)	[120, 121]
13d 3-Methyl	2.98 (H-2 *cis*) 3.80 (H-2 *trans*) 1.68 (H-3) 1.12 (H-4 *cis*) 1.81 (H-4 *trans*) 1.53–1.65 (H-5) 3.32 (H-6 *cis*) 3.87 (H-6 *trans*)	74.8 (C-2) 32.2 (C-3) 26.2 (C-4) 31.2 (C-5) 68.2 (C-6)	[122, 123]
13e 4-Hydroxy	3.94 (H-2 *cis*) 3.43 (H-2 *trans*) 1.55 (H-3 *cis*) 1.87 (H-3 *trans*) 3.80 (H-4)	65.7 (C-2) 35.4 (C-3) 66.6 (C-4)	[124, 125]

Table 13.14 (Continued)

Compound/substituent	^{1}H (δ, ppm)	^{13}C (δ, ppm)	References
13f (2*S*,4*S*)-2-(4-Chlorophenyl)-4-hydroxy	4.72 (H-2) 1.90 (H-3 *eq*) 1.81 (H-3 *ax*) 4.27 (H-4) 1.63 (H-5 *eq*) 1.57 (H-5 *ax*) 4.06 (H-6 *eq*) 3.90 (H-6 *ax*)	73.8 (C-2) 40.6 (C-3) 64.2 (C-4) 32.8 (C-5) 62.8 (C-6)	[114]
13g (2*R*,4*S*)-2-(4-Chlorophenyl)-4-hydroxy	4.24 (H-2) 2.15 (H-3 *trans*) 1.93 (H-3 *cis*) 3.87 (H-4) 1.30–1.68 (H-5) 4.14 (H-6 *cis*) 3.52 (H-6 *trans*)	73.8 (C-2) 40.6 (C-3) 64.2 (C-4) 32.8 (C-5) 62.8 (C-6)	[114]

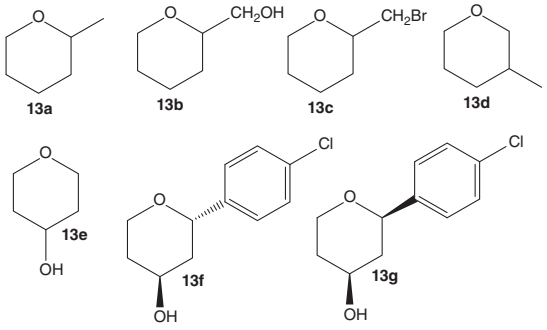

Figure 13.22 Derivatives of oxane (**13**): 2-methyloxane (**13a**), 2-(hydroxymethyl)oxane (**13b**), 2-(bromomethyl)oxane (**13c**), 3-methyloxane (**13d**), 4-hydroxyoxane (**13e**), (2*S*,4*S*)-2-(4-chlorophenyl)-4-hydroxyoxane (**13f**), and (2*R*,4*S*)-2-(4-chlorophenyl)-4-hydroxyoxane (**13g**).

equatorial (δ 1.81 ppm) and axial, the most shielded proton δ (1.12 ppm). The rest of the protons behave as usual.

In the case of 4-hydroxyoxane (**13e**) (Figure 13.22), the symmetry in the structure reduces the number of signals. Hence, the one with lower integral value corresponds to one proton (H-4), and it is at δ 3.80 ppm. The others' integral values should be around the double, being the most deshielded at δ 3.94 and 3.43 ppm for the equatorial and axial positions, respectively (H-2 and H-5). Thus, the H-3 and H-4 appear between δ 1.5 and 1.9 ppm.

Yadav et al. studied some 2-substituted derivatives of 4-hydroxyoxanes for the two diastereomers possible in each case [114]. (2*S*,4*S*)-2-(4-Chlorophenyl)-4-hydroxyoxane (**13f**) with the substituents on opposite sides of the ring and (2*R*,4*S*)-2-(4-chlorophenyl)-4-hydroxyoxane (**13g**) with the substituents at the same side of the ring were selected as example.

With the addition of the 2-aryl group, the H-2 signal is the most deshielded, with δ 4.72 ppm for **13f** and δ 4.24 ppm for **13g**. A significant change in resonance frequency is visible for H-4, which is δ 4.27 ppm for **13f** and δ 3.87 ppm for **13g**, and for the axial H-6, whose chemical shifts are δ 3.90 and 3.52 ppm, respectively. In position 6 (H-6 *eq*), the proton maintains the signal at δ 4.14 ppm, and the H-5 appears at δ 1.30–1.68 ppm. The H-3 appears at δ 1.93 and 2.15 ppm in compound **13g**, and these proton signals are shifted upfield in compound **13f** (δ 1.81 and 1.90 ppm), where only one substituent is in the equatorial position.

In the ^{13}C spectra, a 2-methyl substituent shifts the signals of C-2 and C-3 significantly upfield to δ 73.9 and 33.9 ppm, respectively. The other values are similar to oxane (**13**) (δ 23.8 ppm for C-4, δ 26.1 ppm for C-5, and δ 68.5 ppm for C-6). Curiously, for the 2-hydroxymethyl derivative **13b** and the 2-bromomethyl derivative **13c**, the C-2 is further shifted downfield to δ 78.5 and 76.9 ppm, respectively, but the C-3 appears at values similar to those observed for oxane (**13**). In the case of 3-methyloxane (**13d**), only the C-6 keeps the original resonance frequency (Figure 13.23); the other ones are shifted downfield between $\Delta\delta$ 2 and 5 ppm. For the 4-hydroxy substituted oxane (**13e**), C-2 becomes more shielded and appears at δ 65.7 ppm, while the resonance of C-3 and C-4 increased to δ 35.4 ppm and δ 66.6 ppm, respectively.

In the study involving the diastereomers **13f** and **13g** (Figure 13.22), it is strange that both C-2 and C-3 have the same chemical shift [114]. The C-2 is the most unshielded carbon, with a chemical shift at δ 73.8 ppm, followed by C-4 (δ 64.2 ppm) and C-6 (δ 62.8 ppm). The C-3 appears at δ 40.6 ppm, and the C-5 is the most shielded one, at δ 32.8 ppm.

The pyranoses are monosaccharides with the oxane heterocyclic scaffold, and they can be formed by hexoses and pentoses, aldoses, and ketoses. Furthermore, their anomeric isomers can occur in equilibrium under the NMR analysis. Hence, the NMR frequently changes with the conditions used during analysis because the concentration of each configuration changes with the equilibrium constant in each condition. This also has its advantages, as the ratio between the anomers can be

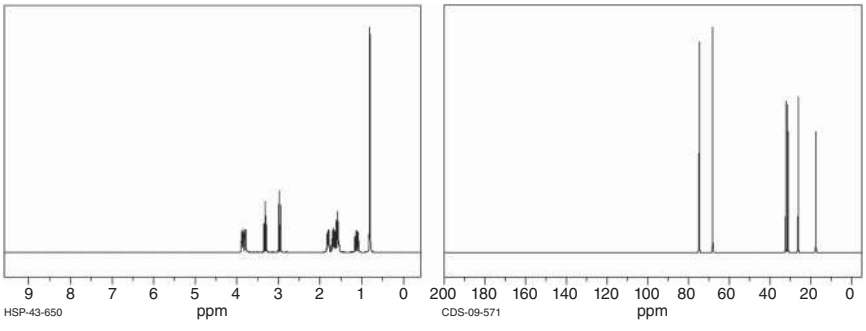

Figure 13.23 3-Methyloxane (**13d**) ^{1}H and ^{13}C NMR spectra. Source: SDBSWeb: https://sdbs.db.aist.go.jp. National Institute of Advanced Industrial Science and Technology, accessed 05 December 2021.

Table 13.15 ^{1}H and ^{13}C NMR chemical shifts and coupling frequencies of pyranoses, in certain solvents.

Compound	^{1}H (δ, ppm) (J, Hz)	^{13}C (δ, ppm)	Solvent	References
13h β-D-Arabinopyranose	4.86 (H-2) 3.48 (H-3) 3.60 (H-4) 3.68 (H-5) 3.69 (H-6 *eq*) 3.38 (H-6 *ax*) ($J_{H,OH}$ 4.2–6.6 Hz J_{gem} −12.1 Hz J_{cis} 2.3–3.3 Hz J_{trans} 5.0–8.3 Hz)	—	DMSO-d_6	[127, 128]
	—	93.4 (C-2) 69.4 (C-3) 69.5 (C-4) 69.3 (C-5) 63.3 (C-6)	D_2O	
13i α-D-Arabinopyranose	—	97.6 (C-2) 69.3 (C-3) 73.3 (C-4) 72.7 (C-5) 67.2 (C-6)	D_2O	[129]
13j β-L-Lyxopyranose	4.61 (H-2) 3.58 (H-3) 3.39 (H-4) 3.54 (H-5) 3.74 (H-6 *eq*) 3.04 (H-6 *ax*)	—	DMSO-d_6	[130, 131]
	—	95.3 (C-2) ~70 (C-3) 73.8 (C-4) 67.6 (C-5) 65.2 (C-6)	D_2O	
13k α-L-Lyxopyranose	—	95.2 (C-2) 71.1 (C-3) 71.6 (C-4) 68.6 (C-5) 64.1 (C-6)	D_2O	[131]

Table 13.15 (Continued)

Compound	^{1}H (δ, ppm) (J, Hz)	^{13}C (δ, ppm)	Solvent	References
13l β-D-Galactopyranose	4.59 (H-2) 3.49 (H-3) 3.65 (H-4) 3.93 (H-5) 3.72–3.78 (H-6)	97.5 (C-2) 73.0 (C-3) 73.9 (C-4) 69.8 (C-5) 76.1 (C-6)	D_2O	[132, 133]
13m α-D-Galactopyranose	5.27 (H-2) 3.85 (H-3) 3.82 (H-4) 3.99 (H-5) 4.09 (H-6)	93.3 (C-2) 69.4 (C-3) 70.3 (C-4) 70.4 (C-5) 71.4 (C-6)	D_2O	[132, 133]
13n β-D-Glucopyranose	6.58 (H-2) 2.89 (H-3) 3.10 (H-4,5) 3.04 (H-6)	—	DMSO-d_6	[126, 134, 135]
	—	97.0 (C-2) 75.2 (C-3) 76.9 (C-4) 70.5–71.0 (C-5) 77.01 (C-6)	D_2O	
13o α-D-Glucopyranose	6.20 (H-2) 3.10 (H-3) 3.42 (H-4) 3.04 (H-5) 3.57 (H-6)	—	DMSO-d_6	[126, 134, 135]
	—	93.2 (C-2) 72.6 (C-3) 73.9 (C-4) 70.8 (C-5) 72.0–72.5 (C-6)	D_2O	
13p β-D-Fructopyranose	3.55–3.59 (H-3,4) 3.65 (H-5) 3.43 (H-6 *ax*) 3.78 (H-6 *eq*)	—	DMSO-d_6	[136, 137]
	—	98.9 (C-2) 68.4 (C-3) 70.5 (C-4) 70.0 (C-5) 64.2 (C-6)	D_2O	

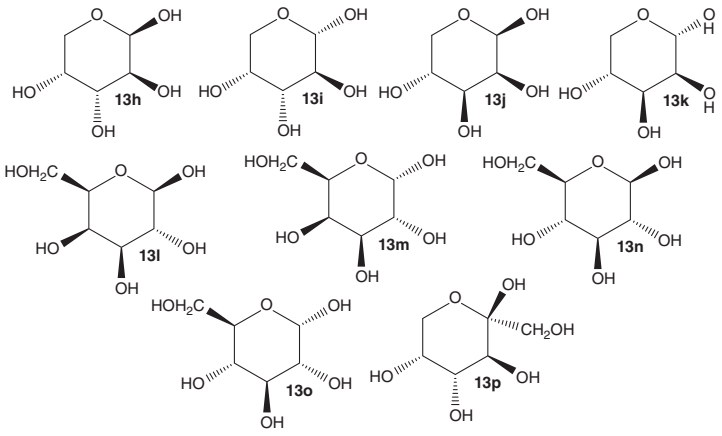

Figure 13.24 Monosaccharides derivatives of oxane (**13**): β-D-arabinopyranose (**13h**), α-D-arabinopyranose (**13i**), β-L-lyxopyranose (**13j**), α-L-lyxopyranose (**13k**), β-D-galactopyranose (**13l**), α-D-galactopyranose (**13m**), β-D-glucopyranose (**13n**), α-D-glucopyranose (**13o**), and β-D-fructopyranose (**13p**).

determined using the NMR techniques [126]. In Table 13.15, several monosaccharide examples and their resonance frequencies are shown. Unfortunately, they are not exhaustive, and a review on that topic is still not available.

Starting with β-D-arabinopyranose (**13h**) (Figure 13.24), the most deshielded proton is the H-2, with a chemical shift at δ 4.86 ppm. The rest of the protons are in the range δ 3.3–3.7 ppm. The lowest resonance frequency belongs to the H-6 in the axial position (δ 3.38 ppm) and the second to the H-3 (δ 3.48 ppm). The coupling constants help in the identification of the signals. The coupling between the proton from the hydroxy group and the proton bonded to the carbon in the same position is $J_{\mathrm{H,OH}}$ 4.2–6.6 Hz. The geminal coupling was assigned as J_{gem} 12.1 Hz, and the calculated *cis*- and *trans*-couplings are J_{cis} 2.3–3.3 Hz and J_{trans} 5.0–8.3 Hz (the attribution of the signals was done using the ^{1}H–^{1}H COSY technique).

For the β-L-lyxopyranose (**13j**), the structural differences are in the hydroxy group locations from C-3 and C-5 compared with **13h**. In the ^{1}H NMR spectrum, the H-2 appears at δ 4.61 ppm, and the equatorial H-6 is the second most deshielded signal at δ 3.74 ppm. The ones more shifted upfield are the axial H-6 (δ 3.04 ppm) and the H-4 (δ 3.39 ppm).

In the aldohexose spectra, the main difference is at C-6, as expected from the new hydroxymethyl group attached to it. Compound **13l** still has the most deshielded proton at δ 4.59 ppm (H-2). Then, the H-5 appears at $\delta > 3.9$ ppm and the H-6 at δ 3.75 ppm. On the opposite side of the spectrum, the H-3 is the most shielded at δ 3.49 ppm. The resonances frequencies shift downfield overall in the ^{1}H NMR spectrum of the α-anomer **13m**. The H-2 reaches δ 5.27 ppm, and the H-6 is at δ 4.09 ppm. The smallest chemical shift now belongs to H-4 (δ 3.82 ppm).

In the β-D-glucopyranose (**13n**) spectrum, the H-2 is extremely deshielded compared with other monosaccharides in Table 13.15 (δ 6.58 ppm). The rest of the signals are around δ 3 ppm, with the smallest belonging to H-3 (δ 2.89 ppm). In the α-anomer

13o, the H-3 and H-5 are still near δ 3 ppm. The H-2 is shifted upfield to δ 6.20 ppm, and the H-4 and H-6 are now in the range δ 3.4–3.6 ppm.

β-D-Fructopyranose (**13p**), an example of a ketohexose, has a methylene group at C-6 with no substitution and two substituents at C-2. The H-3, H-4, and H-5 signals have resonance frequencies between δ 3.55 and 3.65 ppm. The axial H-6 is the most shielded proton at δ 3.43 ppm, and the equatorial H-6 is the most deshielded one (δ 3.78 ppm). Thus, all the signals are very close in range.

In the ^{13}C NMR spectra, the chemical shifts of monosaccharides are significantly higher than those of simple oxane (**13**) due to the presence of the hydroxy groups. The C-2 often appears above δ 90 ppm and the rest between δ 60 and 80 ppm.

Compound **13h** has the C-2 peak at δ 93.40 ppm. The chemical shifts of C-3 to C-5 are slightly above δ 69 ppm, and the methylene C-6 appears at δ 63.3 ppm, being the most shielded. In the α-anomer, the C-3 signal keeps its chemical shift approximately constant, at δ 69.3 ppm, while all the other peaks are shifted downfield around $\Delta\delta$ 4 ppm.

In the case of L-lyxopyranose, only slight differences between the anomers, spectra are observed. In both cases, the C-2 appears around δ 95 ppm; C-3 and C-4 are above δ 70 ppm (the C-3 data is missing in the report of **13j**; it can be deduced to be around δ 70 ppm); and the other carbons appear between δ 64 and 69 ppm. The more straightforward method to differentiate the configurations is through the spacing between the C-3 and C-6 signals. In the case of the β-anomers, they seem to be equally spaced. In the α-anomer case, the carbon C-3 signal is very close to the C-4 ($\Delta\delta \sim 0.5$ ppm), and the C-5 is apart from C-6 by $\Delta\delta \sim 4.5$ ppm.

From the analysis of Table 13.15, it is possible to conclude that the signal of C-2 of hexoses is above δ 97 ppm for the β-anomer and around δ 93 ppm for the α-anomer.

For compound **13l**, the C-5 is the most shielded at δ 69.8 ppm, the C-3 appears at δ 73.0 ppm, the C-4 is near it at δ 73.9 ppm, and the C-6 is the second most deshielded carbon at δ 76.1 ppm. In the α-anomer, **13m**, all the signals are shifted upfield except for C-5, which remains around δ 70 ppm. Therefore, the C-3 is at δ 69.4 ppm, C-4 at δ 70.3 ppm, and the C-6 is still the second most deshielded carbon at δ 71.4 ppm.

Bubb's review provides some NMR data on glucopyranoses **13n** and **13o** [126]. In the ^{13}C NMR spectra of both anomers, the C-5 appears at δ 70.8 ppm. In the case of the β-anomer, C-6 is the second most deshielded carbon, with a chemical shift at δ 77.0 ppm, followed by C-4 (δ 76.9 ppm) and C-3 (δ 75.2 ppm). In the case of the α-anomer, the resonance frequencies are lower, with the C-4 signal appearing at δ 73.9 ppm and then the C-3 at δ 72.6 ppm, and the C-6 being the second most shielded carbon in this case, with chemical shift probably between δ 72.0 and 72.5 ppm. This conclusion is based on the published data [126], where the difference between the C-3 and C-6 signals is minimal (the solvent used was not specified).

In the case of β-D-fructopyranose (**13p**), the C-2 chemical shift reaches δ 98.9 ppm, the C-4 and C-5 are slightly above δ 70 ppm, the C-3 resonates at δ 68.4 ppm, and the methylene C-6 is the most shielded carbon (δ 64.2 ppm).

NMR spectra for fluorinated carbohydrates are available in the review of Michalik et al. [138].

The unsaturated form of oxane is pyran, and two isomeric structures exist, 2*H*-pyran (**14**) and 4*H*-pyran (**15**) (Figure 13.21). Their NMR spectra should be similar, so finding the key features is essential to discriminate between the isomers. Unfortunately, there are few reports about pyran NMR; however, there are many data published for pyranones, as presented in Table 13.16.

To the best of our knowledge, the NMR spectra of 2*H*-pyran derivatives without the carbonyl at C-2 has not been reported. Therefore, the most straightforward structure is 2*H*-pyran-2-one (**14a**) (Figure 13.25); its ^{1}H NMR presents two signals below δ 7 ppm and two above. The H-6 is the most deshielded proton (δ 7.77 ppm), followed by H-4 (δ 7.56 ppm), which can be explained by the electron-withdrawing ability of the carbonyl group via conjugation, along with the double bonds' anisotropy and the ethereal oxygen's inductive effect (position 1). The H-3 has an upfield shift of δ 6.38 ppm, and the H-5 resonates at δ 6.43 ppm. The coupling frequencies J_3 range between 5.0 and 9.4 Hz, and smaller coupling constants at J_4 may also appear (J_4 1.5–2.4 Hz).

Goel and Ram [139] have reviewed a series of halogenated 2*H*-pyran-2-ones, namely, with chloro, bromo, and iodo substituents at C-3, C-4, and C-5. From the NMR data gathered by them, two examples are presented in Table 13.16; 5-chloro-2*H*-pyran-2-one (**14b**) has protons resonating at slightly lower frequencies than in 2*H*-pyran-2-one (**14a**) (Figure 13.25). The difference is more significant in H-6, decreasing to 7.59 ppm, while the shift of the other protons is smaller than $\Delta\delta$ 0.1 ppm. The data regarding other compounds summarized by the authors show that they have similar chemical shifts, except for some cases when the iodine atom is the halogen present. The 3-iodo-2*H*-pyran-2-one (**14d**) has the H-4 shielded at δ 6.52 ppm, and the H-5 is also under some shielding effect of the iodo substituent (δ 6.01 ppm). The H-6 has an increase in the resonance frequency to δ 7.95 ppm. When there are two chlorine atoms at C-3 and C-5, compound **14e**, the ^{1}H NMR signals are shifted downfield compared with 5-chloro-2*H*-pyran-2-one (**14b**), but the values still stay below those of 2*H*-pyran-2-one (**14a**). The chemical shifts of δ 7.55 and 7.65 ppm correspond to H-4 and H-6, respectively.

Kepe et al. [142] have synthesized many 3-amido-2*H*-pyran-2-one derivatives and characterized them by ^{1}H and ^{13}C NMR. The selected compound **14e** (Figure 13.25) has the H-4 signal at δ 8.35 ppm and the H-5 at δ 6.09 ppm. When a nitro substituent is present, the signals are shifted downfield. In compound **14f**, the H-4 and H-5 are both above δ 8 ppm, only the H-3 remains at δ 6.45 ppm.

In the ^{13}C NMR spectra, five signals generally occur, the two most shifted upfield correspond to C-3 and C-5. Hence, in compound **14b** (Figure 13.25), the C-5 has the lowest resonance frequency (δ 101.2 ppm), followed by C-3 (δ 118.0 ppm). The C-2 and C-6 lay in the range δ 150–160 ppm, with C-2 being more deshielded. The C-4 chemical shift is in the middle of the others at δ 146.4 ppm. Finally, bearing an iodine atom as substituent, **14c**, the anomalous C-3 resonates at δ 86.8 ppm, while the others are slightly shifted downfield.

In the Kepe et al. study [143], it is possible to observe that the 3-benzamide group mainly changes the chemical shifts of C-3 and C-4 (both around δ 133 ppm). The former is shifted downfield due to the nitrogen's inductive effect, whereas the latter

Table 13.16 ^{1}H and ^{13}C NMR chemical shifts and coupling frequencies of 2*H*-pyran (**14**) and 4*H*-pyran (**15**) derivatives, in certain solvents.

Compound/substituent	^{1}H (δ, ppm) (J, Hz)	^{13}C (δ, ppm)	Solvent	References
14a 2-Oxo	6.38 (H-3) 7.56 (H-4) 6.43 (H-5) 7.77 (H-6) (J_3 5.0–9.4 Hz J_4 1.5–2.4 Hz)	—	$CDCl_3$	[139, 140]
14b 5-Chloro-2-oxo	6.30 (H-3) 7.34 (H-4) 7.59 (H-6)	159.9 (C-2) 118.0 (C-3) 146.4 (C-4) 101.2 (C-5) 150.1 (C-6)	$CDCl_3$	[139]
14c 3-Iodo-2-oxo	6.52 (H-4) 6.01 (H-5) 7.95 (H-6)	158.6 (C-2) 86.8 (C-3) 151.6 (C-4) 107.3 (C-5) 152.0 (C-6)	$CDCl_3$	[139]
14d 3,5-Dichloro-2-oxo	7.55 (H-4) 7.65 (H-6)	—	CCl_4	[141]
14e 3-Benzamido-6-methyl-2-oxo	8.35 (H-4) 6.09 (H-5)	160.5 (C-2) 133.8 (C-3/4) 132.4 (C-3/4) 104.0 (C-5) 155.1 (C-6)	$CDCl_3$	[142]
14f 5-Nitro-2-oxo	6.45 (H-3) 8.10 (H-4) 8.80 (H-5)	—	$CDCl_3$	[143]
15a 2-Amino-3-cyano-4,5,6-triphenyl	—	160.1 (C-2) 57.8 (C-3) 45.0 (C-4) 116.4 (C-5) 144.4 (C-6)	DMSO-d_6	[144]
15b 4-Oxo	7.88 (H-2) 6.38 (H-3) J_3 5.96 Hz	155.6 (C-2) 118.2 (C-3) 178.2 (C-4)	$CDCl_3$	[145, 146]
15c 3-Methyl-4-oxo	7.50 (H-2) 6.15 (H-5) 7.53 (H-6)	—	$CDCl_3$	[147]
15d 2,6-Dimethyl-4-oxo	6.04 (H-3)	165.6 (C-2) 113.7 (C-3) 180.1 (C-4)	$CDCl_3$	[148, 149]
15e 2-Ethyl-3-hydroxy-4-oxo	—	154.2 (C-2) 142.8 (C-3) 173.6 (C-4) 113.4 (C-5) 154.3 (C-6)	$CDCl_3$	[150]

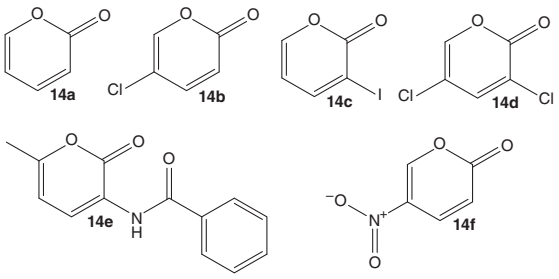

Figure 13.25 Derivatives of 2*H*-pyran (**14**): 2*H*-pyan-2-one (**14a**), 5-chloro-2*H*-pyran-2-one (**14b**), 3-iodo-2*H*-pyran-2-one (**14c**), 3,5-dichloro-2*H*-pyran-2-one (**14d**), *N*-(6-methyl-2*H*-pyran-2-on-3-yl) benzamide (**14e**), and 5-nitro-2*H*-pyran-2-one (**14f**).

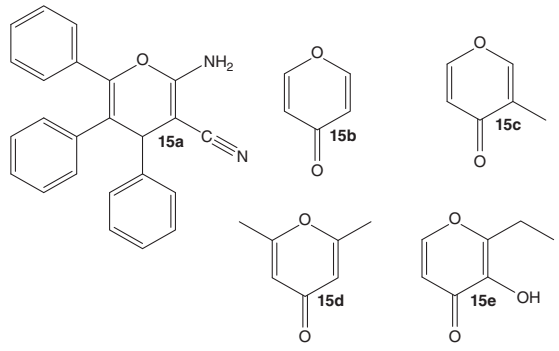

Figure 13.26 Derivatives of 4*H*-pyran (**15**): 2-amino-3-cyano-4,5,6-triphenyl-4*H*-pyran (**15a**), 4*H*-pyran-4-one (**15b**), 3-methyl-4*H*-pyran-4-one (**15c**), 2,6-dimethyl-4*H*-pyran-4-one (**15d**), and 2-ethyl-3-hydroxy-4*H*-pyran-4-one (**15e**).

is shifted upfield due to the change in the electronic distribution that could be rationalized through the resonance structures. Therefore, for proper identification of the signals, multidimensional analysis was needed.

As in the previous case, to the best of our knowledge the NMR spectra of 4*H*-pyran without carbonyl or substituents has not been not reported. The corresponding pyranone, **15b,** (Figures 13.26 and 13.27) only has two signals due to the molecular geometry that makes H-2 and H-3 equivalent to H-6 and H-5, respectively. The H-2 is the most deshielded at δ 7.88 ppm, and the H-3 appears at δ 6.38 ppm. The coupling frequency between neighbor protons is J_3 5.96 Hz. With a 3-methyl substituent, **15c**, the symmetry is lost. The H-6 is the most unshielded proton, at δ 7.53 ppm. Nearby is H-2, with a chemical shift at δ 7.50 ppm. The shielded H-5 appears at δ 6.15 ppm. When there are two methyl groups at C-2 and C-6, **15d**, there is only the H-5 signal around δ 6.0 ppm.

Regarding the ^{13}C NMR an example was found in literature for the 4*H*-pyran isomer with a high substitution pattern and without the carbonyl group **15a** (Figure 13.26). The C-2 appears at δ 160.1 ppm, and the C-6 is close behind (δ 144.4 ppm). The C-5 signal is also at typical values, δ 116.4 ppm. Since the C-4 is sp^3 hybridized, its chemical shift is the lowest (δ 45.0 ppm). The C-3 is below δ 60 ppm, probably because of the resonance of the molecule involving the 2-amino group and the ethereal oxygen (position 1). Other similar examples are available in Reference [144].

The 4*H*-pyran-4-one (**15b**) has three signals at δ 155.6 (C-2), 118.2 (C-3), and 178.2 (C-4) ppm (Figure 13.27). The last one belongs to the carbonyl group, which is more

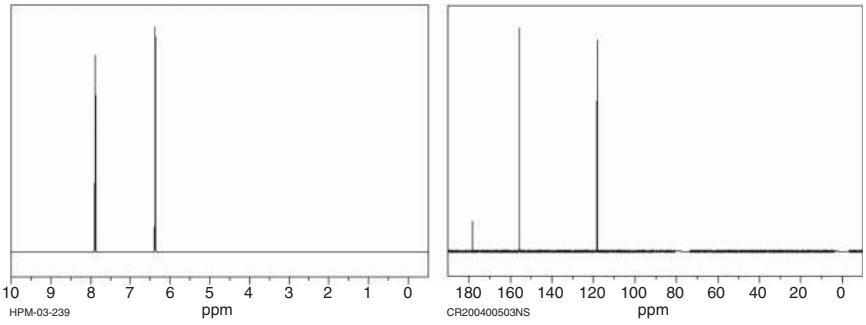

Figure 13.27 4*H*-Pyran-4-one (**15b**) ^{1}H and ^{13}C NMR spectra. Source: SDBSWeb: https://sdbs.db.aist.go.jp. National Institute of Advanced Industrial Science and Technology, accessed 05 December 2021.

deshielded than the corresponding carbon in 2*H*-pyran-2-one. The methyl derivative **15d** has similar values, with C-2 and C-4 shifted downfield and C-3 upfield.

Compound **15e** is asymmetrically substituted. Therefore, C-4 appears at δ 173.6 ppm, C-2 and C-6 at δ 154.2–154.3 ppm, and C-5 is at δ 113.4 ppm. The C-3 signal, bearing a hydroxy group, appears at δ 142.8 ppm.

The pyrylium structure (**16**) is entirely different from pyran (Figure 13.21), due to the fact that it is an aromatic cation. Therefore, an increment in chemical shifts is expected (Table 13.17). Moreover, the counterion used during analysis also influences the NMR results.

Having the tetrafluoroborate as counterion (e.g. **16_1** in Figure 13.28), in deuterated acetonitrile, the pyrylium H-2 reaches δ 9.58 ppm. Because of the resonance structures with the positively charged oxygen, the H-4 appears at δ 9.20 ppm. The H-3 is the most deshielded proton, with a chemical shift of δ 8.38 ppm. Sándor and Radics determined the coupling constants in the range J_3 4.2–8.1 Hz and J_4 1.4–1.8 Hz [151]. The same pyrylium salt produced ^{13}C NMR signals at δ 169.3 and 161.1 ppm for C-2 and C-4, respectively. The C-3 is the most shielded at δ 127.7 ppm, with values resembling benzene. The salt formed with perchlorate, **16_2**, solubilized in deuterated trifluoroacetic acid, has more shielded proton signals. The difference in chemical shift approximates $\Delta\delta$ −0.3 ppm for each proton compared to the previous compound.

Balaban and Wray reported the ^{13}C NMR spectra of many alkyl and phenyl pyrylium perchlorate derivatives [152]. Among them, compound **16b** shows higher chemical shifts for C-2 and C-4 (δ 180.2 and 177.2 ppm), whereas C-3 appears at a lower chemical shift (δ 124.9 ppm). With every position methylated except for C-4, this carbon is the only one that keeps the chemical shift of pyrylium (**16**). In this case, C-3 appears around δ 135 ppm and the C-2 at δ 178.3 ppm. When the substituents are phenyl groups, **16c**, the change in resonance frequencies is smoother. The C-2 is around δ 175 ppm, and the rest of the carbons are shifted upfield compared with pyrylium. In the last example from the table, the resonance frequencies of C-3 and C-4 (δ 120.6 and 171.1 ppm, respectively) are significantly

Table 13.17 ^{1}H and ^{13}C NMR chemical shifts and coupling frequencies of pyrylium **16** salt derivatives.

Compound/counterion	^{1}H (δ, ppm) (J, Hz)	^{13}C (δ, ppm)	Solvent	References
16_1 Tetrafluoroborate	9.58 (H-2) 8.38 (H-3) 9.20 (H-4) (J_3 4.2–8.1 Hz J_4 1.4–1.8 Hz)	169.3 (C-2) 127.7 (C-3) 161.1 (C-4)	CD_3CN	[151, 152]
16_2 Perchlorate	9.22 (H-2) 8.08 (H-3) 8.91 (H-4)	—	CF_3CO_2D	[151]
16a 2,4,6-Trimethyl perchlorate	—	180.2 (C-2) 124.9 (C-3) 177.2 (C-4)	CF_3CO_2H/ CD_2Cl_2 (80 : 20)	[152]
16b 2,3,5,6-Tetramethyl perchlorate	—	178.3 (C-2) 134.9 (C-3) 160.0 (C-4)	CF_3CO_2H/ CD_2Cl_2 (80 : 20)	[152]
16c 2,6-Diphenyl perchlorate	—	175.3 (C-2) 120.2 (C-3) 158.4 (C-4)	CF_3CO_2H/ CD_2Cl_2 (80 : 20)	[152]
16d 2,6-Dimethyl-4-phenyl perchlorate	—	181.2 (C-2) 120.6 (C-3) 171.1 (C-4)	CF_3CO_2H/ CD_2Cl_2 (80 : 20)	[152]

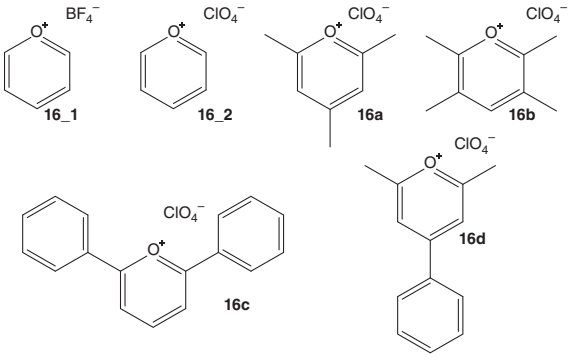

Figure 13.28 Derivatives of pyrylium (**16**): pyrylium tetrafluoroborate (**16_1**), pyrylium perchlorate (**16_2**), 2,4,6-trimethylpyrylium perchlorate (**16a**), 2,3,5,6-tetramethylpyrylium perchlorate (**16b**), 2,6-diphenylpyrylium perchlorate (**16c**), and 2,6-dimethyl-4-phenylpyrylium perchlorate (**16d**).

lower than when C-4 was also substituted by a methyl group (comparison with **16a**).

There are three types of dioxanes with two oxygen nuclei in the same ring and two dioxins. For 1,2-dioxane (**17**) (Figure 13.29), only ab initio values of NMR frequencies are known [153]. So, the focus is passed on to 1,3-dioxanes (**18**) (Table 13.18).

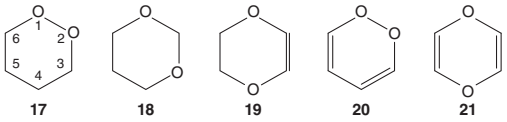

Figure 13.29 Six-membered O-heterocycles with two oxygens: 1,2-dioxane (**17**), 1,3-dioxane (**18**), 1,4-dioxane (**19**), 1,2-dioxin (**20**), and 1,4-dioxin (**21**).

Table 13.18 ^{1}H and ^{13}C NMR chemical shifts and coupling constants of 1,3-dioxane (**18**) derivatives, in certain solvents.

Compound/ substituent	^{1}H (δ, ppm) (J, Hz)	^{13}C (δ, ppm)	Solvent	References
18	4.85 (H-2)	94.3 (C-2)		[154, 155]
	3.91 (H-4)	66.9 (C-4)		
	1.78 (H-5)	26.6 (C-5)		
18a	4.50 (H-2)	—	CCl_4	[156]
2-Methyl	3.95 (H-4 *cis*)			
	3.61 (H-4 *trans*)			
	1.95 (H-5 *cis*)			
	1.23 (H-5 *trans*)			
	(J_{gem} −11.7 to −13.3 Hz			
	J_{cis} 2.6–5.3 Hz			
	J_{trans} 1.3–12.4 Hz)			
18b	5.03 (H-2 *cis*)	93.8 (C-2)	$CDCl_3$	[157, 158]
4-Methyl	4.70 (H-2 *trans*)	72.8 (C-4)		
	3.73 (H-4)	33.8 (C-5)		
	1.74 (H-5 *cis*)	66.6 (C-6)		
	1.48 (H-5 *trans*)			
	4.08 (H-6 *cis*)			
	3.70 (H-6 *trans*)			
18c	5.20 (H-2 *cis*)	94.1 (C-2)	$CDCl_3$	[159, 160]
4-Phenyl	4.88 (H-2 *trans*)	78.6 (C-4)		
	4.62 (H-4)	34.0 (C-5)		
	1.71 (H-5 *cis*)	66.8 (C-6)		
	2.07 (H-5 *trans*)			
	4.16 (H-6 *cis*)			
	3.86 (H-6 *trans*)			

In 1,3-dioxanes (**18**) (Figure 13.29), the most deshielded position is 2, both in ^{1}H and ^{13}C NMR spectra. Conversely, the methylene C-5 that is not bonded to any oxygen is the most shielded one. Hence, H-2 appears at δ 4.85 ppm, the H-4 is in the middle (δ 3.91 ppm), and the H-5 is at δ 1.78 ppm. In the ^{13}C NMR spectrum, the C-2 almost reaches δ 100 ppm (δ 94.3 ppm), while C-4 and C-5 resonate at δ 66.9 and 26.6 ppm, respectively (Table 13.18).

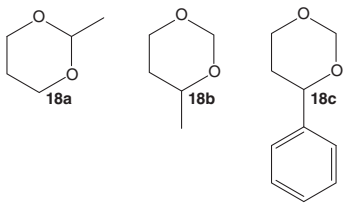

Figure 13.30 Derivatives of 1,3-dioxane (**18**): 2-methyl-1,3-dioxane (**18a**), 4-methyl-1,3-dioxane (**18b**), and 4-phenyl-1,3-dioxane (**18c**).

Methyl group substitution at C-2, **18a** (Figure 13.30), causes a split of the H-4 and H-5 signals due to their *cis*- or *trans*-configuration relative to the substituent. The H-2 is still shifted downfield to δ 4.50 ppm, but less if compared with compound **18**. The protons on the same side of the methyl group (*cis*) are more deshielded than those in a *trans*-configuration (δ 3.95 and 3.65 ppm for H-3 and below δ 2 ppm for the rest). The geminal coupling constant is smaller than $J_{gem} < -10$ Hz, and the coupling between the *cis*-protons in the range J_{cis} 2.6–5.3 Hz. The J_{trans} is smaller when the coupling is between equatorial protons (1.3 Hz) and larger for coupling between axial protons (12.4 Hz). Substitution at C-4 (methyl) increases the number of signals to seven, with each proton having a unique resonance frequency. In compound **18b** (Figure 13.30), the H-2 *cis* is the most deshielded signal at δ 5.03 ppm, followed by the other H-2 (δ 4.70 ppm). The axial H-4 and H-6 are around δ 3.7 ppm, with H-4 slightly more deshielded, while the equatorial H-6 resonates at δ 4.08 ppm. The H-5 chemical shift is below δ 2 ppm. With a 4-phenyl group instead, compound **18c** (Figure 13.25), H-2 signals are shifted downfield by $\Delta\delta$ 0.18 ppm, and the H-4 reaches δ 4.62 ppm. The H-5 *cis* and both H-6 keep the same chemical shifts as in **18b**, approximately. The H-5 *trans*, which is in the equatorial position, is shifted downfield to δ 2.07 ppm.

In the ^{13}C NMR, the 4-alkyl or 4-aryl substitution increases the resonance frequency of both C-4 and C-5. The first one appears at δ 72.8 and 78.6 ppm for compounds **18b** and **18c**, respectively. The C-5 maintains a value near δ 34 ppm for both cases. The C-2 and C-6 chemical shifts do not change when comparing with 1,3-dioxane (**18**).

There are not many NMR results on 1,4-dioxane (**19**) and their derivatives (Figure 13.29) in the literature. The unsubstituted compound **19** has only one signal both in ^{1}H and ^{13}C NMR spectra due to the molecular symmetry. They are at δ 3.69 and 67.2 ppm, respectively (Table 13.19).

The 2,3-dichloro derivative, **19a** (Figure 13.31), has three inequivalent protons. The H-2 and H-3 are the most deshielded ones because of the chlorine's inductive effect (δ 5.96 ppm). The equatorial H-5 and H-6, on the other side of the ring, have chemical shifts of δ 4.39 ppm, and the axial ones resonate at δ 3.74 ppm. In the ^{13}C NMR spectrum, the C-2 and C-3 are more deshielded, reaching δ 90.5 ppm. The other carbons appear as a single peak around δ 60 ppm, lower than in 1,4-dioxane (**19**) (Table 13.19). Another example is the racemic dilactide **19b** (Figure 13.31). The protons have a downfield shift to δ 5.09 ppm due to the anisotropy of the carbonyl group and the inductive effect of oxygens. The same applies to the carbons, where C-2 is above δ 160 ppm (typical of carbonyls) and the C-3 appears at δ 72.5 ppm. The aliphatic zone of the benzo-1,4-dioxane (**19c**) also has only one proton signal at δ

Table 13.19 ^{1}H and ^{13}C NMR chemical shifts of 1,4-dioxane (**19**) derivatives, in $CDCl_3$.

Compound/substituent	^{1}H (δ, ppm)	^{13}C (δ, ppm)	References
19	3.69	67.2	[161, 162]
19a 2,3-Dichloro	5.96 (H-2) 4.39 (H-5 *eq*) 3.74 (H-5 *ax*)	90.5 (C-2) 59.5 (C-5)	[163, 164]
19b 3,6-Dimethyl-2,5-dioxo	5.09	167.5 (C-2) 72.5 (C-3)	[165, 166]
19c Benzo[*b*]	4.18	143.7 (C-4a) 64.3 (C-2)	[167, 168]

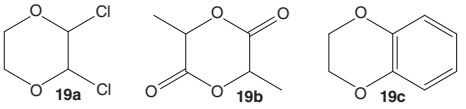

Figure 13.31 Derivatives of 1,4-dioxane (**19**): 2,3-dichloro-1,4-dioxane (**19a**), 3,6-dimethyl-1,4-dioxane-2,5-dione (**19b**), and benzo-1,4-dioxane (**19c**).

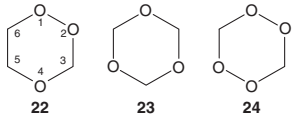

Figure 13.32 Six-membered O-heterocycles with three and four oxygens: 1,2,4-trioxane (**22**), 1,3,5-trioxane (**23**), and 1,2,4,5-tetraoxane (**24**).

4.18 ppm. The aromatic C-4a and C-8a are shifted downfield to δ 143.7 ppm, and the methylene signal is at δ 64.3 ppm.

The NMR spectra of dioxins (derivatives of compounds **20** and **21**, in Figure 13.29) could not be found in the literature. In the few cases of derivatives that could be found, they were instead a hydrogenated form, which resembles the dioxane results. Posner and Oh synthesized and characterized by NMR some 1,2,4-trioxanes (**22**) (Figure 13.32), However, the compound structures are complex, and the assignment of NMR signals to the corresponding protons or carbons was not done [169].

The 1,3,5-trioxanes (**23**) (Figure 13.32) are more common, and several ^{13}C NMR spectra of 1,2,4-alkyl derivatives are available in the AIST's spectral database [9].

From the results summarized in Table 13.20, it can be observed that the ^{13}C NMR signal appears above δ 90 ppm. The example with the lower chemical shift is the 1,3,5-trioxane (δ 93.7 ppm). The addition of alkyl groups shifts it downfield, with a more significant shift for bulkier substituents. For example, in compound **23c** (Figure 13.33), bearing isopropyl groups, the ring-carbons resonate at δ 104.8 ppm.

With the addition of electronegative atoms, such as halogens, the chemical shift increases further. For example, in compound **23d** (Figure 13.33), the signal is at δ 99.8 ppm above the δ 98.65 ppm of 2,4,6-trimethyl-1,3,5-trioxane.

The 1,2,4,5-tetraoxanes (**24**) (Figure 13.32) have been studied for malaria treatment, and Dong and Vennerstrom published a series of NMR results of alkyl and bis-spiro-derivatives, which are compiled in Table 13.21 [175].

The ^{13}C NMR signals of 1,2,4,5-tetraoxanes (**24**) always appear above δ 100 ppm, with the lower value for the tetramethylated compound (δ 107.5 ppm). The chemical

Table 13.20 ^{13}C NMR chemical shifts of the ring-carbons of 1,3,5-trioxane (**23**) derivatives, in $CDCl_3$.

Compound/substituent	^{13}C (δ, ppm)	References
23	93.7	[170]
23a 2,4,6-Trimethyl	98.6	[171]
23b 2,4,6-Triethyl	102.5	[172]
23c 2,4,6-Triisopropyl	104.8	[173]
23d 2,4,6-Tris(chloromethyl)	99.8	[174]

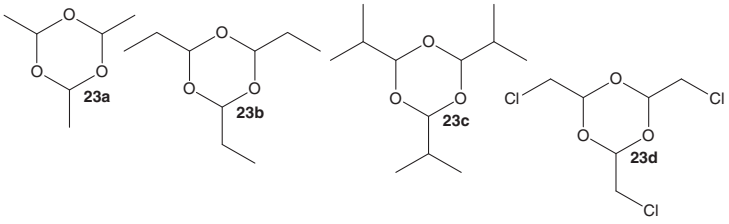

Figure 13.33 Derivatives of 1,3,5-trioxane (**23**): 2,4,6-trimethyl-1,3,5-trioxane (**23a**), 2,4,6-triethyl-1,3,5-trioxane (**23b**), 2,4,6-triisopropyl-1,3,5-trioxane (**23c**), and 2,4,6-tris (chloromethyl)-1,3,5-trioxane (**23d**).

Table 13.21 ^{13}C NMR chemical shifts of the ring-carbons of 1,2,4,5-tetraoxane (**24**) derivatives, in $CDCl_3$.

Compound/substituent	^{13}C (δ, ppm)
24a 3,3,6,6-Tetramethyl	107.5
24b 3,3,6,6-Tetrapropyl	110.4
24c 3,3,6,6-Tetrabutyl	110.6
24d 3,3,6,6-Tetrapentyl	110.6
24e 3,6-Bis(buta-1,4-diyl)	119.7
24f 3,6-Bis(penta-1,4-diyl)	108.1
24g 3,6-Bis(hexa-1,4-diyl)	112.4

Source: Modified from Dong and Vennerstrom [175].

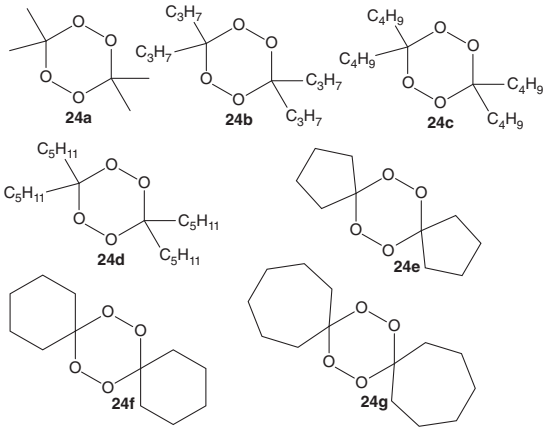

Figure 13.34 Derivatives of 1,2,4,5-tetraoxane (**24**): 3,3,6,6-tetramethyl-1,2,4,5-tetraoxane (**24a**), 3,3,6,6-tetrapropyl-1,2,4,5-tetraoxane (**24b**), 3,3,6,6-tetrabutyl-1,2,4,5-tetraoxane (**24c**), 3,3,6,6-tetrapentyl-1,2,4,5-tetraoxane (**24d**), 6,7,13,14-tetraoxadispiro [4.2.4^{8}.2^{5}]tetradecane (**24e**), 7,8,15,16-tetraoxadispiro [5.2.5^{9}.2^{6}]hexadecane (**24f**), and 8,9,17,18-tetraoxadispiro [6.2.6^{10}.2^{7}]octadecane (**24g**).

shift of carbons at the tetraoxane ring with longer chain alkyl substituents seems to stabilize around δ 110.5 ppm. For the bis-spiro-compounds, the resonance frequencies change with steric restriction of the side rings. With six-membered rings attached to the tetraoxane (compound **24f**, Figure 13.34), the chemical shift is lower (δ 108.1 ppm). For smaller side rings, as in the compound **24e** (Figure 13.34), the signal is shifted downfield (δ 119.7 ppm for compound **24e**), and the same happens for larger rings, as in the seven-membered side rings of compound **24g** (δ 112.4 ppm).

13.6 Chromene and Xanthene-Related Compounds

There are plenty of O-heterocycles in nature that are studied and explored. However, two essential families are related to the chromene and the xanthene structures (Figure 13.35). Fundamentally, they are composed of one pyran ring, fused with one or two benzenes, respectively.

The discussion on these O-heterocycles starts with the chromene scaffold, also known as benzopyran (**25**), and the main related chemical structures isochromene (**26**) and chromenium (**27**) (Figure 13.35). For unsubstituted chromene, we found no NMR data in the literature. The synthesized compounds usually have a ring at C-4 and other smaller substituents at C-2, C-3, C-6, or C-7 [176–178]. An example is compound **25_1** (Tables 13.22 and 13.23, Figure 13.36). This compound can be identified by the signal at δ 5.13 ppm assigned to H-4 and the relatively shielded aromatic protons in the range δ 6.40–7.39 ppm. In the ^{13}C NMR spectrum, the C-2

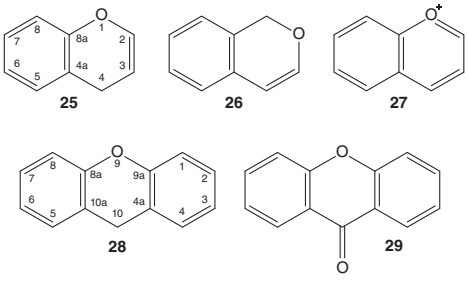

Figure 13.35 Chromene and xanthene-related O-heterocycles: 4*H*-chromene (**25**), 1*H*-isochromene (**26**), chromenium (**27**), 10*H*-xanthene (**28**), and xanthone (**29**).

Table 13.22 ^{1}H NMR chemical shifts (δ, ppm) of chromene-related O-heterocycles, in certain solvents.

Compound	H-(2–4)	H-(5–8)	Solvent	References
25_1 2-Amino-4-(2-chlorophenyl)-3-cyano-7-hydroxy-4*H*-chromene	5.13	6.40–7.39	DMSO-d_6	[176]
25a1 3-Chlorocoumarin	7.88	7.47 (H-5) 7.33 (H-6) 7.55 (H-7) 7.36 (H-8)	$CDCl_3$	[180]
25a2 6,7-Dimethoxy-4-methylcoumarin	6.16	6.94 (H-5) 6.83 (H-8)	$CDCl_3$	[181]
25b Chromone	8.06 (H-2) 6.38 (H-3)	8.32 (H-5) 7.50 (H-6) 7.81 (H-7) 7.65 (H-8)	DMSO-d_6	[182]
25b1 6-Chlorochromone	7.85 (H-2) 6.35 (H-3)	8.17 (H-5) 7.61 (H-7) 7.42 (H-8)	$CDCl_3$	[182, 183]
25b2 2-(Hydroxymethanoyl)-chromone	6.93	8.06 (H-5) 7.55 (H-6) 7.89 (H-7) 7.74 (H-8)	DMSO-d_6	[184]
25b3 (*E*)-5-Hydroxy-2-styrylchromone	6.24	6.79 (H-6) 7.52 (H-7) 6.96 (H-8)	$CDCl_3$	[185]
25c1 6-Methylflavanone	5.50 (H-2) 2.90 (H-3 *cis*) 3.10 (H-3 *trans*)	6.9–7.7	$CDCl_3$	[186]
25c2 7-Hydroxyflavanone	5.59 (H-2) 2.74 (H-3 *cis*) 3.11 (H-3 *trans*)	7.67 (H-5) 6.54 (H-6) 6.39 (H-8)	DMSO-d_6	[187]
25d1 5,7,3′,4′-Tetrahydroxyflavan-3-ol	4.60 (H-2) 3.93 (H-3) 2.40, 2.60 (H-4)	5.82 (H-6) 5.65 (H-8)	DMSO-d_6	[188]
25e Flavone	6.84	8.24 (H-5) 7.43 (H-6) 7.71 (H-7) 7.60 (H-8)	$CDCl_3$	[189]

Table 13.22 (Continued)

Compound	H-(2–4)	H-(5–8)	Solvent	References
25e1 5-Hydroxyflavone	6.74	6.82 (H-6) 7.55 (H-7) 7.00 (H-8)	$CDCl_3$	[190]
25f1 7-Isopropyloxy-isoflavone	7.92	8.20 (H-5) 6.95 (H-6) 6.83 (H-8)	$CDCl_3$	[191]
25 g Flavonol	—	8.10 (H-5) 7.42 (H-6) 7.76 (H-7) 7.71 (H-8)	DMSO-d_6	[192]
25 g1 5,7,3′,4′-Tetrahydroxyflavan-3-ol	—	6.20 (H-6) 6.42 (H-8)	DMSO-d_6	[193]
26_1 1-Allyl-3-propyl-1*H*-isochromene	5.58 (H-1) 5.85–5.93 (H-4)	6.92–7.18	$CDCl_3$	[189]
26_2 1-Allyl-3-phenyl-1*H*-isochromene	5.90 (H-1) 6.33 (H-4)	6.95–7.15	$CDCl_3$	[194]
27a 5,7,4′-Trihydroxy-anthocyanidin chloride	8.01 (H-3) 9.04 (H-4)	6.63 (H-6) 6.91 (H-8)	DMSO-d_6	[195]

and C-8a are the most deshielded signals, at δ 160.5 and 157.6 ppm, respectively. The rest of the aromatic carbons follow them in the order C-7 > C-5 > C-6 ~ C-4a > C-8. The inductive effect of the hydroxy group influences the C-7 chemical shift, and the resonances structures with both oxygens stabilize and shift upfield the last three carbon signals. Finally, the C-3 appears at δ 54.9 ppm and the C-4 at 37.2 ppm.

Coumarins have been intensively studied by ^{13}C NMR spectroscopy, and Duddeck and Kaiser gathered the results for more than 200 spectra in 1982 [179]. For the coumarin itself (**25a**), the carbonyl C-2 resonates at δ 160.4 ppm. The C-8a is the second most deshielded carbon (δ 153.9 ppm), and the C-4 is the third (δ 143.6 ppm) because it resonates with the carbonyl group. The C-5 and C-7 appear around δ 130 ppm, the C-6 appears at δ 124.4 ppm, and the rest are in the range δ 116–119 ppm.

To have an idea of the ^{1}H NMR spectrum's typical signals, we chose two examples from AIST's spectral database [9]. The 3-chlorocoumarin (**25a1**) has the H-4 signal very deshielded at δ 7.88 ppm. The H-3 shows a lower value for the chemical shift in compound **25a2** (δ 6.16 ppm). The H-7 and H-5 are the less shielded protons in the aromatic ring, but this difference seems small ($\Delta\delta$ 0.2 ppm). They are shifted downfield in the compound **25a1** (around δ 7.4 ppm) and keep values below δ 7 ppm in the compound **25a2** (Figure 13.36). In the ^{13}C NMR spectra of these compounds, the only noticeable differences can be found in the substituted carbons.

Table 13.23 ^{13}C NMR chemical shifts (δ, ppm) of chromene-related O-heterocycles, in certain solvents.

Compound	C-(2–4a,8a)	C-(5–8)	Solvent	References
25_1 2-Amino-4-(2-chlorophenyl)-3-cyano-7-hydroxy-4*H*-chromene	160.5 (C-2) 54.9 (C-3) 37.2 (C-4) 112.6 (C-4a) 157.6 (C-8a)	129.2 (C-5) 112.7 (C-6) 149.0 (C-7) 102.3 (C-8)	DMSO-d_6	[176]
25a Coumarin	160.4 (C-2) 116.4 (C-3) 143.6 (C-4) 118.8 (C-4a) 153.9 (C-8a)	128.1 (C-5) 124.4 (C-6) 131.8 (C-7) 116.4 (C-8)	$CDCl_3$	[179]
25a1 3-Chlorocoumarin	157.3 (C-2) 122.4 (C-3) 140.0 (C-4) 118.8 (C-4a) 152.7 (C-8a)	127.3 (C-5) 125.1 (C-6) 131.9 (C-7) 116.8 (C-8)	$CDCl_3$	[195]
25a2 6,7-Dimethoxy-4-methylcoumarin	161.5 (C-2) 112.4 (C-3) 152.4 (C-4) 112.5 (C-4a) 149.5 (C-8a)	105.3 (C-5) 146.2 (C-6) 152.8 (C-7) 100.1 (C-8)	$CDCl_3$	[196]
25b Chromone	157.3 (C-2) 112.7 (C-3) 176.7 (C-4) 124.6 (C-4a) 156.3 (C-8a)	125.8 (C-5) 125.3 (C-6) 134.6 (C-7) 118.8 (C-8)	DMSO-d_6	[182]
25b1 6-Chlorochromone	155.4 (C-2) 113.0 (C-3) 176.3 (C-4) 125.9 (C-4a) 154.9 (C-8a)	125.3 (C-5) 131.3 (C-6) 134.0 (C-7) 120.0 (C-8)	$CDCl_3$	[182, 197]
25b2 2-(Hydroxymethanoyl)-chromone	155.4 (C-2) 113.5 (C-3) 177.5 (C-4) 123.7 (C-4a) 153.2 (C-8a)	124.9 (C-5) 126.0 (C-6) 135.1 (C-7) 118.8 (C-8)	DMSO-d_6	[198]
25b3 (*E*)-5-Hydroxy-2-styrylchromone	162.8 (C-2) 109.0 (C-3) 183.6 (C-4) 110.9 (C-4a) 156.2 (C-8a)	160.8 (C-5) 111.3 (C-6) 135.3 (C-7) 106.8 (C-8)	$CDCl_3$	[185]

Table 13.23 (Continued)

Compound	C-(2–4a,8a)	C-(5–8)	Solvent	References
25c1 6-Methylflavanone	79.7 (C-2) 44.8 (C-3) 192.3 (C-4) 126.2 (C-4a) 159.7 (C-8a)	137.4 (C-5) 131.4 (C-6) 139.0 (C-7) 118.0 (C-8)	$CDCl_3$	[186]
25c2 7-Hydroxyflavanone	78.7 (C-2) 43.0 (C-3) 189.4 (C-4) 113.3 (C-4a) 162.7 (C-8a)	128.1 (C-5) 110.4 (C-6) 164.4 (C-7) 102.4 (C-8)	DMSO-d_6	[199]
25d1 5,7,3′,4′-Tetra hydroxyflavan-3-ol	78.0 (C-2) 64.9 (C-3) 28.1 (C-4) 98.5 (C-4a) 155.7 (C-8a)	156.2 (C-5) 95.1 (C-6) 156.4 (C-7) 94.1 (C-8)	DMSO-d_6	[200]
25e Flavone	163.4 (C-2) 107.6 (C-3) 178.5 (C-4) 124.0 (C-4a) 156.3 (C-8a)	125.7 (C-5) 125.3 (C-6) 133.8 (C-7) 118.1 (C-8)	$CDCl_3$	[189]
25e1 5-Hydroxyflavone	164.6 (C-2) 106.1 (C-3) 183.6 (C-4) 110.9 (C-4a) 156.5 (C-8a)	160.9 (C-5) 111.5 (C-6) 135.4 (C-7) 107.1 (C-8)	$CDCl_3$	[201]
25f1 7-Isopropyloxy-isoflavone	152.6 (C-2) 125.2 (C-3) 175.6 (C-4) 118.2 (C-4a) 158.0 (C-8a)	128.0 (C-5) 115.6 (C-6) 162.5 (C-7) 101.6 (C-8)	$CDCl_3$	[202]
25g Flavonol	145.1 (C-2) 139.1 (C-3) 173.0 (C-4) 121.3 (C-4a) 154.5 (C-8a)	124.8 (C-5) 124.5 (C-6) 133.6 (C-7) 118.3 (C-8)	DMSO-d_6	[192]
25g1 5,7,3′,4′-Tetra hydroxyflavon-3-ol	147.6 (C-2) 136.6 (C-3) 176.7 (C-4) 103.9 (C-4a) 161.6 (C-8a)	157.0 (C-5) 99.0 (C-6) 164.7 (C-7) 94.2 (C-8)	DMSO-d_6	[193, 203]

Table 13.23 (Continued)

Compound	C-(2–4a,8a)	C-(5–8)	Solvent	References
26_1 1-Allyl-3-propyl-1*H*-isochromene	77.4 (C-1) 117.5–134.3 (C-3) 100.3 (C-4)	117.5–134.3	$CDCl_3$	[194]
26_2 1-Allyl-3-phenyl-1*H*-isochromene	77.7 (C-1) 151.4 (C-3) 100.3 (C-4)	117.8–134.6	$CDCl_3$	[194]
27a 5,7,4′-Trihydroxy-anthocyanidin chloride	172.3 (C-2) 110 (C-3) 149.6 (C-4) 113.9 (C-4a) 160 (C-8a)	160.5 (C-5) 103 (C-6) 172.4 (C-7) 96.2 (C-8)	DMSO-d_6	[195]

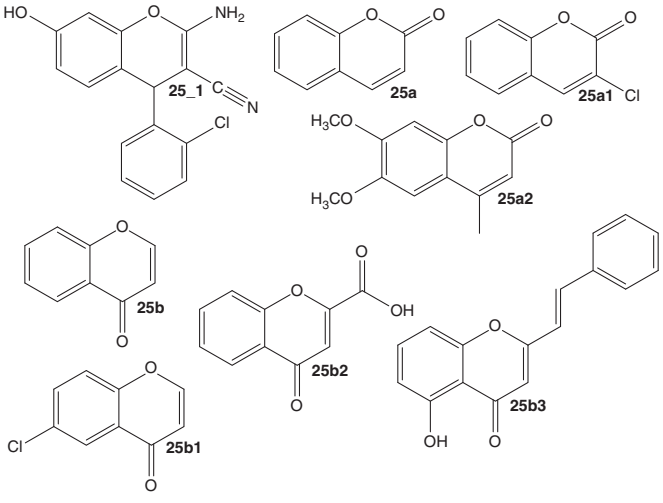

Figure 13.36 Derivatives of chromene: 2-amino-4-(2-chlorophenyl)-3-cyano-7-hydroxy-4*H*-chromene (**25_1**), coumarin (**25a**), 3-chlorocoumarin (**25a1**), 6,7-dimethoxy-4-methylcoumarin (**25a2**), chromone (**25b**), 6-chlorochromone (**25b1**), chromone-2-carboxylic acid (**25b2**), and 5-hydroxy-2-styrylchromone (**25b3**).

The chromones have also been regularly researched, but no review of their NMR spectra was found. The spectrum of compound **25b** (Figure 13.36) was found in a paper by Erdogdu et al. [182], along with 6-halochromones. The H-3 is the most shielded proton, below δ 7 ppm. The impact of the conjugation of the carbonyl at C-4 is higher on its neighbor H-2, deshielding it to a chemical shift around δ 8 ppm. In the aromatic ring, the H-5 appears at 8.32 ppm and the H-7 at δ 7.81 ppm. Both are influenced by the presence of the carbonyl group. The other two protons are

more shielded at δ 7.50 and 7.65 ppm (H-6 and H-8, respectively). In the ^{13}C NMR spectrum, the characteristic carbonyl signal is at δ 176.7 ppm, and the C-2 and C-8a peaks also appear above δ 150 ppm and the C-7 at δ 134.6 ppm. Three signals appear around δ 125 ppm, corresponding to C-5, C-6, and C-4a. The C-8 and C-3 are the most shielded protons, at δ 118.8 and 112.7 ppm, respectively.

The inclusion of a 6-halogen, **25b1**, shifts all the protons' resonance frequencies (around $\Delta\delta$ −0.2 ppm). In the ^{13}C NMR spectrum, the changes are also small, with $\Delta\delta < 2$ ppm. The exception is in the substituted C-6, whose signal is at δ 131.3 ppm due to chlorine's inductive effect. In **25b2**, the only relevant difference compared with chromone **25b** is the H-3 signal, which is shifted downfield to δ 6.93 ppm. 2-Styrylchromones have an opposite effect in H-3, which is shifted upfield to δ 6.24 ppm (Table 13.22, compound **25b3**) due to the resonance of the styryl substituent. The hydroxy group at C-5 shifts H-6 and H-8 frequencies to 6.79 and 6.96 ppm, respectively. The same resonance effects have visible results in the ^{13}C NMR spectrum. The C-3, C-4a, C-6, and C-8 are all shifted upfield. The C-4 reaches δ 183.6 ppm, and the C-5 is now shifted downfield due to the inductive effect of the hydroxy substituent (δ 160.8 ppm).

The following compounds are flavanones, which are the first type of flavonoids to be discussed here. Some NMR results are also available, but unfortunately, not always the complete discrimination of the signals is done, and no spectrum for flavanone itself (compound **25c**) was found [186, 204–206]. In the example, **25c1** (Figure 13.37), the aromatic protons appear in the region δ 6.9–7.7 ppm. However, the signals of the non-aromatic protons make the identification of the compound easier. The most unshielded is the H-2 (δ 5.5 ppm), while the other two can be

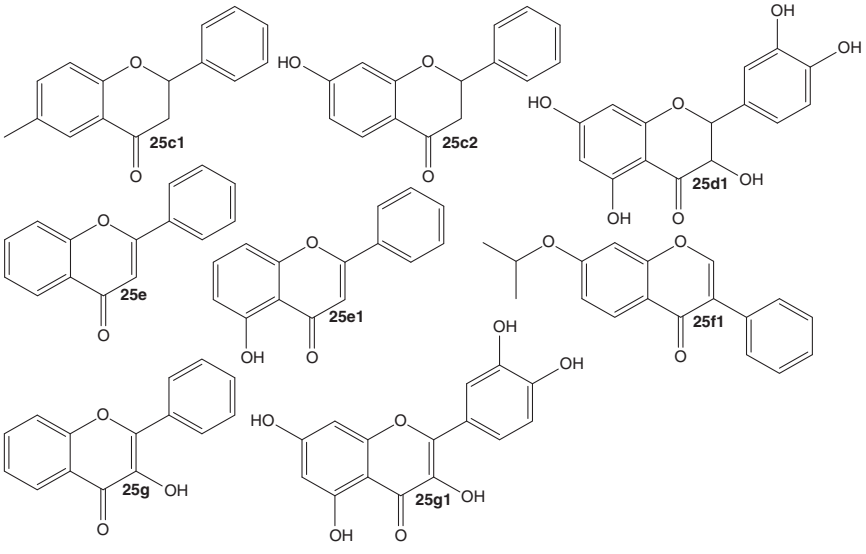

Figure 13.37 Flavonoids' derivatives: 6-methylflavanone (**25c1**), 7-hydroxyflavanone (**25c2**), 5,7,3′,4′-tetrahydroxyflavan-3-ol (**25d1**), flavone (**25e**), 5-hydroxyflavone (**25e1**), 7-isopropyloxy-isoflavone (**25f1**), flavonol (**25g**), and 5,7,3′,4′-tetrahydroflavon-3-ol (**25g1**).

discriminated from the coupling constants. The geminal coupling is the highest (J_{gem} 16.8 Hz), followed by the *cis* and *trans* (J_{cis} 13.2 Hz and J_{trans} 2.9 Hz). Hence, the δ 3.1 ppm signal belongs to the proton on the opposite side of the phenyl substituent (*trans*) and the δ 2.9 ppm to the one on the same side (*cis*). In the ^{13}C NMR spectrum, the methylene carbons are easily assigned to their signals, at δ 79.7 ppm for C-2 and δ 44.8 ppm for the C-3. The most unshielded peak belongs to the carbonyl (δ 192.3 ppm) and the second most unshielded to the C-8a (δ 159.7 ppm). The rest is more challenging to characterize, and multidimensional analysis should be done for a proper correlation. In any case, it is expected that C-5 (*ortho*-position) and C-7 (*para*-position) be shifted downfield due to presence of the electron-withdrawing carbonyl group.

The other flavanone example, **25c2**, has a 7-hydroxy substituent. The proton results are similar. The H-5 (δ 7.67 ppm) is far from the other two aromatic signals (around δ 6.5 ppm). In the ^{13}C NMR spectrum, there is a big difference in the chemical shift of C-7 (δ 164.4 ppm), being now the second most deshielded carbon. Carbons C-4a, C-6, and C-8 are shifted upfield due to the substituent's resonance (within the range δ 102–114 ppm).

The flavan-3-ol presented in Tables 13.22 and 13.23 has many hydroxy substituents, like the natural flavonoids that exist in nature. Its common name is catechin (**25d1**). The ^{1}H NMR spectrum can be highlighted where the H-3 is shifted downfield to δ 3.93 ppm and the H-2 is shielded by resonance with the aromatic substituent (δ 4.60 ppm). H-4 is the most shielded of all protons, with a chemical shift around δ 2.5 ppm. The H-6 and H-8, in the fused aromatic ring, are out of the usual aromatic region in the spectrum. The resonance with the 5- and 7-hydroxy groups shield it to values below δ 6 ppm. In the ^{13}C NMR spectrum, carbon C-3 is shifted downfield to δ 64.9 ppm, and the C-4 appears at δ 28.1 ppm. The C-4a, C-6, and C-8 are all below δ 100 ppm for the same reasons as in the ^{1}H NMR spectrum. The C-5, C-7, and C-8a resonate between δ 155 and 157 ppm mainly due to the inductive effect of oxygens bonded to the respective carbons.

The complete characterization of flavone (2-phenylchromone) (**25e**) (Figure 13.37), the main flavonoid structure, has been reported [189]. In the ^{1}H NMR spectrum, the characteristic H-3 signal has the chemical shift at δ 6.84 ppm. In the aromatic region, the H-5 at δ 8.24 ppm is the most deshielded one. The other double doublets belongs to H-8, at δ 7.6 ppm. The H-6 and H-7 protons are both double doublet of doublets, with δ 7.43 and 7.71 ppm, respectively. In the ^{13}C NMR spectrum, the carbonyl signal is at δ 178.5 ppm. Then, the C-2 is the second most deshielded carbon (δ 163.4 ppm), and the C-8a resonates above δ 150 ppm, as usual. On the opposite side of the spectrum, the C-3 chemical shift appears at δ 107.6 ppm. The C-4a, C-6, and C-8 are all around at δ 125 ppm, and the C-7 appears at δ 133.8 ppm.

The addition of a 5-hydroxy group, **25e1**, shifts the signals of C-4a, C-6, and C-8 to values up to δ 111.5 ppm. The C-5 is at δ 160.9 ppm and is now the second most deshielded carbon. The carbonyl signal is also shifted downfield (δ 183.6 ppm), which may be due to hydrogen bonding with the 5-hydroxy group. In the ^{1}H NMR spectrum, all the resonance frequencies are lower than the ones of flavone (**25e**). A conspicuous effect is seen in protons H-6 and H-8 (the difference is around $\Delta\delta$ −0.6 ppm) due to the resonance structures.

In isoflavones, the phenyl substituent is at C-3, so there is no H-3, and the H-2 signal is very deshielded (near δ 8 ppm). In compound **25f1** (Figure 13.37), the higher resonance frequency belongs to the H-5. The H-6 and H-8 are influenced by the conjugation of the 7-isopropyloxy substituent, resulting in upfield shifted signals (below δ 7 ppm). The ^{1}H NMR spectrum of natural isoflavones daidzein and genistein can be found in the paper of Caligiani et al. [207]. In the ^{13}C NMR spectrum, the C-4a, C-6, and C-8 are all below δ 120 ppm, while C-3 and C-5 are at δ 125.2 and 128.0 ppm, respectively. On the opposite side of the spectrum, the most unshielded carbon has the chemical shift of δ 175.6 ppm and belongs to the carbonyl group, and there are three signals between δ 150 and 165 ppm, which correspond to the C-2, C-8a, and C-7 in increasing resonance frequency order.

Moving on to flavonols, many NMR results are published for different hydroxy and methoxy substituents' positions [192, 193, 203, 208]. For the flavonol (**25g**) (Figure 13.37), the H-5 signal is above δ 8 ppm, the H-7 and H-8 are around δ 7.7 ppm, with the H-7 slightly more deshielded, and the H-6 appears at δ 7.42 ppm. The ^{13}C NMR spectrum contains more information. Comparatively to flavone (**25e**) (Figure 13.37), the C-5 to C-8 signals have similar resonance frequencies. The carbonyl C-4 is now at δ 173.0 ppm, and the C-4a and C-8a are shifted upfield about $\Delta\delta$ −2 ppm. The main differences are in C-3, which is shifted downfield to δ 139.1 ppm, and in C-2, whose resonance with the hydroxy group shifts it upfield (δ 145.1 ppm).

The natural flavonol quercetin (**25 g1**) (Figure 13.37) has two signals below δ 6.5 ppm in the ^{1}H NMR spectrum, corresponding to H-6 and H-8. Besides the chemical shifts of the aromatic protons from the phenyl ring (δ 6.9–7.7 ppm), five other signals appear above δ 9 ppm, belonging to the hydroxy substituents. In the ^{13}C NMR spectrum, C-5 and C-7 are deshielded by the inductive effect of oxygens to δ 157.0 and 164.7 ppm, respectively. Shifted upfield are carbons C-4a, C-6, and C-8, with the first one having the highest value of the three (δ 103.9 ppm). The rest have similar values to compound **25g**.

With a completely different structure, the isochromene (**26**) (Figure 13.35) is not so well studied, and NMR spectra of some derivatives were only found in some papers focused on organic synthesis, in which assignment was not disclosed [194, 209, 210]. The H-1 signal is the most shielded of the isochromene scaffold, appearing at δ 5.58 ppm for **26_1** and δ 5.90 ppm for **26_2** (Figure 13.38). The H-4 is under the double bond anisotropy, but it is stabilized by resonance (δ 5.85–5.93 and 6.33 ppm, for **26_1** and **26_2**, respectively). The aromatic protons are around δ 7 ppm for both cases. In the ^{13}C NMR spectra, the signal near δ 78 ppm should belong to C-1 because it is the only sp^{3} carbon. The C-4 is expected to be around δ 100 ppm, and most of the peaks fall in the range δ 117–135 ppm, being impossible to discern without previous knowledge or 2D analysis. Only in the compound **26_2**, the C-3 chemical shift might be above δ 150 ppm.

As the last example of chromene-related compounds, the anthocyanidin (**27a**) (Figure 13.38) contains the chromenium core (**27**) (Figure 13.35), and it is the aglycone form of anthocyanin. The salt presented is with the chloride counterion. The H-3 and H-4 are more deshielded due to the proximity to the positively charged

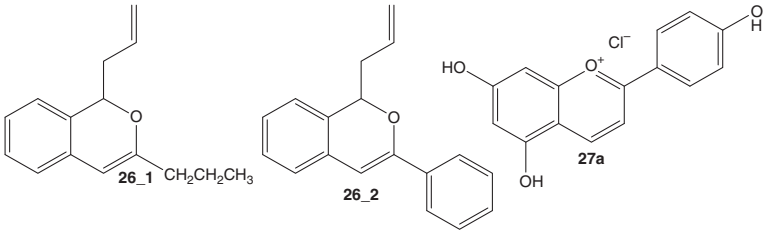

Figure 13.38 Derivatives of isochromene (**26**) and chromenium (**27**): 1-allyl-3-propyl-1*H*-isochromene (**26_1**), 1-allyl-3-phenyl-1*H*-isochromene (**26_2**), and 5,7,4′-trihydroxy-anthocyanidin chloride.

oxygen, and their resonance is δ 8.01 and 9.04 ppm, respectively. The H-6 and H-8 signals are shifted upfield (δ 6.63 and 6.91 ppm, respectively) due to the presence of hydroxy substituents at C-5 and C-7. In the ^{13}C NMR spectrum, the C-2 and C-7 are both above δ 172 ppm. Next are the C-5 and C-8, around δ 160 ppm. The C-4 is still shifted downfield due to the resonance structures formed (δ 149.6 ppm). The rest of the carbons stay below δ 115 ppm, with the C-8 being the lowest (δ 96.2 ppm).

Other chromene, flavanone, and flavone derivatives' NMR can be found in literature, especially of (*Z*/*E*)-2-aryl-4-chloro-3-styryl-2*H*-chromenes and 3-methylflavones, whose complete characterization was done for more than five derivatives by Rocha et al. [211–213].

The xanthene (**28**) (Figure 13.35) is a symmetric molecule, which reduces the number of peaks in NMR spectra and increases their intensities. However, when different substituents are attached to the aromatic rings, those signals are split into several ones. The chemical shifts of xanthene and two derivatives, including xanthone (**29**) (Figure 13.35), are gathered in Tables 13.24 and 13.25. We suggest an earlier publication in literature for a more detailed xanthone derivatives characterization [214].

Table 13.24 ^{1}H NMR chemical shifts (δ, ppm) of xanthene-related O-heterocycles, in certain solvents.

Compound	H-10	H-(1–4)	H-(5–8)	Solvent	References
28 10*H*-Xanthene	4.031	6.89–7.32	—	$CDCl_3$	[215]
28a 10-Phenyl-10*H*-xanthen-10-ol	—	7.18 (H-1) 7.28 (H-2) 7.042 (H-3) 7.340 (H-4)	—	$CDCl_3$	[216]
29a 1,6-Dimethoxy-4-hydroxy-7-(3-oxobutyl)-xanthone	—	7.50 (H-2) 7.02 (H-3)	7.61 (H-5) 7.41 (H-8)	Acetone-d_6	[217]

Table 13.25 ^{13}C NMR chemical shifts (δ, ppm) of xanthene-related O-heterocycles, in certain solvents.

Compound	C-(4a,8a–10a)	C-(1–4)	C-(5–8)	Solvent	References
28 10*H*-Xanthene	120.5 (C-4a) 152.0 (C-8a) 27.8 (C-10)	116.4 (C-1) 127.6 (C-2) 122.9 (C-3) 128.8 (C-4)	—	$CDCl_3$	[218]
28a 10-Phenyl-10*H*-xanthen-10-ol	127.2 (C-4a) 149.6 (C-8a) 70.4 (C-10)	116.4 (C-1) 127.9 (C-2) 123.5 (C-3) 129.0 (C-4)	—	$CDCl_3$	[219]
29a 1,6-Dimethoxy-4-hydroxy-7-(3-oxobutyl)-xanthone	107.6 (C-4a) 149.9 (C-8a) 148.4 (C-9a) 181.9 (C-10) 120.6 (C-10a)	145.8 (C-1) 120.4 (C-2) 108.3 (C-3) 154.1 (C-4)	116.1 (C-5) 152.2 (C-6) 132.2 (C-7) 117.4 (C-8)	Acetone-d_6	[217]

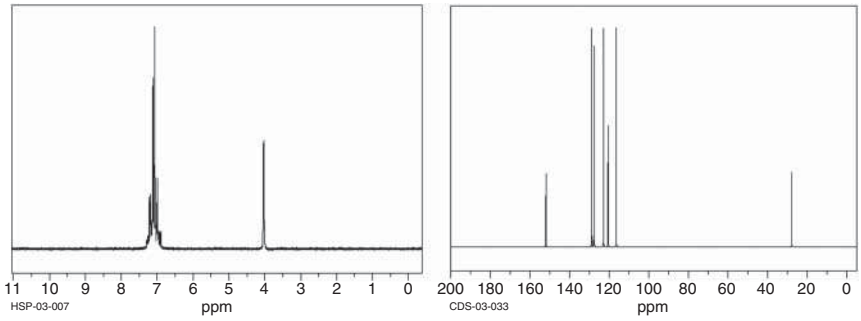

Figure 13.39 10H-Xanthene (**28**) ^{1}H and ^{13}C NMR spectra. Source: SDBSWeb: https://sdbs.db.aist.go.jp. National Institute of Advanced Industrial Science and Technology, accessed 05 December 2021.

For compound **28** (Figure 13.35), the aromatic protons resonate between δ 6.89 and 7.32 ppm, whereas the methylene protons appear at δ 4.03 ppm (Figure 13.39). In derivative **28a** (Figure 13.40), H-10 has been substituted by a phenyl and a hydroxy group. The aromatic protons range between δ 7.04 and 7.34 ppm, with the chemical shift increasing in the order H-3 < H-1 < H-2 < H-4.

In the xanthone derivative **29a**, only four protons from the heterocycle remain in the structure. The H-3 is the most shielded with a chemical shift of δ 7.02 ppm. The H-2 and H-5 are shifted downfield by the carbonyl's resonance to δ 7.50 and 7.61 ppm. Finally, the H-8 signal appears at δ 7.41 ppm.

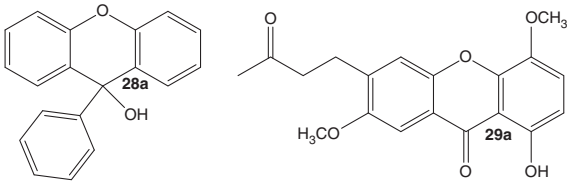

Figure 13.40 Derivatives of 10*H*-xanthene (**28**) and xanthone (**29**): 10-phenyl-10*H*-xanthen-10-ol (**28a**), 4,8-dimethoxy-1-hydroxy-7-(3-oxobutyl)xanthone (**29a**).

The ^{13}C NMR spectra are more complex than the ^{1}H NMR spectra, but usually, 2D experiments are used to obtain the complete assignment. In the xanthene (**28**), the carbons next to the oxygen (C-8a) are the most deshielded (δ 152.0 ppm) (Figure 13.39). On the opposite side of the spectrum, methylene carbon is the most shielded one (δ 27.8 ppm). The last carbon from the central ring resonates at δ 120.5 ppm, close to the signals of the other rings' carbons. The C-1 and C-3 are affected by the resonance involving the ethereal oxygen, therefore having lower chemical shifts (δ 116.4 and 122.9 ppm, respectively). The other two carbons resonate around δ 128 ppm. In derivative **28a**, the C-10 becomes more deshielded due to the phenyl group and the hydroxyl's inductive effect (δ 70.4 ppm). The C-4a also seems to be affected by the substituents, although to a lesser extent (δ 127.2 ppm is a smaller increase in the chemical shift comparatively to C-10). The other carbons resonate practically at the same frequencies as in compound **28**.

The last example, compound **29a**, has a very unshielded signal for C-10 (δ 181.9 ppm), which is now a carbonyl group. The presence of this carbonyl group also shifts downfield the C-8a and C-9a to values around δ 149 ppm. The substituted C-1, C-4, and C-8 have higher chemical shifts due to the inductive effect of the substituents (around $\Delta\delta$ 29 ppm for the methoxy and $\Delta\delta$ 25 ppm for the hydroxy groups). Significant upfield shifts are the carbons C-4a, C-3 (both in resonance with the hydroxy substituent), and C-9 (resonates with the 8-methoxy substituent), and the remaining carbons have similar chemical shifts to the ones observed for xanthene (**28**).

13.7 Conclusions and Perspectives

It is evident that heterocyclic oxygen compounds are necessary scaffolds, and so their NMR characterization is crucial. However, the gathered data showed that some oxygen heterocycles are less studied, in particular 1,3-dioxetanes (**7**) and dioxins (**20** and **21**). Another flaw that we can highlight is the missing data concerning ^{17}O NMR spectra. Moreover, recent NMR studies involving the complete characterization of several O-heterocycle derivatives are scarce, particularly those to establish their stereochemistry. In fact, several of these O-heterocycles have stereocenters that induce non-equivalence in the adjacent protons and the assignment of these diastereotopic protons is vital to establish a compound's stereochemistry.

Acknowledgments

Thanks are due to the University of Aveiro and Fundação para a Ciência e Tecnologia/Ministério da Ciência, Tecnologia e Ensino Superior (FCT/MCTES) for the financial support to LAQV-REQUIMTE (UIDB/50006/2020) research unit through national funds and, where applicable, co-financed by the Fundo Europeu de Desenvolvimento Regional (FEDER), within the PT2020 Partnership Agreement. The authors acknowledge SDBSWeb: https://sdbs.db.aist.go.jp (National Institute of Advanced Industrial Science and Technology, accessed 05 December 2021) for the ^{1}H and ^{13}C NMR spectra.

References

1 Pinto, D.C.G.A., Santos, C.M.M., and Silva, A.M.S. (2007). Advanced NMR techniques for structural characterization of heterocyclic structures. In: *Recent Research Developments in Heterocyclic Chemistry* (ed. T. M. V. D. Pinho e Melo), 397–475. Research Signpost.

2 Karak, N. (2012). 7 – Vegetable oil-based epoxies. In: *Vegetable Oil-Based Polymers* (ed. N. Karak), 180–207. Woodhead Publishing.

3 Aerts, H.A.J. and Jacobs, P.A. (2004). Epoxide yield determination of oils and fatty acid methyl esters using ^{1}H NMR. *J. Am. Oil Chem. Soc.* 81 (9): 841–846. https://doi.org/10.1007/s11746-004-0989-1.

4 Stille, J.K. and Whitehurst, D.D. (1964). Oxirene. An intermediate in the peroxyacid oxidation of acetylenes. *J. Am. Chem. Soc.* 86 (22): 4871–4876. https://doi.org/10.1021/ja01076a029.

5 AIST: Spectral Database for Organic Compounds, SDBS (1999). SDBS-^{1}H NMRSDBS No. 9291HPM-02-720. https://sdbs.db.aist.go.jp/sdbs/cgi-bin/cre_frame_disp.cgi?spectrum_type=hnmr&sdbsno=9291 (accessed 05 December 2021).

6 Davies, S.G. and Whitham, G.H. (1975). Carbon-13 nuclear magnetic resonance spectra of some epoxides. *J. Chem. Soc. Perkin Trans. 2* (8): 861. https://doi.org/10.1039/p29750000861.

7 Iwamura, H., Sugawara, T., Kawada, Y. et al. (1979). ^{17}O NMR chemical shifts versus structure relationships in oxiranes. *Tetrahedron Lett.* 20 (36): 3449–3452. https://doi.org/10.1016/S0040-4039(01)95432-2.

8 Creegan, K.M., Robbins, J.L., Robbins, W.K. et al. (1992). Synthesis and characterization of $C_{60}O$, the first fullerene epoxide. *J. Am. Chem. Soc.* 114 (3): 1103–1105. https://doi.org/10.1021/ja00029a058.

9 AIST: Spectral Database for Organic Compounds, SDBS https://sdbs.db.aist.go.jp/sdbs/cgi-bin/direct_frame_top.cgi (accessed 05 December 2021).

10 AIST: Spectral Database for Organic Compounds, SDBS (1999). SDBS-^{13}C NMRSDBS No. 2907CDS-03-945. https://sdbs.db.aist.go.jp/sdbs/cgi-bin/cre_frame_disp.cgi?spectrum_type=cnmr&sdbsno=2907 (accessed 05 December 2021).

11 AIST: Spectral Database for Organic Compounds, SDBS (1999). SDBS-^{1}H NMRSDBS No. 2907HSP-01-259. https://sdbs.db.aist.go.jp/sdbs/cgi-bin/cre_frame_disp.cgi?spectrum_type=hnmr&sdbsno=2907 (accessed 05 December 2021).

12 AIST: Spectral Database for Organic Compounds, SDBS (1999). SDBS-^{1}H NMRSDBS No. 11268HSP-04-393. https://sdbs.db.aist.go.jp/sdbs/cgi-bin/cre_frame_disp.cgi?spectrum_type=hnmr&sdbsno=11268 (accessed 05 December 2021).

13 Tarhouni, R., Kirschleger, B., Rambaud, M., and Villieras, J. (1984). Monohalomethyllithium XCH2Li: stabilization of a potential synthetic reagent. *Tetrahedron Lett.* 25 (8): 835–838. https://doi.org/10.1016/S0040-4039(01)80040-X.

14 Sadhu, K.M. and Matteson, D.S. (1986). (Chloromethyl) lithium in an efficient conversion of carbonyl compounds to chlorohydrins or oxiranes. *Tetrahedron Lett.* 27 (7): 795–798. https://doi.org/10.1016/S0040-4039(00)84103-9.

15 AIST: Spectral Database for Organic Compounds, SDBS (1999). SDBS-^{1}H NMRSDBS No. 6341HSP-01-211. https://sdbs.db.aist.go.jp/sdbs/cgi-bin/cre_frame_disp.cgi?spectrum_type=hnmr&sdbsno=6341 (accessed 05 December 2021).

16 Villa, L., Schenetti, L., and Taddei, F. (1973). ^{1}H NMR spectra of oxiranes. *cis*-Arylmethyl oxiranes substituted in the phenyl ring. *Org. Magn. Reson.* 5 (12): 593–594. https://doi.org/10.1002/mrc.1270051209.

17 Benassi, R., Lazzeretti, P., Moretti, I. et al. (1973). Substituent effect on the ^{1}H NMR Spectra of trans aryl methyl oxiranes and arylpropenes. *Org. Magn. Reson.* 5 (8): 391–396. https://doi.org/10.1002/mrc.1270050809.

18 AIST: Spectral Database for Organic Compounds, SDBS (1999). SDBS-^{1}H NMRSDBS No. 9288HPM-02-727. https://sdbs.db.aist.go.jp/sdbs/cgi-bin/cre_frame_disp.cgi?spectrum_type=hnmr&sdbsno=9288 (accessed 05 December 2021).

19 AIST: Spectral Database for Organic Compounds, SDBS (1999). SDBS-^{1}H NMRSDBS No. 9285HPM-02-730. https://sdbs.db.aist.go.jp/sdbs/cgi-bin/cre_frame_disp.cgi?spectrum_type=hnmr&sdbsno=9285 (accessed 05 December 2021).

20 AIST: Spectral Database for Organic Compounds, SDBS (1999). SDBS-^{1}H NMRSDBS No. 9287HPM-02-728. https://sdbs.db.aist.go.jp/sdbs/cgi-bin/cre_frame_disp.cgi?spectrum_type=hnmr&sdbsno=9287 (accessed 05 December 2021).

21 Adam, W., Curci, R., and Edwards, J.O. (1989). Dioxiranes: a new class of powerful oxidants. *Acc. Chem. Res.* 22 (6): 205–211. https://doi.org/10.1021/ar00162a002.

22 Wuitschik, G., Rogers-Evans, M., Müller, K. et al. (2006). Oxetanes as promising modules in drug discovery. *Angew. Chem. Int. Ed.* 45 (46): 7736–7739. https://doi.org/10.1002/anie.200602343.

23 Nájera, C., Foubelo, F., Sansano, J.M., and Yus, M. (2020). Stereodivergent routes in organic synthesis: marine natural products, lactones, other natural

products, heterocycles and unnatural compounds. *Org. Biomol. Chem.* 18 (7): 1279–1336. https://doi.org/10.1039/C9OB02597A.

24 Dejaegher, Y., Kuz'menok, N.M., Zvonok, A.M., and De Kimpe, N. (2002). The chemistry of Azetidin-3-ones, Oxetan-3-ones, and Thietan-3-ones. *Chem. Rev.* 102 (1): 29–60. https://doi.org/10.1021/cr990134z.

25 Ducruix, A., Pascard, C., David, S., and Fischer, J.-C. (1975). Crystal and molecular structure of a carbohydrate-derived oxetan-3-one. Definitive evidence for a novel participation of a pyranose ring oxygen atom. *J. Chem. Soc. Perkin Trans. 2* (14): 1678–1682. https://doi.org/10.1039/P29760001678.

26 AIST: Spectral Database for Organic Compounds, SDBS (1999). SDBS-^{1}H NMRSDBS No. 4097HSP-00-242. https://sdbs.db.aist.go.jp/sdbs/cgi-bin/cre_frame_disp.cgi?spectrum_type=hnmr&sdbsno=4097 (accessed 05 December 2021).

27 Wynberg, H. and Staring, E.G.J. (1985). Catalytic asymmetric synthesis of chiral 4-substituted 2-oxetanones. *J. Org. Chem.* 50 (11): 1977–1979. https://doi.org/10.1021/jo00211a039.

28 Thijs, L., Cillissen, P.J.M., and Zwanenburg, B. (1992). An efficient synthesis of oxetanones from α,β-epoxy diazomethyl ketones. *Tetrahedron* 48 (45): 9985–9990. https://doi.org/10.1016/S0040-4020(01)92288-4.

29 Perrin, C.L. and Arrhenius, T. (1978). Malonic anhydride. *J. Am. Chem. Soc.* 100 (16): 5249–5251. https://doi.org/10.1021/ja00484a078.

30 AIST: Spectral Database for Organic Compounds, SDBS (1999). SDBS-^{13}C NMRSDBS No. 4097CDS-03-702. https://sdbs.db.aist.go.jp/sdbs/cgi-bin/cre_frame_disp.cgi?spectrum_type=cnmr&sdbsno=4097 (accessed 05 December 2021).

31 AIST: Spectral Database for Organic Compounds, SDBS (1999). SDBS-^{1}H NMRSDBS No. 8840HPM-02-579. https://sdbs.db.aist.go.jp/sdbs/cgi-bin/cre_frame_disp.cgi?spectrum_type=hnmr&sdbsno=8840 (accessed 05 December 2021).

32 AIST: Spectral Database for Organic Compounds, SDBS (1999). SDBS-^{1}H NMRSDBS No. 8841HPM-02-580. https://sdbs.db.aist.go.jp/sdbs/cgi-bin/cre_frame_disp.cgi?spectrum_type=hnmr&sdbsno=8841 (accessed 05 December 2021).

33 AIST: Spectral Database for Organic Compounds, SDBS (1999). SDBS-^{1}H NMRSDBS No. 19930HPM-00-723. https://sdbs.db.aist.go.jp/sdbs/cgi-bin/cre_frame_disp.cgi?spectrum_type=hnmr&sdbsno=19930 (accessed 05 December 2021).

34 AIST: Spectral Database for Organic Compounds, SDBS (1999). SDBS-^{13}C NMRSDBS No. 19930CDS-12-139. https://sdbs.db.aist.go.jp/sdbs/cgi-bin/cre_frame_disp.cgi?spectrum_type=cnmr&sdbsno=19930 (accessed 05 December 2021).

35 AIST: Spectral Database for Organic Compounds, SDBS (1999). SDBS-^{1}H NMRSDBS No. 3667HSP-05-067. https://sdbs.db.aist.go.jp/sdbs/cgi-bin/cre_frame_disp.cgi?spectrum_type=hnmr&sdbsno=3667 (accessed 05 December 2021).

36 AIST: Spectral Database for Organic Compounds, SDBS (1999). SDBS-^{13}C NMRSDBS No. 3667CDS-07-117. https://sdbs.db.aist.go.jp/sdbs/cgi-bin/cre_frame_disp.cgi?spectrum_type=cnmr&sdbsno=3667 (accessed 05 December 2021).

37 AIST: Spectral Database for Organic Compounds, SDBS (1999). SDBS-^{1}H NMRSDBS No. 5306HPM-00-285. https://sdbs.db.aist.go.jp/sdbs/cgi-bin/cre_frame_disp.cgi?spectrum_type=hnmr&sdbsno=5306 (accessed 05 December 2021).

38 AIST: Spectral Database for Organic Compounds, SDBS (1999). SDBS-^{13}C NMRSDBS No. 5306CDS-05-898. https://sdbs.db.aist.go.jp/sdbs/cgi-bin/cre_frame_disp.cgi?spectrum_type=cnmr&sdbsno=5306 (accessed 05 December 2021).

39 Friedrich, L.E. and Lam, P.Y.-S. (1981). Syntheses and reactions of 3-phenyloxete and the parent unsubstituted oxete. *J. Org. Chem.* 46 (2): 306–311. https://doi.org/10.1021/jo00315a016.

40 Asghari, S. and Habibi, A.K. (2005). Triphenylphosphine-catalyzed synthesis of stable, functionalized 2*H*-oxetes. *Phosphorus Sulfur Silicon Relat. Elem.* 180 (11): 2451–2456. https://doi.org/10.1080/104265090921182.

41 Adam, W., Sauter, M., and Zünkler, C. (1994). Preparation of 2*H*-benzoxetes by photoinduced [2+2] cycloaddition of quinone methides, accessible by dimethyldioxirane (DMD) oxidation of 2,3-dimethylbenzofurans. *Chem. Ber.* 127 (6): 1115–1118. https://doi.org/10.1002/cber.19941270622.

42 Ohkubo, K., Nanjo, T., and Fukuzumi, S. (2005). Efficient photocatalytic oxygenation of aromatic alkene to 1,2-dioxetane with oxygen via electron transfer. *Org. Lett.* 7 (19): 4265–4268. https://doi.org/10.1021/ol051696+.

43 Bartlett, P.D. and Schaap, A.P. (1970). Stereospecific formation of 1,2-dioxetanes from *cis*- and *trans*-diethoxyethylenes by singlet oxygen. *J. Am. Chem. Soc.* 92 (10): 3223–3225. https://doi.org/10.1021/ja00713a072.

44 Schaap, A.P. and Gagnon, S.D. (1982). Chemiluminescence from a phenoxide-substituted 1,2-dioxetane: a model for firefly bioluminescence. *J. Am. Chem. Soc.* 104 (12): 3504–3506. https://doi.org/10.1021/ja00376a044.

45 Schaap, A.P., Handley, R.S., and Giri, B.P. (1987). Chemical and enzymatic triggering of 1,2-dioxetanes. 1: aryl esterase-catalyzed chemiluminescence from a naphthyl acetate-substituted dioxetane. *Tetrahedron Lett.* 28 (9): 935–938. https://doi.org/10.1016/S0040-4039(00)95878-7.

46 Schaap, A.P., Chen, T.-S., Handley, R.S. et al. (1987). Chemical and enzymatic triggering of 1,2-dioxetanes. 2: fluoride-induced chemiluminescence from *tert*-butyldimethylsilyloxy-substituted dioxetanes. *Tetrahedron Lett.* 28 (11): 1155–1158. https://doi.org/10.1016/S0040-4039(00)95313-9.

47 Schaap, A.P., Sandison, M.D., and Handley, R.S. (1987). Chemical and enzymatic triggering of 1,2-dioxetanes. 3: alkaline phosphatase-catalyzed chemiluminescence from an aryl phosphate-substituted dioxetane. *Tetrahedron Lett.* 28 (11): 1159–1162. https://doi.org/10.1016/S0040-4039(00)95314-0.

48 Bos, R., Barnett, N.W., Dyson, G.A. et al. (2004). Studies on the mechanism of the peroxyoxalate chemiluminescence reaction: Part 1. Confirmation of

1,2-dioxetanedione as an intermediate using ^{13}C nuclear magnetic resonance spectroscopy. *Anal. Chim. Acta* 502 (2): 141–147. https://doi.org/10.1016/j.aca.2003.10.014.

49 Cordier, C., Leach, S., and Nelson, A. (2014). Product class 7: 1,3-dioxetanes and 1,3-dioxolanes. In: *Science of Synthesis: Houben-Weyl Methods of Molecular Transformations Vol. 29: Acetals: Hal/X and O/O, S, Se, Te*, vol. 29 (ed. S.L. Warriner), 407–486. Georg Thieme Verlag.

50 Wikipedia (2021). Tetrahydrofuran. https://en.wikipedia.org/w/index.php?title=Tetrahydrofuran&oldid=998143682 (accessed 05 December 2021).

51 AIST: Spectral Database for Organic Compounds, SDBS (1999). SDBS-^{1}H NMRSDBS No. 497HSP-05-077. https://sdbs.db.aist.go.jp/sdbs/cgi-bin/cre_frame_disp.cgi?spectrum_type=hnmr&sdbsno=497 (accessed 05 December 2021).

52 AIST: Spectral Database for Organic Compounds, SDBS (1999). SDBS-^{13}C NMRSDBS No. 497CDS-03-462. https://sdbs.db.aist.go.jp/sdbs/cgi-bin/cre_frame_disp.cgi?spectrum_type=cnmr&sdbsno=497 (accessed 05 December 2021).

53 AIST: Spectral Database for Organic Compounds, SDBS (1999). SDBS-^{1}H NMRSDBS No. 2397HSP-47-025. https://sdbs.db.aist.go.jp/sdbs/cgi-bin/cre_frame_disp.cgi?spectrum_type=hnmr&sdbsno=2397 (accessed 05 December 2021).

54 AIST: Spectral Database for Organic Compounds, SDBS (1999). SDBS-^{13}C NMRSDBS No. 2397CDS-00-577. https://sdbs.db.aist.go.jp/sdbs/cgi-bin/cre_frame_disp.cgi?spectrum_type=cnmr&sdbsno=2397 (accessed 05 December 2021).

55 AIST: Spectral Database for Organic Compounds, SDBS (1999). SDBS-^{13}C NMRSDBS No. 15553CDS-09-403. https://sdbs.db.aist.go.jp/sdbs/cgi-bin/cre_frame_disp.cgi?spectrum_type=cnmr&sdbsno=15553 (accessed 05 December 2021).

56 AIST: Spectral Database for Organic Compounds, SDBS (1999). SDBS-^{1}H NMRSDBS No. 5314HSP-04-084. https://sdbs.db.aist.go.jp/sdbs/cgi-bin/cre_frame_disp.cgi?spectrum_type=hnmr&sdbsno=5314 (accessed 05 December 2021).

57 AIST: Spectral Database for Organic Compounds, SDBS (1999). SDBS-^{13}C NMRSDBS No. 5314CDS-06-071. https://sdbs.db.aist.go.jp/sdbs/cgi-bin/cre_frame_disp.cgi?spectrum_type=cnmr&sdbsno=5314 (accessed 05 December 2021).

58 AIST: Spectral Database for Organic Compounds, SDBS (1999). SDBS-^{13}C NMRSDBS No. 8999CDS-04-540. https://sdbs.db.aist.go.jp/sdbs/cgi-bin/cre_frame_disp.cgi?spectrum_type=cnmr&sdbsno=8999 (accessed 05 December 2021).

59 AIST: Spectral Database for Organic Compounds, SDBS (1999). SDBS-^{1}H NMRSDBS No. 12809HSP-03-321. https://sdbs.db.aist.go.jp/sdbs/cgi-bin/cre_frame_disp.cgi?spectrum_type=hnmr&sdbsno=12809 (accessed 05 December 2021).

60 AIST: Spectral Database for Organic Compounds, SDBS (1999). SDBS-^{13}C NMRSDBS No. 12809CDS-05-557. https://sdbs.db.aist.go.jp/sdbs/cgi-bin/cre_frame_disp.cgi?spectrum_type=cnmr&sdbsno=12809 (accessed 05 December 2021).

61 AIST: Spectral Database for Organic Compounds, SDBS (1999). SDBS-^{1}H NMRSDBS No. 6229HSP-01-240. https://sdbs.db.aist.go.jp/sdbs/cgi-bin/cre_frame_disp.cgi?spectrum_type=hnmr&sdbsno=6229 (accessed 05 December 2021).

62 AIST: Spectral Database for Organic Compounds, SDBS (1999). SDBS-^{13}C NMRSDBS No. 6229CDS-04-475. https://sdbs.db.aist.go.jp/sdbs/cgi-bin/cre_frame_disp.cgi?spectrum_type=cnmr&sdbsno=6229 (accessed 05 December 2021).

63 AIST: Spectral Database for Organic Compounds, SDBS (1999). SDBS-^{1}H NMRSDBS No. 1325HSP-47-023. https://sdbs.db.aist.go.jp/sdbs/cgi-bin/cre_frame_disp.cgi?spectrum_type=hnmr&sdbsno=1325 (accessed 05 December 2021).

64 AIST: Spectral Database for Organic Compounds, SDBS (1999). SDBS-^{13}C NMRSDBS No. 1325CDS-00-277. https://sdbs.db.aist.go.jp/sdbs/cgi-bin/cre_frame_disp.cgi?spectrum_type=cnmr&sdbsno=1325 (accessed 05 December 2021).

65 Achmatowicz, O. and Bialecka-Florjańczyk, E. (1996). Mechanism of the carbonyl-ene reaction. *Tetrahedron* 52 (26): 8827–8834. https://doi.org/10.1016/0040-4020(96)00424-3.

66 Wu, J., Serianni, A.S., and Vuorinen, T. (1990). Furanose ring anomerization: kinetic and thermodynamic studies of the d-2-pentuloses by ^{13}C-NMR spectroscopy. *Carbohydr. Res.* 206 (1): 1–12. https://doi.org/10.1016/0008-6215(90)84001-B.

67 AIST: Spectral Database for Organic Compounds, SDBS (1999). SDBS-^{1}H NMRSDBS No. 41161HR2002-00190TS. https://sdbs.db.aist.go.jp/sdbs/cgi-bin/cre_frame_disp.cgi?spectrum_type=hnmr&sdbsno=41161 (accessed 05 December 2021).

68 AIST: Spectral Database for Organic Compounds, SDBS (1999). SDBS-^{13}C NMRSDBS No. 41161CR2002-00190TS. https://sdbs.db.aist.go.jp/sdbs/cgi-bin/cre_frame_disp.cgi?spectrum_type=cnmr&sdbsno=41161 (accessed 05 December 2021).

69 AIST: Spectral Database for Organic Compounds, SDBS (1999). SDBS-^{1}H NMRSDBS No. 13357HSP-48-886. https://sdbs.db.aist.go.jp/sdbs/cgi-bin/cre_frame_disp.cgi?spectrum_type=hnmr&sdbsno=13357 (accessed 05 December 2021).

70 AIST: Spectral Database for Organic Compounds, SDBS (1999). SDBS-^{13}C NMRSDBS No. 13357CDS-12-019. https://sdbs.db.aist.go.jp/sdbs/cgi-bin/cre_frame_disp.cgi?spectrum_type=cnmr&sdbsno=13357 (accessed 05 December 2021).

71 AIST: Spectral Database for Organic Compounds, SDBS (1999). SDBS-^{1}H NMRSDBS No. 1313HSP-01-913. https://sdbs.db.aist.go.jp/sdbs/cgi-bin/

cre_frame_disp.cgi?spectrum_type=hnmr&sdbsno=1313 (accessed 05 December 2021).

72 AIST: Spectral Database for Organic Compounds, SDBS (1999). SDBS-^{13}C NMRSDBS No. 1313CDS-00-261. https://sdbs.db.aist.go.jp/sdbs/cgi-bin/cre_frame_disp.cgi?spectrum_type=cnmr&sdbsno=1313 (accessed 05 December 2021).

73 AIST: Spectral Database for Organic Compounds, SDBS (1999). SDBS-^{1}H NMRSDBS No. 2803HSP-47-024. https://sdbs.db.aist.go.jp/sdbs/cgi-bin/cre_frame_disp.cgi?spectrum_type=hnmr&sdbsno=2803 (accessed 05 December 2021).

74 AIST: Spectral Database for Organic Compounds, SDBS (1999). SDBS-^{13}C NMRSDBS No. 2803CDS-00-848. https://sdbs.db.aist.go.jp/sdbs/cgi-bin/cre_frame_disp.cgi?spectrum_type=cnmr&sdbsno=2803 (accessed 05 December 2021).

75 AIST: Spectral Database for Organic Compounds, SDBS (1999). SDBS-^{1}H NMRSDBS No. 9353HSP-06-162. https://sdbs.db.aist.go.jp/sdbs/cgi-bin/cre_frame_disp.cgi?spectrum_type=hnmr&sdbsno=9353 (accessed 05 December 2021).

76 AIST: Spectral Database for Organic Compounds, SDBS (1999). SDBS-^{13}C NMRSDBS No. 9353CDS-09-935. https://sdbs.db.aist.go.jp/sdbs/cgi-bin/cre_frame_disp.cgi?spectrum_type=cnmr&sdbsno=9353 (accessed 05 December 2021).

77 AIST: Spectral Database for Organic Compounds, SDBS (1999). SDBS-^{1}H NMRSDBS No. 10444HPM-00-546. https://sdbs.db.aist.go.jp/sdbs/cgi-bin/cre_frame_disp.cgi?spectrum_type=hnmr&sdbsno=10444 (accessed 05 December 2021).

78 *AIST: Spectral Database for Organic Compounds, SDBS* (1999). SDBS-^{13}C NMRSDBS No. 10444CDS-12-541. https://sdbs.db.aist.go.jp/sdbs/cgi-bin/cre_frame_disp.cgi?spectrum_type=cnmr&sdbsno=10444 (accessed 05 December 2021).

79 AIST: Spectral Database for Organic Compounds, SDBS (1999). SDBS-^{1}H NMRSDBS No. 1309HSP-05-839. https://sdbs.db.aist.go.jp/sdbs/cgi-bin/cre_frame_disp.cgi?spectrum_type=hnmr&sdbsno=1309 (accessed 05 December 2021).

80 AIST: Spectral Database for Organic Compounds, SDBS (1999). SDBS-^{13}C NMRSDBS No. 1309CDS-00-257. https://sdbs.db.aist.go.jp/sdbs/cgi-bin/cre_frame_disp.cgi?spectrum_type=cnmr&sdbsno=1309 (accessed 05 December 2021).

81 AIST: Spectral Database for Organic Compounds, SDBS (1999). SDBS-^{1}H NMRSDBS No. 1HSP-05-139. https://sdbs.db.aist.go.jp/sdbs/cgi-bin/cre_frame_disp.cgi?spectrum_type=hnmr&sdbsno=1 (accessed 05 December 2021).

82 AIST: Spectral Database for Organic Compounds, SDBS (1999). SDBS-^{13}C NMRSDBS No. 1CDS-07-852. https://sdbs.db.aist.go.jp/sdbs/cgi-bin/cre_frame_disp.cgi?spectrum_type=cnmr&sdbsno=1 (accessed 05 December 2021).

83 AIST: Spectral Database for Organic Compounds, SDBS (1999). SDBS-^{1}H NMRSDBS No. 9409HPM-02-815. https://sdbs.db.aist.go.jp/sdbs/cgi-bin/cre_frame_disp.cgi?spectrum_type=hnmr&sdbsno=9409 (accessed 05 December 2021).

84 Harper, J.K., Arif, A.M., Ford, E.J. et al. (2003). Pestacin: a 1,3-dihydro isobenzofuran from Pestalotiopsis microspora possessing antioxidant and antimycotic activities. *Tetrahedron* 59 (14): 2471–2476. https://doi.org/10.1016/S0040-4020(03)00255-2.

85 AIST: Spectral Database for Organic Compounds, SDBS (1999). SDBS-^{1}H NMRSDBS No. 1353HSP-02-707. https://sdbs.db.aist.go.jp/sdbs/cgi-bin/cre_frame_disp.cgi?spectrum_type=hnmr&sdbsno=1353 (accessed 05 December 2021).

86 AIST: Spectral Database for Organic Compounds, SDBS (1999). SDBS-^{13}C NMRSDBS No. 1353CDS-00-315. https://sdbs.db.aist.go.jp/sdbs/cgi-bin/cre_frame_disp.cgi?spectrum_type=cnmr&sdbsno=1353 (accessed 05 December 2021).

87 AIST: Spectral Database for Organic Compounds, SDBS (1999). SDBS-^{1}H NMRSDBS No. 8873HSP-40-320. https://sdbs.db.aist.go.jp/sdbs/cgi-bin/cre_frame_disp.cgi?spectrum_type=hnmr&sdbsno=8873 (accessed 05 December 2021).

88 AIST: Spectral Database for Organic Compounds, SDBS (1999). SDBS-^{13}C NMRSDBS No. 8873CDS-04-327. https://sdbs.db.aist.go.jp/sdbs/cgi-bin/cre_frame_disp.cgi?spectrum_type=cnmr&sdbsno=8873 (accessed 05 December 2021).

89 AIST: Spectral Database for Organic Compounds, SDBS (1999). SDBS-^{1}H NMRSDBS No. 16812HSP-40-920. https://sdbs.db.aist.go.jp/sdbs/cgi-bin/cre_frame_disp.cgi?spectrum_type=hnmr&sdbsno=16812 (accessed 05 December 2021).

90 AIST: Spectral Database for Organic Compounds, SDBS (1999). SDBS-^{13}C NMRSDBS No. 16812CDS-13-072. https://sdbs.db.aist.go.jp/sdbs/cgi-bin/cre_frame_disp.cgi?spectrum_type=cnmr&sdbsno=16812 (accessed 05 December 2021).

91 Shubin, D.A., Kuznetsov, D.N., Kobrakov, K.I. et al. (2019). Synthesis of aurone derivatives on the basis of 2,4,6-trihydroxytoluene. *Chem. Heterocycl. Compd.* 55 (12): 1174–1178. https://doi.org/10.1007/s10593-019-02597-0.

92 AIST: Spectral Database for Organic Compounds, SDBS (1999). SDBS-^{1}H NMRSDBS No. 1180HSP-40-203. https://sdbs.db.aist.go.jp/sdbs/cgi-bin/cre_frame_disp.cgi?spectrum_type=hnmr&sdbsno=1180 (accessed 05 December 2021).

93 AIST: Spectral Database for Organic Compounds, SDBS (1999). SDBS-^{13}C NMRSDBS No. 1180CDS-03-034. https://sdbs.db.aist.go.jp/sdbs/cgi-bin/cre_frame_disp.cgi?spectrum_type=cnmr&sdbsno=1180 (accessed 05 December 2021).

94 Keul, H., Kuczkowski, R.L., and Choi, H.-S. (1985). Ozonolysis of enol ethers: formation of 3-alkoxy-1,2-dioxolanes by concerted addition of a carbonyl oxide

to an enol ether. *J. Org. Chem.* 50 (18): 3365–3371. https://doi.org/10.1021/jo00218a024.

95 Wojciechowski, B.J., Chiang, C.Y., and Kuczkowski, R.L. (1990). Ozonolysis of 1,1-dimethoxyethene, 1,2-dimethoxyethene and vinyl acetate. *J. Org. Chem.* 55 (3): 1120–1122. https://doi.org/10.1021/jo00290a062.

96 Okada, M., Mita, K., and Sumitomo, H. (1975). Polymerizability of methyl substituted 1,3-dioxolanes. *Makromol. Chem.* 176 (4): 859–872. https://doi.org/10.1002/macp.1975.021760403.

97 Chen, R., Jiang, Y., Li, J. et al. (2015). Dielectric and optical anisotropy enhanced by 1,3-dioxolane terminal substitution on tolane-liquid crystals. *J. Mater. Chem. C* 3 (33): 8706–8711. https://doi.org/10.1039/C5TC01712B.

98 AIST: Spectral Database for Organic Compounds, SDBS (1999). SDBS-^{1}H NMRSDBS No. 4103HPM-00-064. https://sdbs.db.aist.go.jp/sdbs/cgi-bin/cre_frame_disp.cgi?spectrum_type=hnmr&sdbsno=4103 (accessed 05 December 2021).

99 AIST: Spectral Database for Organic Compounds, SDBS (1999). SDBS-^{13}C NMRSDBS No. 4103CDS-03-841. https://sdbs.db.aist.go.jp/sdbs/cgi-bin/cre_frame_disp.cgi?spectrum_type=cnmr&sdbsno=4103 (accessed 05 December 2021).

100 AIST: Spectral Database for Organic Compounds, SDBS (1999). SDBS-^{1}H NMRSDBS No. 4471HSP-00-230. https://sdbs.db.aist.go.jp/sdbs/cgi-bin/cre_frame_disp.cgi?spectrum_type=hnmr&sdbsno=4471 (accessed 05 December 2021).

101 AIST: Spectral Database for Organic Compounds, SDBS (1999). SDBS-^{13}C NMRSDBS No. 4471CDS-04-108. https://sdbs.db.aist.go.jp/sdbs/cgi-bin/cre_frame_disp.cgi?spectrum_type=cnmr&sdbsno=4471 (accessed 05 December 2021).

102 AIST: Spectral Database for Organic Compounds, SDBS (1999). SDBS-^{1}H NMRSDBS No. 11296HSP-44-230. https://sdbs.db.aist.go.jp/sdbs/cgi-bin/cre_frame_disp.cgi?spectrum_type=hnmr&sdbsno=11296 (accessed 05 December 2021).

103 AIST: Spectral Database for Organic Compounds, SDBS (1999). SDBS-^{13}C NMRSDBS No. 11296CDS-02-855. https://sdbs.db.aist.go.jp/sdbs/cgi-bin/cre_frame_disp.cgi?spectrum_type=cnmr&sdbsno=11296 (accessed 05 December 2021).

104 AIST: Spectral Database for Organic Compounds, SDBS (1999). SDBS-^{1}H NMRSDBS No. 15510HSP-48-695. https://sdbs.db.aist.go.jp/sdbs/cgi-bin/cre_frame_disp.cgi?spectrum_type=hnmr&sdbsno=15510 (accessed 05 December 2021).

105 AIST: Spectral Database for Organic Compounds, SDBS (1999). SDBS-^{13}C NMRSDBS No. 15510CDS-07-978. https://sdbs.db.aist.go.jp/sdbs/cgi-bin/cre_frame_disp.cgi?spectrum_type=cnmr&sdbsno=15510 (accessed 05 December 2021).

106 AIST: Spectral Database for Organic Compounds, SDBS (1999). SDBS-^{1}H NMRSDBS No. 19320HSP-46-674. https://sdbs.db.aist.go.jp/sdbs/cgi-bin/

cre_frame_disp.cgi?spectrum_type=hnmr&sdbsno=19320 (accessed 05 December 2021).

107 AIST: Spectral Database for Organic Compounds, SDBS (1999). SDBS-^{13}C NMRSDBS No. 19320CDS-01-082. https://sdbs.db.aist.go.jp/sdbs/cgi-bin/cre_frame_disp.cgi?spectrum_type=cnmr&sdbsno=19320 (accessed 05 December 2021).

108 IST: Spectral Database for Organic Compounds, SDBS (1999). SDBS-^{1}H NMRSDBS No. 51056HR2003-00385TS. https://sdbs.db.aist.go.jp/sdbs/cgi-bin/cre_frame_disp.cgi?spectrum_type=hnmr&sdbsno=51056 (accessed 05 December 2021).

109 AIST: Spectral Database for Organic Compounds, SDBS (1999). SDBS-^{13}C NMRSDBS No. 51056CR2003-00385TS. https://sdbs.db.aist.go.jp/sdbs/cgi-bin/cre_frame_disp.cgi?spectrum_type=cnmr&sdbsno=51056 (accessed 05 December 2021).

110 AIST: Spectral Database for Organic Compounds, SDBS (1999). SDBS-^{1}H NMRSDBS No. 8465HPM-02-520. https://sdbs.db.aist.go.jp/sdbs/cgi-bin/cre_frame_disp.cgi?spectrum_type=hnmr&sdbsno=8465 (accessed 05 December 2021).

111 Soriano, N.U., Migo, V.P., and Matsumura, M. (2003). Functional group analysis during ozonation of sunflower oil methyl esters by FT-IR and NMR. *Chem. Phys. Lipids* 126 (2): 133–140. https://doi.org/10.1016/j.chemphyslip.2003.07.001.

112 Ewing, J.C., Cosgrove, J.P., Giamalva, D.H. et al. (1989). Autoxidation of methyl linoleate initiated by the ozonide of allylbenzene. *Lipids* 24 (7): 609. https://doi.org/10.1007/BF02535077.

113 Wu, M., Church, D.F., Mahier, T.J. et al. (1992). Separation and spectral data of the six isomeric ozonides from methyl oleate. *Lipids* 27 (2): 129–135. https://doi.org/10.1007/BF02535812.

114 Yadav, J.S., Reddy, B.V.S., Sreelakshmi, C. et al. (2008). Enantioselective reduction of 2-substituted tetrahydropyran-4-ones using Daucus carota plant cells. *Tetrahedron Lett.* 49 (17): 2768–2771. https://doi.org/10.1016/j.tetlet.2008.02.131.

115 AIST: Spectral Database for Organic Compounds, SDBS (1999). SDBS-^{1}H NMRSDBS No. 2399HSP-00-510. https://sdbs.db.aist.go.jp/sdbs/cgi-bin/cre_frame_disp.cgi?spectrum_type=hnmr&sdbsno=2399 (accessed 05 December 2021).

116 AIST: Spectral Database for Organic Compounds, SDBS (1999). SDBS-^{13}C NMRSDBS No. 2399CDS-00-579. https://sdbs.db.aist.go.jp/sdbs/cgi-bin/cre_frame_disp.cgi?spectrum_type=cnmr&sdbsno=2399 (accessed 05 December 2021).

117 AIST: Spectral Database for Organic Compounds, SDBS (1999). SDBS-^{13}C NMRSDBS No. 1827CDS-00-440. https://sdbs.db.aist.go.jp/sdbs/cgi-bin/cre_frame_disp.cgi?spectrum_type=cnmr&sdbsno=1827 (accessed 05 December 2021).

118 AIST: Spectral Database for Organic Compounds, SDBS (1999). SDBS-^{1}H NMRSDBS No. 10334HSP-00-684. https://sdbs.db.aist.go.jp/sdbs/cgi-bin/

cre_frame_disp.cgi?spectrum_type=hnmr&sdbsno=10334 (accessed 05 December 2021).

119 AIST: Spectral Database for Organic Compounds, SDBS (1999). SDBS-^{13}C NMRSDBS No. 10334CDS-04-233. https://sdbs.db.aist.go.jp/sdbs/cgi-bin/cre_frame_disp.cgi?spectrum_type=cnmr&sdbsno=10334 (accessed 05 December 2021).

120 AIST: Spectral Database for Organic Compounds, SDBS (1999). SDBS-^{1}H NMRSDBS No. 21841HSP-40-511. https://sdbs.db.aist.go.jp/sdbs/cgi-bin/cre_frame_disp.cgi?spectrum_type=hnmr&sdbsno=21841 (accessed 05 December 2021).

121 AIST: Spectral Database for Organic Compounds, SDBS (1999). SDBS-^{13}C NMRSDBS No. 21841CDS-07-681. https://sdbs.db.aist.go.jp/sdbs/cgi-bin/cre_frame_disp.cgi?spectrum_type=cnmr&sdbsno=21841 (accessed 05 December 2021).

122 AIST: Spectral Database for Organic Compounds, SDBS (1999). SDBS-^{1}H NMRSDBS No. 21907HSP-43-650. https://sdbs.db.aist.go.jp/sdbs/cgi-bin/cre_frame_disp.cgi?spectrum_type=hnmr&sdbsno=21907 (accessed 05 December 2021).

123 AIST: Spectral Database for Organic Compounds, SDBS (1999). SDBS-^{13}C NMRSDBS No. 21907CDS-09-571. https://sdbs.db.aist.go.jp/sdbs/cgi-bin/cre_frame_disp.cgi?spectrum_type=cnmr&sdbsno=21907 (accessed 05 December 2021).

124 AIST: Spectral Database for Organic Compounds, SDBS (1999). SDBS-^{1}H NMRSDBS No. 15725HSP-41-165. https://sdbs.db.aist.go.jp/sdbs/cgi-bin/cre_frame_disp.cgi?spectrum_type=hnmr&sdbsno=15725 (accessed 05 December 2021).

125 AIST: Spectral Database for Organic Compounds, SDBS (1999). SDBS-^{13}C NMRSDBS No. 15725CDS-09-875. https://sdbs.db.aist.go.jp/sdbs/cgi-bin/cre_frame_disp.cgi?spectrum_type=cnmr&sdbsno=15725 (accessed 05 December 2021).

126 Bubb, W.A. (2003). NMR spectroscopy in the study of carbohydrates: Characterizing the structural complexity. *Concepts Magn. Reson. Part A* 19A (1): 1–19. https://doi.org/10.1002/cmr.a.10080.

127 AIST: Spectral Database for Organic Compounds, SDBS (1999). SDBS-^{1}H NMRSDBS No. 11512HSP-43-749. https://sdbs.db.aist.go.jp/sdbs/cgi-bin/cre_frame_disp.cgi?spectrum_type=hnmr&sdbsno=11512 (accessed 05 December 2021).

128 AIST: Spectral Database for Organic Compounds, SDBS (1999). SDBS-^{13}C NMRSDBS No. 11512CDS-02-653. https://sdbs.db.aist.go.jp/sdbs/cgi-bin/cre_frame_disp.cgi?spectrum_type=cnmr&sdbsno=11512 (accessed 05 December 2021).

129 AIST: Spectral Database for Organic Compounds, SDBS (1999). SDBS-^{13}C NMRSDBS No. 16040CDS-02-652. https://sdbs.db.aist.go.jp/sdbs/cgi-bin/cre_frame_disp.cgi?spectrum_type=cnmr&sdbsno=16040 (accessed 05 December 2021).

130 AIST: Spectral Database for Organic Compounds, SDBS (1999). SDBS-^{1}H NMRSDBS No. 15490HSP-48-993. https://sdbs.db.aist.go.jp/sdbs/cgi-bin/cre_frame_disp.cgi?spectrum_type=hnmr&sdbsno=15490 (accessed 05 December 2021).

131 AIST: Spectral Database for Organic Compounds, SDBS (1999). SDBS-^{13}C NMRSDBS No. 15490CDS-07-009. https://sdbs.db.aist.go.jp/sdbs/cgi-bin/cre_frame_disp.cgi?spectrum_type=cnmr&sdbsno=15490 (accessed 05 December 2021).

132 AIST: Spectral Database for Organic Compounds, SDBS (1999). SDBS-^{1}H NMRSDBS No. 1183HSP-49-668. https://sdbs.db.aist.go.jp/sdbs/cgi-bin/cre_frame_disp.cgi?spectrum_type=hnmr&sdbsno=1183 (accessed 05 December 2021).

133 AIST: Spectral Database for Organic Compounds, SDBS (1999). SDBS-^{13}C NMRSDBS No. 1183CDS-07-026. https://sdbs.db.aist.go.jp/sdbs/cgi-bin/cre_frame_disp.cgi?spectrum_type=cnmr&sdbsno=1183 (accessed 05 December 2021).

134 AIST: Spectral Database for Organic Compounds, SDBS (1999). SDBS-^{1}H NMRSDBS No. 2023HSP-47-803. https://sdbs.db.aist.go.jp/sdbs/cgi-bin/cre_frame_disp.cgi?spectrum_type=hnmr&sdbsno=2023 (accessed 05 December 2021).

135 AIST: Spectral Database for Organic Compounds, SDBS (1999). SDBS-^{13}C NMRSDBS No. 2023CDS-07-025. https://sdbs.db.aist.go.jp/sdbs/cgi-bin/cre_frame_disp.cgi?spectrum_type=cnmr&sdbsno=2023 (accessed 05 December 2021).

136 AIST: Spectral Database for Organic Compounds, SDBS (1999). SDBS-^{1}H NMRSDBS No. 16041HSP-45-786. https://sdbs.db.aist.go.jp/sdbs/cgi-bin/cre_frame_disp.cgi?spectrum_type=hnmr&sdbsno=16041 (accessed 05 December 2021).

137 AIST: Spectral Database for Organic Compounds, SDBS (1999). SDBS-^{13}C NMRSDBS No. 16041CDS-10-028. https://sdbs.db.aist.go.jp/sdbs/cgi-bin/cre_frame_disp.cgi?spectrum_type=cnmr&sdbsno=16041 (accessed 05 December 2021).

138 Michalik, M., Hein, M., and Frank, M. (2000). NMR spectra of fluorinated carbohydrates. *Carbohydr. Res.* 327 (1): 185–218. https://doi.org/10.1016/S0008-6215(99)00323-7.

139 Goel, A. and Ram, V.J. (2009). Natural and synthetic 2*H*-pyran-2-ones and their versatility in organic synthesis. *Tetrahedron* 65 (38): 7865–7913. https://doi.org/10.1016/j.tet.2009.06.031.

140 AIST: Spectral Database for Organic Compounds, SDBS (1999). SDBS-^{1}H NMRSDBS No. 9839HPM-03-217. https://sdbs.db.aist.go.jp/sdbs/cgi-bin/cre_frame_disp.cgi?spectrum_type=hnmr&sdbsno=9839 (accessed 05 December 2021).

141 AIST: Spectral Database for Organic Compounds, SDBS (1999). SDBS-^{1}H NMRSDBS No. 9848HPM-03-226. https://sdbs.db.aist.go.jp/sdbs/cgi-bin/

cre_frame_disp.cgi?spectrum_type=hnmr&sdbsno=9848 (accessed 05 December 2021).

142 Kepe, V., Kočevar, M., and Polanc, S. (1996). One-pot synthesis of some 2*H*-Pyran-2-one derivatives. *J. Heterocycl. Chem.* 33 (6): 1707–1710. https://doi.org/10.1002/jhet.5570330626.

143 AIST: Spectral Database for Organic Compounds, SDBS (1999). SDBS-^{1}H NMRSDBS No. 9844HPM-03-222. https://sdbs.db.aist.go.jp/sdbs/cgi-bin/cre_frame_disp.cgi?spectrum_type=hnmr&sdbsno=9844 (accessed 05 December 2021).

144 Pascual, C., Martin, N., and Seoane, C. (1985). ^{13}C NMR spectra of 2-amino-4*H*-pyran derivatives. *Magn. Reson. Chem.* 23 (9): 793–794. https://doi.org/10.1002/mrc.1260230924.

145 AIST: Spectral Database for Organic Compounds, SDBS (1999). SDBS-^{1}H NMRSDBS No. 13662HPM-03-239. https://sdbs.db.aist.go.jp/sdbs/cgi-bin/cre_frame_disp.cgi?spectrum_type=hnmr&sdbsno=13662 (accessed 05 December 2021).

146 AIST: Spectral Database for Organic Compounds, SDBS (1999). SDBS-^{13}C NMRSDBS No. 13662CR2004-00503NS. https://sdbs.db.aist.go.jp/sdbs/cgi-bin/cre_frame_disp.cgi?spectrum_type=cnmr&sdbsno=13662 (accessed 05 December 2021).

147 AIST: Spectral Database for Organic Compounds, SDBS (1999). SDBS-^{1}H NMRSDBS No. 9861HPM-03-240. https://sdbs.db.aist.go.jp/sdbs/cgi-bin/cre_frame_disp.cgi?spectrum_type=hnmr&sdbsno=9861 (accessed 05 December 2021).

148 AIST: Spectral Database for Organic Compounds, SDBS (1999). SDBS-^{1}H NMRSDBS No. 2292HSP-04-491. https://sdbs.db.aist.go.jp/sdbs/cgi-bin/cre_frame_disp.cgi?spectrum_type=hnmr&sdbsno=2292 (accessed 05 December 2021).

149 AIST: Spectral Database for Organic Compounds, SDBS (1999). SDBS-^{13}C NMRSDBS No. 2292CDS-06-430. https://sdbs.db.aist.go.jp/sdbs/cgi-bin/cre_frame_disp.cgi?spectrum_type=cnmr&sdbsno=2292 (accessed 05 December 2021).

150 AIST: Spectral Database for Organic Compounds, SDBS (1999). SDBS-^{13}C NMRSDBS No. 5706CDS-09-010. https://sdbs.db.aist.go.jp/sdbs/cgi-bin/cre_frame_disp.cgi?spectrum_type=cnmr&sdbsno=5706 (accessed 05 December 2021).

151 Sándor, P. and Radics, L. (1981). High resolution NMR spectroscopy of heteroaromatic cations. II—Pyrylium, thiapyrylium and seleninium cations. *Org. Magn. Reson.* 16 (2): 148–155. https://doi.org/10.1002/mrc.1270160218.

152 Balaban, A.T. and Wray, V. (1977). ^{13}C NMR spectra of some pyrylium salts and related compounds. *Org. Magn. Reson.* 9 (1): 16–22. https://doi.org/10.1002/mrc.1270090105.

153 Senthilkumar, K. and Kolandaivel, P. (2003). Structure, conformation and NMR studies on 1,2-dioxane and halogen substituted 1,2-dioxane molecules. *Comput. Biol. Chem.* 27 (3): 173–183. https://doi.org/10.1016/S0097-8485(02)00019-0.

154 AIST: Spectral Database for Organic Compounds, SDBS (1999). SDBS-^{1}H NMRSDBS No. 1231HSP-03-850. https://sdbs.db.aist.go.jp/sdbs/cgi-bin/cre_frame_disp.cgi?spectrum_type=hnmr&sdbsno=1231 (accessed 05 December 2021).

155 AIST: Spectral Database for Organic Compounds, SDBS (1999). SDBS-^{13}C NMRSDBS No. 1231CDS-00-148. https://sdbs.db.aist.go.jp/sdbs/cgi-bin/cre_frame_disp.cgi?spectrum_type=cnmr&sdbsno=1231 (accessed 05 December 2021).

156 AIST: Spectral Database for Organic Compounds, SDBS 1999.Available on https://sdbs.db.aist.go.jp/sdbs/cgi-bin/cre_frame_disp.cgi?spectrum_type=hnmr&sdbsno=8427 (accessed 05 December 2021).

157 AIST: Spectral Database for Organic Compounds, SDBS (1999). SDBS-^{1}H NMRSDBS No. 10201HSP-47-591. https://sdbs.db.aist.go.jp/sdbs/cgi-bin/cre_frame_disp.cgi?spectrum_type=hnmr&sdbsno=10201 (accessed 05 December 2021).

158 AIST: Spectral Database for Organic Compounds, SDBS (1999). SDBS-^{13}C NMRSDBS No. 10201CDS-04-102. https://sdbs.db.aist.go.jp/sdbs/cgi-bin/cre_frame_disp.cgi?spectrum_type=cnmr&sdbsno=10201 (accessed 05 December 2021).

159 AIST: Spectral Database for Organic Compounds, SDBS (1999). SDBS-^{1}H NMRSDBS No. 6701HSP-01-376. https://sdbs.db.aist.go.jp/sdbs/cgi-bin/cre_frame_disp.cgi?spectrum_type=hnmr&sdbsno=6701 (accessed 05 December 2021).

160 AIST: Spectral Database for Organic Compounds, SDBS (1999). SDBS-^{13}C NMRSDBS No. 6701CDS-04-892. https://sdbs.db.aist.go.jp/sdbs/cgi-bin/cre_frame_disp.cgi?spectrum_type=cnmr&sdbsno=6701 (accessed 05 December 2021).

161 AIST: Spectral Database for Organic Compounds, SDBS (1999). SDBS-^{1}H NMRSDBS No. 890HPM-00-024. https://sdbs.db.aist.go.jp/sdbs/cgi-bin/cre_frame_disp.cgi?spectrum_type=hnmr&sdbsno=890 (accessed 05 December 2021).

162 AIST: Spectral Database for Organic Compounds, SDBS (1999). SDBS-^{13}C NMRSDBS No. 890CDS-00-116. https://sdbs.db.aist.go.jp/sdbs/cgi-bin/cre_frame_disp.cgi?spectrum_type=cnmr&sdbsno=890 (accessed 05 December 2021).

163 AIST: Spectral Database for Organic Compounds, SDBS (1999). SDBS-^{1}H NMRSDBS No. 4252HSP-02-264. https://sdbs.db.aist.go.jp/sdbs/cgi-bin/cre_frame_disp.cgi?spectrum_type=hnmr&sdbsno=4252 (accessed 05 December 2021).

164 AIST: Spectral Database for Organic Compounds, SDBS (1999). SDBS-^{13}C NMRSDBS No. 4252CDS-07-260. https://sdbs.db.aist.go.jp/sdbs/cgi-bin/cre_frame_disp.cgi?spectrum_type=cnmr&sdbsno=4252 (accessed 05 December 2021).

165 AIST: Spectral Database for Organic Compounds, SDBS (1999). SDBS-^{1}H NMRSDBS No. 5501HPM-00-354. https://sdbs.db.aist.go.jp/sdbs/cgi-bin/cre_frame_disp.cgi?spectrum_type=hnmr&sdbsno=5501 (accessed 05 December 2021).

166 AIST: Spectral Database for Organic Compounds, SDBS (1999). SDBS-^{13}C NMRSDBS No. 5501CDS-07-522. https://sdbs.db.aist.go.jp/sdbs/cgi-bin/cre_frame_disp.cgi?spectrum_type=cnmr&sdbsno=5501 (accessed 05 December 2021).

167 AIST: Spectral Database for Organic Compounds, SDBS (1999). SDBS-^{1}H NMRSDBS No. 2428HSP-48-781. https://sdbs.db.aist.go.jp/sdbs/cgi-bin/cre_frame_disp.cgi?spectrum_type=hnmr&sdbsno=2428 (accessed 05 December 2021).

168 AIST: Spectral Database for Organic Compounds, SDBS (1999). SDBS-^{13}C NMRSDBS No. 2428CDS-00-616. https://sdbs.db.aist.go.jp/sdbs/cgi-bin/cre_frame_disp.cgi?spectrum_type=cnmr&sdbsno=2428 (accessed 05 December 2021).

169 Posner, G.H. and Oh, C.H. (1992). Regiospecifically oxygen-18 labeled 1,2,4-trioxane: a simple chemical model system to probe the mechanism(s) for the antimalarial activity of artemisinin (qinghaosu). *J. Am. Chem. Soc.* 114 (21): 8328–8329. https://doi.org/10.1021/ja00047a076.

170 AIST: Spectral Database for Organic Compounds, SDBS (1999). SDBS-^{13}C NMRSDBS No. 2156CDS-00-530. https://sdbs.db.aist.go.jp/sdbs/cgi-bin/cre_frame_disp.cgi?spectrum_type=cnmr&sdbsno=2156 (accessed 05 December 2021).

171 AIST: Spectral Database for Organic Compounds, SDBS (1999). SDBS-^{13}C NMRSDBS No. 1320CDS-00-269. https://sdbs.db.aist.go.jp/sdbs/cgi-bin/cre_frame_disp.cgi?spectrum_type=cnmr&sdbsno=1320 (accessed 05 December 2021).

172 AIST: Spectral Database for Organic Compounds, SDBS (1999). SDBS-^{13}C NMRSDBS No. 7991CDS-02-596. https://sdbs.db.aist.go.jp/sdbs/cgi-bin/cre_frame_disp.cgi?spectrum_type=cnmr&sdbsno=7991 (accessed 05 December 2021).

173 AIST: Spectral Database for Organic Compounds, SDBS 1999. SDBS-^{13}C NMRSDBS No. 17092CDS-02-478. https://sdbs.db.aist.go.jp/sdbs/cgi-bin/cre_frame_disp.cgi?spectrum_type=cnmr&sdbsno=17092 (accessed 05 December 2021).

174 AIST: Spectral Database for Organic Compounds, SDBS (1999). SDBS-^{13}C NMRSDBS No. 7990CDS-13-414 https://sdbs.db.aist.go.jp/sdbs/cgi-bin/cre_frame_disp.cgi?spectrum_type=cnmr&sdbsno=7990 (accessed 05 December 2021).

175 Dong, Y. and Vennerstrom, J.L. (2001). Differentiation between 1,2,4,5-tetraoxanes and 1,2,4,5,7,8-hexaoxonanes using ^{1}H and ^{13}C NMR analyses. *J. Heterocycl. Chem.* 38 (2): 463–466. https://doi.org/10.1002/jhet.5570380224.

176 Fouda, A.M. (2016). Synthesis of several 4*H*-chromene derivatives of expected antitumor activity. *Med. Chem. Res.* 25 (6): 1229–1238.

177 Sabry, N.M., Mohamed, H.M., Khattab, E.S.A.E.H. et al. (2011). Synthesis of 4*H*-chromene, coumarin, 12*H*-chromeno[2,3-*d*]pyrimidine derivatives and some of their antimicrobial and cytotoxicity activities. *Eur. J. Med. Chem.* 46 (2): 765–772. https://doi.org/10.1016/j.ejmech.2010.12.015.

178 Dige, N.C., Mahajan, P.G., Raza, H. et al. (2020). Synthesis and characterization of new 4*H*-chromene-3-carboxylates ensuring potent elastase inhibition activity along with their molecular docking and chemoinformatics properties. *Bioorganic Chem.* 100: 103906. https://doi.org/10.1016/j.bioorg.2020.103906.

179 Duddeck, H. and Kaiser, M. (1982). ^{13}C NMR spectroscopy of coumarin derivatives. *Org. Magn. Reson.* 20 (2): 55–72. https://doi.org/10.1002/mrc.1270200202.

180 AIST: Spectral Database for Organic Compounds, SDBS (1999). SDBS-^{1}H NMRSDBS No. 52372HR2009-01886NS. https://sdbs.db.aist.go.jp/sdbs/cgi-bin/cre_frame_disp.cgi?spectrum_type=hnmr&sdbsno=52372 (accessed 05 December 2021).

181 AIST: Spectral Database for Organic Compounds, SDBS (1999). SDBS-^{1}H NMRSDBS No. 53384HR2014-02952NS. https://sdbs.db.aist.go.jp/sdbs/cgi-bin/cre_frame_disp.cgi?spectrum_type=hnmr&sdbsno=53384 (accessed 05 December 2021).

182 Erdogdu, Y., Yurdakul, Ş., Badoglu, S., and Güllüoğlu, M.T. (2019). Electronic [UV–visible] and vibrational [FT-IR] investigation and NMR spectroscopic analysis of some halogen substituted chromone (6-Fluorochromone, 6-Chlorochromone, 6-Bromochromone). *J. Mol. Struct.* 1184: 364–374. https://doi.org/10.1016/j.molstruc.2019.02.016.

183 AIST: Spectral Database for Organic Compounds, SDBS (1999). SDBS-^{1}H NMRSDBS No. 53440HR2016-03287NS. https://sdbs.db.aist.go.jp/sdbs/cgi-bin/cre_frame_disp.cgi?spectrum_type=hnmr&sdbsno=53440 (accessed 05 December 2021).

184 AIST: Spectral Database for Organic Compounds, SDBS (1999). SDBS-^{1}H NMRSDBS No. 23664HSP-45-562. https://sdbs.db.aist.go.jp/sdbs/cgi-bin/cre_frame_disp.cgi?spectrum_type=hnmr&sdbsno=23664 (accessed 05 December 2021).

185 Pinto, D.C.G.A., Silva, A.M.S., and Cavaleiro, J.A.S. (2000). A convenient synthesis of new (*E*)-5-hydroxy-2-styrylchromones by modifications of the Baker–Venkataraman method. *New J. Chem.* 24 (2): 85–92. https://doi.org/10.1039/A908539D.

186 Albogami, A., Karama, U., Mousa, A. et al. (2012). Simple and efficient one step synthesis of functionalized flavanones and chalcones. *Orient. J. Chem.* 28: 619–626. https://doi.org/10.13005/ojc/280201.

187 AIST: Spectral Database for Organic Compounds, SDBS (1999). SDBS-^{1}H NMRSDBS No. 41407HR2009-01932NS. https://sdbs.db.aist.go.jp/sdbs/cgi-bin/cre_frame_disp.cgi?spectrum_type=hnmr&sdbsno=41407 (accessed 05 December 2021).

188 AIST: Spectral Database for Organic Compounds, SDBS (1999). SDBS-^{1}H NMRSDBS No. 22007HSP-44-526. https://sdbs.db.aist.go.jp/sdbs/cgi-bin/cre_frame_disp.cgi?spectrum_type=hnmr&sdbsno=22007 (accessed 05 December 2021).

189 Santos, R.A.L.S. (2020). *A DMPU's Study: Characterization and Applicability as Solvent in Organic Reactions*. University of Aveiro.

190 AIST: Spectral Database for Organic Compounds, SDBS (1999). SDBS-^{1}H NMRSDBS No. 52202HR2009-01839NS. https://sdbs.db.aist.go.jp/sdbs/cgi-bin/cre_frame_disp.cgi?spectrum_type=hnmr&sdbsno=52202 (accessed 05 December 2021).

191 AIST: Spectral Database for Organic Compounds, SDBS (1999). SDBS-^{1}H NMRSDBS No. 51754HR2007-01366NY. https://sdbs.db.aist.go.jp/sdbs/cgi-bin/cre_frame_disp.cgi?spectrum_type=hnmr&sdbsno=51754 (accessed 05 December 2021).

192 Lee, E.-J., Moon, B.-H., Park, Y. et al. (2008). Effects of hydroxy and methoxy substituents on NMR data in Flavonols. *Bull. Korean Chem. Soc.* 29 (2): 507–510. https://doi.org/10.5012/bkcs.2008.29.2.507.

193 Fathiazad, F., Delazar, A., Amiri, R., and Sarker, S.D. (2010). Extraction of flavonoids and quantification of rutin from waste tobacco leaves. *Iran. J. Pharm. Res.* 5 (3): 222–227. https://doi.org/10.22037/ijpr.2010.680.

194 Obika, S., Kono, H., Yasui, Y. et al. (2007). Concise synthesis of 1,2-dihydroisoquinolines and 1*H*-isochromenes by carbophilic Lewis acid-catalyzed tandem nucleophilic addition and cyclization of 2-(1-alkynyl)arylaldimines and 2-(1-alkynyl)arylaldehydes. *J. Org. Chem.* 72 (12): 4462–4468. https://doi.org/10.1021/jo070615f.

195 Kouda-Bonafos, M., Nacro, M., and Ancian, B. (1996). Total assignment of ^{1}H and ^{13}C NMR chemical shifts of a natural anthocyanidin, apigeninidin, using two-dimensional COLOC and HMBC techniques. *Magn. Reson. Chem.* 34 (5): 389–392. https://doi.org/10.1002/(SICI)1097-458X(199605)34:5<389::AID-OMR888>3.0.CO;2-9.

196 AIST: Spectral Database for Organic Compounds, SDBS (1999). SDBS-^{13}C NMRSDBS No. 52372CR2009-01886NS. https://sdbs.db.aist.go.jp/sdbs/cgi-bin/cre_frame_disp.cgi?spectrum_type=cnmr&sdbsno=52372 (accessed 05 December 2021).

197 AIST: Spectral Database for Organic Compounds, SDBS (1999). SDBS-^{13}C NMRSDBS No. 53440CR2016-03287NS. https://sdbs.db.aist.go.jp/sdbs/cgi-bin/cre_frame_disp.cgi?spectrum_type=cnmr&sdbsno=53440 (accessed 05 December 2021).

198 AIST: Spectral Database for Organic Compounds, SDBS (1999). SDBS-^{13}C NMRSDBS No. 23664CDS-11-876. https://sdbs.db.aist.go.jp/sdbs/cgi-bin/cre_frame_disp.cgi?spectrum_type=cnmr&sdbsno=23664 (accessed 05 December 2021).

199 AIST: Spectral Database for Organic Compounds, SDBS (1999). SDBS-^{13}C NMRSDBS No. 41407CR2009-01932NS. https://sdbs.db.aist.go.jp/sdbs/cgi-bin/

cre_frame_disp.cgi?spectrum_type=cnmr&sdbsno=41407 (accessed 05 December 2021).

200 AIST: Spectral Database for Organic Compounds, SDBS (1999). SDBS-^{13}C NMRSDBS No. 22007CDS-11-083. https://sdbs.db.aist.go.jp/sdbs/cgi-bin/cre_frame_disp.cgi?spectrum_type=cnmr&sdbsno=22007 (accessed 05 December 2021).

201 AIST: Spectral Database for Organic Compounds, SDBS (1999). SDBS-^{13}C NMRSDBS No. 52202CR2009-01839NS. https://sdbs.db.aist.go.jp/sdbs/cgi-bin/cre_frame_disp.cgi?spectrum_type=cnmr&sdbsno=52202 (accessed 05 December 2021).

202 AIST: Spectral Database for Organic Compounds, SDBS (1999). SDBS-^{13}C NMRSDBS No. 51754CR2007-01366NY. https://sdbs.db.aist.go.jp/sdbs/cgi-bin/cre_frame_disp.cgi?spectrum_type=cnmr&sdbsno=51754 (accessed 05 December 2021).

203 Markham, K.R. and Ternai, B. (1976). ^{13}C NMR of flavonoids—II: flavonoids other then flavone and flavonol aglycones. *Tetrahedron* 32 (21): 2607–2612. https://doi.org/10.1016/0040-4020(76)88036-2.

204 Bovicelli, P., Bernini, R., Antonioletti, R., and Mincione, E. (2002). Selective halogenation of flavanones. *Tetrahedron Lett.* 43 (32): 5563–5567. https://doi.org/10.1016/S0040-4039(02)01117-6.

205 Bano, S., Javed, K., Ahmad, S. et al. (2013). Synthesis of some novel chalcones, flavanones and flavones and evaluation of their anti-inflammatory activity. *Eur. J. Med. Chem.* 65: 51–59. https://doi.org/10.1016/j.ejmech.2013.04.056.

206 Maltese, F., Erkelens, C., van der Kooy, F. et al. (2009). Identification of natural epimeric flavanone glycosides by NMR spectroscopy. *Food Chem.* 116 (2): 575–579. https://doi.org/10.1016/j.foodchem.2009.03.023.

207 Caligiani, A., Palla, G., Maietti, A. et al. (2010). ^{1}H NMR fingerprinting of soybean extracts, with emphasis on identification and quantification of isoflavones. *Nutrients* 2 (3): Art. no. 3. https://doi.org/10.3390/nu2030280.

208 Kim, H., Moon, B.-H., Ahn, J.-H., and Lim, Y. (2006). Complete NMR signal assignments of flavonol derivatives. *Magn. Reson. Chem.* 44 (2): 188–190. https://doi.org/10.1002/mrc.1733.

209 Morimoto, K., Hirano, K., Satoh, T., and Miura, M. (2011). Synthesis of isochromene and related derivatives by rhodium-catalyzed oxidative coupling of benzyl and allyl alcohols with alkynes. *J. Org. Chem.* 76 (22): 9548–9551. https://doi.org/10.1021/jo201923d.

210 Dell'Acqua, M., Castano, B., Cecchini, C. et al. (2014). Mild regiospecific synthesis of 1-alkoxy-isochromenes catalyzed by well-defined [silver(I)(pyridine-containing ligand)] complexes. *J. Org. Chem.* 79 (8): 3494–3505. https://doi.org/10.1021/jo5002559.

211 Rocha, D.H.A., Pinto, D.C.G.A., Seixas, R.S.G.R., and Silva, A.M.S. (2014). 3-Methylflavones characterization revisited: complete assignment of ^{1}H and ^{13}C NMR data. *Magn. Reson. Chem.* 52 (1, 2): 47–50. https://doi.org/10.1002/mrc.4026.

212 Rocha, D.H.A., Vaz, P.A.A.M., Pinto, D.C.G.A., and AMS, S. (2019). Synthesis chalones and their isomerization into flavanones and azaflavanones. *Methods Protoc.* 2: 70. https://doi.org/10.3390/mps2030070.

213 Rocha, D.H.A., Batista, V.F., Balsa, E.J.F. et al. (2020). Chromene- and quinoline-3-carbaldehydes: useful intermediates in the synthesis of heterocyclic scaffolds. *Molecules* 25: 3791. https://doi.org/10.3390/molecules25173791.

214 Silva, A.M.S. and Pinto, D.C.G.A. (2005). Structure elucidation of xanthone derivatives: studies of nuclear magnetic resonance spectroscopy. *Curr. Med. Chem.* 12 (21): 2481–2497. https://doi.org/10.2174/092986705774370718.

215 AIST: Spectral Database for Organic Compounds, SDBS (1999). SDBS-^{1}H NMRSDBS No. 1192HSP-03-007. https://sdbs.db.aist.go.jp/sdbs/cgi-bin/cre_frame_disp.cgi?spectrum_type=hnmr&sdbsno=1192 (accessed 05 December 2021).

216 AIST: Spectral Database for Organic Compounds, SDBS 1999. SDBS-^{1}H NMRSDBS No. 15631HSP-44-176. https://sdbs.db.aist.go.jp/sdbs/cgi-bin/cre_frame_disp.cgi?spectrum_type=hnmr&sdbsno=15631 (accessed 05 December 2021).

217 Huang, Z., Yang, R., Yin, X. et al. (2010). Structure elucidation and NMR assignments for two xanthone derivatives from a mangrove endophytic fungus (No. ZH19). *Magn. Reson. Chem.* 48 (1): 80–82. https://doi.org/10.1002/mrc.2539.

218 AIST: Spectral Database for Organic Compounds, SDBS (1999). SDBS-^{13}C NMRSDBS No. 1192CDS-03-033. https://sdbs.db.aist.go.jp/sdbs/cgi-bin/cre_frame_disp.cgi?spectrum_type=cnmr&sdbsno=1192 (accessed 05 December 2021).

219 AIST: Spectral Database for Organic Compounds, SDBS (1999). SDBS-^{13}C NMRSDBS No. 15631CDS-07-342. https://sdbs.db.aist.go.jp/sdbs/cgi-bin/cre_frame_disp.cgi?spectrum_type=cnmr&sdbsno=15631 (accessed 05 December 2021).

Index

Heterocycles: Synthesis, Catalysis, Sustainability, and Characterization, First Edition.
Edited by Teresa M.V.D. Pinho e Melo and Marta Pineiro.

b

C

d

e

f

g

h

n

p

t